NASA Conference Publication 2413

1+12

Laminar Flow Aircraft Certification

(NASA-CP-2413) LAMINAR FLOW AIRCRAFT
CERTIFICATION (NASA) 325 p CSCL 01A
N88-23737
--THRU--
N88-23749
Unclas
H1/02 0146390

Date for general release May 31, 1988

Proceedings of a workshop
held at Wichita, Kansas
April 15-16, 1985

AIAA SAE FAA NASA

NASA Conference Publication 2413

Laminar Flow Aircraft Certification

Compiled by
Louis J. Williams
Langley Research Center
Hampton, Virginia

Proceedings of a workshop sponsored by
the National Aeronautics and Space
Administration, the American Institute
of Aeronautics and Astronautics, the
Society of Automotive Engineers, and the
Federal Aviation Administration and held at
Wichita, Kansas
April 15-16, 1985

NASA
National Aeronautics
and Space Administration

Scientific and Technical
Information Branch

1986

PREFACE

This workshop on laminar flow aircraft certification was an outgrowth of the NASA/AIAA General Aviation Technology Conference held at the NASA Langley Research Center in 1984. At that conference, several people from NASA Langley, the Federal Aviation Administration, industry, and universities expressed the desire for a forum to discuss the effect of laminar flow aerodynamics on certification procedures for future aircraft. It was felt that such a forum should bring together researchers concerned with maximizing the benefits of laminar flow aerodynamics, manufacturers concerned with developing significantly improved new aircraft, and regulators concerned with applying proper certification procedures to insure safety. By bringing together these diverse interests to address the common goal of developing new aircraft with superior efficiency, it was hoped that an improved understanding of laminar flow aerodynamics technology would be obtained and that improved communications between the participants would serve to guide future efforts.

The workshop was structured to review the state of the art in laminar flow aerodynamics technology and explore technology needs in four areas: test techniques, aerodynamic research, operational procedures, and manufacturing technology. Each participant at the workshop was assigned to a working group in one of these four areas. In order to provide a foundation for these working groups, the workshop began with invited papers addressing each area.

The papers included in this report are largely as presented. The recommendations of each working group are also included. Identification of commercial products in this report does not constitute official endorsement, expressed or implied, of such products by NASA. The special efforts of Frances E. Sabo of the NASA Langley Research Center in organizing the workshop and of Richard A. Vandame of the SAE in providing meeting facilities for this workshop in conjunction with the 1985 SAE General Aviation Aircraft Meeting and Exposition are gratefully acknowledged.

PRECEDING PAGE BLANK NOT FILMED

CONTENTS

PREFACE iii

WORKING GROUP MEMBERS vii

SESSION I

BOUNDARY-LAYER STABILITY AND AIRFOIL DESIGN 1
Jeffrey K. Viken

HIGH-LIFT FLAPS FOR NATURAL LAMINAR FLOW AIRFOILS 31
Harry L. Morgan

COMPUTATIONAL WING DESIGN STUDIES RELATING TO NATURAL LAMINAR FLOW 67
Edgar G. Waggoner

ACOUSTIC DISTURBANCE EFFECTS (Paper unavailable at time of publication)
Parma Mungur

SESSION II

WIND TUNNEL TESTING OF LOW-DRAG AIRFOILS 89
W. D. Harvey, R. J. McGhee, and C. D. Harris

BOUNDARY-LAYER FLOW VISUALIZATION FOR FLIGHT TESTING 129
Clifford J. Obara

BOUNDARY LAYER MEASUREMENTS USING HOT-FILM SENSORS 141
Harlan K. Holmes and Debra L. Carraway

FLIGHT EXPERIENCES WITH LAMINAR FLOW 155
Bruce J. Holmes

SESSION III

MANUFACTURING REQUIREMENTS 171
Bruce J. Holmes, Clifford J. Obara, Glenn L. Martin, and
Christopher S. Domack

PRELIMINARY AERODYNAMIC DESIGN CONSIDERATIONS FOR ADVANCED LAMINAR FLOW AIRCRAFT CONFIGURATIONS 185
Joseph L. Johnson, Jr., Long P. Yip, and Frank L. Jordan, Jr.

NATURAL LAMINAR FLOW AND AIRPLANE STABILITY AND CONTROL 227
C. P. van Dam

OPERATIONAL CONSIDERATIONS FOR LAMINAR FLOW AIRCRAFT 247
Dal V. Maddalon and Richard D. Wagner

PRECEDING PAGE BLANK NOT FILMED

SESSION IV

INDUSTRY PERSPECTIVE 267
Stanley J. Green

CERTIFICATION ASPECTS OF AIRPLANES WHICH MAY OPERATE WITH SIGNIFICANT NATURAL LAMINAR FLOW 269
Edward A. Gabriel and Earsa L. Tankesley

WORKING GROUP SUMMARIES AND RECOMMENDATIONS

TEST TECHNIQUES WORKING GROUP SUMMARY AND RECOMMENDATIONS 279
Bruce J. Holmes, Chairman

AERODYNAMIC RESEARCH WORKING GROUP SUMMARY AND RECOMMENDATIONS 281
Percy J. Bobbitt, Chairman

OPERATIONAL PROCEDURES WORKING GROUP SUMMARY AND RECOMMENDATIONS 317
Charles E. Arnold, Chairman

MANUFACTURING TECHNOLOGY WORKING GROUP SUMMARY AND RECOMMENDATIONS 321
Bert Overfield, Chairman

TEST TECHNIQUES WORKING GROUP MEMBERS

ARCHER Donald D.
Boeing Commercial Airplane Company
Mail Stop 24-13
P.O. Box 3707
Seattle WA 98127-2207

BARNES Terence J.
FAA, C68966
17900 Pacific Highway South
Seattle WA 98168

BARRETT Bruce G.
Cessna Aircraft Company
P.O. Box 1521
Wichita KS 67201

BOPPE Charles W.
Grumman Aerospace Corporation
Mail Stop B-19/35
Bethpage NY 11714

CROOM Cindy C.
NASA Langley Research Center
Mail Stop 286
Hampton VA 23665-5225

HARVEY W. Donald
NASA Langley Research Center
Mail Stop 359
Hampton VA 23665-5225

HEFNER Jerry N.
NASA Langley Research Center
Mail Stop 410
Hampton VA 23665-5225

HOLMES Bruce J. (Chairman)
NASA Langley Research Center
Mail Stop 286
Hampton VA 23665-5225

HOLMES Harlan K.
NASA Langley Research Center
Mail Stop 238
Hampton VA 23665-5225

JOHANSEN Louis
Beech Aircraft Corporation
Mail Station 90-406
P.O. Box 85
Wichita KS 67201

LORD Wesley K.
Pratt & Whitney
Mail Stop 118-25
East Hartford CT 06108

MAGENHEIM Bert
Ideal Research, Inc.
1810 Parklawn Drive
Rockville MD 20852

MAPLE Charles J.
DOT/FAA/ACE-160W
1801 Airport Road
Wichita KS 67209

MILEY Stanley J.
Texas A&M University
Department of Aerospace Engineering
College Station TX 77843

MUELLER Dr. T. J.
University of Notre Dame
Aerospace & Mechanical Engineering
Notre Dame IN 46556

NYENHUIS Roger J.
Cessna Aircraft Company
P.O. Box 7704
Wichita KS 67277

OBARA Clifford J.
PRC Kentron, Inc.
NASA Langley Research Center
Mail Stop 286
Hampton VA 23665-5225

RONCZ John G.
Gemini Technologies, Inc.
1510 E. Colfax Avenue
South Bend IN 46617

TAYLOR Fen
Mooney Aircraft Corporation
Louis Schrener Field
P.O. Box 72
Kerrville TX 78028

TUMLINSON Richard
Beech Aircraft Corporation
9709 East Central Avenue
Wichita KS 67201

WARD Donald T.
Texas A&M University
2702 Teakwood Court
College Station TX 77840

WENTZ William H.
Wichita State University
Aero. Engineering Department
Wichita KS 67208

AERODYNAMIC RESEARCH WORKING GROUP MEMBERS

BOBBITT Percy J. (Chairman)
NASA Langley Research Center
Mail Stop 285
Hampton VA 23665-5225

BRAGG Michael B.
Ohio State University
Aero-Astro Research Lab
2300 W. Case Road
Columbus OH 43220

CARLINE Ken
Fairchild Aircraft Corporation
P.O. Box 32486
San Antonio TX 78284

CLAY James T.
Beech Aircraft Corporation
Mail Stop E5
P.O. Box 85
Wichita KS 67201

GABRIEL Edward A.
FAA
ACE 111
601 East 12th Street
Kansas City MO 64106

HINSON Mike
Gates Learjet Corporation
Mail Stop 45
P.O. Box 7707
Wichita KS 67277

INGRAM Wyatt C.
OMAC, Inc.
P.O. Box 3530
Albany GA 31708

JOHNSON Joseph
NASA Langley Research Center
Mail Stop 355
Hampton VA 23665-5225

KENDALL Eric R.
Gates Learjet Corporation
P.O. Box 7707
Wichita KS 67277

MITCHELL Charles M.
USAF ASD/ENFTA
Wright-Patterson AFB
Wright-Patterson AFB OH 45433-6503

NICKS Oran
Texas A&M University
Aerospace Engineering Division
College Station TX 77843

O'CONNER Mike
11913 Somerville Drive
Yukon OK 73099

PEARCE W. E.
Douglas Aircraft Company
Mail Stop 36-55
3855 Lakewood Boulevard
Long Beach CA 90846

PFEIFFER Neal J.
Beech Aircraft Corporation
P.O. Box 85
Wichita KS 67201

PUTT James C.
BF Goodrich
Aero. & Def. Div., Z/1832, 17-F
500 South Main Street
Akron OH 44318

SELBERG Bruce P.
University of Missouri-Rolla
232 Mechanical Engineering Building
Rolla MO 65401

STEWART Eric
NASA Langley Research Center
Mail Stop 355
Hampton VA 23665-5225

VAN DAM Cornelis
Vigyan Research Associates, Inc.
Mail Stop 286
Langley Research Center
Hampton VA 23665-5225

VIJGEN Paul
University of Kansas
Mail Stop 286
NASA Langley Research Center
Hampton VA 23665-5225

VIKEN Jeff
ESCON
Mail Stop 339
NASA Langley Research Center
Hampton VA 23665-5225

WAGGONER Edward G.
NASA Langley Research Center
Mail Stop 294
Hampton VA 23665-5225

OPERATIONAL PROCEDURES WORKING GROUP MEMBERS

ARNOLD Charles E. (Chairman)
FAA, ACE-106
601 E. 12th Street
Kansas City MO 64106

BAKER Robert
FAA, ACE
Mid-Continental Airport
Wichita KS

ELLIS David R.
Cessna Aircraft Company
Dept. 178
P.O. Box 1521
Wichita KS 67201

HANSMAN R. John
MIT
Mail Code 33-115
Cambridge MS 02139

JORDAN Jerry L.
Kohlman Systems Research
319 Perry Street
Lawrence KS 66044

KALBERER Paul
Cessna Aircraft
P.O. Box 7704
Wichita KS 67277

KOENIG Robert
NASA Langley Research Center
Mail Stop 249
Hampton VA 23665-5225

MADDALON Dal V.
NASA Langley Research Center
Mail Stop 261
Hampton VA 23665-5225

MCSWEENEY Thomas E.
DOT/FAA
AWS-100 Office of Airworthiness
800 Independence Avenue, S.W.
Washington DC 20591

MUNGUR Parma
General Electric
1 Neumann Way
Cincinnati OH 45215

ROSKAM Jan
University of Kansas
Route 4, Box 274
Ottawa KS 66067

SCHROEDER Donald A.
FAA Washington Headquarters
APM-710
800 Independence Avenue
Washington DC 20591

STICKLE Joseph W.
NASA Langley Research Center
Mail Stop 246A
Hampton VA 23665-5225

TERRY James E.
Beech Aircraft
9709 East Central Avenue
Wichita KS 67201

THELANDER Jack A.
Douglas Aircraft Company
3855 Lakewood Boulevard
Long Beach CA 90808

VERSTYNEN Harry A.
FAA/Langley D&L Field Office
Mail Stop 250
NASA Langley Research Center
Hampton VA 23665-5225

WILLIAMS Louis J.
NASA Langley Research Center
Mail Stop 286
Hampton VA 23665-5225

MANUFACTURING TECHNOLOGY WORKING GROUP MEMBERS

BENNETT John A.
Lockheed-Georgia Company
86 S. Cobb Drive
Marietta GA 30060

BERNSTORF David J.
Beech Aircraft Corporation
P.O. Box 85
Wichita KS 67201

CARMICHAEL Bruce H.
Rockwell International
Autonetics Division
34795 Camino Capistrano
Capistrano Beach CA 92624

CAVINESS A. C.
FAA
Apt. 622S
2111 Jefferson Davis Highway
Arlington VA 22202

EKLUND Richard C.
LOCUS, Inc.
2560 Huntington Avenue
Alexandria VA 22309

GREEN Stanley J.
General Aviation Manufacturers Association
Suite 801
1400 K. Street, N.W.
Washington DC 20005

GREGOREK Dr. Gerald M.
Ohio State University
Aero-Astro Research Laboratory
2300 West Case Road
Columbus OH 43220

HAIG Douglas W.
FAA
ACE 120W
1801 Airport Road
Wichita KS 67209

KLAPPROTT Robert
FAA
Mid-Continental Airport
Wichita KS

MORGAN Harry L.
NASA Langley Research Center
Mail Stop 339
Hampton VA 23665-5225

MOUNT Joseph S.
ROHR Industries, Inc.
P.O. Box 878, MZ 19T
Chula Vista CA 92045

OVERFIELD Bert B. (Chairman)
Gates Learjet Corporation
P.O. Box 7707
Wichita KS 67277

SCHULTZ Bill
Beech Aircraft Corporation
9709 East Central
Wichita KS

SMITH A. J.
804 N. Evans
Tecumseh MI 49286

TANKESLEY Earsa
FAA
ACE-110
610 E. 12th Street
Kansas City MO 64106

WATSON-VIKEN Sally
ESCON
Mail Stop 339
NASA Langley Research Center
Hampton VA 23665-5225

51-02

N88-23738

BOUNDARY-LAYER STABILITY AND AIRFOIL DESIGN*

Jeffrey K. Viken
ESCON
Grafton, Virginia 23692

SUMMARY

Several different natural laminar flow (NLF) airfoils have been analyzed for stability of the laminar boundary layer using linear stability codes. The NLF airfoils analyzed come from three different design conditions: incompressible, compressible with no sweep, and compressible with sweep. Some of the design problems are discussed, concentrating on those problems associated with keeping the boundary layer laminar. Also, there is a discussion on how a linear stability analysis was effectively used to improve the design for some of the airfoils.

INTRODUCTION

The problem of designing an airfoil to perform well over a range of conditions instead of just one point is a significant one and is well appreciated by anyone associated with airfoil design. In many cases an airfoil has been chosen for its high-lift characteristics even though it has a high profile drag at cruise. Presently, performance gains associated with low cruise profile drags are being emphasized. The challenge here is to design an airfoil to perform well at cruise while retaining good high-lift performance.

A key element in the design of low-drag laminar flow airfoils is linear stability theory which offers a quantitative method of examining the growth of disturbances in the laminar boundary layer. This tool allows the airfoil designer to design the airfoil for the desired amount of laminar foil. In addition, by designing the laminar boundary layer with just enough stability for the desired conditions, the compromises with other performance areas of the airfoil can be minimized.

This paper uses linear stability theory to illustrate some of the problems associated with designing an airfoil for extensive laminar flow and emphasizes the problems at the cruise condition. Laminar boundary-layer stability analysis is conducted on airfoils for three different design conditions: incompressible, compressible with no sweep, and compressible with sweep. The specific design considerations associated with each flying condition are discussed.

---

*Research by the author was supported by the National Aeronautics and Space Administration under NASA Contract No. NAS1-17670.

SYMBOLS

A/A_o	amplitude ratio of disturbance from initial point of instability
c	chord length
c_d	profile drag coefficient
c_ℓ	section lift coefficient (listed in figures as CL)
c_m	section pitching moment coefficient about the quarter chord point (listed in figures as CM C/4)
C_p	pressure coefficient, $(p - p_\infty)/q_\infty$
f	disturbance frequency, Hz
M	free-stream Mach number
n	logarithmic amplification, $n = \ln(A/A_o)$
p	static pressure
q	dynamic pressure, $\rho U^2/2$
R	chord Reynolds number, $\rho_\infty U_\infty c/\mu_\infty$
s	surface distance
t/c	thickness ratio of airfoil, thickness/chord (listed in figures as T/C)
u'	perturbation velocity in the x direction
U	potential flow velocity in the x direction
x,y	two-dimensional Cartesian coordinate axes
α	angle of attack, deg (listed in figures as ALP)
δ_f	trailing-edge flap deflection in degrees (+: up) (listed in figures as DELTA F)
Λ	wing sweep, deg (listed in figures as SW)
λ	wavelength
ρ	mass density
ψ	wave angle of perturbation vortices with respect to potential flow direction, deg

Subscripts:

max	maximum value
∞	free-stream conditions

Other:

CF	crossflow
LFC	laminar flow control
LS	lower surface
NLF	natural laminar flow
TS	Tollmien-Schlichting
US	upper surface
DESB159	airfoil designation
DESB165	airfoil designation
NLF(1)-0414F	airfoil designation
HSNLF(1)-0313	airfoil designation
SAL8EYO	airfoil designation

LINEAR STABILITY THEORY

Free-stream turbulence, vibrating boundaries, sound from the propulsion system, or surface roughness may introduce disturbances into the laminar boundary layer which can be amplified. At present, there is no quantitative analysis for calculating a given amplitude of disturbance generated by a given flow environment. Fortunately, because there are such large amplifications of disturbances in the laminar boundary layer before transition, we are still able to give a reasonably good prediction of the transition location. This transition prediction method examines the degree of amplification of a disturbance from the initial point of instability using a linearized form of the Navier-Stokes equations. Linear theory represents a good approximation when the perturbations are weak because the nonlinear stress terms are negligible as compared to those driving the mean flow. The disturbance is assumed to be harmonic and monochromatic. When the flow is essentially two-dimensional, the selectivity of the allowable amplified disturbances dampens all but a narrow range of frequencies which makes the monochromatic assumption reasonable. But seldom are these disturbance waves propagated naturally in a periodic fashion. A more realistic model is a modulated wave packet. Gaster (ref. 1) states that these modulated waves will break down the ordered laminar boundary layer at a lower growth rate than a periodic wave would. The reason he gives is that nonlinear stresses induced by the modulated wave are very much different from those created in the periodic wave train. Naturally, if prediction is to be improved, this aspect must be taken into account.

For two-dimensional airfoils (no sweep), only Tollmien-Schlichting (TS) type disturbances occur. However, on wings with sweep, an instability due to spanwise flow also arises. This problem was discovered by Gray but was illustrated by Dagenhart (ref. 2) when he analyzed the temporal amplification rate versus orientation angle at a specific chord location on a swept airfoil. He showed that there was a sharp peak in the amplification at approximately 90° relative to the local potential flow. Also there was another broad amplification region with a maximum in the direction of the local potential flow. Thus, the boundary-layer stability problem on a swept wing can be broken up into two parts according to wave orientation. Disturbance waves with $\psi = 0^{\circ}$ travel in the local potential flow direction, while those with an orientation angle within a few degrees of $\psi = 90^{\circ}$ progress nearly normal to the potential flow direction. The former, which are associated with the tangential boundary layer, are often referred to as TS waves since they are similar to the two-dimensional waves studied by Tollmien and Schlichting. The latter are generally called crossflow disturbances since they are associated with the crossflow boundary layer. These disturbances arise from the three-dimensional character of the boundary layer on a swept wing. They are not present in two-dimensional flows. Pfenninger (ref. 3) notes that this separation of the stability problem into two independent parts is physically acceptable as long as strongly amplified crossflow and TS waves do not occur simultaneously. Raetz (refs. 4 to 6), Reed (refs. 7 and 8), and Saric and Yeates (ref. 9) have shown that relatively weak oblique TS waves can distort and stretch streamwise vortices such as crossflow disturbance vortices to produce rapid, resonance like amplification and transition. For this reason, the mutual interaction of amplified disturbances of the two types should be avoided. This mutual interaction can be minimized when highly amplified TS and crossflow disturbances do not occur simultaneously.

According to Rayleigh and Tollmien (ref. 10), boundary-layer profiles without a point of inflection, i.e., $\partial^2 u/\partial y^2 = 0$, are stable with respect to boundary-layer perturbations when viscosity is neglected. Profiles with an inflection point are dynamically highly unstable, even in frictionless flow. The presence of viscosity introduces a relatively mild frictional type of instability to convex boundary-layer profiles without inflection points. This is illustrated in reference 10, page 443, where curves of neutral stability, for both frictional and inflectional instabilities, are shown on plots of nondimensional disturbance wave number versus the Reynolds number based on boundary-layer thickness. The region of amplified wave numbers is much smaller for frictional instabilities than for inflectional instabilities. The band of unstable wave numbers goes to zero as the Reynolds number based on boundary-layer thickness approaches infinity for frictional instabilities, but remains wide for inflectional instabilities. For TS disturbances, accelerating pressure gradients, $dp/dx < 0$, are termed favorable because they result in velocity profiles without inflection points. The more steep the accelerating gradient, the more the relatively mild frictional instabilities are stabilized. For TS disturbances, decelerating pressure gradients, $dp/dx > 0$, are termed adverse because they result in velocity profiles with inflection points. With respect to crossflow disturbances, the spanwise velocity profiles resulting from wing sweep always have inflection points and are always dynamically highly unstable. The steeper the pressure gradient, accelerating or decelerating, the more unstable the crossflow disturbances.

For incompressible TS instabilities, the SALLY analysis code (refs. 11 to 13) is used to calculate disturbance amplification. This utilizes Chebychev polynomials to find the eigenvalues of the incompressible Orr-Sommerfeld equation. A range of frequencies is analyzed for chordwise disturbance growth, and transition prediction is made from the most unstable frequency. A wave orientation angle of $\psi = 0^{\circ}$ is assumed because Squire (ref. 14) has shown that this is the maximum amplified orientation angle in incompressible flow.

For compressible TS disturbances, the COSAL analysis code (ref. 15) is used to calculate the growth of unstable waves. This code utilizes a finite difference scheme to solve the compressible Orr-Sommerfeld equation. For these cases, a range of frequencies is also analyzed and transition predictions are made on the most unstable frequency. However, in compressible flow $\psi = 0^0$ is not the most unstable orientation angle of disturbance. A maximization procedure in the COSAL program is used to find the orientation angle-wavelength combination of the most unstable disturbance at each computation station. The density change in compressible flow makes the boundary layer more stable with respect to TS disturbances. Roughly, a rule of thumb is that through a compressible analysis ($M_{local} \approx 1$), one will get the same disturbance amplification at twice as high a chord Reynolds number as in the corresponding incompressible analysis.

Only an incompressible crossflow analysis is made for this paper. The MARIA code (ref. 2), developed from Pfenninger's ideas using Brown's curves (ref. 3), is used to calculate crossflow disturbance amplification. This code incorporates an algorithm to approximate crossflow disturbance amplification from amplification rate solution charts generated from the SALLY code for ten typical crossflow velocity profiles. A range of wavelengths is analyzed and transition predictions are made on the most unstable wavelength. This analysis is the fixed wavelength method and assumes the disturbance is a stationary wave ($f = 0$). There are some experimental data which seem to indicate that the crossflow vortices are standing vortices on the wing and that the wavelength does not change along the chord. However, there are also data which indicate that the wavelength of the crossflow vortices increases in the chordwise direction with some vortices eventually disappearing. Neither set of data is conclusive to define the actual state of the disturbances at the present time. Compressibility favorably affects crossflow disturbance growth but not as radically as in the case of TS disturbances. For crossflow disturbance amplifications which are calculated with a compressible analysis, the growth in n_{max} will be approximately 10 percent less than the calculated incompressible value.

ANALYSIS OF EXPERIMENTAL RESULTS

An analysis was made of an existing flight experiment to correlate linear stability theory with predicting the transition process for uninteracted TS disturbances. The analysis is of flight tests made on a smooth NACA 66_{2x}-216 airfoil on a King Cobra World War II airplane (refs. 16 to 18). This airfoil section was designed for approximately 60 percent to 65 percent chord laminar flow on both surfaces. Three experimental pressure distributions were analyzed with the incompressible SALLY stability code for TS amplification. They were first published in reference 19, but a typical one is shown here for comparison.

The case shown here was for the upper surface at $c_\ell = 0.38$, $M = 0.269$, and $R = 12 \times 10^6$ (fig. 1). The pressure distribution is characterized by a leading-edge negative-pressure peak with a local deceleration of 11 percent q_{max}, followed by a very flat negative pressure gradient up to 60 percent chord. The most amplified frequency is 2000 Hz which reaches a logarithmic amplification of $n = 22.958$. This gives a total amplification of $A/A_o = 9.344 \times 10^9$ up to the point of laminar separation. The chord was 6.2 ft and the free-stream velocity was 280 ft/sec. In free flight, as verified by Gray and Fullam (ref. 17), transition occured at or very close after the point of laminar separation ($x/c = 0.625$). Care must be taken when extrapolating this result to other cases. There is a strong amplification along the chord for all the frequencies analyzed, but the logarithmic amplification stays under $n = 13$ up to the 45 percent chord station. The TS disturbances then amplify much quicker in the slight deceleration region from $x/c = 0.45$ to 0.60. If these strong amplifications occurred further upstream in the chord, then the disturbances could become three-dimensional. Once these TS disturbances become three-dimensional, they grow much quicker than the linear theory predicts (refs. 20 to 23).

Another point that should be noted is that the transition location was considerably different in the wind tunnel than in free flight. For the same pressure distribution, in the wind tunnel with a turbulence level of $u'/U = 0.07$ percent, transition occurred downstream of the leading-edge negative-pressure peak at $x/c = 0.15$. Based on this and McCready's results (ref. 24), apparently the scale of atmospheric turbulence in atmospheric boundary layers or jetstream shear layers is so much larger than the microscale turbulence of even the best low turbulence wind tunnels, it is shifted into the region of viscous dissipation. As a result, atmospheric microscale turbulence generally appears too weak to affect transition.

To correlate crossflow disturbance amplification with transition one can look at an experiment of a Northrop modified NACA 66-012 LFC wing swept 30°. Using Brown's theoretical results, Pfenninger calculated total logarithmic amplifications of $n = 6$ to 8 up to $s/c = 0.60$ and transition had not yet occurred (ref. 3). Also, transition experiments of J. Carlson on a 15 percent thick, 33° swept nonsuction wing gave transition values of logarithmic amplification at fully developed turbulent flow of $n = 12$ (ref. 25).

LOW-SPEED (INCOMPRESSIBLE) AIRFOILS

When designing NLF airfoils, there are certain compromises one has to live with, and it is important to maximize the benefits and minimize the losses. When designing for low cruise profile drags, the first thing to be concerned with is the amount of laminar flow desired. This means starting the main pressure rise after that point on each surface. To get extensive laminar flow, for the high Reynolds applications considered in this paper ($R \approx 10 \times 10^6$), a favorable pressure gradient, i.e., accelerated flow, must be designed up to the point of desired transition. For low Reynolds number airfoils it might even be desirable to design a slightly adverse gradient over most of the airfoil. Favorable gradients stabilize the laminar boundary layer with respect to TS disturbance waves, while adverse pressure gradients give velocity profiles with inflection points which are dynamically highly unstable.

As the design Reynolds number increases, more acceleration needs to be designed into the airfoil on each surface to keep the boundary layer laminar up the desired point of transition. To get more acceleration, the airfoil has to be designed thicker overall or with a thinner leading edge, since the pressure gradient in subsonic flow responds inversely with thickness increase. Making the airfoil thicker makes the far aft pressure recovery on the upper surface more critical with respect to separation. Up to a certain point, making the leading edge thinner increases the low drag c_ℓ range at low angles of attack, but increases the chance of laminar separation at the leading edge at high angles of attack. The real problem arises if the leading edge is so sharp that after leading-edge laminar separation the turbulent boundary layer does not reattach to the airfoil. Ideally, the way to design the airfoil is to design as little acceleration into the airfoil as is needed. This helps alleviate the problems in the rear pressure recovery region and helps the designer to get a thicker leading edge for better $c_{\ell_{max}}$ performance.

Airfoil DESB159 (fig. 2), first published in reference 19, was designed using this philosophy and linear stability theory. Based on the logarithmic TS growths up to transition on the King Cobra flight experiment and other wind tunnel experiments, DESB159 was designed using linear theory with enough acceleration to give the desired amplification at the design point, $c_\ell = 0.454$, $M = 0.4$, and $R = 10 \times 10^6$. The negative pressure gradients on both surfaces are much flatter than for most other NLF airfoils previously designed for use at such a high chord Reynolds number.

The results of the stability analysis for the upper surface of DESB159 at the design point are shown in figure 3. The maximum amplified TS disturbance is f = 3500 Hz which reaches a logarithmic amplification of n = 10.917 at the laminar separation point (x/c = 0.70). The chord used in the analysis was 4.0 ft and the free-stream velocity was 414.7 ft/sec. The analyzed TS frequencies do not even become unstable until x/c = 0.17. This is well below the TS amplification calculated in the King Cobra stability analysis, but the airfoil was designed to also get 70 percent chord NLF in a wind tunnel test where the free-stream turbulence unfavorably affects transition. Also, with some margin of stability, one can expect a range of lift coefficients with low drag in flight instead of only a point design.

The lower surface of DESB159 had similar TS amplification at the design point $c_\ell = 0.454$, $M = 0.4$, and $R = 10 \times 10^6$. The maximum amplified frequency was 2750 Hz, which had a maximum logarithmic amplification of n = 9.214 up to the laminar separation point.

An illustration of the TS amplification, caused by the dynamically highly unstable profiles with inflection points in decelerating flow, is shown in figure 4. This is a plot of the stability analysis of the upper surface of DESB159 at $c_\ell = 0.75$, $M = 0.4$, and $R = 10 \times 10^6$. The flow is decelerated from x/c = 0.15 to the laminar separation point of x/c = 0.70. The maximum logarithmic amplification is doubled from that of the design case. The most unstable analyzed frequency was 3375 Hz, which had a logarithmic amplification of n = 20.715. The chord was 4.0 ft and the free-stream velocity was 414.7 ft/sec. This amplification is comparable with that analyzed in the King Cobra experiments. In free flight, on a smooth wing at $c_\ell = 0.75$, $M = 0.4$, and $R = 10 \times 10^6$, transition might be expected at the laminar separation point for this condition. However, the TS disturbances grow to higher values earlier in the chord than in the King Cobra analysis so it is possible that the disturbances could become three-dimensional sooner.

Because of the problems a thin leading edge gave with respect to $c_{\ell_{max}}$ performance in the design of DESB159, an investigation was conducted to examine the effects on low drag that resulted from thickening the leading edge. Thickness was superimposed directly onto the leading edge region of DESB159, changing as little of the rest of the airfoil as possible. The modified airfoil, DESB165, is shown in figure 5, where the change in surface contour from that of DESB159 is plotted. A comparison of the inviscid pressure distributions of both airfoils is shown in figure 6 at $c_\ell = 0.45$ and $M = 0.4$. The flow accelerates quicker in the leading-edge region of DESB165 than in that of the original airfoil, DESB159. There is a flat spot in the pressure distribution from x/c = 0.10 to 0.15 and then the flow again accelerates quicker than that of DESB159, merging into the same pressure distribution at about x/c = 0.50. Stability analysis on this design pressure distribution of DESB165 led to an interesting result. It was found that at the design condition of $c_\ell = 0.45$, $R = 10 \times 10^6$, and $M = 0.4$, this modification to the upper surface resulted in a drop in the maximum TS amplification by approximately a factor of 2.5. This result can be deduced from the stability analysis of the upper surface of DESB165 at the design condition in figure 7. The maximum amplified disturbance frequency is 3500 Hz, which reaches a maximum logarithmic amplification of 9.931 at the laminar separation point. The chord was 4.0 ft and the free-stream velocity was 414.7 ft/sec. The maximum amplified disturbance frequency for DESB159 had a logarithmic amplification of $n = 10.917$. It appears that the acceleration on DESB165 is tailored such that it is concentrated in the correct place to curb the disturbances near the lower branch of the neutral stability curve where they are small, before they have a chance to multiply. Acceleration is wasted if it is used before the disturbances have begun to amplify (ref. 26).

It was known, however, that the thick leading edge of DESB165 would reduce the c_ℓ range with low drag by causing leading-edge negative-pressure peaks sooner than that of DESB159. This can be seen in figure 8, where the inviscid pressure distributions of DESB159 and DESB165 are plotted at $M = 0.4$ and $c_\ell = 0.75$. On DESB165, there is a leading-edge deceleration of $0.15q_{max}$ up to x/c = 0.15, whereas the DESB159 airfoil has a slightly negative gradient up to this point. This leading-edge deceleration gives dynamically highly unstable profiles which will give much greater TS amplifications than those of DESB159 up to x/c = 0.15.

The c_ℓ range with low drag can be increased with the use of a small-chord simple trailing-edge cruise flap that can be deflected both positively and negatively for different flying conditions (ref. 27). This small-chord simple flap trades lift due to angle of attack for lift due to flap deflection. As a result, the stagnation point can be kept near the leading edge for different lift coefficients to keep the gradients favorable on both surfaces. This is illustrated in experimental results from NLF(1)-0414F shown in figure 9. NLF(1)-0414F is a derivative of the DESB165 airfoil that is an attempt to distribute the acceleration on the upper surface after the flat region over a wider distance. The results of the wind tunnel experiment of NLF(1)-0414F conducted in NASA Langley's LTPT are published in reference 28. Figure 9(a) shows the pressure distribution and section characteristics at a section lift coefficient of approximately 0.8, $R = 10 \times 10^6$, and $M = 0.12$ for 0° and 12.5° deflections of the 12.5 percent chord cruise flap. No stability analysis has been conducted on these pressure distributions, but the measured profile drag coefficients show the merit of the cruise flap. With a 0° flap deflection the airfoil needs $\alpha = 3.12^\circ$ to get $c_\ell = 0.837$. The airfoil has a leading edge C_p of -1.85 on the upper surface and the flow decelerates continuously to the trailing edge. The corresponding profile drag coefficient is 0.0084. With the cruise flap deflected 12.5°, the airfoil can get a c_ℓ of 0.794 at $\alpha = -1.99^\circ$. In this case, the upper surface is accelerated continuously up to the main pressure rise at x/c = 0.70. The lower surface is accelerated continuously up to x/c = 0.40, with a slight deceleration from x/c = 0.40 to 0.70, the start of the main pressure rise. The profile drag coefficient at this condition is 0.0032. With the 12.5° flap deflection and the restored favorable gradient, the profile drag is only 38 percent that of the airfoil at approximately the same c_ℓ with no flap deflection. This reduction in profile drag can also be seen at the cruise lift coefficients with a negative flap deflection. The pressure distributions and section characteristics of NLF(1)-0414F at a section lift coefficient of approximately 0.22 ($M = 0.12$ and $R = 10 \times 10^6$) are shown in figure 9(b) for 0° and -5.0° flap deflections. To get down to $c_\ell = 0.236$ with 0° flap deflection, an angle of attack of -2.44° is needed. At this condition there is a leading-edge negative-pressure peak on the lower surface with a local deceleration of 12.4 percent q_{max}. The profile drag coefficient is 0.0041. With a flap deflection of -5.0° the angle of attack can be increased to -0.46° to get $c_\ell = 0.22$. The flow is now accelerated on both surfaces back to the main pressure rise. The profile drag coefficient at $c_\ell = 0.22$, $M = 0.12$, and $R = 10 \times 10^6$ is now 0.0027. This is only 66 percent that of the drag with 0° flap deflection at approximately the same lift coefficient.

A linear stability analysis was conducted for the upper surface of NLF(1)-0414F at the design condition ($c_\ell = 0.45$, $M = 0.12$, and $R = 10 \times 10^6$) to correlate transition measurements with linear TS amplification. The results of this linear stability analysis are shown in figure 10(a). The maximum amplified disturbance frequency is 1400 Hz, which reaches a maximum logarithmic amplification of $n = 12.636$ at the laminar separation point ($x/c = 0.70$). The chord used was 3.0 ft with a free-stream velocity of 121.9 ft/sec. These disturbance growths are very similar to those calculated for the theoretical pressure distribution of the DESB165 airfoil. Transition measurements were made on the experimental model with surface-mounted hot-film gauges. The gauges were placed at x/c's of 0.50, 0.55, 0.60, 0.65, and 0.70. At the design condition the flow over the gauge at 65 percent chord was fully laminar, and the gauge at 70 percent chord had about 50 percent laminar and 50 percent turbulent flow. This would give a logarithmic amplification up to the beginning of transition of about $n = 11$ to 12. A summary plot of n_{max} against frequency is shown in figure 10(b), which illustrates the highly selective process of the laminar boundary layer with respect to the frequency of TS amplification. Only a small range of frequencies from the total spectrum are highly amplified. Remember, this is a logarithmic plot. If actual values were plotted, the selectiveness would seem more dramatic.

HIGH-SPEED (COMPRESSIBLE) AIRFOILS - NO SWEEP

When increasing the Mach number on an airfoil, one must be alert for additional design considerations due to the effects of compressibility. Compressibility has favorable effects with respect to TS instability. The flow is more accelerated around the airfoil which reduces the TS amplification. With no sweep, the added acceleration does not contribute to any crossflow instability. Also, for a given pressure distribution, the change in density in the boundary layer associated with compressibility helps stabilize the flow with respect to TS disturbances.

The problems with compressibility in airfoil design come mainly in decelerating the flow. With this added acceleration the rear pressure recovery becomes steeper and is more prone to separation than in the low-speed case. Also, one has to be careful that the flow does not over-accelerate around the airfoil and develop into a shock. At these high speeds, an airfoil needs to be designed with less camber than in the incompressible case. An illustration of what happens to an incompressible airfoil at high speeds is shown in figure 11.

This is an inviscid pressure distribution of NLF(1)-0414F at $M = 0.70$ and $\alpha = -0.953^\circ$. The upper surface has accelerated strongly and becomes supersonic at $x/c = 0.20$. The accelerated region terminates in a strong shock at $x/c = 0.70$. This airfoil has too much camber for compressible applications. Camber can be taken out over the whole extent of the airfoil or it can be taken out at the trailing edge with a simple flap deflection. Taking out overall camber of the airfoil makes it better transonically but can hurt low speed performance. Taking out camber with a trailing-edge flap still leaves camber in the airfoil for low speed performance, but causes relatively strongly accelerated flow over the airfoil which leads to shocks sooner at higher Mach numbers.

HSNLF(1)-0313 (fig. 12) is a modified version of NLF(1)-0414F. Camber has been taken out of the trailing edge with a flap deflection of -5.24° (12.5 percent chord flap). Also, the beginning of the pressure rise on the upper surface is moved ahead to $x/c = 0.57$ to help alleviate the problems of turbulent separation in the pressure recovery region. The inviscid pressure distribution of HSNLF(1)-0313 is also shown in figure 12 at $M = 0.70$ and $c_\ell = 0.26$. For this condition, the flow on the upper surface is only slightly supersonic from $x/c = 0.34$ to 0.58.

The results of the compressible TS stability analysis for HSNLF(1)-0313 are shown in figure 13 at the design point: $M = 0.70$, $c_\ell = 0.26$, and $R = 10 \times 10^6$. On the upper surface, figure 13(a), the maximum amplified frequency was $f = 5000$ Hz, which reached a maximum logarithmic amplification of $n = 1.688$ at the point of laminar separation. The chord used was 4.0 ft and the free-stream velocity was 711.1 ft/sec. On the lower surface of HSNLF(1)-0313 at the design point, figure 13(b), the maximum amplified frequency, $f = 5000$ Hz, reached a maximum logarithmic amplification of $n = 2.937$ at $x/c = 0.53$. The disturbance was stable from $x/c = 0.53$ to 0.67, the laminar separation point. The lower surface pressure distribution is characterized by a leading-edge deceleration of 2.1 percent q_{max} followed by a strong acceleration up to the laminar separation point. For all the frequencies analyzed, this leading-edge negative-pressure peak does not seem to influence the TS instability.

With such a small TS disturbance amplification at the design chord Reynolds number, chord Reynolds numbers of 15, 20, and 40×10^6 were analyzed on the design pressure distribution of both surfaces. In figure 14(a), the chordwise compressible TS disturbance amplification for the upper surface of HSNLF(1)-0313 at $c_\ell = 0.26$, $M = 0.70$, and $R = 40 \times 10^6$ is shown. The chord is 4.0 ft and the free-stream velocity is 711.1 ft/sec. The maximum amplified disturbance frequency is $f = 8000$ Hz, which reaches a maximum amplification of only $n = 5.357$ at the laminar separation point. The stabilizing effects of compressibility and the strong acceleration give very low TS amplification even at this high chord Reynolds number. To illustrate the stabilizing effects of compressibility, the chordwise TS amplification calculated at the same conditions with incompressible stability computations is shown in figure 14(b). The incompressible calculations predict a maximum logarithmic amplification of $n = 14.036$ up to the laminar separation point. This is a maximum logarithmic amplification that is 2.6 times that calculated in the compressible calculations or a total amplification (A/A_0) of 5,878 times greater. The compressible and incompressible chordwise TS disturbance amplification of the lower surface of HSNLF(1)-0313 is shown in figures 15(a) and 15(b), respectively. The maximum compressible logarithmic amplification was n = 9.793 at f = 8000 Hz. This disturbance became stable at x/c = 0.51 and remained stable up to the laminar separation point at x/c = 0.67.

HIGH-SPEED (COMPRESSIBLE) AIRFOILS - WITH SWEEP

When designing for high cruise Mach numbers, one is inevitably led to designing wings with sweep to keep down the maximum local Mach numbers on the surface. The same benefits and problems arise from compressibility as in the non-swept case; however, with sweep another boundary-layer instability arises from the spanwise flow across the wing. The strong acceleration that stabilizes the boundary layer with respect to TS disturbances leads to crossflow instabilities. For the most part, at high Mach numbers and with any significant sweep, one has to design around the problem of crossflow instability.

The first example of linear stability analysis of a swept wing in compressible flow is the analysis of a flight condition of the NASA glove for the F-14 in the Variable Sweep Transition Flight Experiment. This glove was designed by Waggoner, Campbell, and Phillips (National Transonic Facility, Transonic Aerodynamics Division, NASA Langley). The case shown here is at M = 0.70 and at an altitude of 20,000 ft. This analysis was done at the mid-semispan location with the wing leading edge swept 20^o and the trailing edge swept 2.5^o. The chord here was 8.75 ft and the free-stream velocity was 711.1 ft/sec, which gave a chord Reynolds number of 24.15×10^6. The upper surface pressure distribution used in the stability calculation is a theoretical three-dimensional calculation with viscous effects calculated using the TAWFIVE computer code (ref. 29).

The results of the compressible chordwise logarithmic TS amplification for the F-14 NASA glove calculated by the COSAL program are shown in figure 16. For the analyzed frequencies, the maximum logarithmic amplification is n = 8.74 for a frequency of 4000 Hz. In this case, there is a significant amount of the total amplification after the pressure minimum, when the boundary-layer profiles have inflection points. For the maximum amplified frequency of 4000 Hz, there is a logarithmic amplification of n = 4.0 up to the laminar separation point. The linear TS amplification (uninteracted) is much weaker than that needed to cause transition, but there is a crossflow instability caused by the spanwise flow. The calculated crossflow instability for this case, using the incompressible MARIA code (ref. 2), is shown in figure 17. The most unstable nondimensional wavelength of disturbance, $\lambda/c = 0.0012$, grows to maximum logarithmic amplification of n = 9.497 at x/c = 0.46, decaying slightly up to the laminar separation point at x/c = 0.50. However, smaller wavelengths get amplified to significant values early in the chord. For a nondimensional wavelength of $\lambda/c = 0.0008$, an n of 8 is exceeded at x/c = 0.16. The maximum compressible TS logarithmic amplification at x/c = 0.16 is n = 1.4, for the frequencies analyzed. In this case, one can expect transition after x/c = 0.16 to be solely due to crossflow instability, with essentially no TS interaction. Given that this incompressible calculation could overpredict compressible crossflow amplification by 10 percent, crossflow instability might not cause transition until x/c ≈ 0.30.

Another high-speed airfoil analyzed was SAL8EYO. The two-dimensional inviscid pressure distribution is shown in figure 18. At the design condition, $c_\ell = 0.20$ and M = 0.75, there is slightly accelerated flow over the upper surface back to x/c = 0.60. The lower surface is strongly accelerated back to x/c = 0.55 with a slight deceleration from x/c = 0.55 to 0.60. The main pressure recoveries for both surfaces start at the x/c = 0.60 location. There is a very shallow supersonic zone on the upper surface extending from x/c = 0.10 to 0.60. The design philosophy behind this type of airfoil is that with the flat pressure gradient on the upper surface, one can get a higher design Mach number before shocks start to develop. Also, on most airfoils, the pressure rise on the upper surface is much greater than that on the lower surface. With SAL8EYO, the decelerations on both surfaces are much more equal, thereby somewhat alleviating the problems of turbulent separation on the upper surface. Note that both these pressure recoveries have to be refined. The turbulent boundary layer separates in both recoveries when the flow is fully turbulent at the design condition. This airfoil is included to provide an example of problems associated with boundary-layer stability.

The compressible chordwise TS amplification for the upper surface of SAL8EYO at $M = 0.75$, $c_\ell = 0.20$, and $R = 10 \times 10^6$ is shown in figure 19. For all the SAL8EYO and CBLXF2 cases, the chord is 4.0 ft and the free-stream velocity is 788.3 ft/sec. The maximum amplified disturbance frequency is 5000 Hz, which reaches a maximum logarithmic TS amplification of $n = 7.365$ up to the laminar separation point. This logarithmic growth is still well below transitional levels. The incompressible logarithmic crossflow amplification for the upper surface of SAL8EYO is shown in figure 20. In this case, the analyzed pressure distribution has been transformed applying simple sweep theory to an infinitely swept untapered wing. The wing sweep used, $\Lambda = 20^\circ$, gave a free-stream Mach number of 0.798 and a chord Reynolds number of 10.64×10^6, with the same normal Mach number of 0.75. Note that the pressure distribution shown in the plot is still the two-dimensional inviscid pressure distribution. This is the case for all the pressure distributions shown with SAL8EYO and CBLXF2. The maximum amplified wavelength is $\lambda/c = 0.0006$, which reaches a maximum logarithmic amplification of only $n = 1.644$ at $x/c = 0.035$ decaying to $n = 0.0$ at $x/c = 0.10$. The crossflow amplification here is essentially insignificant. For this case on the upper surface, realizing that the TS amplification will be somewhat greater when analyzed at $\Lambda = 20^\circ$, transition should not occur before the laminar separation point at $x/c = 0.60$.

The compressible chordwise logarithmic TS amplification for the lower surface of SAL8EYO at $M = 0.75$, $c_\ell = 0.20$, and $R = 10 \times 10^6$ is shown in figure 21. For all the frequencies analyzed, the only amplification that occurs is in the slight deceleration region from the pressure minimum ($x/c = 0.55$) up to the laminar separation point at $x/c = 0.60$. The maximum amplified disturbance is at a frequency of 5000 Hz and has a logarithmic amplification of only $n = 2.517$. The incompressible chordwise crossflow amplification, with 20° of sweep (no taper) for the lower surface of SAL8EYO, is shown in figure 22. At a free-stream Mach number of 0.798 and $R = 10.64 \times 10^6$, the maximum amplified wavelength is $\lambda/c = 0.0024$, which reaches a maximum logarithmic amplification of $n = 9.798$ at the laminar separation point. Because of the stabilizing effects of compressibility, transition would probably occur between $x/c = 0.50$ and 0.60.

With swept wings at higher Reynolds numbers, this crossflow instability on the lower surface becomes more of a problem and dominates the transition process. This is illustrated in figure 23, where the incompressible chordwise crossflow instability for the lower surface of SAL8EYO at $R = 15.96 \times 10^6$ is shown. Simple sweep theory was again used to transform the two-dimensional inviscid pressure distribution at $M = 0.75$ into the analyzed pressure distribution on a 20° swept, non-tapered wing at $M = 0.798$. The maximum amplified wavelength is $\lambda/c = 0.0020$, which reaches a maximum logarithmic amplification of $n = 13.604$ at the laminar separation point. For this case, the uninteracted crossflow disturbances can be expected to cause transition between $x/c = 0.20$ and 0.30.

To try and relieve this problem, a new longer surface pressure distribution was sketched and analyzed. This pressure distribution is shown in figure 24, along with the incompressible chordwise crossflow amplification. The pressure distribution is much flatter overall, and the total crossflow amplification is reduced considerably. The maximum logarithmic amplification is $n = 3.157$ ($\lambda/c = 0.0020$) up to the laminar separation point. Uninteracted, this crossflow disturbance amplification should not cause transition. However, with this reduced overall acceleration, the TS amplification is greater than in the SAL8EYO case. This is illustrated in figure 25, where the same CBLXF2 pressure distribution is analyzed for chordwise compressible TS disturbance growth. The maximum amplified disturbance ($f = 5000$ Hz) now has a logarithmic amplification of $n = 7.684$ up to the laminar separation point. There will probably be some interaction between the crossflow vortices and the TS disturbances from $x/c = 0.50$ to $x/c = 0.64$, and transition might occur before the laminar separation point.

CONCLUSIONS

1. When designing an airfoil for extensive NLF, linear stability theory gives a quantitative analysis of disturbance growth in the laminar boundary layer that empirical transition predictions miss. Linear stability theory allows the tailoring of the airfoil for specific design conditions, minimizing the off-design compromises.

2. In view of the King Cobra flight results (NACA 66_{2x}-216), where uninteracted linear TS logarithmic amplifications were in excess of $n = 20$, it appears that TS disturbance amplifications can rise to much higher levels than are commonly expected, before transition occurs. These much higher disturbance amplifications can be gained from the much lower free-stream disturbances encountered in flight than in even the best low turbulence wind tunnels. This is provided that there are no acoustic disturbances generated by the airplane in the highly amplified TS frequency range.

3. The negative pressure gradient should be tailored so that acceleration is concentrated near the lower branch of the neutral stability curve of the most amplified TS disturbance. The concentrated acceleration curbs the disturbances when they are small, before they have had a chance to grow, and results in much lower maximum TS amplifications than when acceleration is wasted in a stable region or when the acceleration is used after the disturbances have grown to a high level.

4. When designing an NLF airfoil with a relatively thick leading edge for favorable high-lift performance, the use of a cruise flap is necessary to increase the low-drag range of the airfoil. For different c_ℓ values, favorable gradients can be maintained on both surfaces by keeping the stagnation point at the leading edge and varying the deflection of the cruise flap.

5. As the Mach number increases, compressibility stabilizes the laminar boundary layer and also gives more acceleration on the airfoil. As long as there is no sweep, the main design problem changes from obtaining laminar flow to designing against shock formation and turbulent separation in the pressure recoveries.

6. For swept wings at high Mach numbers, the crossflow instability in the laminar boundary layer seems to be the major deciding factor in determining the amount of laminar flow, especially on the lower surface.

REFERENCES

1. Gaster, M.: Propagation of Linear Wave Packets in Laminar Boundary Layers. AIAA Journal, Vol. 19, No. 4, April 1981, pp. 419-423.

2. Dagenhart, J. Ray: Amplified Crossflow Disturbances in the Laminar Boundary Layer on Swept Wings with Suction. NASA TP-1902, November 1981.

3. Pfenninger, Werner: Laminar Flow Control Laminarization. Special Course on Concepts for Drag Reduction, AGARD-R-654, June 1977, pp. 3-1 thru 3-75.

4. Raetz, G. S.: A New Theory of the Cause of Transition in Fluid Flows, Northrop Norair Report NOR 59-383 (BLC-121), June 1959.

5. Raetz, G. S.: 'Current Status of Resonance Theory of Transition,' Summary of Boundary Layer Control Research, ASD-TDR-63-554, Part I, Chapter A, March 1964.

6. Raetz, G. S.: 'Calculation of Precise Proper Solutions for the Resonance Theory of Transition,' Theoretical Investigations Task 3.3, AFFDL-TR-64-185, Part I, December 1964.

7. Reed, H. L.: Wave Interactions in Swept Wing Flows. AIAA Paper No. 84-1678, 1984.

8. Reed, H. L.: Disturbance Wave Interactions in Flows with Crossflow. AIAA Paper No. 85-0494, 1985.

9. Saric, W. S.; and Yeates, L. G.: Experiments on the Stability of Crossflow Vortices in Swept Wing Flows. AIAA Paper No. 85-0493, 1985.

10. Schlichting, Herman (J. Kestin, transl.): Boundary-Layer Theory. New York: McGraw-Hill Book Co., Sixth Edition, 1968.

11. Srokowski, Andrew J.; and Orszag, Steven A.: Mass Flow Requirements for LFC Wing Design. AIAA Paper No. 77-1222, 1977.

12. Orszag, Steven A.: Accurate Solution of the Orr-Sommerfeld Stability Equation. Journal of Fluid Mech., Vol. 50, Part 4, 1971, pp. 689-703.

13. Srokowski, Andrew J.: SALLY User's Guide. LAR-12556. Available through COSMIC, 112 Barrow Hall, The University of Georgia, Athens, Ga. 30602, 1979.

14. Squire, H. B.: On the Stability of Three-Dimensional Distribution of Viscous Fluid Between Parallel Walls. Proc. Roy. Soc. London A142, pp. 621-628, 1933.

15. Malik, Mujeeb R.: COSAL--A Black Box Compressible Stability Analysis Code for Transition Prediction in Three-Dimensional Boundary Layers. NASA CR-165925, May 1982.

16. Gray, W. E.: Transition in Flight on a Laminar-Flow Wing of Low Waviness (King Cobra). R.A.E. Report No. 2364, March 1950.

17. Gray, W.E.; and Fullam, P. W. J.: Comparison of Flight and Wind Tunnel Measurements of Transition on a Highly Finished Wing (King Cobra). R.A.E. Report No. 2383, June 1950.

18. Smith, F.; and Higton, D. J.: Flight Tests on 'King Cobra' F.Z.440 to Investigate the Practical Requirements for the Achievement of Low Profile Drag Coefficients on a 'Low Drag' Aerofoil. R.A.E. Report No. 2078, A.R.C. 9043, August 1945.

19. Viken, Jeffrey K.: Aerodynamic Considerations and Theoretical Results for a High Reynolds Number NLF Airfoil. Master's Thesis, George Washington University, January 1983.

20. Schubauer, G. B.; and Klebanoff, P. S.: Contributions on the Mechanics of Boundary Layer Transition. NACA Rep. 1289, 1956.

21. Saric, W. S.; Kozlov, V. V.; and Levchenko, V. Y.: Forced and Unforced Subharmonic Resonance in Boundary Layer Transition. AIAA Paper No. 84-0007, 1984.

22. Saric, W. S.; and Thomas, A. S. W.: Experiments on the Subharmonic Route to Turbulence in the Boundary Layer. Turbulence and Chaotic Phenomena in Fluids. Edited by Tatusmi, North Holland, 1984.

23. Reynolds, G. A.; and Saric, W. S.: Experiments on the Stability of a Flat Plate Boundary Layer with Suction. AIAA Paper No. 82-1026, 1982.

24. McCready, P.: Turbulence Measurements by Sailplane. Journal of Geophysical Research, vol. 67, no. 3, pp. 1041-1050, 1962.

25. Carlson, J. C.: Results of a Low Speed Wind-Tunnel Test to Investigate the Influence of Leading Edge Radius and Angle of Attack on the Spanwise Spread of Turbulence Along the Leading Edge of a Sweptback Wing. Northrop Report NOR-64-30, 1964.

26. Reed, H. L.; and Nayfeh, A. H.: Stability of Flow Over Plates with Porous Suction Strips. AIAA Paper No. 81-1280, 1981.

27. Pfenninger, W.: Investigations on Reductions of Friction on Wings in Particular by Means of Boundary Layer Suction. NACA Technical Memorandum 1181, August 1947.

28. McGhee, Robert J.; Viken, Jeffrey K.; Pfenninger, Werner; Beasley, William D.; and Harvey, William D.: Experimental Results for a Flapped NLF Airfoil with High Lift/Drag Ratio. NASA TM-85788, May 1984.

29. Melson, N.D.; and Street, C.L.: TAWFIVE: A User's Guide. NASA TM-84619, September 1983.

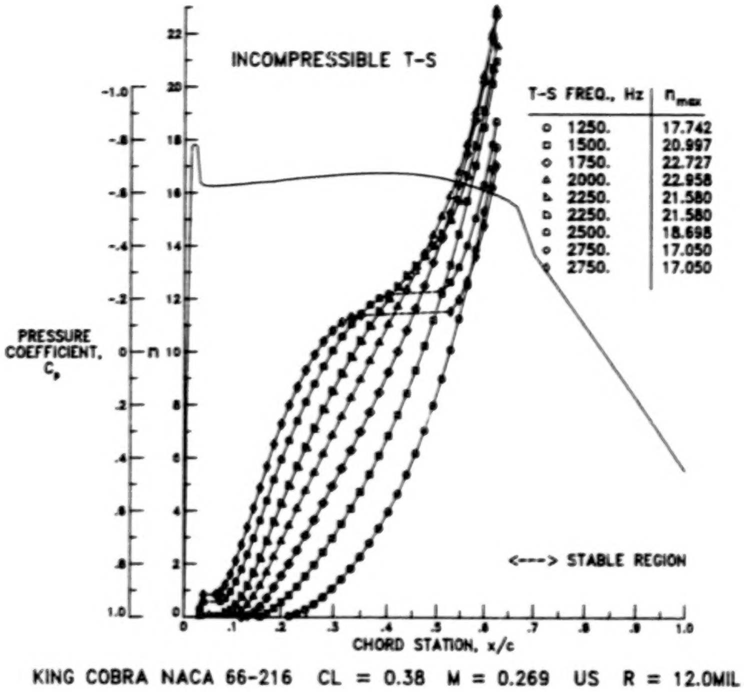

Figure 1.- Pressure distribution and the incompressible logarithmic amplification of various TS disturbance frequencies of Gray and Fullam's experiments on an NACA 66_{2x}-216 airfoil.

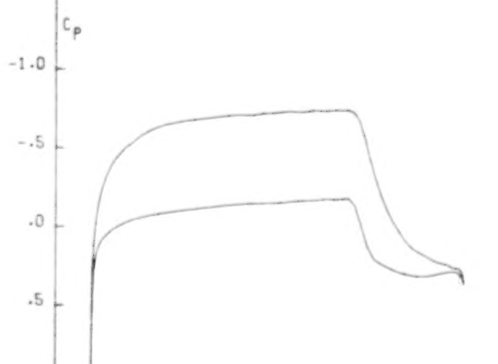

Figure 2.- Calculated inviscid pressure distribution of DESB159 at the design case.

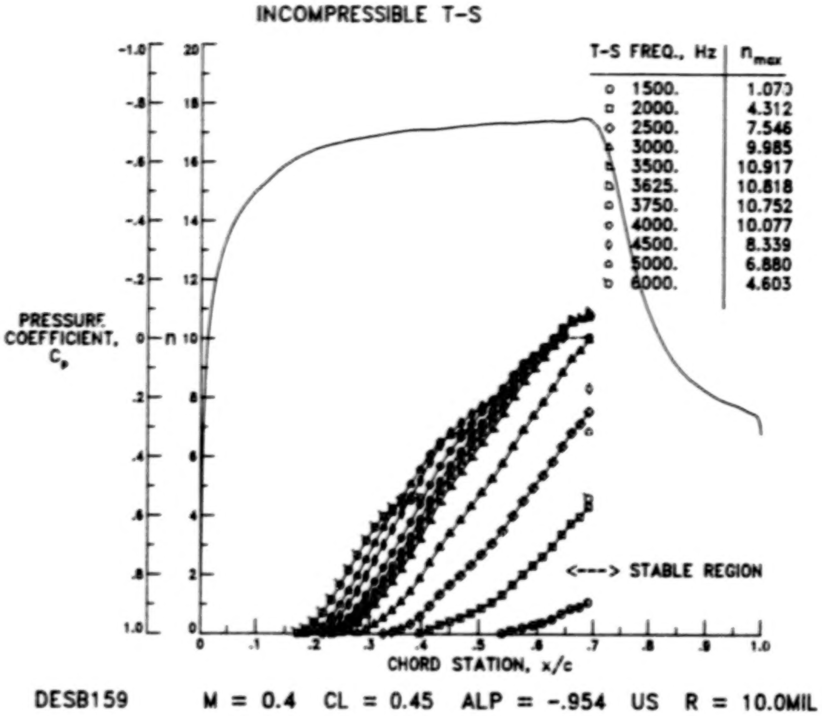

Figure 3.- Calculated pressure distribution and the incompressible logarithmic amplification of various TS disturbance frequencies for the upper surface of DESB159 at design.

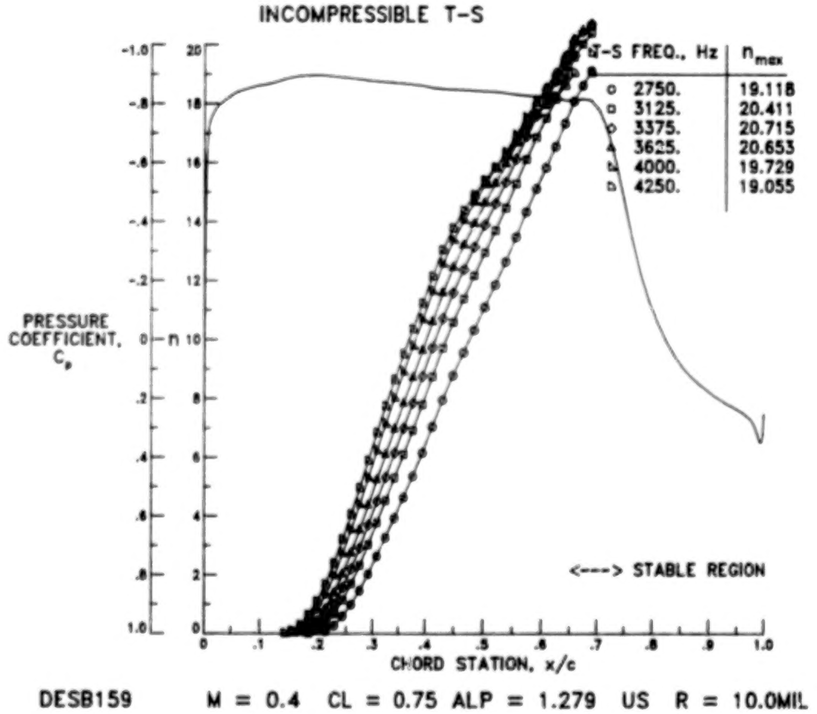

Figure 4.- Calculated pressure distribution and the incompressible logarithmic amplification of various TS disturbance frequencies for the upper surface of DESB159 at climb conditions.

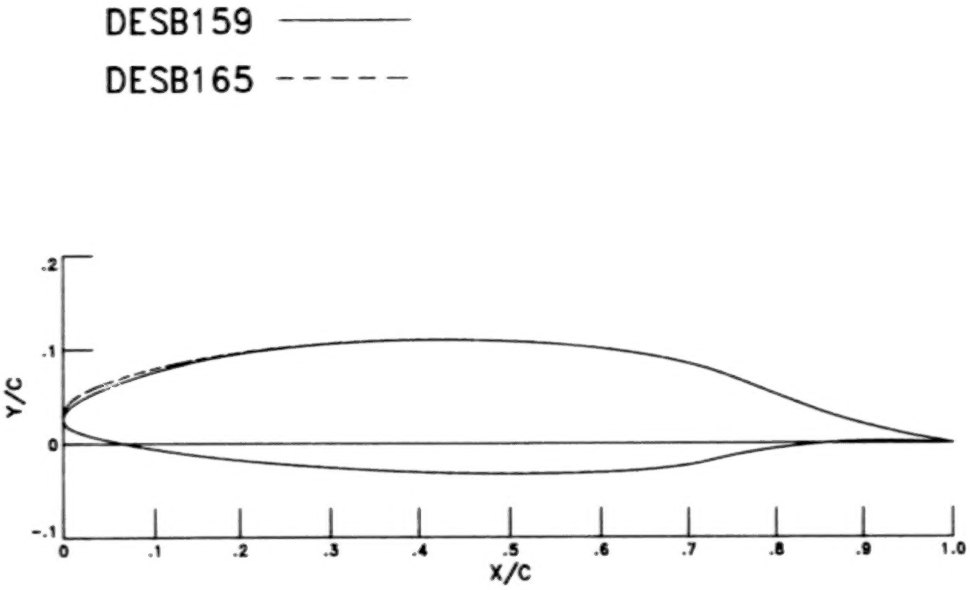

Figure 5.- Comparison of airfoil profile DESB165 with the baseline profile DESB159.

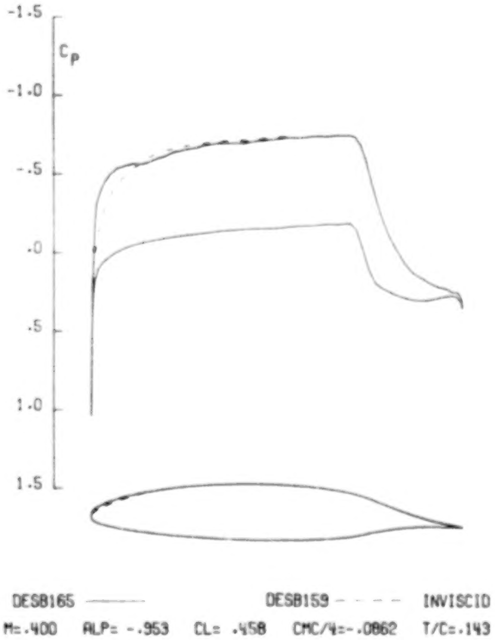

Figure 6.- Comparison of inviscid pressure distributions of DESB165 airfoil with the DESB159 airfoil at the design condition.

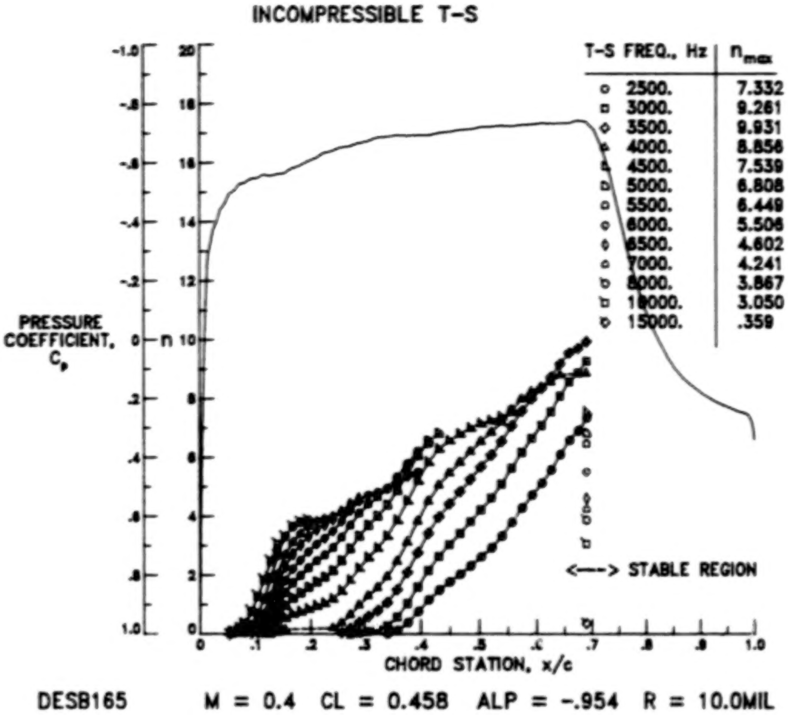

Figure 7.- Calculated pressure distribution and the incompressible logarithmic amplification of various TS disturbance frequencies for the upper surface of DESB165 at design.

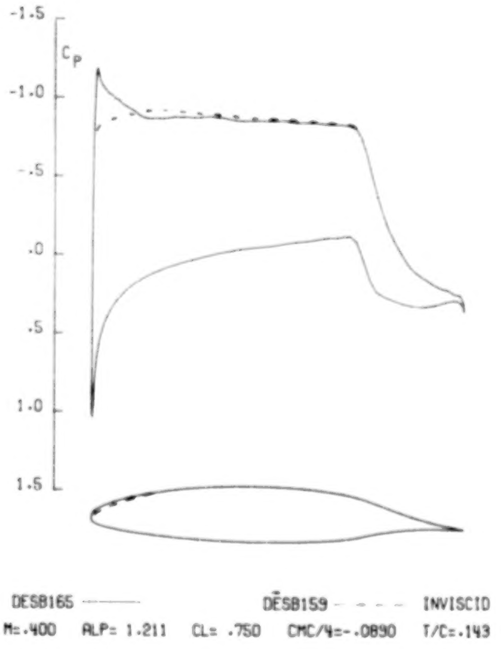

Figure 8.- Comparison of inviscid pressure distributions of DESB165 airfoil with the DESB159 airfoil at the climb condition.

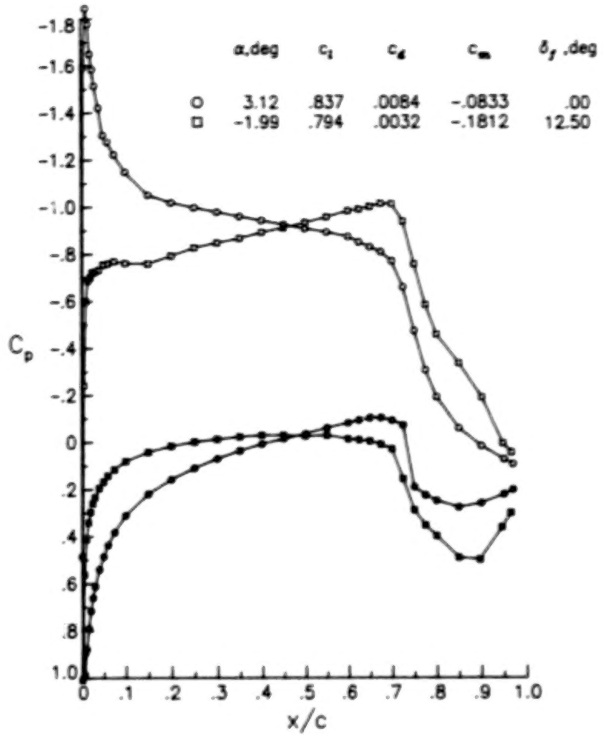

(a) Cruise flap deflection for low drag in climb.

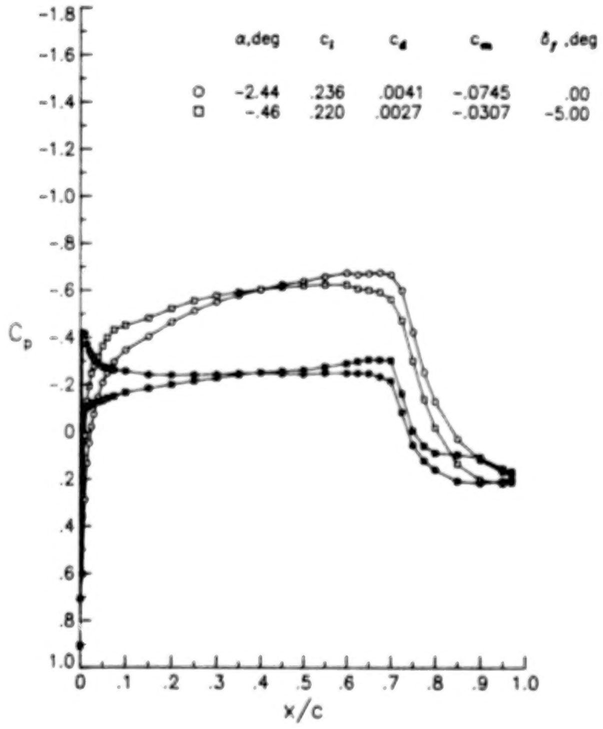

(b) Cruise flap deflection for low drag in cruise.

Figure 9.- Experimental pressure distributions on the NLF(1)-0414F airfoil at nearly constant section lift coefficients.

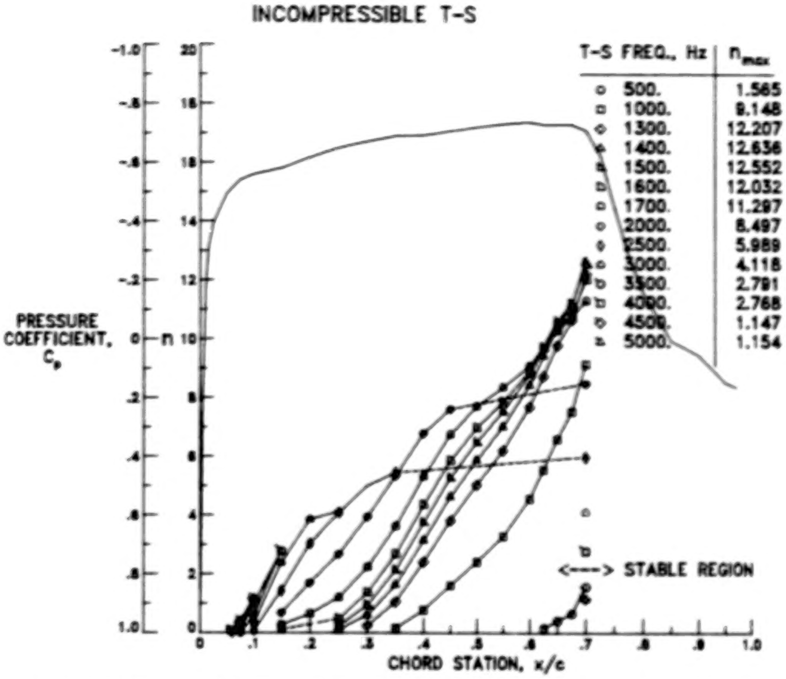

NLF1-0414F DELTA F = 0.0DEG M=0.12 ALP = -.97 US R = 10.0MIL

(a) Experimental pressure distribution and the incompressible amplification of various TS disturbance frequencies.

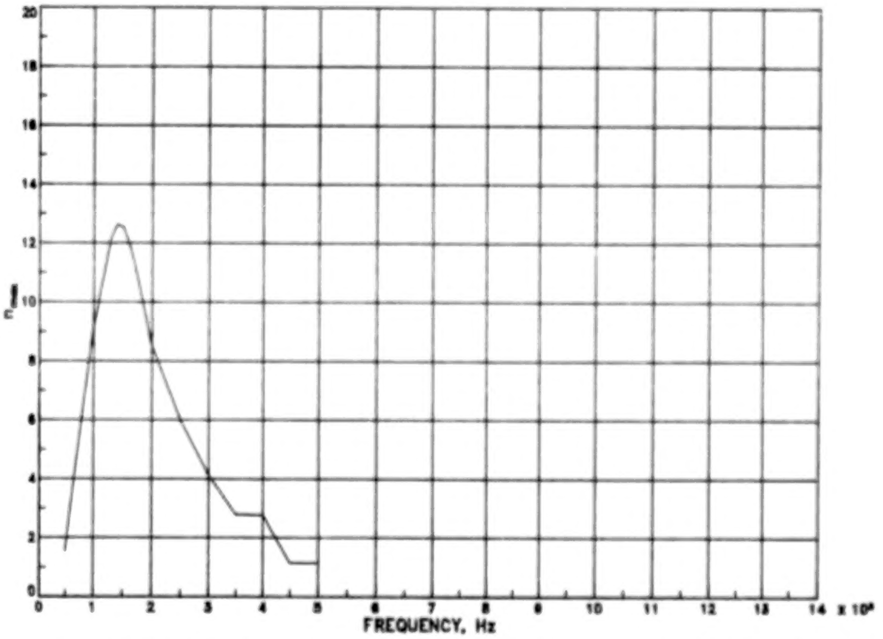

NLF1-0414F DELTA F = 0.0DEG M=0.12 ALP = -.97 US R = 10.0MIL

(b) Maximum incompressible logarithmic amplification versus TS disturbance frequency.

Figure 10.- Results of stability calculations at design conditions for the upper surface of NLF(1)-0414F.

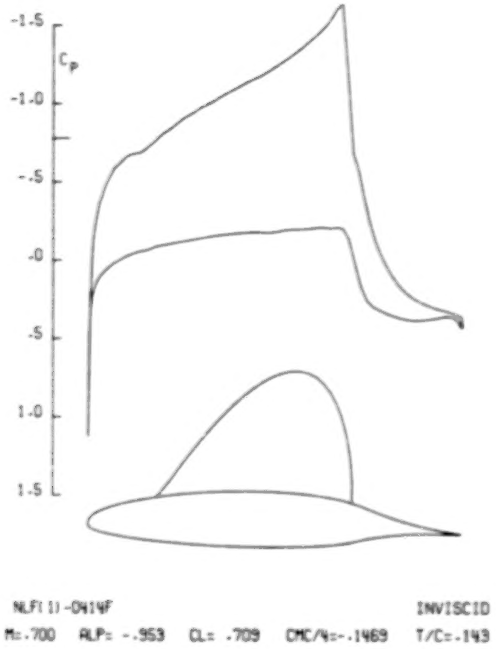

Figure 11.- Calculated inviscid pressure distribution of incompressible NLF(1)-0414F at compressible conditions.

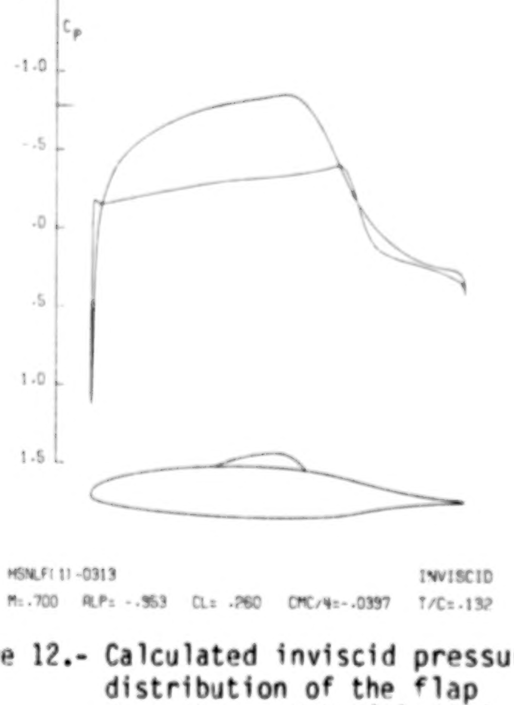

Figure 12.- Calculated inviscid pressure distribution of the flap de-cambered HSNLF(1)-0313 airfoil.

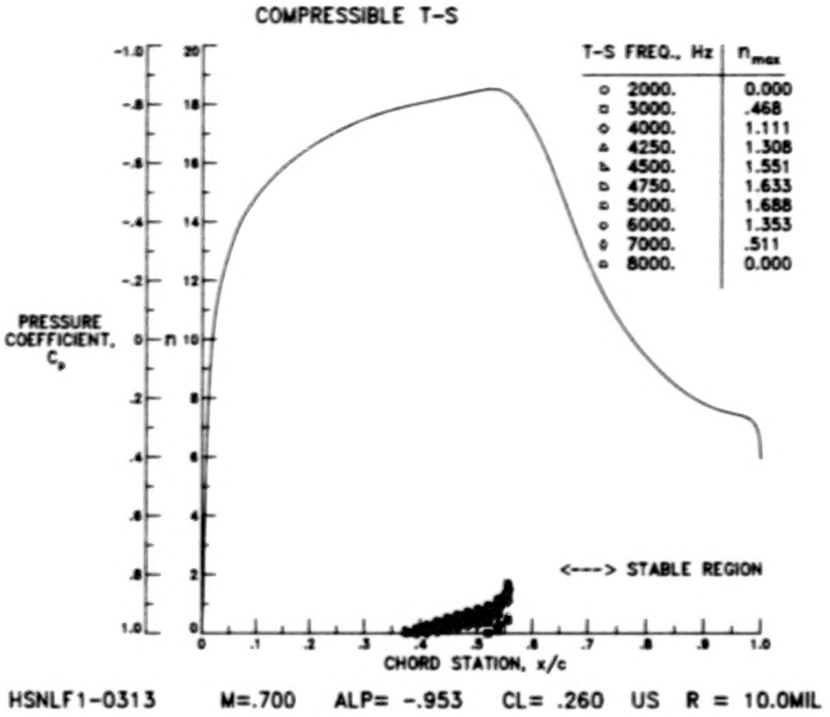

(a) Upper surface.

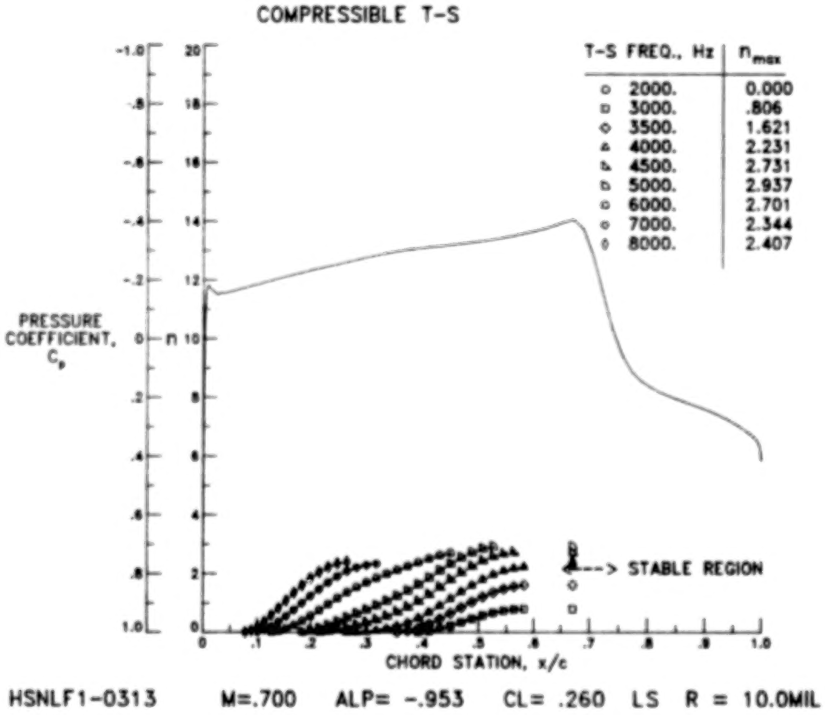

(b) Lower surface.

Figure 13.- Calculated pressure distribution and the compressible logarithmic amplification of various TS disturbance frequencies for HSNLF(1)-0313 at design.

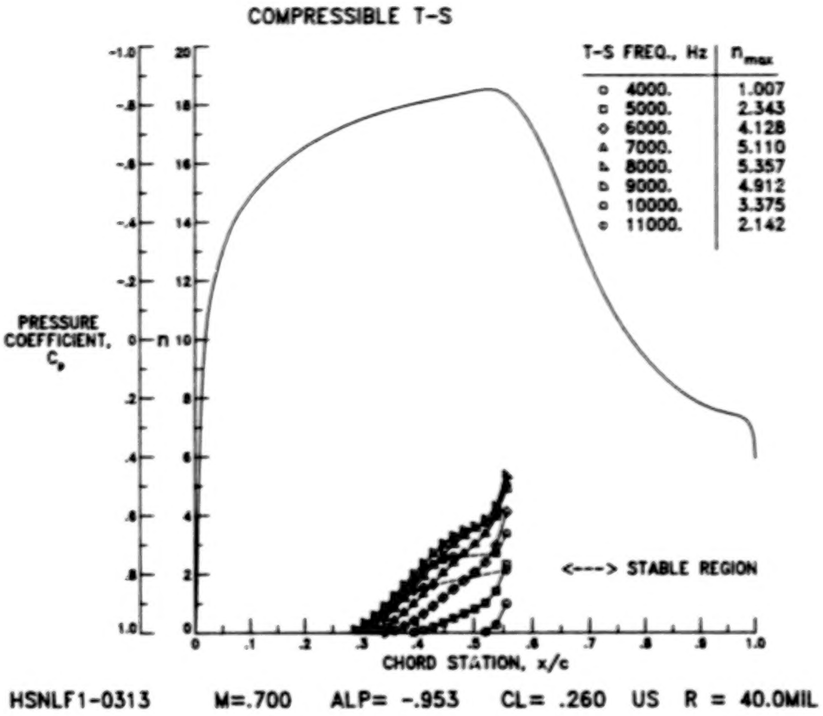

(a) Compressible logarithmic amplification.

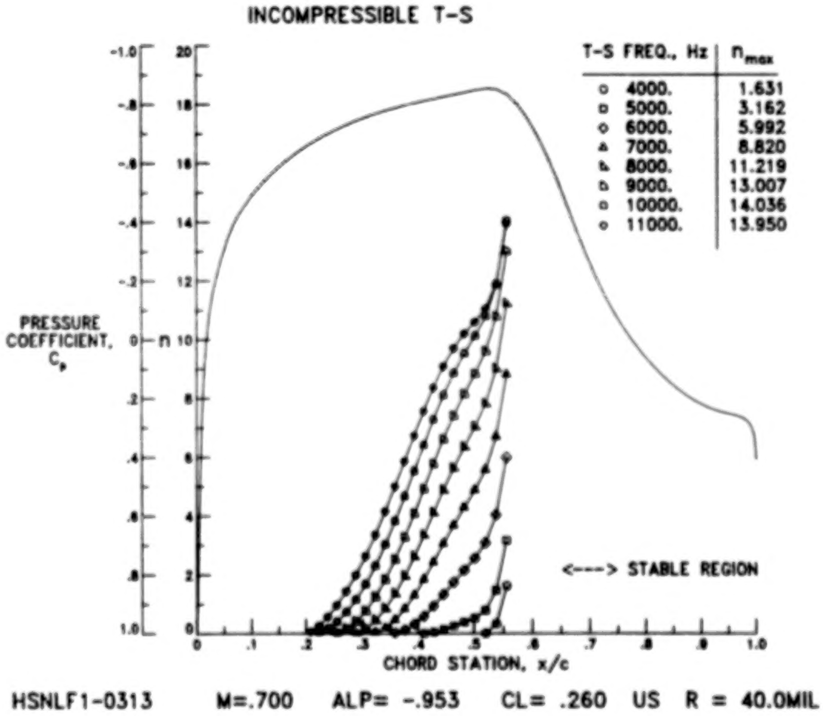

(b) Incompressible logarithmic amplification.

Figure 14.- Calculated pressure distribution and the logarithmic amplification of various TS disturbance frequencies for the upper surface of HSNLF(1)-0313 at $R = 40 \times 10^6$.

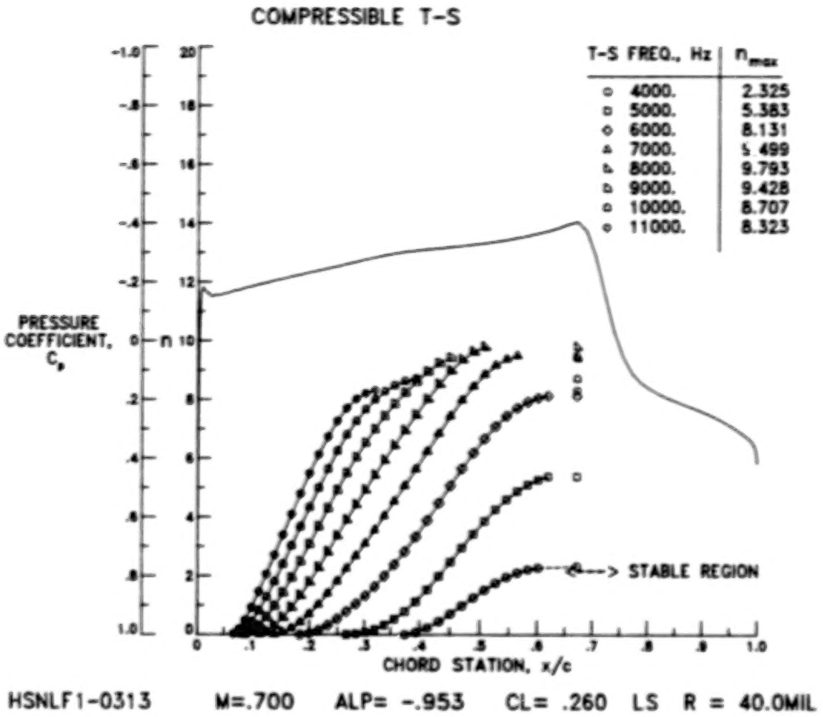

(a) Compressible logarithmic amplification.

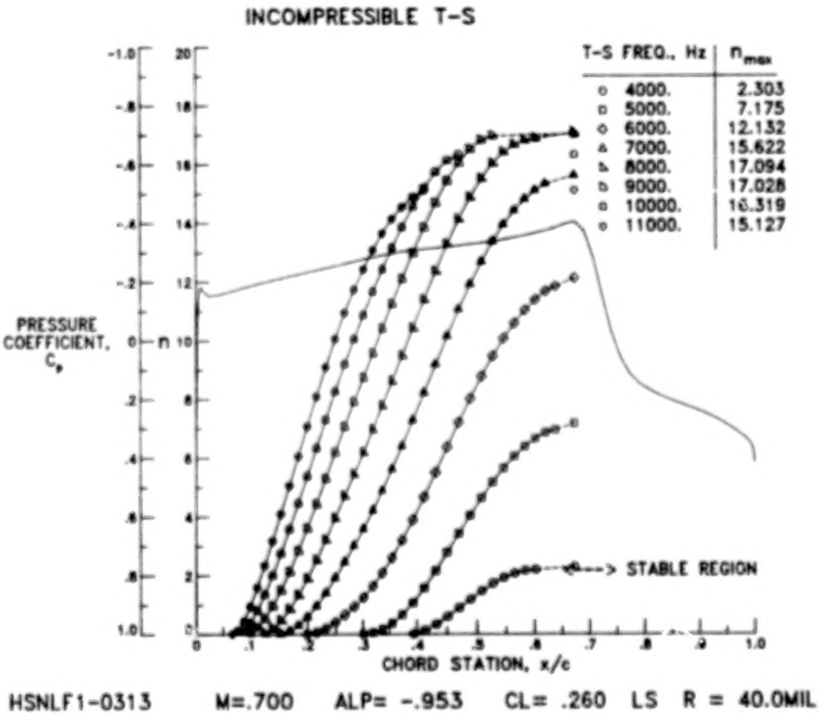

(b) Incompressible logarithmic amplification.

Figure 15.- Calculated pressure distribution and the logarithmic amplification of various TS disturbance frequencies for the lower surface of HSNLF(1)-0313 at $R = 40 \times 10^6$.

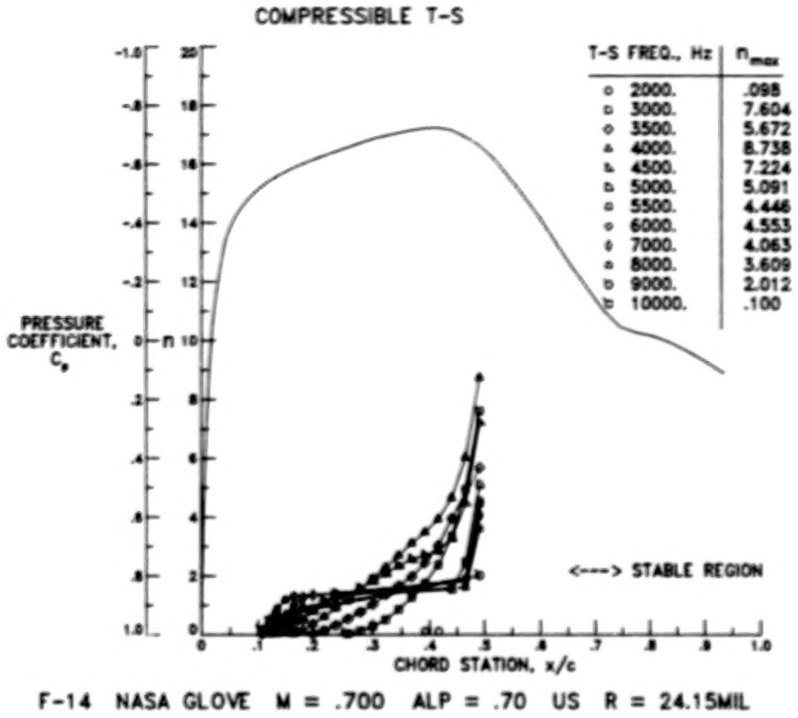

Figure 16.- Calculated three-dimensional pressure distribution and the compressible logarithmic amplification of various TS disturbance frequencies for the upper surface of the F-14 NASA glove.

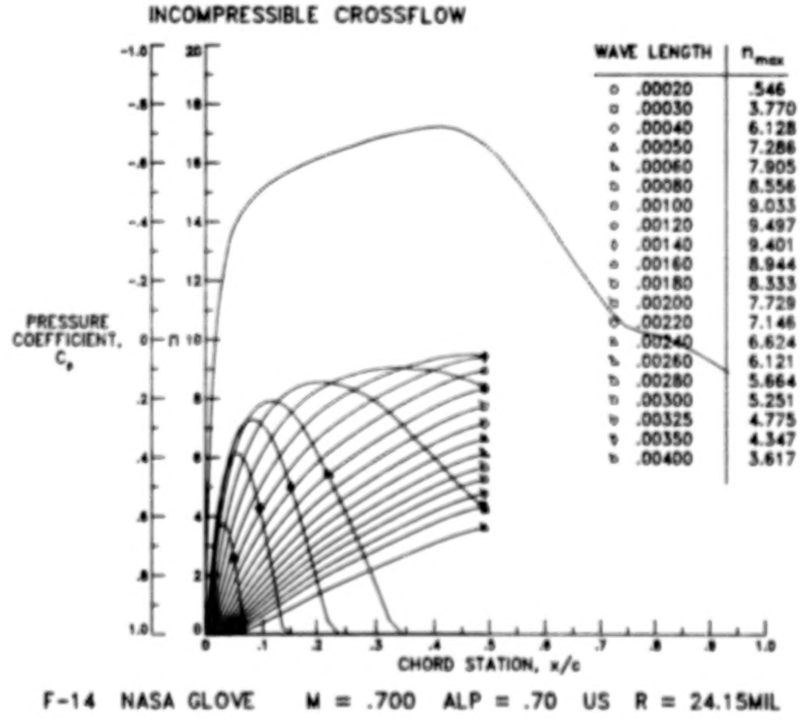

Figure 17.- Calculated three-dimensional pressure distribution and the incompressible logarithmic amplification of various crossflow disturbance wavelengths for the upper surface of the F-14 NASA glove.

ORIGINAL PAGE IS
OF POOR QUALITY

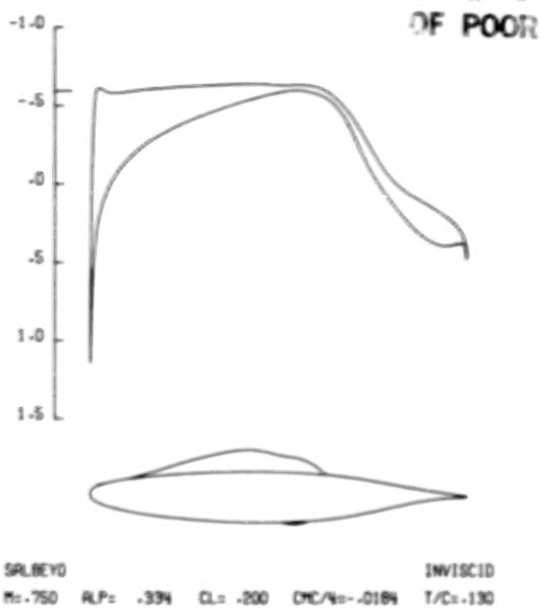

Figure 18.- Calculated inviscid pressure distribution of SALBEYO at the design case.

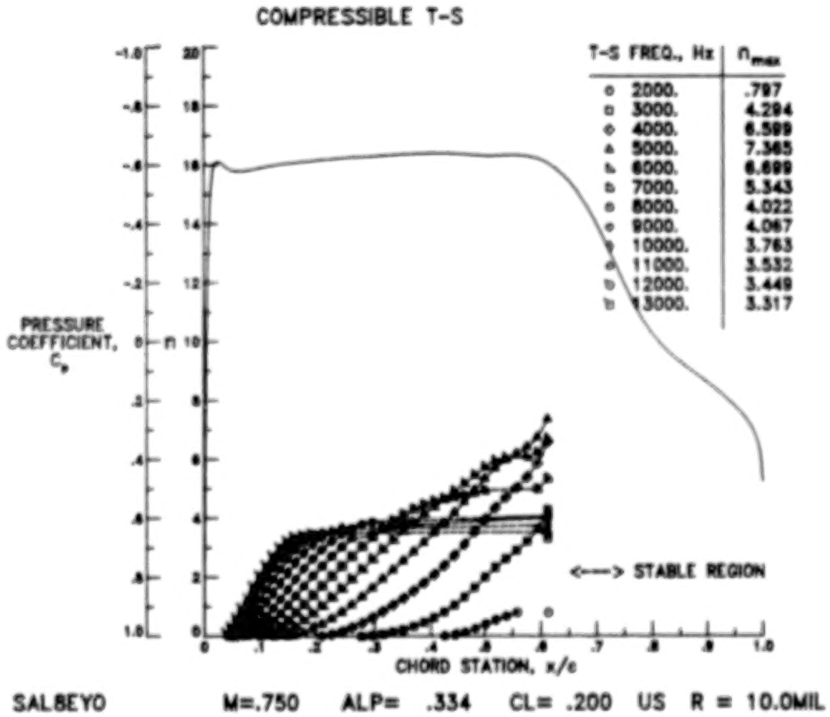

T-S FREQ., Hz	n_{max}
○ 2000.	.797
□ 3000.	4.294
◇ 4000.	6.599
△ 5000.	7.365
◺ 6000.	6.699
▷ 7000.	5.343
● 8000.	4.022
◆ 9000.	4.067
▼ 10000.	3.763
▲ 11000.	3.532
▶ 12000.	3.449
▶ 13000.	3.317

Figure 19.- Calculated inviscid pressure distribution and the compressible logarithmic amplification of various TS disturbance frequencies for the upper surface of the SALBEYO airfoil at design.

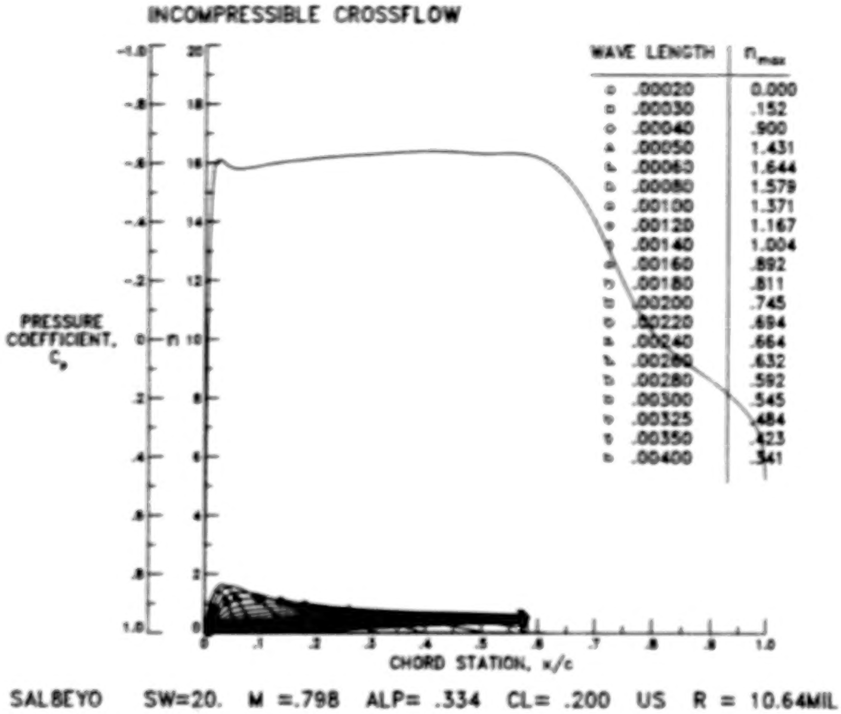

Figure 20.- Calculated inviscid pressure distribution and the incompressible logarithmic amplification of various crossflow disturbance wavelengths for the upper surface of the SALBEYO airfoil at design.

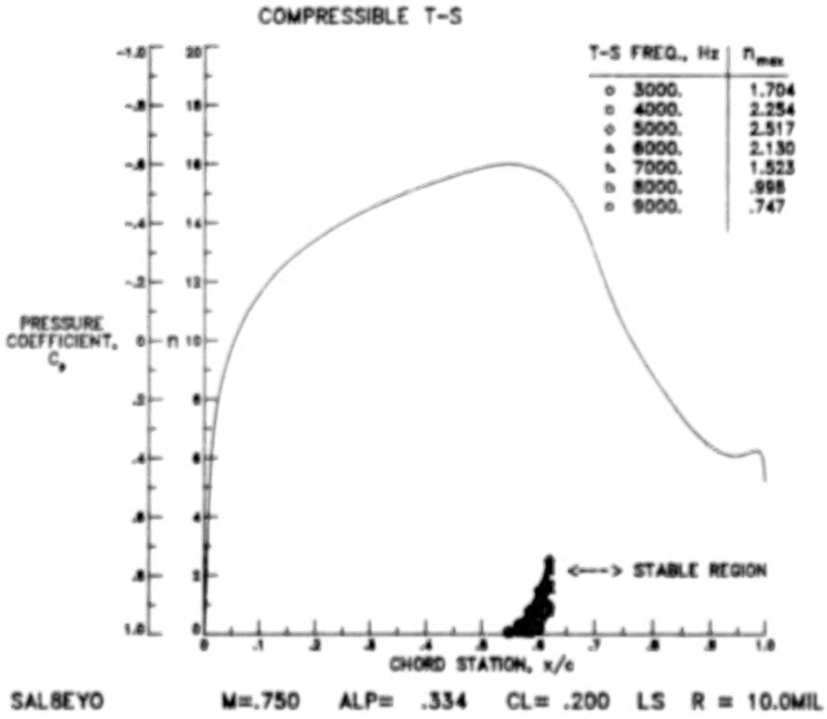

Figure 21.- Calculated inviscid pressure distribution and the compressible logarithmic amplification of various TS disturbance frequencies for the lower surface of the SALBEYO airfoil at design.

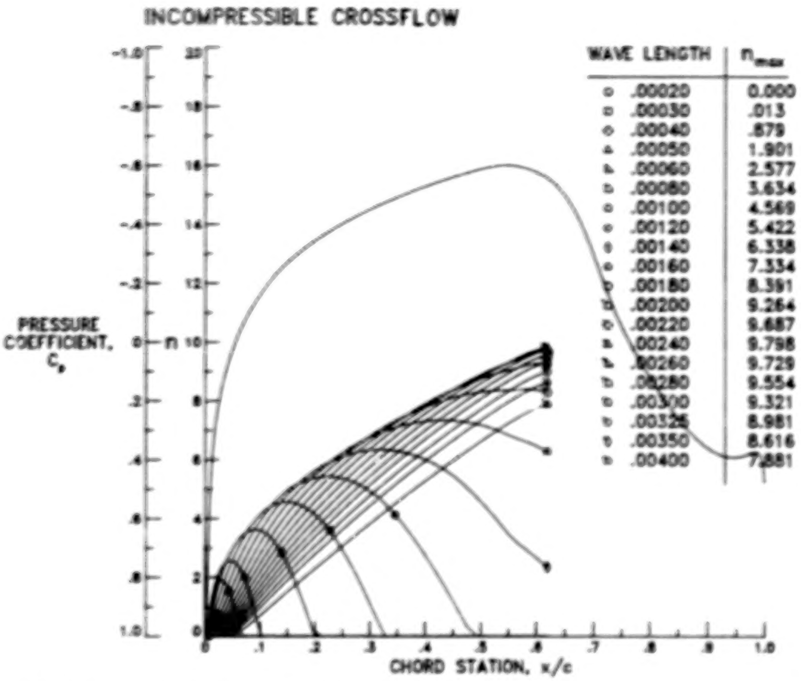

SALBEYO SW=20. M=.798 ALP= .334 CL= .200 LS R = 10.64MIL

Figure 22.- Calculated inviscid pressure distribution and the incompressible logarithmic amplification of various crossflow disturbance wavelengths for the lower surface of the SALBEYO airfoil at design.

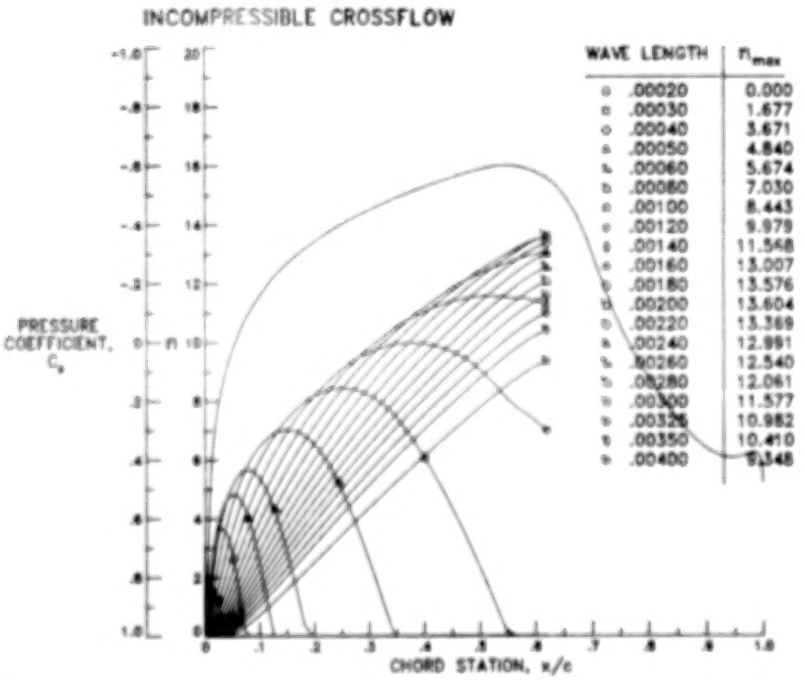

SALBEYO SW=20. M=.798 ALP= .334 CL= .200 LS R = 15.96MIL

Figure 23.- Calculated inviscid pressure distribution and the incompressible logarithmic amplification of various crossflow disturbance wavelengths for the lower surface of the SALBEYO airfoil at $R = 15.96 \times 10^6$.

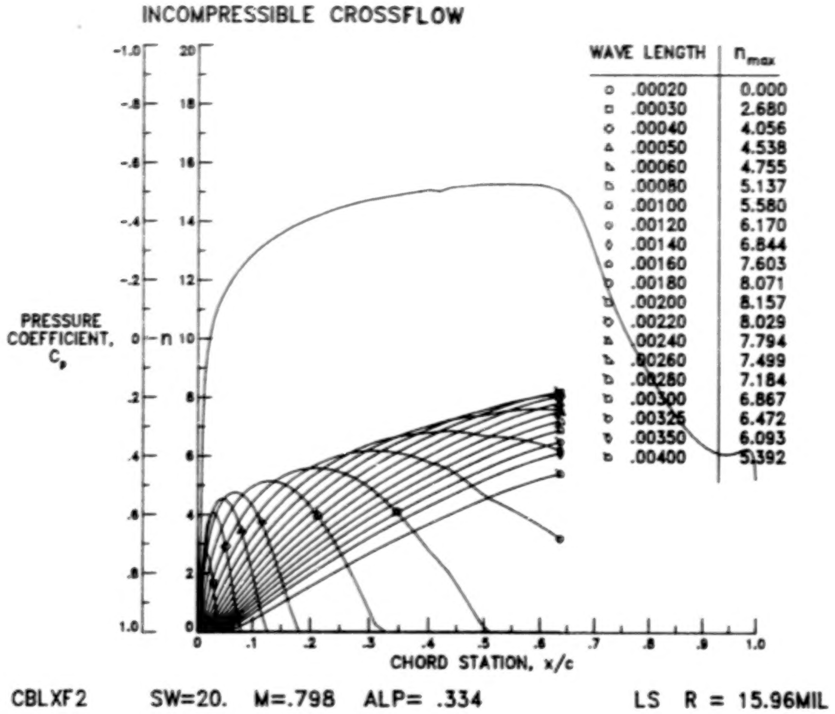

Figure 24.- Calculated inviscid pressure distribution and the incompressible logarithmic amplification of various crossflow disturbance wavelengths for the lower surface of CBLXF2 at R = 15.96 × 10^6.

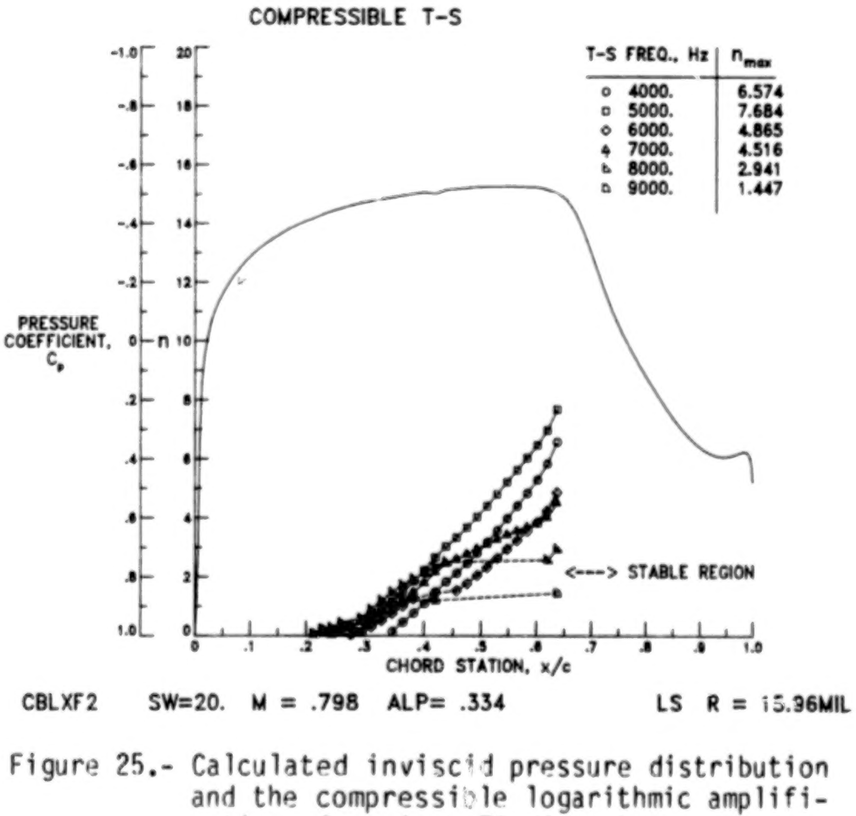

Figure 25.- Calculated inviscid pressure distribution and the compressible logarithmic amplification of various TS disturbance frequencies for the lower surface of CBLXF2 at R = 15.96 × 10^6.

S2-02

N88-23739

HIGH-LIFT FLAPS FOR NATURAL LAMINAR FLOW AIRFOILS

Harry L. Morgan
NASA Langley Research Center
Hampton, Virginia 23665

SUMMARY

A review of the NACA and NASA low-drag airfoil research is presented with particular emphasis given to the development of mechanical high-lift flap systems and their application to general aviation aircraft. These flap systems include split, plain, single-slotted, and double-slotted trailing-edge flaps plus slat and Krueger leading-edge devices. The recently developed continuous variable-camber high-lift mechanism is also described. The state-of-the-art of theoretical methods for the design and analysis of multi-component airfoils in two-dimensional subsonic flow is discussed, and a detailed description of the Langley MCARF (Multi-Component Airfoil Analysis Program) computer code is presented. The results of a recent effort to design a single- and double-slotted flap system for the NASA HSNLF(1)-0213 airfoil using the MCARF code are presented to demonstrate the capabilities and limitations of the code.

INTRODUCTION

The NASA has in recent years undertaken an extensive research effort aimed at improving the aerodynamic performance of a wide range of military and civil aircraft. A large part of this research effort has been focused on improvements in cruise performance by reducing the total aircraft drag and by increasing the drag-rise Mach number of the wing. Extensive development work was performed under the leadership of NASA's Dr. Richard T. Whitcomb during the 1960's and 1970's on the NASA supercritical airfoils which have greatly improved high-speed characteristics compared to the earlier NACA 65- and 66-series airfoils developed during the 1940's wartime effort. The current NASA research effort aimed at reducing total aircraft drag involves synergetic research in the interrelated disciplines of wing aerodynamics, aircraft structures, propulsion integration, and flight control systems.

Considerable improvements in cruise performance can be achieved by reducing overall wetted-area skin-friction drag. A large percentage of the skin-friction drag associated with the high-velocity flows around the lift-producing wing and tail surfaces can be reduced by either actively or passively delaying the transition of the surface boundary layer from laminar to turbulent flow. The best active approach involves the use of distributed surface suction either through spanwise slots or porous skins. Laminar flow control (LFC) research on both forms of suction is currently being conducted in the Langley 8-Foot Transonic Pressure Tunnel. The primary objective of this research is to demonstrate the feasibility of obtaining large amounts of laminar flow on a typical moderately swept transport wing at transonic speeds and high Reynolds number.

08607 -

The best passive means of controlling boundary-layer transition involves shaping the airfoil to have favorable upper and lower surface pressure gradients and carefully manufacturing the wing to eliminate surface roughness and waviness. The natural laminar flow (NLF) airfoils currently being developed at Langley (refs. 1, 2, and 3) are based on this passive means of boundary-layer control. As Mach number and Reynolds number are increased, the effects of shock-boundary-layer interaction and surface smoothness become more pronounced, and as a result, transition is more difficult to control passively. The NLF airfoils, therefore, are being designed for a subsonic Mach number range of 0.2 to 0.7 and for Reynolds numbers up to 10 million, which makes them ideally suited for application to general aviation aircraft. The greater drag reductions possible with active LFC-type airfoils are not generally applicable to general aviation aircraft because of the enormous complexity and weight penalties associated with the suction mechanisms.

In general, no matter how much effort is devoted to improving the cruise performance characteristics of an airfoil, the airfoil cannot be utilized unless it can be equipped with a flap system that will produce maximum lift coefficients great enough to prevent the necessity of unreasonable increases in wing area to meet take-off and landing performance requirements. This fact is often overlooked by airfoil designers, and as a result, many otherwise excellent airfoil designs are never put into practical use. There are very few applications for a particular airfoil that will not involve the need for some type of control surface such as flaps, slats, spoilers, and ailerons. The purpose of this paper is to present a summary of the types of flap systems that were developed for the earlier NACA low-drag and NASA supercritical airfoils and to discuss their possible application to the new NLF airfoils. The currently available theoretical methods for the analysis and design of two-dimensional flap systems will also be discussed and sample comparisons presented. Finally, the results of a recently completed effort to apply these methods to the design of a trailing-edge flap system for the HSNLF(1)-0213 airfoil will be presented and the limitations of the methods discussed.

SYMBOLS

Values are given in both SI and U.S. Customary Units. All measurements and calculations were made in U.S. Customary Units.

c	airfoil chord, cm (in.)
C_p	pressure coefficient, $\frac{p_\ell - p_\infty}{q_\infty}$
c_ℓ	section lift coefficient
c_d	section drag coefficient

C_m	section pitching-moment coefficient about quarter-chord point
M	free-stream Mach number
M_ℓ	local Mach number at a point on the airfoil
M'_ℓ	$\frac{dM_\ell}{d(s/c)}$
p	static pressure, Pa (lb/ft^2)
q	dynamic pressure, Pa (lb/ft^2)
R	Reynolds number based on free-stream conditions and airfoil chord
R_θ	Reynolds number based on local velocity and boundary-layer momentum thickness
s	distance along surface of airfoil, cm (in.)
x	airfoil abscissa, cm (in.)
z	airfoil ordinate, cm (in.)
α	geometric angle of attack, deg.
δ_f	flap deflection, deg.

Subscripts:

max	maximum
∞	free-stream conditions

Abbreviations:

F	flap
HSNLF	high speed natural laminar flow
LE	leading edge
LS	low speed
MCARF	Multi-Component Airfoil Analysis Program
MS	medium speed
NLF	natural laminar flow
SEP	separation point
TE	trailing edge

HISTORY OF NACA AND NASA LOW-DRAG AIRFOIL DEVELOPMENT

The NACA and NASA have been actively involved in the design and testing of low-drag airfoils since the early 1930's. (See reference 4.) The NACA 1-series airfoil sections were the first attempts to develop sections with prescribed pressure distributions and were the first family of NACA low-drag high-speed wing sections. The development of these first airfoils was so hampered by lack of adequate theoretical tools that they only operated well over a very small lift coefficient range. The next successive attempts were the NACA 2- to 5-series airfoil sections. These sections had relatively low maximum lift coefficients and exhibited extreme sensitivity to surface roughness. The rather large extent of laminar flow obtained on these airfoils was considered to be impractical at that time. This led to the development of the NACA 6-series airfoils which were designed for smaller extents of laminar flow and higher maximum lift coefficients. A large number of these airfoils were designed and tested due to the wartime environment of the 1940's, and many sections are still in use today. The final NACA-developed sections were those of the 7-series. These sections were designed for a greater extent of laminar flow on the lower than the upper surface, which led to lower pitching moments and higher design lift coefficients at the expense of reduced maximum lift and critical Mach number.

The NASA continued development of the low-drag airfoils beginning in the early 1970's due to the renewed interest in airfoil design as a result of the supercritical wing development work under the leadership of Langley's Dr. Richard T. Whitcomb. The low- and medium-speed (LS- and MS-series) airfoils developed during that time were intended primarily for application to general aviation and exhibited the highly aft-loaded characteristics of the supercritical sections. These sections were designed for a small extent of laminar flow on the upper and lower surfaces and for relatively high maxmimum lift coefficients, high climb lift-drag ratios, and docile stall behavior. More recently, NASA has shifted emphasis toward the NLF airfoils in an attempt to lower the cruise drag of the LS and MS airfoils, while retaining high maximum lift capability. The primary difference between these NLF airfoils and the earlier NACA 6-series airfoils is not so much in the overall design objectives but more in the theoretical methods used to design them. Today's airfoil design and analysis methods are very accurate, which means that it is no longer necessary to design and test a large number of airfoils to obtain an airfoil with the desired performance characteristics.

To date, the NASA has developed four NLF airfoils which vary in thickness, cruise lift coefficient, extent of laminar flow, and cruise Mach number. The first two of these airfoils are the NLF(1)-0416 and NLF(1)-0215F and are reported in references 1 and 2. The NLF(1)-0416 was designed for a Mach number of 0.2 with approximately 30-percent laminar flow on the upper surface and 40-percent laminar flow on the lower surface, and likewise, the NLF(1)-0215F was designed for 40-percent laminar flow on the upper surface and 60-percent on the lower surface. The third airfoil is the NLF(1)-0414F and is reported in reference 3. This airfoil was designed for a higher Mach number of 0.4 with 70-percent laminar flow on both surfaces. The fourth airfoil is the HSNLF(1)-0213 (High-Speed NLF) which has recently undergone preliminary low- and high-speed verification tests in the Langley Low-Turbulence Pressure and 6- by 28-Inch transonic tunnels. This airfoil was designed for a cruise Mach number of 0.7 with 56-percent laminar flow on the upper surface and 67-percent on the lower surface.

Each of these four airfoils has design pressure distributions similar to that illustrated in figure 1 for the NLF(1)-0414F. The pressure gradients forward of the transition point are favorable to promote a steady growth of the laminar boundary layer and slightly adverse aft of the transition point to promote efficient transition to turbulent flow without separation. The further aft the transition point, the steeper the recovery and the more difficult it is to avoid trailing-edge separation. All of these NLF sections have less thickness and camber in the trailing-edge region than the LS and MS airfoils. These characteristics have an adverse effect on the design, and therefore, it is more difficult to design an efficient high-lift system for NLF sections. These NLF airfoils are very similar to the 6-series airfoils, but have the advantage of improved leading-edge shapes to increase maximum lift capability. When equipped with similar high-lift systems, these new NLF airfoils should perform as well, if not slightly better, than similarly equipped 6-series airfoils. The next section of this paper will present a brief review of the types of flap systems that were developed for the early NACA airfoils and the general performance characteristics associated with each.

TYPES OF MECHANICAL FLAPS

Almost all aircraft wings require some type of auxiliary device to modulate aerodynamic lift, drag, pitch, and roll in order to satisfy cruise, takeoff, and landing performance requirements. Wing sizing is perhaps the most critical item the designer of a new aircraft must consider because it directly affects wing weight, ride quality, and growth potential. Wings with poor maximum lift capability are much larger and heavier and tend to have increased friction drag which inhibits cruise performance. Since the first flight by the Wright Brothers, airfoil and high-lift system development have continued to evolve due to tremendous increases in aircraft size and cruise speeds. In recent years, a great deal of emphasis has been given to improvements in the fuel efficiency of aircraft. This emphasis has brought about a renewed interest in smaller wings producing lower drag. These smaller wings generally have high aspect ratios and operate at high cruise lift coefficients and wing loadings which require smaller, more efficient, and more complex high-lift systems to meet takeoff and landing requirements.

Smaller and more efficient wings are especially of interest to the manufacturers of military and commercial transports who are particularly concerned with the payload capability and operational costs of new aircraft. The design, manufacture, and operational maintenance difficulties associated with the more complex high-lift systems required for these wings are overshadowed by the potential benefit of increased performance capability. In contrast, the manufacturers of the smaller general aviation aircraft are more interested in low initial costs, low maintenance requirements, and high reliability. Due to the highly competitive market for new general aviation aircraft, complex high-lift systems are not considered generally applicable. Another more desirable, although less effective, way to reduce wing drag and increase cruise performance is to reduce the skin-friction drag of the basic wing section, which has led to a renewed interest by general aviation in the development of natural laminar flow airfoils.

In general, there are four basic methods to increase the maximum lift of an airfoil: 1) increase leading- and trailing-edge camber, 2) extend the chord, 3) delay boundary layer separation, and 4) energize the external flow field. The latter two methods which encompass selective boundary layer suction and/or blowing and powered-lift concepts are extremely complex and costly to maintain and are understandably not applicable to general aviation aircraft. The discussion of high-lift systems will therefore be limited to those that utilize the first two methods.

The trailing-edge flap systems generally applicable to general aviation are presented in figure 2. The split flap is the simplest of the trailing-edge flap systems and is formed by deflecting an aft portion of the lower surface about a hinge point at the forward edge of the deflected portion. The hinge point can be located to provide a slot at the leading edge of the flap. The split flap can produce maximum C_ℓ increments in the range of 0.9 to 1.5 and possibly as high as 1.9 for very thick airfoils with large leading-edge radii. Deflecting the split flap results in a large bluff body which creates a large separation region with accompanying high drag. As an example, the performance of the several NACA 6-series and NASA NLF airfoils equipped with a 20% chord split flap is presented in figure 3 and shows average maximum C_ℓ increments of approximately 1.0.

Plain flaps are formed by hinging the trailing-edge region of the airfoil about a point within the contour and by pivoting with a downward deflection to increase the trailng-edge camber of the airfoil. This flap, like the split flap, can produce maximum C_ℓ increments in the range of 0.9 to 1.5 and are generally more effective when applied to airfoils with small amounts of camber. The drag produced by the plain flap is considerably less than that for a corresponding split flap because the upper surface is also deflected and the large bluff body with its corresponding separation is avoided. The plain flap has been used on many vintage and current production aircraft because it is easy to build, to actuate, and to maintain, and it is very reliable. As an example, the performance of the NACA 65,3-618 and NACA 66(215)-216 airfoils equipped with a 20-percent chord plain flap is presented in figure 4 and shows maximum C_ℓ increments of 0.9 and 1.0 for corresponding flap deflections of 60° and 65°, respectively. Split flaps usually produce slightly higher maximum C_ℓ increments than an equal-chord plain flap due to the loss of effective chord associated with the deflected plain flap.

The next level of trailing-edge flap system complexity is the slotted flap which is similar to the plain flap except that the flap hinge point is located external to the airfoil and produces a slot when deflected. The slot ducts the high-energy air from the lower surface to the low-energy air on the upper surface of the downstream element to delay separation and increase flap effectiveness. The rearward motion to produce the slot also results in a chord extension which in turn increases flap effectiveness. The amount of chord extension is dependent on the cutoff point on the forward element and the deflection of the aft element. In other words, the smaller the amount of the upper surface of the flap that is exposed when nested, the greater will be the chord extension when the flap is deflected. This type of flap is extremely effective and the most widely used on existing aircraft. Many commercial transports and commuter aircraft are equipped with single-, double-, or triple-slotted flap systems. The mechanical complexity of the slotted flap varies from the simple external fixed-hinge-point arrangement, which combines rotation and translation in the same movement, to the external flap-track arrangement, which separates rotation and translation allowing for greater possible chord extension.

Although a great deal of experimental data have been accumulated over the years, a general statement concerning the maximum C_ℓ increments obtainable with slotted flaps is not possible because of the sensitivity of flap effectiveness to the number of flap elements, Reynolds number, gap and overlap settings, and element deflection. In general, however, increasing the number of flap elements tends to increase the maximum obtainable C_ℓ increments. More than two flap elements rarely provide enough additional C_ℓ to warrant the additional complexity and weight, unless the airfoil is equipped with some type of leading-edge device. An examination of the data presented in reference 3 for the NACA 6-series airfoils shows maximum C_ℓ increments in the range of 1.0 to 1.4 for single-slotted flaps and 1.4 to 1.7 for double-slotted flaps. As an example, the performance of the NACA 63_4-420 airfoil equipped with a 25-percent chord slotted flap is presented in figure 5 and shows maximum C_ℓ increments of 1.5 and 1.56 for two flap-hinge locations. Likewise, the performance of the NACA 65_3-118 airfoil equipped with a 30.9-percent chord double-slotted flap is presented in figure 6 and shows a maximum C_ℓ increment of 1.7. It is reasonable to expect the NLF airfoils, which have slightly improved leading-edge designs, to obtain maximum C_ℓ increments of 1.5 to 1.6 with a properly designed single-slotted flap and increments of 1.8 to 1.9 with a double-slotted flap.

Although not generally considered during the design of general aviation aircraft, leading-edge devices are required in order to take full advantage of the trailing-edge flap system. Four types of mechanical leading-edge devices in use on many current military and commercial aircraft are presented in figure 7. These devices are mounted ahead of the leading edge to assist in turning the flow around the leading edge, thereby, delaying flow separation to a much higher angle of attack. The complexity of these devices ranges from the rather simple drooped-leading-edge device with a single lower surface hinge point to the very sophisticated variable-camber Krueger device actuated by complex four-bar linkages. The chord of a leading-edge device nominally ranges from 10 to 20 percent of the nested chord and rarely consists of more than a single element. Like the trailing-edge flap, a slotted leading-edge device is preferred because of the beneficial ducting effect of the high-energy lower surface air into the leading-edge boundary layer on the main element. The increment in maximum C_ℓ due to the addition of a leading-edge device is also very difficult to estimate because of the interaction of the wake from the device with the boundary layers and wakes on the downstream elements. It is not uncommon to see additional increments 30 to 40 percent greater due to the addition of a leading-edge device. As an example, the performance of an NACA 64A010 airfoil equipped with a split and a double-slotted flap and a 17-percent chord leading-edge slat is presented in figure 8 and shows incredible performance gains attributable to the slat.

As stated before, the manufacturers of general aviation aircraft have avoided the use of leading-edge devices because of the complexity and weight penalty associated with the device and because of the extensive maintenance schedule required to insure safe and reliable operation. They are not generally considered applicable to low-drag airfoils due to the adverse effects on the stability of the leading-edge laminar boundary layer resulting from surface irregularities with the device nested. These irregularities can possibly cause premature transition and a corresponding increase in trailing-edge separation with a possible loss in maximum C_ℓ capability. The Krueger leading-edge devices, which fold out from the lower surface, should not adversely affect the upper surface laminar boundary layer and possibly not the lower surface boundary layer because of the mildness of the lower-surface pressure gradient. In view of the recent advances in composite materials and de-icing mechanisms, it is reasonable to consider the use of leading-edge devices with the new NLF airfoils.

Another type of leading- and trailing-edge device, which has recently received considerable attention by transport manufacturers, is the continuous variable-camber device. These devices consist of internal shape-altering mechanisms that deflect and smoothly recontour (without steps and gaps) the leading and trailing edges of the airfoil surface. These devices can produce small deflections to optimize wing camber during climb, cruise, and descent and large deflections to provide high lift for takeoff and landing. A detailed discussion of the development of a continuous variable-camber device for application to short- and long-range commercial transports is presented in reference 5. A photograph of a working model of this concept is presented in figure 9, and details of the leading- and trailing-edge internal mechanisms are presented in figures 10 and 11, respectively. The continuous skin of the leading edge is flexed by the variable-camber mechanism to maintain a constant leading-edge radius through the entire range of deflections. In the trailing-edge region, the overall length of the upper surface skin remains constant, and an overlapping seal on the lower surface allows for articulation. These devices are particularly attractive for application to NLF airfoils because they eliminate surface discontinuities that exist with conventional high-lift devices and offer opportunity for a continuously optimized shape during the entire flight envelope.

The results of the study presented in reference 5 showed overall fuel savings as high as 4 percent utilizing variable-camber devices on existing conventional transport wings. Add to this the fuel savings possible using NLF airfoil sections and the net fuel savings can be substantial. There are, of course, greater weight penalities associated with continuous variable-camber devices compared to the other less complex high-lift systems. However, recent advances in composite materials technology are making this type of high-lift device more feasible, at least for application to transport aircraft. Variable-camber trailing-edge devices do not generally produce maximum C_ℓ increments as great as those of conventional slotted-flap devices because there are no slots to duct high-energy air from the lower surface of the main wing to the upper surface of the flap. The variable-camber mechanism can be modified to create a single- or double-slotted flap by allowing several linkage pivot-points to be located external to the airfoil contour as illustrated in figure 12. This double-slotted flap mechanism also allows for positive deflections which will allow the pilot to continuously alter the wing shape to optimize cruise performance.

As previously mentioned, it is very difficult to empirically formulate performance estimates for slotted-flap systems because of their sensitivity to Reynolds number and position. There are, however, theoretical methods and corresponding computer codes that attempt to model the complex flow around high-lift flaps and provide the designer with valuable tools to estimate performance. The next section of this paper will discuss some currently available and widely used methods to analyze high-lift flap systems.

THEORETICAL DESIGN AND ANALYSIS METHODS

The flow field around an airfoil with a deflected slotted leading- and trailing-edge flap system is very complex as illustrated in figure 13. Ordinary laminar and turbulent boundary layers and downstream wakes exist on each element. For optimum performance, the elements must be located in close proximity to one another which results in the interaction of the downstream wake of the forward elements with the boundary layers on the downstream elements. These interacting merged flows are called confluent boundary layers. Usually, at or near the maximum C_ℓ conditions, one or more regions of separated, highly rotational flow exist. The cove geometric discontinuities associated with the main-element flap cutout also create local separation and reattachment regions.

Both linear and nonlinear methods have been used to model the complex flow field around slotted flap systems. The nonlinear methods which directly couple viscid and inviscid flow regions involve the use of finite-element or finite-difference numerical techniques to solve some form of the time-dependent Navier-Stokes equations. These nonlinear methods require rather dense field grid networks to adequately represent the viscous effects, which in turn require rather large computer capacity for solution. Although excellent progress has been made applying these methods to the analysis of unflapped airfoils and wings, very little progress has been made applying them to the flapped configurations. Computer capacity and execution speeds are increasing at a phenomenal rate, and hopefully, complete nonlinear solutions will be possible within the next decade. Even then, this type of solution method will probably not be used on a routine basis for some further period of time because of the large computation time and high costs involved. A more logical application would be to use linear methods to improve the models used in the nonlinear methods.

The linear methods assume that, although the shear forces are interrelated with the pressure forces through the boundary layer, the viscid and inviscid regions can be solved separately and then iteratively interacted with each other. One such method that uses this solution philosophy is the NASA-developed Multi-Component Airfoil Analysis computer code (MCARF) which was the product of a joint effort with NASA, Lockheed-Georgia Company, and Boeing Commercial Airplane Company and is documented in references 6 and 7. The current version of this program is only applicable to flapped airfoils with smooth geometry and no separated flow regions in subsonic flow. The Laplace equation is used to solve the inviscid potential flow which is assumed to be irrotational. Utilizing the Biot-Savart law, the airfoil components are represented by a series of connected constant or linearly varying vortex and source singularities whose strengths are determined using matrix inversion techniques. The viscous displacement effects due to the wake and surface boundary layers are computed using integral techniques to solve the ordinary and confluent boundary layer equations. During successive iterations, the viscous displacement effects are accounted for by either decambering the airfoil shape or by imposing an additional source distribution whose strength is proportional to the rate of change of the boundary-layer displacement thickness. The current version of MCARF uses the decambering technique because it requires less computational time and provides an answer approximately 90-percent that obtained using the distributed source technique. It is believed, however, that use of the distributed source technique will be necessary to properly simulate massive separation regions. The output from the MCARF computer code consists of surface pressure and velocity distributions, boundary-layer properties, and integrated force and moment coefficients. An auxiliary computer code called TRACE is available to map streamline patterns around a multi-component airfoil and uses the vortex and source strengths computed by MCARF as input. Work is currently underway on a version of MCARF which can account for fixed external boundaries such as wind-tunnel floors and ceilings. Preliminary results from this improved version are presented in figure 14 showing the streamline pattern for a typical single-slotted flap with simulated floor and ceiling boundaries corresponding to that for the Langley Low-Turbulence Pressure Tunnel (LTPT).

Although the current version of the MCARF code does not contain a separated flow model, the code can be used to predict the maximum C_ℓ of airfoils with leading-edge stall properties which are characteristic of many supercritical and NLF airfoils. Leading-edge stall occurs when the angle of attack is great enough to induce sufficient instability of the laminar boundary layer to prevent transition to a reattached turbulent boundary layer. At lower angles of attack, the reattached turbulent boundary layer will remain attached to the trailing edge of the airfoil. At the stall angle, the laminar boundary layer separates and a massive separation region forms resulting in a dramatic loss in C_ℓ. The integral laminar boundary layer method of Cohen-Reshotko (ref. 8) transformed for compressible flow by Stewartson's transformation (ref. 9) is used in the MCARF program to compute the laminar boundary-layer properties. The Schlichting-Ulrich-Granville method (refs. 10 and 11) is used to predict the point of laminar instability and subsequent point of transition.

To date, no exact method exists to determine whether the laminar boundary layer will remain completely separate or reattach as a turbulent boundary layer. The Goradia-Lyman laminar stall criterion (ref. 12) suggests that a pair of nondimensional parameters based on the Mach number, Mach number gradient, and momentum Reynolds number at the separation point can be used to predict the existence of turbulent reattachment. Extensive correlations between available experimental data and theory predictions have generally shown poor agreement using the pair of parameters proposed by Goradia-Lyman. Better agreement has been obtained by formulating the following modified pair of parameters which also incorporates the influence of free-stream Mach number and Reynolds number:

$$\left(\frac{R_\theta}{\sqrt{R/10^6 - R_\theta/10^3}}\right)^{1/2} \qquad (1)$$

$$\frac{-M'_\ell}{\sqrt{M_\ell - M}} \qquad (2)$$

Figure 15 shows a curve for predicting laminar stall based on the theoretical predictions from the MCARF code. The primary data used to develop this laminar separation curve included experimental-theory correlations for the NACA 0012, NACA 23012, NACA 65_2-215, and the NASA NLF(1)-0416 airfoils.

Additional experiment-theory correlations have been performed to determine the validity of using the laminar separation curve to predict laminar stall and corresponding maximum C_ℓ for flapped airfoils. The most comprehensive data available on a laminar-stall-type airfoil equipped with a wide variety of the leading- and trailing-edge high-lift devices are those for the 9.3-percent-thick supercritical airfoil reported in reference 13. Figure 16 shows the theory-experiment comparison for the basic unflapped section. Lift, drag, and pitching-moment agreement is good until the turbulent boundary layer begins to separate near the trailing edge. Although the separation method predicts the correct maximum C_ℓ, the predicted stall angle is approximately 2° less than the experimental value. However, the separation method is not expected to perform as well for unflapped airfoils that may have rather large regions of trailing-edge separation at maximum C_ℓ, which is typical of many of the NASA-developed low- and medium-speed general aviation airfoils or the recently developed NLF(1)-414 and HSNLF(1)-0213 airfoils.

Presented in figures 17 and 18 are theory-experiment comparisons for the supercritical airfoil equipped with a single-slotted flap deflected 20° and 30°, respectively. The agreement with the flap deflected 20° is excellent. Although the overall agreement for C_ℓ is poor with the flap deflected 30°, the predicted maximum C_ℓ agrees well with the experimental value. An examination of the experimental flap pressure distributions for the 30° case shows that the flow is separated on approximately 10% of the upper surface near the trailing edge which accounts for the poor agreement between experiment and theory. It should not be generally concluded, however, that the code will predict the correct maximum C_ℓ with flap separation present. Without proper modelling of the separation region on the flap, the predicted flap loads are too high and produce a greater circulation around the main element and more adverse pressure gradient in the leading-edge region than occurs experimentally. The code will, therefore, predict a lower stall angle than that obtained experimentally. In order to incorporate a separation model in the MCARF code for flapped airfoils, a criterion for the accurate prediction of the separation point for merging confluent boundary layers is needed. To date, no such criterion has been developed; therefore, only ordinary turbulent boundary layer methods can be used to indicate possible flow separation.

The theory-experiment comparison for the supercritical airfoil equipped with a leading-edge device is presented in figure 19 and shows good agreement for lift and pitching moment. Maximum C_ℓ prediction is based on laminar boundary layer separation on the leading-edge device and shows good agreement, even though the experimental data show separation present near the trailing edge of the main element. The rather poor drag agreement can be attributed to errors in the downstream wake measurements caused by flow disturbances from the support brackets for the leading-edge device. The theory-experiment comparisons for the airfoil equipped with a triple-slotted trailing-edge flap and no leading-edge device and with a double-slotted trailing-edge flap and leading-edge slat are presented in figures 20 and 21, respectively. The agreement is good for both flapped airfoils shown, and again, the maximum C_ℓ in each case is based on the laminar stall of the most forward element. The two flap configurations shown are at relatively low deflections and the flow is attached on all flap elements. Additional correlations have shown that the prediction accuracy of the MCARF code deteriorates rapidly with increased flap deflection and accompanying flap separation.

FLAP SYSTEM FOR HSNLF(1)-0213 AIRFOIL

A large percentage of the experimental tests conducted by the NACA during the development of flap systems for the 6-series airfoils were performed in the Langley LTPT facility. This unique two-dimensional test facility can obtain a maximum Mach number of approximately 0.45 and a maximum Reynolds number of approximately 18 million per foot. The LTPT has recently undergone extensive renovation to improve the facility's operating characteristics. (See reference 14.) A new model-support and force-balance system and a sidewall boundary-layer control system were included in the renovation to improve the high-lift testing capability of the tunnel. The cooling coils were replaced to extend the cold weather operating pressures of the facility and the antiturbulence screens replaced to reduce the free-stream turbulence of the flow. As a result of these modifications, the LTPT facility is now considered to be one of the best tunnels in existence for the development of low- and medium-speed NLF airfoils and low-speed high-lift flap systems.

Due to the unique operational characteristics of the LTPT, the facility is in heavy demand by government and non-government organizations conducting research on a wide range of laminar flow and high-lift-related topics. The Langley 6- by 28-Inch Transonic Tunnel, which is a blowdown facility and uses the LTPT as a primary high-pressure air-storage tank, is also in heavy demand by researchers developing high-speed and transonic airfoils. Due to the heavy demand on both facilities and due to a limitation on the number of operating personnel, the test time available for any given experiment is rather limited and the test objectives very selective. Tunnel time is no longer readily available to conduct tests on large families of airfoils or high-lift systems; therefore, design and analysis methods are used extensively to reduce the development time. In fact, in many instances the primary objective of a typical test scheduled for the LTPT and the 6- by 28-Inch Transonic Tunnel is to either verify a particular theoretically designed airfoil system or to provide data needed to improve the design and analysis methods. The remaining discussion in this paper will describe one such research effort and involves the design of a trailing-edge flap system for the recently developed HSNLF(1)-0213 airfoil. The single- and double-slotted flap systems designed for this airfoil have not been experimentally verified to date.

The structural wing box for most high-speed general-aviation and transport aircraft has a length which is nominally 50 percent of the local wing chord and is positioned with 20 percent of the chord forward of the wing box available for leading-edge devices and 30 percent aft available for trailing-edge devices. For the HSNLF(1)-0213, an additional 2 percent immediately aft of the wing box was allowed for structural interface with a flap actuation system which resulted in a nested trailing-edge flap chord length of 28 percent of the total wing chord. The recessed cove region formed in the lower surface trailing edge of the main element when the flap is deflected produces a local separation bubble with a reattachment point at the exit of the slot between the main and flap elements. It is desirable to locate the cutoff point as far forward as possible on the lower surface of the main element to insure smooth pressure recovery through the slot region. The lower surface geometry of the single-slotted flap design is, therefore, the same as that of the aft 26 percent of the lower surface of the basic section. The bulk of the flap design effort is therefore centered around contouring the upper surface of the flap. After selecting the upper surface cutoff point for the main element, the flap design contour is further limited to that enclosed within the flap cove region of the main element.

The flap contours for the HSNLF(1)-0213 airfoil that result from selecting upper main element cutoff points at 88, 92, 96, and 98 percent of the total chord are presented in figure 22. The advantage of moving the cutoff point further aft toward the trailing edge is an increase in the effective chord with the flap extended which should produce a corresponding incremental increase in C_ℓ. The primary disadvantage to moving the cutoff further aft is that, in order to obtain an acceptable structural thickness in the trailing-edge region of the main element, the maximum thickness and leading-edge camber of the flap must decrease, which will result in a possible incremental decrease in C_ℓ. The performance of each of the four flap designs was determined using the MCARF computer code for flap deflections of 35° and 40° with a 2-percent gap and a 0-percent overlap at a Mach number of 0.1 and a Reynolds number of 4 million. The stall angle for each case was assumed to occur at the angle corresponding to separation of the laminar boundary layer at the upper surface transition point. A check for flap separation was made by performing an ordinary turbulent boundary layer analysis of the upper surface flap pressure distribution for all four cutoff designs at the same flap deflection. It was assumed for comparison purposes that the more forward the predicted separation point, the greater the loss in the maximum C_ℓ. Until a separation model can be formulated and incorporated into the MCARF computer code, only empirical estimates can be made of the exact loss in maximum C_ℓ due to flap separation. No attempt was made during this design effort to determine an empirical correlation; therefore, the maximum C_ℓ values presented are probably higher than those which could be obtained experimentally.

A comparison of the lift and drag performance predictions for the 88- and 92-percent flap designs is presented in figure 23 for flap deflections of 35° and 40°. At a given angle of attack, the C_ℓ for the 92-percent flap design was approximately 0.1 higher than that for the 88-percent design and the corresponding increment in maximum C_ℓ was approximately the same. Examination of the lift-drag polars shows slightly higher drag for the 92-percent design with 35° flap deflection and very little difference at 40° deflection. These results indicate a slight performance advantage of the 92-percent flap design over the 88-percent flap design. A comparison of the corresponding lift and drag performance predictions for the 92- and 96-percent and the 92- and 98-percent flap designs are presented in figures 24 and 25, respectively. Both comparisons show a negligible increase in maximum C_ℓ at 35° deflection and an approximate 0.2 increase at 40° deflection. The drag polars, however, show a variation in the increase in drag coefficient of 25 percent at low C_ℓ values to approximately 5 percent near maximum C_ℓ. A turbulent boundary-layer analysis of the flap pressure distributions of each flap design at 35° deflection indicated that approximately 31, 21, and 17 percent of the upper surface was separated for the 88-, 96-, and 98-percent designs as compared to 14 percent for the 92-percent design. A comparison of the geometries and of the flap pressure distributions for the four designs at an angle of attack of 0° and a flap deflection of 35° is presented in figure 26. The comparison of the flap geometries shows a forward movement of the maximum thickness location as the cutoff point is moved further aft, which results in higher overall velocities in the slot region and reduced flap separation. The 92-percent flap is proportionally thicker aft of the maximum thickness point compared to the others, which reduces the upper surface pressure recovery and further decreases flap separation.

The results of the analysis of the performance predictions for the four flap designs indicate a slight advantage of the 92-percent design over the other three. The reduction in flap thickness that occurred by moving the cutoff location from 88 to 92 percent results in a slight structural disadvantage for the flap element but not for its corresponding main element which is thicker in the trailing-edge region. The 92-percent design is, therefore, recommended for application with the HSNLF(1)-0213 airfoil.

The next phase of the design effort was the design of a double-slotted flap with the same 28-percent nested chord length. The vane (forward flap element) had to be concealed in the cove region of the main element which meant that its geometry was completely arbitrary. The design of the aft flap had the same type of constraints as that for the single-slotted flap design. It was decided to design the vane-flap combination so that the vane remained in a fixed position relative to the aft flap element as the flap combination deflects. The simplest type of actuation system is a fixed external-hinge mechanism. The 88-percent single-slotted flap was selected as the starting geometry. After many hours of trial-and-error vane and flap contouring, the geometries presented in figure 27 were finalized. The vane element has a chord of approximately 8 percent and the aft flap element a chord of 20.5 percent. The upper surface cutoff point for the main element had to be moved forward to 87 percent to allow for the passage of the vane element through the cove opening for flap deflections greater than 20°. At a deflection of 20°, the lower surface of the vane forms a smooth contour between the upper- and lower-surface cutoff points on the main element. For flap deflections greater than 25°, the lower-surface trailing-edge deflector can be deflected upward into the cove approximately 15° to provide for a smoother cove region which should improve the acceleration of the flow through the slot and the pressure recovery on the upper surface of the vane and aft-flap elements.

The primary advantage of the double-slotted flap over the single-slotted flap is that the second slot allows for additional energization of the flap boundary layer which should delay separation and increase flap effectiveness. In other words, the vane performs the same function for the aft-flap as a leading-edge device would for the main element. A sample predicted C_p distribution for the double-slotted flap at 55° deflection is presented in figure 28. An analysis of the predicted performance data showed a very small increase in the load on the aft-flap element with an increase in deflection greater than 35°. The load on the vane element, on the other hand, increased substantially for deflections greater than 25° and reached unrealistic suction C_p values of -11 at 60° flap deflection. It is doubtful that the flow on the vane will remain attached at deflections greater than approximately 55°. A prediction of the maximum C_ℓ based on output from the MCARF computer code for the double-slotted flap through a range of deflections from 20° to 65° and for the single-slotted flap at deflections of 35° and 40° is presented in figure 29. Both the double-slotted flap at 55° deflection and the single-slotted flap at 40° deflection have the same maximum C_ℓ of approximately 3.7. An analysis of the turbulent boundary layer for the double- and single-slotted flaps at this equivalent condition showed no separation on the vane and aft-flap of the double-slotted flap and approximately 30-percent upper-surface separation for the single-slotted flap. This indicates that the double-slotted flap is a much more effective flap than the single-slotted flap and should be used for applications requiring relatively high maximum wing lift. Another factor which should be considered before selecting the double- over the single-slotted flap is that the double-slotted flap will be heavier and more difficult to actuate than the single-slotted flap.

The effects of Reynolds number on the maximum C_ℓ of the double-slotted flap at 55° deflection and the single-slotted flap at 40° deflection are presented in figure 30. The maximum C_ℓ values presented were based on separation of the leading-edge laminar boundary layer on the main element and do not include corrections for the effects of trailing-edge flap separation. As shown in figure 30, the Reynolds number effect on both flap designs is very large with a substantial loss in maximum C_ℓ occurring at Reynolds number less than 4 million. This type of trend is common for NLF airfoil sections due to the relative sensitivity of the stability and separation of the leading-edge laminar boundary layer to a reduction in Reynolds number. This trend was also noted during the NACA tests of a 64_1A212 airfoil equipped with a leading-edge slat and a double-slotted flap as reported in reference 15. A summary of the maximum C_ℓ values obtained as a function of Reynolds number for this particular airfoil is presented in figure 31 and show trends similar to those noted for the HSNLF(1)-0213 airfoil.

CONCLUDING REMARKS

The theoretical methods available for the design and analysis of multi-component airfoils are readily available and are generally easy to use. The linearized singularity-type methods do not model the flow as accurately as the nonlinear finite-difference-type methods, but they are less costly to execute and are better suited to preliminary design and analysis tasks. Most of the currently available linearized methods do not contain separation models, which prevents reliable maximum lift predictions for airfoils and flaps with trailing-edge separation. Although several separation models are available, they cannot be used until reliable methods are developed for the prediction of the separation point for both turbulent and confluent boundary layers. The development of these methods will require the acquisition of detailed experimental data on separating boundary layers which is now possible due to the advances in the non-intrusive laser velocimetry instrumentation.

The recently completed task to design a flap system for the HSNLF airfoil demonstrated the usefulness of these theoretical methods. The selection of either the single- or double-slotted flap is dependent on the particular aircraft performance requirements. The double-slotted flap is better suited to aircraft which require low approach speeds or have relatively high wing loadings. The single-slotted flap, which will produce less maximum C_ℓ, is better suited to aircraft with low wing loadings and higher approach speeds. The theoretical analysis methods cannot reliably predict the exact maximum C_ℓ; therefore, experimental tests need to be conducted prior to the selection of either flap system. High-lift airfoil models are considerably more complex and expensive to build than conventional airfoils and should only be tested in facilities with adequate tunnel sidewall boundary-layer treatment in order to obtain the correct performance characteristics, especially near stall.

REFERENCES

1. Somers, Dan M.: Design and Experimental Results for a Flapped Natural-Laminar-Flow Airfoil for General Aviation Applications. NASA TP-1865, 1981.

2. Somers, Dan M.: Design and Experimental Results for a Natural-Laminar-Flow Airfoil for General Aviation Applications. NASA TP-1861, 1981.

3. McGhee, Robert J.; Viken, Jeffrey K.; Pfenninger, Werner; Beasley William D.; and Harvey, William D.: Experimental Results for a Flapped Natural-Laminar-Flow Airfoil with High Lift/Drag Ratio. NASA TM-85788, 1984.

4. Abbott, Ira H.; and Von Doenhoff, Albert E.: Theory of Wing Sections. Dover Publications, New York, 1959.

5. Preliminary Design Department of the Boeing Commercial Airplane Company: Assessment of Variable Camber for Application to Transport Aircraft. NASA CR-158930, 1980.

6. Stevens, W. A.; Goradia, S. H.; and Braden, J. A.: Mathematical Model for Two-Dimensional Multi-Component Airfoils in Viscous Flow. NASA CR-1843, 1971.

7. Brune, G. W.; and Manke, J. W.: An Improved Version of the NASA-Lockheed Multielement Airfoil Analysis Computer Program. NASA CR-145323, 1978.

8. Cohen, Clarence B.; and Reshotko, Eli: The Compressible Laminar Boundary Layer with Heat Transfer and Arbitrary Pressure Gradient. NACA TR-1294, 1956.

9. Stewartson, K.: Correlated Incompressible and Compressible Boundary Layers. Proc. Roy. Soc. (London), Ser. A, Vol. 200, No. 1060, Dec. 22, 1949, pp. 84-100.

10. Schlichting, H.; and Ulrich A.: Zur Berechnung des Umschlages Laminar-Turbulent. Jahrbuch d. dt. Luftfahrtforschung, No. 1, 1942, pp. 8-35.

11. Granville, Paul S.: The Calculation of the Viscous Drag of Bodies of Revolution. Rep. 849, David Taylor Model Basin, July 1953.

12. Goradia, Suresh H.; and Lyman, Victor: Laminar Stall Prediction and Estimation of Maximum Lift Coefficient. Journal of Aircraft, Vol. 11, No. 9, Sept. 1974, pp. 528-536.

13. Omar, Z.; Zierten, T.; Hahn, M.; Szpiro, E.; and Mahal, A.: Two-Dimensional Wind-Tunnel Tests of a NASA Supercritical Airfoil with Various High-Lift Systems. Volume II - Test Data. NASA CR-2215, 1977.

14. McGhee, Robert J.; Beasley, William D.; and Foster, Jean M.: Recent Modifications and Calibration of the Langley Low-Turbulence Pressure Tunnel. NASA TP-2328, 1984.

15. Quinn, John H., Jr.: Tests of the NACA 64_1-A212 Airfoil Section with a Slat, A Double Slotted Flap, and Boundary Layer Control by Suction. NACA TN 1293, 1947.

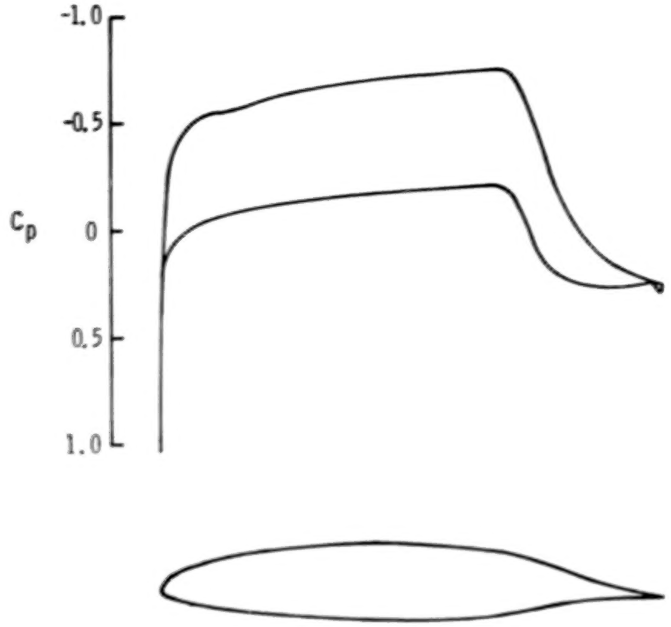

Figure 1.- Calculated pressure distribution for NLF(1)-0414F airfoil at design conditions. ($C_\ell = 0.43$, $M = 0.40$, $R = 10 \times 10^6$)

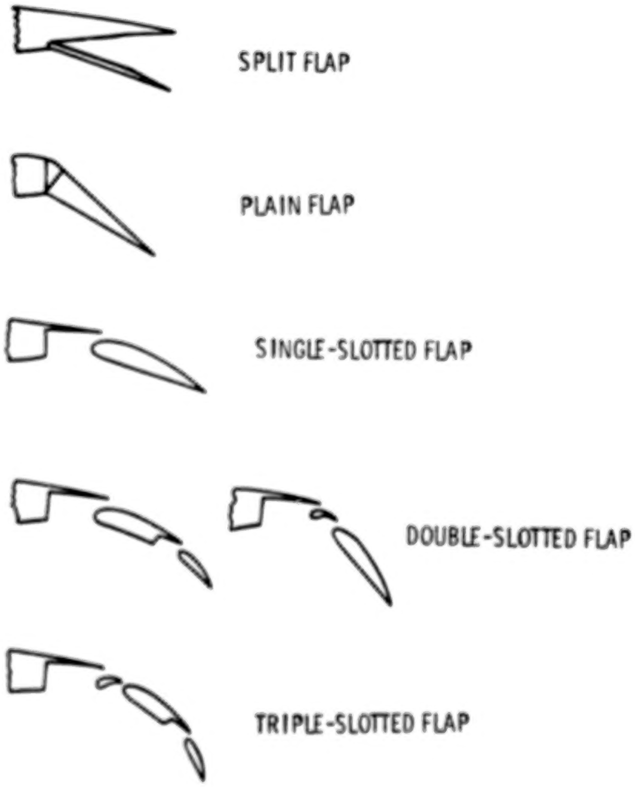
SPLIT FLAP
PLAIN FLAP
SINGLE-SLOTTED FLAP
DOUBLE-SLOTTED FLAP
TRIPLE-SLOTTED FLAP

Figure 2.- Mechanical high-lift trailing-edge devices.

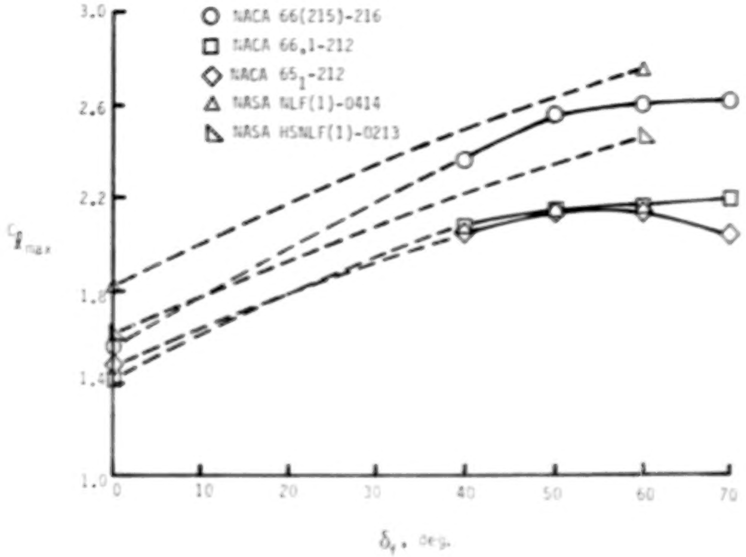

Figure 3.- Maximum lift coefficients for several NACA and NASA airfoils equipped with 0.20-chord split flaps. ($R = 6 \times 10^6$)

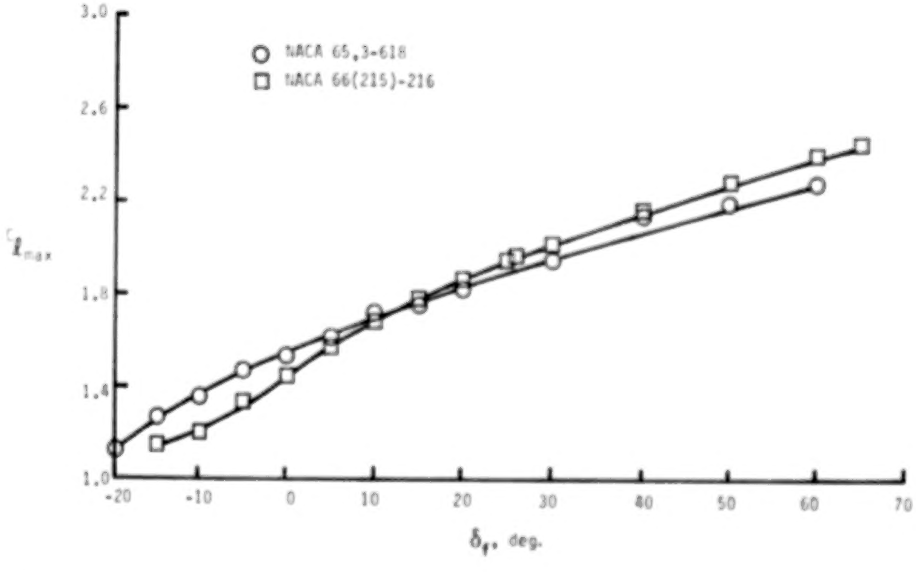

Figure 4.- Maximum lift coefficients for two NACA airfoils equipped with 0.20-chord plain flaps. ($R = 6 \times 10^6$)

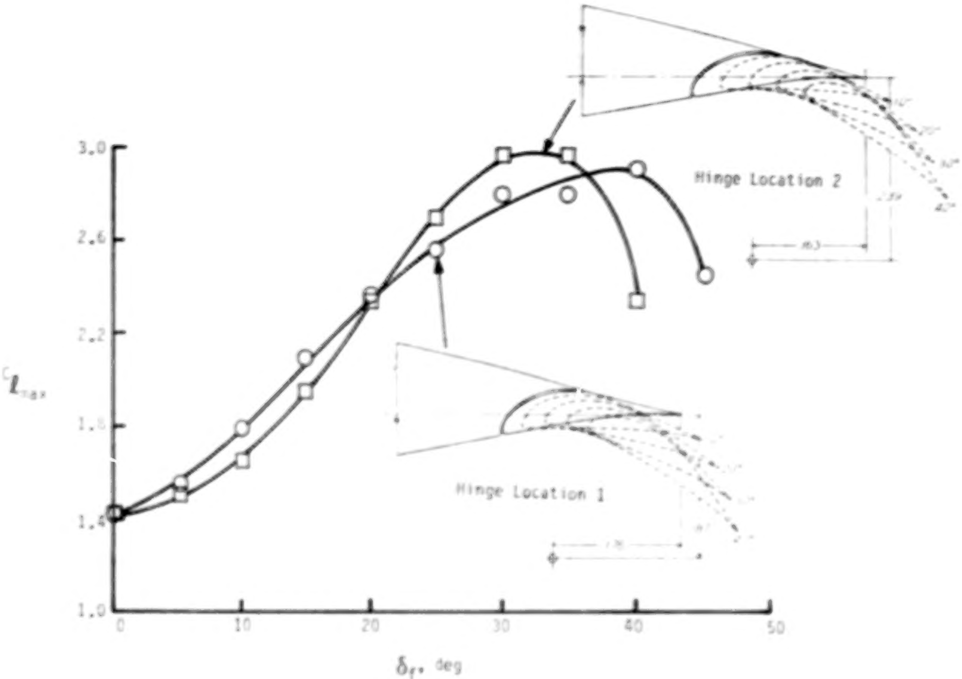

Figure 5.- Maximum lift coefficients for the NACA 63_4-420 airfoil equipped with 0.25-chord single-slotted flap. ($R = 6 \times 10^6$)

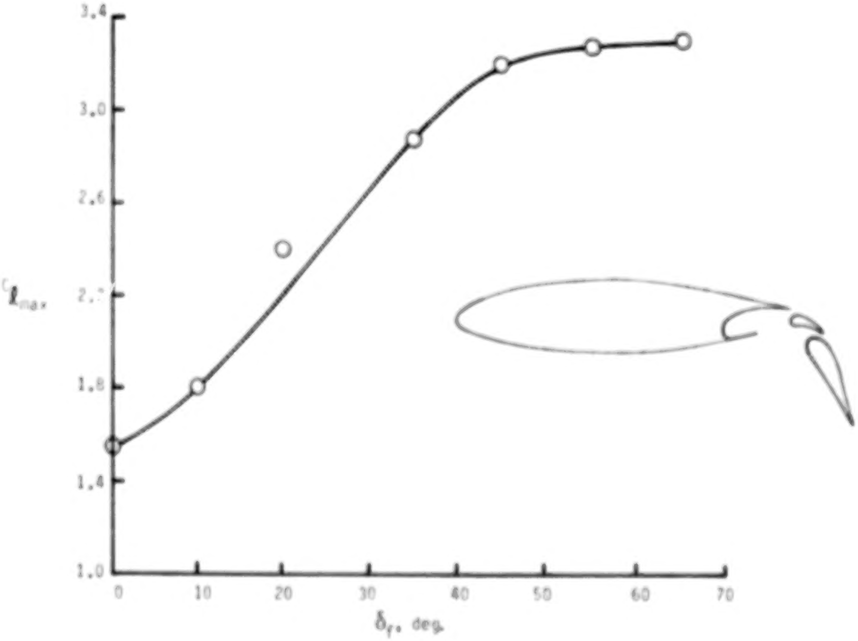

Figure 6.- Maximum lift coefficients for NACA 65_3-118 airfoil equipped with double-slotted flap. ($R = 6 \times 10^6$)

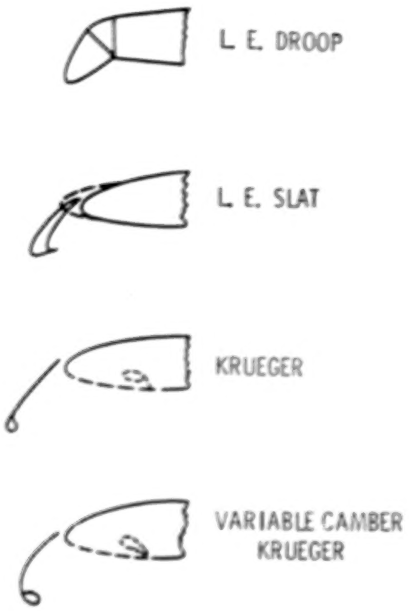
L. E. DROOP
L. E. SLAT
KRUEGER
VARIABLE CAMBER KRUEGER

Figure 7.- Mechanical high-lift leading-edge devices.

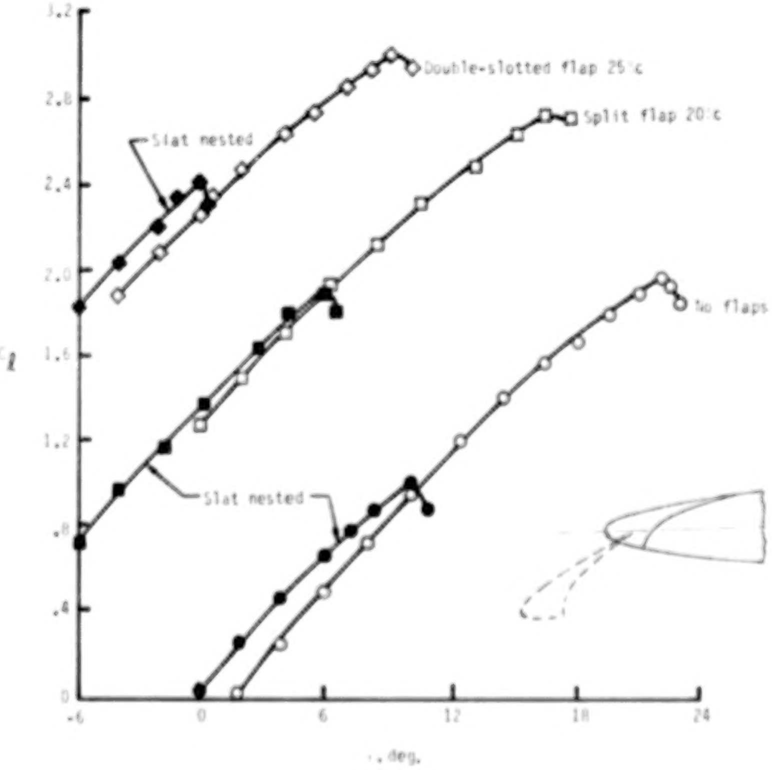

Figure 8.- Effect of leading-edge slat on performance of NACA 64A010 airfoil with and without flaps. ($R = 6 \times 10^6$)

ORIGINAL PAGE IS
OF POOR QUALITY

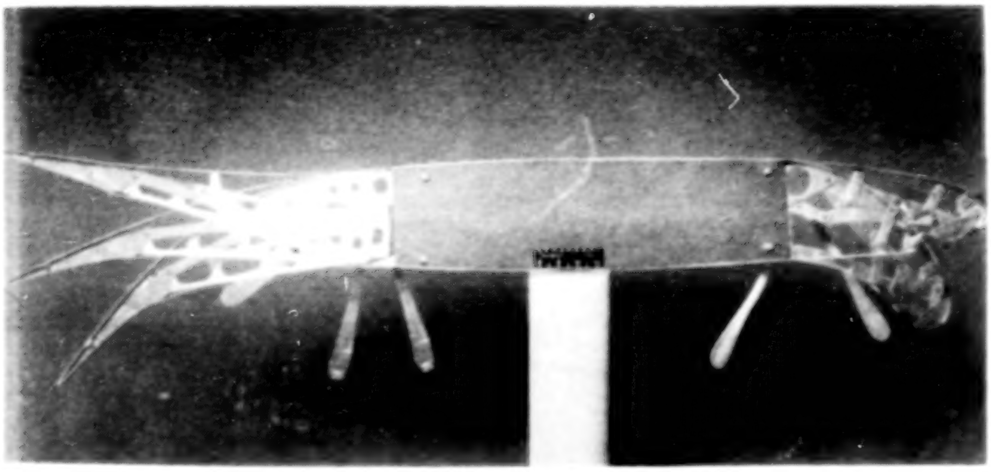

Figure 9.- Photograph of variable-camber high-lift mechanism.

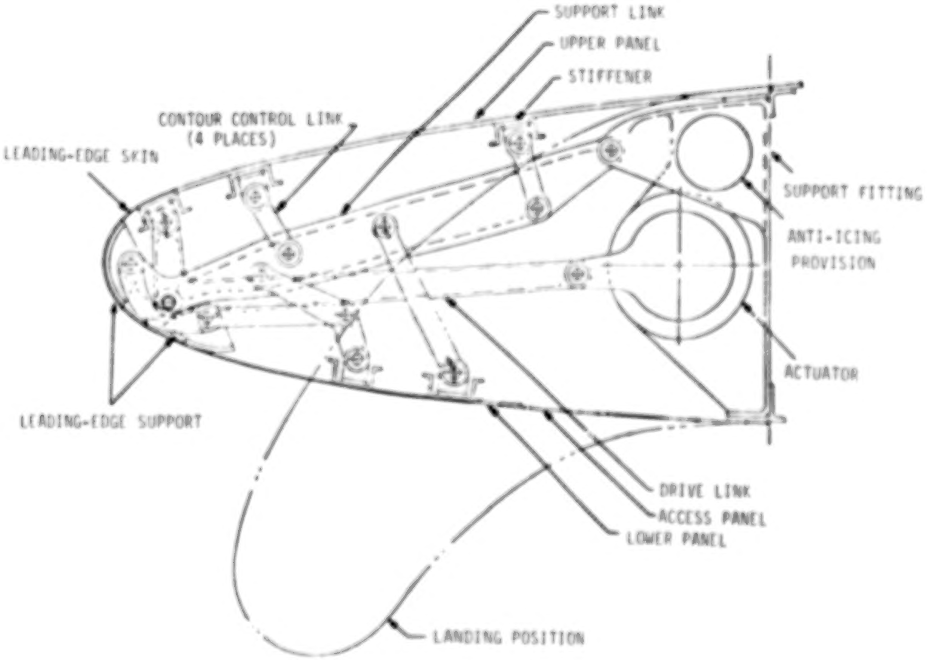
SUPPORT LINK
UPPER PANEL
STIFFENER
CONTOUR CONTROL LINK
(4 PLACES)
LEADING-EDGE SKIN
SUPPORT FITTING
ANTI-ICING
PROVISION
ACTUATOR
LEADING-EDGE SUPPORT
DRIVE LINK
ACCESS PANEL
LOWER PANEL
LANDING POSITION

Figure 10.- Sketch of variable-camber leading-edge device.

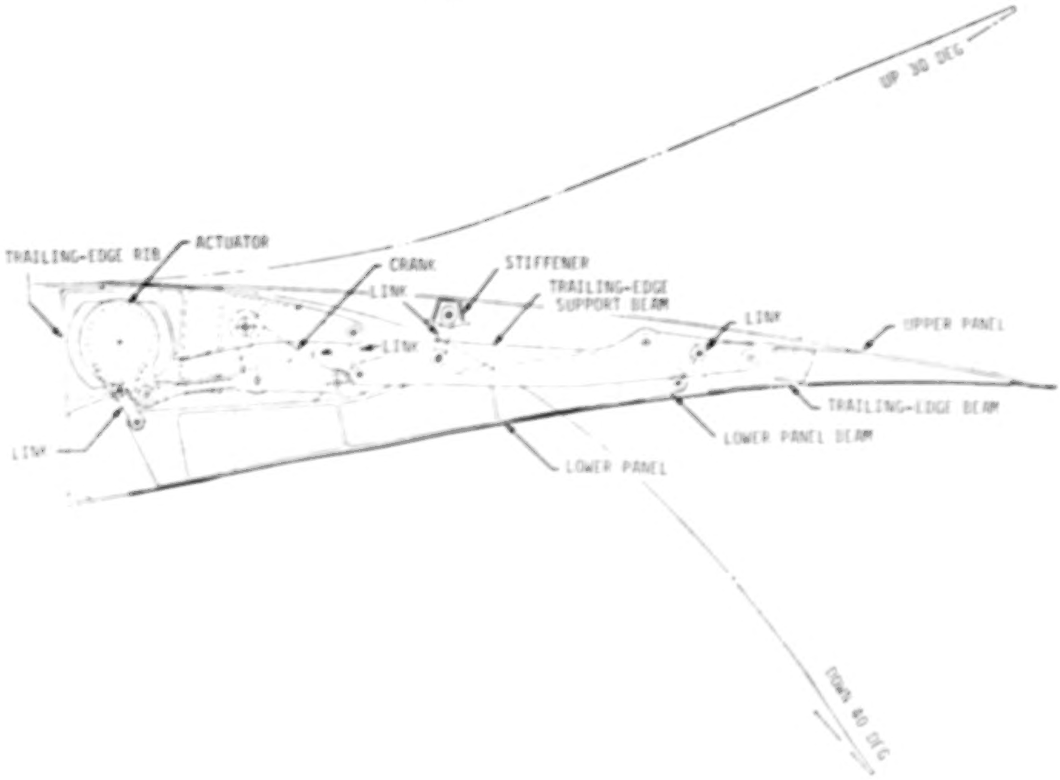
UP 30 DEG
TRAILING-EDGE RIB
ACTUATOR
CRANK
STIFFENER
LINK
TRAILING-EDGE SUPPORT BEAM
LINK
LINK
UPPER PANEL
LINK
TRAILING-EDGE BEAM
LOWER PANEL BEAM
LOWER PANEL
DOWN 40 DEG

Figure 11.- Sketch of variable-camber trailing-edge device.

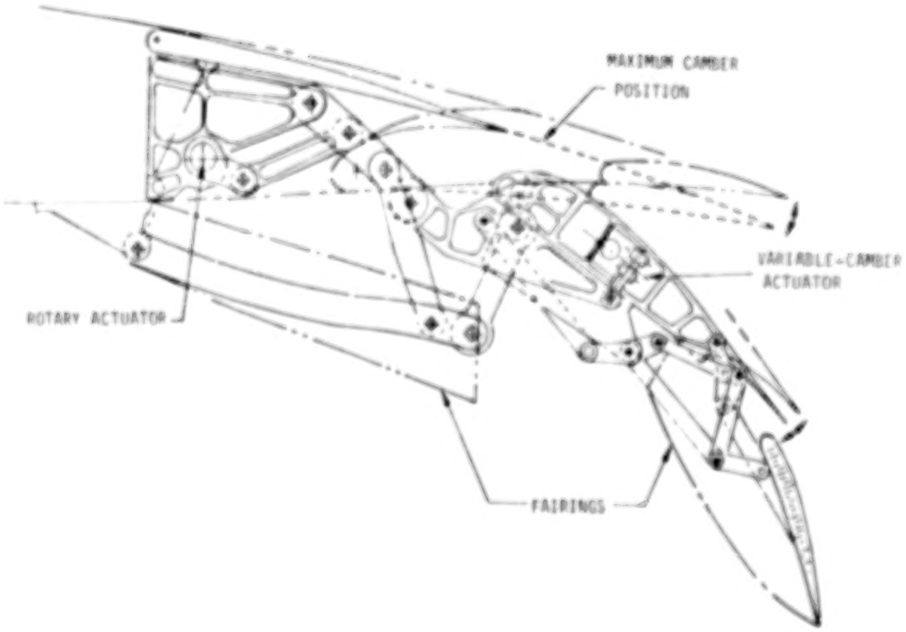
MAXIMUM CAMBER POSITION
VARIABLE-CAMBER ACTUATOR
ROTARY ACTUATOR
FAIRINGS

Figure 12.- Sketch of double-slotted, variable-camber trailing-edge device.

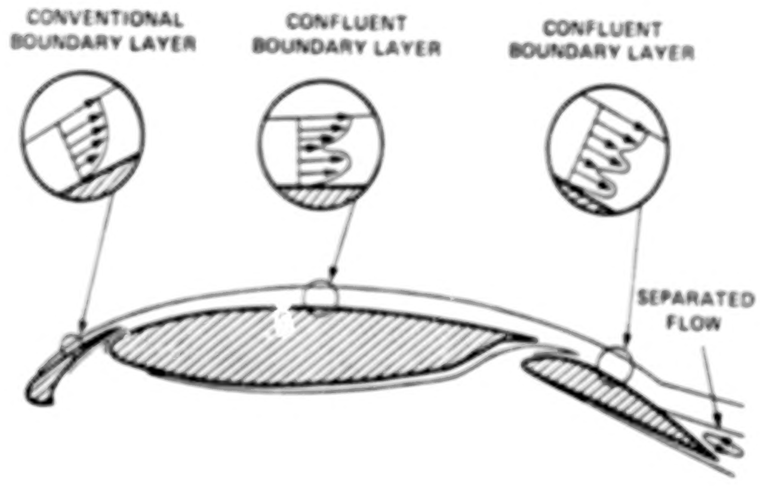

FLOW ABOUT MULTI-COMPONENT AIRFOIL

CONVENTIONAL BOUNDARY LAYER
CONFLUENT BOUNDARY LAYER
CONFLUENT BOUNDARY LAYER
SEPARATED FLOW

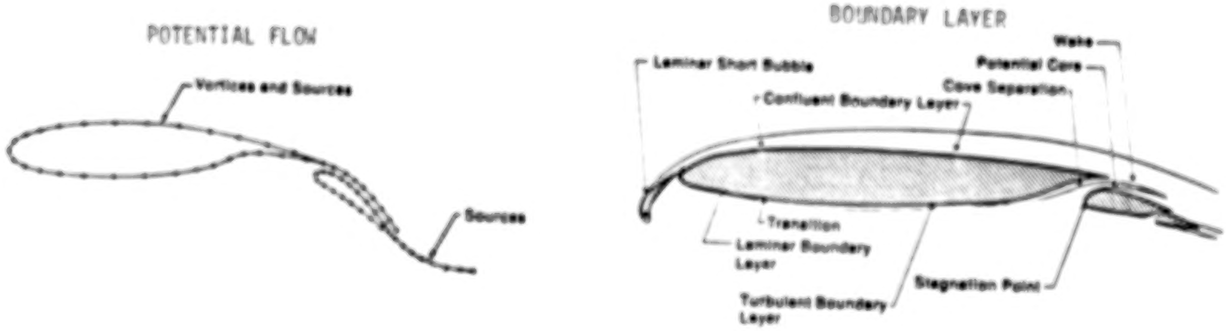

LINEAR THEORY FLOW MODEL

POTENTIAL FLOW
Vortices and Sources
Sources
BOUNDARY LAYER
Wake
Laminar Short Bubble
Potential Core
Cove Separation
Confluent Boundary Layer
Transition
Laminar Boundary Layer
Stagnation Point
Turbulent Boundary Layer

Figure 13.- Flow field and theoretical model for multi-component airfoils.

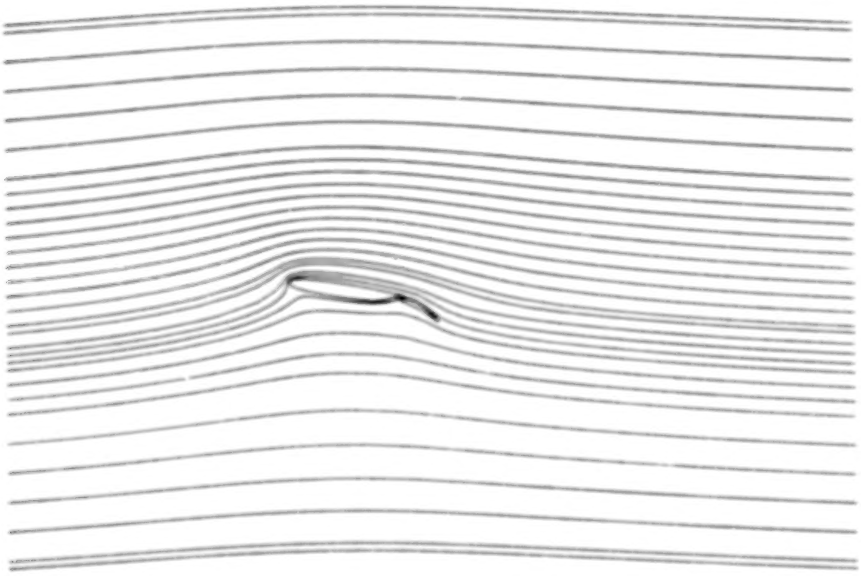

(a) Without floor and ceiling.

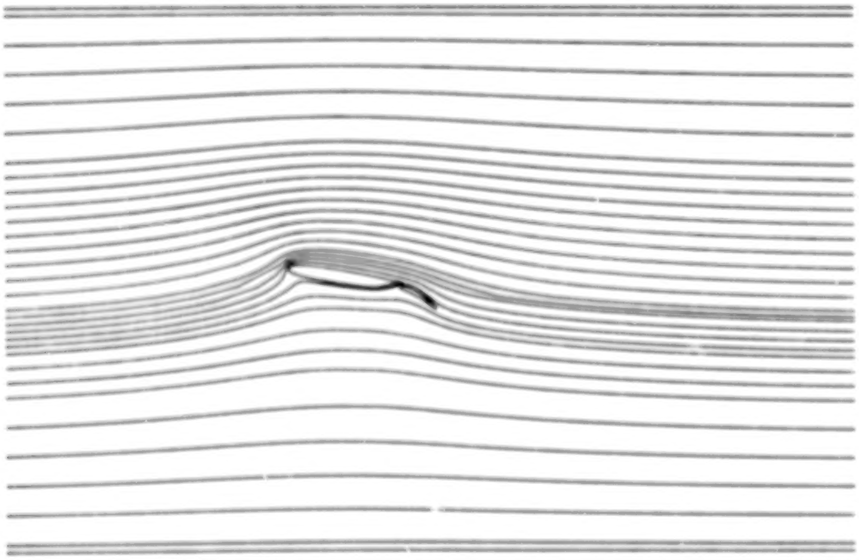

(b) With floor and ceiling.

Figure 14.- Streamline trace for typical single-slotted flap with and without floor and ceiling simulation.

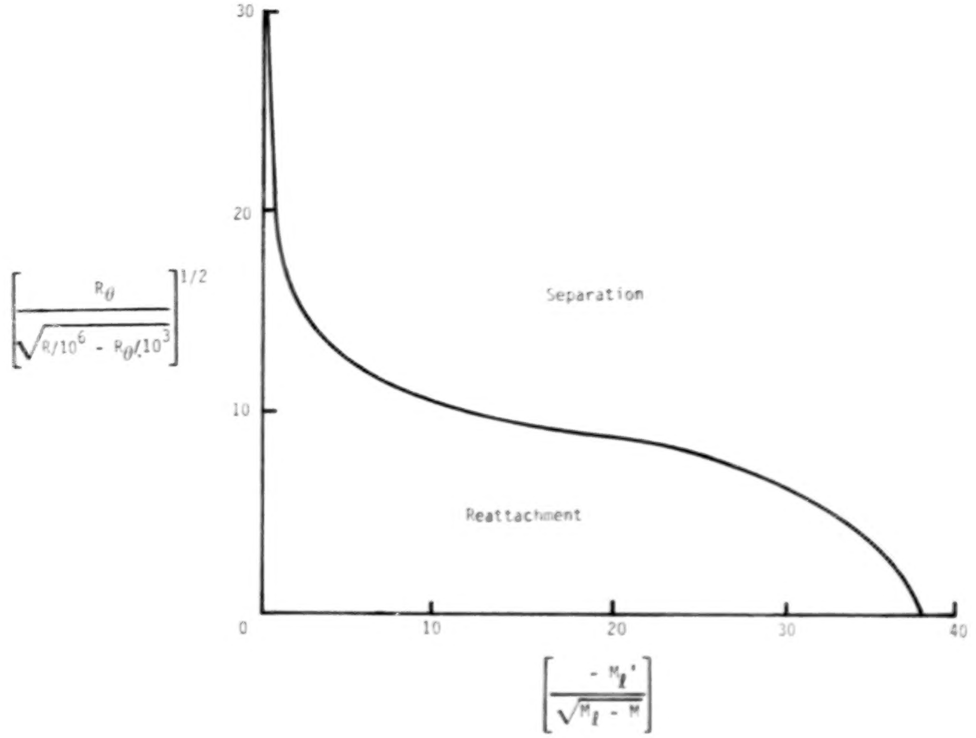

Figure 15.- Laminar boundary layer separation-reattachment curve.

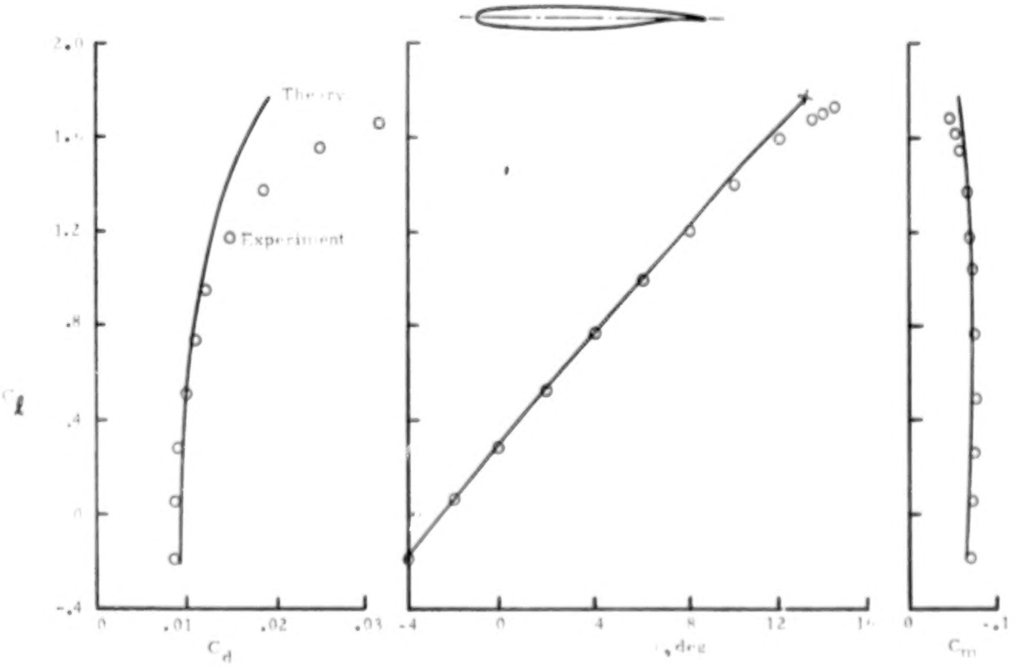

Figure 16.- Theory-experiment comparison for 9.3% thick supercritical airfoil.

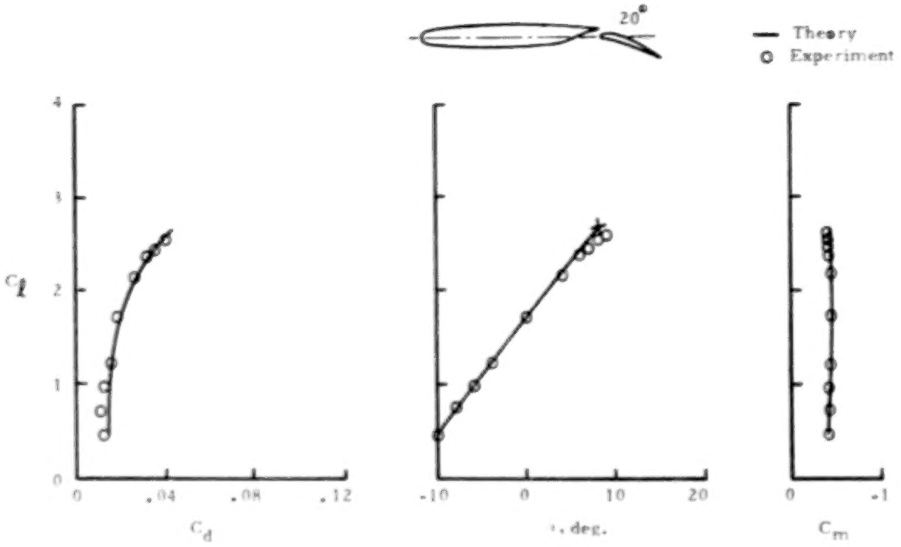

Figure 17.- Theory-experiment comparison for 9.3% thick supercritical airfoil equipped with a single-slotted flap at 20° deflection.

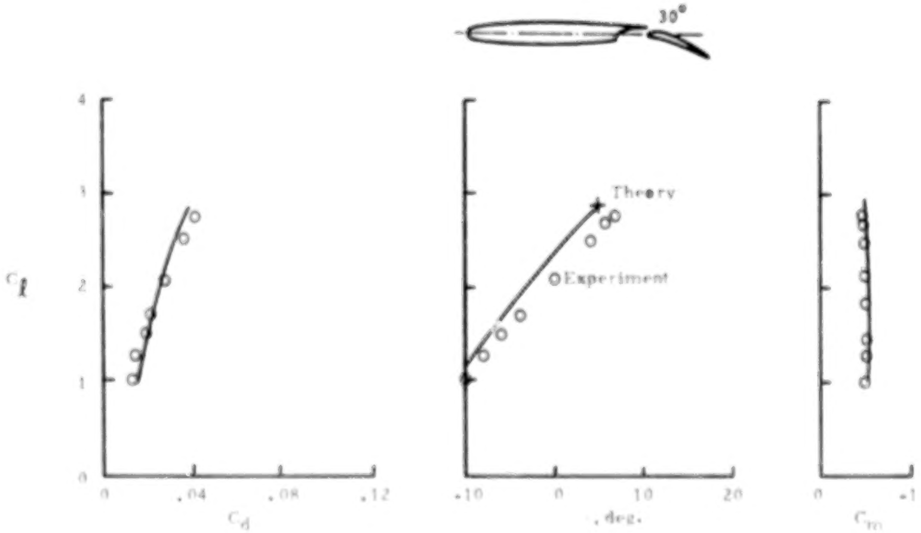

Figure 18.- Theory-experiment comparison for 9.3% thick supercritical airfoil equipped with a single-slotted flap at 30° deflection.

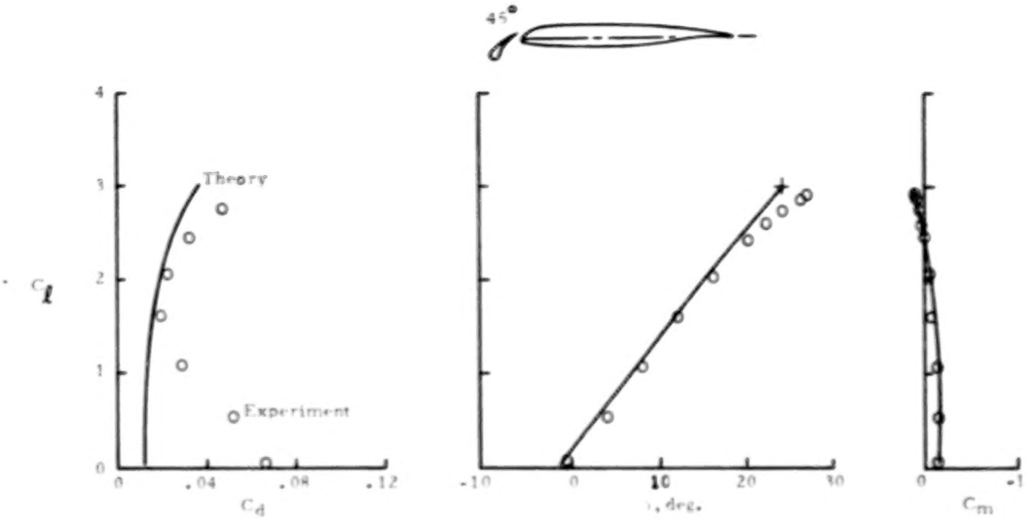

Figure 19.- Theory-experiment comparison for 9.3% thick supercritical airfoil equipped with a leading-edge Krueger.

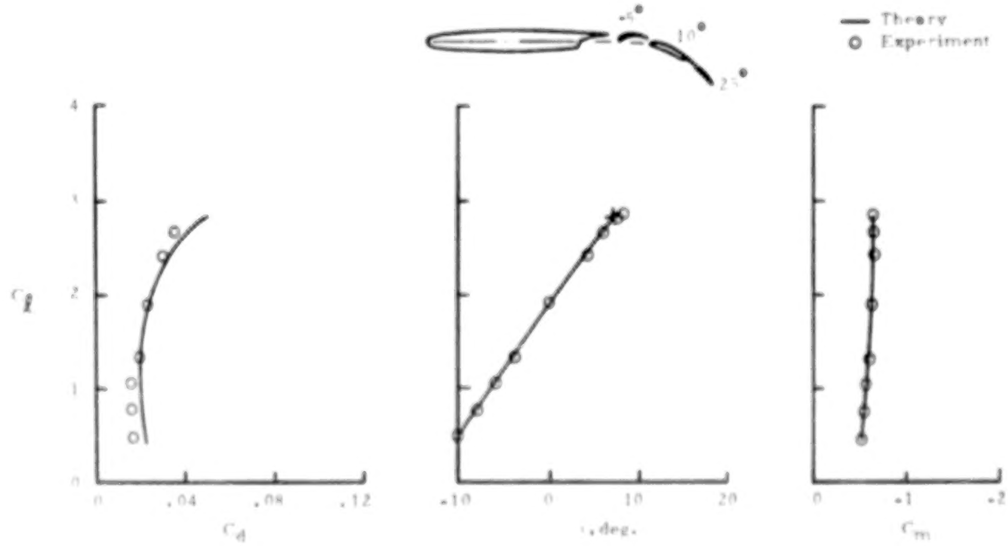

Figure 20.- Theory-experiment comparison for 9.3% thick supercritical airfoil equipped with a triple-slotted flap.

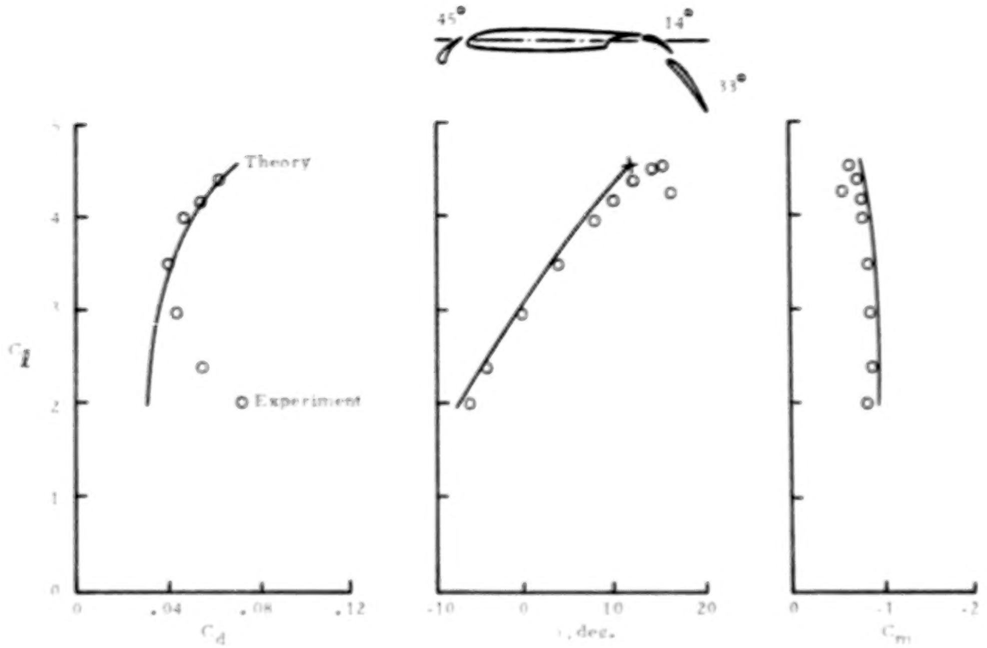

Figure 21.- Theory-experiment comparison for 9.3% thick supercritical airfoil equipped with a leading-edge Krueger and a double-slotted trailing-edge flap.

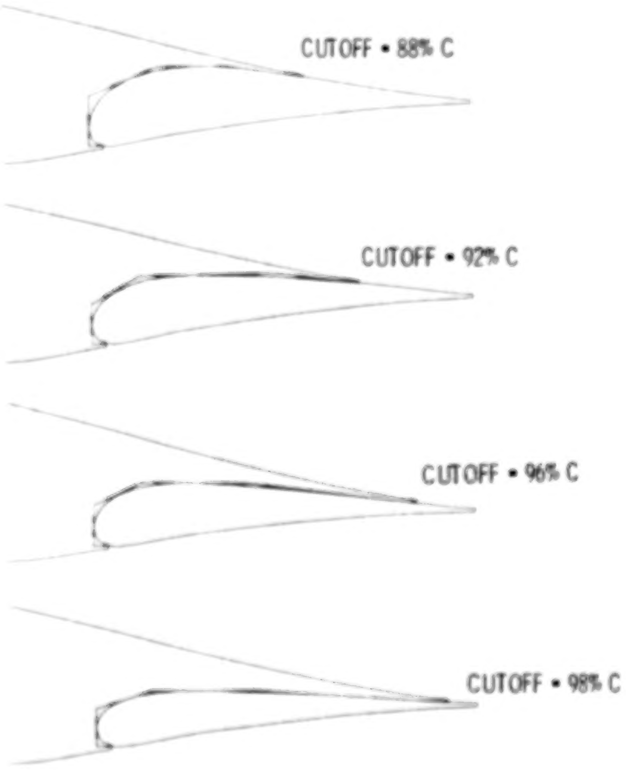
CUTOFF = 88% C
CUTOFF = 92% C
CUTOFF = 96% C
CUTOFF = 98% C

Figure 22.- Single-slotted flap designs for HSNLF(1)-0213 airfoil.

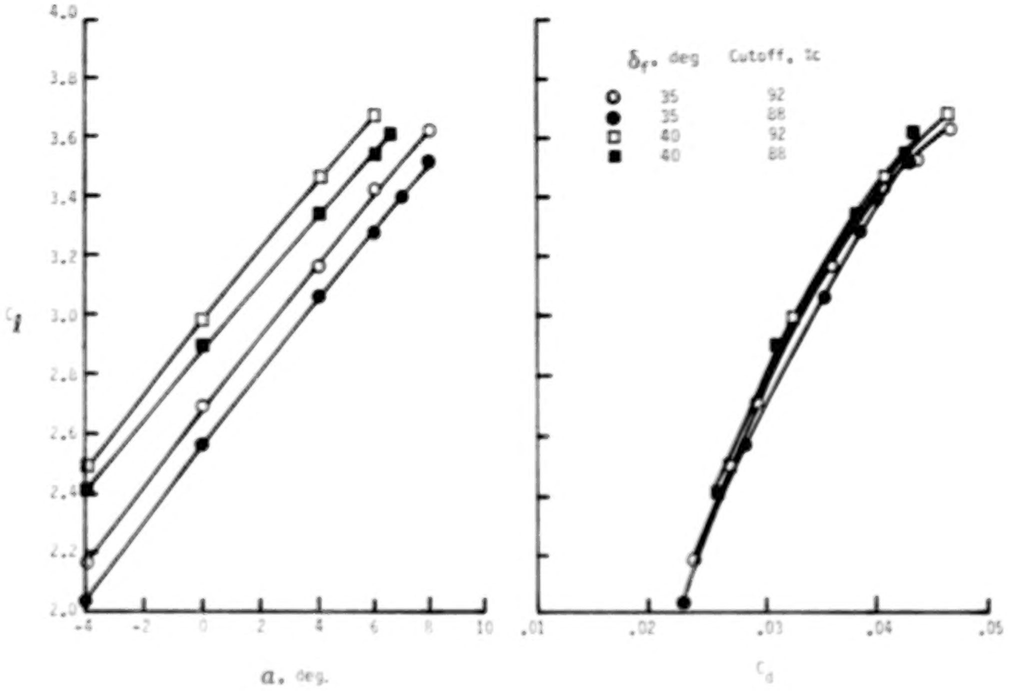

Figure 23.- Effect of 88- and 92-percent chord cutoff on lift and drag coefficient for HSNLF(1)-0213 airfoil. (R = 4×10^6)

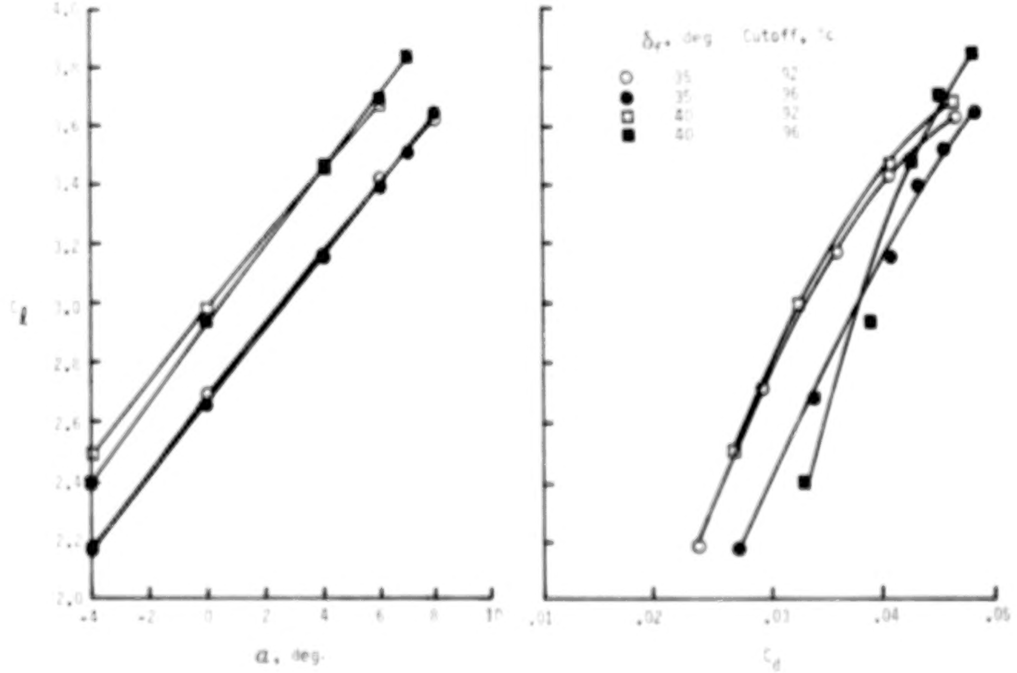

Figure 24.- Effect of 92- and 96-percent chord cutoff on lift and drag coefficient for HSNLF(1)-0213 airfoil. (R = 4×10^6)

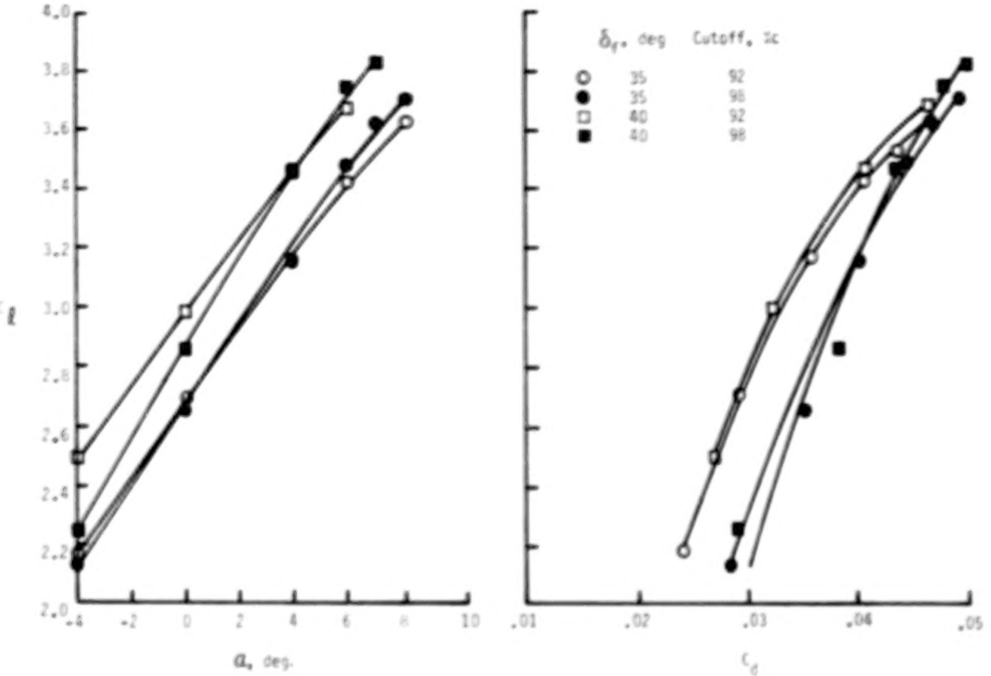

Figure 25.- Effect of 92- and 98-percent chord cutoff on lift and drag coefficient for HSNLF(1)-0213 airfoil. ($R = 4 \times 10^6$)

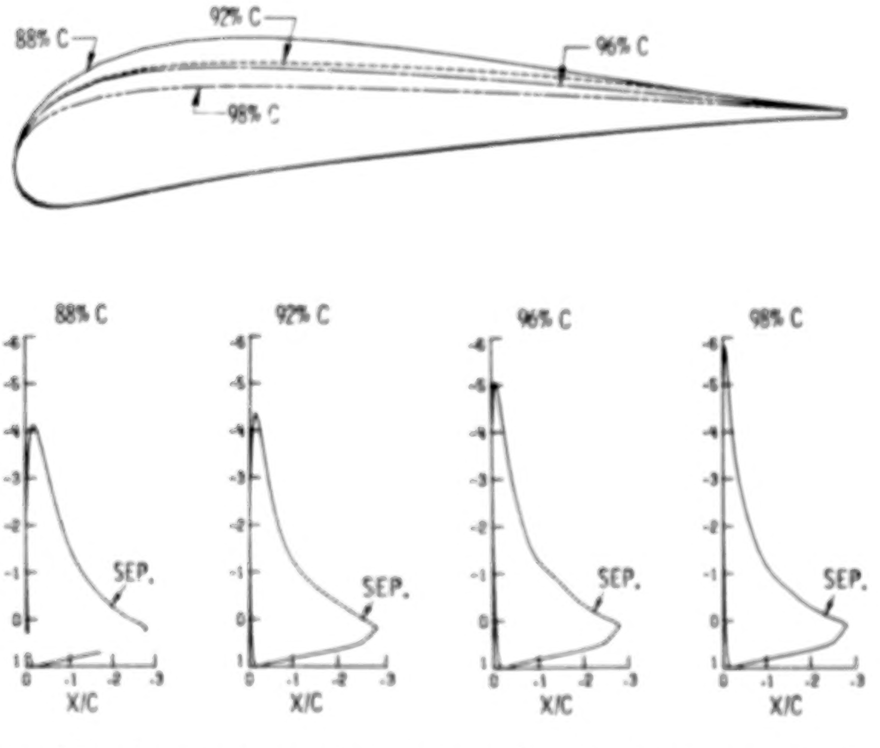

Figure 26.- Geometries and pressure distributions for single-slotted flap designs for HSNLF(1)-0213 airfoil. ($\alpha = 0°$, $R = 4 \times 10^6$, $\delta_f = 35°$)

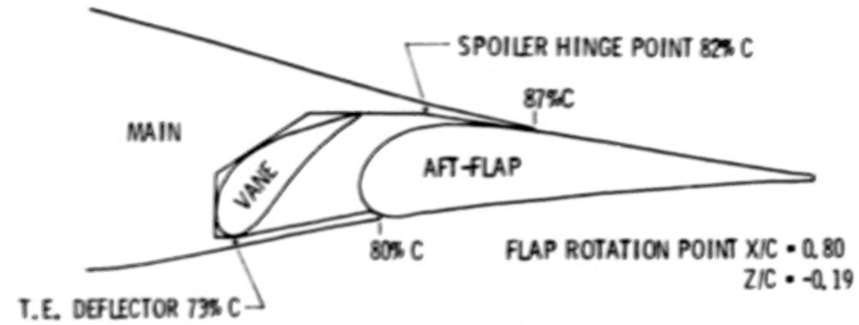
SPOILER HINGE POINT 82% C
87% C
MAIN
VANE
AFT-FLAP
80% C
FLAP ROTATION POINT X/C = 0.80
Z/C = -0.19
T.E. DEFLECTOR 73% C

(a) DOUBLE-SLOTTED FLAP

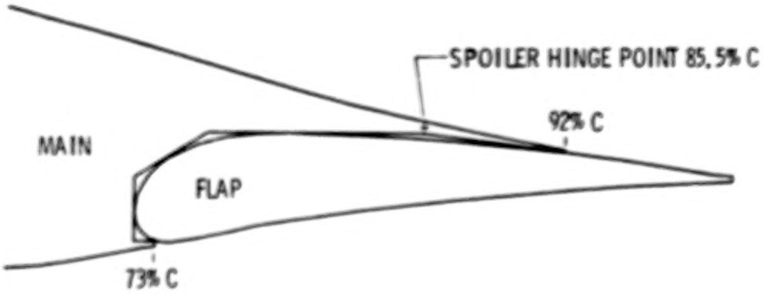
SPOILER HINGE POINT 85.5% C
92% C
MAIN
FLAP
73% C

(b) SINGLE-SLOTTED FLAP

Figure 27.- Details of double- and single-slotted flap designs for HSNLF(1)-0213 airfoil.

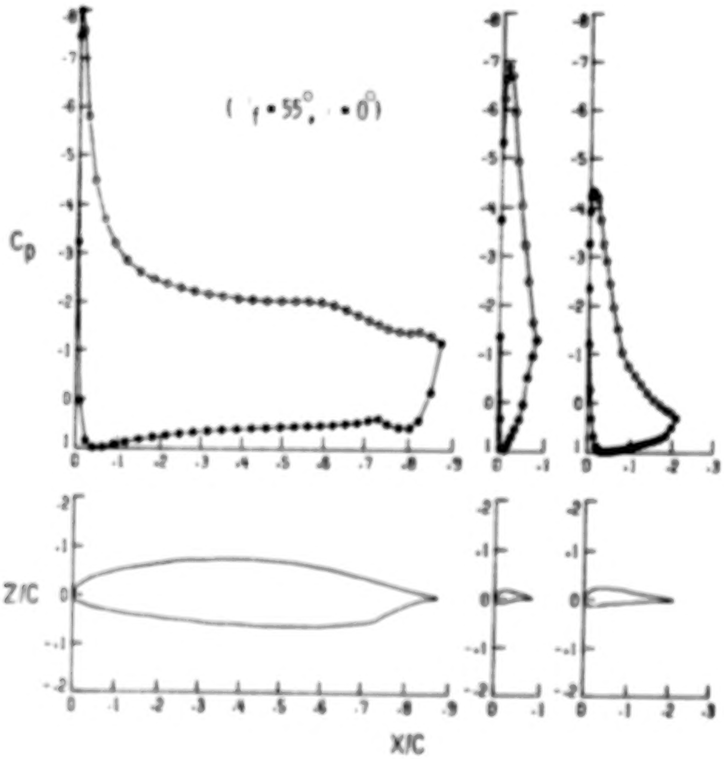

Figure 28.- Sample pressure distribution for HSNLF(1)-0213 airfoil equipped with double-slotted flap. ($R = 4 \times 10^6$)

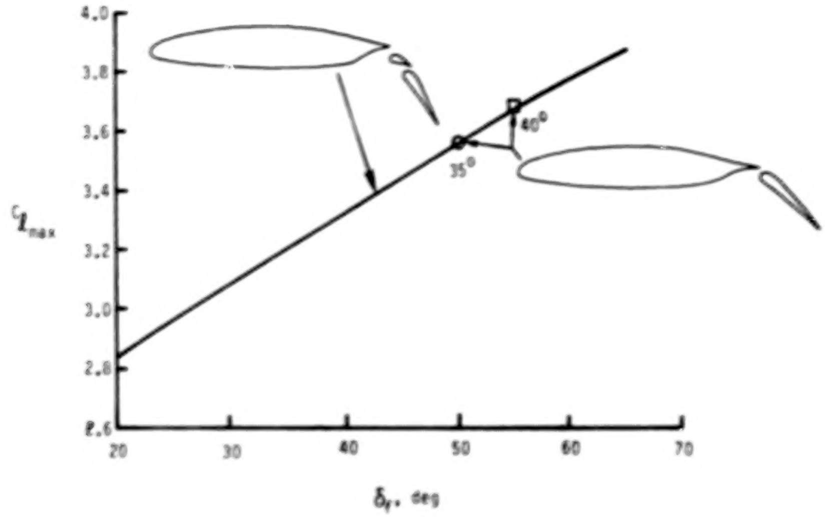

Figure 29.- Effect of flap deflection on maximum lift coefficient for single- and double-slotted flaps. (R = 4 × 10^6)

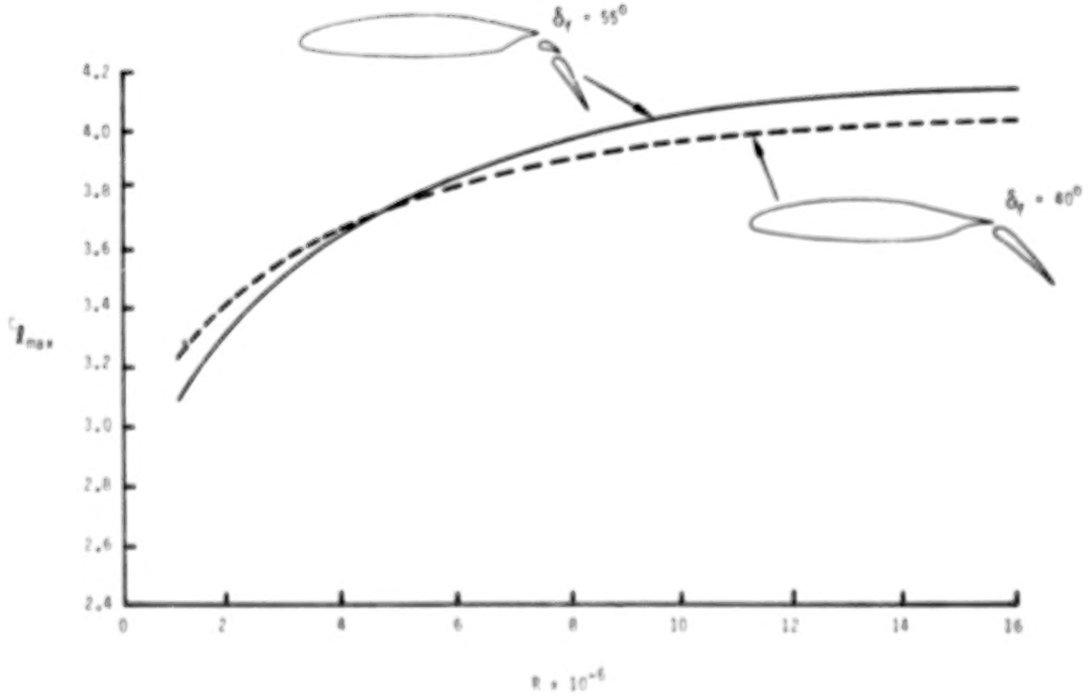

Figure 30.- Effect of Reynolds number on maximum lift coefficient for 55° double-slotted flap and 40° single-slotted flap.

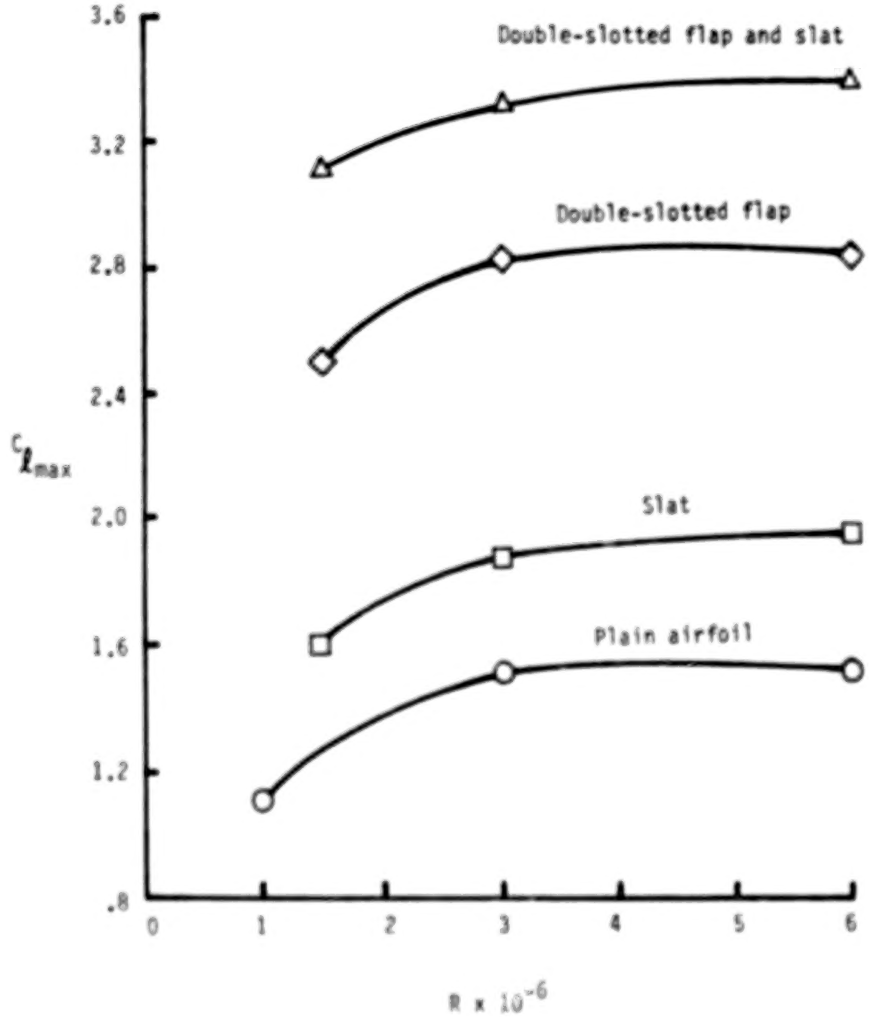

Figure 31.- Effect of slat on maximum lift coefficients for NACA 64_1A212 airfoil with and without double-slotted flap.

53-02 18

N88-23740

COMPUTATIONAL WING DESIGN STUDIES RELATING TO NATURAL LAMINAR FLOW

Edgar G. Waggoner
NASA Langley Research Center
Hampton, Virginia 23665

SUMMARY

Two research studies are described which directly relate to the application of natural laminar flow (NLF) technology to transonic transport-type wing planforms. Each involved using state-of-the-art computational methods to design three-dimensional wing contours which generate significant runs of favorable pressure gradients. The first study supported the Variable Sweep Transition Flight Experiment and involves design of a full-span glove which extends from the leading edge to the spoiler hinge line on the upper surface of an F-14 outer wing panel. Boundary-layer and static-pressure data will be measured on this design during the supporting wind-tunnel and flight tests. These data will then be analyzed and used to infer the relationship between crossflow and Tollmien-Schlichting disturbances on laminar boundary-layer transition. A wing was designed computationally for a corporate transport aircraft in the second study. The resulting wing design generated favorable pressure gradients from the leading edge aft to the mid-chord on both upper and lower surfaces at the cruise design point. Detailed descriptions of the computational design approach are presented along with the various constraints imposed on each of the designs. Wing surface pressure distributions, which support the design objectives and were derived from transonic three-dimensional analysis codes, are also presented. Current status of each of the research studies is included in the summary.

INTRODUCTION

Computational fluid dynamics (CFD) is playing an increasingly important role in the aircraft design process. All major airframers are using CFD as a complement to wind-tunnel and flight testing. This can increase the efficiency of test facility utilization as well as significantly reduce the risks associated with a development program. Increases in computer speed and storage capabilities, in conjunction with developments in code solution algorithms and grid generation, have fostered development of powerful computer codes. Codes have been developed which can solve the complex transonic flow field around a multi-component aircraft configuration (refs. 1 and 2). In addition, these codes have proven to be robust and reliable, and they can be routinely relied upon in a preliminary design environment.

Two studies are described in this paper. The first is concerned with understanding the interaction of crossflow and Tollmien-Schlichting (TS) instabilities on laminar boundary-layer transition. The second study is an actual design of a natural laminar flow wing. Although each of these studies is concerned with various aspects of laminar flow, the theme of this discussion is the application of computational techniques in support of each of these programs.

Each study involved designing a wing or portion of a wing to generate a pressure distribution with certain characteristics. State-of-the-art computational techniques were used to accomplish the design tasks associated with each study. The designs will be experimentally verified through wind-tunnel testing at the NASA Langley Research Center.

A brief description of the various two- and three-dimensional computer codes is included in the following section. Subsequent sections describe each of the studies in some detail. Included are descriptions of study objectives and constraints which impacted the design. A rather detailed description of the design process is included, along with appropriate examples of results at key stages during the design. Current status of the

PRECEDING PAGE BLANK NOT FILMED

studies is discussed, and a summary of the salient observations made during the two studies is included in the conclusion.

COMPUTATIONAL METHODS USED IN THE STUDIES

Several computer codes have been used to analyze the various configuration models and designs which have been evaluated during the present studies. Three-dimensional analyses have utilized both a full potential code, which is coupled with a three-dimensional integral boundary-layer code (TAWFIVE) (ref. 1) and an extended small-disturbance analysis code (WBPPW) (ref. 2) which has been verified extensively at NASA Langley Research Center (refs. 3 and 4). Three-dimensional automated design capability was realized using a Lockheed Georgia modified version of the FLO-22NM code (ref. 5). The code has McFadden's design algorithm (ref. 6) and a quasi-Newton's method optimization procedure as an integral part of the code. The NYU airfoil code (ref. 7) and the two-dimensional option in the WBPPW code were used to provide the two-dimensional analyses. High-lift characteristics of airfoil designs were predicted with a subsonic panel code which includes an integral boundary-layer calculation (ref. 8).

WBPPW Analysis Code

The Wing-Body-Pod-Pylon-Winglet code, developed by Charles Boppe of Grumman Aerospace Corporation, is characterized by a unique grid-embedding technique which provides excellent flow-field resolution about various configuration components. The code solves for the flow field about a wing-fuselage configuration which can include engine pods or stores, wing pylons, and wingtip-mounted winglets at transonic speeds. Using finite-difference approximations, a modified small-disturbance potential-flow equation is iteratively solved in a system of multiple embedded grids. The modifications to the classical small-disturbance equation are in the form of extra terms, which, when added to the equation, provide more accurate resolution of shock waves with large sweep angles and a better approximation of the critical velocity where the full potential equation changes from elliptic to hyperbolic in type.

The computational space used in the method is filled with a relatively crude global grid system. This grid is stretched to planes corresponding to infinity in all directions. The global grid basically serves two purposes. It provides the proper representation of the effects of the configuration on the far-field and, conversely, the effects of the far-field conditions on the flow field near the configuration. In addition, the crude grid provides the channels of communication between the various embedded fine grids.

Fine grid regions around components of interest are embedded into the global continuous grid. The fine grids are distributed along the wing span and, if desired, may also encompass the fuselage, engine pods or stores, pylons, and/or a winglet. Within the fine grids, the resolution is much enhanced relative to the global grids. This allows far greater resolution in areas where flow-field gradients are large.

Viscous effects are approximated in the code by coupling a modified Bradshaw boundary-layer computation to the finite-difference potential-flow solution. The modified method provides a technique to extend a two-dimensional boundary-layer calculation to account for first-order sweep effects (ref. 9). The viscous effects are incorporated in the solution by adding the boundary-layer displacement slopes to the wing surface slopes. This modifies the wing surface to an equivalent "fluid" wing shape which is then analyzed by the potential flow code.

TAWFIVE Analysis Code

A computer code for the Transonic Analysis of a Wing and Fuselage with Interacted Viscous Effects (TAWFIVE) was also used in the study. The code utilizes the interaction of an inviscid and a viscous flow solver to obtain transonic flow-field solutions about wing-fuselage combinations. The outer inviscid flow field is solved using a conservative, finite-volume, full-potential method based on FLO-30 by Caughey and Jameson. No modifications were made to the internal grid-generation algorithm in FLO-30, which is a body-fitted, sheared, parabolic coordinate system.

Viscous effects are computed using a compressible integral method which calculates three-dimensional boundary layers for wings. The code has the capability of computing laminar or turbulent boundary layers with the methods of Stock (ref. 10) and Smith (ref. 11), respectively. An important addition to the code is Streett's treatment of the wake (ref. 12). The wake model used in FLO-30 was replaced with a model which satisfies flow tangency on the wake displacement body and the pressure jump condition resulting from wake curvature. These changes in the code can make significant differences in results obtained on various configurations (ref. 12).

FLO-22NM Design and Analysis Code

The FLO-22NM (ref. 6) code is a wing alone transonic code which has the application of design and optimization algorithms included as solution options. The FLO-22 (ref. 13) solver has provided reliable nonconservative solutions to the full potential equation for a number of years. A design algorithm is included in the code based on the work of Bauer, Garabedian, and McFadden (ref. 6). By relating wing section contour changes to incremental changes in surface pressure distributions, a systematic procedure is established to modify a wing contour to achieve a desired target pressure distribution. Modifications to the original algorithm were made at Lockheed Georgia Company to extend the regions of the wing where the algorithm is applied. An option to employ a quasi-Newton's method optimization procedure (ref. 14) is available in the code. However, this option was not exercised during this study.

NYU Airfoil Code

The New York University airfoil analysis code written by Bauer, Garabedian, Korn, and Jameson (ref. 7) is used extensively by many researchers to provide two-dimensional viscous analyses of airfoils. The inviscid solution solves for the steady, isentropic, irrotational flow about an airfoil contour. Viscous corrections are provided by adding the turbulent displacement thickness to the airfoil surface. There is no laminar boundary layer calculated by the code. The momentum thickness is initialized at the transition point, which can be set arbitrarily. Using the turbulent boundary-layer method of Nash and Macdonald (ref. 15), the boundary-layer characteristics are computed using the results from the potential flow analysis and the airfoil geometric characteristics.

High-Lift Code

The high-lift code (ref. 8) developed at Lockheed Georgia Company and modified at NASA-Langley defines the subsonic viscid attached flow about two-dimensional multicomponent airfoils. The viscous solution is obtained by interacting potential flow and a boundary-layer solution for the flow field. Potential flow approximations are made using a distributed vortex concept with the vortex singularity comprising the fundamental solution to the Laplace equation. Boundary-layer solutions employ representations of the laminar and turbulent boundary layer along with a transition model. Laminar boundary-layer separation criteria have also been included in the code and are used in the present study as an indication of low-speed maximum lift coefficients.

F-14 VARIABLE SWEEP TRANSITION FLIGHT EXPERIMENT

During the mid 1970's, NASA began the Aircraft Energy Efficiency (ACEE) program to develop fuel conservation technology for commercial transports (ref. 16). One aspect of the ACEE program that has received considerable research attention is the development of technology for viscous-drag reduction through natural laminar flow (NLF) and laminar flow control (LFC). Recent research at NASA has been encouraging relative to obtaining significant extents of laminar flow with either method or a combination of both.

An important question which must be answered in order to design wings which effectively utilize natural laminar flow relates to boundary-layer transition. It is known that for boundary layers in a three-dimensional flow environment there is an interaction between crossflow (CF) and TS instabilities that can cause transition to occur in an otherwise favorable environment (i.e., favorable pressure gradient, smooth surface, etc.) (ref. 17). In order to assist in identifying and quantifying the influence of the CF-TS interaction on wing boundary-layer transition, data are needed for various combinations of favorable pressure gradients, Reynolds numbers, and wing sweep angles.

To establish a data base for the transition data, NASA Langley and NASA Ames-Dryden have defined a variable sweep transition flight experiment (VSTFE) utilizing the F-14 aircraft. The objectives of this flight test are to obtain in-flight wing pressure and boundary-layer data which will be used to develop a reliable laminar boundary-layer transition prediction method. The approach to obtaining the flight data is to modify the F-14 wing outer panel by 'gloving' on a foam and fiberglass panel contoured such that it generates favorable pressure gradients on the upper surface over a wide range of flight conditions (fig. 1). By using data obtained from analyses of the wing pressure distributions with a boundary-layer stability code and from flight-measured transition data, inferences will be made relative to the interaction of CF and TS instabilities on boundary-layer transition.

Extensive computations have been performed in support of the proposed flight-test program. These range from verification of the potential flow methods to the actual design of the contour for the outer panel glove. Many of the preliminary computations are reported in reference 18. One of the intents of this paper is to demonstrate how the computations have been utilized and relied upon during the glove design phase of the VSTFE. Initially pertinent questions were answered regarding the use of small-disturbance and full-potential transonic analysis codes. Questions were addressed relative to geometric considerations resulting from the complexity of the F-14 aircraft (figs. 1 and 2), the applicability of two-dimensional codes to the design problem, and the ability of the three-dimensional codes to accurately predict the flow field on the configuration. Although these questions are discussed in reference 18, in the interest of completeness of the present discussion it seems appropriate to include a brief discussion of the code validation efforts which involved comparison of code prediction with flight test data.

Comparison of Computations and Flight-Test Data

Some wind-tunnel pressure data existed for the F-14; however, the data were sparse for the primary wing sweep angle (Λ_{LE} = 20°), the Mach number, and the lift range of interest in this study. In January 1984, a flight test was conducted on NASA's F-14A aircraft 1-X at the Dryden Flight Research Facility (ref. 19). The objective of the flight test was to explore the proposed flight envelope for the VSTFE and to obtain wing pressure data on the baseline aircraft. 'Strip-A-Tubes' were bonded to the wing surface at four locations along the wing span. The pressure tubes were aligned with the free-stream flow when the wing leading edge was swept 19°. For this sweep angle, the tube spanwise positions corresponded to 40, 56, 73, and 87 percent of the semispan.

Wing pressure data were obtained over a wide range of Mach numbers, lift coefficients, altitudes, and wing sweeps. The ranges of the various parameters are summarized in the table below.

Table 1. - Flight-Test Conditions

Leading-edge sweep	20°-30°
Mach number	0.6-0.85
Altitude, ft	25K-35K
Lift coefficient	1-2g flight

From these data, four flight points were designated to be of primary interest. Three of these points correspond to corners of the flight envelope for the VSTFE, and the remaining point was an intermediate flight condition. The four points are listed as follows:

Point	M	Altitude, ft	C_L
1	0.70	25,000	0.35
2	0.70	35,000	0.52
3	0.75	25,000	0.33
4	0.80	35,000	0.39

Points 1 and 2 correspond to the minimum and maximum altitudes where data will be obtained for level flight at $M = 0.7$, while point 4 corresponds to the maximum altitude level flight at $M = 0.80$. All of these data are for a wing sweep angle of 19°. Although data were obtained at sweep angles to 35°, the 'Strip-A-Tubes' were not aligned with the free-stream flow at the higher sweep angles. This misalignment could easily have compromised the corresponding data, since the tubes are raised off the wing surface.

These data were used to compare predictions from the TAWFIVE and WBPPW codes. The computational models for each of these codes included a wing and fuselage; however, the models did not include either horizontal or vertical tails. Therefore, in order to circumvent the problem of matching the total lift coefficient, all analyses were performed at the flight Mach number and measured angle of attack. The WBPPW code was run for 100 crude and 200 crude/fine iterations. Transition was specified at 5-percent of the chord on the upper and lower surfaces. The 2-D strip boundary-layer solution was interacted with the inviscid solution every 20 iterations. The TAWFIVE code was run for 100 crude, 100 medium, and 200 fine-mesh iterations. Transition was specified at the leading edge on both surfaces. Viscous effects were incorporated into the solution by calculating the full 3-D boundary layer three times (at iterations 100, 150, and 200) on the finest mesh. Solution residuals obtained were of the order of 10^{-4}.

The comparisons between the computations and the flight-test data are presented to discern the types of correlation possible between the experimental and computational data obtained in an engineering environment rather than to judge which code is 'best' or 'worst.' Two important points need to be reiterated in this regard:

1. The codes were not run to ultimate convergence, rather, they were converged to engineering accuracy.

2. No attempt was made to match lift coefficient, leading-edge pressure expansion, etc. Solutions were obtained at the flight Mach number, angle of attack, and altitude.

Overall, the comparisons presented in figures 3 to 6 are quite good. Before addressing specific points observed in the comparisons, several broad observations are appropriate. There are indications that the leading-edge slat is deflecting under flight load conditions. Evidence of this is apparent to some degree in each of the figures. Notice the pressure distributions over the forward 10 percent of the chord on the upper surface. The characteristic of the flow expansion at the leading edge followed by a compression is suspicious, particularly, since neither code predicts this type of characteristic. Evidence to support this hypothesis was obtained when static loadings corresponding to the flight loads were applied to the wing. By measuring surface deflections, it was obvious the slat was deflecting relative to the main wing structure.

The other observation concerns differences in the code predictions. Where differences in leading-edge expansion are observed (i.e., fig. 4), the full-potential code predicts more expansion at the leading edge than the small-disturbance code. This is consistent with the code formulation. Two points should be mentioned concerning shock waves (figs. 5 and 6). The grid in the WBPPW code has approximately three times higher resolution near the shock location than the TAWFIVE code (0.01x/c vs. 0.03x/c). This accounts for the 'sharper' shock resolution observed in the WBPPW results. In addition, the shock is located forward in the WBPPW code relative to the TAWFIVE code. This difference can be traced to the basic differencing scheme formulations employed in the code. The WBPPW code uses nonconservative differencing, while the TAWFIVE code uses a conservative differencing scheme. The most obvious effect of this difference is the location of shock waves. Nonconservative differencing tends to affect the solution in the same manner as viscous effects so that shock waves tend to be predicted further forward.

The data for level flight at M = 0.7 and 25,000 feet are presented in figure 3. The comparisons between these data and experiment are excellent at both span locations presented. The loading at the outboard span location is slightly overpredicted by each of the analysis codes.

The high altitude (35,000 feet), M = 0.70 data are presented in figure 4. This case shows the maximum effect of leading-edge slat deflection on the pressure distributions. Note also that the maximum difference in the computational predictions at the leading edge is observed here. Aft of 20-percent chord, the comparisons are excellent on the upper surface. However, the predictions of lower surface pressure distributions are significantly different from the experiment at the inboard station. The mechanism driving these differences is not fully understood at this time.

Quite good comparisons of computations and experiment are obtained for the intermediate (M = 0.75) case presented in figure 5. Evidence of the differences in shock prediction is observed at the inboard span location. However, the data for the high altitude (35,000 feet), high Mach (M = 0.80) case present a more graphic example of the code differences in figure 6. Note the agreement between the codes and the data over the forward part of the upper surface ahead of the shock. The shock predicted from the TAWFIVE code is approximately 5-percent chord aft and smeared relative to the shock predicted by the WBPPW code. This is consistent with the previous discussion.

Overall, the agreement between the flight-test data and the computational predictions from each code is excellent. All the differences observed between the computational results and between the computational results and experiment can be accounted for, except those shown in figure 4 for the pressure distributions on the rear part of the lower surface. These particular differences will not impact the way the codes will be applied in the design procedures.

Glove Design Constraints

Before a detailed description of the design steps and the supporting data are presented, the physical constraints of the actual modification should be addressed. These constraints had a significant impact on the design process. Although the constraints changed often over the course of the design study, only the final constraints and supporting rationale will be presented herein.

The wing upper surface was allowed to be modified from the leading edge aft to approximately the 60-percent chord line. Modifications to the lower surface were limited to the first 10 percent of the chord. The upper surface constraint was imposed to stop the glove modification in front of the spoiler hinge line, since the spoilers are used for roll control over a portion of the flight envelope. Consideration of the techniques employed in manufacturing the glove was responsible for the lower surface constraint being imposed.

Instrumentation leads were to be routed inside the leading edge of the glove, hence it was necessary to extend the glove leading edge 2 inches in front of the actual leading edge of the wing. There was also concern over slat movement under flight-loading conditions. This could have possibly caused undesirable contour changes in the glove shape. To minimize this possibility, the glove thickness was constrained to be a minimum of 0.65 inches over the upper surface. Under static loading conditions this thickness of foam and fiberglass was sufficient to absorb any relative movement of the slot and the main wing element. This minimum thickness constraint in turn posed another constraint. In order to maintain adequate spoiler effectiveness, the thickness of the glove at the spoiler hinge line was limited to a maximum of 1 inch.

It is obvious that these are quite stringent constraints from a design standpoint. Detailed descriptions of the design steps and supporting data are included in the following discussion.

Glove Design Procedures

Based on the trends which were observed in the wing pressure data and the excellent comparisons which were obtained with the potential flow analysis codes, it was felt that an integrated two-dimensional/three-dimensional analysis and design process could be effectively formulated. The procedure, which evolved during the design effort, was not formulated a priori but did follow this loosely defined integrated approach.

The design point was chosen which corresponded to a 'worst case' condition for the targeted Mach number of interest (M = 0.70). Because of the difficulty of maintaining favorable pressure gradients near the wing leading edge, the angle of attack for 1-g flight at the highest altitude in the test envelope was designated the design point. If a slightly favorable pressure gradient could be generated from the leading edge to the pressure rise at that condition, then reducing the altitude, hence the total lift coefficient and angle of attack required for level flight, would yield a more favorable pressure gradient. The design point corresponded to 1-g flight at M = 0.70 and 35,000 feet.

Five defining stations were chosen to be recontoured with linear lofting utilized between the defining stations. These corresponded to the inboard and outboard extent of the gloved region, where laminar flow was desired, and three intermediate defining stations. By relying on two-dimensional analyses, simple sweep corrections, and design procedures which generate modifications to pressure distributions within specified physical constraints, upper surface contours were defined for each defining station which met the aerodynamic and physical constraints. The design procedure employed was a relatively simple algorithm which relates changes in local surface curvature to increments in surface pressure coefficients. The resulting curvature changes could be integrated to yield surface ordinate increments while monitoring the various physical constraints on the glove contour. Pressure distributions for a range of lift coefficients for the mid-span defining station are presented in figure 7. A sectional lift coefficient of 0.60 corresponds to the 'worst case,' and the other values to less severe cases. Note the favorable pressure gradient aft to the pressure rise for the range of lift coefficients presented.

After two-dimensional designs were completed for the five defining stations, the question of three-dimensional effects was addressed. The recontoured outer panel was modeled and analyzed in a three-dimensional analysis and design code (ref. 5). This allowed the identification of adverse three-dimensional effects resulting from the wing planform, twist distribution, etc. Two adverse characteristics were observed in the three-dimensional pressure distribution (fig. 8) which were not evident in the two-dimensional analyses. This includes a pressure peak at the wing leading edge and a flow expansion just forward of the shock. Of course, it was desirable to remove the adverse pressure gradient associated with the leading-edge pressure peak and to minimize the flow acceleration just forward of the shock. As described previously, the code has a design option available. A target pressure distribution was defined at each of the defining stations to minimize the adverse effects (fig. 8). The design option in the code was then employed to modify the wing outer panel to minimize the difference between the predicted and target pressure distributions. This step in the design process yielded modified contours for each of the defining stations.

These five new defining station airfoils were examined relative to the smoothness of their curvature distributions and constraint violations. Where appropriate, refairing and smoothing of the new contours were employed. This yielded final smoothed contours which met the design constraints at each of the defining stations. A typical contour is presented in figure 9 showing its relationship to the F-14 baseline contour at that wing station. Two-dimensional analyses were used to verify that no adverse effects had inadvertently shown up in the pressure distributions (fig. 10).

However, final computational verification of the design was realized by analyzing the entire configuration (fuselage, nacelles, strake, and outer panel) in the TAWFIVE code. Results presented in figure 11 show that the design objectives were realized over the range of lift coefficients corresponding to the altitudes of interest at M = 0.7. Data are also presented for a glove designed by Boeing for a design Mach number of 0.8. This glove will be flown concurrently with the NASA-designed glove. Data are presented for the M = 0.7 and M = 0.8 flight conditions. The boundary-layer analysis for the high altitude case at M = 0.8 (fig. 11(c)), gave no evidence of flow separation. Since the computational analysis predicted acceptable results and the design constraints were met, the glove design was frozen at this point.

VSTFE Status

Glove design has been completed for the VSTFE, and fabrication is underway for a wind-tunnel test to be conducted in the NTF during the early summer of 1985. The objectives of the test are to obtain data to verify the glove design and safety-of-flight data for support of the flight test program. Flight test instrumentation techniques will be validated in a program which will be flown in the late summer or early fall of 1985. A 'clean-up' glove has been fabricated for the F-14 outer panel which employs the physical constraints described previously and corresponds to the baseline F-14 outer panel contour. Any manufacturing or instrumentation problems uncovered during this program can be addressed before the NLF glove experiment is flown. Manufacture of the NLF glove will commence in the last quarter of 1985 with the flight test following 9 to 12 months later.

HIGH ASPECT RATIO NLF WING

NASA has been interested in extending the applicability of the concept of natural laminar flow into the transonic speed regime, in addition to low- and medium-speed applications (ref. 16). In support of this objective, a program was undertaken to incorporate the concept of NLF into a high aspect ratio, low sweep wing designed for a corporate transport configuration. Much of the design work had been accomplished prior to NASA's involvement in the program including identification of the configuration characteristics such as fuselage geometry and wing planform (fig. 12). However, the wing section contour had not been defined, and this provided the basis for this discussion. An objective was identified to design a wing contour which would generate a significant extent of laminar flow on both the upper and lower surfaces at a transonic cruise design point. In addition, there were aerodynamic and geometric constraints imposed on the design. In order to provide adequate volume for fuel and for landing gear storage, the wing was required to have a minimum thickness to chord ratio of 12.5 percent. The configuration was powered by a single engine which dictated a rather low landing speed requirement. To meet this requirement, a large wing area had been specified along with airfoils which had a maximum sectional lift coefficient of 3.8. The large wing area translated to a cruise design point at M = 0.7 at a wing lift coefficient of 0.25. A self-imposed constraint was that the design offer acceptable aerodynamic characteristics with a fully turbulent boundary layer on the wing (as opposed to the long runs of laminar flow) over the flight envelope.

Computational Design

Again an integrated two- and three-dimensional computational design approach was identified. Both two-dimensional and three-dimensional analysis codes which had been verified for transport application were identified to be used. This includes the two-dimensional Garabedian and Korn (ref. 7) and high-lift codes (ref. 8). Three-dimensional analyses were provided by the small-disturbance WBPPW code (ref. 2) and the full-potential TAWFIVE code (ref. 1).

As previously discussed, the wing planform had been specified as having a wing area of 250 ft^2, an aspect ratio of 8.0, and a taper ratio of 0.35. The quarter-chord of the wing had essentially no sweep, which minimized crossflow influences on the laminar boundary layer. In addition, except for interactions in the wing-body juncture regions and near the wing tip, the flow field was essentially two-dimensional. This allowed much of the contour modification work to be accomplished two dimensionally, employing three-dimensional analyses to verify the configuration characteristics.

The initial airfoil design was a derivative of a medium-speed NLF airfoil design by Viken (ref. 20). This airfoil had been designed for a lift coefficient of 0.4, $M = 0.4$, and a Reynolds number of 10 million. At the design condition, the airfoil generated favorable pressure gradients back to approximately 70 percent of the chord on the upper and lower surfaces. Viken's medium-speed design was scaled down for the higher speed applications, and the trailing edge was modified to account for the lower design lift coefficient. Analysis of the resulting airfoil is included in figure 13 for $M = 0.70$ and a sectional lift coefficient of 0.25. Two features of the flow over the airfoil at these conditions caused concern. The slight pressure peak at the lower surface leading edge was not desirable from a laminar flow standpoint. Of greater concern, however, was the pressure gradient through the pressure rise (at approximately 70 percent of the chord). Computational analyses predicted boundary-layer separation at these conditions. At overspeed conditions, the boundary-layer separation would be worse.

A computational 'cut and try' approach was employed to modify the initial airfoil contour. Using two-dimensional analysis as a guide, the mid-chord region of the upper and lower surfaces and the leading edge of the lower surface were modified to eliminate the undesirable flow characteristics at the design condition. Two-dimensional analysis of the final airfoil design is presented in figure 14 along with the pressure distribution from the initial design. Note the softening of the gradients through the pressure rise and the modification of the lower surface leading-edge pressure expansion. It is also important to note that the extent of favorable pressure gradient has been reduced to approximately 50 percent of the chord on the upper surface and 60 percent of the chord on the lower surface. Analysis indicated no evidence of flow separation at the design condition.

The two-dimensional analysis calculates a turbulent boundary-layer skin-friction drag coefficient as part of the viscous solution. Estimates of skin-friction drag reduction can be inferred from figure 15 based on an analysis at two Mach numbers over a range of sectional lift coefficients. Transition was fixed at 10 percent of the chord for both surfaces for the forward transition case and 50 to 65 percent of the chord on the upper and lower surfaces for the aft transition case. These show a reduction of turbulent skin-friction drag ranging from 50 to 70 percent. Note that there is no estimate of the contribution from the laminar boundary layer. In addition, the reader should use the absolute levels judiciously; however, the relative differences are representative.

Up to this point, the discussion has centered around two-dimensional design and analysis. Three-dimensional analyses were employed at appropriate checkpoints in the design process to monitor the possible generation of adverse three-dimensional effects. An example of the three-dimensional analysis is included in figure 16. The data presented show the effect of varying the boundary-layer transition location on the pressure distribution on the inboard portion of the wing span. As expected, these data show little change in the pressure distribution; however, more important is the fact that no boundary-layer separation is predicted with the forward transition location. These same characteristics were evident at higher free-stream Mach numbers for cruise conditions.

Computational Wing Design Effort

Only a small amount of data directly concerned with the wing section design has been included in this paper. However, several areas were addressed during this study which are not described in detail or supported with data presentations herein. It seems appropriate to describe the complete wing design effort so that the reader can obtain an appreciation for the various design areas deemed important.

While the initial two-dimensional design effort was underway, three-dimensional analyses yielded initial spanwise loading distributions. This led to a rather involved study to define an appropriate twist distribution for the wing. Tradeoffs were made among various twist and airfoil section distributions along the span. Final decision will have to be made by factoring in economic and manufacturing considerations. During the study, an evaluation was made on a proposed planform modification. Analyses yielded the effect of the modification on design decisions which had already been made.

As the airfoil modifications were completed, they were analyzed as part of the complete configuration in the three-dimensional codes. Although the majority of the analyses were near the design point, off-design analyses were performed and monitored to ensure that design goals were being met. Of primary importance for the off-design case was the shock strength associated with the overspeed flight conditions.

In anticipation of improvements in the configuration stall characteristics, two drooped leading-edge extensions were designed. Outboard leading-edge extensions have been found to improve stability levels in the vicinity of stall for certain classes of general aviation aircraft. The two extensions designed corresponded to 2- and 3-percent chord extensions and were employed in the outboard 25 percent of the wing semispan. Transonic and low-speed analysis codes were used to analyze these modifications.

Final Design Characteristics

The wing designed through the use of computational procedures yielded excellent aerodynamic characteristics. At the cruise design point, favorable pressure gradients were generated on the upper and lower surfaces to 50 and 60 percent of the chord, respectively. This should yield significant runs of laminar flow and reductions in viscous drag. In addition, there was no indication of boundary-layer separation when transition was specified at the wing leading edge. The wing possessed good aerodynamic characteristics from low-speed conditions up to $M = 0.80$. Analyses indicated a drag divergence Mach number of 0.75 at cruise. A trade-off between the aerodynamic and propulsion characteristics might yield a cruise Mach number slightly higher than 0.70. Through the use of airfoil modification techniques, the drooped leading-edge extensions were smoothly incorporated into the airfoil contours. Overall, the computational analyses indicated the wing achieved or exceeded the originally specified performance goals.

SUMMARY AND CONCLUSIONS

State-of-the-art potential flow analysis techniques have been relied on to support two design studies involving natural laminar flow. Two- and three-dimensional small-disturbance and full-potential equation analysis codes have been verified for application to the present studies by comparison with experimental data. The various codes were used in analysis and design modes to meet the design objectives and constraints. A process evolved during the studies which effectively integrated the two- and three-dimensional codes. Results proved the potential flow codes to be accurate and reliable, and provided significant confidence in the design to be investigated.

During the course of this preliminary study, several salient observations were made concerning the computer codes exercised. These are summarized below:

1. TAWFIVE and WBPPW analyses each provided excellent prediction of flight-test results when compared at flight angle of attack, Mach number, and Reynolds number for the F-14 aircraft.

2. The integrated two- and three-dimensional design process proved to be efficient. Detailed contour modifications were made utilizing two-dimensional codes. Adverse three-dimensional effects were identified and appropriate contour modifications incorporated using three-dimensional design and analysis codes.

3. The automated three-dimensional design code was reliable. However, when contour changes were required near shock locations, additional fairing and smoothing were required.

In conclusion, computational wing design methodologies were successfully applied in two unique programs. The two- and three-dimensional aerodynamic codes used in these studies proved to be robust and reliable in a stringent schedule environment. The automated design procedure yielded excellent results, and the inclusion of that procedure or a similar one in the three-dimensional analysis codes is being pursued. Some deficiencies in the capabilities of the codes were identified, and possible corrections and improved running strategies are being addressed. The final accuracy of the design methods will be evaluated when wind-tunnel tests of both configurations are completed.

REFERENCES

1. Melson, N. D.; and Streett, C. L.: TAWFIVE: A User's Guide. NASA TM-84619, September 1983.

2. Boppe, C. W.; and Stern, M.: Simulated Transonic Flows for Aircraft With Nacelles, Pylons, and Winglets. AIAA Paper 80-130, January 1980.

3. Waggoner, E. G.: Computational Transonic Analysis for a Supercritical Transport Wing-Body Configuration. AIAA Paper 80-0129, January 1980.

4. Waggoner, E. G.: Computational Transonic Analysis for an Advanced Transport Configuration with Engine Nacelles. AIAA Paper 83-1851, July 1983.

5. Raj, P.; and Reaser, J. S.: An Improved Full-Potential Finite-Difference Transonic-Flow Code (FLO22.5) for Wing Analysis and Design. Lockeed California Company Report 29759, November 1981.

6. Bauer, F.; Garabedian, P.; and McFadden, G.: The NYU Inverse Swept Wing Code. NASA CR-3662, January 1983.

7. Bauer, F.; et al.: Supercritical Wing Sections II. Lecture Notes in Economics and Mathematical Systems, vol. 108, Springer-Verlag , 1975.

8. Stevens, W. A.; Goradia, S. M.; and Braden, J. A.: Mathematical Model for Two-Dimensional Multi-Component Airfoils in Viscous Flow. NASA CR-1843, July 1971.

9. Mason, W. H.; et al.: An Automated Procedure for Computing the Three-Dimensional Transonic Flow Over Wing-Body Combinations, Including Viscous Effects. Air Force Flight Dynamics Laboratory Report AFFDL-TR-122, vol. I, October 1977.

10. Stock, W. H.: Integral Method for the Calculation of Three-Dimensional Laminar and Turbulent Boundary Layers. NASA TM 75320, 1978.

11. Smith, P. D.: An Integral Prediction Method for Three-Dimensional Compressible Turbulent Boundary Layers. RAE R&M 3739, 1974.

12. Streett, C. L.: Viscous-Inviscid Interaction for Transonic Wing-Body Configurations Including Wake Effects. AIAA Paper 81-1266, July 1981.

13. Jameson, A.; and Caughey, D. A.: Numerical Calculation of the Transonic Flow Past a Swept Wing. COO-3077-140, ERDA Math and Computer Laboratory, New York University, June 1977.

14. Kennelly, R. A.: Improved Method for Transonic Airfoil Design by Optimization. AIAA 83-1844, July 1983.

15. Nash, J. B.; and Macdonald, A. G. J.: The Calculation of Momentum Thickness in a Turbulent Boundary Layer at Mach Numbers up to Unity. Aeronautical Research Council C.P. No. 963, London, 1967.

16. James, R. L.; and Maddalon, D. V.: The Drive for Aircraft Energy Efficiency. Aerospace America, vol. 22, no. 2, February 1984, p. 54.

17. Hanks, G. W.; et al.: F-111 Natural Laminar Flow Glove Flight Test Data Analysis and Boundary Layer Stability Analysis. NASA CR-166051, January 1984.

18. Waggoner, E. G., et al.: Potential Flow Calculations and Preliminary Wing Design in Support of an NLF Variable Sweep Transition Flight Experiment. AIAA Paper 85-0426, January 1985.

19. Moes, T. R.; and Myer, R. R.: In-Flight Wing Pressure Distributions for the F-14A. NASA TM 85921, June 1985.

20. Viken, J. K.: Aerodynamic Design Considerations and Theoretical Results for a High Reynolds Number Natural Laminar Flow Airfoil. M.S. Thesis, George Washington University, January 1983.

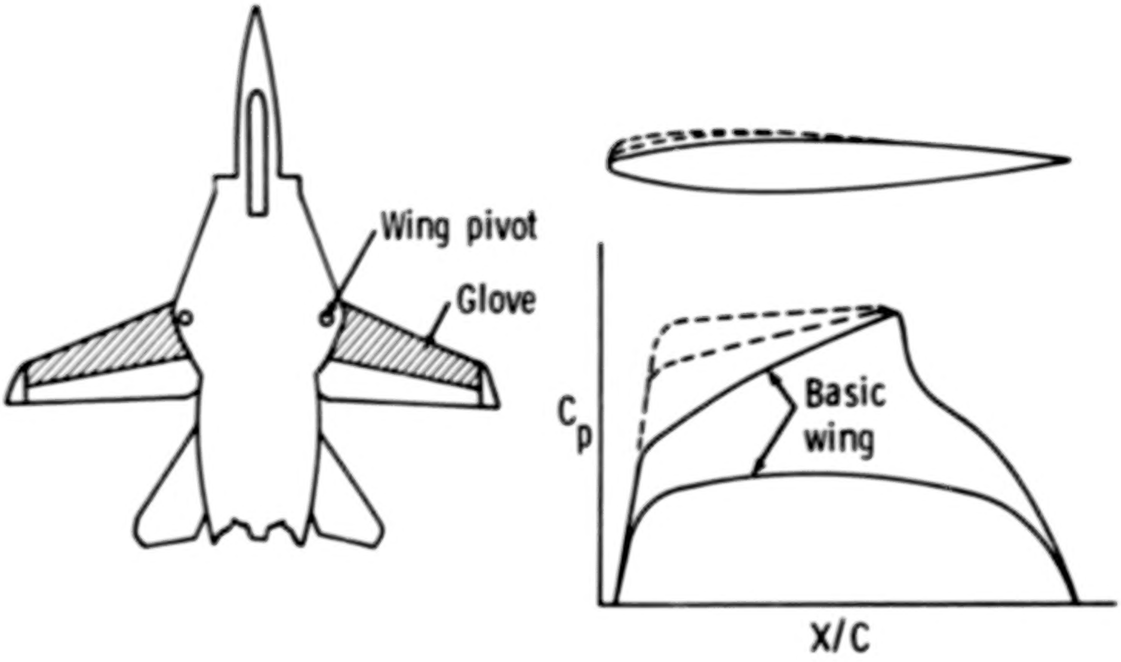
Wing pivot
Glove
C
p
Basic
wing
X/C

Figure 1.- F-14 planform and wing glove region.

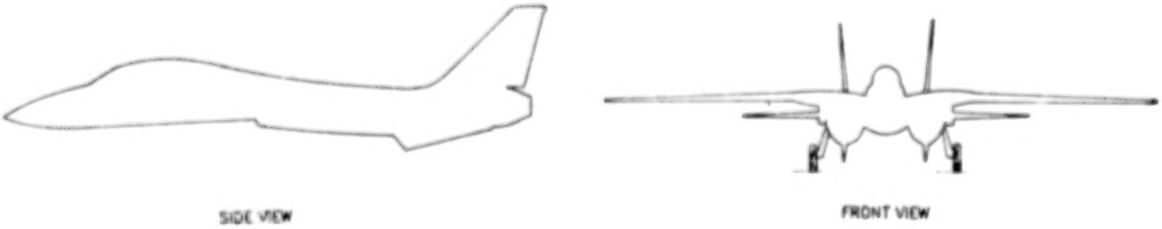
SIDE VIEW
FRONT VIEW

Figure 2.- F-14 variable-sweep aircraft configuration.

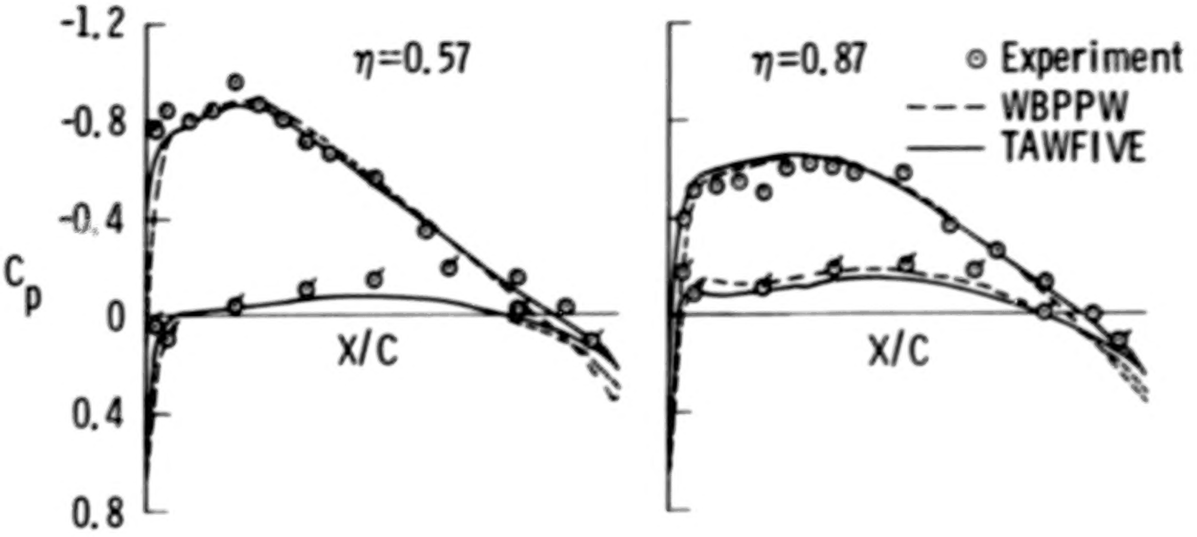

Figure 3.- Comparison of computational results and flight test data at an altitude of 25,000 ft for M = 0.70 and α = 2.1°.

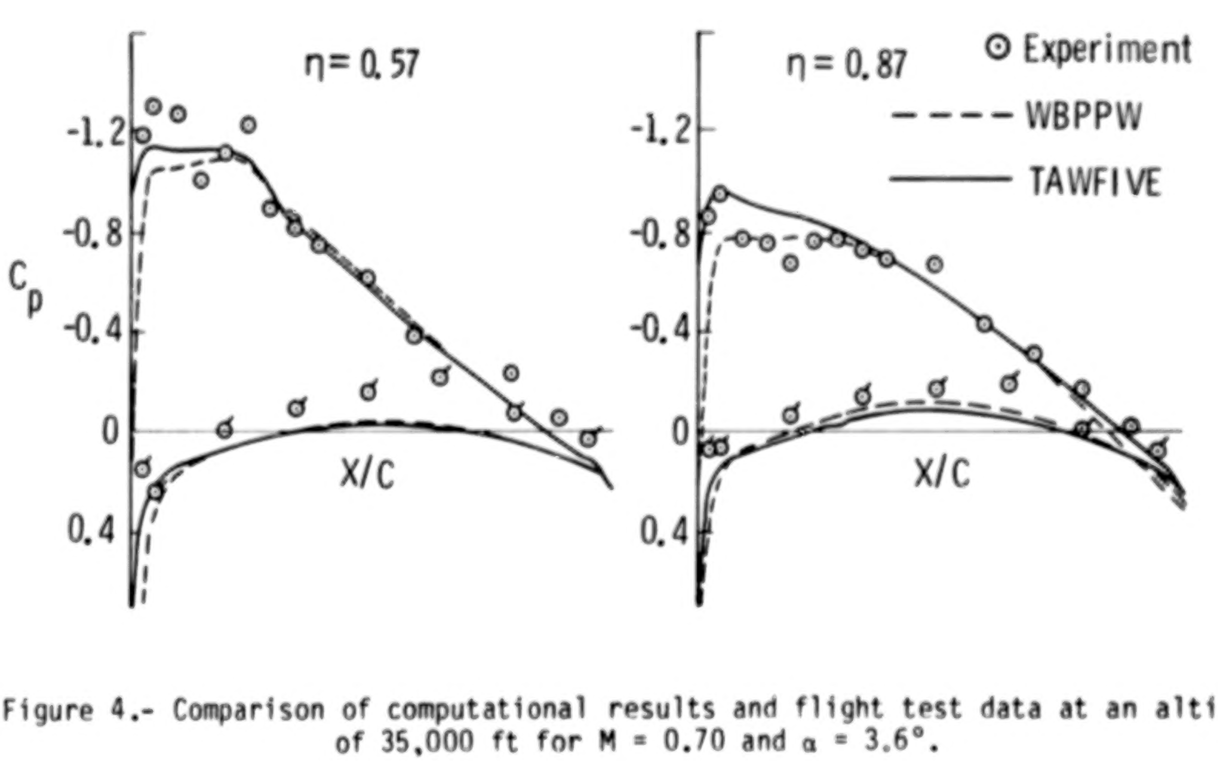

Figure 4.- Comparison of computational results and flight test data at an altitude of 35,000 ft for M = 0.70 and α = 3.6°.

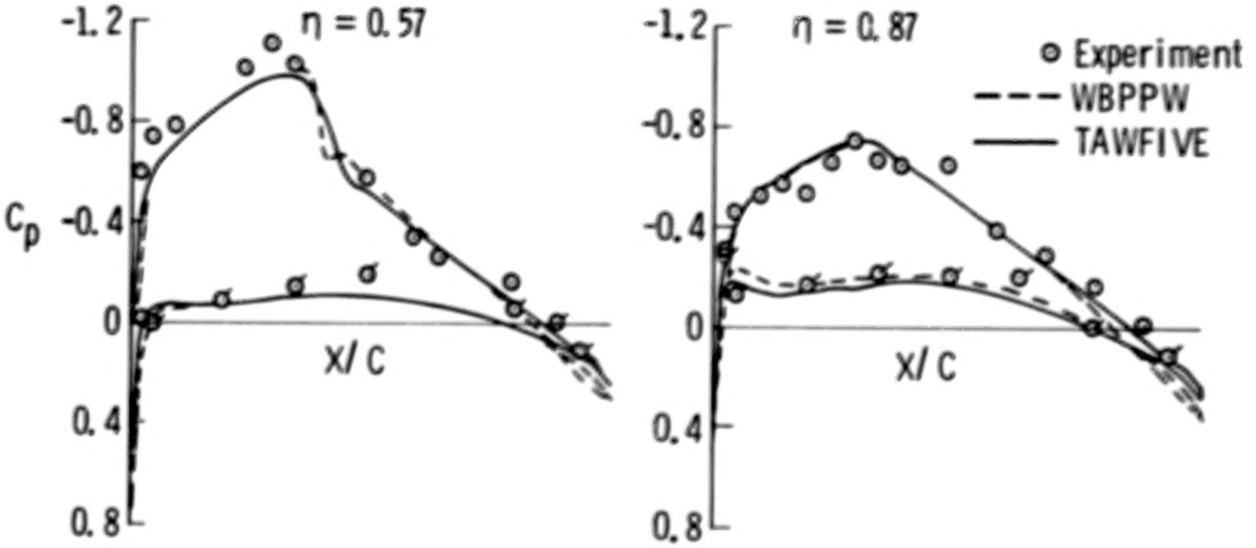

Figure 5.- Comparison of computational results and flight test data at an altitude of 25,000 ft for M = 0.75 and α = 1.7°.

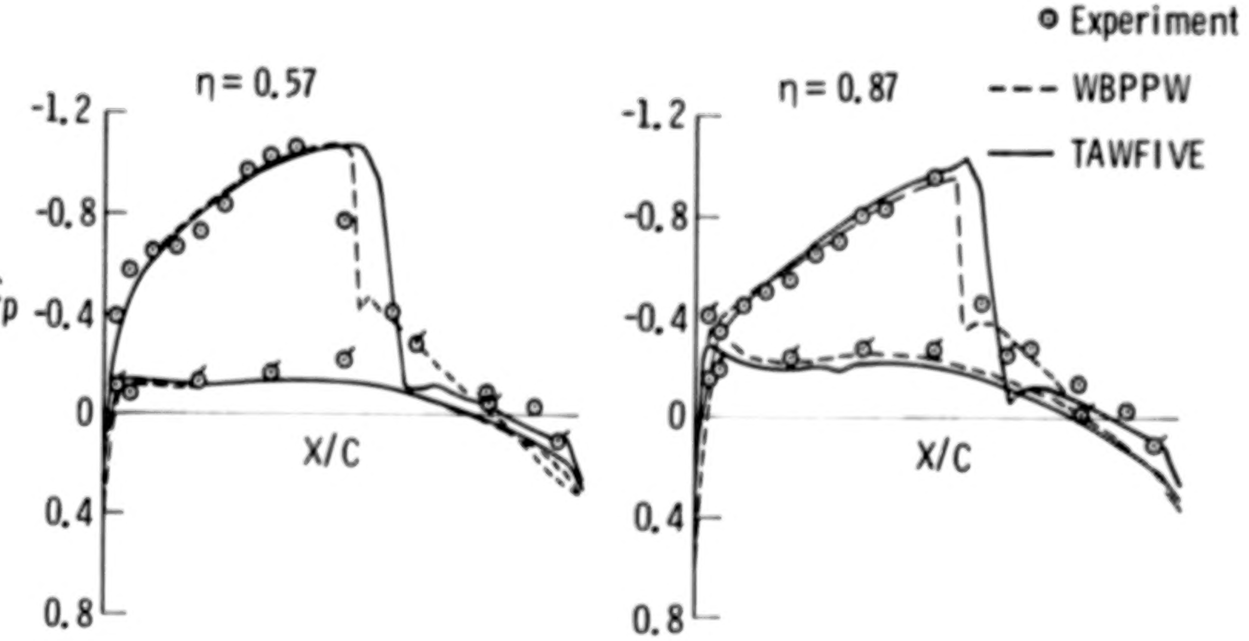

Figure 6.- Comparison of computational results and flight test data at an altitude of 35,000 ft for M = 0.80 and α = 1.4°.

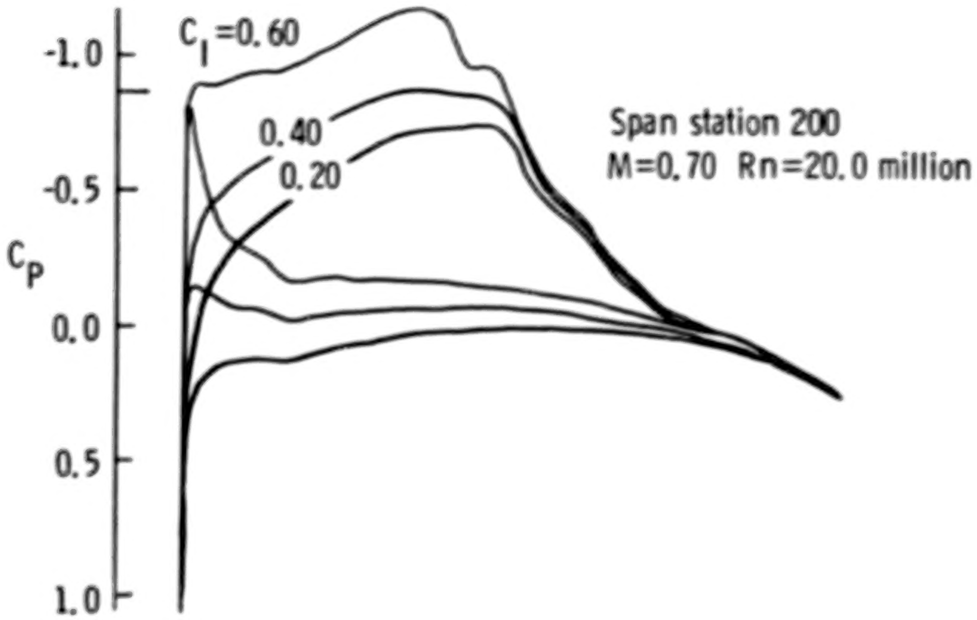

Figure 7.- Two-dimensional analysis of design airfoil meeting final constraints.

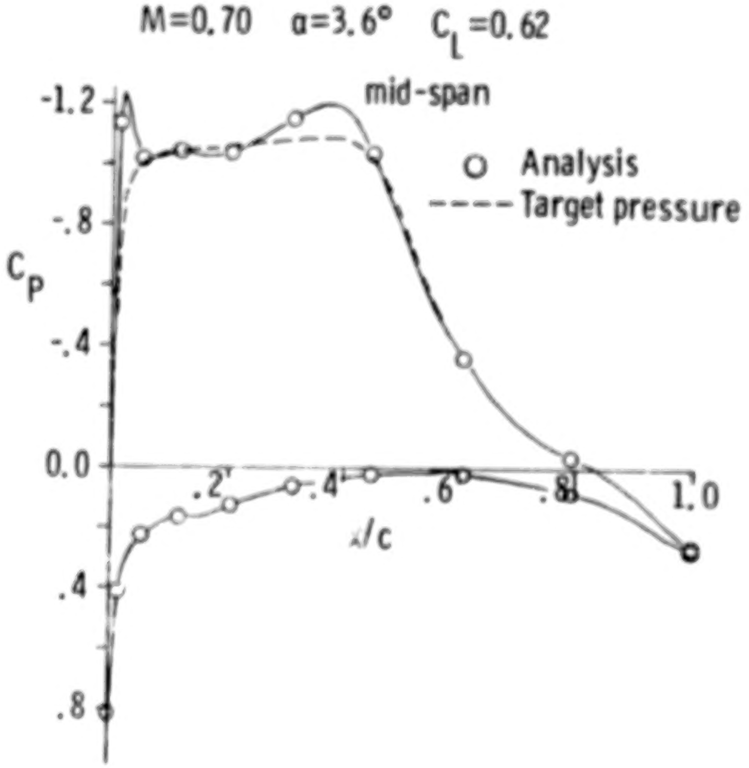

Figure 8.- Three-dimensional analysis and target pressures.

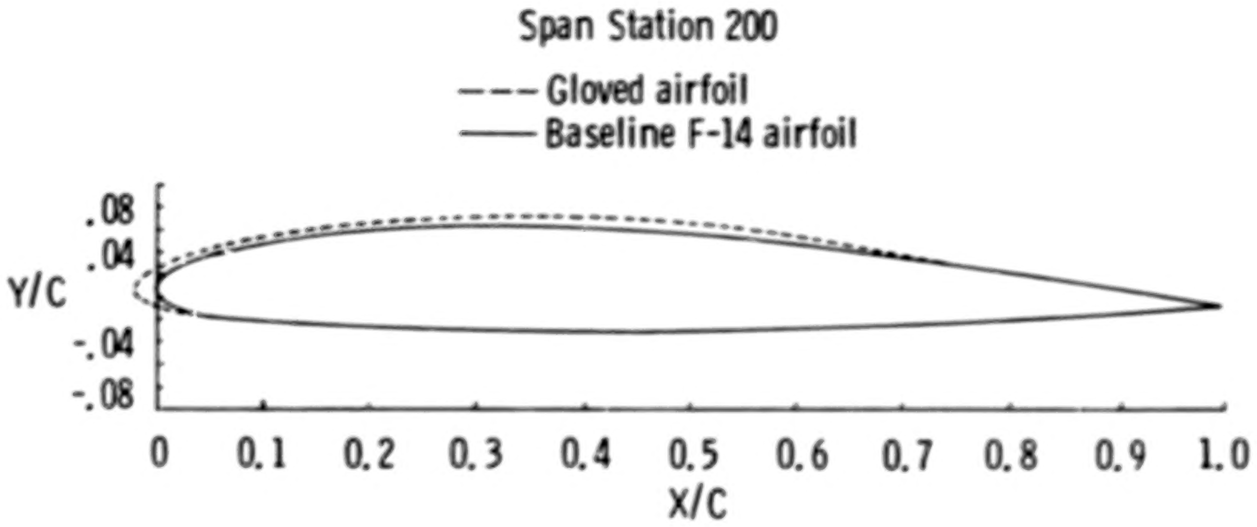

Figure 9.- Baseline F-14 section and glove design.

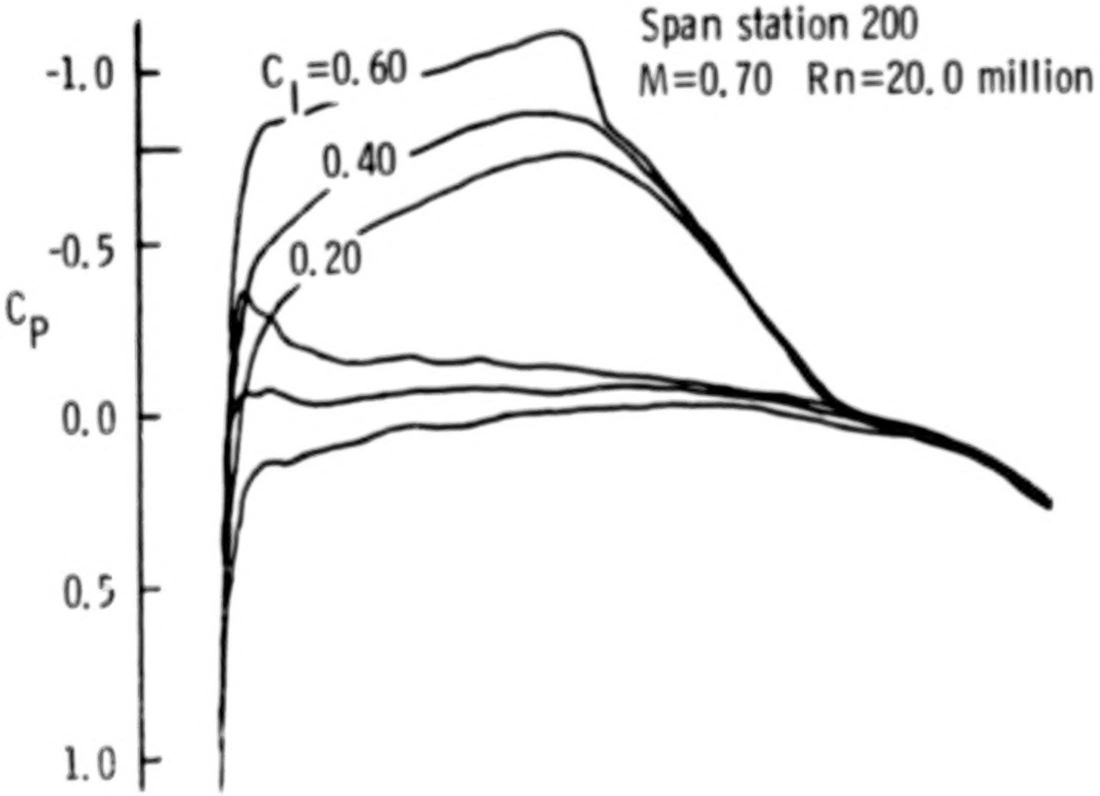

Figure 10.- Two-dimensional analysis of final F-14 glove design.

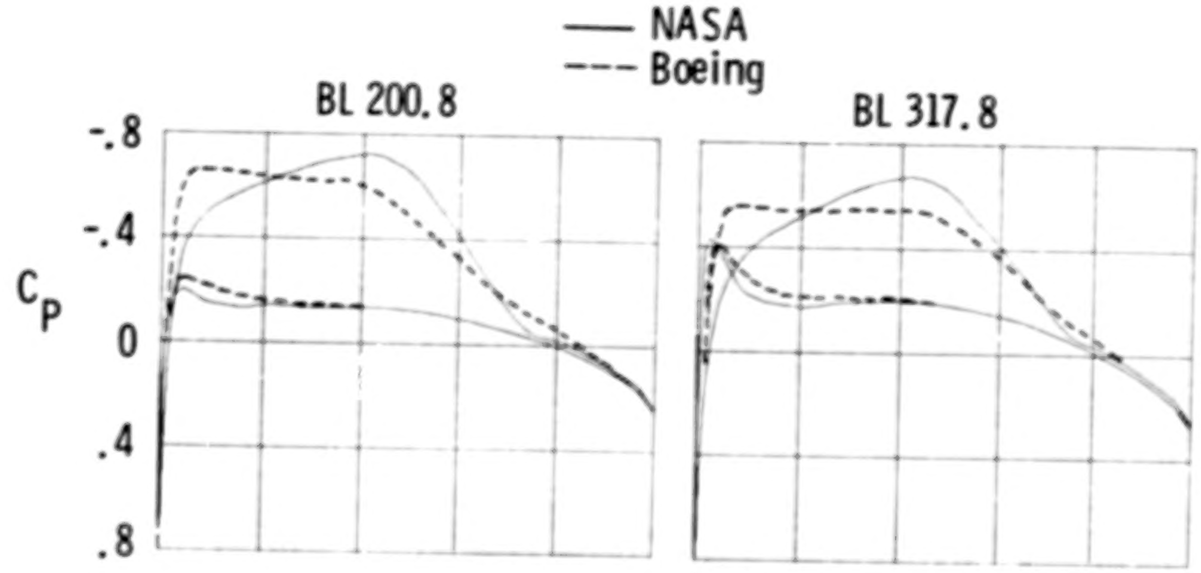

(a) M = 0.7; α = 0.7°.

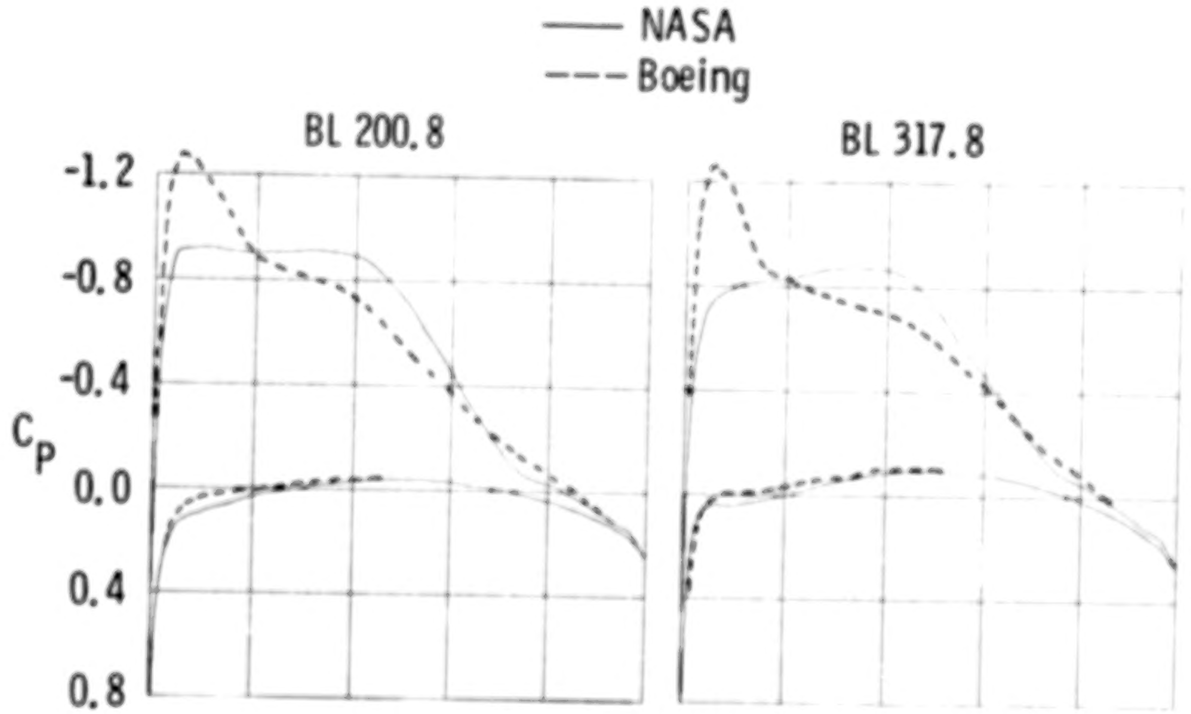

(b) M = 0.7; α = 2.95°.

Figure 11.- Three-dimensional analysis of F-14 glove design.

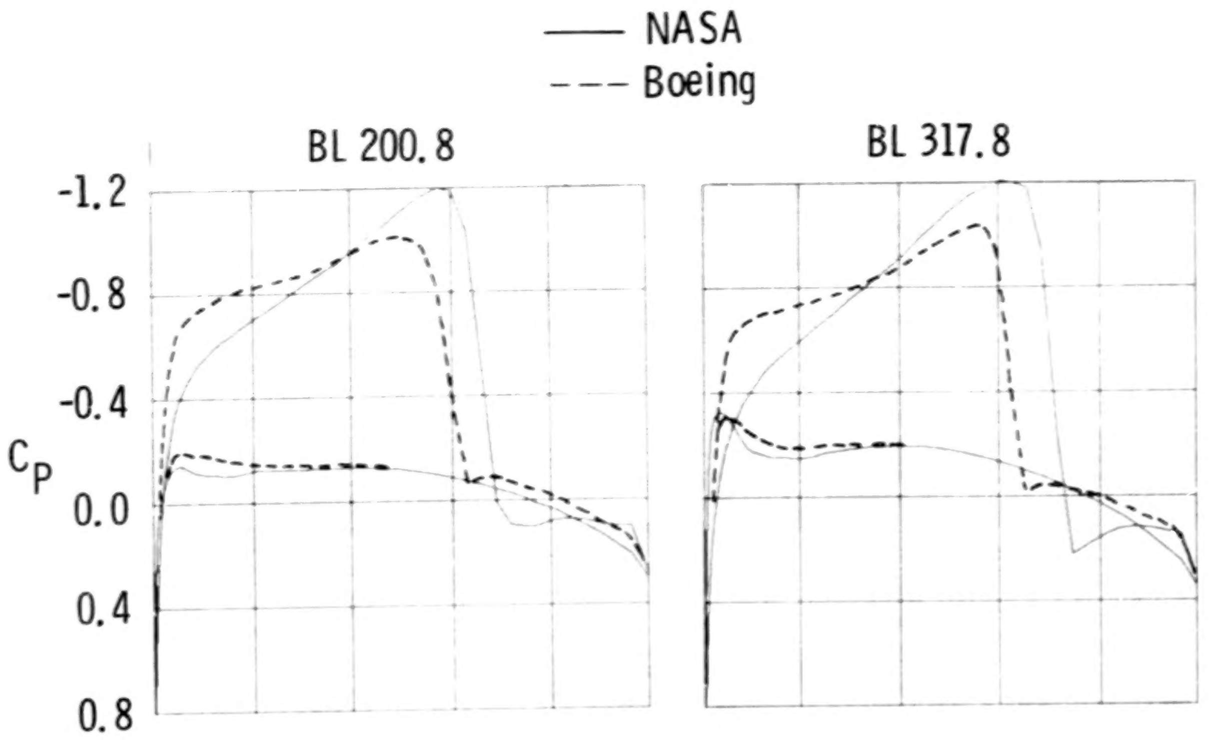

(c) M = 0.8; α = 1.3°.

Figure 11.- Concluded.

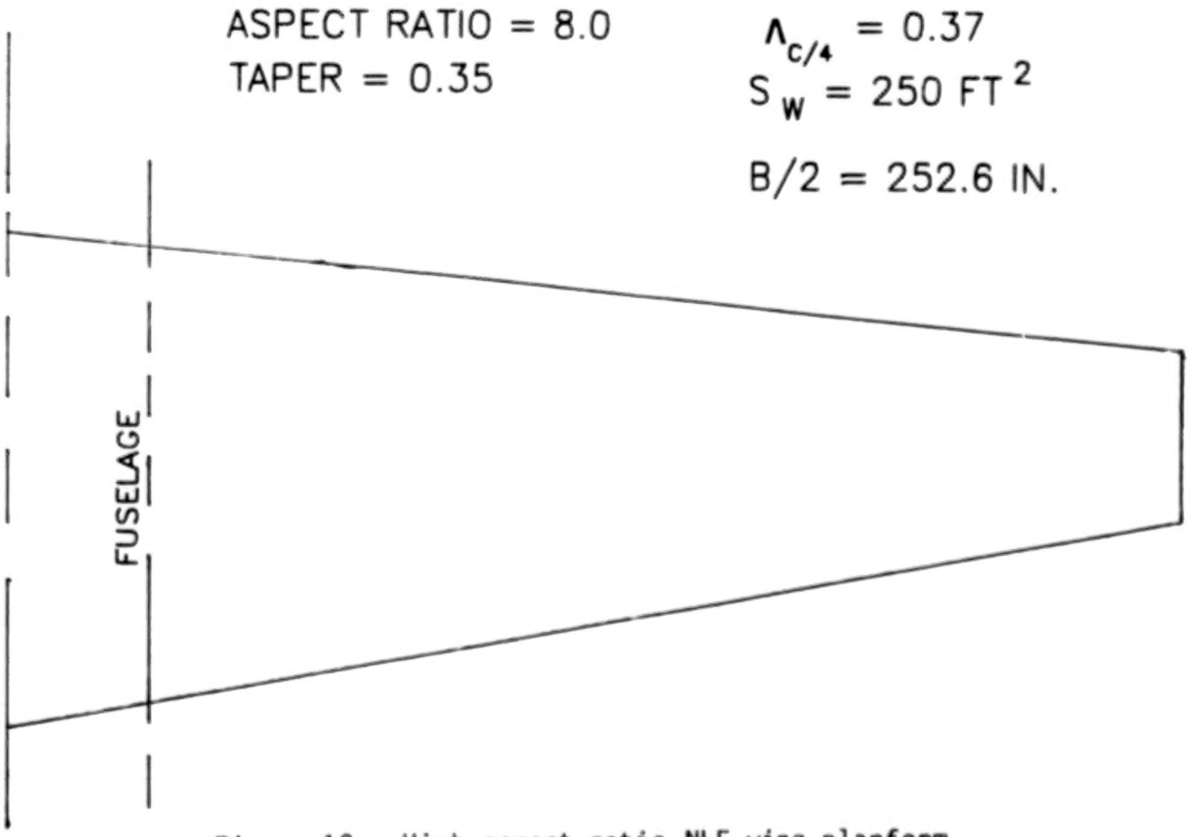
ASPECT RATIO = 8.0
TAPER = 0.35
$\Lambda_{c/4}$ = 0.37
S_W = 250 FT^2
B/2 = 252.6 IN.
FUSELAGE

Figure 12.- High-aspect-ratio NLF wing planform.

C-2

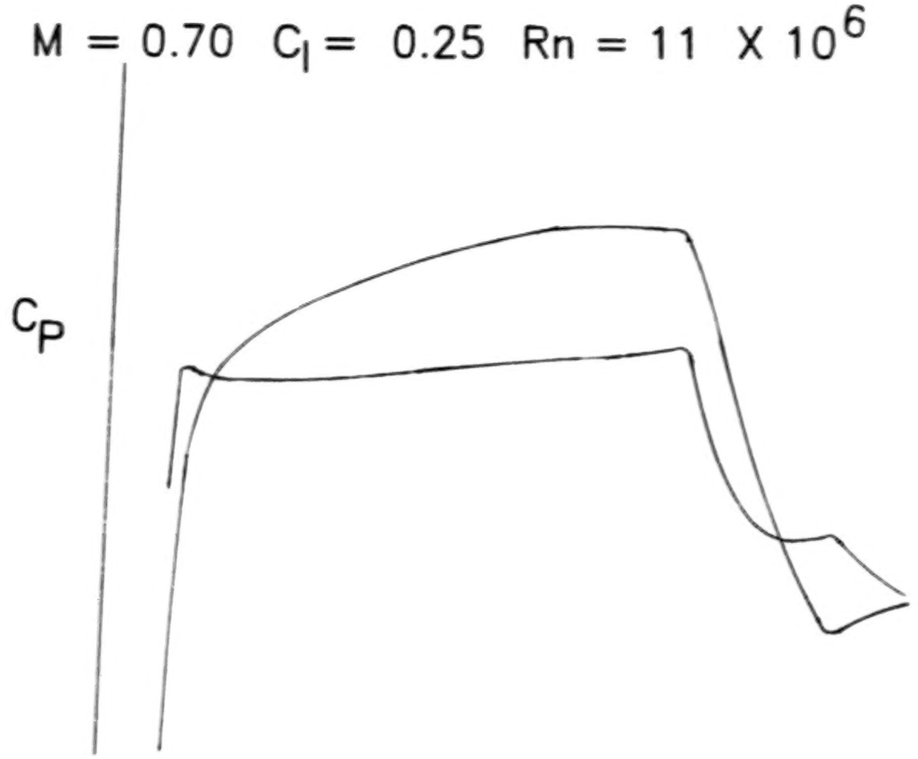

Figure 13.- Two-dimensional analysis of initial airfoil design.

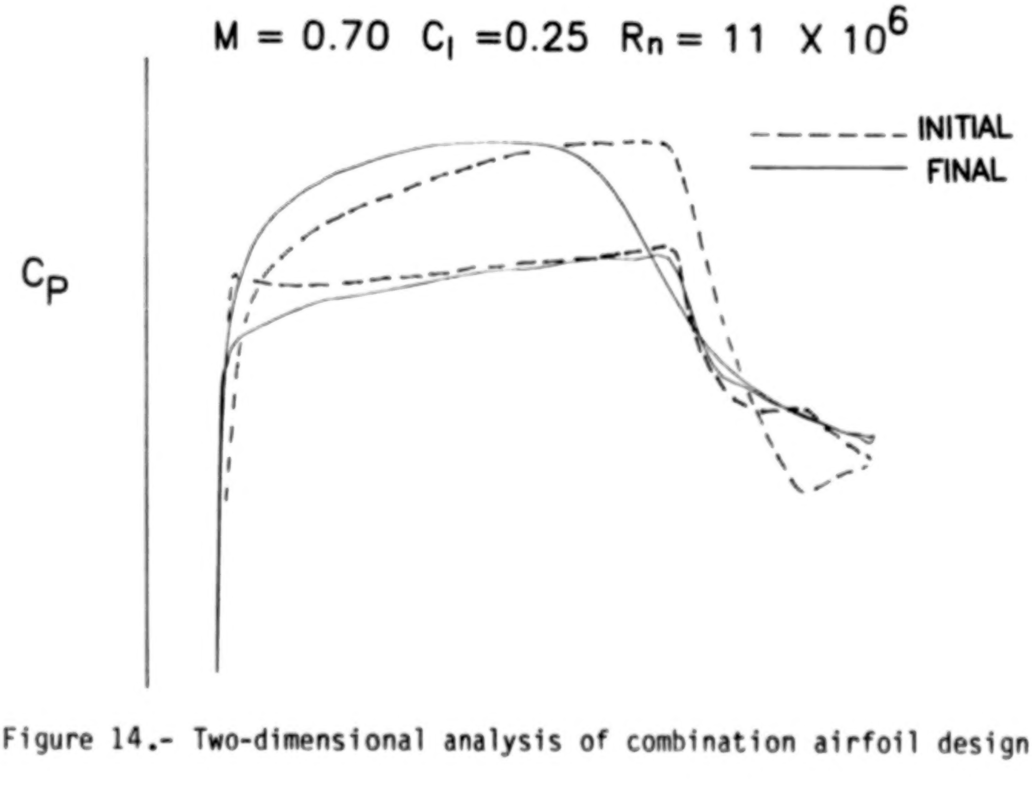

Figure 14.- Two-dimensional analysis of combination airfoil design.

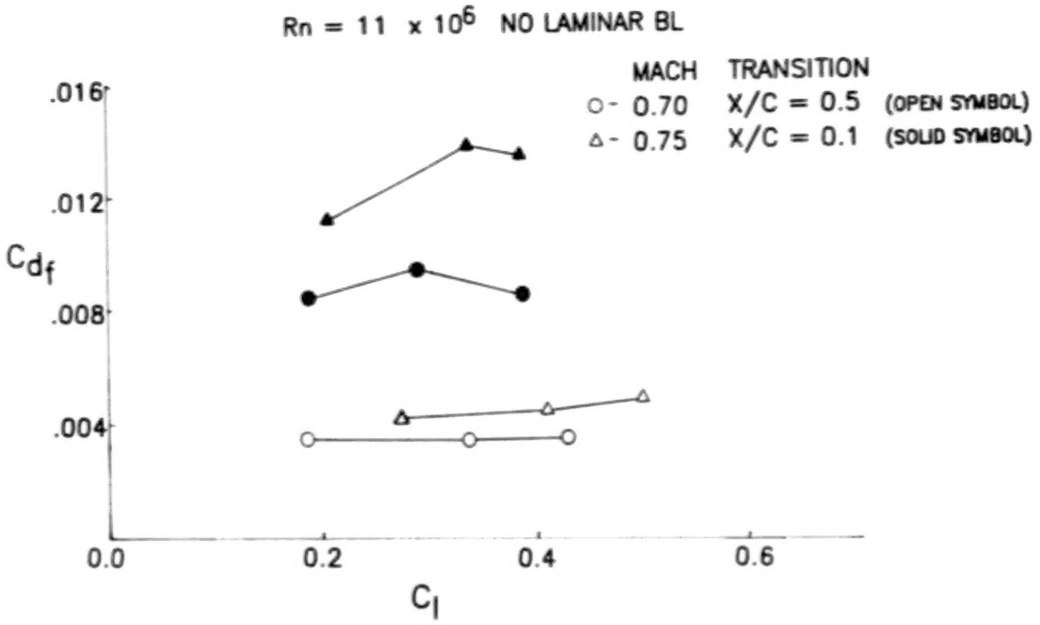

Figure 15.- Variation of skin-friction drag coefficient with sectional lift coefficient.

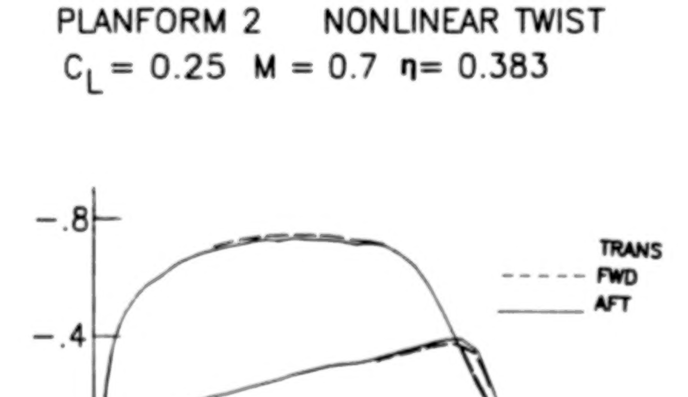

Figure 16.- Three-dimensional analysis of final wing design.

4-02
U18

N88-23741

WIND TUNNEL TESTING OF LOW-DRAG AIRFOILS

W. D. Harvey, R. J. McGhee, and C. D. Harris
NASA Langley Research Center
Hampton, Virginia 23665

ABSTRACT

Results are presented for the measured performance recently obtained on several airfoil concepts designed to achieve low drag by maintaining extensive regions of laminar flow without compromising high-lift performance. The wind tunnel results extend from subsonic to transonic speeds and include boundary-layer control through shaping and suction. The research was conducted in the NASA Langley 8-Ft. Transonic Pressure Tunnel (TPT) and Low Turbulence Pressure Tunnel (LTPT) which have been developed for testing such low-drag airfoils. Emphasis is placed on identifying some of the major factors influencing the anticipated performance of low-drag airfoils.

INTRODUCTION

Application of laminar flow concepts to aircraft design depends on fabrication, materials, and ease of maintaining laminar flow. The benefits of laminar flow are measured by achievement of very low drag which depends on the total wetted surface that is maintained laminar under various flight conditions. Performance at off-design conditions and surface maintenance tolerances are also of importance. Successful laminar flow application may cause significant changes in the trend of future aircraft design.

Whereas wing loadings on recent aircraft designs have been increasing, a laminar flow airplane will generally have a lower wing loading than a turbulent one. This effect occurs because of the type of pressure distribution required to yield the insensitivity to surface conditions and provides for long runs of laminar flow. Large laminar flow airplanes (transports) will almost surely operate at high altitudes to minimize Reynolds number effects and thus maximize performance.

Considerable basic research and technology, with and without boundary-layer control, is available (refs. 1-12) and believed suitable for design and construction of an aircraft wing to achieve laminar flow with reasonable success at subsonic speeds. Interest in this capability has been renewed by the inflight and wind tunnel test results obtained on several aircraft to establish the existence of natural laminar flow (NLF) on recent production-quality general-aviation airframe surfaces in typical operating environments (refs. 13-15). These results were based primarily on flow visualization (sublimating chemicals) techniques to define transition location and provide increased knowledge and understanding for present day aircraft. However, many of the wings investigated incorporated turbulent airfoil sections and were not designed to achieve laminar flow.

PRECEDING PAGE BLANK NOT FILMED

Laminarization has proven to be an inherently difficult boundary-layer stability problem to analyze and control due to influences of various local and external disturbances. This difficulty becomes more acute when sweep effects are included at high speeds. For this reason, a good understanding of the various stability theories along with advanced design technology will be required for the development and certification of future high performance aircraft with laminar flow aerodynamics. The emergence of advanced design codes, boundary-layer stability analysis methods, composite materials, and new fabrication technology can substantially alleviate previous laminarization concerns and encourage aerodynamicists to design better airfoils with higher lift-to-drag ratios. The Airfoil Aerodynamics Branch at Langley Research Center is currently involved in utilizing these emerging technologies to develop low-drag airfoils over a wide range of conditions. One such effort is directed toward developing natural laminar flow (NLF) airfoils for general-aviation applications which combine the high maximum lift capability of new NASA high-lift airfoils (refs. 16-18) with the low-drag characteristics of the NACA 6-series airfoils. A major design goal of these airfoils is to avoid degradation of high-lift performance characteristics if the flow becomes fully turbulent. Another effort is directed toward research on large-scale swept laminar flow control (LFC) airfoils at transonic speeds to evaluate the compatibility of suction laminarization and supercritical technology at conditions which are typical of high-performance transport aircraft (refs. 6, 19).

The purpose of this paper is to develop a better understanding of the wind tunnel testing environment and its influences on the measured performance of several advanced low-drag airfoil concepts designed to achieve extensive regions of laminar flow. The wind tunnel results extend from subsonic to transonic speeds and include boundary-layer control. The low-speed research was conducted in the Langley Low Turbulence Pressure Tunnel (LTPT), and the transonic research was conducted in the NASA Langley 8-Ft. Transonic Pressure Tunnel. These tunnels were developed or modified for testing low-drag airfoils.

SYMBOLS

c	airfoil chord
c_d	section profile-drag coefficient
c_ℓ	section lift coefficient
c_m	section pitching-moment coefficient at quarter-chord
C_p	pressure coefficient, $(p-p_\infty)/q_\infty$
$C_p{}^*$	pressure coefficient for local sonic velocity

C_Q	suction coefficient
h	height
L/D	lift-to-drag-ratio, c_ℓ/c_d
M_∞	free-stream Mach number
p	static pressure
$\tilde{p}$	rms pressure fluctuation
q	dynamic pressure
R	unit Reynolds number
R_c	Reynolds number based on chord
$(R_x)_{tr}$	Reynolds number based on transition location
t	section maximum thickness
u,v	velocity
$\tilde{u}$	rms velocity fluctuations
x,y	chordwise and spanwise coordinate system
α	angle of attack
δ_f	flap deflection angle, degrees
Λ	leading-edge sweep, degrees
λ	wavelength

Subscripts:

B	balance
c	corrected
max	maximum
s	suction
tot	total
tr	transition
w	wake
∞	free-stream conditions

LOW-DRAG CHARACTERISTICS

The drag due to friction on a current transport aircraft at cruise conditions with turbulent boundary layers is approximately 60% of the total drag. Induced drag accounts for most of the balance. The friction drag approaches nearly 90% of the total drag for submersible vehicles. It is clear, then, that there is room for performance improvements in either case by reducing the drag.

In principle, the most promising approach towards achieving significant drag reduction is through the stabilization and maintenance of the laminar boundary layer as long as possible such that most of the friction drag remains at the laminar rather than the turbulent level. It is expected (ref. 20) that techniques involving local flow manipulators may soon be available for reduction of the turbulent friction drag of regions of the aircraft that are not laminarized. However, such techniques are not anticipated to give drag reduction levels comparable to that of maintaining laminar flow. These techniques will not be discussed herein and only pre-transition concepts are considered.

Past and present wind tunnel research and development and wing-glove flight testing have established pressure and friction as the two major sources of aerodynamic drag. The most effective approach of reducing drag is by geometric shaping (passive) and minimization of wetted area (active), respectively. These approaches have provided a means of maintaining laminar flow over extensive lengths with subsequent low drag.

Passive Method - Geometric Shaping Control

The passive or natural laminar flow (NLF) approach involves stabilizing laminar boundary layers by producing a favorable pressure gradient through geometric shaping and requires no active system for control. The exploitation of favorable pressure gradient can be traced back to the development of the NACA 6-series airfoils and sailplane airfoils as well as more recent airfoils developed by Somers (ref. 16) and Viken (ref. 17).

If flow can be maintained laminar over the entire favorable pressure gradient region, it will either undergo transition just beyond the pressure minimum or else proceed to laminar separation with subsequent transition to turbulent flow. Which of these flow processes occurs will depend on several factors that include the geometric shape, angle of attack, local Reynolds number, and surface conditions. These combined factors can also produce a hysteresis effect in the lift performance that is often observed for low Reynolds number airfoils (ref. 21). Thus the major objective is to shape the airfoil contour to have as extensive a region of favorable pressure gradient as possible to ensure laminar flow followed by an appropriate recovery in the adverse pressure gradient region for maintaining attached flow. This becomes more difficult to accomplish the more rearward the favorable pressure gradient is retained. As one approaches transonic speeds, shaping becomes more important in order to minimize pressure peaks in the nose region and shock formation in the rear adverse pressure gradient (ref. 22). In addition, inherent instabilities due to boundary-layer crossflow at the leading edge of swept wings and in the rear pressure rise regions become very difficult to control passively (refs. 5-8, 23-24).

Active Method - Suction Control

A detailed discussion and summary review of a large number of suction control (LFC) investigations, including both wind tunnels and flight results, have been presented by Pfenninger (ref. 5). In general, large reductions in friction and profile drag were achieved with LFC as compared with turbulent flow.

Active approaches usually depend on both shaping and mass transfer through local suction or blowing concepts. This concept appears to be the most attractive way of laminarization for low drag, especially when sweep is required at the higher speeds. Flight experience has shown that on swept wings the transition location is considerably further forward than on unswept wings as reported earlier (refs. 7-10) and recently by Holmes et al. (ref. 13). Earlier transition on swept wings is probably caused by unstable boundary-layer profiles in the direction normal to the potential streamlines that create a crossflow in the immediate leading-edge region and rear pressure rise regions (refs. 6, 23-24). These crossflow instabilities are less responsive to suction control than Tollmien-Schlichting instabilities which develop in the streamwise direction or constant pressure regions. Weakly amplified oblique Tollmien-Schlichting waves can superimpose on crossflow disturbances causing distortion of the crossflow vortices that are stretched and converged downstream. The resulting nonlinear interaction of different disturbance modes will cause the less stable crossflow vortices to grow considerably faster than predicted by linearized stability theory. It is anticipated that this interaction can be minimized by designing swept low-drag wings so that crossflow is only critical over a small percentage of the chord. In the nose region, this may be accomplished by reducing both the sweep angle and nose radius to acceptable design values. In the aft region, control of adverse pressure gradient should be the objective.

The boundary-layer development and stability limits of these crossflow profiles, as well as the Tollmien-Schlichting instabilities, and the boundary-layer air which must be removed to stabilize either can be calculated by numerous available theories (refs. 6, 23-27). However, these methods require arbitrary choice of the growth limitation of the disturbances or transition location as input to the theory. Thus, these methods should serve only as a guide in the design process.

Because one of the key elements to the successful achievement of very low drag with or without boundary-layer control is the question of surface tolerance, it is important to recognize that no easing of tolerances is afforded by boundary-layer suction or shaping if both the speed and unit Reynolds number increase (refs. 5, 7, 8, 14, 28, 29). In attainment of low drag by NLF, success depends on surface shape and ability to control smoothness. Similarly, for suction surfaces, the boundary-layer stability Reynolds number is held to below limiting values by keeping the boundary layer thin. However, thin boundary layers are inherently developed by increasing Reynolds number and suction and require surfaces with correspondingly smaller roughness and waviness (refs. 5-6, 19).

The turbulent boundary-layer flow over the fuselage of an aircraft can spread from the wing juncture along the attachment line causing contamination. This effect will increase with sweep. Such leading-edge contamination can be avoided by keeping the critical momentum thickness Reynolds number below 100 (ref. 30). This may be accomplished by applying a fence for shielding the inboard turbulent boundary layer from spreading, or reducing sweep angle and leading-edge radius (ref. 5).

Steep pressure gradients due to shock waves can cause separation of the boundary layer and substantial increases in drag. Earlier efforts (ref. 5) and recent in-house analysis and tests (ref. 19) suggest that suction laminarization appears basically feasible in regions of weak shocks at transonic conditions. Apparently, the pressure rise which a laminar boundary layer with suction can sustain in regions of shock interaction decreases with length Reynolds number, unless the upstream boundary-layer thickness is reduced by appropriate suction (ref. 31). In summary, the above discussed effects (sweep, disturbances, contamination, shocks, etc.) impose design challenges to maintaining extensive laminar flow and low drag.

LAMINARIZATION ASPECTS

Some of the major factors known to affect transition on low-drag airfoils are surface roughness, waviness, pressure gradient, Reynolds number, suction-induced disturbances, crossflow instability, and wind tunnel or flight environment. A prerequisite for laminarization is a surface finish compatible with the boundary-layer thickness for which the investigation is undertaken. Three-dimensional surface-induced disturbances become primary sources for distortion of growth disturbances in the absence of sweep-induced crossflow effects. However, in comparison with small scale experiments in low turbulence wind tunnels, somewhat increased two- and three-dimensional surface roughness seems permissible in flight (refs. 5, 7, 8, 14, 28, 29). Thus, conclusions from low-drag experiments in wind tunnels often result in misleading and/or unduly pessimistic views about surface roughness or waviness requirements.

Wind tunnel turbulence and noise influence the transition process, and the isolation of these effects requires the total elimination or control of the other known factors (refs. 32-34). The objective of achieving very low wind tunnel disturbance levels approaching anticipated flight simulation levels becomes increasingly difficult as one moves from subsonic to transonic speeds or increases Reynolds number at a given speed. The characteristic disturbances increase in proportion to the tunnel speed or pressure level. Thus, the ability to simulate a free air environment diminishes with the existence and increased level of stream turbulence, radiated sound from the wall boundary layer or drive system, diffuser flow separation disturbances, mechanical vibrations, etc. Previous investigations in wind tunnels and flight have clearly shown that the maximum transition Reynolds numbers obtained with and without suction (ref. 19) on simple and complex geometries critically depend on the characteristic disturbance level and broadband frequency present. Figure 1 summarizes a large quantity of experimental data from previous investigations (refs. 19, 34) that show the effect of disturbance level on transition Reynolds number. The data indicate that low disturbance levels are required ($\bar{u}/u \ll 0.1\%$) for maximum transition Reynolds numbers in wind tunnels. However, there may be limitations in the ability of facilities to achieve diminished disturbance levels and scales compared with flight.

Laminarizing the flow on subscale airfoil models in wind tunnels is generally a more difficult aerodynamic problem than on full scale wing surfaces in flight as previously discussed. In particular, the achievement of moderately high chord Reynolds number simulation on practical size models in most wind tunnels requires testing at high unit Reynolds numbers where characteristic tunnel disturbances dominate, causing early transition. Laminar separation without reattachment may occur at very low Reynolds numbers causing difficulty in measuring airfoil performance (ref. 21). Wind tunnel testing at high unit Reynolds numbers adversely influences the surface tolerance critieria for both NLF and LFC and will strongly affect the suction surface and metering system design; physical dimensions are frequently so small that practical fabrication tolerances for certain model features become difficult to accomplish (refs. 6, 19). Thus, wind tunnel selection is very important for low-drag testing. The major objective is to be able to test large chord and aspect ratio models to reduce scale effects and to have good flow quality.

Establishing the lift performance of low-drag or even turbulent airfoils is very important. Lift performance can be influenced in wind tunnels by large adverse pressure gradients induced by the airfoil at high angles of attack which can cause sidewall juncture boundary-layer separation. Obviously, this separated flow can influence the pressure distribution on the wing and spread across the airfoil span, causing both loss of laminar flow and lift performance. This influence can be compounded by the addition of leading- and trailing-edge high-lift devices on the airfoil during wind tunnel testing. Thus, consideration must be given to model aspect ratio and to sidewall boundary-layer control for high-lift testing.

FACILITIES FOR LOW-DRAG TESTING

Low-Turbulence Pressure Tunnel (LTPT)

The Langley Low-Turbulence Pressure Tunnel (LTPT) is a single-return closed-circuit tunnel which can be operated at pressures from near-vacuum to 10 atmospheres. The test section is rectangular in shape (3 feet wide and 7.5 feet in height and length) and the contraction ratio is 17.6:1. The LTPT is capable of testing at Mach numbers from 0.05 to 0.50 and unit Reynolds numbers from 0.1×10^6 to 15×10^6 per foot. This tunnel has provisions for removal of the sidewall boundary layer by means of a closed-loop suction system mounted inside the pressure chamber. This system utilizes slotted vertical sidewalls just ahead of the model test section, and the removed air is reinjected through an annular slot downstream of the test section. A flow control system allows the flow and pressure requirements to be varied as dictated by tunnel operation. This system can be used to provide boundary-layer control (BLC) for airfoil research.

A BLC system for high-lift airfoil testing is also available. This system utilizes compressed dry air and involves tangential blowing from slots located on the sidewall mounting endplates. Flowmeters can be used to monitor the amount of air blown into the tunnel. An automatically controlled vent valve is utilized to remove the air injected into the tunnel by this system. A high-lift model support and force balance system is provided to handle both single-element and multiple-element airfoils.

The measured turbulence level of the LTPT is very low due to the large contraction ratio and the nine fine-mesh antiturbulence screens. This excellent flow quality facility is particularly suitable for testing low-drag airfoils. Recent flow quality measurements in the LTPT indicate that the velocity fluctuations in the test section range from 0.025 percent at Mach 0.05 to 0.30 percent at Mach 0.20 at the highest unit Reynolds number (refs. 35, 36).

The drive system is a 2000-horsepower direct-current motor with power supplied from a motor-generator set. The tunnel stagnation temperature is controlled by a heat exchanger which provides both heating and cooling using steam injectors and modulated valves that control the flow volume of water through a set of coils. A complete description and calibration of the tunnel are reported in reference 37.

8-Ft. Transonic Pressure Tunnel (8-Ft. TPT)

The Langley 8-Foot Transonic Pressure Tunnel is a closed-circuit single-return variable density continuous-flow wind tunnel with a contraction ratio of 20:1. The test section walls are slotted (5 percent porosity) top and bottom, with solid sidewalls fitted with windows for schlieren flow visualization. In 1981 the facility was modified for flow quality improvements and reconfigured for low-drag testing of a large-chord swept laminar-flow-control airfoil at transonic speeds (ref. 19). A honeycomb and five screens were permanently installed in the settling chamber to suppress the turbulence level in the test section. A contoured liner was installed on all four walls of the test section to simulate interference-free flow about an infinite yawed wing. This contoured liner produces a contraction ratio of 25:1 and covers existing floor and ceiling slots. An adjustable sonic throat is also located at the end of the test section to block upstream propagation of diffuser noise.

The combination of honeycomb, screens, and choke provides a very low disturbance level ($\tilde{p}/p \approx 0.05\%$) in the test region at transonic speeds. Except for the honeycomb and screens, the modifications are reversible. In the current configuration, the stagnation pressure can be varied from about 0.25 to 1.25 atmospheres up to a Mach number of less than 0.85 with the transonic slots closed by the liner. The stagnation temperature is controlled by a water-cooled radiator upstream of the settling chamber. Tunnel air can be dried by a dryer using silica gel desiccant to prevent fogging due to expansion in the high-speed nozzle.

RESULTS AND DISCUSSION

Past and present wind tunnel and in-flight testing has shown that the maintenance of extensive regions of laminar flow by the use of NLF or LFC approaches can provide significant drag reduction for improved aircraft performance. The following discussion is a review of recent wind tunnel tests of advanced design concepts (refs. 17, 19, 38) for low-drag airfoils and some of the effects that the wind tunnel environment has on those results. Also, it is intended to identify influences that are known to affect performance results obtained in wind tunnels that, if not taken into account, can cause concern and rejection of such low-drag airfoils for future application. Several of the 2-D/3-D designed airfoil configurations (refs. 17, 38, 39) shown herein were discussed in detail earlier in this workshop along with discussions of integrated trailing-edge flap designs (ref. 40) for the medium- to high-speed NLF airfoil designs. Thus, no detailed discussion of design concepts will be presented here, only background information, experimental verification, and factors that influence overall results.

Tunnel Flow Quality

Aside from other factors known to affect transition on low-drag airfoils, the maximum transition Reynolds number, with or without boundary-layer control, critically depends on the characteristic disturbance level and broadband frequencies generated in wind tunnels utilized for testing (fig. 1). An example of this effect is shown in figure 2 for several airfoils recently tested in the two NASA Langley wind tunnels developed and used for low drag research. Both facilities operate above and below atmospheric pressure, providing a wide range of Reynolds numbers and Mach numbers from $0.05 < M_\infty < 0.85$ as currently configured. The present flow quality values were measured with conventional hot-wire and acoustic probe techniques (ref. 33). Transition location on the airfoils was measured using surface thin film gages (ref. 41) and is a routine requirement for assessment of laminar patterns or state of the local boundary layer.

For either the NLF or LFC airfoil results in figure 2, the measured logarithm of transition-length Reynolds number varies inversely in proportion to the logarithm of the tunnel disturbance level. As expected, the indicated levels for $(R_X)_{tr}$ with LFC applications are significantly higher than those without suction control as can be seen by comparing past (ref. 12) and present results obtained in the LTPT ($M \approx 0.20$). It should be noted that the extensive lengths of laminar flow measured on the new NASA airfoils (figure 2) generally agree with expectations and that this achievement may in part be attributed to excellent flow quality. Thus, the achievement of high transition Reynolds numbers for low-drag testing may not be possible if acceptable flow quality cannot be realized in test facilities. The selection of suitable facilities would, of course, imply the need for measured and documented flow quality for assessment.

Low-Speed Airfoils - Surface Tolerances

Figure 3 illustrates the airfoil shape and near design velocity distribution over both surfaces and represents a concept developed by industry for long endurance operation requiring high L/D. This configuration was shaped to provide a velocity profile or favorable pressure gradient suitable for maintaining laminar flow back to $x/c \approx 0.30$ on the upper and $x/c \approx 0.75$ on the lower surfaces at a chord Reynolds number of 14×10^6 with zero sweep. This geometry type and velocity distribution are not entirely unfamiliar to today's aerodynamicists in that they resemble those which may be found on sailplanes, low-speed aircraft, and business jets that have utilized NLF for drag reduction and improved performances.

A model of the long endurance airfoil concept was constructed of metal with a 2.7 foot chord and aspect ratio near 1 and instrumented with pressure orifices. The photograph in figure 4 shows the model removed from the tunnel and is a view of the underside leading-edge region illustrating the removable metal cover plate located at near mid-span for access to internal instrumentation and leads. The model was initially tested as received with only minor cleaning of the surface with diluted alcohol.

Wake-rake drag measurements were obtained in the LTPT at one model chord length downstream of the trailing edge at spanwise stations of $y/c = 0$ (mid-span) and $y/c = 0.325$ (10.4 inches from mid-span). The measured surface pressures were integrated to obtain airfoil section lift coefficients. Performance of the low endurance airfoil is summarized in figure 5 for $M_\infty = 0.1$ and $R_c = 14 \times 10^6$ with and without fixed transition. The results clearly indicate that the drag levels obtained at mid-span ($y/c = 0.0$) with free transition were extremely high, indicative of only small lengths of laminar flow. This result is supported by a comparison of the drag levels obtained at mid-span with free or fixed transition on the upper and lower surfaces at $x = 0.03c$.

Visual inspection of the model prior to this initial test revealed that the lower surface may have had adverse roughness effects due to the model cover plate. Therefore, the model was sanded on both surfaces with number 600 carborundum paper and thoroughly cleaned with diluted alcohol in an effort to eliminate the suspected cause for loss of laminar flow. Further precaution was taken by also lightly wiping the surface with a special cloth (tack rag) to remove lint and dust settlement on the horizontally mounted model. Drag measurements were then made at the spanwise station $y/c = 0.325$ to minimize possible lower-surface cover-plate disturbance effects. Figure 5 shows that a drag coefficient of about 0.0055 was measured at a lift coefficient of about 1.2 ($L/D \approx 218$), signifying a large gain in the extent of laminar flow for the improved surface conditions. Upon completion of the test, surface waviness measurements were made at both spanwise stations using a surface dial indicator with fixed legs on a solid base spaced 2 inches apart. The resolution of the dial indicator was determined to be 0.0005 inches. The measured waviness on the long endurance airfoil indicated possible excessive waviness at the mid-span station on both surfaces that would be unacceptable for wind tunnel models and low-drag tests. For example, several waves with height-to-wavelength ratio of $h/\lambda = 0.003$ were measured on both surfaces near $x/c = 0.15$.

Previous research by Carmichael (refs. 28, 29) on low-drag airfoils with and without sweep has provided an empirical expression that represents local allowable waviness for single waves. Carmichael further suggested that one could estimate tolerances for closely spaced multiple waves by multiplying the single wave expression by a factor of 1/3. Since multiple waves were present on the long endurance model surface, the measured $h/\lambda = 0.003$ for single waves was reduced by this factor and compared to Carmichael's empirical expression for several Reynolds numbers and constant sweep angle of 30° (figure 6). Carmichael has shown that only a small reduction in allowable multiple waviness exists for a swept wing compared to unswept wings at low speeds. Also, included in figure 6 are measured values of allowable waviness obtained for other low-drag airfoil models tested in the NASA Langley 8-Ft. TPT and LTPT and subsequently discussed herein. The present results clearly indicate the need for tight control of fabrication tolerances on low-drag wind tunnel models due to scale effects. These tolerances, however, may be relaxed for full scale aircraft surfaces, as suggested in a recent review by Holmes et al. (ref. 14), since scale effects are greatly reduced both by wing chord and low unit Reynolds numbers at cruise conditions ($R/ft < 2 \times 10^6$). The extent of laminar flow at mid-span on the long endurance airfoil model at $R_c = 14 \times 10^6$ ($R/ft = 5.2 \times 10^6$) was probably influenced by increased tunnel turbulence level associated with high unit Reynolds number, in addition to sensitivity of surface conditions.

Low-Speed Airfoils - Shaping

Recent experimental performance results have been obtained in the LTPT for a low-speed NLF airfoil (ref. 18), designated NLF(1)-0414F, and details of the design features are given by Viken (ref. 38). In general, the design objective for this airfoil was to obtain very low cruise drag coefficients by selective shaping of the contour to provide a favorable pressure gradient with extensive laminar flow regions over both upper and lower surfaces and high maximum lift. The design conditions were $c_\ell = 0.43$, $R_c = 10\times10^6$, $M_\infty < 0.40$, and thickness ratio of $t/c = 0.14$. Figure 7 illustrates the calculated design pressure distribution and airfoil section shape. A simple trailing-edge flap having a length equal to 0.125c was incorporated to substantially increase the low-drag c_ℓ range. As can be seen from the design favorable pressure gradient (figure 7), laminar flow is anticipated over both upper and lower surfaces rearward to $x/c = 0.70$. Furthermore, design considerations were given to the achievement of gentle stall characteristics and to maintaining an acceptable lift performance if the airfoil becomes turbulent.

Representative airfoil section data obtained with wake rake and surface pressures are presented in figure 8 for the design Reynolds number with and without fixed transition in the indicated nose regions. For the free transition case, laminar flow was measured on both surfaces back to $x/c = 0.70$ and will be subsequently shown and discussed. Figure 8 shows that a minimum drag coefficient of about 0.0027 was measured at the design lift of about 0.40. This corresponds to $L/D \approx 160$ with zero flap deflection. Furthermore, a value of 1.8 for the maximum lift coefficient was obtained at an angle of attack of 18° while the pitching moment remained relatively constant. However, of major significance is the fact that fixing transition near the leading edge had only a very small effect on the lift performance and $(c_\ell)_{max}$ value at the expense of drag increase. This finding is believed to be a very important improvement over the previous NACA 6-series airfoils which have adverse stall characteristics. In other words, this new NLF airfoil design can also be classified as a very good turbulent flow airfoil in terms of lift performance as well as drag level and pitching moment.

Transition location on the airfoil upper surface was determined by using small thin-film gages that were glued to the model surface at several chordwise and spanwise locations and spaced to eliminate interference effects from one another. These instruments basically operate on the same principle as hot-wire anemometry with overheat ratio set for the sensitivity required for the detection of the state of the local boundary layer where they are placed (ref. 41). This is accomplished by utilizing characteristic behavior of the gages for detection of local changes in heating due to shear stresses of either a laminar, transitional, or turbulent boundary layer. These local changes are recorded as variation of rms output signals with time and require a sufficient number of these gages to be spatially located on the surface to properly identify patterns.

It is essential that each thin-film gage experience a known laminar, transitional, and turbulent flow output signal for a given investigation in order to reference and properly interpret results. This may either be accomplished by starting at sufficiently low Reynolds number test conditions where the output signals for all gages are known to be laminar or by locating a reference gage where it always senses a known turbulent or laminar boundary layer for comparison. Caution should be used when these conventional type gages are located in separated flow zones as to interpretation of results. The output signals in such a zone may indicate similar signals to those for turbulent attached flow.

Figure 9 shows example results taken by J. P. Stack (NASA Langley) from surface mounted thin-film gages on an NLF airfoil model in the LTPT. The gage located at $x/c = 0.40$ and in a known laminar flow region indicates a time-dependent low-level rms output signal with essentially no deviations above or below the mean. As the laminar boundary layer approaches its stability limit, laminar-to-turbulent bursts are locally detected with elapsed time as indicated for $x/c = 0.5$ location. The flow becomes progressively unstable downstream (or with increased Reynolds number) until peak transition occurs with a higher rms level and very random signal with time as seen for $x/c = 0.6$. Once the flow goes through transition to fully turbulent flow ($x/c = 0.7$), the output signal remains high, but the deviations above and below the mean become more consistent. From these type signals obtained over a series of test conditions, the extent of laminar flow could be determined. Figure 10 shows the measured upper surface transition location on the NLF(1)-0414F airfoil with lift coefficient for constant R_c's. The results confirm that the existence of laminar flow was maintained rearward to $x/c = 0.70$ at design $c_\ell = 0.40$ and $R_c = 10\times10^6$. The corresponding wake-rake drag measurements (fig. 8) with free transition support the thin-film results. However, as the lift coefficient is increased above design c_ℓ, transition gradually moves forward, and at $c_\ell = 0.50$, $(x/c)_{tr} = 0.50$. The successful verification of this airfoil's performance is attributed to holding very tight surface tolerances during fabrication and obtaining test results in a wind tunnel with good flow quality. The fabricated and measured surface waviness was held to $h/\lambda = 1/3000$ for single waves and is shown in figure 6 ($h/\lambda = 0.00033$ at $\lambda/c = 0.056$) to be well below other data and that allowable for multiple waves at design $R_c = 10\times10^6$.

The measured drag variation with lift for different flap deflections from $-10° < \delta_f < 20°$ is summarized in figure 11 at $R_c = 6\times10^6$ and $M_\infty = 0.07$. The results indicate that very low drag values can be maintained over a lift coefficient range from $0 < c_\ell < 1.0$. These results were obtained with a simple flap of 0.125c length and offer the potential for long runs of laminar flow over a wide c_ℓ range. Because the NLF(1)-0414F airfoil was shaped (fig. 7) for long regions of accelerated flow necessary to achieve laminarization followed by a rather steep pressure gradient downstream, a laminar separation bubble was anticipated beyond the pressure minimum at low Reynolds numbers. Such bubbles have inherently unstable characteristics that generally cause transition to rapidly move forward with significant lift losses. The existence of a laminar separation bubble on either surface was detected by comparison of measured and predicted pressure distributions (not shown) and associated drag level increase from lift-drag polars. These comparisons clearly indicated that a laminar bubble which existed aft of $x/c = 0.70$ for $R_c < 3\times10^6$ was nonexistent for $R_c > 4\times10^6$.

It is well known that a significant reduction in drag can be realized if flow can be kept attached. One method for reducing the drag associated with the presence of a laminar bubble is to force boundary-layer transition to occur ahead of the bubble causing the flow to remain attached (refs. 42-44). This can be accomplished by the use of turbulators (2D-3D trips, spoilers, sound, passive or active blowing and suction, etc.). Of course, one must account for the "device drag" of the turbulator used. Tests were conducted to evaluate the effectiveness of several turbulators on the NLF(1)-0414F airfoil in the LTPT. Figure 12 illustrates the effect of using simple 2D strips of commercial tape placed at $x = 0.68c$ on both upper and lower surfaces of the model to force transition and eliminate separation bubbles ($R_c = 3\times10^6$, $M_\infty < 0.2$, and $\delta_f = 0°$). A tape 0.012 inch thick and 0.25 inch wide was used. The results (figure 12) clearly show a measured reduction in drag coefficient of about 0.0010 at $c_\ell = 0.40$ with the turbulator tape. Apparently, only a small amount of induced energy by turbulators is required to force transition and attachment of laminar separation bubbles.

The effectiveness of turbulators strongly depends both on their geometry and location since they function like trips or roughness which scale with local boundary-layer properties. Other turbulator devices (not shown) were tested aside from the tape and found to be effective. For example, small vortex generators of $h/c = 0.25$, and 15° leading-edge sweep with respect to flow direction, were spaced ($\Delta y/h = 8$) along the model span at $x/c = 0.60$ and $x/c = 0.70$. Results from using these devices proved very effective in forcing transition and bubble attachment but produced undesirable drag penalty. Probably the most effective turbulator, in terms of both forcing laminar bubble attachment and reducing wake drag with no apparent device drag, was a spanwise row of holes (ref. 42) ahead of $x/c = 0.70$. The holes of diameter $d = 0.0018$ inches, located 0.25 inches apart, were drilled through from the top to bottom surface. Since the design pressure distribution (figure 7) generated a pressure differential across the upper and lower surfaces, passive suction and blowing occur, providing a method for energizing the boundary layer that was sufficient to be effective in these tests. In summary, such devices and techniques as described above appear very promising and economically feasible for application and control of laminar separation bubble attachment with subsequent drag reduction.

High-Speed Airfoils - Shaping

It is well known that the subsonic cruise speeds of high performance aircraft are limited by the onset of the transonic drag rise and that the use of wing sweepback delays this onset (ref. 22). Another method for increasing the cruise Mach number is through the use of geometric shaping which delays the drag rise Mach number. The first airfoils developed in the U.S.A. to delay drag rise were the NACA 1-series (ref. 45). These airfoils were designed to delay the Mach numbers at which supersonic flow first develops locally on the airfoil. These airfoils have significantly higher drag-rise Mach numbers than the earlier NACA four-digit series; however, the low-speed high-lift characteristics are much poorer than those of the earlier airfoils. The NACA 6-series airfoils also provided increased critical speeds with improved drag-rise characteristics compared to the four-digit series but also have small degraded low-speed characteristics. Such airfoils or their derivatives have been used on many first generation subsonic jet aircraft.

The first airfoils designed to purposely delay drag rise by improving the supercritical flow over the upper surface were the "peaky" airfoils. These airfoil shapes generate an isentropic recompression of the supersonic flow on the forward airfoil region and provide some delay in drag rise but also have degraded low-speed characteristics compared to the NACA 6-series airfoils. Whitcomb's research efforts (ref. 22) led to designs which allowed the recompression to move far rearward on the airfoil at transonic speeds and resulted in significant delays in drag-rise Mach number without degrading low-speed characteristics.

Based on the encouraging results obtained by geometric shaping to achieve extensive laminar flow on both surfaces of the low-speed NLF(1)-0414F airfoil, effort has been recently directed towards extension of the concepts to higher speed NLF airfoils. Details of the two-dimensional design concepts have been given by Viken (ref. 38) along with wing body integration by Waggoner (ref. 39) and integrated trailing-edge flap design by Morgan (ref. 40). One of the more promising high-speed NLF airfoil concepts has been fabricated and tested in the NASA Langley LTPT and 6x28-inch transonic tunnel (TT) complex to investigate its low-speed high-lift and drag-rise characteristics. This NASA high-speed natural laminar flow airfoil is designated HSNLF(1)-0213. The airfoil was designed for a lift coefficient of 0.25, Mach number of 0.70, chord Reynolds number of $R_c = 10 \times 10^6$, and $t/c = 0.134$. This particular design was for essentially zero sweep.

The HSNLF(1)-0213 airfoil design pressure distribution and section shape are shown in figure 13. Geometric shaping was expected to provide laminar flow rearward to $x/c = 0.55$ on the upper and $x/c = 0.70$ on the lower surfaces up to $R_c < 10 \times 10^6$. In general, the bottom side of the nose was slightly modified from the NLF(1)-0414F to minimize off-design pressure peaks on the lower surface, and upper surface aft camber was reduced to minimize the possibility of turbulent separation.

Results obtained (not shown) from tests in the 6x28-inch TT indicated good agreement between measured and predicted pressure profiles and that drag rise occurred at about $M_\infty = 0.72$ for $c_\ell \approx 0.2$, and design $R_c = 10 \times 10^6$. The level before drag rise, with and without fixed transition at $x/c = 0.05$, was about 20 to 30 percent below that of a good turbulent airfoil. It should be noted that the turbulence and noise levels are believed to be high in the 6x28-inch TT which operates as a blowdown facility. Thus, poor flow quality contributed to the inability to achieve extensive laminar flow over the model, especially at the higher Reynolds numbers. However, the drag rise characteristics can still be approximated. Surface contour accuracy was measured for the 6-inch chord steel model fabricated and found to be acceptable.

A second HSNLF(1)-0213 airfoil model, fabricated with fiberglass external surfaces, had a 2-foot chord and no flap. This model was tested in the LTPT for low-speed performance evaluation. An example of the results is shown in figure 14 for $M_\infty = 0.168$ and $R_c = 4\times10^6$ with and without fixed transition at $x/c = 0.05$. Figure 14 shows that a minimum drag coefficient of about 0.0038 was measured at $c_\ell = 0.2$ or $L/D \approx 53$. The results indicate that the airfoil displayed trailing-edge-type stall characteristics, and a value of $(c_\ell)_{max} \approx 1.55$ was obtained for $R_c = 4\times10^6$. It is also apparent that fixing transition had only small effects on the lift performance. Figure 15 shows the effect of Mach number and Reynolds number on the maximum lift performance. While the $(c_\ell)_{max}$ increases with increasing R_c for constant Mach number as expected, there is a small effect of Mach number on the maximum lift. For example, results at $M_\infty = 0.1$ are consistently 0.05 higher than results at $M_\infty = 0.2$ over the Reynolds number range tested. Thus, one cannot simulate Reynolds number effects on $(c_\ell)_{max}$ by increasing Mach number at the same time Reynolds number is increased since they have opposing influences.

Boundary-layer transition locations were also obtained by J. P. Stack (NASA Langley) on both surfaces of the HSNLF(1)-0213 airfoil in the LTPT using surface-mounted thin-film gages. A summary of the transition locations on the upper and lower surfaces compared with predictions from the Eppler theory (refs. 46-47) is shown in figure 16 for $\alpha = 0°$ and chord Reynolds number from 3.0×10^6 to 9×10^6. The data clearly indicate that laminar flow was maintained rearward to about $x/c \approx 0.5$ and $x/c \approx 0.70$ on the upper and lower surface, respectively, up to $R_c = 8\times10^6$, before any forward movement of transition was measured.

Low Reynolds Number Airfoils

For airfoils designed to operate at low Reynolds numbers ($R_c < 500\times10^3$), the existence of a laminar separation bubble and turbulent separation significantly increase the drag and decrease the lift, both of which contribute to low lift-to-drag ratios. This phenomenon has previously been extensively investigated and discussed (refs. 21, 48-51). Increasing the Reynolds number will reduce the length of the laminar separation bubble and extent of turbulent separation. At positive incidence, the boundary layer, which is laminar along the airfoil's upper-forward surface, separates at the downstream adverse pressure-gradient recovery region. It then quickly undergoes transition to turbulent flow in the separated shear layer.

Depending on the Reynolds number and the severity of the adverse pressure gradient, this separated turbulent boundary layer may or may not reattach to the airfoil surface. If reattachment occurs, the turbulent boundary layer may then separate again near the trailing edge. If the Reynolds number is sufficiently low such that reattachment does not occur, increasing the Reynolds number to some critical value will cause reattachment that corresponds to a dramatic increase in L/D. Thus, the possible existence of both laminar and turbulent separation should be considered in the design and wind tunnel testing of airfoils in the low Reynolds number regime. For example, such airfoils are typical of those on current RPVs, sailplanes, and general aviation aircraft canards.

Mangalam and Pfenninger (ref. 52) have recently designed a low Reynolds number airfoil and tested it in the 12"x18" open-circuit tunnel at the NASA Langley 8-Ft. TPT complex at low speeds. The airfoil section shape and an example of the measured and predicted pressure distributions are shown in figure 17 for $R_c = 100\times10^3$, $c_\ell = 1.0$, and $\alpha = 4°$. Basically, the airfoil was shaped to have moderate negative camber in the nose region to reduce pressure peaks at off-design and attached flow. The forward lower surface cusp is due to combined leading-edge thickness and camber and requirement for increased mid-chord thickness for structural strength. This airfoil is designated LRN(1)-1007 and represents about a 40% increase in t/c and an appreciable increase in c_ℓ/c_d at design (fig. 18) above previous similar airfoils (ref. 51).

Except for the upper surface aft region, good agreement is shown between the measured and predicted pressures using the Eppler theory (ref. 46) for the smooth model. The measured data indicate a long separation bubble in the rear upper-surface pressure-rise region, with reattachment near the trailing edge. Mangalam and Pfenninger (ref. 52) concluded from these results that at low Reynolds number the laminar boundary layer is highly stable and a number of trips are required in several locations along the chord to promote transition. Applications of the 2-D spanwise trips (ref. 52) eliminated the laminar separation bubble and provided about a 25% increase in lift-drag ratio. Subsequent flow visualization photographs were obtained of the model flow field in the same tunnel, using smoke wire techniques*, and are shown in figure 19 illustrating the occurrence of laminar separation with incidence angle for $R_c = 40{,}000$. Figure 19 shows attached flow over most of the airfoil surface at $\alpha = 3°$. However, for $\alpha = 18°$, separation occurs at the leading edge and never reattaches. Similarly, for $\alpha = -12°$, the lower surface separates without reattachment. It can be seen from these photographs that the measurement and verification of the performance of low Reynolds number airfoils with separated flow become highly questionable.

---

*Smoke wire technique was developed and results obtained by Amir Bar-Sever and Dr. S. Mangalam, under contract to AAB, NASA Langley.

High-Lift Testing - Sidewall Effects

Depending upon model aspect ratio and facility utilized, testing of airfoils at high angles of attack can result in severe tunnel sidewall interference effects. Large adverse pressure gradients can be induced by the airfoil at incidence that cause the oncoming tunnel sidewall boundary layer to separate, spread downstream and spanwise, and result in a large decrease in airfoil lift. The following results and discussion attempt to illustrate this influence on high-lift performance for low-drag or turbulent airfoils.

Figure 20 shows lift performance results for the same single-element airfoil tested in two different NASA Langley facilities at $M_\infty = 0.30$ and $R_c = 6x10^6$. The models tested in the LTPT and 6x28-inch TT had aspect ratios of 1.5 and 1.0, respectively. The results indicate that severe sidewall interference effects occur in the 6x28-inch TT for angles of attack greater than about 10°. This resulted in measured maximum lift coefficient for this airfoil in the 6x28-inch TT that was about 17 percent lower than in the LTPT. Figure 21 shows photographs of oil flow patterns obtained in the 6x28-inch TT with the airfoil having an aspect ratio of 1.0 for $8^\circ < \alpha < 12^\circ$. A complex secondary flow field that nearly dominates the entire model span is seen to develop due to sidewall interference as model incidence is increased. Separated flow occurs on either side of mid-span for $\alpha = 12^\circ$ causing drastic lift loss (fig. 20).

To ensure that models experience uniform, two-dimensional, interference-free air flow when testing multi-element airfoils, some feasible concept is required for tunnel sidewall boundary-layer control (BLC). The LTPT has recently been modified to incorporate a BLC system (ref. 37) which includes both upstream sidewall suction slots ahead of the model and tangential blowing slots located on the same tunnel walls near the model juncture region. This system provides a means for reducing the oncoming boundary-layer thickness as well as energizing the boundary layer locally around the model for maintaining attached flow as incidence is increased.

The effects of sidewall BLC on the lift performance of a multi-element airfoil using tangential slot blowing near the nose and flap regions are shown in figure 22. Slot blowing is applied until the lift at mid-span (obtained from surface pressure data) is approximately matched with the lift near the tunnel sidewalls. The results shown in figure 22 indicate large differences in lift coefficient at high incidence between the mid-span and near wall regions without blowing compared to the results with blowing. With blowing, the measured lift values at mid-span and near wall regions are essentially the same. Thus, one should use caution in conducting high-lift performance testing or verification to select a facility that accommodates large-aspect-ratio models or that has sidewall control for reducing interference effects to insure meaningful results.

In addition to the interference effects produced by separation of the boundary layer on the vertical sidewalls, corrections are required to account for model and wake blockage and interference due to test section floor and ceiling constraints on streamline curvature. Tests are planned in the LTPT to evaluate these interference effects by testing high-lift models with chord lengths of 1 and 2 feet. Lift coefficients up to about 4.0 are expected from these models.

High-Speed Airfoils - Shaping and Suction

The concept of combining geometric shaping and suction laminarization on airfoils to achieve very low drag dates back to the late 1930's (refs. 4-5). The basic feasibility of achieving full chord laminar flow with very low drag on swept nonsupercritical LFC wings was pioneered by Pfenninger (ref. 5) with suction applied through many closely spaced surface slots on the wings. Results were obtained on large chord wing sections (modified 66012) of 30° sweep and $t/c = 0.12$ in three different wind tunnels. These studies confirmed earlier beliefs that results were dependent on the characteristic turbulent and acoustic disturbance levels in each facility. Since this research demonstrated the potential for significant drag reduction through application of LFC, an interest in evaluating the feasibility of combined suction laminarization and supercritical airfoil technology at conditions which are typical of high-performance transports has been generated. Therefore, a large chord ($c = 7.07$ ft.) swept supercritical LFC airfoil with suction slots has been designed, constructed, and recently tested in the NASA Langley 8-Ft. TPT. This NASA airfoil is designated SCLFC(1)-0513F. Details of the airfoil and suction system design along with the test setup have been reported (ref. 19). Requirements for this test also included modification of the wind tunnel to achieve the desired flow quality and test section wall contouring to simulate free air flow about an infinitely yawed model at transonic speeds.

Figure 23 shows the design pressure distribution for the swept supercritical LFC airfoil. Attempts were made to minimize suction laminarization through a highly tailored pressure distribution and choices of leading-edge sweep, chord Reynolds number, and crossflow Reynolds number (ref. 6). Depending on geometry, boundary-layer instabilities that can occur on swept wings are leading-edge instability, Tollmien-Schlichting tangential instability, crossflow instability, and Taylor-Goertler instability due to surface concave curvature. These instability regions are shown in figure 23 for the LFC airfoil and indicate where combined shaping and suction were applied for control. A rather large supercritical zone (aspect ratio = 0.37) exists over the upper surface flat-pressure region followed by a steep rear pressure rise. The lower surface is seen to be heavily loaded in the fore and aft regions with a small supercritical zone in between.

Figure 24 shows the measured and designed chordwise pressure distributions for two chord Reynolds numbers at $M_\infty = 0.82$ on the LFC airfoil that are generally in good agreement. Essentially shock-free flow was obtained for the results shown. The slightly overall higher velocities on the upper surface and chordwise deviations from design are attributed to classical problems associated with transonic wind tunnel testing, wall interference, and model deformation under design air loads. The velocity field between the upper surface-tunnel wall channel (supersonic bubble zone) was higher than predicted due to the contoured liner wall and inability to completely account for three-dimensional boundary-layer displacement thickness effects in the design analysis. Measured coordinate deviations from design, obtained with a dial indicator under applied simulated design airloads, were about 0.003-inch on the model forward upper surface at mid-span. This deviation corresponds to $h/\lambda = 0.0015$ for multiple waves and is shown in figure 6 to meet allowable criteria based on earlier results at low speeds but well above the projected goal for supercritical airfoils (ref. 19). The data in figure 24 indicate that flow separation occurs on the lower surface at about $x/c = 0.80$ when the Reynolds number is increased from $R_c = 10 \times 10^6$ to 20×10^6. Since transition correspondingly moved rapidly forward on the lower surface, the flow into the trailing-edge cusp apparently was unable to sustain the adverse pressure gradient. This separated flow changes the local effective area distribution of the test section resulting in a slightly higher freestream Mach number and increased sensitivity to local surface conditions and pressure variations.

The measured chordwise suction coefficient (C_Q) distribution required to maintain full-chord laminar flow over both surfaces at the design Mach number and $R_c = 10 \times 10^6$ is shown in figure 25 compared to prediction. The measured required suction was higher than the theory over most of the upper and lower surfaces. The higher suction requirements were attributed to the previously discussed higher than anticipated velocities and surface pressure irregularities, the higher suction control required to overcome cross-flow instabilities associated with the steep pressure gradients on the upper and lower surface nose and aft regions, and the minimization of centrifugal Taylor-Goertler type boundary-layer instabilities and interactions with crossflow in the concave regions of the lower surfaces.

A summary of the measured transition locations on the LFC airfoil upper surface for several Mach numbers is shown in figure 26. These results were obtained from a grid of flush-mounted surface thin-film gages to detect the state of the local boundary layer. Full chord laminar flow was maintained on both surfaces up to $R_c = 10 \times 10^6$ for all Mach numbers. As Reynolds number was increased for constant Mach number, transition moved gradually forward on the upper surface. The Reynolds number at which this forward movement began was dependent on Mach number. It was concluded that suction laminarization over a large supercritical zone is feasible to high chord Reynolds numbers even under nonideal surface conditions on a swept LFC airfoil at high-lift conditions.

Analysis of both spanwise pressure distributions and transition patterns revealed that the flow over the yawed wing was not two-dimensional at $M_\infty < 0.80$. It is believed that the resulting spanwise gradients influenced suction requirements and laminarization at the lower speeds.

The total drag at $M_\infty = 0.40$ and 0.82 for $R_c = 10 \times 10^6$ with full chord laminar flow is seen in figure 27 to be equal to about $(c_d)_{tot} = 0.0030$. This represents about 60-percent drag reduction as compared to an equivalent turbulent airfoil drag level of about $c_{dw} = 0.0080$ and a lift-to-drag ratio of about 180 based on design c_ℓ. Total drag is the sum of measured wake rake drag (c_{dw}) at mid-span and the suction drag (c_{d_s}) penalty required to maintain laminar flow. The suction required to maintain full chord LFC was somewhat higher than anticipated (figure 25) and the contribution of suction drag penalty was about 40-percent for the upper and 60-percent for the lower surface. The increase in wake drag for $M_\infty > 0.70$ was attributed to the formation of a weak shock wave at the leading-edge region as the supersonic bubble began to develop. As the bubble develops ($0.78 < M_\infty < 0.80$), full chord laminar flow still exists, but periodic turbulent bursts occur over the upper surface causing an increase in wake drag. As Mach number is increased to 0.82, the supersonic zone spreads rearward to about 80-percent chord, the bursts disappear, and the wake drag returns to near its subsonic level (figure 27). It is concluded that the basic phenomenon of applying suction laminarization over an extensive supercritical zone is feasible up to high chord Reynolds numbers as demonstrated on a swept LFC airfoil at high lift conditions. The major difficulty or influence in achieving this result was that of overcoming the classic "non-ideal" wind tunnel test environment and hardware tolerances.

CONCLUDING REMARKS

Laminarization through passive or active methods is a boundary-layer stability problem which has been proven to be difficult to analyze, control, and verify. This is especially true as one moves from low to high speeds where swept-back wings and higher lift-to-drag ratios are desirable for improved aircraft performance.

In an effort to simulate flight conditions on models in wind tunnels, we need to better understand the environment and its influences on high-lift and low-drag testing. Several factors influencing the performance of low-drag airfoils have been identified which are primarily involved with overcoming the classic "nonideal" wind tunnel test environment and hardware tolerances.

NASA Langley has recently developed several advanced low-drag airfoil concepts with and without boundary-layer suction control for achieving extensive laminar flow with very low drag. Verification of the anticipated performance of these concepts through wind tunnel testing, from subsonic to transonic speeds, has shown significant improvements in lift-to-drag ratio over previous airfoils designed for low drag. Probably the most significant result at subsonic speeds is that the lift performance for these lower drag airfoil concepts is not degraded with fully turbulent flow over the airfoil surface. This provides a factor of safety in aircraft operation, should laminar flow be lost due to contamination. Suction laminarization over a large supercritical zone has been shown to be feasible to high chord Reynolds numbers even under non-ideal surface conditions on a swept LFC airfoil at high lift.

REFERENCES

1. Jacobs, Eastman N.: "Preliminary Report on Laminar Flow Airfoils Method Adopted for Airfoil and Boundary Layer Investigations", NASA WR L-345, June 1939.

2. Abbot, Ira H.; and von Doehhoff, Albert E.: "Theory of Wing Sections", New York, Dover Publications. 1959.

3. Pfenninger, W.: "Investigations on Reduction of Friction on Wings, in Particular by Means of Boundary Layer Suction." NASA Technical Memorandum 181, August 1947.

4. Lachmann, G. V. (Editor): Boundary Layer and Flow Control, Vol. 2, Pergamon Press, 1961.

5. Pfenninger, W.: Laminar Flow Control, Laminarization. AGARD-R-654, Von Karmon Institute, Belgium, 1977.

6. Pfenninger, W.; Reed, H. L.; and Dagenhart, J. R.: "Design Considerations of Advanced Supercritical Low Drag Suction Airfoils." Viscous Flow Drag Reduction, Vol. 72, Progress in Astronautics and Aeronautics, 1980.

7. Gray, W. E.: "Transition in Flight on a Laminar-Flow Wing of Low Waviness (King Cobra)". R.A.E. Report N. 2364, March 1950.

8. Gray, W. E.; and Fullam, P. W. J.: "Comparison of Flight and Wind Tunnel Measurements of Transition on a Highly Finished Wing (King Cobra)". R.A.E. Report No. 2383, June 1950.

9. Pfenninger, W.; and Growth, E.: "Low Drag Boundary Layer Suction Experiments in Flight on a Wing Glove of an F-94A Airplane with Suction Through a Large Number of Fine Slots". Boundary Layer and Flow Control, Vol. 2, G. V. Lachmann, ed., 1961, pp. 981-999.

10. Fowell, L. R.; and Antonatos, P. P.: "Laminar Flow Control Flight Test Results, Some Results from the X-21A Program". Part 2, Recent Developments in Boundary Layer Research, Part IV, May 1965. AGARDograph 97, pp. 1-76.

11. Loftin, L. K. Jr.; and Burrows, D. L.: "Investigations Relating to the Extension of Laminar Flow by Means of Boundary-Layer Suction Through Slots". NACA TN 1961, 1949.

12. Braslow, A. L.; Burrows, D. L.; Tetervin, N.; and Visconti, F.: "Experimental and Theoretical Studies of Area Suction for the Control of the Laminar Boundary Layer on an NACA 64A010 Airfoil". NACA Rept. 1025, 1951.

13. Holmes, Bruce J.; Obara, Clifford, J.; and Yip, Long P.: "Natural Laminar Flow Experiments on Modern Airplane Surfaces." NASA TP-2256, June 1984.

14. Holmes, Bruce J.; Obara, Clifford J.; Martin, Glenn L.; and Domack, Christopher S.: "Manufacturing Tolerance for Natural Laminar Flow Airplane Surfaces." SAE Paper 850863, April 1985.

15. Croom, C. C.; and Holmes, B. J.: "Flight Evaluation of an Insect Contamination Protection System for Laminar Flow Wings." SAE Paper 850860, April 1985.

16. Somers, Dan M.: "Design and Experimental Results for a Flapped Natural Laminar Flow Airfoil for General Aviation Applications." NASA Technical Paper, 1965.

17. Viken, Jeffrey K.: "Aerodynamic Design Considerations and Theoretical Results for a High Reynolds Number NLF Airfoil." Master's Thesis. George Washington University. January 1983.

18. McGhee, Robert J.; Viken, Jeffrey K.; Pfenninger, W.; Beasley, William D.; and Harvey, William D.: "Experimental Results for a Flapped NLF Airfoil with High Lift/Drag Ratio." NASA TM-85788, May 1984.

19. Harvey, W. D.; and Pride, J. D.: "The NASA Langley Laminar Flow Control Airfoil Experiment." AIAA Paper No. 82-0567, March 1982.

20. Reshotko, Eli: "Control of Boundary Layer Transition." AIAA-85-0562, 1985.

21. Mueller, T. J.: "The Influence of Laminar Separation and Transition on Low Reynolds Number Airfoil Hysteresis." AIAA-84-1617, 1984.

22. Whitcomb, R. T.: "Review of NASA Supercritical Airfoils." ICAS Paper No. 74-10, Aug. 1974.

23. Dagenhart, J. R.: "Amplified Crossflow Disturbances in the Laminar Boundary Layer on Swept Wings with Suction." NASA TP-1902, November 1981.

24. El-Hady, Nabil M.: "HADY-I, a FORTRAN Program for the Compressible Stability Analysis of Three-Dimensional Boundary Layers." NASA CR-3467, 1981.

25. Srokowski, A. J.; and Orszag, S. A.: "Mass Flow Requirements for LFC Wing Design." AIAA Paper No. 77-1222, Aug. 1977.

26. El-Hady, N. M.: "On the Stability of Three-Dimensional Compressible Nonparallel Boundary Layers." AIAA Paper No. 80-1374, July 1980.

27. Mack, L. M.: "On the Stability of the Boundary Layer on a Transonic Swept Wing." AIAA Paper No. 79-0264, Jan. 1979.

28. Carmichael, B. H.: "Surface Waviness Criteria for Swept and Unswept Laminar Suction Wings." NOR-59-438, 1959.

29. Carmichael, B. H.: "Surface Imperfection Experiments on a Swept Laminar Suction Wing." Northrop Rept. BLC-124, NOR-59-454, 1959.

30. Poll, D. I. A.: "Leading Edge Transition on Swept Wings." AGARD CP-224, pp. 21-1-21-11, 1977.

31. Ram, R. B.; Vemuru, C. S.; and Harvey, W. D.: "Hybrid Approach to Steady Transonic Normal Shock-Compressible Laminar Boundary Layer Interactions over Airfoils with Suction." AIAA 85-0522, 1985.

32. Pate, S. R.: "Effects of Wind Tunnel Disturbances on Boundary-Layer Transition with Emphasis on Radiated Noise: A Review." AIAA Paper No. 80-0431, March 1980.

33. Owen, F. K.; Stainback, P. C.; and Harvey, W. D.: "An Evaluation of Factors Affecting the Flow Quality in Wind Tunnels." AGARD Conference Proceedings No. 348 on Wind Tunnels and Testing Techniques, July 1979.

34. Harvey, W. D.; and Bobbitt, P. J.: "Some Anomalies Between Wind Tunnel and Flight Transition Results." AIAA Paper 81-1225, 1981.

35. Harvey, W. D.; Stainback, P. C.; and Owen, F. K.: "An Evaluation and Assessment of Flow Quality in Selected NASA Wind Tunnels." NASA TM-85659, August 1983.

36. Stainback, P. Calvin; and Owen, F. Kevin: "Dynamic Flow Quality Measurements in the Langley Low Turbulence Pressure Tunnel." AIAA-84-0621, 1984.

37. McGhee, Robert J.; Beasley, William D.; and Foster, Jean M.: "Recent Modifications and Calibration of the Langley Low-Turbulence Pressure Tunnel." NASA TP-2328, July 1984.

38. Viken, J. K.: "Boundary Layer Stability and Airfoil Design." NASA CP-2413, 1986.

39. Waggoner, E. G.: "Computational Wing Design Studies Relating to Natural Laminar Flow." NASA CP-2413, 1986.

40. Morgan, Harry L.: "High-Lift Flaps for Natural Laminar Flow Airfoils." NASA CP-2413, 1986.

41. Dagenhart, J. Ray; and Stack, John P.: "Boundary-Layer Transition Detection Using Flush-Mounted Hot-Film Gages and Semiconductor Dynamic Pressure Transducers." AIAA Paper No. 82-0593, March 1982.

42. Horstmann, K. H.; and Quast, A.: "Reduction of Section Drag by Blowing Through Rows of Holes in Areas of Laminar Separation Bubbles," Technical Soaring, Vol. VII, No. 1, September 1981.

43. Pfenninger, W.: "Investigation on Reductions of Friction on Wings in Particular by Means of of Boundary Layer Suction. NACA TM 1181, August 1947. (Translated from the German "Untersuchungen uber Reibungsverminderungen an Tragflugeln, insbesondere mit Hilfe von Grenzschtabsaugung," Mitteilungen aus dem Inst. fur Aerodynamik, Nr. 13, Zurich, 1946).

44. Champine, R.; and Blanchard, W.: "Airplane Model Experiments with Wedge-Shaped Strips Mounted on the Upper Wing Surface." Soaring, vol. 18-19, 1955.)

45. Stack, John.: "Tests of Airfoils Designed to Delay the Compressibility Bubble. NACA TN-976, 1944.

46. Eppler, Richard; and Somers, Dan M.: "A Computer Program for the Design and Analysis of Low-Speed Airfoils," NASA TM-80210, August 1980.

47. Eppler, Richard; and Somers, Dan M.: "Low Speed Airfoil Design and Analysis." Proceedings of the NASA Advanced Technology Airfoil Research Conference, NASA CP-2045, Part 1, March 1978.

48. Mueller, T. J.; and Pohlen, L. J.: "Boundary Layer Characteristics of the Miley Airfoil at Low Reynolds Numbers," AIAA-83-1795, July 1983.

49. Miley, S. J.: "On the Design of Airfoil for Low Reynolds Numbers," Proceedings of the Second International Symposium on the Technology and Science of Low-Speed Motorless Flight, The Soaring Society of America, Inc., September 1974.

50. Lissaman, P. B. S.: Low Reynolds Number Airfoils. Annual Review of Fluid Mechanics, Vol. 15, 1983.

51. Pfenninger, W.: Experimental Investigation of an Airfoil with High Lift-To-Drag Ratios at Low Reynolds Numbers. Northrop BLC-Report 84 (NAI 560188), 1956.

52. Mangalam, S.; and Pfenninger, W.: "Wind-Tunnel Tests on a High Performance Low-Reynolds Number Airfoil." AIAA-84-0628, 1984.

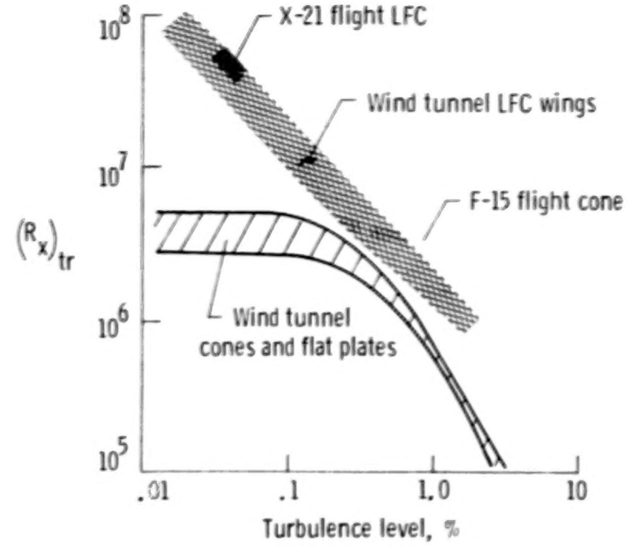

Figure 1.- Influence of turbulence level on transition Reynolds number.

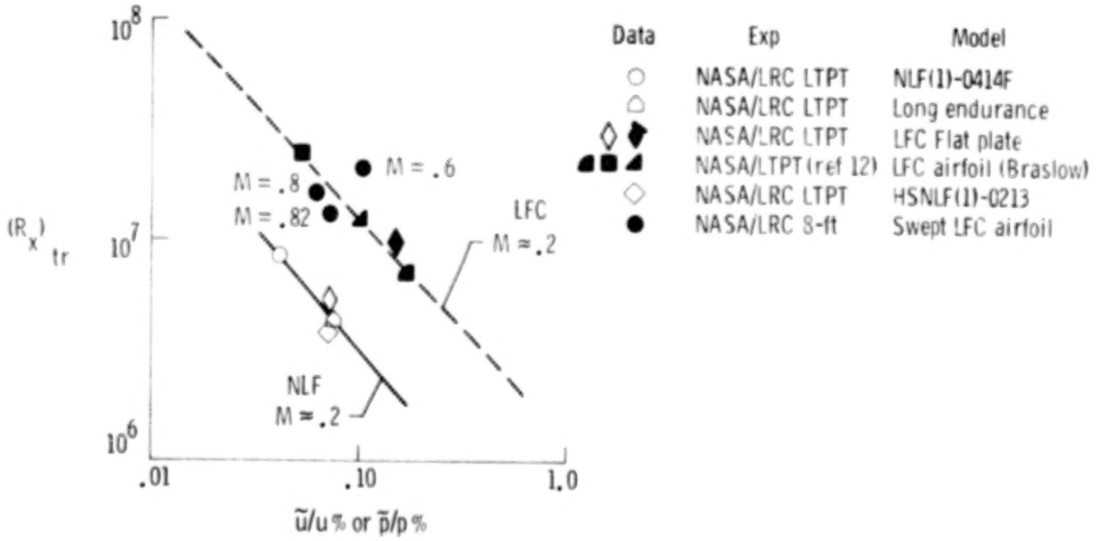

Figure 2.- Influence of tunnel disturbance level on measured maximum transition Reynolds number for low-drag airfoils in two NASA Langley tunnels.

ORIGINAL PAGE IS
OF POOR QUALITY

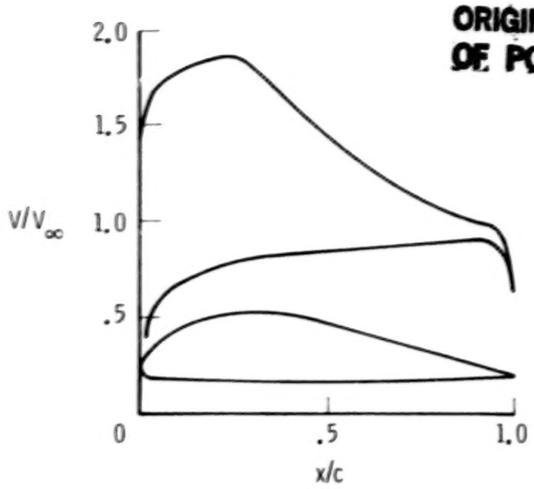

Figure 3.- Velocity distribution for long endurance airfoils.

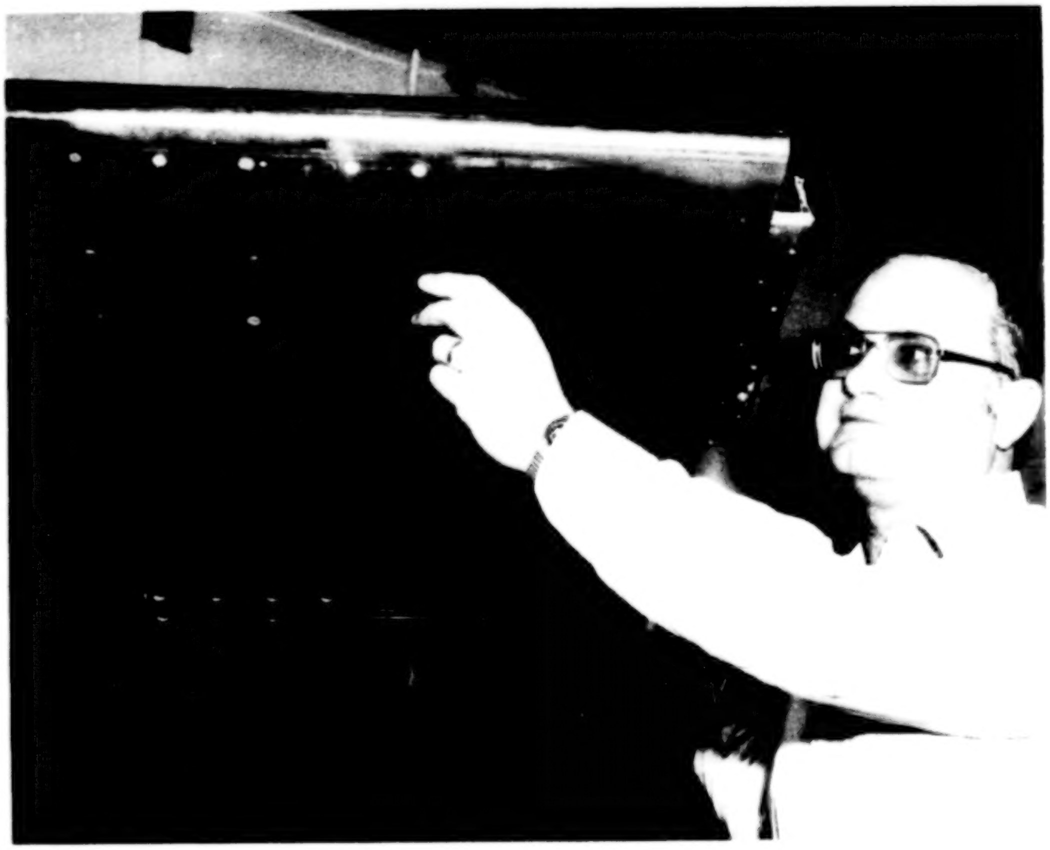

Figure 4.- Long endurance laminar-flow airfoil tested in the Low-Turbulence Pressure Tunnel.

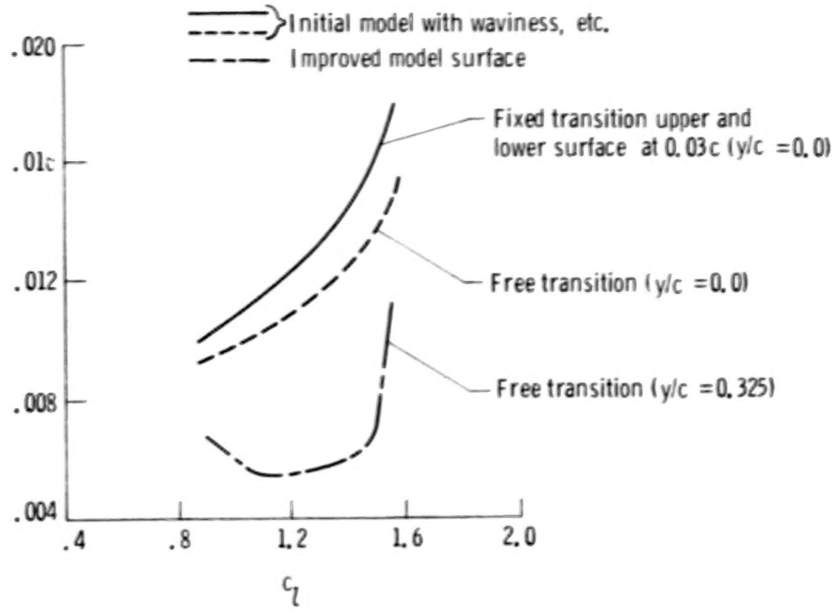

Figure 5.- Long endurance laminar flow airfoil results from LTPT. M = 0.10, $R_c = 14 \times 10^6$.

$$\left(\frac{h}{\lambda}\right) = \frac{1}{3}\left[\frac{59000 \cos^2 \Lambda}{\lambda/c \, (R_c)^{1.5}}\right]^{.5} \quad ; \Lambda = 30°$$

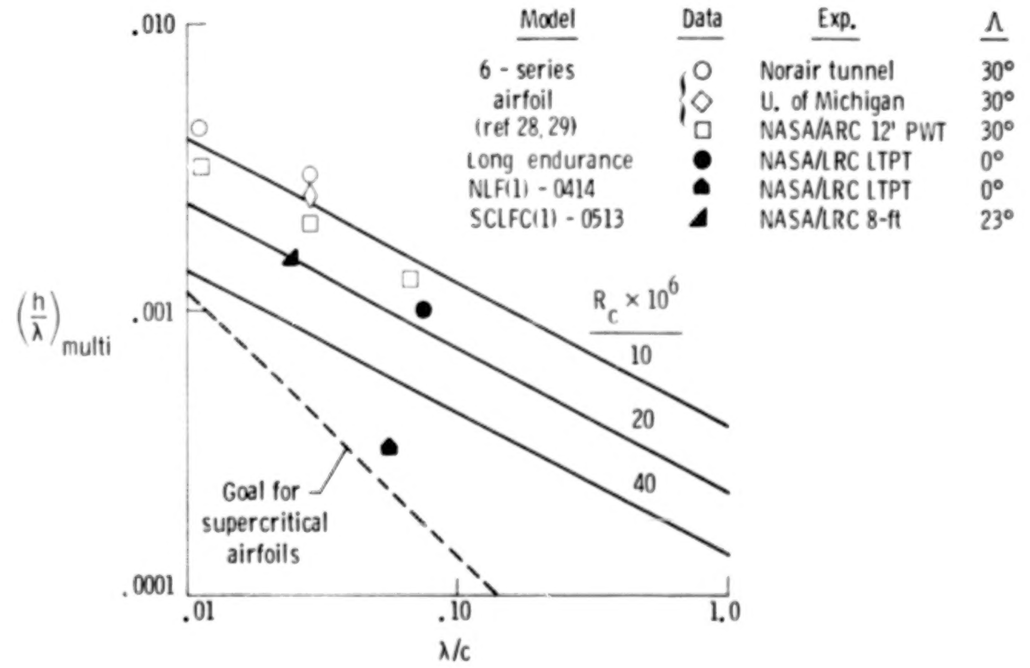

Figure 6.- Permissible amplitude ratio (h/λ) of multiple waves for airfoils in wind tunnels.

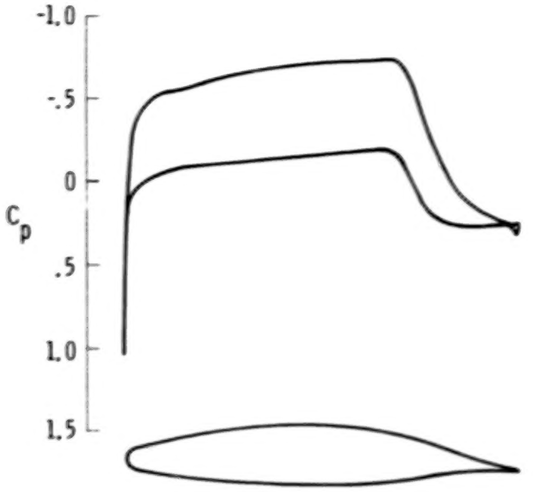

Figure 7.- Calculated pressure distribution for NLF(1)-0414F airfoil at design conditions. $c_\ell = 0.43$, $M = 0.40$; $R = 10.0 \times 10^6$.

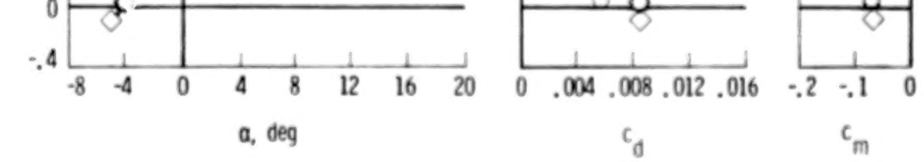

Figure 8.- Section data for NLF(1)-0414F airfoil. $R_c = 10 \times 10^6$, $M = 0.10$.

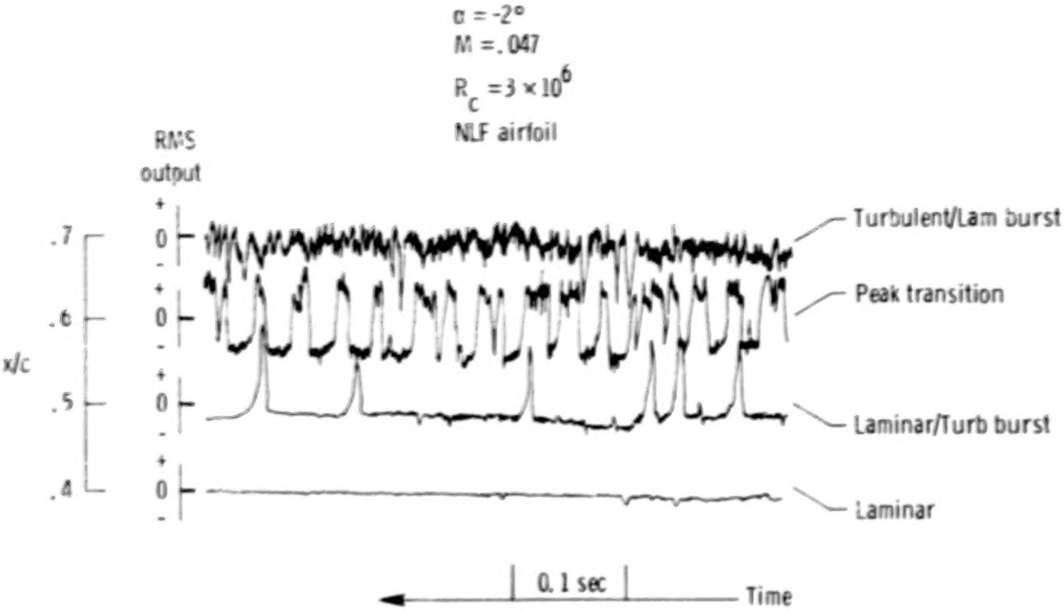

Figure 9.- Example oscillograph recorder traces of thin-film gage RMS output signals with time for state of boundary-layer detection.

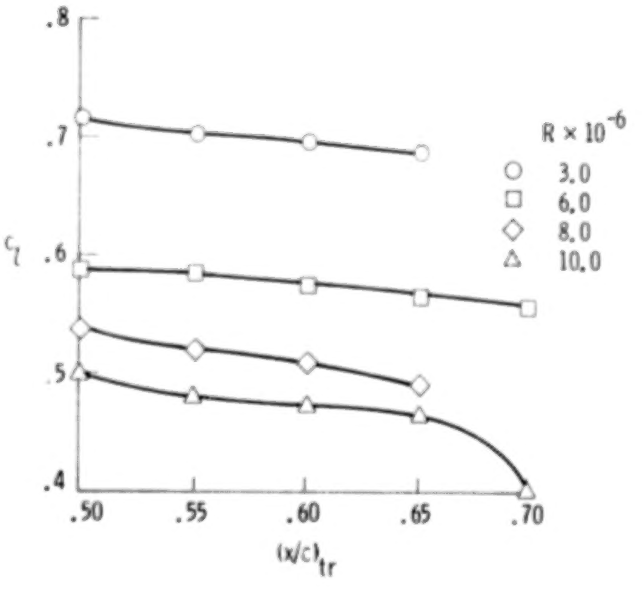

Figure 10.- Upper-surface transition location as determined from thin-film data for NLF(1)-0414F airfoil.

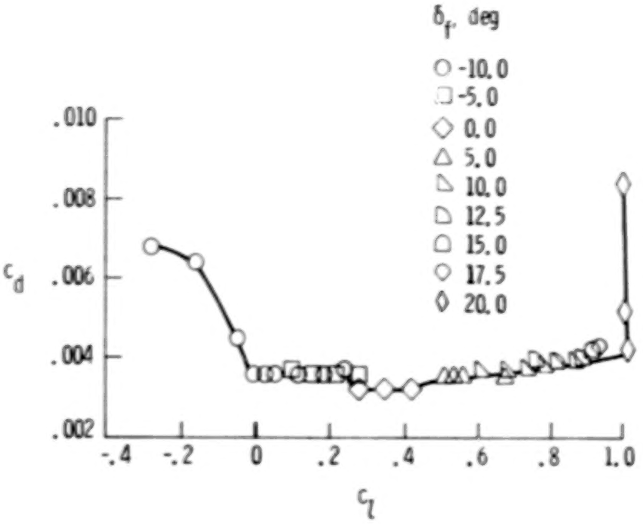

Figure 11.- Effects of flap deflection for NLF(1)-0414F airfoil. $R_c = 6.1 \times 10^6$, M = 0.07.

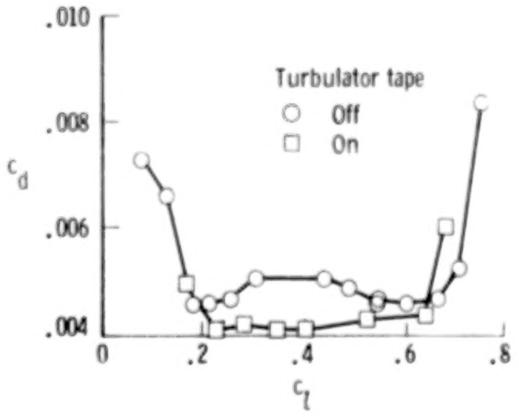

Figure 12.- Effect of turbulator tape on section characteristics for NLF(1)-0414F airfoil. $R_c = 3.0 \times 10^6$; $M < 0.20$; $\delta_f = 0°$.

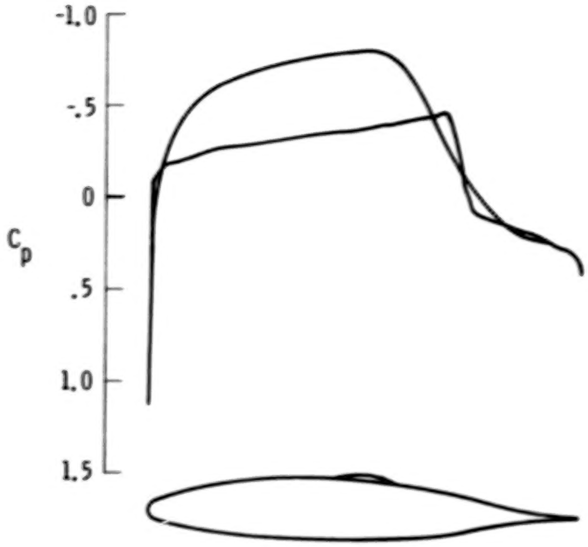

Figure 13.- Design pressure distribution for HSNLF(1)-0213 airfoil. $M = 0.70$; $c_\ell = 0.20$.

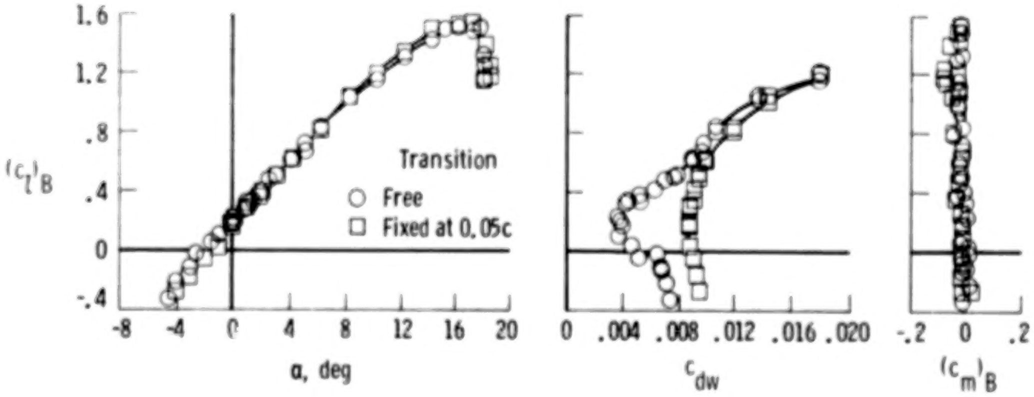

Figure 14.- Section data for HSNLF(1)-0213 airfoil in LTPT. $M = 0.168$; $R_c = 4 \times 10^6$; $\delta_f = 0°$.

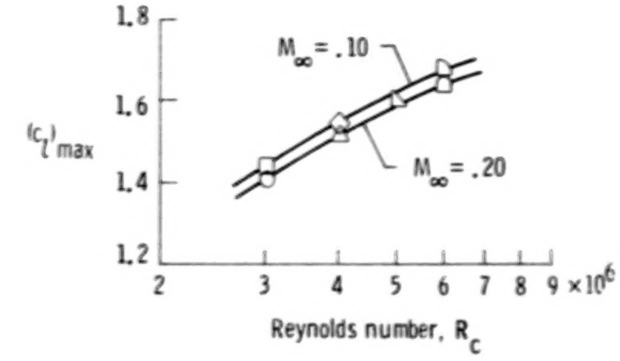

Figure 15.- Effect of Mach number and Reynolds number on maximum lift coefficient performance for NASA HSNLF(1)-0213 airfoil; $\delta_f = 0°$.

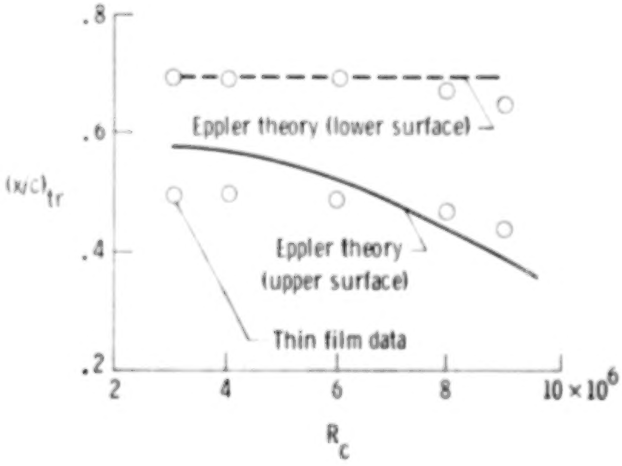

Figure 16.- Transition location for HSNLF(1)-0213 airfoil; $M < 0.20$, $\alpha = 0°$.

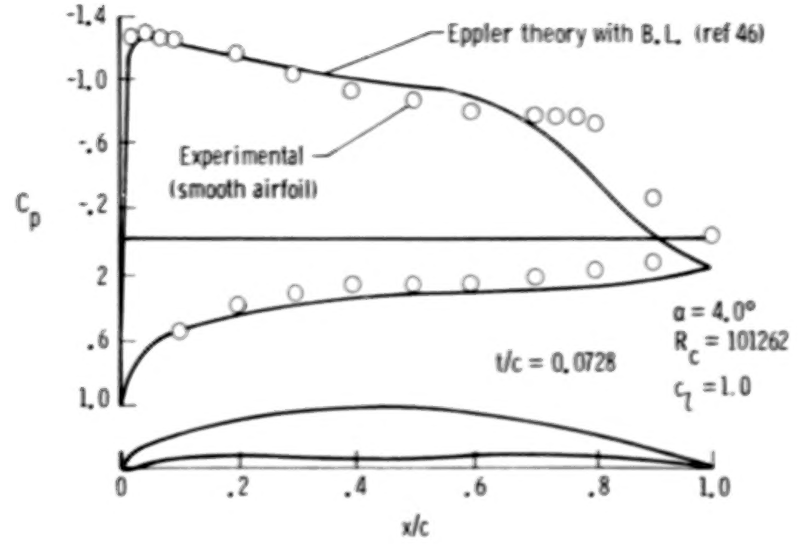

Figure 17.- Measured and predicted pressure distribution for LRN(1)-1007 airfoil.

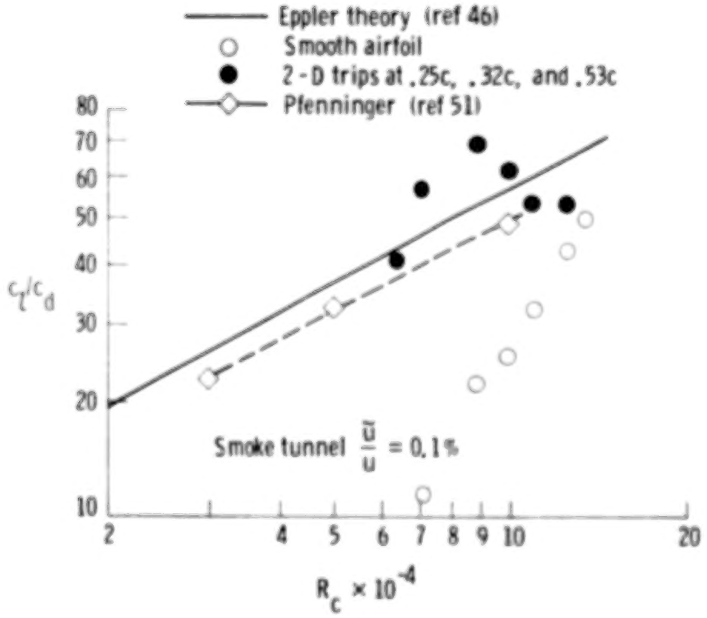

Figure 18.- Maximum lift/drag variation with Reynolds number on LRN(1)-1007 airfoil.

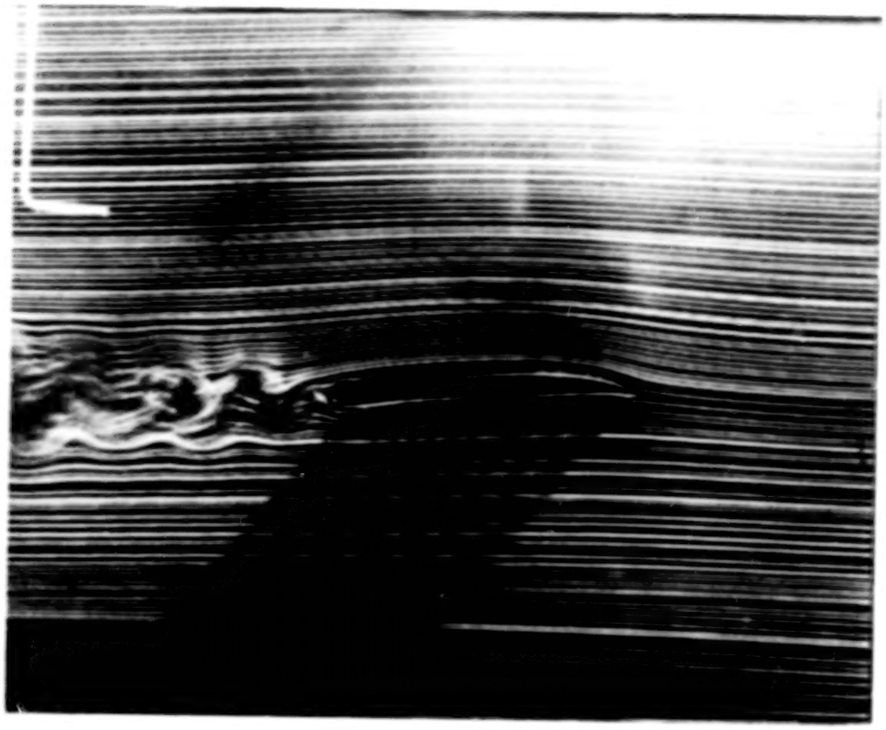

(a) α = 3°.

ORIGINAL PAGE IS
OF POOR QUALITY

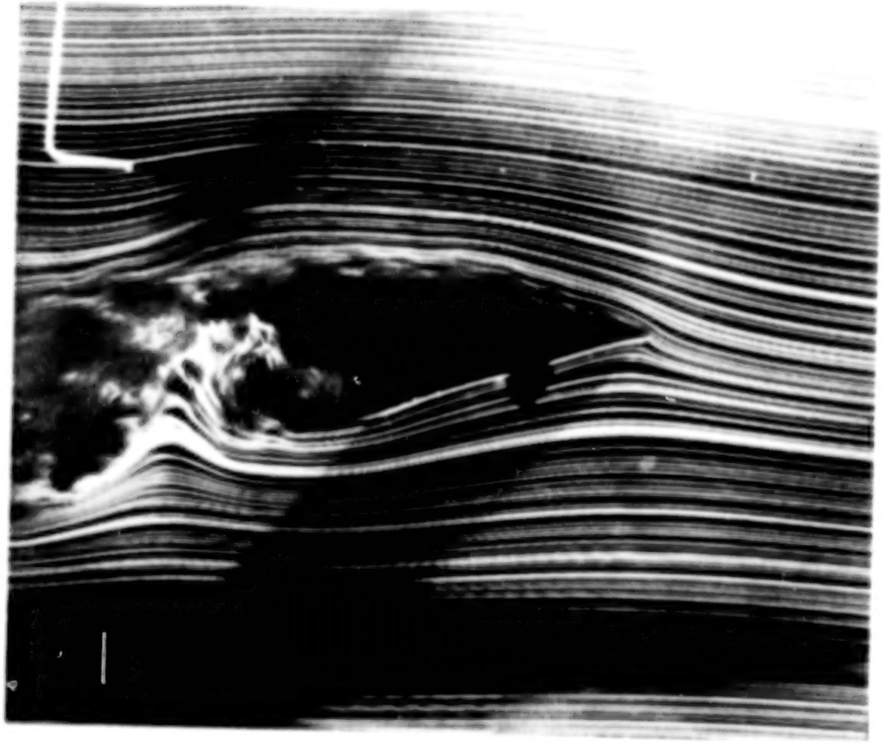

(b) α = 18°.

Figure 19.- Smoke-wire flow visualization photographs for LRN(1)-1007 airfoil. R_c = 40,000.

ORIGINAL PAGE IS
OF POOR QUALITY

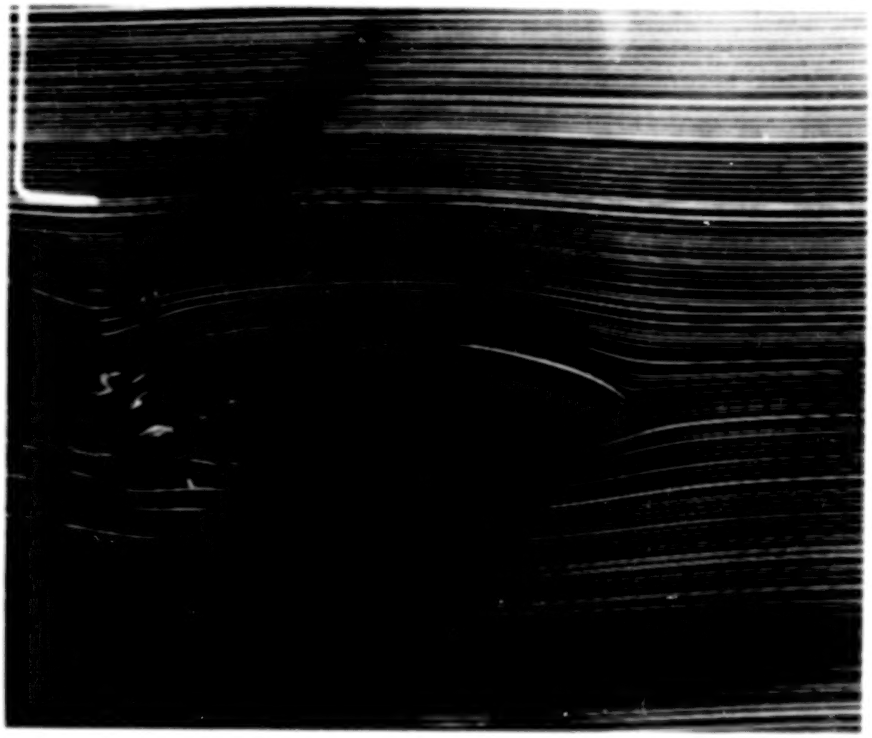

(c) $\alpha = -12°$.

Figure 19.- Concluded.

ORIGINAL PAGE IS
OF POOR QUALITY

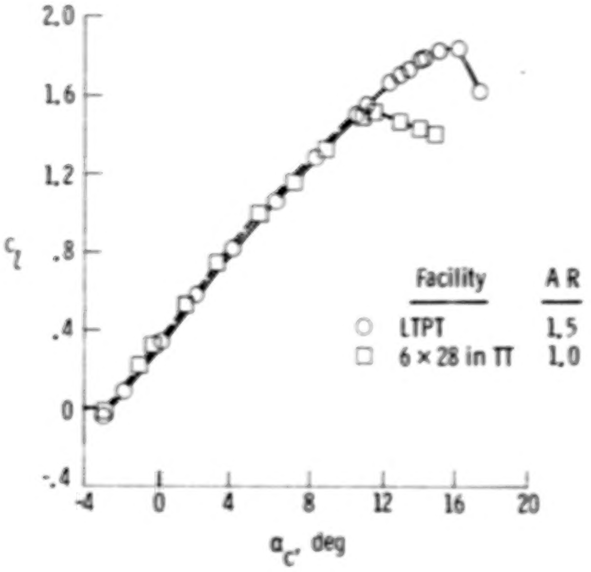

Figure 20.- Tunnel sidewall effects for single-element airfoil. $M = 0.30$; $R_c = 6.0 \times 10^6$.

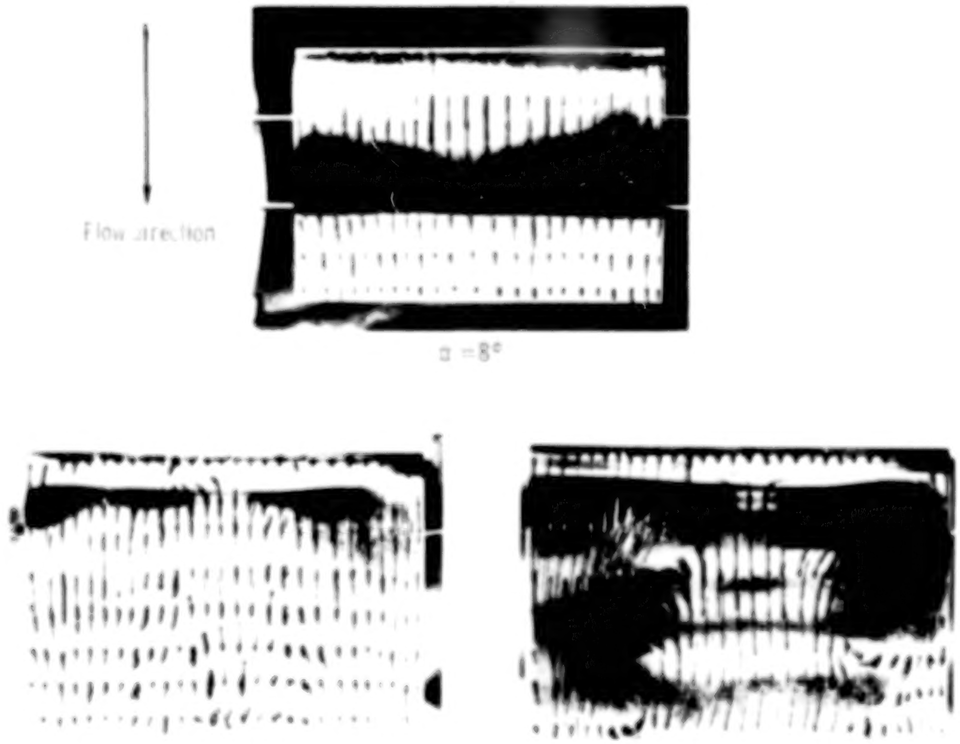

$\alpha = 8°$

$\alpha = 10°$

$\alpha = 12°$

Figure 21.- Oil flow pattern of single-element airfoil illustrating tunnel sidewall effects in 6 × 28-inch TT.

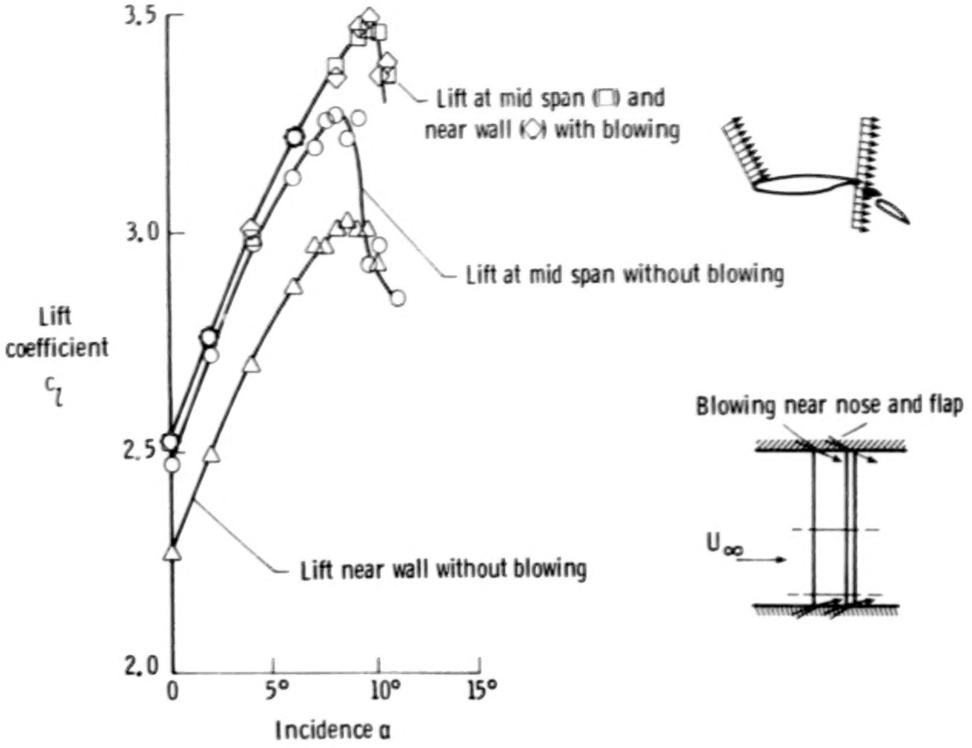

Figure 22.- Typical tunnel sidewall effects for multi-element airfoil showing requirement for sidewall boundary-layer control.

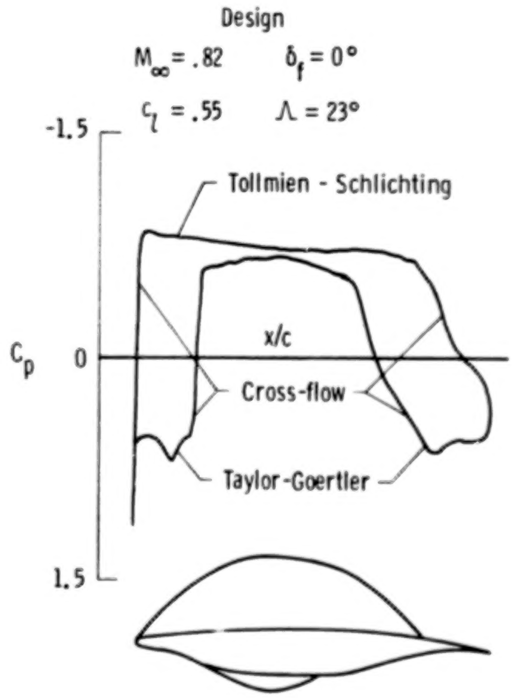

Figure 23.- Design chordwise pressure distributions and sonic lines on the LFC airfoil section.

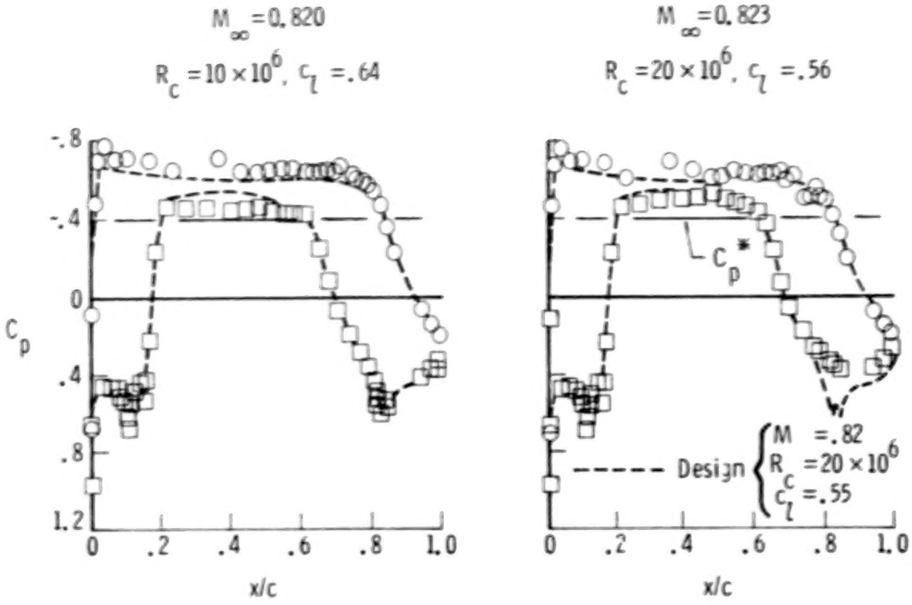

Figure 24.- Comparison of measured and design pressure distribution for swept LFC airfoils.

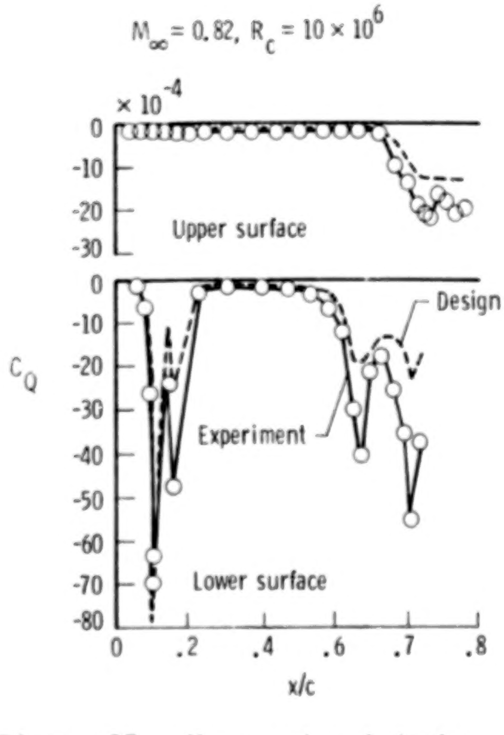

Figure 25.- Measured and design suction distributions for swept LFC airfoil.

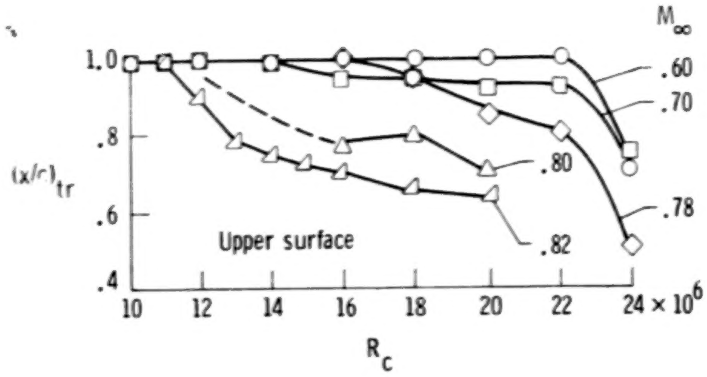

Figure 26.- Variation of measured transition location with Reynolds number for swept LFC airfoil.

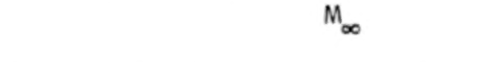

Figure 27.- Measured variation of drag with Mach number for swept LFC wing. $R_c = 10 \times 10^6$.

55-34 ,9P

N88-23742

BOUNDARY-LAYER FLOW VISUALIZATION FOR FLIGHT TESTING

Clifford J. Obara
PRC Kentron, Inc.
Aerospace Technologies Division
Hampton, Virginia 23666

SUMMARY

Flow visualization is used extensively in flight testing to determine aerodynamic characteristics such as surface flow direction and boundary layer state. Several visualization techniques are available to the aerodynamicist. Two of the most popular are oil flows and sublimating chemicals. Oil is used to visualize boundary-layer transition, shock wave location, regions of separated flow, and surface flow direction. Boundary-layer transition can also be visualized with sublimating chemicals. A summary of these two techniques is discussed, and the use of sublimating chemicals is examined in some detail. The different modes of boundary-layer transition are characterized by different patterns in the sublimating chemical coating. The discussion includes interpretation of these chemical patterns and the temperature and velocity operating limitations of the chemical substances. Information for selection of appropriate chemicals for a desired set of flight conditions is provided. With the introduction of new aircraft utilizing laminar flow for drag reduction, flow visualization is an important diagnostic tool which supplements other analytical measurements for validation of aerodynamic design behavior.

INTRODUCTION

Past flight research has made extensive use of flow visualization for determining aerodynamic characteristics such as boundary-layer state (laminar, transitional, turbulent, or separated), shock wave location, and surface flow direction. Measurement of these characteristics becomes important to the aerodynamicist with the introduction of modern smooth aircraft surfaces which are compatible with laminar flow requirements. Flow visualization can be used for determining the boundary-layer transition characteristics while supplementing other analytical measurements for validation of aerodynamic design behavior.

Several techniques have been developed for in-flight flow visualization including sublimating chemicals (refs. 1 and 2) and oil flow (ref. 3). Each technique has its own advantages and disadvantages. The oil flow technique can provide information for a wide variety of flow conditions from boundary-layer transition to flow separation and shock wave location. At the same time oils can be very messy and must be viewed during flight. The sublimating chemical method provides a detailed pattern of boundary-layer transition that can be examined on the ground following the flight test. Whereas oil flow can show regions of laminar and turbulent separation, sublimating chemicals are far more useful for determining transition modes including the cases of crossflow and Tollmien-Schlichting types of instabilities, as well as laminar separation.

The purpose of this paper is to describe the sublimating chemical technique for flow visualization. A method for selecting appropriate chemicals based on a set of flight conditions is provided. A brief description on the use of oils for flow visualization is included. The advantages of both flow visualization techniques for testing modern aircraft are discussed.

SYMBOLS

a	constant used in determining vapor pressure
b	constant used in determining vapor pressure
c	constant used in determining vapor pressure
g_s	rate of transfer of mass from unit area of surface, oz/s-ft^2
K_g	local mass transfer coefficient
m	molecular weight of a substance
m_∞	molecular weight of the free stream
M	Mach number
p	static pressure, mm Hg
p_s	absolute vapor pressure, mm Hg
R	recovery factor
R'	unit Reynolds number, ft^{-1}
T	temperature, °C or °F
T_{aw}	adiabatic wall temperature, °C or °F
V_∞	free-stream velocity, fps
γ	specific heat ratio, $\gamma = 1.4$
ρ	density of diffusing vapor, slugs/ft^3
ρ_∞	free-stream density, slugs/ft^3
ψ	concentration, ρ/ρ_∞
ψ_∞	concentration in the free stream
ψ_s	concentration corresponding to saturation

SUBLIMATING CHEMICALS

Description of Technique

The chemical sublimation method for indicating boundary-layer transition was developed at the Royal Aircraft Establishment by W. E. Gray in 1944 (ref. 1). Originally devised for low-speed wind tunnel testing, the method was extended to aircraft in flight with the introduction of more durable coating materials. The sublimation method has the advantages of simplicity, rapidity, low cost in operation, and ability to provide a very detailed graphic record of the transition from laminar to turbulent flow over the surface. For many flight applications, the chemical pattern developed at the desired test condition can be viewed on the ground following the flight. The method has been effective at subsonic speeds for temperatures down to -20°F and altitudes up to about 20,000 ft and at supersonic speeds up to Mach 2 for temperatures down to -70°F and altitudes up to 55,000 ft (ref. 4).

The sublimation method for indicating boundary-layer transition involves coating the surface to be observed with a very thin film of a volatile chemical solid. During exposure to a free-stream airflow, areas develop in which the chemical film evaporates more rapidly due to greater local shear stress within the boundary layer as depicted in figure 1. Greater rates of sublimation will occur in regions of high shear stress or skin friction such as that found in turbulent flow. The regions near stagnation on the surface will also have high shear stresses and hence greater rates of sublimation.

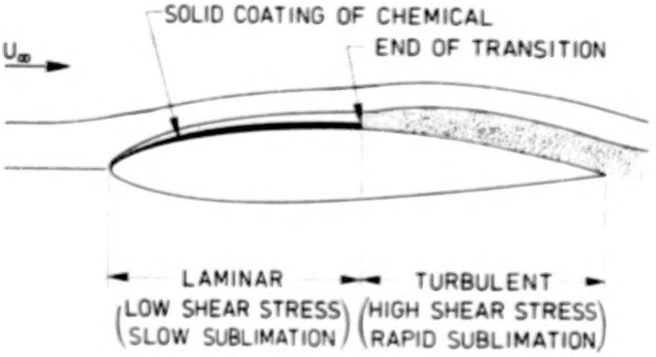
SOLID COATING OF CHEMICAL
END OF TRANSITION
U_∞
LAMINAR
(LOW SHEAR STRESS SLOW SUBLIMATION)
TURBULENT
(HIGH SHEAR STRESS RAPID SUBLIMATION)

Figure 1.- How sublimating chemicals indicate boundary-layer transition.

There are several criteria necessary for the coatings to remain solid, opaque, and durable at temperatures for which transition indications are obtained and examined. The chemicals must have high melting points, be resistant to moisture, have no adverse effects on surface finishes, have low vapor pressures for aerodynamic use, and be soluble in a fast evaporating carrier. These considerations restrict the possible compounds to solids with melting points above 50°C, of low or medium molecular weights, and high hydrogen content. The types of solid compounds suitable are hydrocarbons, esters, alcohols, ethers, ketones, acylamines, and azohydrocarbons (ref. 2). Another consideration for selecting appropriate chemicals is safety from health hazards associated with the use of such compounds. Four useful compounds which meet these requirements and provide a practical range of operating characteristics (sublimation rates) are naphthalene, biphenyl, acenaphthene, and fluorene, listed in Table 1. An added feature of fluorene is its fluorescent properties, which make it possible to obtain high quality photographic transition pattern data by using ultraviolet lighting.

Table 1. Practical Sublimating Chemicals for Transition Visualization

Chemical Substance	Chemical Formula Molecular Weight
Naphthalene	$C_{10}H_8$ 128.17
Biphenyl	$C_6H_5C_6H_5$ 154.21
Acenaphthene	$C_{10}H_6$-1,8-CH_2CH_2 154.21
Fluorene	$C_6H_4CH_2C_6H_4$ 166.22

The solvents used must have low toxicity, low corrosiveness, and high volatility. Water and the low-volatility alcohols have insufficient vaporizing characteristics to be used as solvents. Some of the esters which are low in toxicity are corrosive to metals in long-term use. The solvents found to be most suitable are acetone and light petroleum fractions such as 1,1,1 trichloroethane and trichlorotrifluoroethane (Freon TF). The requirement for a highly volatile solvent is a result of the process by which the sublimating chemicals are applied to the surface. A technique called "dry-spraying" is used whereby the chemical solute is dissolved in the solvent and the solution is sprayed onto the surface. It is necessary that the solvent be almost completely evaporated before the spray solution has time to wet the surface, leaving the sublimating chemical coating on the surface.

The chemical is applied to the test surface by compressed-air spraying. A solution of 8 parts solvent to 1 part solute (by volume) has been found to be nearly optimum for uniform application. The solution is ready for spraying when the solute has completely dissolved. When using standard compressed-air spray equipment, good control in uniform thickness of the chemical coating is best achieved using a spray gun with a flat fan nozzle of minimum size orifice and needle (orifice diameter between 0.030 and 0.040 in.). Spraying is done using about 25 psi air pressure, for either siphon feed or pressure feed equipment. If pressure feed equipment is used, the reservoir pressure should be about 5 psi. The spray nozzle should be held between 10 to 20 in. from the surface being coated for proper dry-spraying. Proper spray technique will produce a powdery matte appearance of the chemical coating, whereas when the spray goes on too wet, the coating appears crystalline. After spraying, the chemical coating is brushed with a large soft bristle brush, wiped with cheesecloth, and rubbed by hand (using rubber gloves) to loosen chemical particles which can adhere to the coating and cause turbulent wedges.

A standard rate of chemical solution application is one quart per 20 to 30 ft^2. At the application rate of 20 ft^2 per quart, a very heavy coating will result. Depending on temperature and airspeed, such a coating thickness has a sufficiently long reaction time to permit ample off-condition flight time for takeoff, climb, descent, and landing without affecting the chemical pattern developed at the test condition. This feature permits transition data to be observed and recorded on the ground. Extra thick coatings can be applied by brushing the surface between repeated applications of a "standard" thickness. This technique can be useful for thick applications of rapidly sublimating chemicals to extend the allowable off-condition time for climb to high altitude test conditions, for example.

During the test flight, airspeed and altitude should be held as long as needed to obtain a transition pattern. If the fuel burn at the test condition changes airplane weight by more than about ten percent, a speed schedule should be worked out to keep the airplane lift coefficient constant (for conditions where compressibility can be ignored). For high-speed tests where compressibility is a factor, an altitude schedule should be flown to maintain a constant Mach number at constant indicated airspeed. For most flight measurements of transition using the sublimating chemicals, response time is sufficiently rapid that constant speeds and altitudes can be flown, and weight changes have an insignificant effect on transition location.

The use of an intentional boundary-layer trip, such as a very small piece of tape located within 6 in. of the leading edge, is a useful method of providing a "calibrated" indication of the rate of transition pattern development in the chemical coating. When the chemical pattern appears mature, the descent and approach should be flown as near to the indicated test speed and as close in to the landing as is safe. Since at most test conditions of interest, pattern development times are greater than 10 minutes, ample time is usually available for normal approaches and landings.

Selection of Chemicals

Selecting an appropriate chemical for a given flight condition requires an understanding of the chemical process involved. The rate of sublimation is simply the rate of transport of a foreign gas through the boundary layer. Thus, the rate of mass transfer will depend on the surface concentration of the diffusing gas. The sublimation rates can be approximated by considering the relationships between diffusion, heat transfer, and skin friction. This paper covers only the principal equations for predicting sublimation rates; a more detailed analysis appears in reference 5.

The rate at which mass is transferred across a unit area of the surface, g_s, is given by

$$g_s = K_g \rho_\infty V_\infty (\psi_s - \psi_\infty) \qquad (1)$$

where K_g is the local mass transfer coefficient, ρ_∞ and V_∞ are the free-stream density and velocity, and ψ_s and ψ_∞ are the foreign gas concentrations at the surface and the free stream, respectively. The concentrations can be represented by the general form

$$\psi = \frac{\rho}{\rho_\infty} \qquad (2)$$

where ρ is the density of the diffusing vapor. For the sublimation process occurring in air, ψ_∞ can be taken as zero; however, determination of ψ_s is less obvious. There are two stages for the sublimation of a substance into a stream of air (ref. 5). The first stage is purely molecular and takes place in a very thin layer near the surface. It involves a continuous evaporation and recondensation of gas molecules in the surface layer of chemicals. The second stage can be represented by the diffusion through the boundary layer of those molecules which escape from the surface layer. The number of molecules that do escape can be determined by the difference between the partial pressure of the vapor at the surface and the saturation pressure. It has been shown (ref. 5) that the concentration at the surface corresponds closely to saturation. This can account for the fact that relatively smaller amounts of molecules are carried away from the surface as compared to the larger quantity evaporating and recondensing in the surface layer. For the sublimation of substances used for boundary-layer observation, the concentration at the surface can be approximated by

$$\psi_s = \frac{m\ p_s}{m_\infty\ p_\infty} \qquad (3)$$

where m and m_∞ are the molecular weights of the substance and the air, respectively, p_s is the absolute vapor pressure, and p_∞ is the free-stream static pressure.

By combining equations (1) and (3) and assuming that $\psi_\infty = 0$, the rate of sublimation can be rewritten as

$$g_s = K_g\ \rho_\infty\ V_\infty\ \left(\frac{m}{m_\infty}\right)\ \left(\frac{p_s}{p_\infty}\right) \qquad (4)$$

Rearranging equation 4 using the ideal gas law yields

$$g_s = \frac{K_g}{R}\ \left(\frac{m}{m_\infty}\right)\ \frac{V_\infty\ p_s}{T} \qquad (5)$$

For most liquids and solids, the variation of vapor pressure with temperature will follow the Clasius-Clapeyron law and is expressed as

$$\log_{10}\ p_s = -52.23\ \frac{a}{(T + b)} + c \qquad (6)$$

where p_s is the vapor pressure in millimeters of Hg at temperature T in °C, and a, b, and c are constants for a particular substance. Approximate values of a, b, and c for the four solids selected as suitable boundary-layer transition indicators are taken from references 6 and 7 and are reproduced in Table 2. It must be mentioned here that values of p_s for a particular substance are not always consistent from one source to another. Some of these differences result from the difficulty of determining very low (at T < 0°C) vapor pressures. Figure 2 shows the relation between vapor pressure and temperature from equation (6) over a range of temperatures compatible with flight operations.

Table 2. Vapor Pressure Constants for Selected Sublimating Chemicals

Chemical Substance	a	b	c
Naphthalene	30.759	187.22	6.846
Biphenyl	53.942	273.10	8.221
Acenaphthene	54.279	273.10	8.033
Fluorene	56.615	273.10	8.059

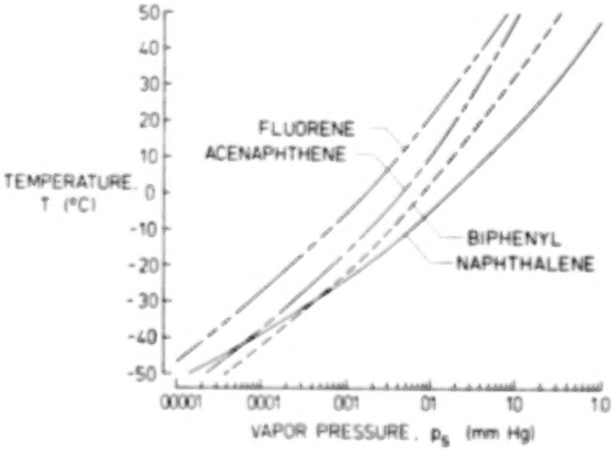

Figure 2.- Vapor pressures of sublimable solids.

For first approximations, the local mass transfer coefficient K_g is proportional to the local skin friction. In regions of high skin friction such as near the stagnation or attachment line or in the turbulent boundary layer, values of the local mass transfer coefficient will also be high. A complete description and analysis of this mechanism are available in reference 5.

Based on past flight experiments, a practical summary is provided in figures 3 and 4 to guide selection of suitable chemicals for given test conditions. These recommendations will allow reasonable times for chemical pattern development at the test conditions and still provide adequate time for off-condition (climb and descent) portions of a flight profile. As given by equation 5, the rate of sublimation is proportional to ambient temperature, free-stream velocity, and local skin friction.

Figure 3 presents the operating temperature ranges of the four chemicals. Each solid bar represents typical limits, while the dashed ends suggest variability resulting from coating thickness. For the fastest sublimating solid, naphthalene, the useful temperature range at subsonic speeds is from -50°F < T < 32°F. Biphenyl and acenaphthene have subsonic temperature ranges of -20°F < T < 80°F and 32°F < T < 100°F, respectively. A subsonic temperature range for fluorene would be 60°F < T < 120°F. The additional data point for fluorene at the low temperature was for a supersonic aircraft (M = 2.0) tested by McTique et al. (ref. 4). One of the factors that allow the use of sublimating chemicals at supersonic speeds is that the adiabatic wall temperature rises with compressibility. Since the chemicals are affected by this wall temperature, rates of sublimation are higher than would be normal at the free-stream temperature. The relationship between the adiabatic wall temperature and the free stream is

$$T_{aw} = T \left(1 + R \left(\frac{\gamma-1}{2}\right) M^2\right) \qquad (7)$$

where γ is taken as 1.4 and R is the recovery factor. For a laminar boundary layer, the recovery factor is approximately 0.84, whereas for a turbulent boundary layer, the recovery factor is approximately 0.88. These suggested practical temperature ranges are based on the experiences of the author and on other published flight results.

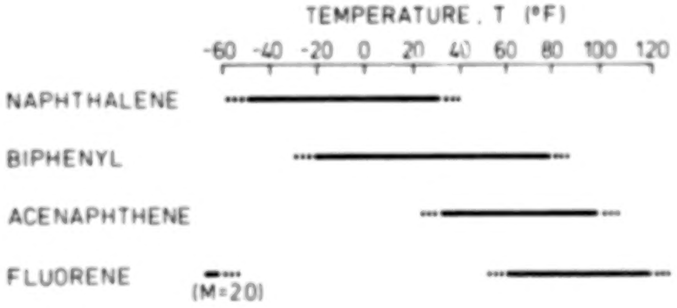

- SUBLIMATION RATE IS ALSO PROPORTIONAL TO DYNAMIC PRESSURE (SKIN FRICTION)

Figure 3.- Temperature operating ranges for selecting sublimable chemicals.

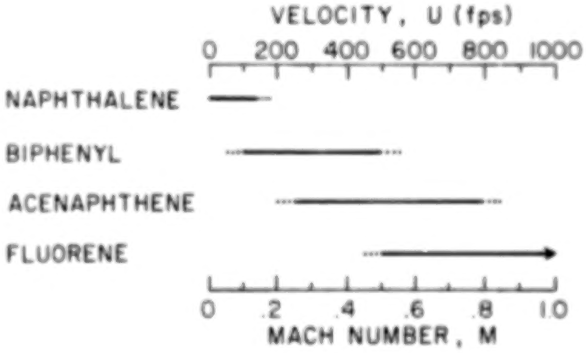

- BASED ON SEA LEVEL STANDARD DAY CONDITIONS

Figure 4.- Velocity operating ranges for selecting sublimating chemicals.

As previously mentioned, the free-stream velocity affects the sublimation rate of a particular chemical. Based on the author's experience, suggested practical velocity ranges for each of the selected chemicals are presented in figure 4. These ranges are valid for sea-level standard day conditions. It is important to remember that the solid bar represents typical limits with standard coating thicknesses. Naphthalene can be used up to about 150 fps. Biphenyl works well in the low subsonic range of 50 fps to 500 fps, whereas acenaphthene is useful from 250 fps on up to transonic speeds of around 800 fps. A practical velocity range for fluorene would start from around 500 fps and go up to supersonic speeds.

The transition mechanism or mode can be determined by analysis of the chemical patterns which develop. Typical patterns for four modes of transition are shown in figure 5. Tollmien-Schlichting instability transition is characterized by a ragged transition line. A crisp straight line is indicative of the presence of laminar separation. When there are streamwise striations in the chemical coating followed by a very jagged transition line, crossflow or Görtler instability is the transition mechanism. The fourth type of transition pattern is formed by roughness. A typical shape would be a thin trail behind the element quickly followed by a turbulent wedge, usually having an included angle of about 15°.

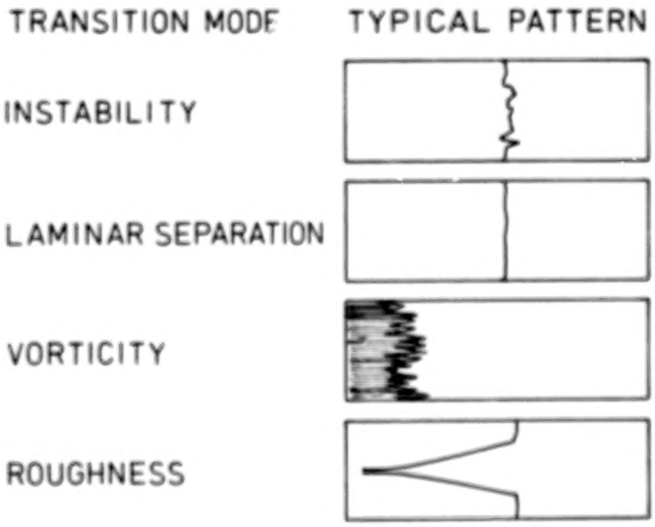

Figure 5.- Transition mode characteristics in sublimating chemical patterns.

Sublimating Chemical Flow Visualization Examples

Sublimating chemicals have been used extensively in recent years by NASA Langley personnel to document boundary-layer transition locations in flight on a variety of aircraft. Complete documentation of the results of the flight tests is presented in reference 8. The sublimating chemical technique has been used successfully on all surfaces of an aircraft including wings, fuselages, empennages, and propellers.

Figure 6 shows a chemical pattern on the lower surface of a wing. The unit Reynolds number for the test was $R' = 1.9 \times 10^6 \text{ ft}^{-1}$, and the chemical was acenaphthene. The figure shows the effect of insect strikes, propeller slipstream, and roughness in the form of inspection cover plates, screws, and selected tape trips on boundary-layer transition. There were several additional insect strikes which did not cause transition, whereas the ones shown did, as indicated by the turbulent wedges in the chemical pattern. The middle inspection cover had an aft-facing step which caused boundary-layer transition. Although it cannot be seen, the wing root caused transition because of the screw heads holding the plate rather than by the step height. Two additional turbulent wedges appear from intentional tape trips which served to calibrate the photograph. Another noticeable effect is that the propeller slipstream caused the mean transition front to move slightly forward. The natural transition front shows the smooth, uniform pattern characteristic of laminar separation.

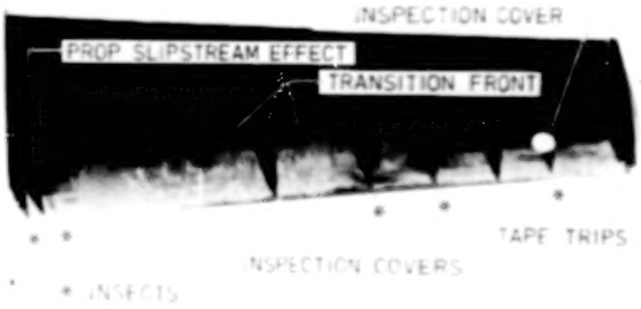

Figure 6.- Boundary-layer transition on a wing lower surface indicated by sublimating chemicals (acenaphthene), $R' = 1.9 \times 10^6$ ft^{-1} (ref. 8).

As noted previously above, it is possible to measure the extent of laminar flow on a rotating propeller. Figure 7 shows an example of the suction side of a propeller and its boundary-layer transition location. Another useful application of sublimating chemicals for flow visualization is in determining crossflow vortices, as shown in figure 8. The figure shows the development of crossflow vortices in the laminar boundary layer on the lower surface of a 27° swept wing at $R' = 2.4 \times 10^6$ ft^{-1}. Prior to causing boundary-layer transition, the vortices were spaced at 8-10 per inch.

In separate unpublished tests, a comparison between oil flows and sublimating chemicals was conducted in flight and in a wind tunnel. The results showed that sublimating chemicals indicate the location of turbulent reattachment following laminar separation.

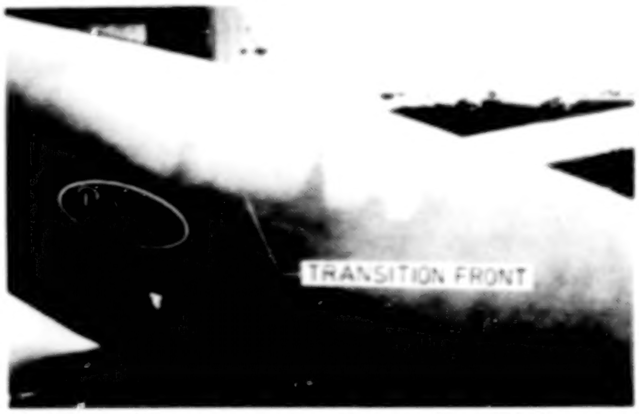

Figure 7.- Boundary-layer transition on the suction side of a propeller indicated by sublimating chemicals (acenaphthene), $R' = 2.77 \times 10^6$ ft^{-1}.

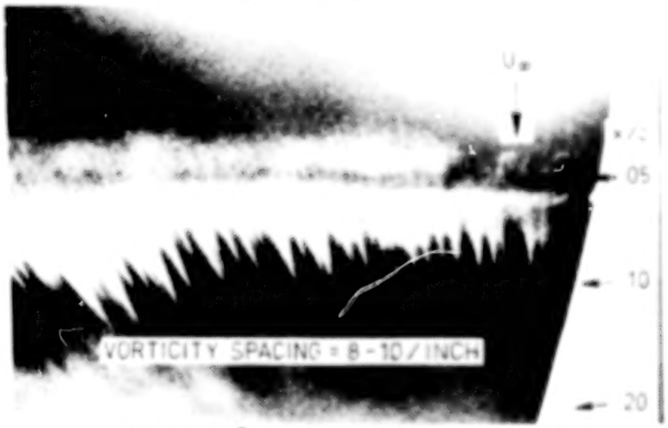

Figure 8.- Crossflow vortices indicated by sublimating chemicals (acenaphthene), $\Lambda = 27°$, $R' = 2.4 \times 10^6$ ft^{-1}.

Safety Precautions

There are several precautions which should be followed in order to insure safe use of sublimating chemicals. The chemicals discussed here were selected because of their low health hazards. However, these chemicals should still be treated with caution. Persons within close use of the chemicals should wear an organic-vapor-type respirator (carbon filter). Eye and skin contact should be avoided whenever possible. Rubber gloves are recommended for handling. (Wash after use.) Always provide adequate ventilation when applying the chemicals. Biphenyl and naphthalene have been found to have low short-term and low long-term toxicity. Currently, fluorene and acenaphthene are known to have low short-term toxicity, but long-term toxicity has not been extensively studied. For further health safety information on these and other chemicals, consult the American Society for Testing and Materials or request a materials safety data sheet from the chemical supplier.

A recent safety alert has been announced regarding the use of 1,1,1-trichloroethane and other halogenated hydrocarbons in pressurized fluid systems having aluminum or galvanized wetted parts. Under certain circumstances, these solvents can corrode the aluminum or galvanized parts. In pressurized spraying systems, this corrosive action could result in a pressure vessel explosion. Unless a stainless steel canister and spray gun are used, a siphon cup sprayer should be used when applying the chemical with a halogenated hydrocarbon solvent. Inspect aluminum parts regularly for corrosion. Acetone can be used as a solvent; however, it does affect fiberglass and plexiglass and is a greater fire hazard than 1,1,1-trichloroethane. Proper cleaning of any fluid system will minimize the potential hazard. For further information on potential corrosion hazards, it is best to consult the manufacturer of the spray equipment.

OIL FLOW

Description of Technique

A second useful flow visualization technique for determining the state and nature of the flow over a surface is that of oil flow. Oils can identify regions of laminar and turbulent flow, regions of separated flow, location of shocks, and the location of laminar separation bubbles. One advantage of field flows over sublimating chemicals is the ability to detect laminar separation bubbles.

The technique of applying and using oils differs somewhat from that for sublimating chemicals. The oil is brushed onto the surface to be tested. The aircraft is then flown to the desired flight conditions and held there until an oil pattern has developed. The oil will flow in the direction of the surface flow, collecting in regions of reverse flow, as shown in figure 9.

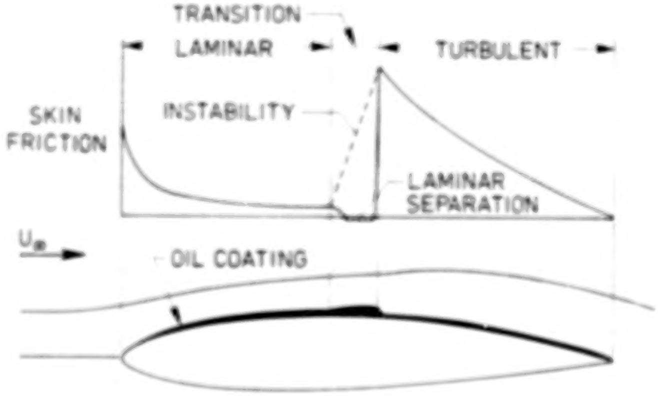

Figure 9.- How oil flows indicate boundary-layer transition.

Rapid movement of the oil will occur in regions of high skin friction and shear. Ambient temperature has a large effect on the flow characteristics of the oil. The oil becomes less responsive at lower temperatures which occur at higher altitudes. This requires that the flight test conditions be held longer to insure that the oil patterns have adapted to the flow field. Unlike sublimating chemicals, with oil any photographs of the developed pattern must be taken during flight at the desired test conditions, since transition patterns in oil coatings are difficult to preserve through off-condition flight regimes. For this same reason, the use of a less viscous oil may not help the low temperature effect, since the climb portion of the flight would generally remove the thinner oils. For most flight conditions, the use of a 1:1 mixture of AMS/Oil Para-Synthetic and Mobil 1, combined with a pigment to provide a contrast with the surface, has been recommended (ref. 3). Suggested pigments include ferric oxide (FeO_2) for visualization on lighter surfaces and titanium dioxide (TiO_2) for contrast on darker surfaces. Useful ratios of pigment to oil are 1:10 for ferric oxide and 1:1 for titanium dioxide. The pigment should be completely dissolved into the oil before application to any surface. Further information on the use of oil flow can be obtained from reference 3.

Oil Flow Visualization Examples

Some of the results of Curry et al. (ref. 3) in using oils for in-flight flow visualization are reproduced here. Figure 10 shows an oil flow pattern indicating boundary-layer transition. The unit Reynolds number for this test was $R' = 630{,}000\ ft^{-1}$, and the oil was the mixture of AMS/Oil and Mobil 1 recommended above. The effect of fixed transition, followed further downstream by a region of flow separation, is also shown. An example of a shock location indicated by oil flow is shown in figure 11. For the faster speed, $M = .85$, $R' = 2.9 \times 10^6\ ft^{-1}$, a more viscous oil was used.

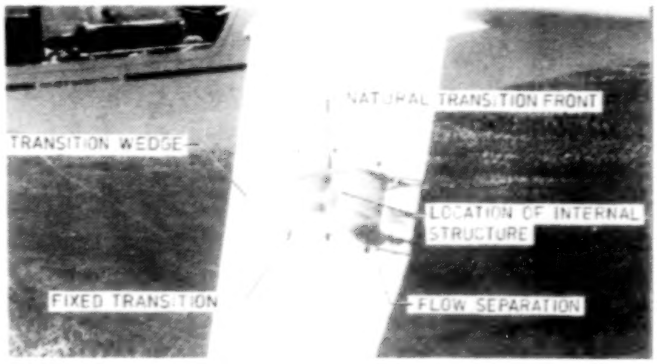

Figure 10.- Boundary-layer transition indicated by oil flow, $R' = 0.63 \times 10^6\ ft^{-1}$.

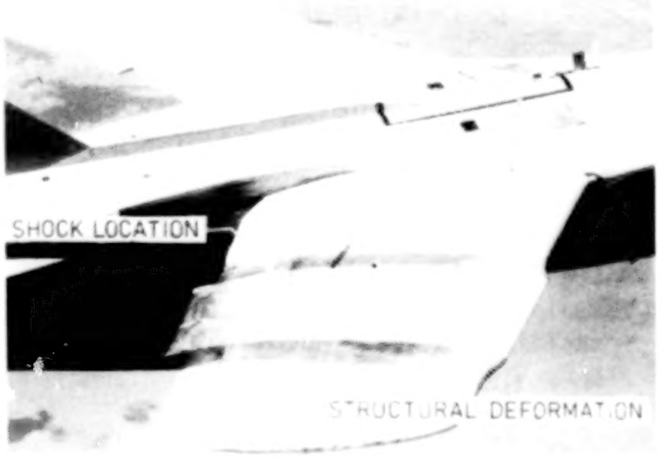

Figure 11.- Shock wave location indicated by oil flow, $M = 0.85$, $R' = 2.9 \times 10^6\ ft^{-1}$ (ref. 3).

CONCLUSIONS

Combined use of both oil flows and sublimating chemicals provides extensive boundary-layer data for use in design validation or certification flight testing. Each method of flow visualization has its advantages and disadvantages. Oil flows can be used to determine boundary-layer transition, shock wave locations, regions of separated flow, and surface flow direction. However, they must be photographed in flight following pattern development and are somewhat untidy. Sublimating chemicals are useful for visualizing boundary-layer transition patterns from several modes of transition, including Tollmien-Schlichting instability, laminar separation, crossflow instability, and transition due to roughness. With the advent of new aircraft utilizing laminar flow for drag reduction, flow visualization is a valuable diagnostic tool to supplement other analytical measurements.

REFERENCES

1. Gray, W. E.: A Chemical Method of Indicating Transition in the Boundary Layer. RAE TN Aero 1466, June 1944.

2. Main-Smith, J. D.: Chemical Solids as Diffusible Coating Films for Visual Indications of Boundary-Layer Transition in Air and Water. R&M 2755, February 1950.

3. Curry, Robert E.; Meyer, Robert R., Jr.; and O'Connor, Maureen: The Use of Oil for In-Flight Flow Visualization. NASA TM 84915, revised January 1984.

4. McTigue, John G.; Overton, John D.; and Petty, Gilbert, Jr.: Two Techniques for Detecting Boundary-Layer Transition in Flight at Supersonic Speeds and at Altitudes above 20,000 ft. NASA TN D-18, August 1959.

5. Owen, P. R.; and Ormerod, A. O.: Evaporation from the Surface of a Body in an Airstream. R&M 2875, September 1951.

6. Dean, John A., ed.: Lange's Handbook of Chemistry. 11th Edtiion, McGraw-Hill Book Co., New York, 1973.

7. Weast, Robert C., ed.: CRC Handbook of Chemistry and Physics. 65th Edition, CRC Press, Inc., Boca Raton, FL, 1984.

8. Holmes, Bruce J.; Obara, Clifford, J.; and Yip, Long P.: Natural Laminar Flow Experiments on Modern Airplane Surfaces. NASA TP-2256, June 1984.

56-34

N88-23743

BOUNDARY LAYER MEASUREMENTS USING HOT-FILM SENSORS

Harlan K. Holmes
NASA Langley Research Center
Hampton, Virginia 23665

Debra L. Carraway
Old Dominion University Research Foundation
Norfolk, Virginia 23508

SUMMARY

Measurements in the aerodynamic boundary layer using heat transfer, hot-film sensors are receiving a significant amount of effort at the Langley Research Center. A description of the basic sensor, the signal conditioning employed, and several manifestations of the sensor are given. Results of a flow reversal sensor development are presented, and future work areas are outlined.

INTRODUCTION

Aerodynamic viscous drag is the focus of an intensifying research and development effort at the Langley Research Center. The objectives of this research are to identify and quantify the origins of that drag and to implement means for its reduction whether by profile modifications or through surface treatments. Providing the aerodynamicist with a diversity of sensors and supporting electronics to perform these studies is also receiving a significantly increased development effort, particularly within the Instrument Research Division (IRD) at Langley. Past developments have resulted in a miniaturized, mechanical force balance-type skin-friction sensor which has been used in both supersonic and cryogenic flows, and an improved design is now being readied for use in the National Transonic Facility (NTF). A high sensitivity design is being constructed for use in a low speed, quiet tunnel, and units are being fabricated for an upcoming flight test program. More recently, a major effort into the development and understanding of hot-film, heat transfer sensors has begun.

Figure 1 is a conceptualization of several boundary layer sensors under development by the Instrument Research Division. Extensive development of mechanical, force balance skin-friction sensors has been completed with numerous designs having been built and tested. Devices have been fabricated of several different materials, and many have been tested at cryogenic temperatures. These units operate on a closed-loop servo principle where the current to restore the sensing element to its null position is a measure of the aerodynamic friction on the surface. A two-dimensional sensor utilizing the same concepts is now in design. The fiber optic sensor, conceptually illustrated, is expected to provide an amplitude variation in response to surface shear forces and is being pursued under a university grant. Polyvinylidine fluoride is a thin (0.0005" - 0.015") piezoelectric copolymer sheet which has the interesting property of providing voltages as a result of surface pressure fluctuations. Illustrated is a concept for a surface dynamic pressure sensor array which will be pursued in a future program. The remaining items, the thermal skin-friction sensor; the flow reversal sensor; the crossflow sensor; and a multi-element transition sensor, will be discussed in more detail in following sections.

SYMBOLS

A	Area, cm^2
Q_a	Heat transfer by forced convection, Btu/sec
Q_c	Heat transfer by conduction to the substrate, Btu/sec
Q_i	Joulean heat input, Btu/sec
Q_r	Heat transfer by radiation to the surroundings, Btu/sec
Q_s	Heat transfer to the substrate, Btu/sec
R_f	Resistance of the film at temperature, T_f, ohms
R_o	Resistance at a reference temperature, T, ohms
$R_{()}$	Resistance as designated by the subscript, ohms
$T_{()}$	Absolute temperature, generally defined with a subscript, $^\circ$C
h	Convective heat transfer coefficient, Btu/m^2-sec-$^\circ$C-cm
I	Current
k	Thermal heat transfer coefficient, Btu/m^2-sec-$^\circ$C-cm
ℓ	Length dimension, cm
α	Temperature coefficient of resistance, ohm/ohm-$^\circ$C
ϵ	Emissivity of the foil sensor
σ_{SB}	Stefan Boltzmann constant, 567 x 10^{-8} W/m^2-$^\circ$C^4
ρ	Coefficient of resistivity, ohm-cm

HOT-FILM SENSOR

Figure 2 is a conceptual representation of a typical metallic foil sensor mounted on a thin insulating blanket which is then bonded to the surface of a structure from which information is desired. The thinness of the insulating blanket is dictated by the requirement for a low sensor profile to prevent premature boundary layer transition. Should this not be a driving influence, a thicker blanket having a lower conductive heat transfer can be employed. Several factors dictate the design of a sensor: the heat transfer relationship between the film and substrate, the heating capacity and controllability of the film, and other physical characteristics of both film and substrate which make them compatible with instrumentation and test surfaces. This is illustrated theoretically by performing a heat balance upon the sensor.

$$\text{Heat In} = \text{Heat Out} + \text{Heat Stored} \tag{1}$$

Symbolically,

$$Q_i = Q_a + Q_s + Q_r + Q_{stored}$$

Where,

$Q_i = J' I^2 R_f$ is the Joulean heat input

$J' = 0.484 \times 10^{-4}$ Btu/sec-W

$$R_f = R_o \, [1 + \alpha(T_f - T_o)] \tag{2}$$

$R_o = \rho_o \ell / A$

$Q_a = hA\Delta T$ is the heat loss due to convection

$Q_s = -kA\partial T/\partial n$ is the conductive losses to the substrate

$Q_r = \epsilon\sigma_{SB} A(T_f^4 - T_a^4)$ is the heat loss by radiation

Combining the separate terms gives

$$J' I^2 R_f = [hA\Delta T] - [kA\partial T/\partial n] + \epsilon\sigma_{SB} [A(T_f^4 - T_a^4)] \tag{3}$$

The terms over which some influence can be effected are as follows:

$$J' I^2 R_f = [hA\Delta T] - [kA\partial T/\partial n] \tag{4}$$

When the sensor is operated in a constant temperature (or resistance) system where the film is generally controlled at a temperature higher than the surroundings (overheat temperature), whatever disturbance (turbulent burst, velocity fluctuation, skin-friction variation, etc.) that arises to perturb the equilibrium temperature (resistance), translates to a change in sensor resistance. The governing electronics then forces the sensor resistance to its original controlled value. Equation (4) reveals the essence of the measurement. The last term deals with conduction to the substrate. Minimization of this term is generally desirable and is accomplished principally through selection of the material for the substrate or the temperature gradient. Since the element temperature is electronically controlled by the "overheat" (resistance) which also governs the sensitivity, the only controllable elements from which benefit can be gained are the material, which specifies the thermal conductivity, and the material thickness, which controls the temperature gradient. Since the thickness of the sensor is generally dictated by aerodynamic considerations, selection of the substrate material is the remaining variable. More discussion on the substrate material will follow later. Looking at the first term on the right hand side of equation (4), modulation of the boundary layer profile causes changes in the temperature which are reflected in a change of film resistance. Thus, it is the task of the electronic control unit to sense this perturbation and to effect the necessary changes in current to the sensor to restore the sensor to its commanded resistance value. Before looking at the control electronics, note that selection of the film material has a profound impact on the sensitivity of the device. To see this, differentiating equation (3) with respect to the film temperature gives

$$dR_f/dT_f = \rho\alpha\ell/A \qquad (5)$$

which for a given physical construction makes maximization of the $\rho\alpha$ product the feature which maximizes the device sensitivity. Table I gives information on several potential film materials.

CONDITIONING ELECTRONICS

Figure 3 describes the functional operation of the "constant temperature" anemometer system and includes a functional relationship between the system's input and output. The sensor, R_4, forms one leg of a basic wheatstone bridge. Examination of the diagram shows the circuit to be a high-gain, wide bandwidth differential measuring system with feedback to the bridge circuit. These characteristics make the circuit prone to oscillate, and care must be taken in its adjustments. The dc offset control biases the current amplifier stage into conduction, which places that stage into a more linear operating region. Knowing the resistance vs. temperature characteristics of the film sensor, one can specify an operating temperature for the film (known as overheat), which translates into a resistance at that temperature. To achieve this overheat, R_3 is increased to that value, unbalancing the bridge and causing a differential input voltage to appear at the input of the amplifier. The amplifier sends a large driving signal to the current amplifier which drives current through all resistors of the bridge, but principally through R_2 and R_4, until the heating in R_4 increases the resistance to match that of R_3 and thereby balances the bridge at the new operating point. Quite frequently, R_1 and R_3 are some multiple of the values in the other half of the bridge so that the major current flows through R_2 and the film sensor. Also shown at the left of the figure is a square (sine) wave generator which can be switched into the bridge circuit so that a signal can be injected to provide for frequency response adjustments. Care must be taken in the system design because the cable connecting the film sensor to the anemometer is also in the bridge circuit, and variations in cable or contact resistance will be indistinguishable from data. The connecting cable has inductance which introduces a reactive component in the balance equations and must be compensated for; otherwise, instabilities result. Also, R_2 must be a high-quality non-inductive temperature-insensitive resistor, or else variations in this element will also appear as data. Increasing the film resistance in order to reduce the current requirements has some restrictions. For example, use of a higher input voltage power supply can raise the differential voltage higher than the common-mode voltage limit of the input amplifier stage.

Also shown in figure 3 is a functional relationship of the input/output characteristic of the system. From this figure and equation (5) it should be apparent that the slope (sensitivity) is largely dependent on the sensor material. Table I lists the thermal parameters of several materials having large rho-alpha ($\rho\alpha$) products. Also apparent from this figure is the effect of heat loss to the substrate and the desirability of minimizing it. Table II lists several substrate materials and their thermal conductivity and linear expansion coefficients. Note that fused quartz and silicon dioxide have a thermal conductivity an order of magnitude greater than that for the polystyrene and polyimide families of thermoplastics. The polyimide family, more readily identified by the E. I. du Pont de Nemours and Company trademark Kapton, has many desirable properties (ref. 1):

> "Polyimide precision parts can be used continuously in air at temperatures up to 500°F. The continuous operating temperature can be raised to 600°F in an inert atmosphere or vacuum. For intermittent, short-term exposures, top temperatures appear to be in the 800° to 900°F range.
>
> The thermal expansion of polyimide parts is between that of metals and conventional plastics.
>
> Tests exposing polyimide parts in liquid nitrogen indicate possible applications in cryogenic systems at -320°F to -420°F. Tensile strength at -320°F shows a 30 percent increase above that at room temperature. Shrinkage at -320°F, for example, is about 7 mils/in."

Figure 4 is a picture of a flight-qualified version of the circuit shown in figure 3.

THERMAL SENSORS

Figure 5 illustrates two prototype sensors, a flow reversal sensor and a 10-element crossflow sensor. Both sensors feature metallic films which are mounted on polyimide film substrates. Both sensors would be oriented as they are in the figure, with flow progressing from top to bottom. Care has been taken that the lead connections are made downstream or to the side of the sensor elements to minimize any interference with the flow. The crossflow sensor is constructed with film elements mounted on a 0.035" center-to-center spacing. This distance was determined from calculations and measurements of the average spacing between crossflow vortices. In sublimating chemicals used to visually detect this phenomenon, crossflow vortices appear as longitudinal streaks. An enlarged view of the sensor is found in figure 6. The solder pads on the terminal strip have significant height, and the connecting wire between the solder tab and the sensing element possesses a surprising amount of resistance. Figure 7 illustrates a continuous multi-element hot-film transition gage that has been developed to overcome the disadvantages of individual hot-film gages. The multi-element sensor integrates a quantity and distribution of hot-film sensing elements into a long, continuous, thin sheet. Transition data acquisition is accomplished using an electronic switching system which allows rapid switching of all sensing elements into the data recording system. The continuous thin sheet of a particular length covers the area of interest for transition measurements beginning at the leading edge and continuing to downstream of the transition region. For example, on an airplane wing of 10 ft chord length, the gage may be as much as 7 to 8 ft in length. The leading edge of a gage mounted on the upper surface of a wing would wrap around and beneath and downstream of the wing leading edge. In this fashion, no disturbance from the film leading edge will cause turbulent wedges to disturb the hot-film sensors in the transition region. For situations where the lateral edges could cause transition, the edges may be filled and faired to correct this difficulty.

Figure 8 illustrates a completely different construction technique for building a thermal skin-friction sensor. Here, a thin foil is sandwiched between beryllium-copper sheets. This foil assembly is then bonded between two plastic cylindrical halves and trimmed. The surface is machined until resistance of the foil rises to approximately 5 ohms. At this point, leads are attached, and it is mounted in an adapter ready for tunnel test. These units have been used several times in a cryogenic test, and when compared against the mechanical force balance instruments, good agreement has been obtained.

Figure 9 is an idealized description of the fluctuating or high-frequency signals from the hot-film sensors. Within the laminar region, where there is a slow, steady heat transfer rate, the sensor requires less current input to keep the temperature constant; hence, there is a low amplitude signal. The low level of signal amplitude in the illustration indicates the presence of noise in the instrumentation system. A noise-free laminar signal would have zero amplitude. In the turbulent region, where there are large current changes with the rapid fluctuating heat transfer rates, a larger voltage change is required and results in signals of greater amplitude. Both the fluctuating and mean values of heating voltage are recorded and observed in real time using a battery-powered oscilloscope.

TUNNEL TEST OF FLOW REVERSAL SENSOR

In figure 10, the top photo is of a laminar airfoil model which was coated with oil containing carbon black and tested in IRD's small tunnel. Inspection reveals that a laminar separation bubble, which is characterized by a flow separation, reversal, and reattachment, has formed between 60 - 70% of chord. A flow reversal sensor was then mounted at this chord position along with several additional sensors mounted strategically around the model as seen in the center photograph. With this sensor configuration, a low-speed test was performed, and typical responses from the various sensors are shown along the line labeled 45 mph. At the far right is the output from the flow reversal sensor which indicates that the flow is in a reverse direction. If the velocity is increased to 185 mph, as seen at the bottom, the separation bubble moves aft because of a low Reynolds number hysteresis effect, and the sensor now shows a forward flow direction.

FUTURE WORK

Development work to date has revealed several areas where additional development is needed. There have been several expressed needs for large numbers of sensors both for models and full scale articles, where switching of the sensors into a limited number of signal conditioning units is required. Response time to arrive at steady state conditions needs additional definition. This may also be required in the case of the crossflow sensor where operating the gages continuously may result in thermal crosstalk because the sensors are so closely spaced. Operation in a pulse mode would reduce the average power consumed per sensor. Calibration techniques must be developed so that the system frequency response can be obtained more easily. The current trends in instrumentation are towards microprocessor involvement to provide more automatic control, monitoring, calibrating, selecting, etc.

CONCLUDING REMARKS

In this paper, several thin film, thermal sensors have been described as being applicable to boundary layer measurements with transition, flow reversal and skin-friction being the more prominent applications. A single sensor element can be used to investigate flow transition. Adding two elements, one upstream and the other downstream, allows flow reversal to be detected. Creating a spanwise array of closely spaced elements allows investigations of crossflow conditions occurring in swept wing situations. Imbedding a single filament in a low thermal conductivity plastic can be used to measure aerodynamic skin-friction if the sensor has been calibrated against a force balance type unit. All of the sensors mentioned utilize the same signal conditioning equipment which indicates that all methods have similar operational characteristics.

REFERENCES

1. Handbook of Materials and Processes for Electronics, Charles A. Harper, Editor, McGraw-Hill, Inc., 1970, pp. 1-64, 65.

2. Holmes, Bruce, J: Progress in Natural Laminar Flow Research. AIAA Paper No. 84-2222, 1984.

3. Obara, Clifford J., and Holmes, Bruce J.: Flight-Measured Laminar Boundary Layer Transition Phenomena Including Stability Theory Analysis. NASA TP 2417, 1985.

TABLE I. - POTENTIAL MATERIAL FOR SENSOR ELEMENTS

Material	Resistivity Micro-ohm-cm	Coef. of Resistivity Per Degree Celsius	Coef. of Expansion Per Degree Celsius
BALCO (1)	19.9	0.0045	0.000015
"A" Nickel	10.0	0.0048	0.000013
Platinum	10.6	0.003	0.0000088
Copper	1.73	0.0039	0.0000166
Columbium	14.2	0.0395	0.0000069
Tungsten	5.49	0.0045	0.0000046
Titanium	55.0	0.0041	0.0000085
Nichrome	105.0	0.0014	-

(1) BALCO is a Trademark of W. B. Driver Company

TABLE II. - MATERIAL FOR INSULATION

Material	Thermal conductivity cal/cm^2-sec-°C-cm	Coef. of Expansion Per Degree Celsius
Fused Quartz	0.0033	0.00000055
Silicon Dioxide	0.00256	-
Balsawood	0.000116	-
Polysulphone	0.000162	0.000056
Polystyrene	0.00030	0.000065
Polyester	0.000363	0.000027
Nylon 6	0.00059	0.00007
Polyimide	0.00035	-

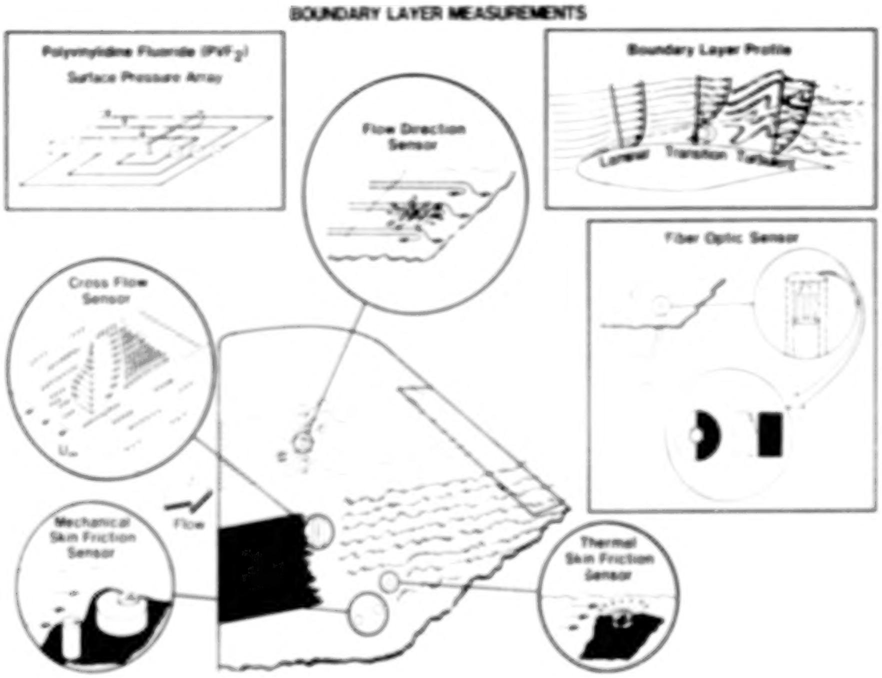
BOUNDARY LAYER MEASUREMENTS
Polyvinylidine Fluoride (PVF_2)
Surface Pressure Array
Flow Direction Sensor
Boundary Layer Profile
Laminar
Transition
Turbulent
Fiber Optic Sensor
Cross Flow Sensor
U_∞
Flow
Mechanical Skin Friction Sensor
Thermal Skin Friction Sensor

Figure 1.- Boundary layer measurement concepts.

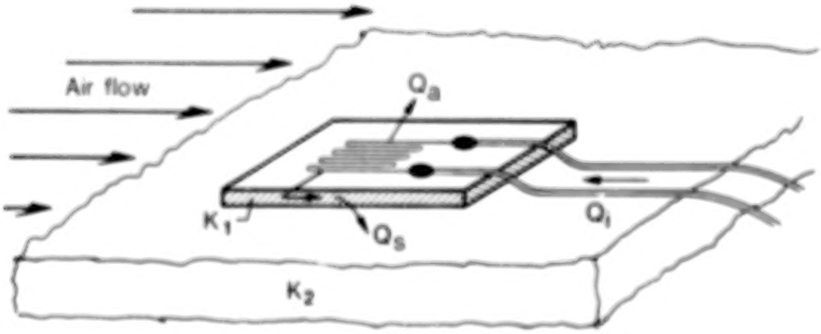
Air flow
Q_a
K_1
Q_s
Q_i
K_2

Q_i = Input electrical power (Joulean heating)

Q_a = Heat transfer by forced convection

Q_s = Heat transfer by conduction to substrate

$K_{1\text{-}2}$ = Thermal heat transfer coefficients

Figure 2.- Metallic foil thermal sensor.

ORIGINAL PAGE IS
OF POOR QUALITY

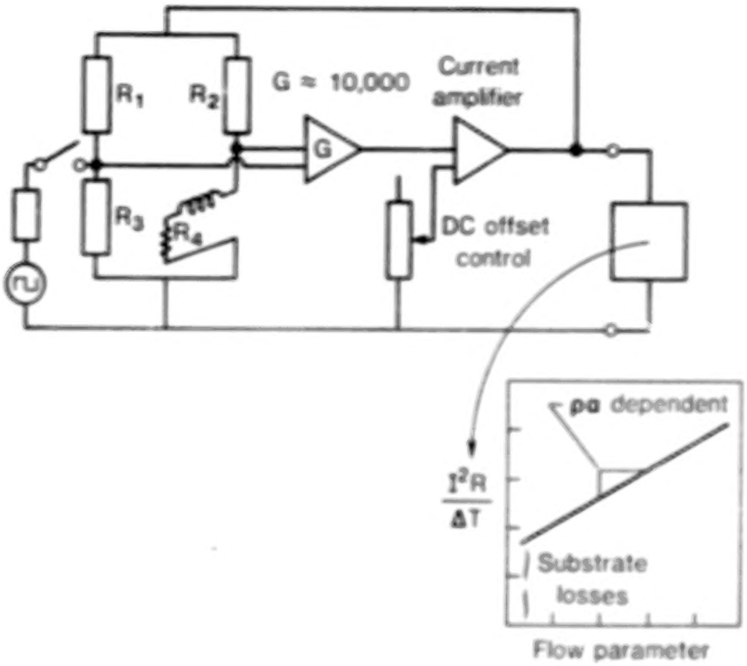
R$_1$
R$_2$
G ≈ 10,000
Current amplifier
G
R$_3$
R$_4$
DC offset control
ρα dependent
I²R / ΔT
Substrate losses
Flow parameter

Figure 3.- Anemometer functional schematic and input/output functional relationship.

ORIGINAL PAGE IS
OF POOR QUALITY

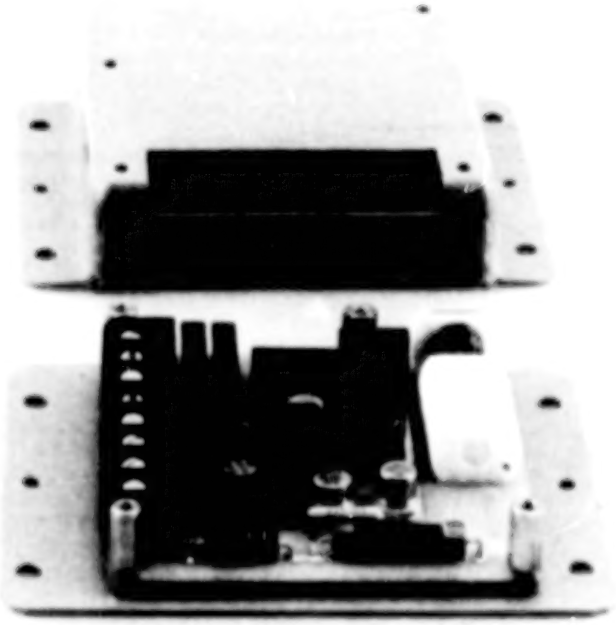

Figure 4.- Flight qualified anemometer package.

ORIGINAL PAGE IS
OF POOR QUALITY

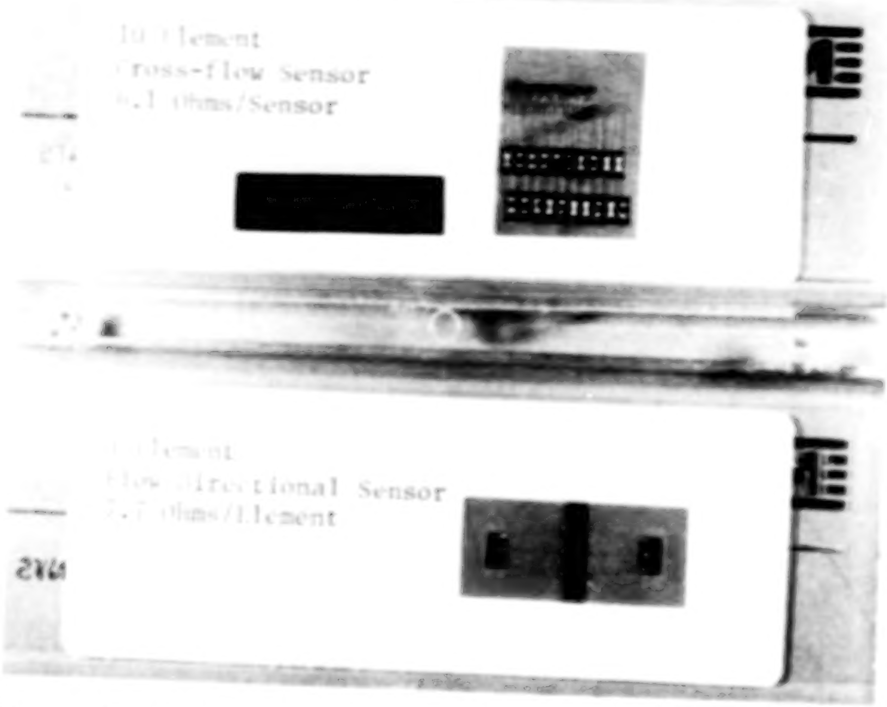
10 Element
Cross-flow Sensor
Ohms/Sensor
Element
Flow Directional Sensor
Ohms/Element

Figure 5.- Prototype flow reversal and cross-flow sensors.

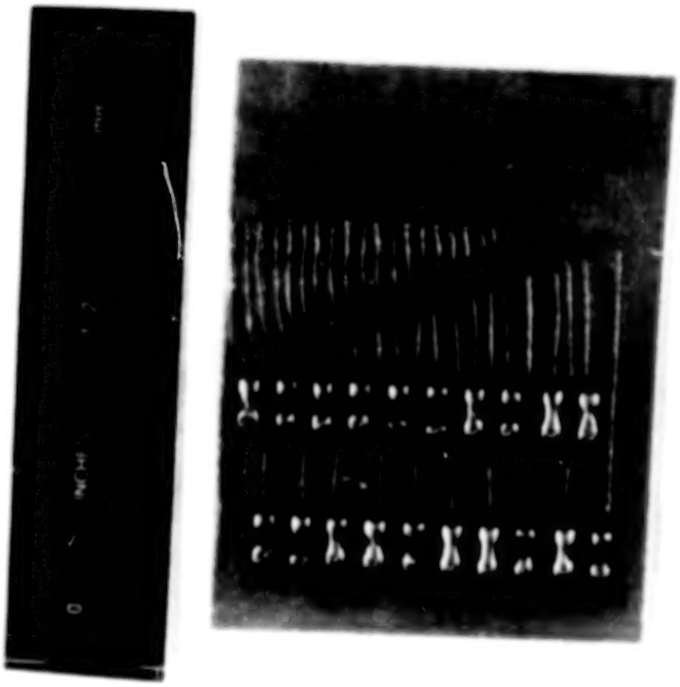

Figure 6.- Prototype cross-flow sensor.

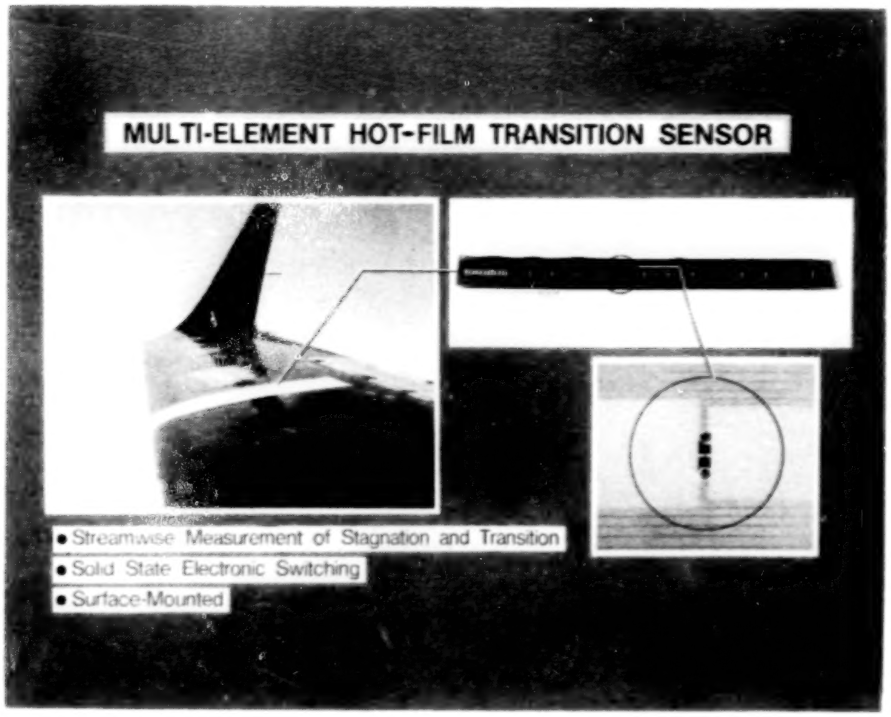

MULTI-ELEMENT HOT-FILM TRANSITION SENSOR

- Streamwise Measurement of Stagnation and Transition
- Solid State Electronic Switching
- Surface-Mounted

Figure 7.- Multi-element hot-film transition sensor (ref. 2).

ORIGINAL PAGE IS
OF POOR QUALITY

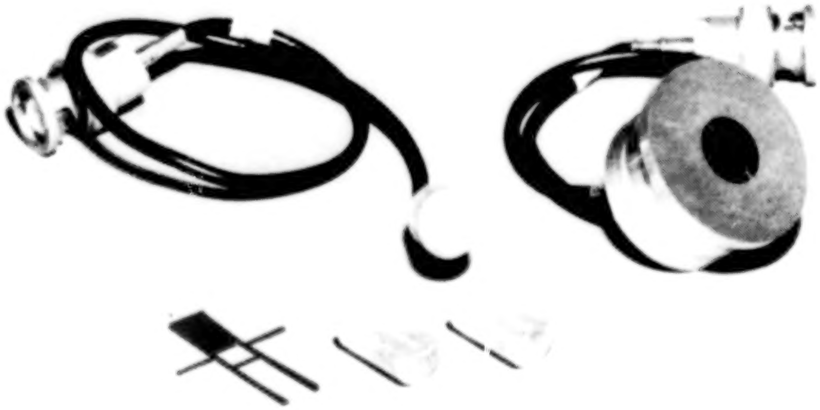

Figure 8.- Thermal skin-friction sensor.

~~ORIGINAL PAGE IS
OF POOR QUALITY~~

ORIGINAL PAGE IS
OF POOR QUALITY

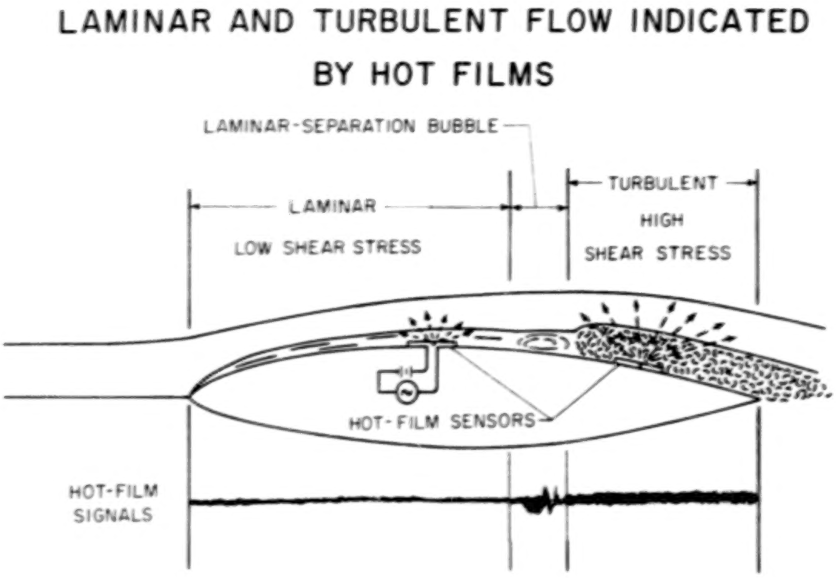
LAMINAR AND TURBULENT FLOW INDICATED
BY HOT FILMS
LAMINAR-SEPARATION BUBBLE
LAMINAR
LOW SHEAR STRESS
TURBULENT
HIGH
SHEAR STRESS
HOT-FILM SENSORS
HOT-FILM
SIGNALS

Figure 9.- Hot-film signal characteristics for laminar, laminar separation, and turbulent boundary layer conditions (ref. 3).

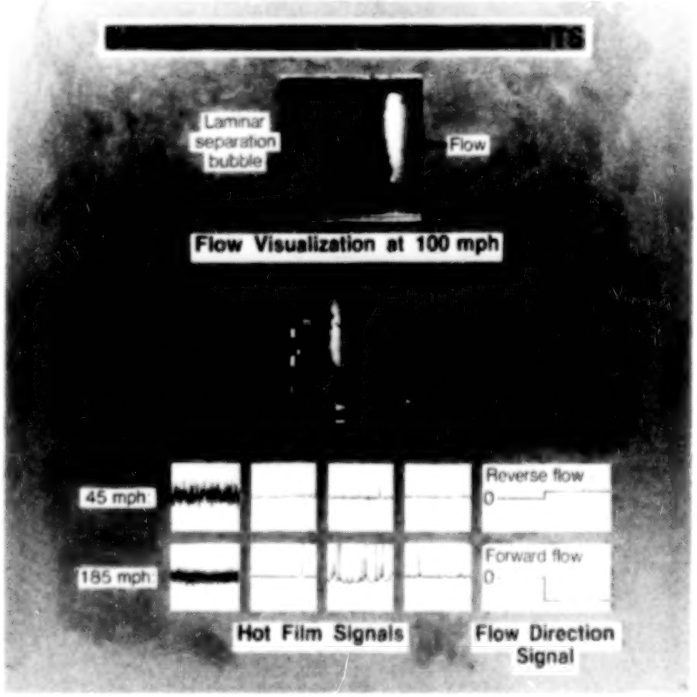
Laminar
separation
bubble
Flow
Flow Visualization at 100 mph
45 mph
185 mph
Reverse flow
0
Forward flow
0
Hot Film Signals
Flow Direction
Signal

Figure 10.- Flow reversal sensor test results.

N88-23744

FLIGHT EXPERIENCES WITH LAMINAR FLOW

57-05
158

by Bruce J. Holmes
NASA Langley Research Center
Hampton, Virginia 23665

INTRODUCTION

Five decades of flight experiences with natural laminar flow (NLF) have provided a basis of understanding how this technology can be used for reduction of viscous drag on modern practical airplanes. The classical concerns about the practicality of NLF have related to achievability and maintainability. The earliest efforts to achieve NLF in flight were uniformly successful on specially prepared and gloved airframe surfaces and unsuccessful on the production metal surfaces of the 1940's and 1950's era. More recent NASA flight experiments have demonstrated the achievability of NLF on modern metal and composite airframe surfaces (ref. 1). These experiments, more than 30 in total, were conducted over a range of free-stream conditions including Mach numbers up to 0.7, transition Reynolds numbers up to 14 x 10^6, chord Reynolds numbers up to 30 x 10^6, and on wings of relatively small leading-edge sweep angles, typically less than 27°.

In contrast to the difficulties encountered on older production airframe surfaces of the 1940's and 1950's, NLF is achievable today because of the small waviness of modern production wings, because of the lower values of unit Reynolds numbers at the higher cruise altitudes of modern airplanes, and because of the favorable influence of subcritical compressibility on two-dimensional laminar stability at the higher cruise Mach numbers of modern airplanes.

A selection of flight-measured transition data from past NLF flight experiments is presented in figures 1 through 7. In figure 1, transition near 65-percent chord is illustrated on the specially prepared wing section in the classic British Royal Aeronautical Establishment King Cobra experiments (ref. 2). In figure 2, flight-measured transition is shown on several surfaces of the Rutan Long-EZ airplane (ref. 1). The figure shows transition near 33-percent chord on the swept wing and winglet. Transition on the fuselage was approximately 1-1/2 ft from the nose, and transition on the wheel fairings (not shown) occurred at about 50 percent of the fairing body length. Transition on the wing of the Bellanca Skyrocket airplane is shown near the 50-percent chord location along the wing span in figure 3 (ref. 3). Extensive runs of more than 50-percent chord length of laminar flow were recorded on the forward and aft faces of the propeller of this airplane as well. Figure 4 (from ref. 1) illustrates transition on the forward face of the propeller of the Beech 24R Sierra airplane at cruise conditions. Laminar flow over nearly the full length of the propeller spinner on the Cessna P210 airplane is shown in figure 5 (ref. 1). From this same flight experiment, transition on the upper surface on the horizontal tail of the P210 is shown near 30-percent chord in figure 6. Finally, in figure 7 (from ref. 1), transition near 45-percent chord is shown at M = 0.7 on the wing of a Learjet Model 28/29. This small selection of results illustrates the wide variety of aircraft surfaces and flight conditions for which NLF has been observed in the past. The significant implications of the past research are the following:

PRECEDING PAGE BLANK NOT FILMED

CLASSICAL NLF FLIGHT EXPERIMENTS

Natural laminar flow to 65% chord
(RAE 1951)

King Cobra; C_L = 0.14, R = 17 × 10^6, 66-series

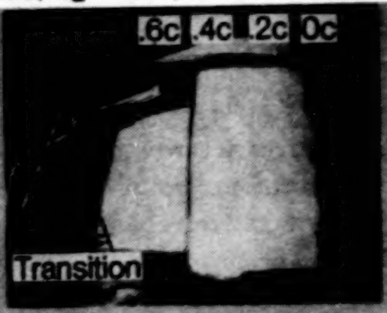

Natural laminar flow at R = 34 × 10^6
(RAE 1951)

Jet fighter; M = 0.72, C_L = 0.07

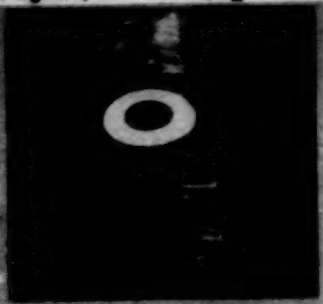

Transition caused by flies
(RAE 1951)

King Cobra; C_L = 0.34, R = 11 × 10^6, 66-series

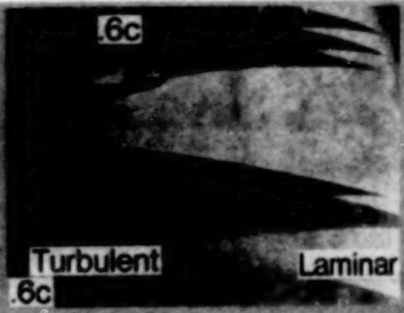

Figure 1.- Natural laminar flow on the specially prepared wing sections of World War II airplanes (ref. 2).

1. Achievability: NLF is a practical drag reduction technology on modern metal and composite airframe surfaces for Mach numbers as high as 0.7, chord Reynolds numbers as large as 30 x 10^6, and wing sweep angles as high as 17° to 27°, depending on length and unit Reynolds numbers and Mach number.

2. Maintainability: NLF is more persistent and durable at high-speed subsonic conditions than previously expected.

Many of the lessons learned from these past NLF flight experiments have significance for current efforts to design, flight test, and operate NLF airplanes. In particular, these lessons relate to the maintainability of NLF in typical airplane operating environments. This paper summarizes these past experiences concerning the following topics:

1. Effects of laminar flow on drag
2. Character of laminar transition in flight
3. Effects of loss of laminar flow on stability and control

ORIGINAL PAGE IS
OF POOR QUALITY

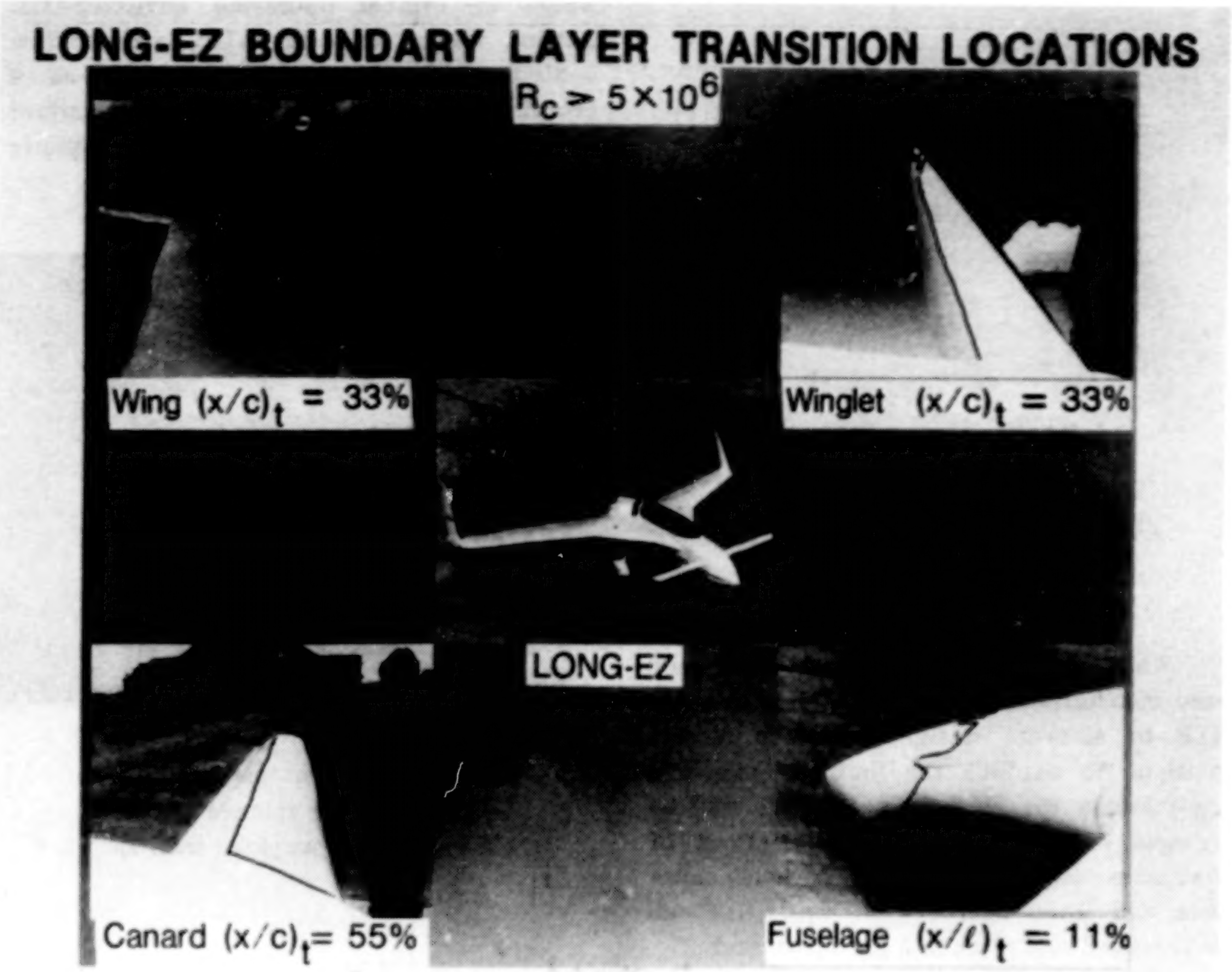
LONG-EZ BOUNDARY LAYER TRANSITION LOCATIONS
$R_c > 5 \times 10^6$
Wing $(x/c)_t = 33\%$
Winglet $(x/c)_t = 33\%$
LONG-EZ
Canard $(x/c)_t = 55\%$
Fuselage $(x/\ell)_t = 11\%$

Figure 2.- Natural laminar flow on the Rutan Long-EZ airframe surfaces (ref.1).

4. Effects of loss of laminar flow on maximum lift
5. Effects of insect accumulation on laminar flow airfoils
6. Effects of flight through clouds and precipitation on laminar flow
7. Laminar flow behavior in propeller slipstreams
8. Fixed transition flight testing

ORIGINAL PAGE IS
OF POOR QUALITY

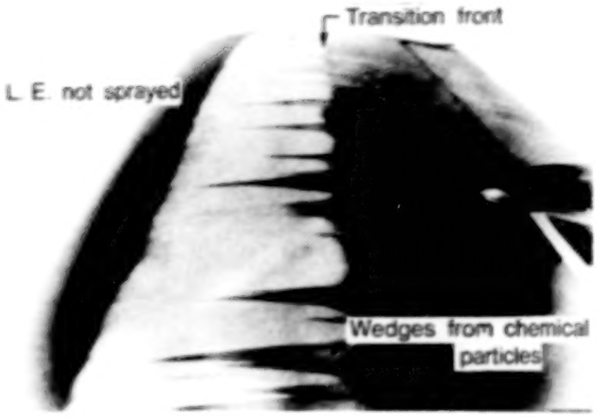
Transition front
L. E. not sprayed
Wedges from chemical particles

Figure 3.- Natural laminar flow on the Bellanca Skyrocket II wing upper surface (ref. 3).

While the lessons of the past have been very instructive for current efforts to apply NLF to aircraft designs, research efforts continue to explore the limits of practical applications for NLF. These limits may be thought of in terms of combinations of maximum angles of sweep, Reynolds numbers, and Mach numbers for which NLF can be achieved and maintained on practical wings in typical operating environments. Beyond these limits for NLF, laminar flow control (LFC) by suction appears as a promising means for achieving laminar viscous drag reduction benefits. This paper concentrates on NLF subjects.

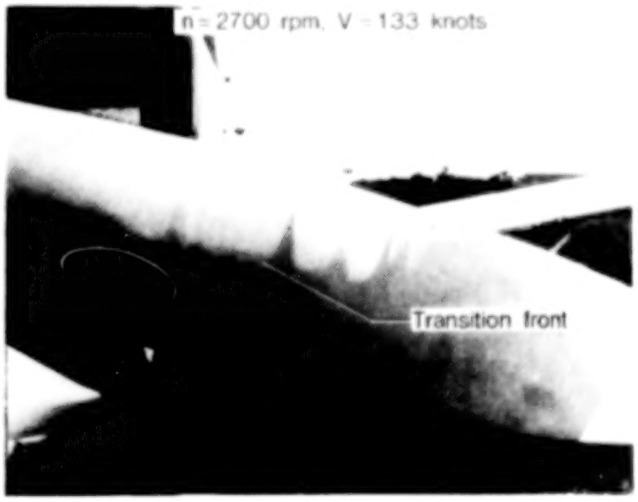
$n = 2700$ rpm, $V = 133$ knots
Transition front

Figure 4.- Natural laminar flow on the propeller of the Beech Model 24R Sierra (ref. 1).

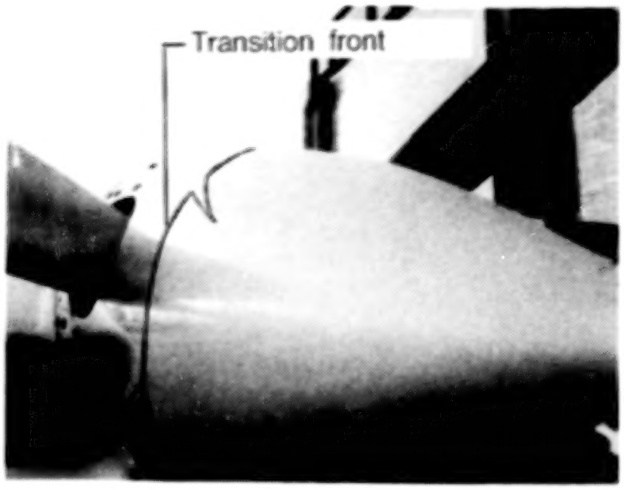
Transition front

Figure 5.- Natural laminar flow on the propeller spinner of the Cessna P210 airplane (ref. 1).

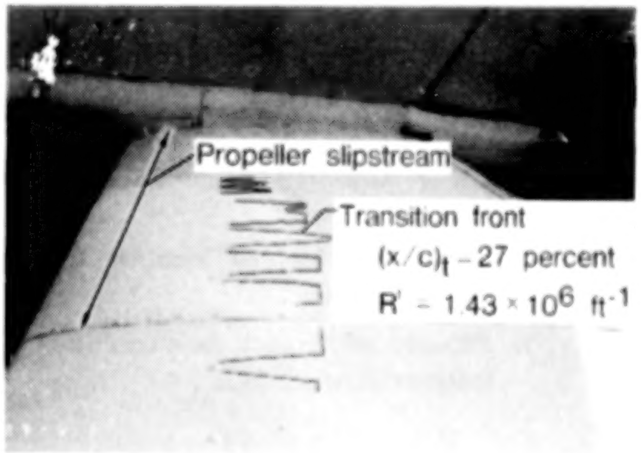
Propeller slipstream
Transition front
$(x/c)_t = 27$ percent
$R' = 1.43 \times 10^6$ ft^{-1}

Figure 6.- Natural laminar flow on the horizontal tail upper surface of the Cessna P210 airplane (ref. 1).

ORIGINAL PAGE IS
OF POOR QUALITY

ORIGINAL PAGE IS
OF POOR QUALITY

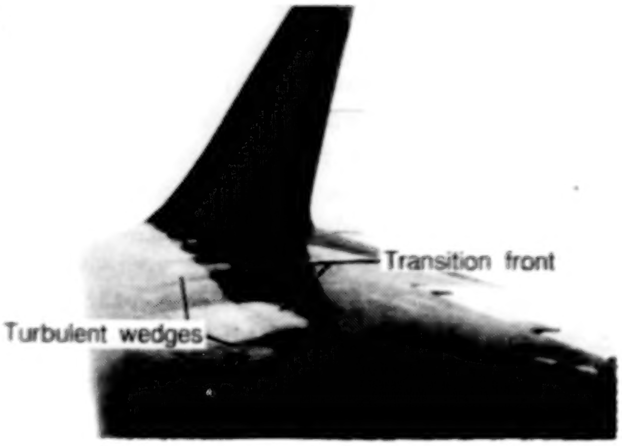

Figure 7.- Natural laminar flow on the Gates Learjet wing upper surface at M = .7 (ref. 1).

LAMINAR FLOW LESSONS OF THE PAST

In certain respects, the design, testing, and operation of NLF airplanes differ from those considerations for turbulent airplanes. Laminar flow airplane designs must include the consideration that for certain environmental conditions, laminar flow will be lost. Testing of these airplanes must include fixing of transition near the leading edges of the laminar surfaces. Operators of laminar flow airplanes must have information concerning the differences in airplane characteristics with and without NLF.

Effects of Laminar Flow on Drag

The reduction of airplane drag with laminar flow results directly from changes in skin friction and pressure drag. Practical boundary-layer considerations limit the maximum lengths of NLF runs to between 50 and 70 percent of the total length of a surface. For these lengths of laminar runs, the potential drag reduction ranges between about 30 and 60 percent compared to the drag of a "good" turbulent airfoil (NACA 23015), as illustrated in figure 8. The figure also illustrates the nearly 100-percent increase in airfoil section cruise drag with turbulent compared to laminar conditions for the NACA 63_2-215 NLF airfoil measured in flight on the Bellanca Skyrocket II airplane (ref. 3).

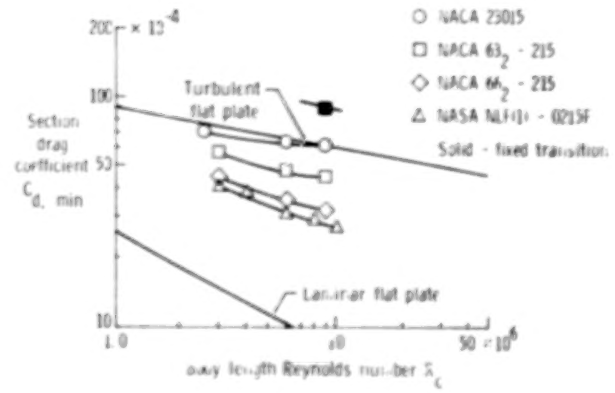

Figure 8.- Natural laminar flow drag reduction for several airfoil sections.

Flight-measured increases in cruise drag of 25 percent caused by loss of laminar flow were reported in reference 1 for three airplanes. These three airplanes were the Rutan VariEze, the Rutan Long-EZ, and the Bellanca Skyrocket II. The drag increases on the first two airplanes were aggravated by flow separation on the thick canard airfoil associated with loss of laminar flow. The Skyrocket NACA 6-series airfoil did not experience significant flow separation with loss of laminar flow; for this airplane, the drag change was dominated by the change in skin friction caused by early transition.

For a high-performance business jet, the potential drag reduction with NLF ranges between about 12 percent (for NLF on the wing only) to about 24 percent (for NLF on the wing fuselage, empennage, and engine nacelles). (See fig. 9.) These drag reductions are calculated for NLF added to an existing

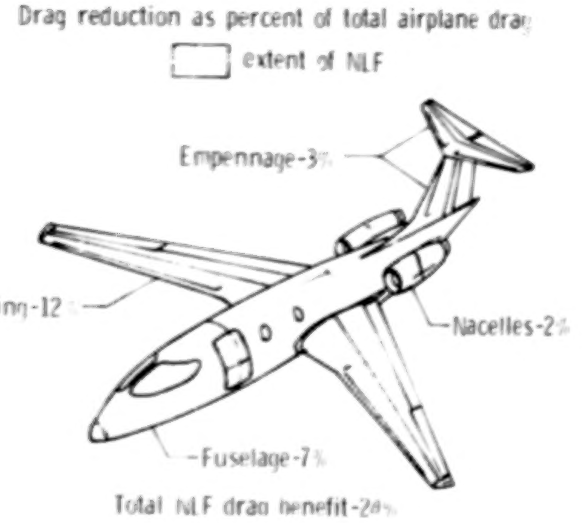
Drag reduction as percent of total airplane drag
extent of NLF
Empennage-3%
Wing-12%
Nacelles-2%
Fuselage-7%
Total NLF drag benefit-24%

Figure 9.- Natural laminar flow drag reduction for a high-performance business airplane.

configuration; larger benefits would accrue for integrated design calculations.

Character of Laminar Transition in Flight

As far back in the literature as 1948, Tani (ref. 4) remarked that transition on smooth surfaces in flight typically occurred downstream of the point of minimum pressure. This observation was repeated in the recent NASA NLF flight experiments (ref. 1) on modern airframe surfaces. Physically, these observations mean that transition resulted either from amplified Tollmien-Schlichting (T-S) waves or laminar separation in the adverse pressure gradient. Analysis of flight transition data in reference 5 leads to the hypothesis that at relatively large values of transition Reynolds numbers (R_t on the order of 6×10^6) on airfoils with moderately favorable pressure gradients, in dominantly two-dimensional incompressible flows, transition in flight can be expected to occur as a consequence of the inflectional instability associated with laminar separation in the adverse pressure gradient.

The natural log of the T-S wave amplitude at transition (A) to the amplitude at the point of instability (A_0) is defined as n; thus $n = \ln(A/A_0)$. Past analyses of T-S stability for flight-measured transition (ref. 5) have produced values of n from 15 to 20 for transition near laminar separation. With sufficient flow acceleration up to the location of the start of pressure recovery, n = 15 may be used as a conservative criterion to avoid T-S instability transition prior to the point where laminar separation can occur. The favorable influence of compressibility on T-S wave damping suggests that this effect may occur even for larger values of transition Reynolds numbers at higher subcritical Mach numbers. Figure 10 illustrates this effect. This analysis shows that for a given moderately favorable pressure distribution, the "n-factor" or amplitude ratio does not exceed a value near 15 for predicted transition at 70-percent chord for the highest chord Reynolds numbers at the increasing value of Mach number. This behavior of T-S amplification means that at these larger chord Reynolds numbers, transition might still be expected to occur at laminar separation.

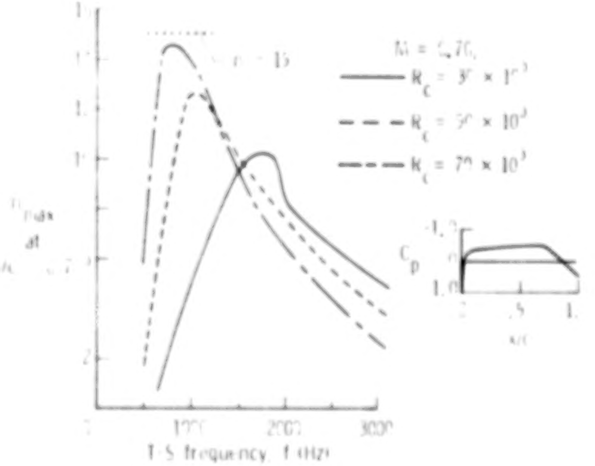

Figure 10.- The influence of compressibility on Tollmien-Schlichting wave amplification at large chord Reynolds numbers.

ORIGINAL PAGE IS
OF POOR QUALITY

Effects of Loss of Laminar Flow on Stability and Control

For several NLF flight experiments, changes in stability and control characteristics caused by the loss of laminar flow have been observed. Reference 1 and this paper present data illustrating such effects. These changes were brought on by the behavior of the particular airfoils selected for use on the forward control surfaces for several canard configuration airplanes. These particular airfoils experienced boundary layer separation near the trailing edge if no laminar flow existed from the leading edge. This design feature is not typical of NLF airfoils. In general, NLF airfoils should be designed or selected which do not experience flow separation and lift loss upon loss of laminar flow.

Figure 11 depicts a Dragonfly airplane which experienced significant changes in stability and control characteristics with the loss of laminar flow on the forward wing. Difficulties were encountered in elevator effectiveness, climb performance, and handling qualities on approach and landing.

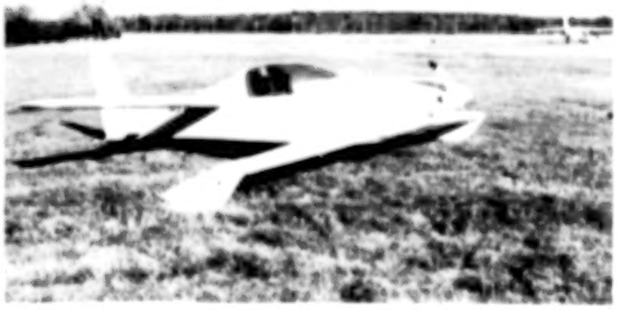

Figure 11.- Dragonfly airplane N 56 DH.

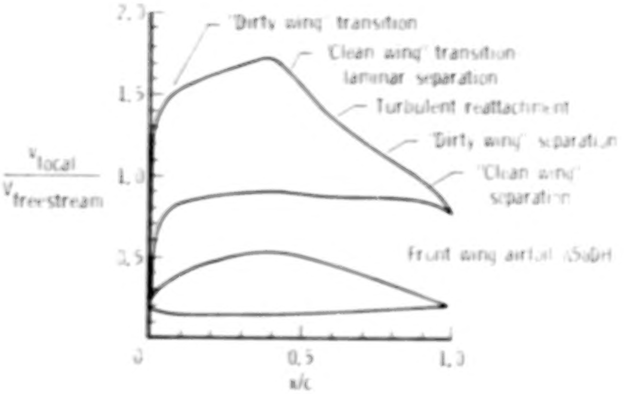

Figure 12.- Boundary-layer characteristics for a thick natural laminar flow airfoil. Angle of attack = 4 °, $R_c = 2 \times 10^6$.

Figure 12 illustrates the predicted velocity distributions and transition locations for the forward wing on this airplane. As illustrated in the figure, free transition (clean wing) is predicted near the 45-percent chord location. In flight, transition occurred at this location where a laminar separation bubble was observed with a length of about 10-percent chord. When transition occurs near the leading edge (dirty wing), the thick turbulent boundary layer is unable to remain attached during the pressure recovery on the aft part of this airfoil, and separation is predicted near the 75-percent chord location. Excellent agreement was observed between these predictions and the flight-measured separation location with transition fixed near the leading edge. Figure 13 illustrates the differences in airfoil performance (lift and drag) which result from these changes in transition. A very large, approximately 100 percent, increase in drag results from the combination of laminar flow loss and the increase in form drag caused by separation near $C_\ell = 1.0$. The effect of loss of laminar flow on forward wing lift is seen as a 15-percent reduction of lift curve slope. This behavior is precisely the cause of pitch-trim changes observed in flight with loss of laminar flow in this airplane.

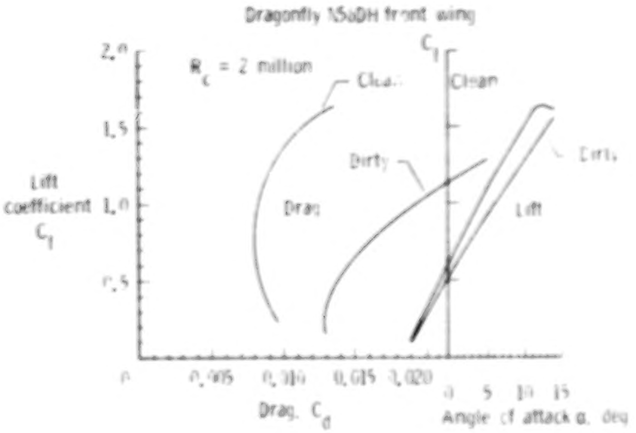

Figure 13.- Effect of fixed transition on performance of a thick NLF airfoil.

Figure 14 shows the configuration of small vortex generators installed at the 45-percent chord location to energize the turbulent boundary layer and alleviate the effects of loss of laminar flow. In addition, these devices increased the top speed of the airplane in the clean wing condition by about 10 mph and decreased the minimum trim speed by about 8 mph. This improvement resulted from the elimination of the relatively large laminar separation bubble on this airfoil and from the ensuing reduction in turbulent separation. Smaller improvements were observed for maximum and minimum speeds with transition fixed near the leading edge. Climb performance was improved by the vortex generators as well. Thus, the devices were very effective in alleviating the flow separation present for this laminar flow airfoil in both the laminar and turbulent conditions. In doing so, the stability and control of the airplane were greatly improved.

On airplanes for which winglets provide substantial levels of directional stability, loss of laminar flow can affect lateral-directional stability and control characteristics. References 6 and 7 explore the potential consequences of loss of laminar flow on stability and control in greater detail.

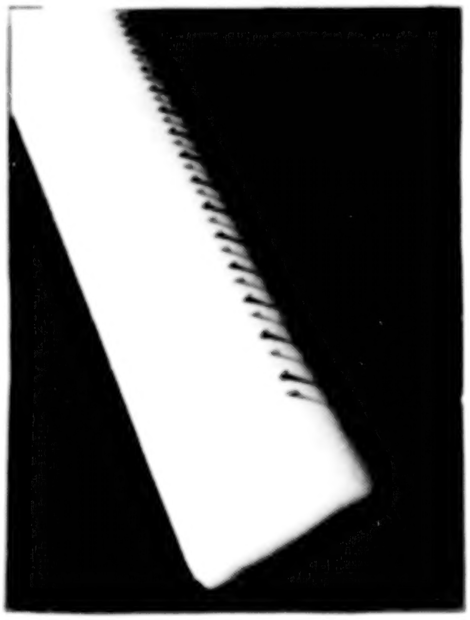

Figure 14.- Vortex generators on forward wing of Dragonfly airplane N 56 DH.

Effects of Loss of Laminar Flow on Maximum Lift

Careful selection of NLF airfoils can preclude difficulties related to maximum lift changes with loss of laminar flow. Two examples given here illustrate two possible outcomes depending on airfoil sections.

The flight data presented in the previous section for the Dragonfly airplane illustrated the effect of loss of laminar flow on minimum trim speed. This effect was caused by the flow separation which resulted from

ORIGINAL PAGE IS
OF POOR QUALITY

early transition, thus affecting section lifting behavior. For the Dragonfly airplane, loss of laminar flow caused an estimated increase in minimum trim speed of 18 mph. This speed change corresponds to a 40-percent reduction in maximum trimmed lift coefficient. Reductions in maximum trimmed lift coefficient between 20 and 27 percent were reported in reference 1 for the VariEze and Long-EZ airplanes using canard airfoils which were sensitive to loss of laminar flow.

By proper airfoil design, the dramatic effects of loss of laminar flow on lifting behavior described above can be avoided. The NACA 6-series airfoil on the Skyrocket wing for example (ref. 3) actually experienced a slight increase in maximum lift in flight with transition artificially fixed near the wing leading edge. This effect is explained by the elimination of an upper-surface leading-edge laminar-separation bubble at high angles of attack by the transition strip. These observations reinforce the need for selection of NLF airfoils which do not experience significant flow separation and lift loss associated with the loss of laminar flow. These examples show that care must be taken during testing of NLF airplanes to account for the effects of transition location.

Effects of Insect Accumulation on Laminar Flow

In spite of the long history of NLF flight research, little quantitative information is in the literature concerning the seriousness of insect contamination on laminar flow airplanes in practical operating environments. Specifically, no data are available which establish the increase in drag which can be expected to occur on laminar flow airplanes flying in representative insect population densities.

In practice, the seriousness of insect debris contamination will likely be dependent on airplane characteristics and mission. The occurrence of insect accumulation on aircraft surfaces varies widely in terms of frequency, location of impact, and resulting debris height. The population density of insects is affected by local terrain, vegetation, temperature, moisture, humidity, wind, and height above ground level (ref. 8). The insect impact pattern, as shown in recent analytical studies by Bragg (ref. 9), is affected by airfoil section geometry.

Insect accumulation on aircraft occurs predominantly at low altitudes (less than 500 ft), mostly on the takeoff roll and initial climb and on final approach and landing (ref. 10). Under many conditions (very cool or very warm temperatures for example), very small rates of insect accumulation will occur even at low altitudes. Maximum rates of insect accumulation will occur for an ambient temperature of 77°F under light wind conditions and high humidity (ref. 11). During recent NASA flight experiments by Croom (ref. 12) on an insect contamination protection system, the ambient conditions noted above were observed to produce maximum rates of insect accumulation. Figure 15 illustrates the sensitivity of rates of insect accumulation to ambient temperature and wind conditions. The results of these flight experiments indicate that below temperatures of about 70°F, insect accumulation rates will be insignificant.

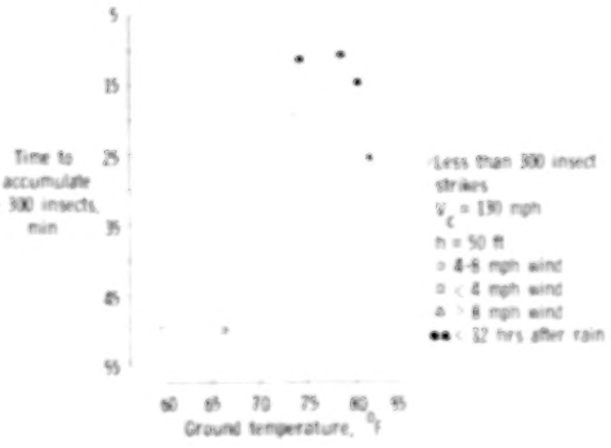

Figure 15.- Effect of ambient conditions on rates of insect accumulation on an airplane in flight.

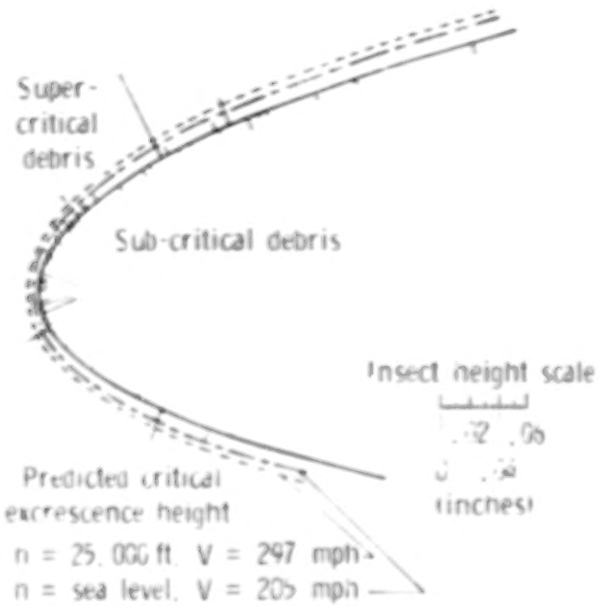
Super-critical debris
Sub-critical debris
Insect height scale
.02 .06
0 .04
(inches)
Predicted critical excrescence height
h = 25,000 ft, V = 297 mph
h = sea level, V = 205 mph

Figure 16.- Insect contamination pattern on Bellanca Skyrocket II NLF wing, accumulated in flight.

Flight-measured insect debris patterns on the Skyrocket airplane provide data illustrating the relative insensitivity of this particular airfoil at the conditions of the test to insect contamination. Figure 16 (from ref. 1) illustrates an insect debris pattern accumulated during a 2.2-hour flight at low altitudes. Sublimating chemicals were used in flight at sea level at 178 knots to determine which insect strikes caused transition. As shown, only about 25 percent of the insects collected were of sufficient or "supercritical" height at the particular airfoil location and caused transition. For illustrative purposes in the figure, supercritical insects are shown as protruding outward from the airfoil surface and subcritical ones protruding inward. Very near the stagnation point, rather large insect remains were recorded which did not cause transition. These insects were located forward of the location where disturbances can begin to amplify in the laminar boundary layer. An analysis using a value of critical roughness height Reynolds number of 600 was conducted to predict which insects would cause transition at a more typical cruise altitude of 25 000 ft. The dashed line in the figure depicts the height of roughness required to cause transition at this altitude. It shows that only about 9 percent of the insects collected would have caused transition. Thus, even though large numbers of insects might be collected on a wing leading edge, relatively few of them can be expected to cause transition at high cruise altitudes.

Effects of Flight Through Clouds and Precipitation on Laminar Flow

Under certain conditions, the operation of a laminar flow airplane can be affected by either precipitation onto the NLF surface or by the flux of free-stream cloud particles through the laminar boundary layer. Precipitation can cause loss of laminar flow by

ORIGINAL PAGE IS
OF POOR QUALITY

creating three-dimensional roughness elements on the airfoil surface which, in sufficient quantity and size, act as a boundary-layer trip near the leading edge. Cloud particles (i.e., ice crystals) can cause loss of laminar flow by the shedding of turbulent wakes from the particles as they traverse the laminar boundary layer. At sufficient flux (particles per unit area per unit time) and sufficient particle Reynolds number, partial or total loss of laminar flow can occur.

The VariEze wind-tunnel experiments of reference 1 provided limited data on the effects of precipitation on NLF. In those experiments the effects of rain were studied by spraying water on the canard and wing. (See fig. 17.) Comparison of the aerodynamic characteristics of the canard in a heavy water spray and with transition fixed by artificial roughness showed that the effect of the water drops on the airfoil was to move transition to near the leading edge.

Spray carriage

Figure 17.- Rain simulation apparatus in the Langley 30- x 60-ft wind tunnel VariEze experiments.

Figure 18 illustrates the effect of water spray on the VariEze canard in the Langley 30- by 60-Foot Tunnel. For these conditions, transition is suspected to occur near the leading edge, with separation of the turbulent boundary layer near the 55-percent chord location (as previously described for this canard airfoil).

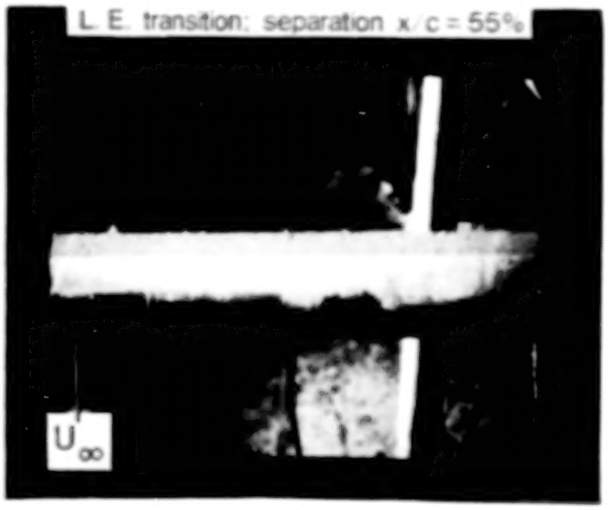

Figure 18.- Effects of water spray on transition and separation of a natural laminar flow airfoil.

Results of two flight experiments have shown that when a mist deposit occurs on a laminar flow surface during flight through clouds, the boundary layer becomes turbulent. During the early Hawcon flights (ref. 13), wake-rake drag measurements were made with a mist deposit from flight through clouds on the wing. The Heinkel measurements (ref. 13) showed a 42-percent increase in section drag (i.e., loss of laminar flow) caused by the mist deposit at chord Reynolds numbers between 6.5×10^6 and 8.5×10^6. During the more recent NASA T-34C NLF glove flight experiments (ref. 5), transition location was measured using hot films with mist deposit on the leading edge during flight through clouds. Transition during these tests was observed to occur near the wing leading edge.

During these same T-34C flights, transition was measured during flight through clouds for which no mist deposit occurred on the wing. For these tests, laminar flow was unaffected by the cloud particles in the free stream. By using Hall's criterion (refs. 14 and 15) for a critical spherical particle Reynolds number of 400 (based on particle diameter), the speed required for an average-size cloud particle of 20 microns to cause transition is estimated as 587 knots at a unit Reynolds number of 1.4×10^6. In the X-21 LFC flight experiments (ref. 14), laminar flow was lost as a result of flight through ice-crystal clouds. For these tests, the critical particle Reynolds number was exceeded for the flight conditions involved. This occurred because of the much lower value of critical particle Reynolds number for the larger and prism-shaped ice crystals encountered in the stratosphere. For the X-21 and the T-34C flights, laminar flow was restored immediately upon exiting from a cloud.

These results indicate the insensitivity of the laminar boundary layer to flight through clouds at low altitudes where the particles do not deposit on the surface and where the critical particle Reynolds number is not exceeded. The mechanism for loss of laminar flow in clouds at lower altitudes involves deposit of mist which creates supercritical roughness in the boundary layer. Rain causes loss of laminar flow probably by a similar roughness mechanism.

Laminar Flow Behavior in Propeller Slipstreams

Recent flight and wind-tunnel investigations have clarified the understanding of the effect which a propeller slipstream has on the laminar boundary layer on a surface immersed in the slipstream (refs. 3 and 16). These recent experiments relied on hot-film and hot-wire measurement techniques to explore the time-dependent characteristics of laminar boundary-layer behavior in propeller slipstreams. These measurements documented the existence of a cyclic turbulent behavior resulting in convected regions of turbulent packets between which the boundary layer remains laminar. A physical model for this behavior is presented in figure 19 (ref. 16). This model illustrates the local changes in boundary-layer thickness and levels of turbulence within the turbulent packets caused by the wake of each propeller passage. The results of the experimental investigation indicate that laminar flow is not totally lost in a propeller slipstream. Furthermore, transition location in the propeller slipstream cannot be determined using pressure probes which give time-averaged information about the boundary-layer velocity profile; time-dependent measurements with hot-film sensors, for example, can provide transition information. As illustrated in figure 20, sublimating chemicals can be used to determine a mean location of boundary-layer transition in the slipstream.

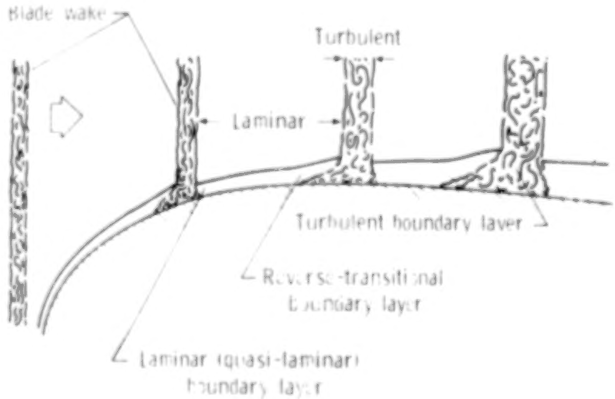
Blade wake
Turbulent
Laminar
Turbulent boundary layer
Reverse-transitional boundary layer
Laminar (quasi-laminar) boundary layer

Figure 19.- Propeller slipstream disturbance flow model showing turbulent response in laminar boundary layer (ref. 16).

ORIGINAL PAGE IS
OF POOR QUALITY

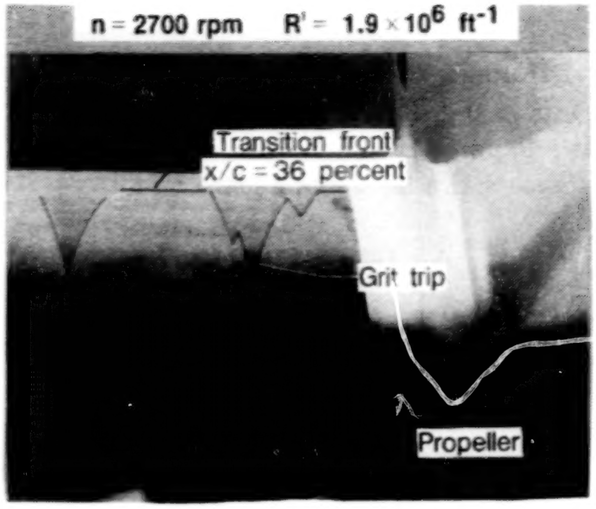

Figure 20.- Laminar boundary-layer transition in a propeller slipstream as indicated by sublimating chemicals.

Howard, Miley, and Holmes (ref. 16) attempted to numerically model the skin-friction changes in response to the propeller slipstream. A finite-difference boundary-layer code was used with the turbulent and laminar solution procedure switched on and off at intervals across the surface. The skin-friction values were integrated to determine sectional-drag coefficient. The resulting cyclic laminar/ turbulent drag coefficient lay between the fully laminar and fully turbulent levels of drag. This theoretical prediction agrees well with the analysis of experimental results presented in figure 21. The figure shows that the wake-rake measured section drag with the propeller rotating lies between the levels of drag with free transition and with fully turbulent flow.

Based on these experiences, it is concluded that some levels of benefit from laminar viscous drag reduction can be achieved on wings in propeller slipstreams. It is not clear whether these benefits extend to laminar flow on fuselages or engine nacelles immersed in propeller slipstreams.

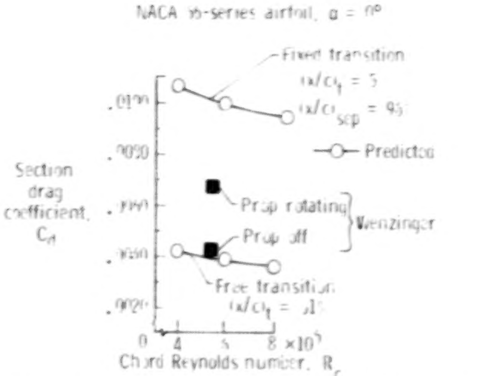

Conclusion: significant NLF drag reduction possible in slipstream

Figure 21.- Effect of propeller slipstream on measured drag for a laminar flow airfoil section.

Fixed Transition Flight Testing

One important conclusion from the recent NASA NLF flight experiments is that fixed transition tests are an important inclusion in flight research or in certification flight testing on airplanes with smooth surfaces and accelerating pressure gradients which can support laminar flow. Fixed transition testing will be increasingly important for correlation of wind tunnel, analytical, and flight test characteristics for laminar flow airplanes. Furthermore, since several propeller surfaces have been observed to support significant runs of NLF, there is additional value in conducting tests with transition fixed on the propeller as well.

Standard wind-tunnel transition fixing procedures are directly applicable to flight testing. Braslow's critical roughness criteria for both two-dimensional and three-dimensional boundary layers (ref. 17) can be used for sizing of grit to produce transition without excessive grit drag. Very thin (0.001

in.) double-back tape is available from large manufacturers of industrial tapes and is very useful for applying grit in a fashion which makes removal easy after testing. Two-dimensional transition strips (e.g., tape or wire) can be used as an alternative to grit. Sizing of two-dimensional trip strips can be accomplished using reference 18 for a tape trip and reference 19 for a wire trip.

CONCLUDING REMARKS

A review of NLF flight experiences over the period from the 1930's to the present has been given to provide information on the achievability and maintainability of NLF in typical airplane operating environments. Significant effects of loss of laminar flow on airplane performance have been observed for several airplanes, indicating the importance of providing information on these changes to laminar flow airplane operators. Significant changes in airplane stability and control and maximum lift were observed in flight experiments with the loss of laminar flow. However, these effects can be avoided by proper selection of airfoils. Conservative laminar flow airfoil designs should be employed which do not experience significant loss of lift (caused by flow separation) upon the loss of laminar flow. Mechanisms have been observed for the effects of insect accumulation, flight through clouds and precipitation, and propeller slipstreams on laminar flow behavior. Fixed transition testing, in addition to free transition testing, is recommended as a new standard procedure for airplanes with surfaces designed to support laminar flow. With care and attention to boundary-layer considerations, NLF can be safely used for practical reduction of viscous drag.

REFERENCES

1. Holmes, Bruce J.; Obara, Clifford J.; and Yip, Long P.: Natural Laminar Flow Flight Experiments on Modern Airplane Surfaces. NASA TP 2256, 1984.

2. Davies, H.: Some Aspects of Flight Research. J. of Royal Aeronautical Society, vol. 55, June 1951, pp. 325-361.

3. Holmes, Bruce J.; Obara, Clifford J.; Gregorek, Gerald M.; Hoffman, Michael J.; and Freuler, Rick J.: Flight Investigation of Natural Laminar Flow on the Bellanca Skyrocket II. SAE Paper 830717, 1983.

4. Tani, I.: On The Design of Airfoils in Which the Transition of the Boundary-Layer is Delayed. NACA TM 1351, 1952.

5. Obara, Clifford J.; and Holmes, Bruce J.: Flight Measured Laminar Boundary-Layer Transition Phenomena Including Stability Theory Analysis. NASA TP 2417, 1985.

6. van Dam, C. P.: Natural Laminar Flow and Airplane Stability and Control. Laminar Flow Aircraft Certification, NASA CP-2413, 1986.

7. Johnson, J. L., Jr.; Yip, L. P.; and Jordan, F. J., Jr.: Preliminary Aerodynamic Design Considerations for Advanced Laminar Flow Aircraft Configurations. Laminar Flow Aircraft Certification, NASA CP-2413, 1986.

8. Atkins, P. B.: Wing Leading Edge Contamination by Insects. Flight Note 17, Aeronautical Research Laboratories, Oct. 1951.

9. Bragg, Michael B.; and Maresh, J. L.: The Role of Airfoil Geometry in Minimizing the Effect of Insect Contamination of Laminar Flow Sections. AIAA Paper no. 84-2170, 1984.

10. Coleman, W. S.: Roughness Due to Insects. Boundary-Layer and Flow Control, vol. 2, Pergamon Press, 1961.

11. Coleman, W. S.: Wind Tunnel Experiments on the Prevention of Insect Contamination by Means of Soluble Films and Liquids Over the Surface. Report to the Boundary-Layer Control Committee, BLCC Note 39, 1952.

12. Croom, Cynthia C.; and Holmes, Bruce J.: Flight Evaluation of an Insect Contamination Protection System for Laminar Flow Wings. SAE Paper No. 850860, 1985.

13. Serby, J. E.; and Morgan, M. B.: Note on the Progress of Flight Experiments on Wing Drag. Rep. No. B.A. 1360, British R.A.E., Dec. 1936.

14. Hall, G. R.: On the Mechanics of Transition Produced by Particles Passing Through an Initially Laminar Boundary Layer and the Estimated Effect on the LFC Performance of the X-21 Aircraft. Northrop Corp., Oct. 1964.

15. Hall, G. R.: Interaction of the Wake From Bluff Bodies With an Initially Laminar Boundary Layer. AIAA J., vol. 5, no. 8, Aug. 1967, pp. 1386-1392.

16. Howard, R. M.; Miley, S. J.; and Holmes B. J.: An Investigation of the Effects of the Propeller Slipstream on the Laminar Boundary Layer. SAE Paper 850859, 1985.

17. Braslow, Albert L.; and Knox, Eugene C.: Simplified Method for Determination of Critical Height of Distributed Roughness Particles for Boundary-Layer Transition at Mach Numbers From 0 to 5. NACA TN 4363, 1958.

18. Fage, A.: The Smallest Size of Spanwise Surface Corrugation Which Affects Boundary Layer Transition on an Airfoil. R&M No. 2120, Brit. A.R.C., 1943.

19. Schlichting, H.: Boundary Layer Theory. McGraw-Hill, 7th ed., 1979, p. 539.

N88-23745

58-01
138

MANUFACTURING REQUIREMENTS

Bruce J. Holmes
NASA Langley Research Center
Hampton, Virginia 23665

Clifford J. Obara, Glenn L. Martin,
and Christopher S. Domack
PRC Kentron, Inc.
Hampton, Virginia 23666

SUMMARY

In recent years, natural laminar flow (NLF) has been proven to be achievable on modern smooth airframe surfaces over a range of cruise flight conditions representative of most current business and commuter aircraft. Published waviness and boundary-layer transition measurements on several modern metal and composite airframes have demonstrated the fact that achievable surface waviness is readily compatible with laminar flow requirements. Currently, the principal challenge to the manufacture of NLF-compatible surfaces is two-dimensional roughness in the form of steps and gaps at structural joints. This paper presents results of recent NASA investigations on manufacturing tolerances for NLF surfaces, including results of a flight experiment. Based on recent research, recommendations are given for conservative manufacturing tolerances for waviness and shaped steps.

INTRODUCTION

Many modern metal and composite airframe manufacturing techniques can provide surface smoothness which is compatible with natural laminar flow (NLF) requirements (ref. 1). Specifically, this has been shown in flight investigations over a range of free-stream conditions including Mach numbers up to 0.7, chord Reynolds numbers up to about 30 million, and transition Reynolds numbers up to about 14 million. Surface smoothness requirements relate to waviness, to two-dimensional steps and gaps, and to three-dimensional roughness elements. The recent flight experiments were conducted on flush-riveted thin aluminum skins, integrally stiffened milled thick aluminum skins, bonded thin aluminum skins, and composite surfaces. The most important conclusion concerning manufacturing to be drawn from these experiences is that the waviness of the surfaces in the tests met the NLF criterion for the free-stream conditions flown. However, in addition to waviness, an equally important consideration is manufacturing roughness of the surface in the form of steps and gaps perpendicular to the free stream. While much work has been done in the past, many unknowns still exist concerning the influences of wing sweep, compressibility, and shapes of steps or gaps on manufacturing tolerances for laminar flow surfaces. Even less information is available concerning NLF requirements related to practical three-dimensional roughness elements such as flush screw head slots and incorrectly installed flush rivets.

The principal challenge to the design and manufacture of laminar flow surfaces today appears to be in the

PRECEDING PAGE BLANK NOT FILMED

installation of leading-edge panels on wings, nacelle, and empennage surfaces. Another similar challenge is in the installation of access panels, doors, windows, and the like on fuselage noses and engine nacelles, where laminar flow may be desired. These surface discontinuities appear to be unavoidable for typical current aircraft; the challenge is, "Can laminar flow be maintained over these discontinuities?" Figure 1 illustrates the drag reduction benefits available from laminar flow on various airframe components on a medium-sized subsonic business jet. These are not integrated benefits, but rather the benefits of adding laminar flow to a fixed airframe geometry. Figure 1 shows that significant fuel efficiency improvements of the order of 25 percent are possible. Such improvements are strong motivation for understanding how to achieve laminar flow over surface discontinuities.

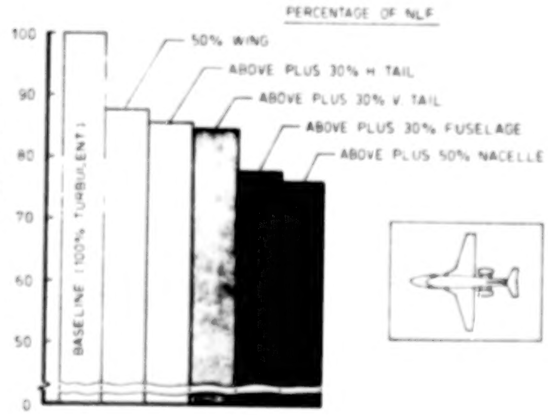

Figure 1. Predicted drag benefits of laminar flow on a subsonic business jet.

The purpose of this paper is to present results and analyses of recent NASA Langley research on manufacturing tolerances for waviness and shaped steps on NLF surfaces for subsonic aircraft. No treatment is given herein of tolerances for three-dimensional roughness effects. The paper includes a review and discussion of past manufacturing tolerances research.

SYMBOLS

C_{D_o}	profile drag coefficient
C_ℓ	section lift coefficient
C_p	pressure coefficient
c	local chord, in.
h	step height, gap width, or double amplitude wave length, in. or ft
h'	height of a bulge above nominal surface, in. or ft
H	altitude, ft
M	Mach number
n	logarithmic exponent of Tollmien-Schlichting amplitude ratio
R'	free-stream unit Reynolds number, ft^{-1}
R_c	chord Reynolds number
R_h	roughness height Reynolds number
s_t	surface length from stagnation to transition, ft
u_e	boundary-layer edge velocity, ft/sec
U_∞	free-stream velocity, ft/sec
x	longitudinal dimension, ft
θ	boundary-layer momentum thickness, in.
ν	kinematic viscosity, ft^2/sec
Λ	wing leading-edge sweep angle, deg
Λ_s	angle between ridge of a step and the free stream
λ	length of wave, bulge, ridge, or hollow, in.

Subscripts:

crit	critical
max	maximum
∞	free stream

LAMINAR BOUNDARY-LAYER TOLERANCES TO SURFACE IMPERFECTIONS

Existing criteria for NLF surfaces deal with waviness and with both two- and three-dimensional roughness. Each of these types of surface imperfections can cause transition by different mechanisms in the boundary layer. The definition of critical height for waviness or roughness is related to the mechanism by which transition is affected. The mechanisms of most practical interest include laminar separation, amplification of Tollmien-Schlichting (T-S) waves, amplification of crossflow vorticity, and interactions between any of these mechanisms. In addition, free-stream turbulence and acoustic disturbances may interact with these mechanisms to influence critical waviness and roughness heights. Criteria exist only for critical waviness and roughness which cause either laminar separation or amplification of T-S waves. No criteria exist which fully address surface-imperfection-induced transition related to crossflow amplification on swept wings or interactions between the various transition mechanisms and free-stream disturbances.

The following definitions appear in the literature and are useful for the present discussion. Critical waviness height to length ratio (h/λ) and critical step height or gap width can be defined as those which produce transition forward of the location where it would occur in the absence of the surface imperfection. Experimentally, premature transition was identified in past work as the first appearance of turbulent bursts downstream of either a waviness or roughness surface imperfection. This is the definition used in references 2 to 5 to establish critical conditions for surface imperfections.

For most common applications in two-dimensional flows, this definition physically relates to the viscous amplification of T-S waves or to (Rayleigh's) inflectional instability growth over a laminar separation bubble. Figure 2 illustrates possible effects of a given two-dimensional surface imperfection on transition. A subcritical condition exists when transition is unaffected by the disturbance (top of figure). The middle of figure 2 illustrates the critical condition at which transition just begins to be affected by the disturbance. In the extreme, a surface imperfection could cause sufficiently rapid T-S wave amplification for transition to occur very near the wave itself, as illustrated at the bottom of figure 2.

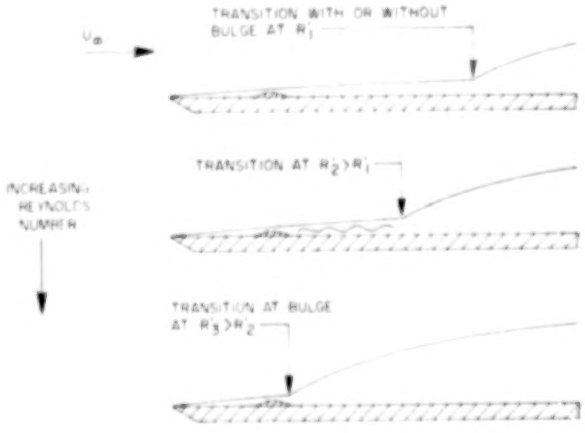
TRANSITION WITH OR WITHOUT BULGE AT R'_1
U_∞
TRANSITION AT $R'_2 > R'_1$
INCREASING REYNOLDS NUMBER
TRANSITION AT BULGE AT $R'_3 > R'_2$

Figure 2. Effects of two-dimensional surface imperfection on laminar flow.

Another limiting condition of practical interest is the occurrence of transition at the surface imperfection caused by the inflectional instability in the free shear layer over the laminar separation bubble formed there. Using flight data (from ref. 6), figure 3 illustrates the predicted local increase in growth rate of T-S instability caused by a surface wave. The surface wave tested was $h = 0.010$ in. and $\lambda = 2.5$ in.; the effects of this wave on the pressure distribution between $0.10 < x/c < 0.13$ and on maximum T-S amplitude ratios are apparent in the figure. In the adverse pressure gradient of the wave, n_{max} is seen to grow from about 1 to near 4. Elsewhere, in favorable pressure gradients, the rate of growth of the T-S disturbance is damped.

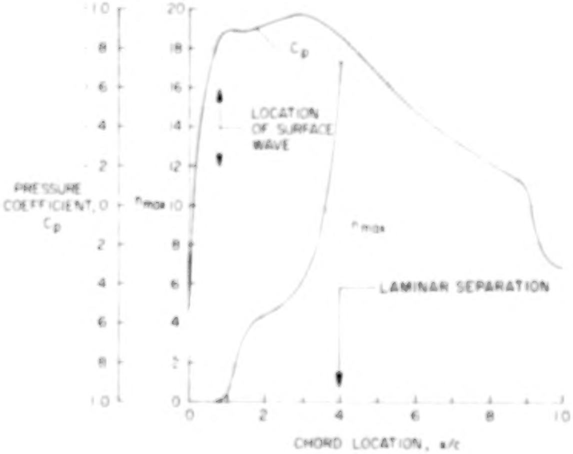

Figure 3. Tollmien-Schlichting instability growth in the presence of a surface wave.

From Schlichting (ref. 7), the laminar boundary layer will separate for $(\theta^2/\nu)\,(du_e/dx) < -0.1567$ where θ is the boundary-layer momentum thickness, ν is the local kinematic viscosity, and u_e is the local potential flow velocity. Calculation of values of $(\theta^2/\nu)\,(du_e/dx)$ for both Fage's and Carmichael's surface imperfections indicates that the critical value for laminar separation was exceeded at most of the test conditions for those studies. For example, at the conditions shown in figure 4 (from Fage), $(\theta^2/\nu)\,(du_e/dx) = -0.19$. Similar results occur for analysis of Carmichael's data from reference 3. It appears then that for many of the critical surface imperfections tested by Fage and Carmichael, laminar separation at the imperfection was present. Thus, the mechanism for forward movement of transition due to a surface imperfection could involve both the effect of local adverse pressure gradient on T-S amplification and the effect of Rayleigh's inflectional instability.

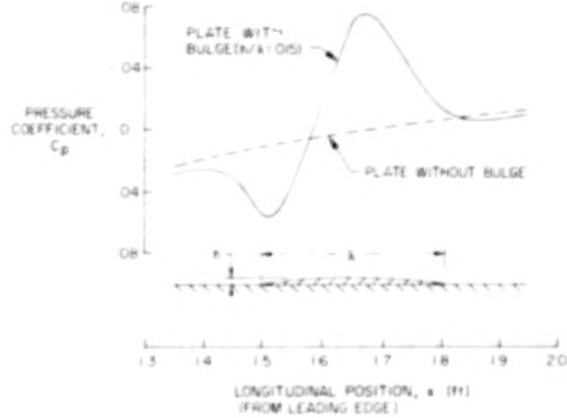

Figure 4. Pressure distributions over a bulge, from Fage (ref. 2).

CRITERIA FOR WAVINESS

The classical research by Fage (ref. 2) provided criteria for critical height of 2-D bulges, ridges, and hollows in incompressible 2-D boundary layers. His shapes, as illustrated in figure 5, do not accurately represent many of the surface imperfections observed on modern airframe surfaces. However, the pressure disturbances over Fage's bulges and hollows do simulate those which will occur over sinusoidal waves. In spite of these limitations, Fage's experiments did provide an understanding of some of the mechanisms associated with transition over these imperfections.

The research of Carmichael (refs. 3 to 5) provided the basis for the existing criterion on allowable waviness for both swept and unswept wing surfaces. Carmichael's criterion applies to single and multiple bulges or sinusoidal waves above the nominal surface which produce sinusoidal-shaped disturbances in the pressure distribution. As previously discussed, transition in Carmichael's surface waviness experiments may have been related to either laminar separation or to amplified Tollmien-Schlichting wave growth. This T-S amplification over a surface wave results from the decreased boundary-layer stability in the adverse pressure gradient on the aft side of a wave, but may also be influenced by resonance between the critical T-S frequency and the surface waviness frequency (wavelength of multiple, closely spaced waves) (refs. 3 and 8). Carmichael's investigations at least partially included the influences of compressibility, boundary-layer stabilization by suction and pressure gradient, multiple waves, and wing sweep.

Compressibility influences allowable waviness in two ways. First, compressibility favorably increases the damping of growth rates for T-S waves. The second unfavorable effect results from the increased pressure peak amplitude over a wave due to compressibility. It is not clear which effect dominates.

With wing sweep, Carmichael and Pfenninger observed a slight reduction in allowable waviness (ref. 5). Furthermore, a slightly greater reduction in allowable (h/λ) was observed for multiple waves on a swept wing than for multiple waves on an unswept wing. This might be expected to result from the interaction between the T-S instability growth in the deceleration on the backside of the wave and the crossflow instability growth due to the spanwise pressure gradient. Carmichael defined a critical wave as the minimum (h/λ) which prevents the attainment of laminar flow to the trailing edge under boundary-layer stabilization using moderate suction. On a non-suction wing, the criterion applies for waves in regions of boundary-layer stabilization using a favorable pressure gradient (flow acceleration). The criterion was based on experimental results for waves located more than 25 percent of the chord downstream of the leading edge. Thus for waves located in very highly accelerated flows closer to the leading edge, the criterion may underpredict allowable waviness. Conversely, the criterion would overpredict the allowable waviness in a region of unaccelerated flow; for this case, the criterion provided by Fage (ref. 2) from his flat plate experiments would provide better information. Fage's criterion is given by

$$\frac{h'}{s_t} = 9 \times 10^6 \left[\frac{u_e s_t}{\nu}\right]^{-3/2} \left[\frac{\lambda}{s_t}\right]^{1/2} \qquad (1)$$

which can be more conveniently written

$$\frac{h'}{\lambda} = 9 \times 10^6 \left[\frac{u_e s_t}{\nu}\right]^{-3/2} \left[\frac{s_t}{\lambda}\right]^{1/2} \qquad (2)$$

where h' is the height of a bulge in feet above the nominal surface, λ is the length of the bulge in feet, s_t is

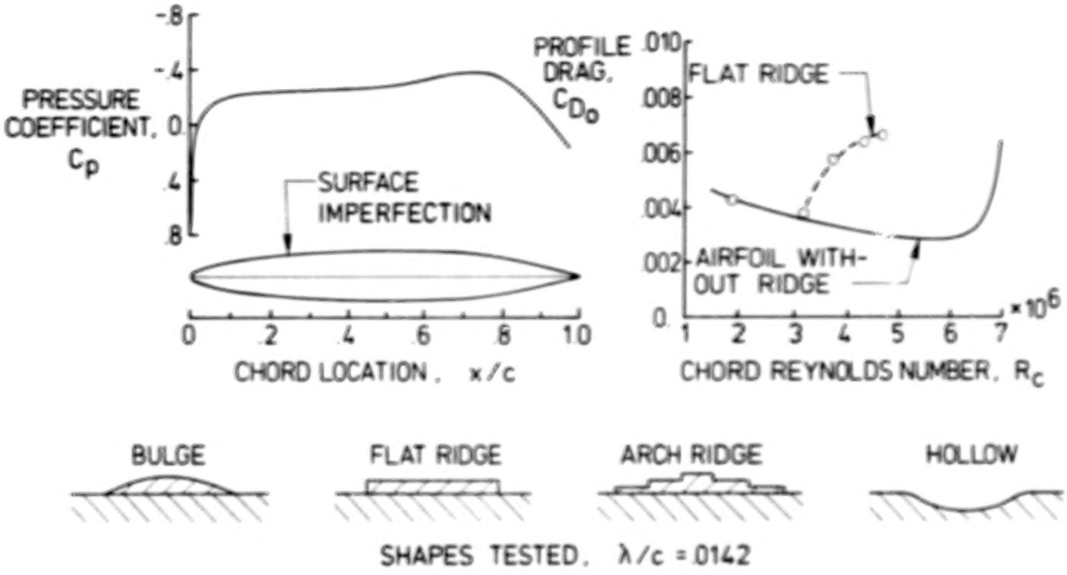

Figure 5. Shapes of two-dimensional surface imperfections tested by Fage (ref. 2).

the surface length to transition in feet, u_e is the boundary-layer edge velocity in feet per second at the location of the center of the bulge for the undistorted surface, and ν is the kinematic viscosity. Using local C_p and free-stream velocity, u_e can be determined directly for use in equation (2). Fage's work covered a range of transition Reynolds numbers from 1 x 10^6 to 3.5 x 10^6 and did not include any effects of compressibility or sweep.

Carmichael's waviness criterion is given as

$$\frac{h}{\lambda} = \left(\frac{59000\ c\ \cos^2 \Lambda}{\lambda\ R_c^{1.5}}\right)^{0.5} \qquad (3)$$

where h is the double-amplitude wave height in inches, λ is the wavelength in inches, c is the streamwise wing chord in inches, Λ is the wing leading-edge sweep, and R_c is the chord Reynolds number based on chord length and airspeed in the free-stream direction. Note the difference in the definition of wave heights, h and h', used in equations (2) and (3). For waves which have their peaks and valleys aligned in the chordwise direction, the recommendation of reference 9 is to double the value of h/λ from equation (3).

The dial indicator mounted on a 2-in. base has been used for decades to document waviness. On a swept wing, both h and λ are most appropriately measured normal to the leading edge since most of the aircraft structure which is responsible for waviness is oriented this way. This practice will only slightly and conservatively affect the measured surface wave height to length ratios for wings of moderate sweep (as compared to measuring waviness in the free-stream direction).

For conservatism, Carmichael proposed that the value of (h/λ) from equation (3) be multiplied by 1/3 to estimate tolerances for multiple waves. However, this multiple waviness criterion was developed using closely spaced waves and does not address any effects due to widely spaced waves. As previously discussed, closely spaced waves may have a T-S resonance effect which might be less likely to occur for widely spaced waves. Furthermore, the wind-tunnel and flight experimental results used to develop the factor of 1/3 actually varied over a range from 1/3 to 3/4, with the flight values being typically greater than the wind-tunnel values. Thus, some uncertainty exists concerning a realistic method for figuring the effect of multiple waves on the allowable (h/λ). Carmichael (ref. 4) notes that "...if the wing design can be accomplished such that waviness is reduced to a low value, then a few waves at major structural points could be permitted with a somewhat larger tolerance than (that calculated using the 1/3 factor)." As discussed in reference 10, most waviness observed on modern airframe surfaces typically consists of only one or two waves, widely spaced, at major structural joints. This observation was also made for very stiff skins (on missiles and on certain supersonic airplanes) as early as 1959. (See ref. 11.)

Consistently in recent flight experiments (ref. 1), the measured aircraft surface waviness was better than required as calculated by Carmichael's criterion, using the single-wave assumption. A selected number of these comparisons are illustrated in figure 6. All but one of the waves shown are significantly smaller than allowable. Since the allowable waviness values were calculated for the low altitudes and high speeds of the flight experiments, the allowable waviness at lower Reynolds numbers for typical cruise conditions for all of the airplanes will be even larger than shown. During the flight experiments on these airplanes at the chord Reynolds numbers indicated in figure 6, no transition due to waviness was observed. Thus, a conservative value for allowable waviness on unswept ($\Lambda < 15°$) NLF wings can be determined using equation (3) for a single wave. Use of a single-wave assumption will result in larger allowable wave heights which are easier and less costly to achieve in production.

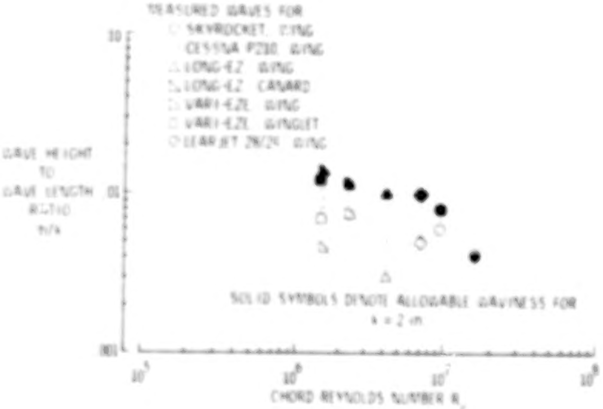

Figure 6. Comparisons of allowable and actual waviness measured on airplanes used for NLF flight experiments.

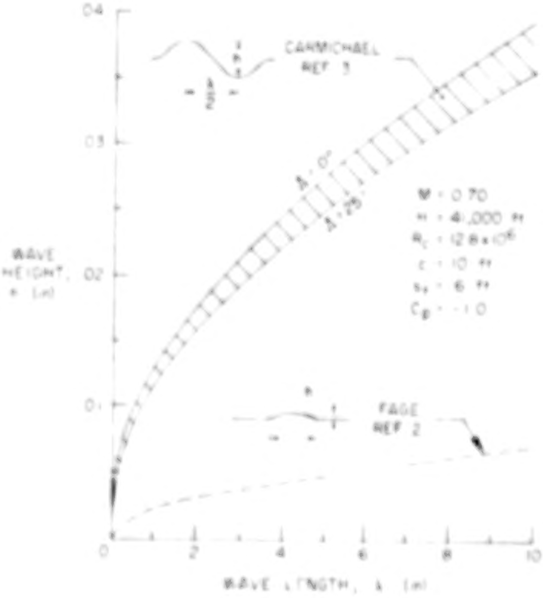

Figure 7. Allowable waviness for a business jet at cruise conditions. From Fage (ref. 2) and Carmichael (ref. 3).

Figure 7 presents examples of allowable waviness for free-stream conditions representative of a high performance business airplane flying at Mach 0.7 at 41,000 ft. The chart shows allowable waviness using both equations (2) and (3). Using Carmichael's criterion (eq. (3)), the effect of sweep on allowable waviness is seen to be on the order of 10 percent. These calculations show that with a wavelength of 6 in., the allowable wave height is 0.025 in. on a 25° swept wing, with a favorable pressure gradient. Such a manufacturing tolerance for waviness is within the capabilities of modern airframe manufacturing methods. Were this same 6-in. wave in a region of unaccelerated flow, the allowable height would be about 0.010 in. This calculation assumes it is reasonable to relate h to h' by a factor of 2; that is, an allowable double amplitude wave height may be estimated using 2 x h' in equation (2) for comparisons with h in equation (3).

The dashed line for Fage's criterion in figure 7 is presented with the caution that it has never been verified for compressible flows. The figure shows the effect of an unaccelerated flow (Fage's criterion) on reducing the allowable waviness significantly compared to allowable waviness in an accelerated flow (Carmichael's criterion). This result illustrates the dominant effect of pressure gradient on waviness tolerances. The reason for this effect is explained by the dominant effect of pressure gradient on boundary velocity profiles and, hence, on T-S stability.

CRITERIA FOR STEPS AND GAPS

A potentially misleading conclusion from Fage (ref. 2) was that shape did not affect the critical size of the surface imperfection. This conclusion resulted, at least in part, from the particular shapes tested by Fage. (See fig. 5.) In the case of his ridges, each shape produced a laminar separation region at the front of the ridge and a second laminar separation at the aft-facing step on the downstream edge of the ridge. Transition behind Fage's ridges could have been dominated by the inflectional instability growth over these two separated flow regions. For modern airframe surfaces, the simple forward-facing step, aft-facing step, or gap (perpendicular to the free stream) is of more practical interest. Figure 8 shows the characteristics of laminar separation over such a step.

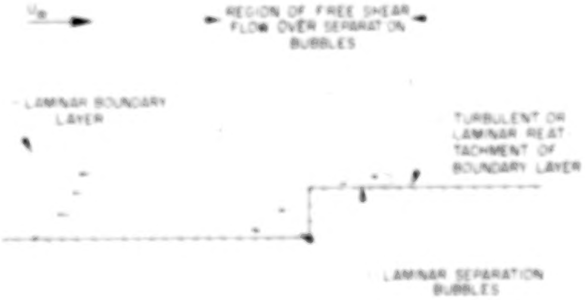
U∞
REGION OF FREE SHEAR FLOW OVER SEPARATION BUBBLES
LAMINAR BOUNDARY LAYER
TURBULENT OR LAMINAR REATTACHMENT OF BOUNDARY LAYER
LAMINAR SEPARATION BUBBLES

Figure 8. Characteristics of laminar separation over a step.

The past work on criteria for step and gap tolerances came from the X-21 experiments (ref. 9). The literature does not state what definition was used to determine critical Reynolds numbers for these surface imperfections. However, according to Dr. Werner Pfenninger, who conducted wind-tunnel experiments to develop these criteria, the critical step height Reynolds number was established based on the conditions where the first turbulent bursts occurred far downstream from the surface imperfection. Thus, these criteria were developed in a manner consistent with that for the waviness criteria. The critical Reynolds number $R_{h,crit} = (U_\infty/\nu)\, h$ is determined by free-stream airspeed (U_∞), kinematic viscosity, and the height of the step or length of the gap (h). The shapes and critical Reynolds numbers for which tolerances were established in the X-21 experiments are illustrated in figure 9.

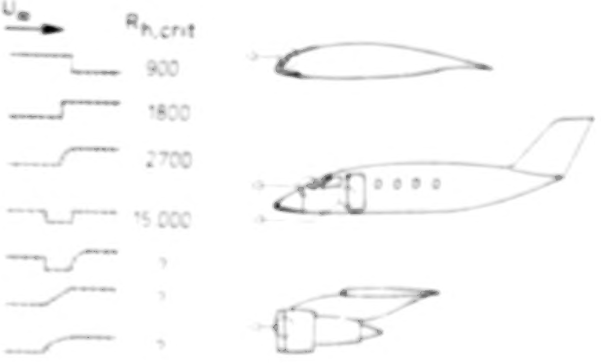

Figure 9. Examples of surface imperfections and tolerances for NLF surfaces.

In addition, figure 9 presents information from recent NASA investigations on the influence of rounded steps on critical Reynolds numbers. For three of the illustrated surface imperfection shapes (indicated by question marks), no criteria exist. The recent NASA flight experiments on shaped steps were conducted on an NLF glove installed on a T-34C airplane. The results are summarized in the following section. Previous flight transition experiments on this glove are described in reference 6.

These recent NASA experiments illustrate (in contrast to Fage's experiments) that shape of the surface imperfection influences the allowable height. The reason for the difference in conclusions of Fage and the recent NASA experiments has to do with sensitivity of the laminar boundary layer to inflectional instability growth over a laminar separation region. In the case of the present experiments, the boundary layer was subjected to smaller regions of laminar separation than in Fage's experiments. This difference occurred because in the NASA experiments, the rounded shape of the step reduced the length of the region of laminar separation over the step; thus, the inflectional instability growth was reduced. Critical step heights may be larger for steps with shapes which reduce the length of the region of laminar separation.

FORWARD-FACING STEP FLIGHT EXPERIMENTS

The forward-facing step was simulated for the NASA flights using a cellulose acetate sheet attached to the lower surface of the glove with double-sided adhesive tape. The thickness of the sheet tested was 0.020 in.; the addition of the adhesive tape produced a total step height of 0.027 in. The sheet had two different leading-edge profiles (see fig. 10); one was a

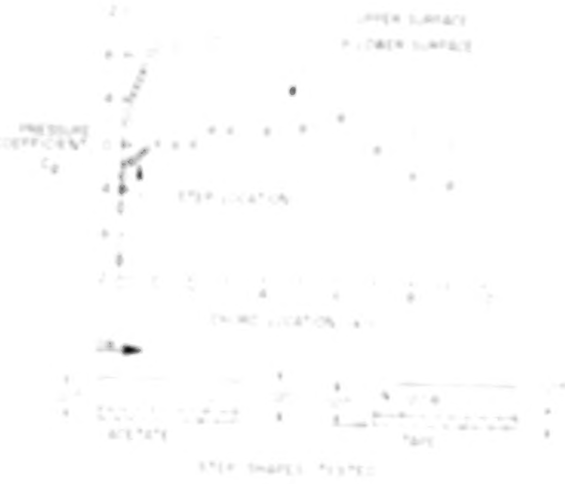

Figure 10. Forward-facing step shapes tested in flight on an NLF glove, $R' = 1.95 \times 10^6$ ft^{-1}. (Dimensions on sketch are in inches.)

ORIGINAL PAGE IS
OF POOR QUALITY

square step, the other a rounded step with a 0.020-in. radius. The testing was done with the sheet positioned such that the step was located at the 5-percent chord location on the lower surface. The lower surface pressure distribution at the test condition was only slightly favorable (accelerating) as shown in figure 10. Determination of critical step height Reynolds number for the square and rounded steps was made by flying both step shapes of equal height on one flight and by using sublimating chemicals to detect transition. A flight condition was chosen to provide a step height Reynolds number which would significantly exceed the critical value of 1800 (from ref. 9) for a square forward-facing step. The condition flown resulted in an R_h of 2720, thus exceeding 1800 by more than 50 percent. At this condition, transition occurred at the square step as expected. For the rounded step, on the other hand, transition occurred far downstream from the step (about 2 ft) as illustrated in figure 11.

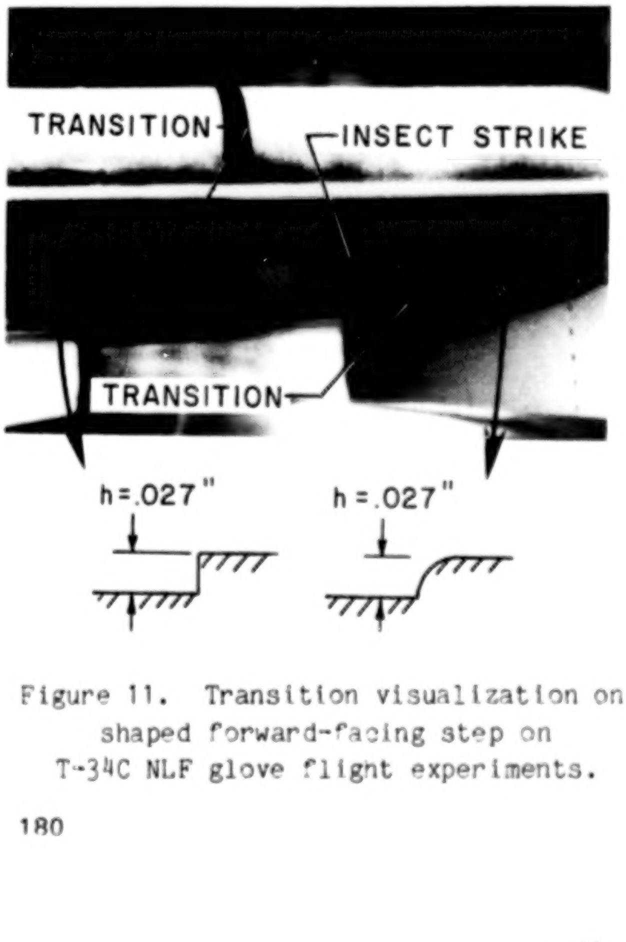

Figure 11. Transition visualization on shaped forward-facing step on T-34C NLF glove flight experiments.

These data establish a conservative value of $R_{h,crit}$ = 2700 for a rounded forward-facing step, close to the leading edge, on an unswept wing, with a radius approximately equal to the step height.

Additional flight experiments were conducted to simulate both forward- and aft-facing steps at several sweep angles. The sweep angle in this context is the angle between the ridge of the step and the free stream. Acetate sheets were attached to the upper surface of the T-34C glove in a fashion similar to the previous tests. The purpose of these experiments was to develop a technique for installation of large thin films carrying flush instrumentation (e.g., hot-film transition sensors) on swept airplane wings for NLF flight experiments. These experiments were designed to crudely simulate the flow which a spanwise facing step would see on a swept wing. On an actual swept lifting surface, the presence of crossflow vorticity would very likely produce smaller critical step sizes. The shape of the steps was varied until the step no longer caused boundary-layer transition. The pressure distribution for these tests was similar to that which appears on the upper surface in figure 10. The results are presented in figures 12 and 13. At a step height of 0.0215 in. and a sweep angle of 73°, it can be seen in

C-3

ORIGINAL PAGE IS
OF POOR QUALITY

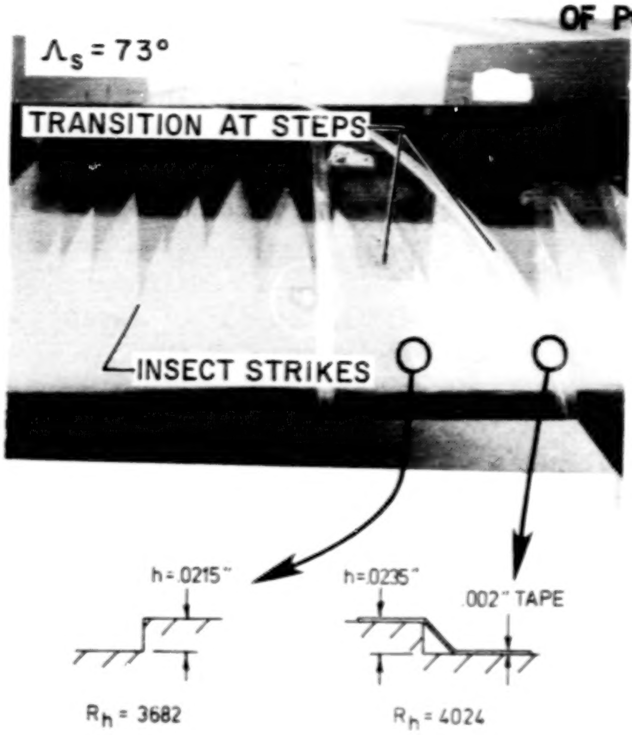
Λ_s = 73°
TRANSITION AT STEPS
INSECT STRIKES
h = .0215"
h = .0235"
.002" TAPE
R_h = 3682
R_h = 4024

Figure 12. Transition visualization on swept shaped steps on T-34C NLF glove flight experiments.

figure 12 that both the forward-facing square step and the aft-facing ramp step caused transition. Figure 13 shows the modified step shapes that did not cause boundary-layer transition at step sweep angles (Λ_s) of 73° and 45°. The step height Reynolds numbers for these two steps were R_h = 4024 and 4110, for the forward ramp step and the aft ramp step, respectively. These values of R_h can be used as a guide to size allowable forward- and aft-facing steps with up to 45° of step sweep in a region of accelerated two-dimensional flow, with steps shaped as shown in figure 13.

For one set of free-stream conditions representative of a high performance business airplane, figure 14 illustrates allowable step heights and gap widths for a range of cruise altitudes. The strong beneficial effect of higher altitudes on allowable step heights and gap widths is readily apparent. The increases in tolerances with increased altitude result directly from the decrease in unit Reynolds number. As the unit Reynolds number decreases, the length of the laminar separation regions associated with the steps decreases, reducing the growth of the inflectional instability and increasing the allowable step height.

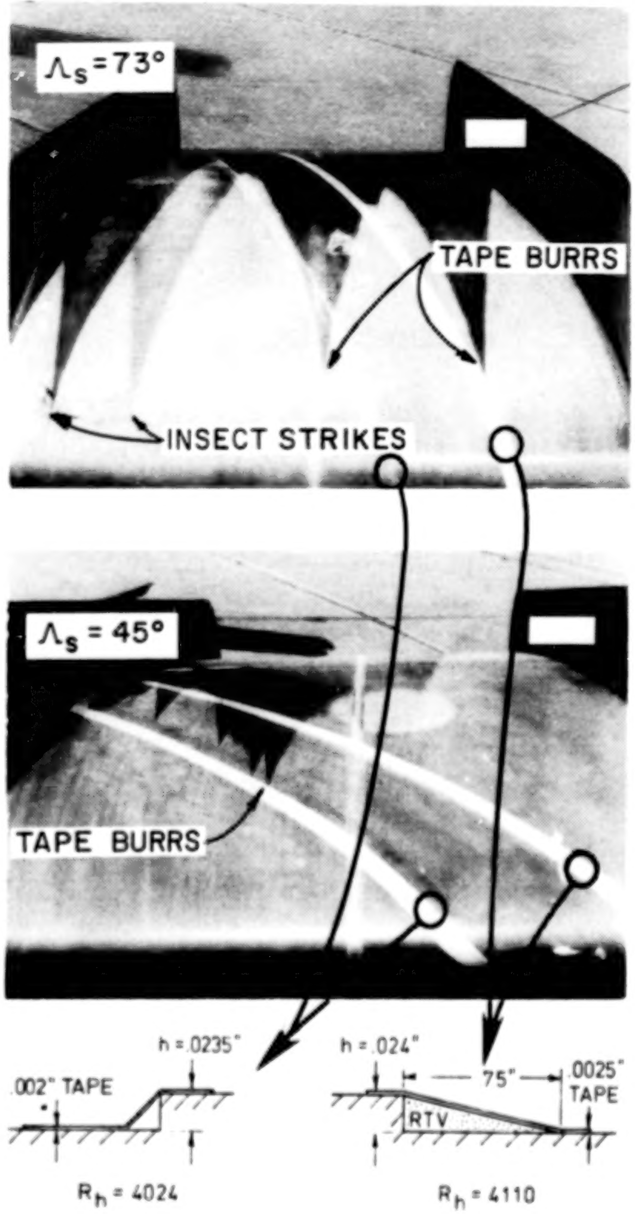
Λ_s = 73°
TAPE BURRS
INSECT STRIKES
Λ_s = 45°
TAPE BURRS
h = .0235"
.002" TAPE
h = .024"
75"
.0025" TAPE
RTV
R_h = 4024
R_h = 4110

Figure 13. Transition visualization on swept shaped steps on T-34C NLF glove flight experiments.

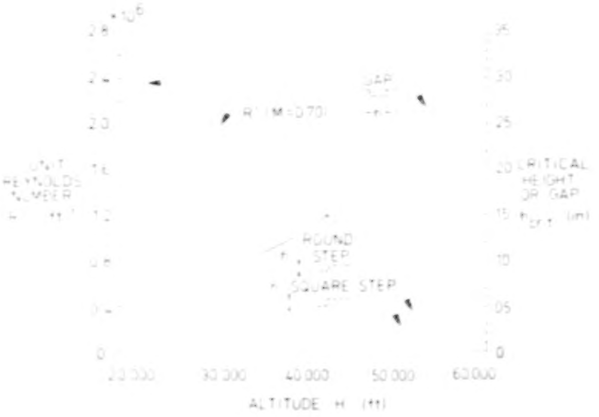

Figure 14. Allowable step heights and gap widths for a range of cruise altitudes at M = 0.7.

CONCLUDING REMARKS

A review of past work on roughness and waviness manufacturing tolerances and comparisons with more recent experiments provided the following conclusions:

1. On modern airframe surfaces where large waves typically occur only at major structural joints, the assumption of multiple waves for use of Carmichael's waviness criterion is too conservative. Based on recent flight experiences with modern airframes, it is recommended that Carmichael's criterion be used with the single-wave assumption.

2. In contrast to Fage's conclusion concerning the unimportance of the shape of a two-dimensional step in a laminar boundary layer, it has been demonstrated experimentally that shape has a significant effect on critical Reynolds numbers.

3. For a forward-facing rounded step, close to the leading edge, with a radius approximately equal to the step height, a conservative value for $R_{h,crit}$ of 2700 is indicated. This value is more than a 50-percent increase over the critical step height Reynolds number for a forward-facing square step.

4. For steps with up to 45° of sweep relative to the free stream in two-dimensional flows, step height Reynolds numbers of 4000 and 4100 can be used as a guide to size foward- and aft-facing steps, respectively. These values apply to swept forward-facing steps with rounded corners and to swept aft-facing ramp steps.

REFERENCES

1. Holmes, B.J., Obara, C.J., and Yip, L.P., "Natural Laminar Flow FLight Experiments on Modern Airplane Surfaces," NASA TP 2256, 1984.

2. Fage, A., "The Smallest Size of Spanwise Surface Corrugation Which Affects Boundary Layer Transition on an Airfoil," R&M No. 2120, Brit. A.R.C., 1943.

3. Carmichael, B.H., Whites, R.C., and Pfenninger, W., "Low Drag Boundary Layer Suction Experiments in Flight on the Wing Glove of an F-94A Airplane," Northrop Aircraft Inc. Rep. No. NAI-57-1163 (BLC-101), 1957.

4. Carmichael, B.H., "Surface Waviness Criteria for Swept and Unswept Laminar Suction Wings," Norair Rep. No. NOR-59-438 (BLC-123), 1959.

5. Carmichael, B.H., and Pfenninger, W., "Surface Imperfection Experiments on a Swept Laminar Suction Wing," Norair Rep. No. NOR-59-454 (BLC-124), 1959.

6. Obara, C.J., and Holmes, B.J., "Flight Measured Laminar Boundary-Layer Transition Phenomena Including Stability Theory Analysis," NASA TP 2417, 1985.

7. Schlichting, H., Boundary Layer Theory, McGraw-Hill, 7th ed., 1979.

8. Spence, D.A., and Randall, D.G., "The Influence of Surface Waves on the Stability of a Laminar Boundary Layer With Uniform Suction," A.R.C. C.P. No. 161 (15.916), T.N. No. AERO 2241, 1953.

9. Anon, "Final Report on LFC Aircraft Design Data Laminar Flow Control Demonstration Program," NOR 67-136 (Contract AF 33(657)-13930), Northrop Corp., June 1967. (Available from DTIC as AD 819 317).

10. Holmes, B.J., "Progress in Natural Laminar Flow Research," AIAA Paper 84-2222, 1984.

11. Stall, C.G., and Pfenninger, W., "Present Status of Production Aircraft Surface Waviness at Norair. Norair Rep. No. NOR-59-444 (BLC-126), 1959.

N88-23746

34-05
418

PRELIMINARY AERODYNAMIC DESIGN CONSIDERATIONS FOR ADVANCED LAMINAR FLOW AIRCRAFT CONFIGURATIONS

Joseph L. Johnson, Jr., Long P. Yip, and Frank L. Jordan, Jr.
NASA Langley Research Center
Hampton, Virginia 23665

SUMMARY

Recent aerodynamic research on advanced aircraft configurations has revealed some important design considerations that affect aerodynamic efficiency and performance, stability and control, and safety of flight. Modern composite manufacturing methods have provided the opportunity for smooth surfaces that can sustain large regions of natural laminar flow (NLF) boundary-layer behavior and have stimulated interest in developing advanced NLF airfoils and improved aircraft designs. The present paper overviews some of the preliminary results obtained in exploratory research investigations on advanced aircraft configurations at the NASA Langley Research Center. Results of the initial studies have shown that the aerodynamic effects of configuration variables such as canard/wing arrangements, airfoils, and pusher-type and tractor-type propeller installations can be particularly significant at high angles of attack. Flow field interactions between aircraft components were shown to produce undesirable aerodynamic effects on a wing behind a heavily loaded canard, and the use of properly designed wing leading-edge modifications, such as a leading-edge droop, offset the undesirable aerodynamic effects by delaying wing stall and providing increased stall/spin resistance with minimum degradation of laminar flow behavior.

INTRODUCTION

In recent years, there have been significant performance improvements in general aviation aircraft from the realization of increased amounts of NLF (see refs. 1 through 8). This result was achieved in part through advanced NLF airfoil design and modern construction materials and fabrication techniques such as composites and milled or bonded aluminum skins. In addition, there have been design trends toward unconventional aircraft arrangements incorporating unusual features such as canards, tandem wings, and multiple surfaces to obtain performance gains. Preliminary results suggest that the use of some of these features provides weight savings, improved cabin layouts, and improved aerodynamic characteristics which can provide significant performance benefits and increased overall operating efficiency and utility. Examples of such advanced designs are the Gates Learjet/Piaggio GP-180, a three-surface configuration with twin-pusher engines mounted on the wing (fig. 1), and the Beech Aircraft Corporation Starship I, a canard configuration with twin-pusher engines mounted on the wing (fig. 2). Although the advanced aircraft designs with new

PRECEDING PAGE BLANK NOT FILMED

technology features and modern construction techniques appear very promising from performance considerations, information on the aerodynamic characteristics of unconventional configurations, particularly those with strong flow-field interactions, is very limited. For this reason, several recent system studies and wind-tunnel investigations have been initiated to provide a technology base for evaluating the aerodynamic characteristics of the advanced designs. The initial results of these wind-tunnel investigations indicate the importance of recognizing the strong aerodynamic interactions that can result from placing propulsion systems or control surfaces in unconventional locations.

Flow-field interactions between aircraft components can produce undesirable aerodynamic effects, and the use of wing leading-edge modifications may be required to offset the undesirable aerodynamic effects and improve stall/spin resistance. Preliminary results have shown that the application of a properly designed wing leading-edge droop to advanced NLF wings can improve the stall/spin resistance of these wings with minimum performance degradation. This paper presents some of the initial results of the exploratory aerodynamic investigations for several of the configurations investigated and discusses the significance of the results from overall performance and stability and control considerations.

SYMBOLS

b	wing span, ft
BL	butt line
C	canard
$\bar{c}$	wing mean aerodynamic chord, ft
c	local chord, ft
C_D	drag coefficient, Drag/qS
C_{D_c}	canard drag coefficient
C_L	lift coefficient, Lift/qS
C_{L_c}	canard lift coefficient, Canard lift/qS_c
C_{l_p}	roll damping
C_m	pitching-moment coefficient, Pitching moment/$qS\bar{c}$
C_{m_c}	canard pitching-moment coefficient
C_n	section normal-force coefficient, Normal force/qc
C_T	propeller thrust coefficient, Thrust/qS
ΔF_c	incremental force on canard due to power, lb
F_p	propeller normal force, lb
ΔF_w	incremental force on wing due to power, lb
LE	leading edge
q	dynamic pressure, lb/ft^2
R_N	Reynolds number
S	wing area, ft$_2$

S_c	canard area, ft^2
WL	water line
x	local wing chord, ft
y	lateral distance from wing centerline, ft
α	angle of attack, deg
β	sideslip angle, deg
δ_e	elevator deflection, deg

Notation:

C.G.	center of gravity

MODELS AND TEST CONDITIONS

The models used to provide aerodynamic information for discussion in this paper include the following configurations:

- Canard, single-engine pusher
- Canard, single-engine tractor
- Conventional single-engine tractor design
- Conventional business jet design
- Three-surface design
- Over-the-wing propeller design

The canard, pusher configuration was a full-scale model of a propeller-driven homebuilt aircraft which has demonstrated good performance and a high level of stall/spin resistance in operational use (see refs. 3 to 5). The canard, tractor configuration was a sub-scale model of an advanced general aviation design which incorporated a relatively close-coupled canard and an aft-mounted wing of relatively low sweep (see ref. 6). A single-slotted elevator on the canard provided pitch control. For the canard models, an auxilary balance was used to measure canard loads independently from the total aerodynamic loads measured on a main balance.

The conventional single-engine tractor model and the conventional business jet model represent configurations incorporating advanced NLF airfoils for improved performance (see refs. 7 and 8). One of the unique features of these configurations was the application of leading-edge droop designs which increased stall/spin resistance without significantly degrading NLF performance (see ref. 9). The three-surface design and the over-the-wing propeller design were configurations derived from a general purpose model used in generic studies to explore low-speed stability and control characteristics of advanced designs including the effects of power with aft-mounted engines (see refs. 10 and 11). The wind-tunnel results presented in this paper were obtained in investigations conducted in the Langley 30- by 60-Foot Wind Tunnel and 12-Foot Low-Speed Wind Tunnel.

RESULTS AND DISCUSSION

Canard, Single-Engine Pusher

Presented in figure 3 is a photograph of the large-scale canard, single-engine pusher configuration investigated in the Langley 30- by 60-Foot Wind Tunnel. The model was constructed with smooth fiberglass surfaces and was equipped with pressure ports in the canard and wing to give detailed pressure distribution data. This investigation revealed many important design considerations for canard aircraft and pointed out the significance of these design features on performance, stability, and control characteristics (see refs. 4 and 5). Some of the more significant results of the investigation include: (1) the influence of the canard downwash on the wing aerodynamics; (2) the large regions of NLF on the smooth fiberglass surfaces; (3) the effect of canard airfoil section on stability and control; and (4) the effect of the engine location on propeller efficiency and stability and control. One of the most important, unexpected findings resulting from the wind-tunnel investigation was the discovery of large regions of NLF boundary-layer behavior. Using a sublimating chemical technique for transition visualization, it was determined that NLF existed back to 55-percent chord on the canard, 65-percent chord on the wing, and 60-percent chord on the winglets for a cruise attitude (see fig. 4). Figure 5 shows the flight vehicles which were used to verify the amount of NLF indicated in the wind-tunnel tests. Figure 5(c) shows the results of chemical sublimation tests conducted in flight and illustrates that the amount of NLF achieved in flight on the canard was similar to that measured in the wind tunnel (back to 55-percent chord station). As part of the 30- by 60-foot wind-tunnel investigation, tests were conducted to force premature boundary-layer transition on the canard by either carborundum grit applied at 5-percent chord or by water spray. These tests were initiated because of pilot reports of such aircraft experiencing a pitch trim change when entering rain. To determine whether this trim change was the result of early laminar to turbulent boundary-layer transition caused by rain, a test apparatus was used for rain simulation as shown in figure 6. The test apparatus consisted of a horizontal boom mounted in the wind tunnel about 4 chord lengths ahead of the canard. Results of the forced boundary-layer transition tests (presented in fig. 7) show that forced transition by either carborundum grit or rain simulation resulted in a significant reduction in the canard lift-curve slope and increased canard drag. Figure 8 shows that fixed boundary-layer transition on the canard caused, as expected on the basis of premature trailing-edge flow separation and reduced canard lift-curve slope, an increase in longitudinal stability and loss of elevator control effectiveness. These results point out the importance of airfoil selection to avoid changes in lift characteristics with loss of laminar flow. Advanced NLF airfoils have been designed to minimize the loss in lift due to premature transition (see ref. 7). Advanced NLF airfoils will be examined in more detail in subsequent sections of this paper.

Included in the investigation of canard airfoil design was a study of the effect of canard configuration on stall/post-stall behavior. Figure 9 shows the two airfoils investigated to illustrate the effects of camber and shape on stability and control. Presented in figure 10(a) are pitching-moment characteristics of the aircraft with the two different canards, and the data show significant differences in the stall/post-stall angle-of-attack range. For either airfoil configuration, the data show a stable break at wing stall, but in the post-stall angle-of-attack range the NACA 0012 airfoil shows a marked destabilizing trend and positive pitching moments at high angles of attack. The significance of such a trend is that for certain landing conditions there may exist the possibility of inadvertently entering the post-stall angle-of-attack region and experiencing a deep-stall trim condition. The data of figure 10(b) show the importance of airfoil design in avoiding undesirable deep-stall characteristics. The significant point of figure 10(b) is that the GU25-5(11)8 airfoil has a relatively flat lift-curve slope following the stall, whereas the NACA 0012 airfoil shows an abrupt loss of lift at the stall and then an increase in lift in the post-stall angle-of-attack range. The increase in canard lift-curve slope in the post-stall angle-of-attack range is very destabilizing because an increase in canard lift tends to aggravate the destabilizing effect of wing stall on pitch stability for a canard arrangement. The stability and control of canard arrangements will be discussed in further detail in the section of this paper dealing with tractor engine arrangements.

Figure 11 presents a sketch to introduce the subject of canard downwash and vortex-wake interaction effects on the main wing. The two main points to be discussed are the canard downwash on the inboard portion of the wing, and the canard vortex flow which introduces an upwash on the wing tip. Figure 12 presents measured section normal-force coefficient data to show the effect of the canard wake on the wing and indicates, as expected, that a reduction in span loading occurs inboard and an increase in span loading occurs at the wing tip. The results of tuft flow studies (fig. 13(a)) show that the aircraft experiences spanwise flow on the wing and severe tip stall at $\alpha = 19.5^\circ$. The use of a leading-edge droop, shown in cross section in figure 13(b), is shown by the tuft photograph of figure 13(a) to provide attached flow at the wing tip.

The importance of wing leading-edge treatment for swept wings is illustrated in a plot of aspect ratio against wing sweep in figure 14. The figure was taken from reference 12 and shows that swept wings with high aspect ratios tend to have an unstable pitching-moment break at the stall due to tip stall. The figure does not take into account the effects of such items as winglets or canard vortex flow on the wing tip stall. Such effects emphasize the need for additional research on the use of wing leading-edge treatment for improved stall characteristics. Figure 15 shows the stabilizing effect of the wing leading-edge droop on the pitching-moment characteristics of the canard single-engine pusher configuration, and figure 16 shows the stabilizing effect of the leading-edge droop on roll damping. Model and airplane flight tests verified the damping-in-roll data of figure 16 and showed that the wing leading-edge droop eliminated a wing rock tendency of the basic airplane configuration for aft center-of-gravity location.

Canard, Single-Engine Tractor

Discussion of the canard, single-engine tractor configuration emphasizes the effects of canard airfoil section and the effects of power on longitudinal stability characteristics. More complete discussion of the overall stability and control characteristics of the tractor configuration is presented in reference 6.

Presented in figure 17 is a photograph of the canard, tractor model mounted for static wind-tunnel tests in the Langley 30- by 60-Foot Wind Tunnel. The model has a closely coupled canard-wing arrangement with the canard placed slightly above the wing. Power for the subject model was supplied by a tip-turbine air motor driven by compressed air.

Figure 18 shows a comparison of the effects of power on the pitching-moment characteristics of the canard, tractor and pusher configurations for climb power ($C_T = 0.4$) and aft center-of-gravity conditions. The data show that the power effects were destabilizing for the tractor model and stabilizing for the pusher model. The large nose-up trim changes for the tractor model were caused by a combination of direct propeller normal force and induced effects on the canard and wing. As indicated in the sketch of figure 18, the rearward location of the propeller results in a propeller normal force which produces a nose-down or stabilizing pitching moment.

Figure 19 shows the effect of canard airfoil section on the pitching-moment characteristics of the tractor configuration. Of particular interest in figure 19 is the relative difference between the pitching-moment data of the NACA 23018 airfoil and two NLF airfoils, the GU25-5(11)8 and the NLF(1)-0416, in the post-stall angle-of-attack range. As noted in the preceding section, the post-stall stability characteristics of canard configurations can be greatly influenced by the canard airfoil. For the three airfoils investigated, the NACA 23018 gives the most destabilizing pitching-moment trends at post-stall angle of attack. The reason for this trend is that the NACA 23018 is a relatively thin airfoil which exhibits a sharp stall and an increase in lift-curve slope at post-stall angles of attack and becomes very destabilizing. The other airfoils of figure 19 tend to have a relatively flat lift curve at stall and, therefore, give more desirable post-stall stability contributions.

As part of the exploratory research on the tractor design, tests were continued to examine in more detail the aerodynamic characteristics of the GU25-5(11)8 and the NLF(1)-0416 airfoils. Presented in figure 20 are the results of some of the exploratory tests to show the effect of Reynolds number, and presented in figure 21 are the effects of forced boundary-layer transition using carborundum grit applied at the 5-percent chord station. The significant results of figures 20 and 21 are that the aerodynamic characteristics of the NLF(1)-0416 are not sensitive to Reynolds number or forced boundary-layer transition; whereas, the GU25-5(11)8 airfoil shows loss of canard lift due to boundary-layer separation at low Reynolds number and, also, loss of lift due to forced boundary-layer transition. The NLF(1)-0416 airfoil aerodynamic characteristics are typical of several advanced NLF airfoils developed in recent years which provide promising performance gains. Application of some of the advanced NLF airfoils to conventional airplane configurations for improved performance will be addressed in subsequent sections.

Included in the canard, tractor investigation were tests to study the effect of relative locations of the canard and wing on longitudinal characteristics of the configuration. Presented in figure 22 is a photograph of the tractor model with the canard lowered on the fuselage and the wing raised to the top of the fuselage. The data of figure 23 show that modifying the configuration to have the canard lowered and the wing raised provided a stabilizing influence on longitudinal stability in the post-stall angle-of-attack range and eliminated the undesirable deep-stall tendency of the basic configuration with power on. The stabilizing effect of the modified design apparently results from moving the canard out of the propeller slipstream and moving the wing out of the canard downwash.

Conventional Single-Engine Tractor Design

The discussion of conventional configurations will emphasize the use of advanced NLF airfoils for improved performance and the application of wing leading-edge droop to the NLF airfoils to improve stall/spin resistance with minimum performance degradation. Before discussing the new airfoil configurations, a brief review of related stall/spin research at Langley is provided to discuss the development of an effective wing leading-edge droop for increased departure resistance.

Shown in figure 24 are the research airplanes flown at Langley in the stall/spin research program. These research airplanes were flown with a modified wing leading-edge droop which proved effective for increased stall/spin resistance. Figure 25 shows some design features of the droop arrangement developed for the T-tail research airplane. An important feature of the droop is the abrupt discontinuity of the droop inboard leading-edge. This discontinuity is effective in generating a vortex which acts as an aerodynamic fence to stop the spanwise flow from the inboard portion of the wing as stall progresses. The leading-edge droop extends to near the wing tip such that the outer position of the wing performs as a low-aspect-ratio wing with a very high stall angle of attack. Flow visualization studies using fluorescent oil provide an excellent means of illustrating the effectiveness of the leading-edge droop. Figure 26 presents the results of oil flow studies and shows the basic wing in a stalled condition with a predominant outward flow direction. The outboard droop is shown to keep the outer wing panel flow attached to $\alpha = 35°$. A summary of the effectiveness of the droop for spin prevention is presented in figure 27 which shows that the leading-edge droop significantly improved the spin resistance of the research airplanes.

The recent trend in general aviation airplane design toward the use of NLF airfoils for improved performance has led to an interest in applying the wing leading-edge technology developed in stall/spin research to the new NLF airfoils. Two NLF airfoils of current interest are the NLF(1)-0215F and the NLF(1)-0414F (see fig. 28). One approach recently studied in exploratory research programs at Langley was to use the NLF(1)-0414F airfoil for enhanced performance, and the NLF(1)-0215F airfoil for the droop required for improved spin resistance. A leading-edge droop was developed from the NLF(1)-0215F airfoil by gloving over the leading-edge outboard panel of the wing. Presented in figure 29 is a sketch of the advanced wing planform, compared to the planform of a more conventional general aviation wing. The advanced wing is of higher aspect ratio, and the droop is smaller in span and located further outboard than that derived for conventional wings in earlier research. The droop was developed in subscale tests in the Langley 12-Foot Low-Speed Wind Tunnel using a wing-tip balance to measure the aerodynamics of the outer wing panel. This research also revealed that the effectiveness of the outboard droop could be enhanced by the addition of a small-span inboard droop located inboard on the wing. A photograph of the model used in the 12-foot tunnel test is presented in figure 30. The final droop geometry developed from the low-speed tests evolved from a number of exploratory studies of different designs. The fact that the most effective location of the droop was relatively far outboard on the wing is probably related to the stall pattern of the higher aspect ratio wing compared to that of previous wings investigated. Some oil flow studies conducted by Professor Allen Winkelman at the University of Maryland have shown that considerable differences occur in the stall behavior of wings of various aspect ratios. For example, presented in figure 31 are results of oil flow studies which show that in separated flow conditions the higher aspect ratio wings tend to have a greater number of stall cells on the wing trailing edge than noted for the lower aspect ratio wings. These differences in surface patterns between wings of different aspect ratio may be one of the reasons for different leading-edge droop requirements as the wing aspect ratio increases. Additional tests are planned to provide research information for use in wing leading-edge droop design for the advanced wing planform. Presented in figure 32 are the results of chemical sublimation tests conducted on a larger scale model of the general aviation advanced wing configuration. Figure 32 shows that the wing had NLF back to about 70-percent chord where transition occurred near the point of minimum pressure. Except for wedges along the edges of the droop, NLF also occurred behind the droop to the 70-percent chord station. Chemical sublimation tests on the lower side of the wing also showed NLF to about the 70-percent chord station. Thus, incorporation of the droop had a minimal impact on the character of the NLF features of the advanced wing.

The results of roll damping tests on the advanced wing, presented in figure 33, show that the leading-edge droop arrangement investigated eliminated the unstable roll damping at the stall for the basic wing and provided stable roll damping for the modified wing over the test angle-of-attack range.

Conventional Business Jet Design

Another configuration employing NLF airfoils for improved performance is the business jet shown in figure 34. The wing NLF airfoil used on the configuration is shown in figure 35. This airfoil is the NLF(1)-0414F and has the departure resistant leading-edge droop developed from the NLF(1)-0215F in a similar manner to that discussed earlier for the advanced NLF wing on the general aviation research aircraft.

In order to determine the effectiveness of the wing leading-edge droop for departure resistance, damping-in-roll tests were made of the business jet configuration, and the results of the tests are presented in figure 36. The data of figure 36(a) show that the damping-in-roll characteristics of the basic wing became unstable near the stall angle of attack, and as the angle of attack increased, a region of stable damping developed and then the damping became unstable again near $\alpha = 35^{\circ}$. The addition of the outboard droop is shown to have eliminated the unstable damping near the stall. Although the configuration was not very heavily damped in the stall angle-of-attack range, the configuration would be expected to show increased departure resistance over that of the basic design. In an attempt to increase the roll damping of the configuration at the initial stall angle of attack, the basic leading-edge droop arrangement was modified to add a small inboard droop segment in combination with the outboard segment (see fig. 36(b)). This segmented droop arrangement was developed for the general aviation research configuration discussed in the preceding section. The data of figure 36(b) show that the modified droop arrangement provided a substantial increase in roll damping at the initial wing stall and provided good roll damping over the test angle-of-attack range. Figure 37 shows the results of chemical sublimation tests of the wing and modified leading-edge droop arrangement. The results show that NLF was maintained relatively far rearward on the wing chord (about 70-percent chord) and was not adversely affected by the wing leading-edge droop. Similar results were obtained for sublimation tests made on the bottom of the wing, indicating that performance penalties associated with the departure resistant wing should be small.

Three-Surface Configuration

Three-surface configurations employing NLF airfoils were recently investigated in exploratory studies at the Langley Research Center. Figure 38 shows plan views of the three-surface designs investigated and also a plan view of a conventional design tested to provide data for comparison purposes. Included in the study were configurations with aft-mounted engines and with wing-mounted pusher engines. All three configurations were derived from the basic model components. The model was equipped with a six-component strain-gage balance for measuring the total aerodynamic characteristics of the configuration and also had separate balances on the wing, canard, and the engine nacelle. More complete model descriptions are presented in reference 10. A photograph showing the model with aft-mounted engines is presented in figure 39. A comparison of the aerodynamic characteristics of the aft-mounted engine configurations with those of the conventional design is shown in figure 40. The lift data of figure 40(a) show a slightly higher lift-curve slope and maximum lift coefficient for the three-surface designs than for the conventional design. This result can be attributed to the lift of the canard and also to the fact that wing-nacelle interference effects of the conventional design were eliminated or minimized in the aft-mounted engine configurations.

The data of figure 40(b) show the effects of power on the longitudinal stability characteristics of the test configurations. Although all three configurations exhibited a pitch-up tendency, which is generally characteristic of a T-tail design, the three-surface configuration tended to have more aggravated pitch-up characteristics. This result can be attributed to the aft location of the wing in the three-surface design, which results in the wing giving relatively large destabilizing pitching-moment changes when the wing stalls. The data of figure 40(b) show a destabilizing effect of power on the longitudinal stability characteristics of the conventional design, whereas a significant stabilizing change in pitching moment due to power is shown for the three-surface configuration with aft-fuselage-mounted engines. Lateral-directional stability tests in sideslip showed that power effects were also very stabilizing characteristics for the aft-mounted engine arrangement.

Over-the-Wing Propeller Design

Presented in figure 41 is a photograph of an advanced configuration recently investigated which uses the propellers in an over-the-wing arrangement to induce large favorable interference effects of the propeller slipstream on the wing for reduced wing drag at high power settings (see ref. 10). This concept, which is based on earlier research with jet-engine aircraft, was derived from the three-surface design shown in figure 38 by rotating the engine nacelles and propellers from the pusher arrangement to the over-the-wing tractor arrangement. The drag data obtained with the over-the-wing propeller arrangement show that the drag of the wing decreases as the propeller thrust coefficient is increased. At the thrust coefficient corresponding to the climb condition, the drag of the wing relative to that for the power-off condition is significantly reduced. Preliminary results of tests to measure the effects of the wing proximity on the propeller efficiency indicated relatively small interference penalties on the propeller performance.

Additional tests with the over-the-wing propeller arrangement are currently planned using a forward-swept arrangement (fig. 42). The forward-swept wing configuration has the advantage of locating the wing root chord and over-the-wing propellers aft on the fuselage for improved structural efficiency and reduced cabin noise. Preliminary results with the forward-swept wing configuration indicate similar performance improvements for the over-the-wing propeller concepts to those determined earlier for straight-wing configurations. Preliminary stability and control studies indicate, however, that careful consideration must be given to tailoring of the forward-swept wing design to minimize pitch-up tendencies associated with early wing root stall and lateral instability (loss of effective dihedral) inherent with forward-swept wings. Follow-on tests at larger scale are planned to provide information for analysis and evaluation of over-the-wing propeller concept and forward-swept wing design at higher Reynolds numbers.

CONCLUDING REMARKS

The results of recent aerodynamic research on advanced configurations have revealed some important design considerations that affect aerodynamic efficiency and performance, stability and control, and safety of flight. Modern composite manufacturing methods have provided large regions of NLF boundary-layer behavior and stimulated interest in developing advanced NLF airfoils and improved aircraft design. Experiments have indicated that selection of canard airfoils can be extremely important to avoid large pitch trim and stability changes between conditions of natural and forced turbulent boundary-layer transition; the canard airfoil characteristics at stall/post-stall angles of attack can determine the susceptibility of an aircraft to pitch-up and deep-stall trim problems. Flow-field interactions between aircraft components were shown to produce undesirable aerodynamic effects on a wing located behind a heavily loaded canard. The use of properly designed wing leading-edge modifications, such as a leading-edge droop, was found to delay wing stall and provide increased stall/spin resistance with minimum performance degradation. Power effects were shown to be generally stabilizing for aft-mounted engine arrangements and destabilizing for tractor-engine arrangements.

REFERENCES

1. Holmes, Bruce J.; Obara, Clifford J.; and Yip, Long P.: Natural Laminar Flow Experiments on Modern Airplane Surfaces. NASA TP-2256, June 1984.

2. Holmes, B. J.; and Obara, C. J.: Observations and Implications of Natural Laminar Flow on Practical Airplane Surfaces. ICAS Paper 82-5.1.1, 1982.

3. Rutan, B.: Development of a Small, High Aspect Ratio Canard Aircraft. Society of Experimental Test Pilots Technical Review, Vol. 13, No. 2, 1976, pp. 93-101.

4. Yip, L. P.; and Coy, P. F.: Wind Tunnel Investigation of a Full-Scale Canard-Configured General Aviation Aircraft. ICAS Paper No. 82-6.8.2, 1982.

5. Yip, Long P.: Wind-Tunnel Investigation of a Full-Scale Canard-Configured General Aviation Airplane. NASA TP-2382, 1985.

6. Chambers, Joseph R.; Yip, Long P.; and Moul, Thomas M.: Wind Tunnel Investigation of an Advanced General Aviation Canard Configuration. NASA TM-85760, April 1984.

7. Somers, Dan M.: Design and Experimental Results for a Natural-Laminar-Flow Airfoil for General Aviation Applications. NASA TP-1861, 1981.

8. Viken, Jeffrey K.: Aerodynamic Design Considerations and Theoretical Results for a High Reynolds Number Natural Laminar Flow Airfoil. M.S. Thesis, George Washington University, January 1983.

9. Staff of the Langley Research Center: Exploratory Study of the Effects of Wing Leading-Edge Modifications on the Stall/Spin Behavior of a Light General Aviation Airplane. NASA TP-1589, 1979.

10. Johnson, J. L., Jr.; and White, E. R.: Exploratory Low-Speed Wind-Tunnel Investigation of Advanced Commuter Configurations Including an Over-the-Wing Propeller Design. AIAA Paper 83-2531, October 1983.

11. Williams, L. J.; Johnson, J. L., Jr.; and Yip, L. P.: Some Aerodynamic Considerations for Advanced Aircraft Configurations. AIAA Paper 84-0562, 1984.

12. Shortal, Joseph. A.; and Maggin, Bernard.: Effect of Sweepback and Aspect Ratio on Longitudinal Stability Characteristics of Wings at Low Speeds. NACA TN-1093, 1946.

ORIGINAL PAGE IS
OF POOR QUALITY

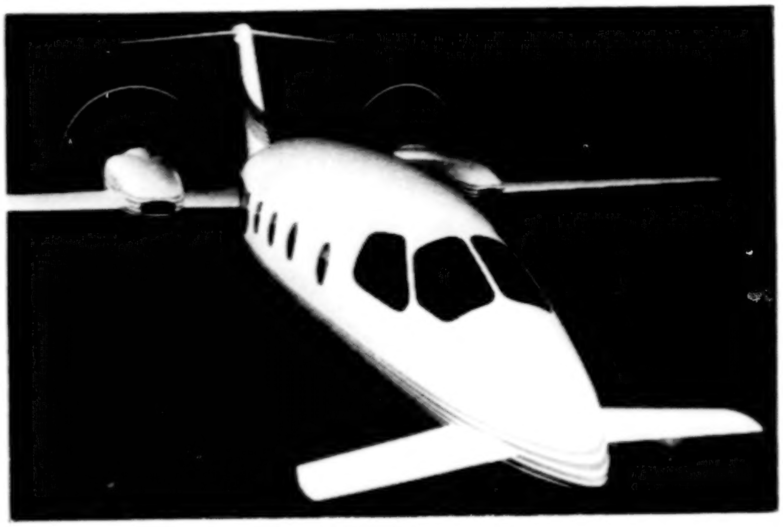

Figure 1.- Learjet/Piaggio GP-180.

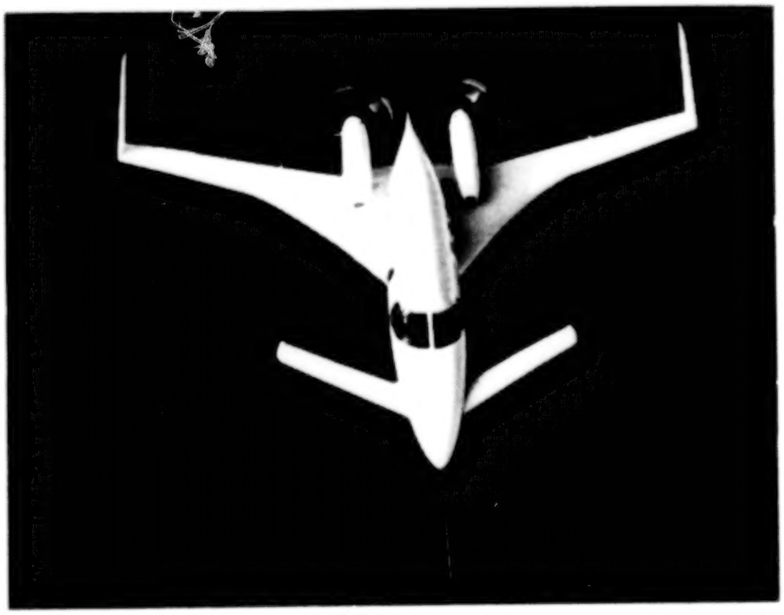

Figure 2.- Beechcraft Starship 1, 85-percent-scale flying prototype.

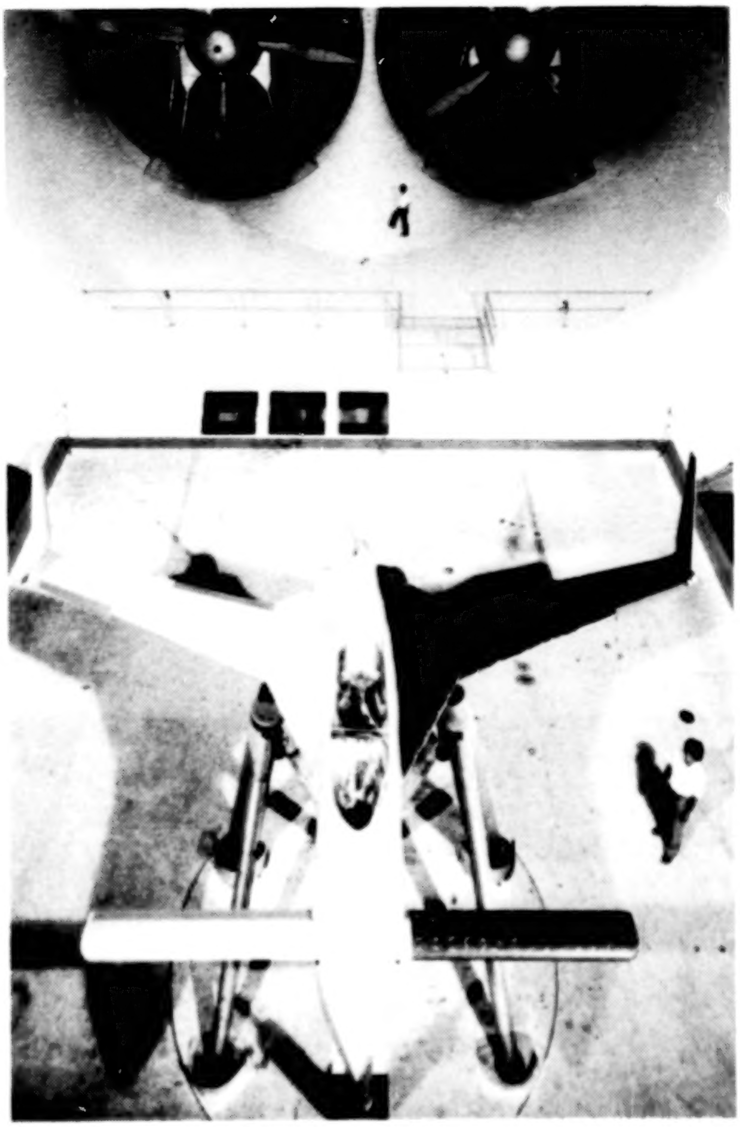

Figure 3.- Canard, single-engine pusher configuration in the Langley 30- by 60-Foot Wind Tunnel.

ORIGINAL PAGE IS
OF POOR QUALITY

ORIGINAL PAGE IS
OF POOR QUALITY

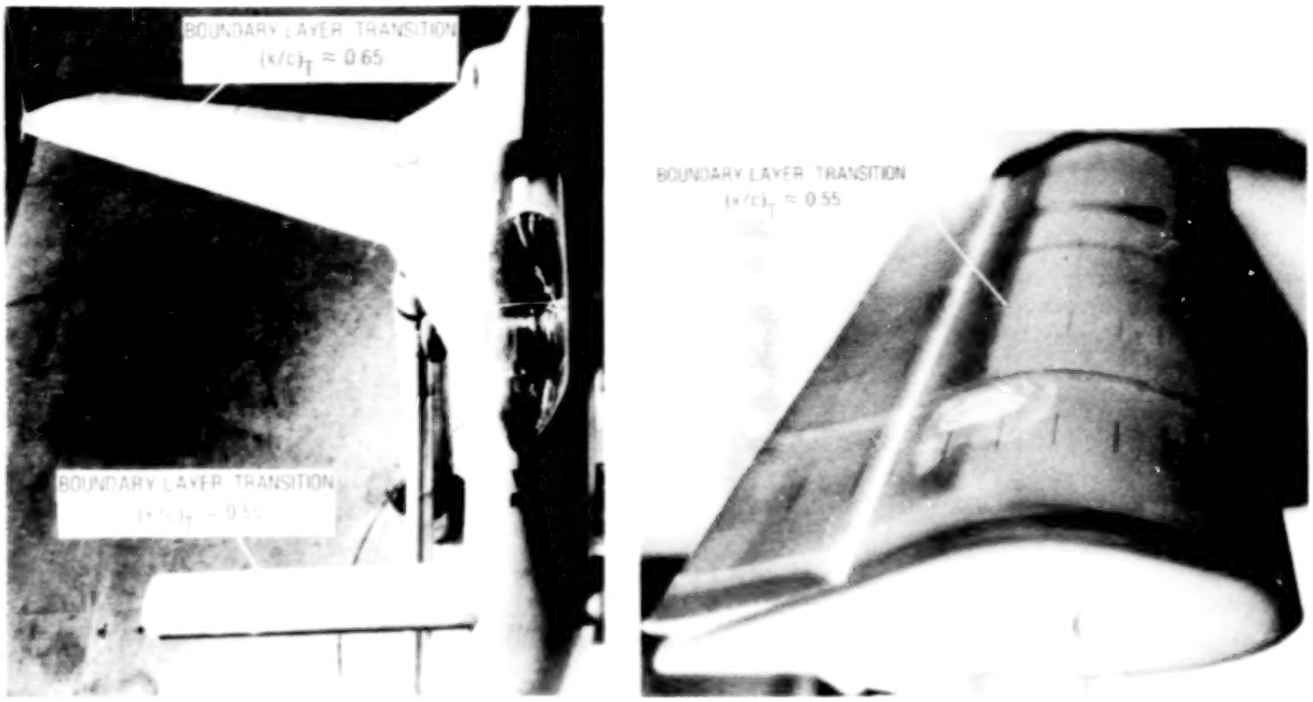
BOUNDARY LAYER TRANSITION
(x/c)T ≈ 0.65
BOUNDARY LAYER TRANSITION
(x/c)T ≈ 0.55
BOUNDARY LAYER TRANSITION
(x/c)T ≈ 0.55

(a) Top view of wing and canard.

(b) Canard.

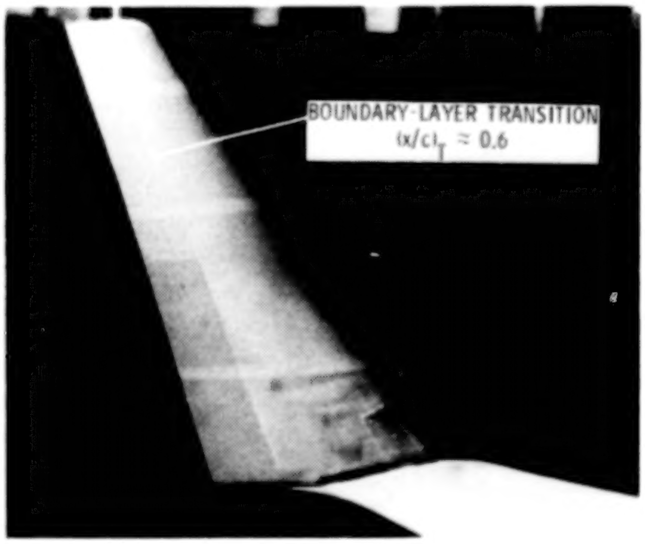
BOUNDARY-LAYER TRANSITION
(x/c)T ≈ 0.6

(c) Winglet.

Figure 4.- Flow visualization using sublimating chemicals to show boundary-layer transition.

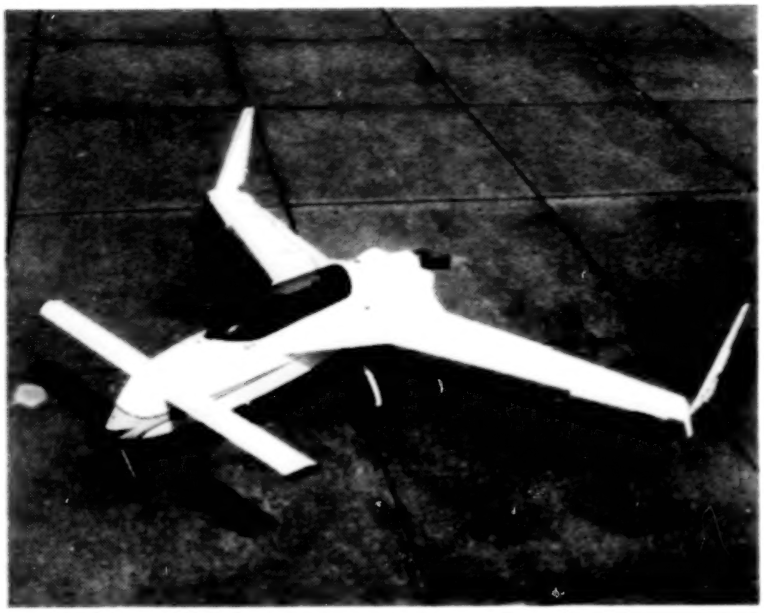

(a) Rutan Vari-eze.

(b) Rutan Long-EZ.

Figure 5.- Canard, single-engine pusher airplanes used for natural laminar flow flight experiments.

ORIGINAL PAGE IS
OF POOR QUALITY

ORIGINAL PAGE IS
OF POOR QUALITY

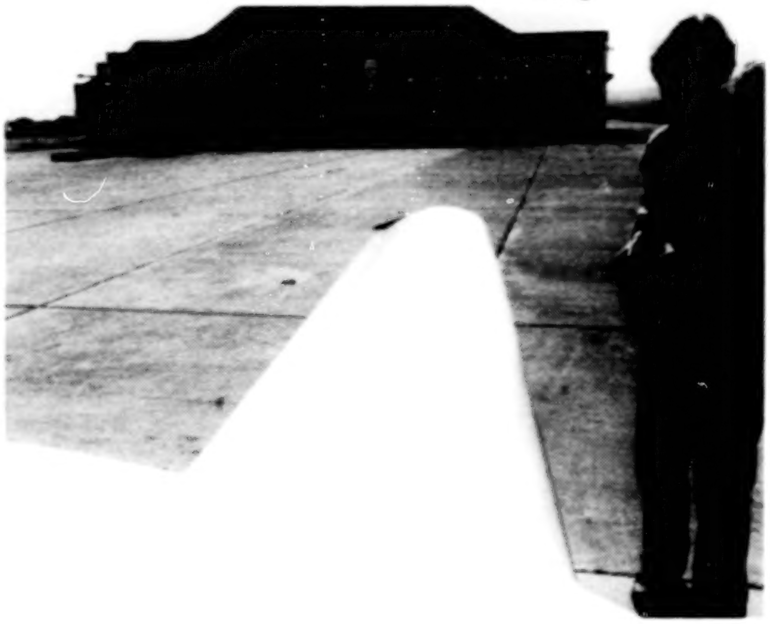

(c) Canard.

Figure 5.- Concluded.

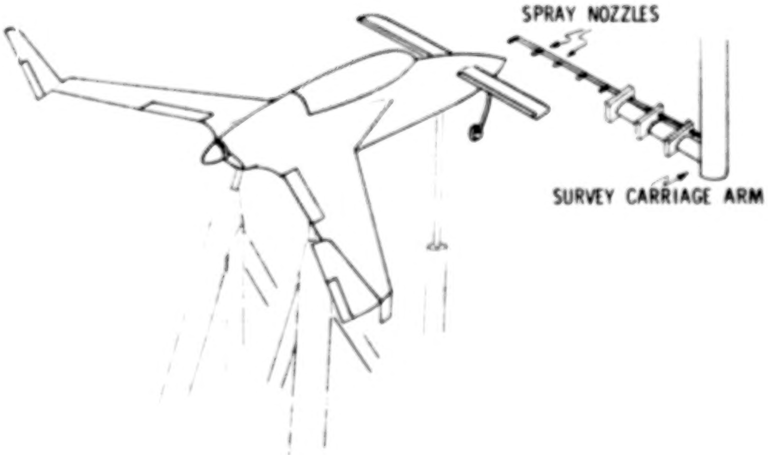
SPRAY NOZZLES
SURVEY CARRIAGE ARM

Figure 6.- Sketch of rain-simulation apparatus.

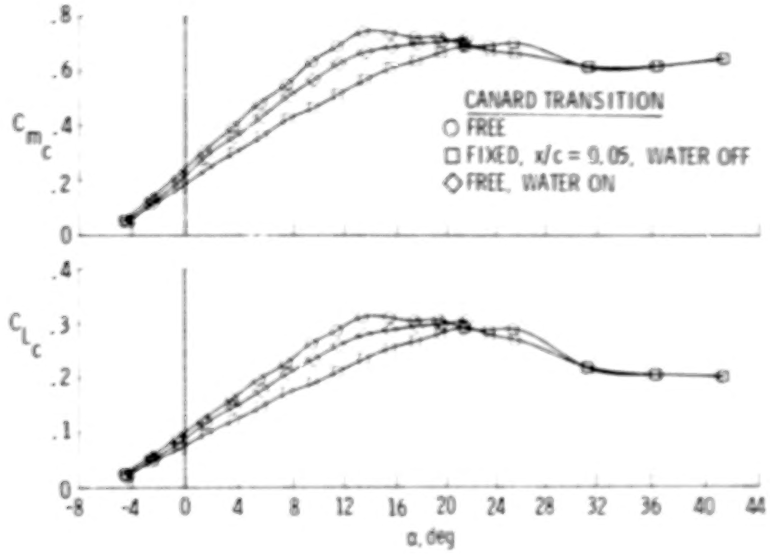

(a) Lift and pitching moments.

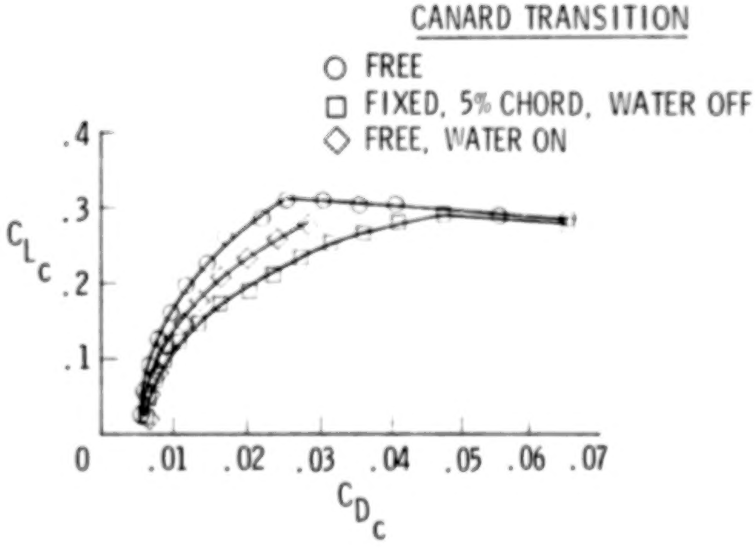

(b) Drag characteristics.

Figure 7.- Effect of water spray on canard aerodynamics.

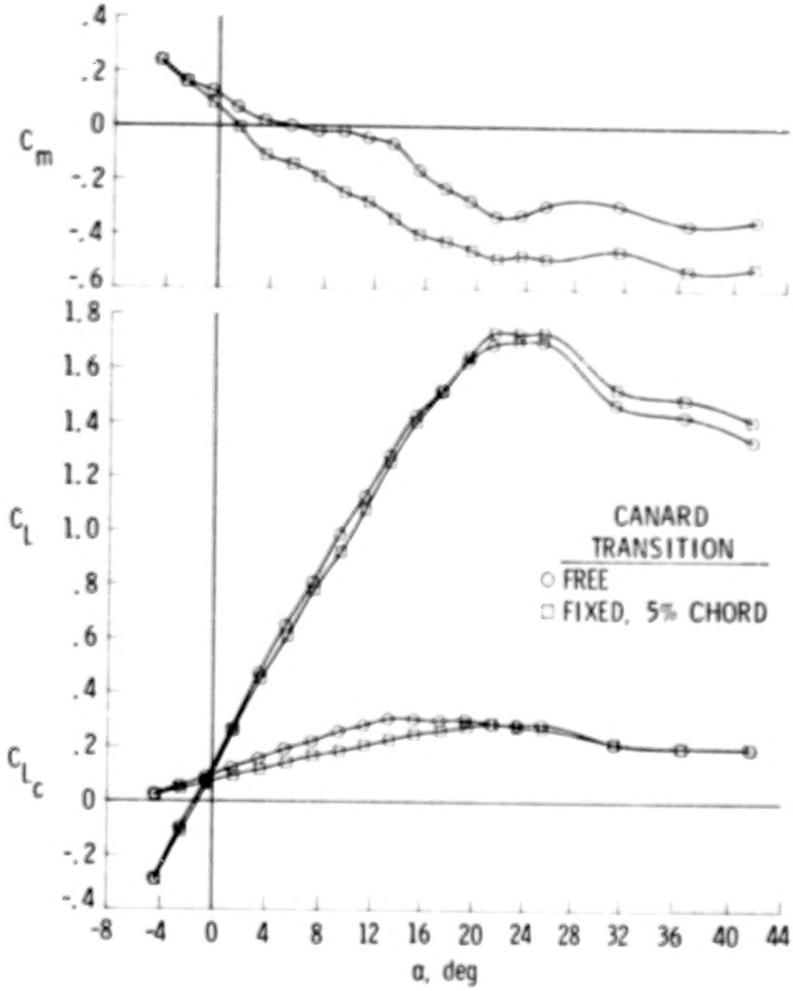

(a) Lift and pitching moments.

Figure 8.- Effect of canard transition on airplane aerodynamics.

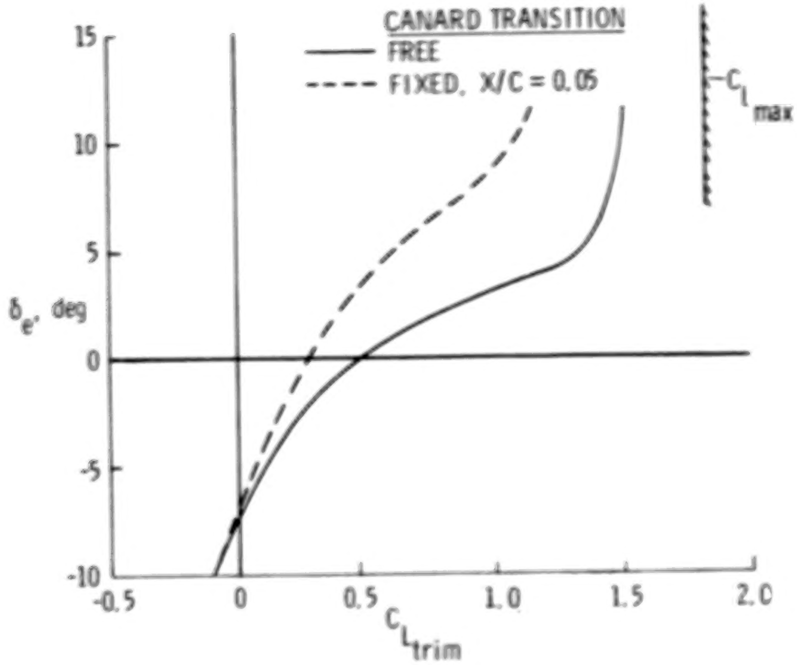

(b) Elevator effectiveness.

Figure 8.- Concluded.

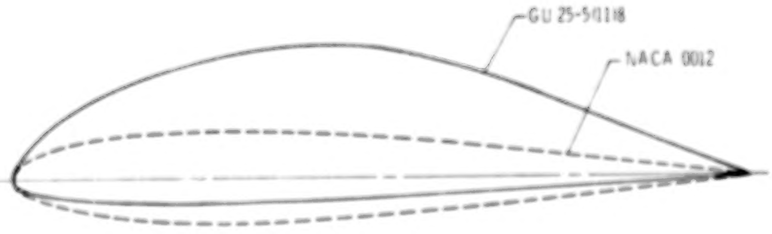
GU 25-5(11)8
NACA 0012

Figure 9.- Canard airfoil contours.

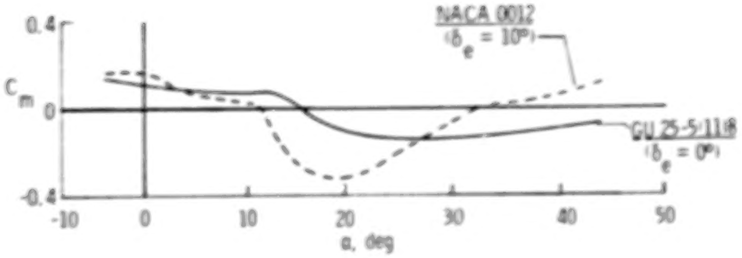

(a) Total pitching-moment characteristics.

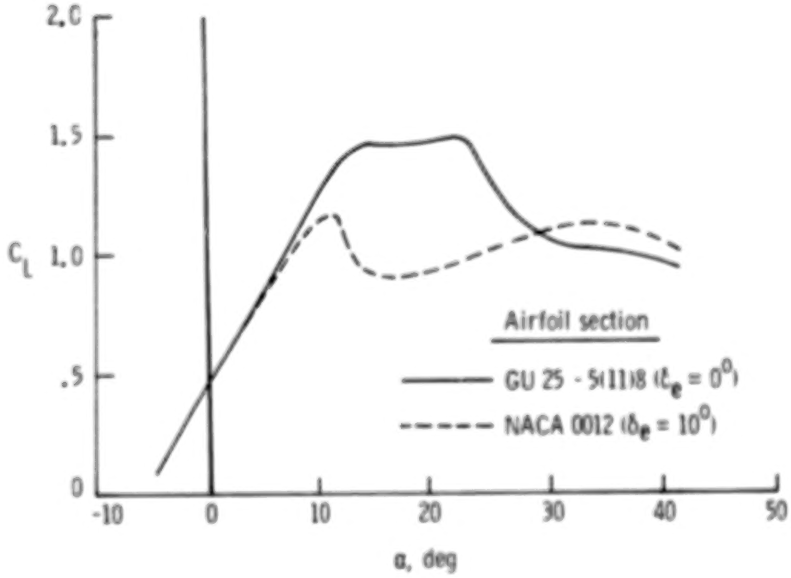

(b) Canard lift characteristics.

Figure 10.- Effect of canard on longitudinal stability of configuration with aft c.g.: Reynolds number = 1.60 million.

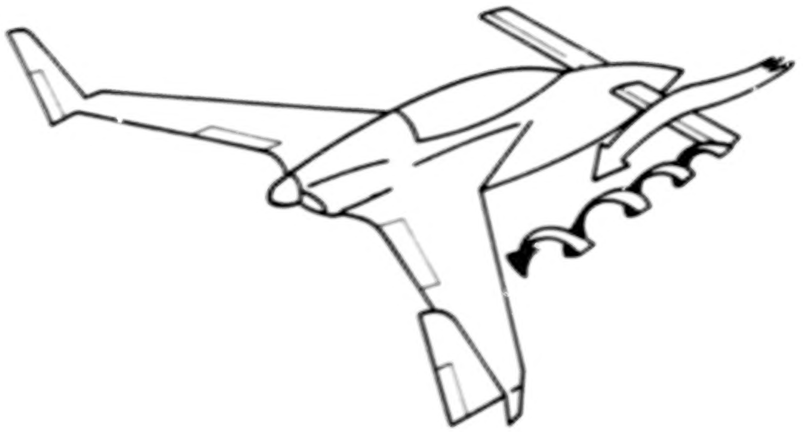

Figure 11.- Sketch of canard-wing aerodynamic flow interactions.

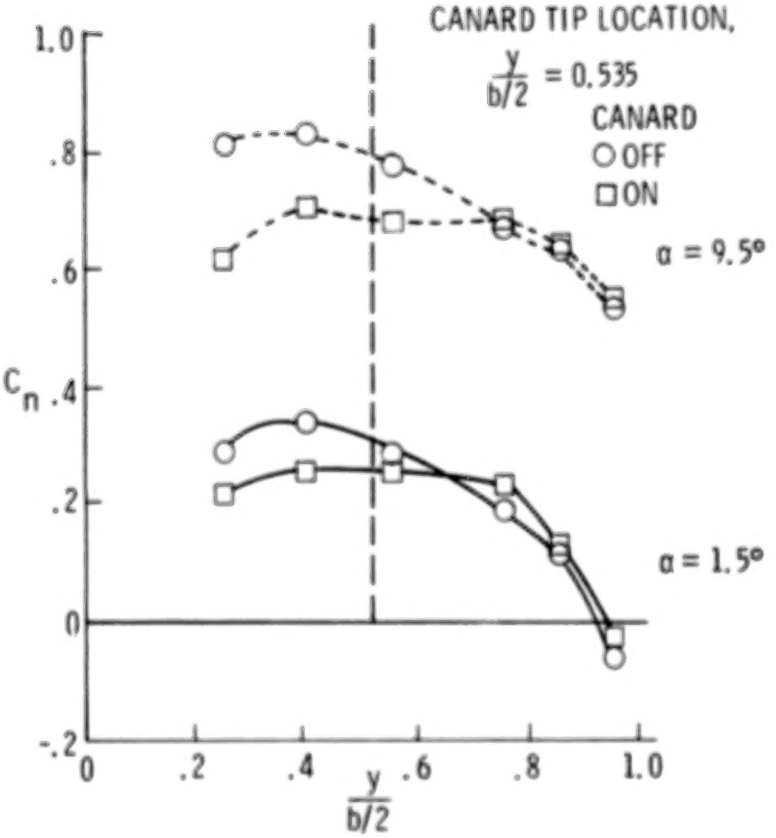

Figure 12.- Effect of canard on spanload distribution of wings.

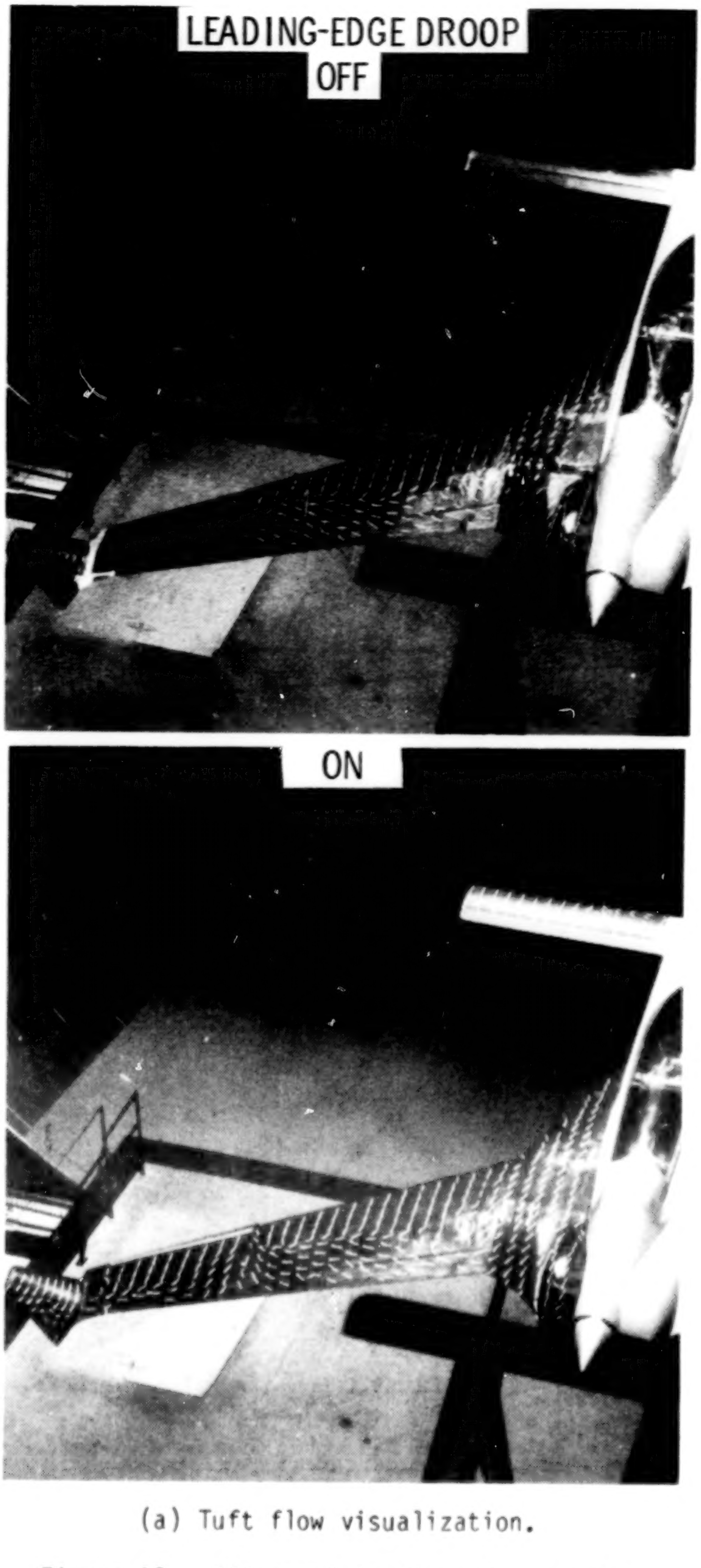
LEADING-EDGE DROOP
OFF
ON

ORIGINAL PAGE IS
OF POOR QUALITY

(a) Tuft flow visualization.

Figure 13.- Effect of leading edge on wing stall patterns, $\alpha = 19.5°$.

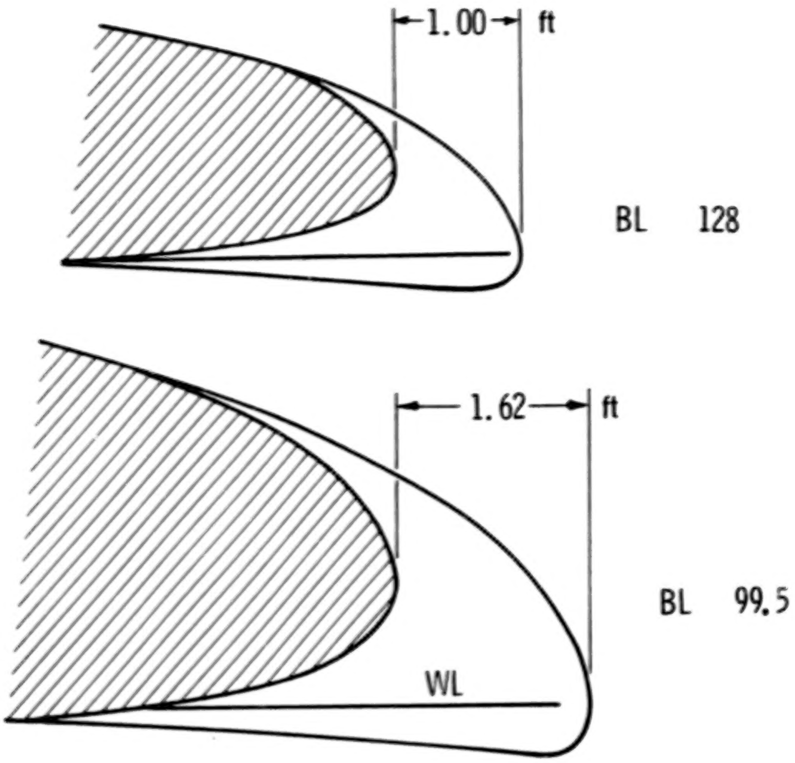
1.00 ft
BL 128
1.62 ft
BL 99.5
WL

(b) Leading-edge droop.

Figure 13.- Concluded.

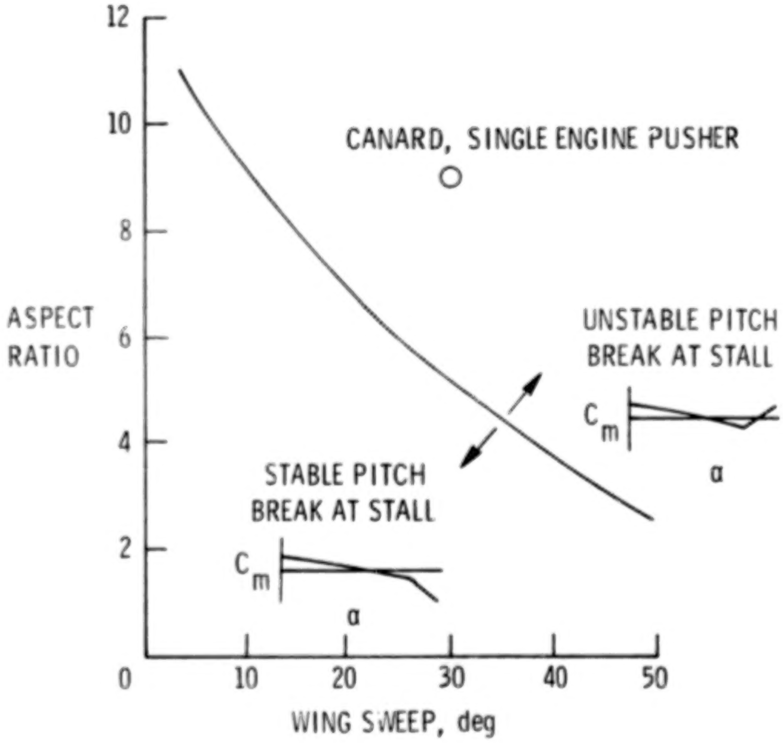

Figure 14.- Effect of wing aspect ratio and sweep on pitching-moment characteristics at stall.

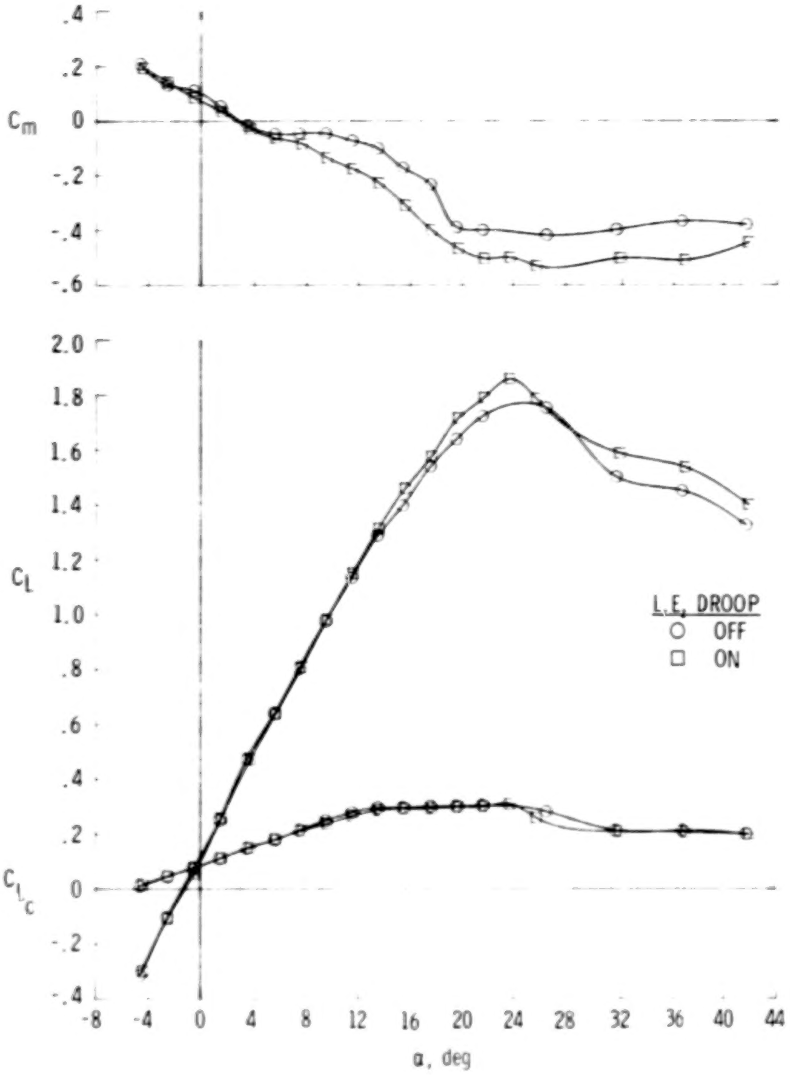

Figure 15.- Effect of leading-edge droop on longitudinal characteristics.

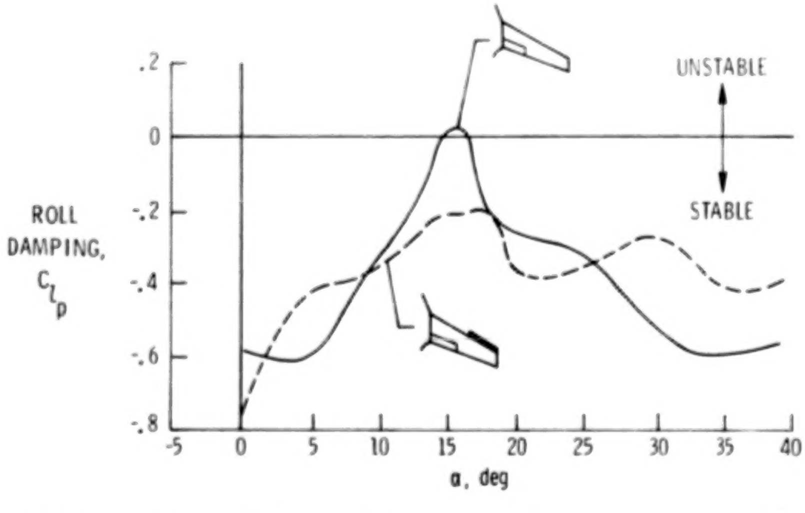

Figure 16.- Effect of leading-edge droop on roll damping characteristics.

ORIGINAL PAGE IS
OF POOR QUALITY

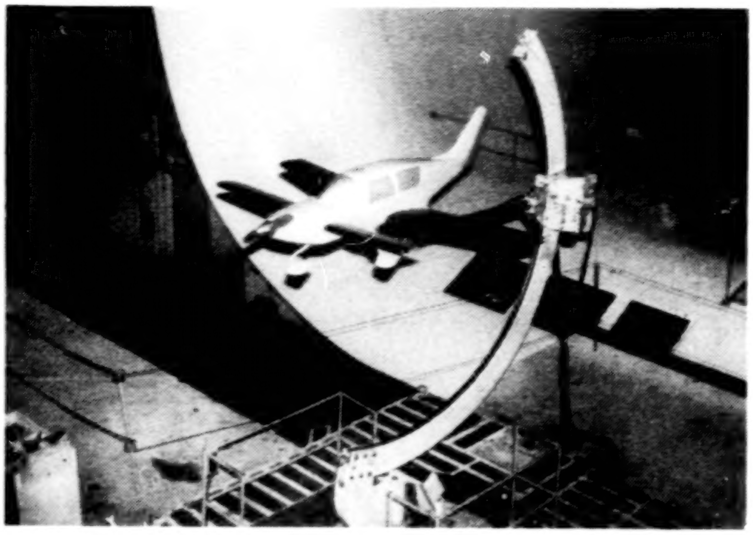

Figure 17.- Canard, tractor configuration mounted in the 30- by 60-Foot Wind Tunnel.

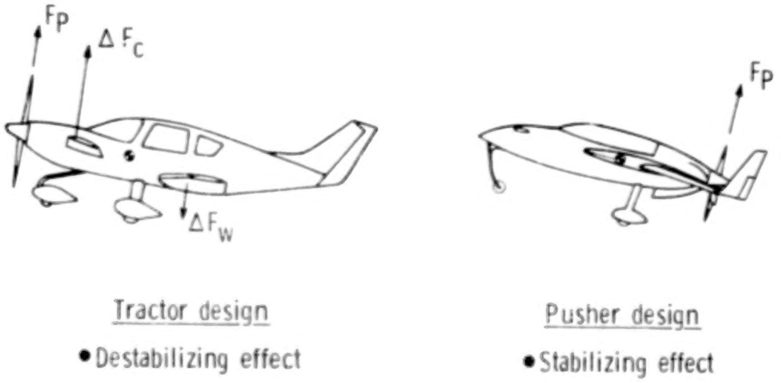
F_P
ΔF_c
ΔF_w
F_P
Tractor design
• Destabilizing effect
Pusher design
• Stabilizing effect

(a) Illustration of power effects.

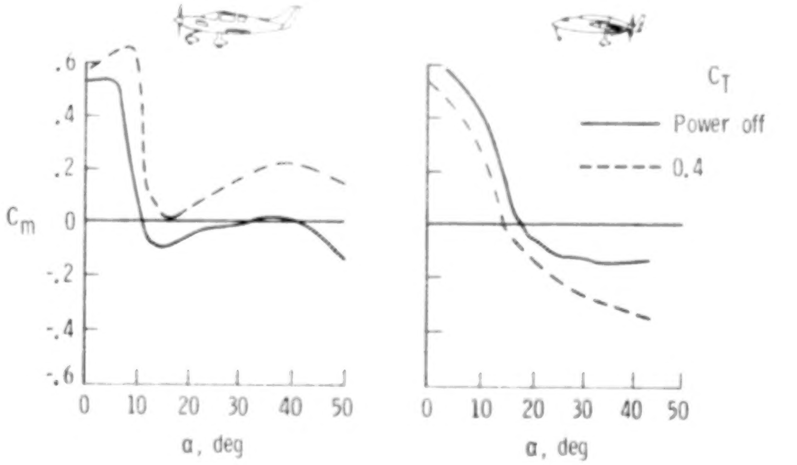

(b) Pitching-moment characteristics.

Figure 18.- Comparison of power effects on pitching-moment characteristics of canard tractor and pusher designs.

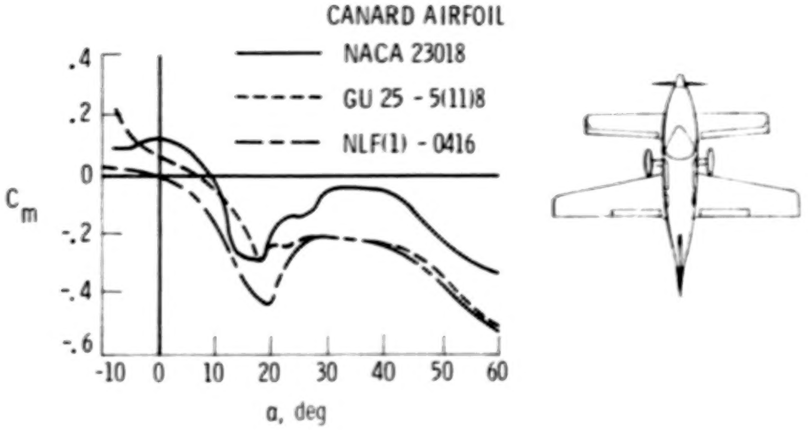

Figure 19.- Effect of canard airfoil on pitching-moment characteristics.

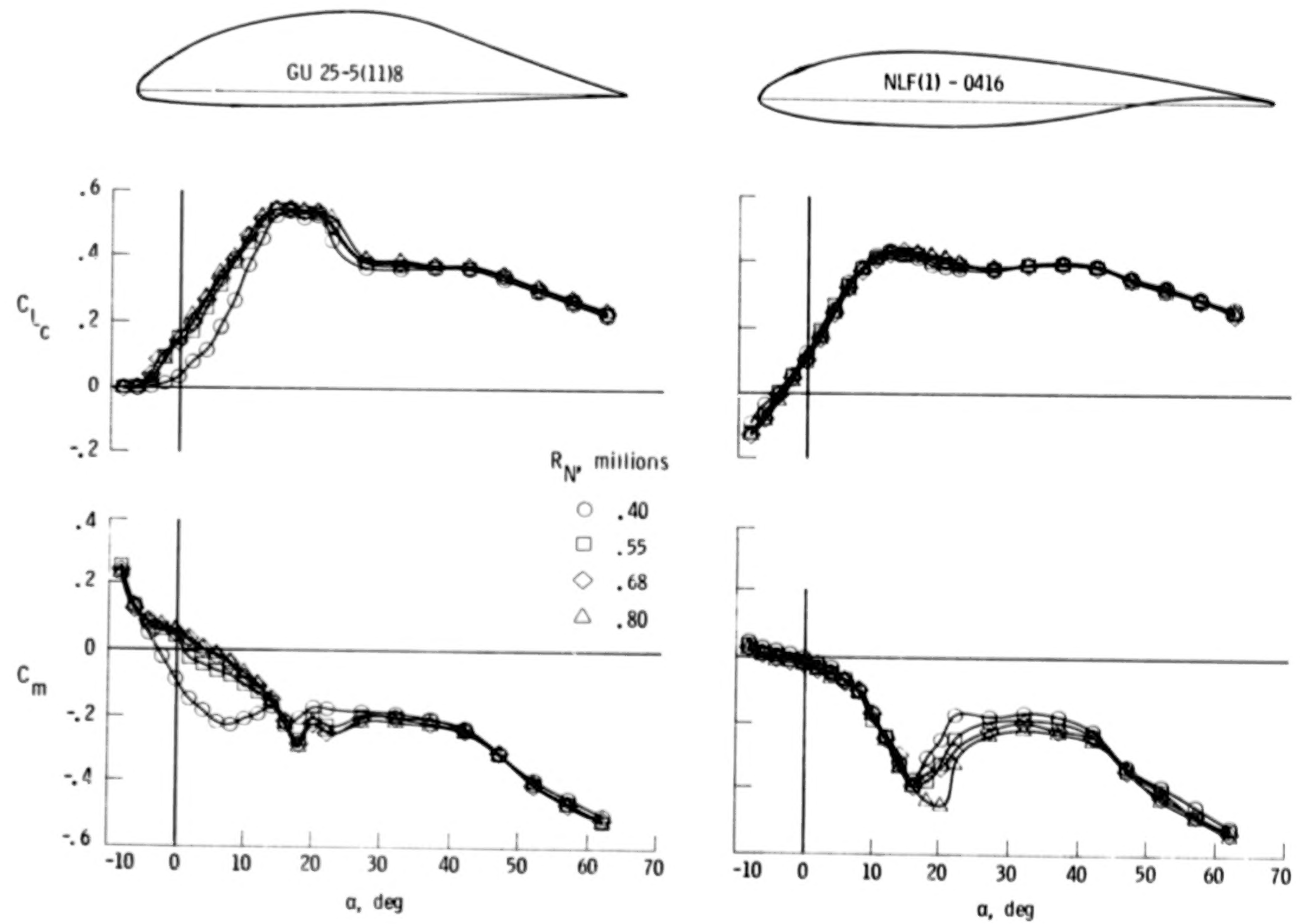

Figure 20.- Effect of Reynolds number on aerodynamic characteristics of canard, tractor configuration for two different canard airfoils.

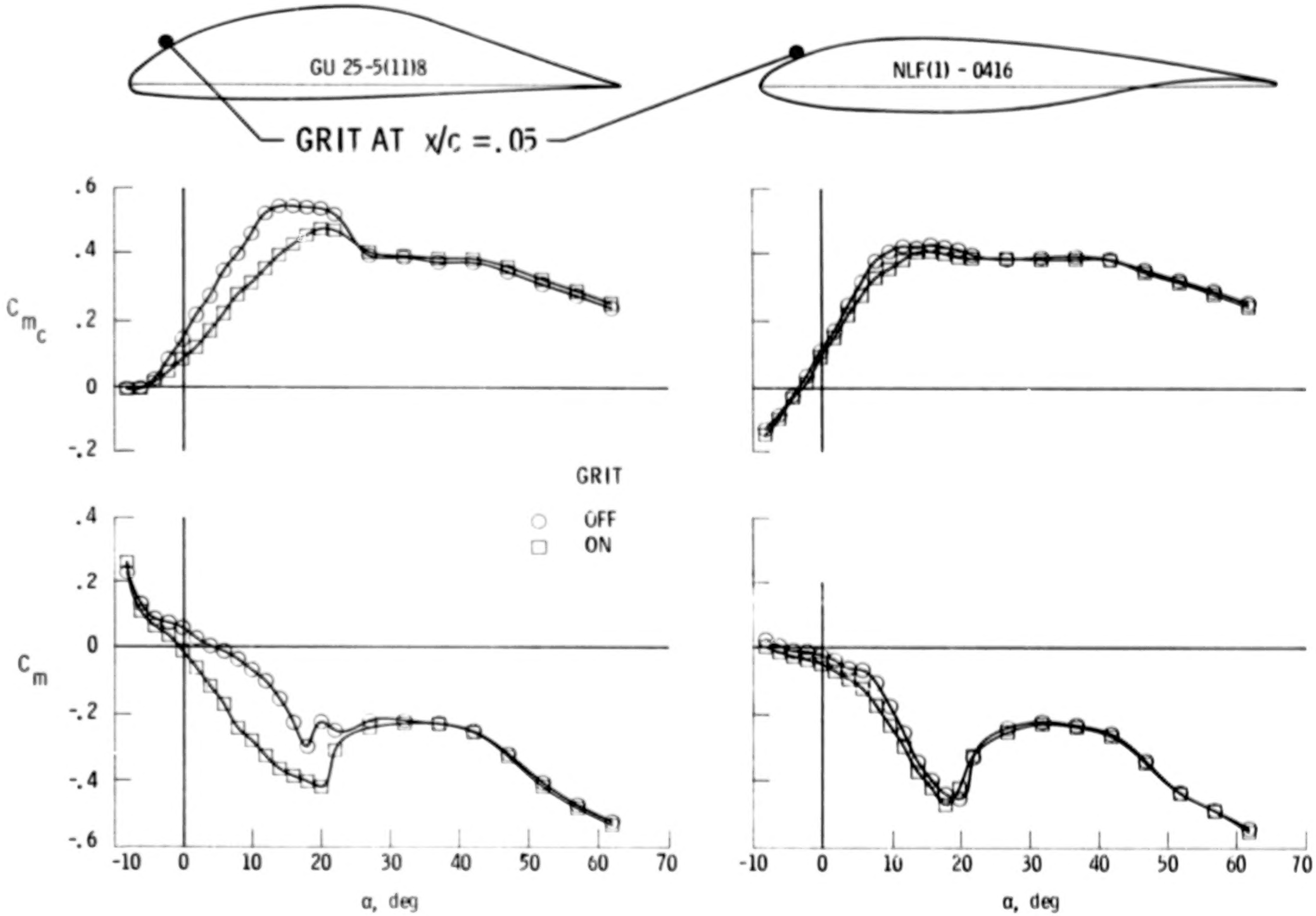

Figure 21.- Effects of fixed-transition on aerodynamic characteristics of canard, tractor configuration for two different canard airfoils. Reynolds number = 800,000.

ORIGINAL PAGE IS
OF POOR QUALITY

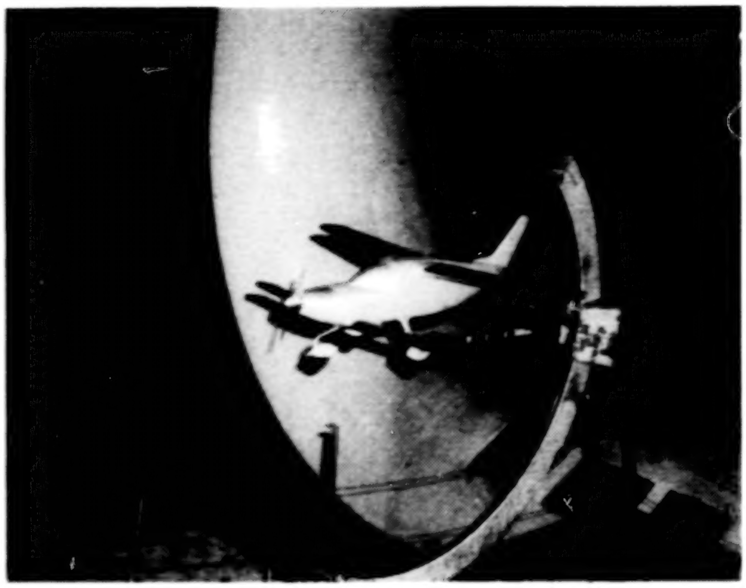

Figure 22.- High-wing, low-canard tractor configuration.

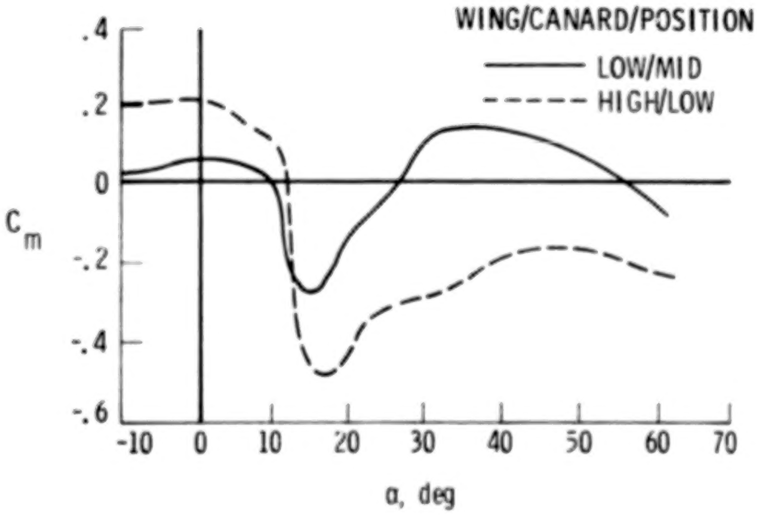

Figure 23.- Effect of canard/wing arrangement on pitching-moment characteristics of canard tractor design.

ORIGINAL PAGE IS
OF POOR QUALITY

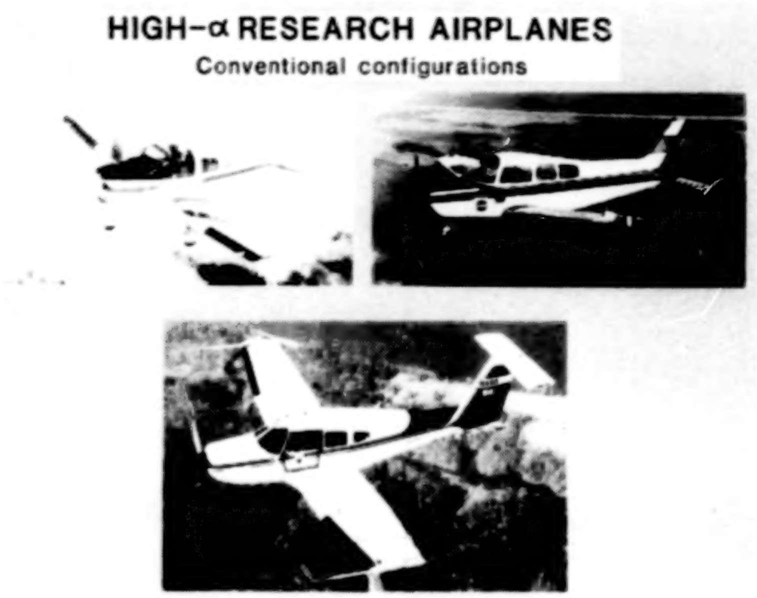

HIGH-α RESEARCH AIRPLANES

Conventional configurations

Figure 24.- Conventional airplanes used in stall/spin research.

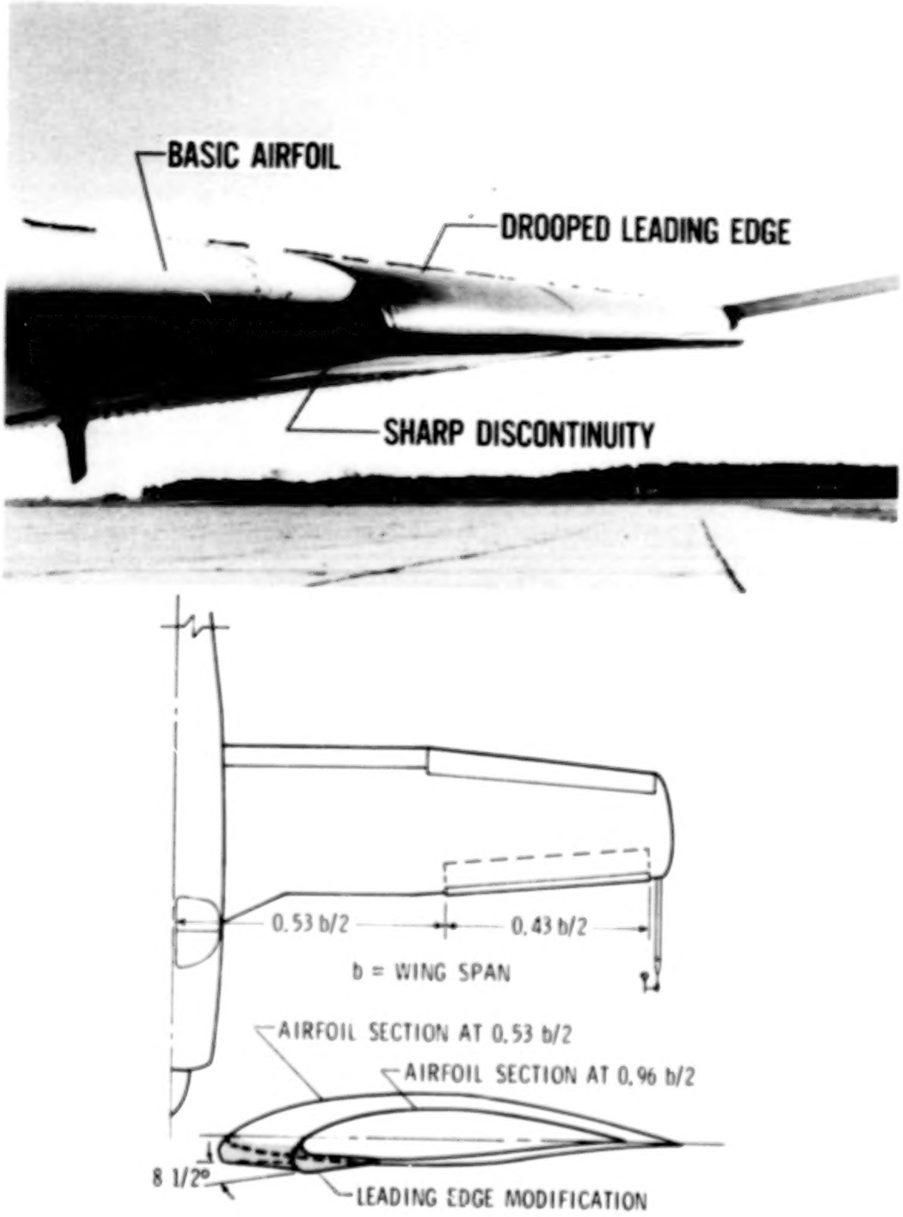
BASIC AIRFOIL
DROOPED LEADING EDGE
SHARP DISCONTINUITY
0.53 b/2
0.43 b/2
b = WING SPAN
AIRFOIL SECTION AT 0.53 b/2
AIRFOIL SECTION AT 0.96 b/2
8 1/2°
LEADING EDGE MODIFICATION

Figure 25.- Wing leading-edge droop used in stall/spin research.

ORIGINAL PAGE IS
OF POOR QUALITY

ORIGINAL PAGE IS
OF POOR QUALITY

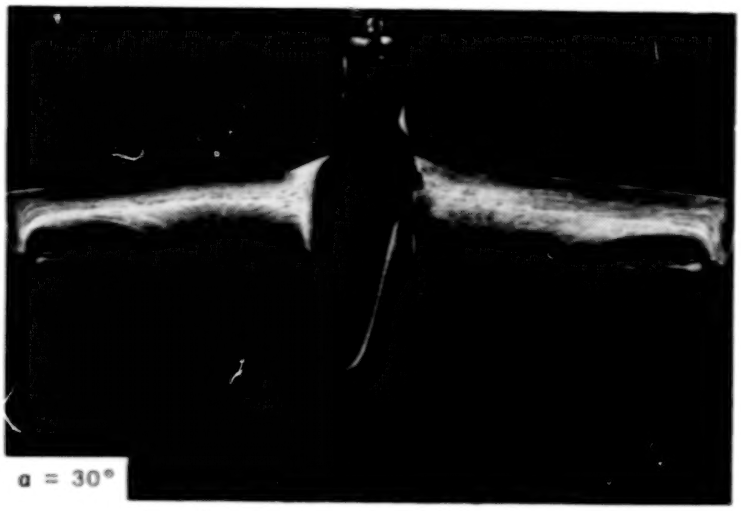

(a) Basic wing, α = 30°.

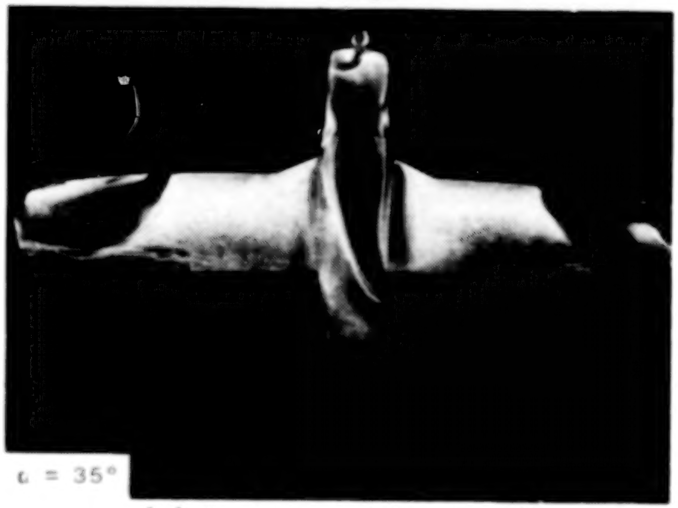

(b) Modified wing, α = 35°.

Figure 26.- Oil flow visualization on tapered-wing model showing effect of leading-edge droop.

	NUMBER OF SPINS / ATTEMPTS	
	BASIC AIRPLANE	MODIFIED AIRPLANE
AA-1X (YANKEE)	$\frac{185}{193} = 96\%$	$\frac{0}{31} = 0\%$
C-23X (SUNDOWNER)	$\frac{127}{129} = 98\%$	$\frac{7}{134} = 5\%$
PA-28RX (ARROW)	$\frac{224}{255} = 88\%$	$\frac{12}{236} = 5\%$

Figure 27.- Summary of stall/spin flight test results showing spin resistance due to wing modifications.

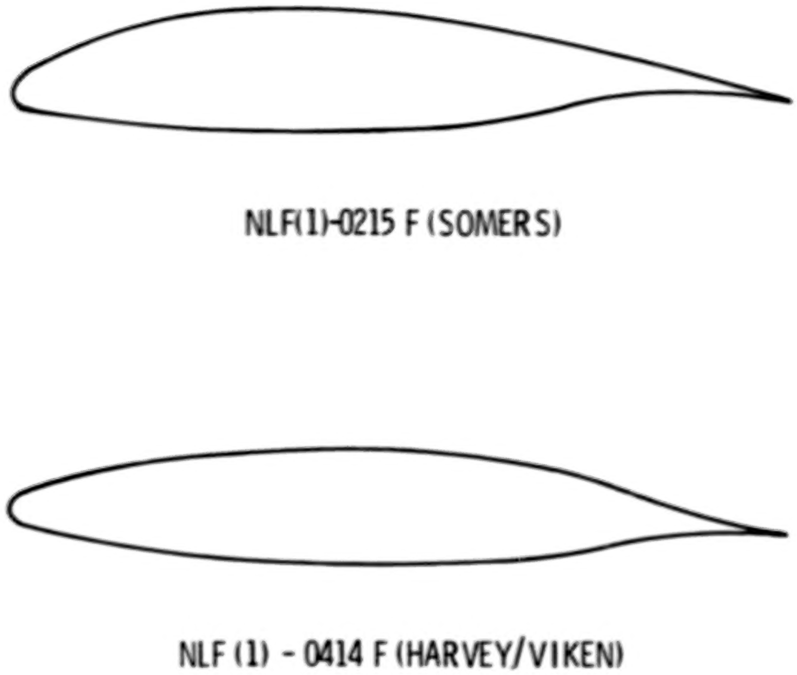
NLF(1)-0215 F (SOMERS)
NLF (1) - 0414 F (HARVEY/VIKEN)

Figure 28.- Sketch of two different airfoils designed for natural laminar flow.

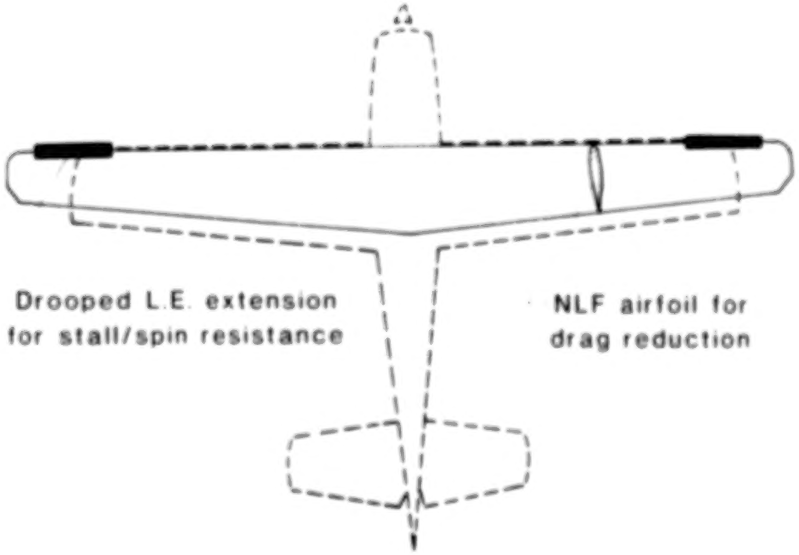
Drooped L.E. extension
for stall/spin resistance
NLF airfoil for
drag reduction

Figure 29.- Leading-edge droop modification applied to advanced wing design.

ORIGINAL PAGE IS
OF POOR QUALITY

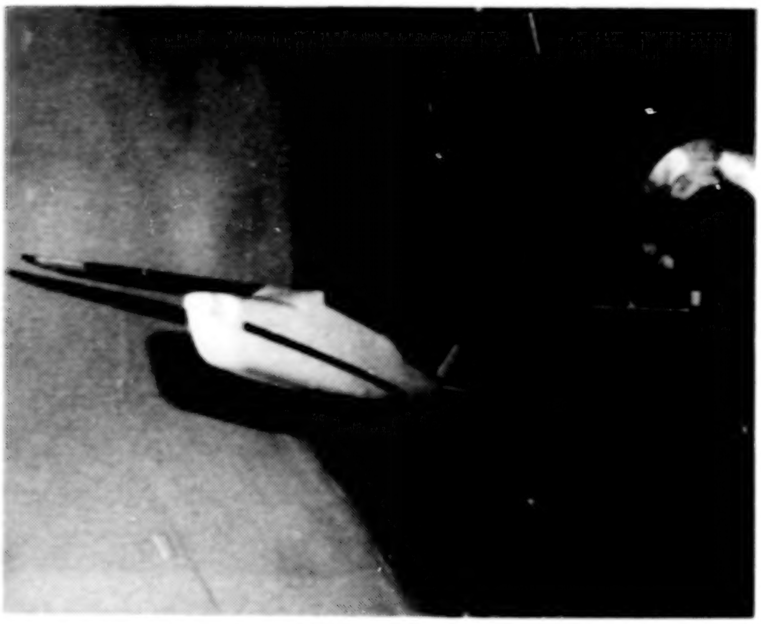

Figure 30.- Photograph of leading-edge droop on advanced wing design in Langley 12-Foot Low-Speed Wind Tunnel.

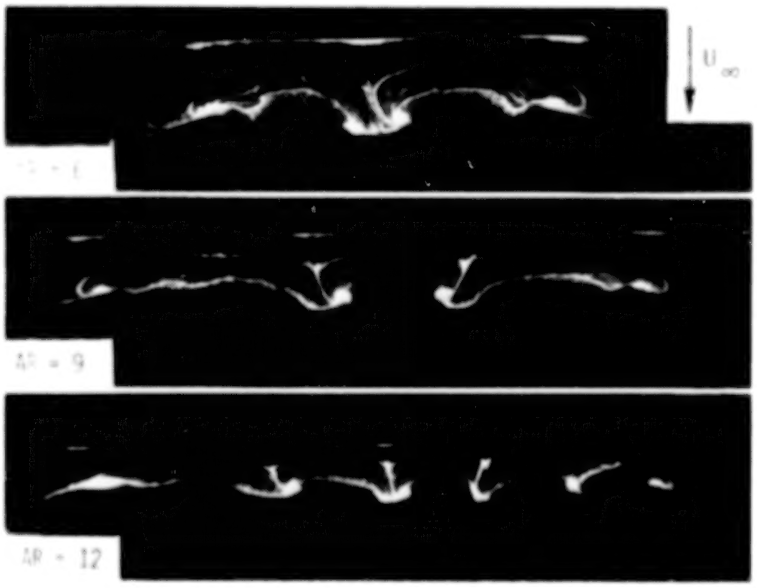

Figure 31.- Oil flow patterns developed on a series of wings (14% Clark Y airfoils of various aspect ratios, α = 18.4°, Reynolds number = 385,000.

ORIGINAL PAGE IS OF POOR QUALITY

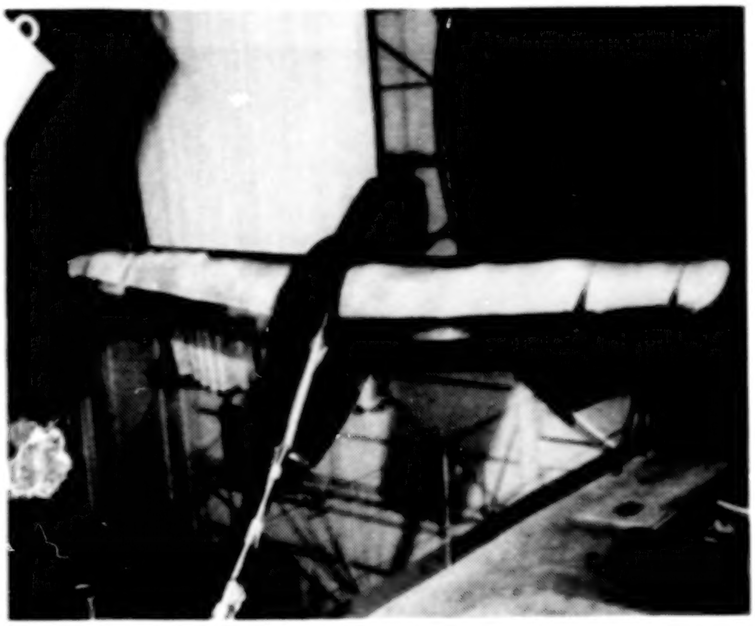

Figure 32.- Chemical sublimation study showing extent of natural laminar flow on advanced wing design.

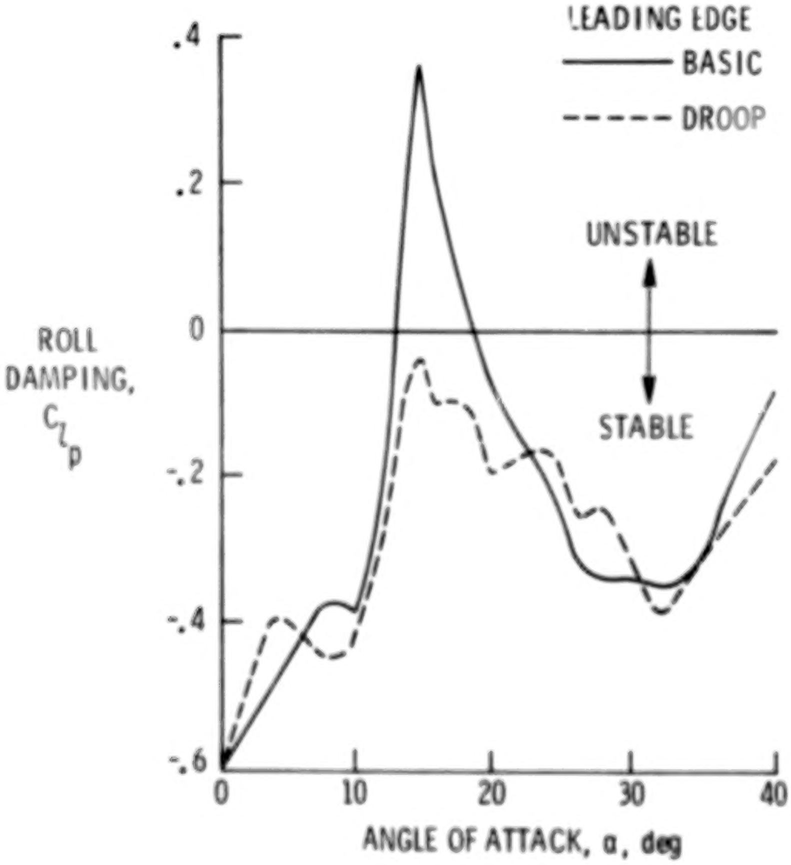

Figure 33.- Effect of leading-edge droop on roll damping characteristics of advanced wing design.

ORIGINAL PAGE IS
OF POOR QUALITY

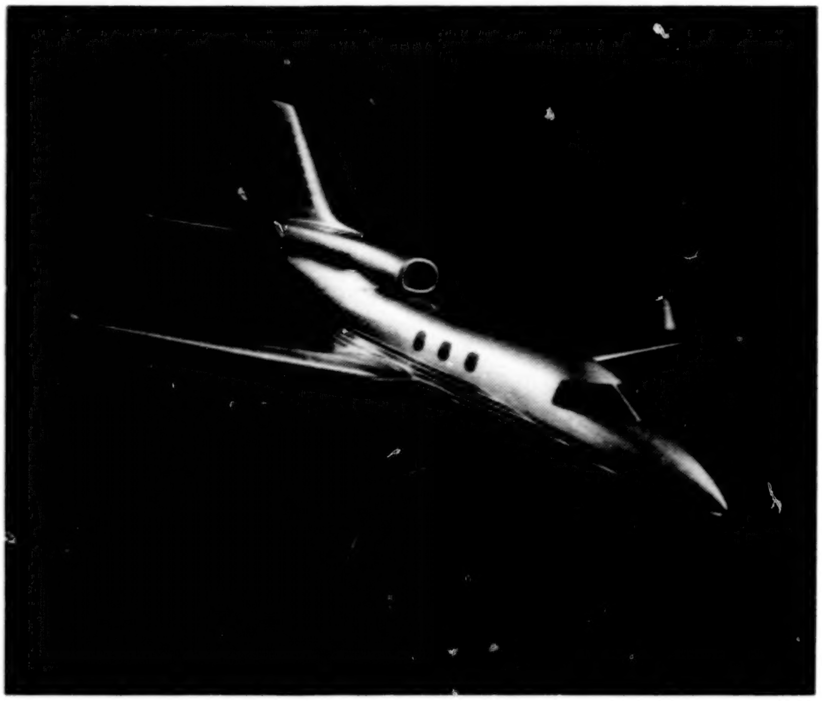

Figure 34.- Photograph of business jet configuration.

ORIGINAL [illegible]
OF POOR QUALITY

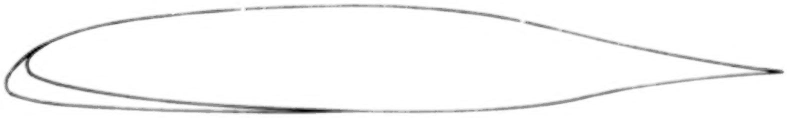

Figure 35.- Sketch of leading-edge droop design used on business jet configuration.

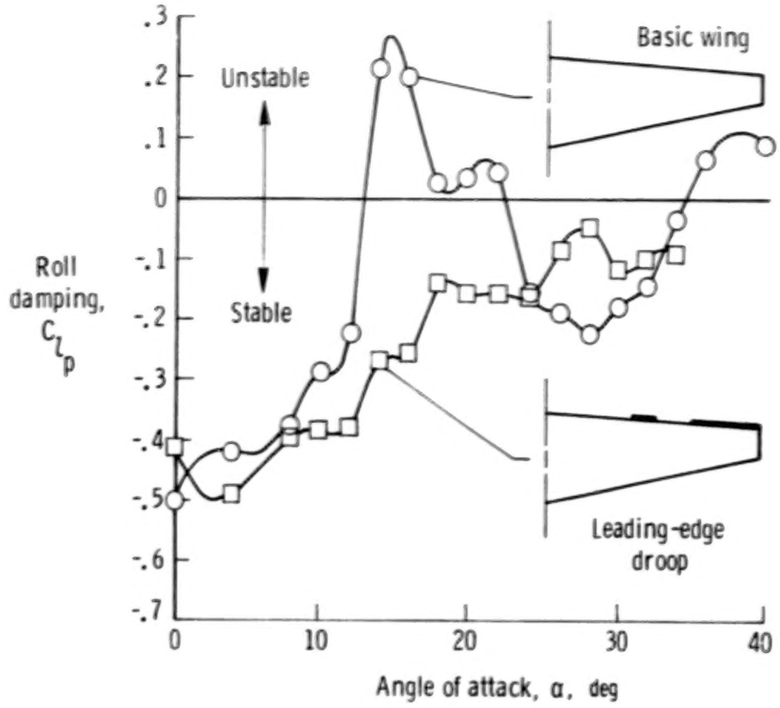

(a) Outboard droop alone.

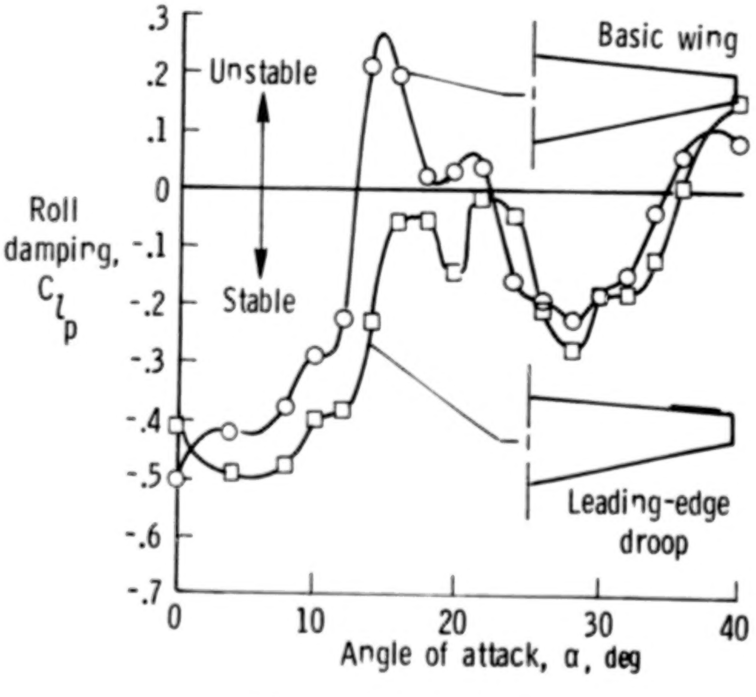

(b) Segmented droop.

Figure 36.- Effects of leading-edge droop on roll damping characteristics of business jet configuration.

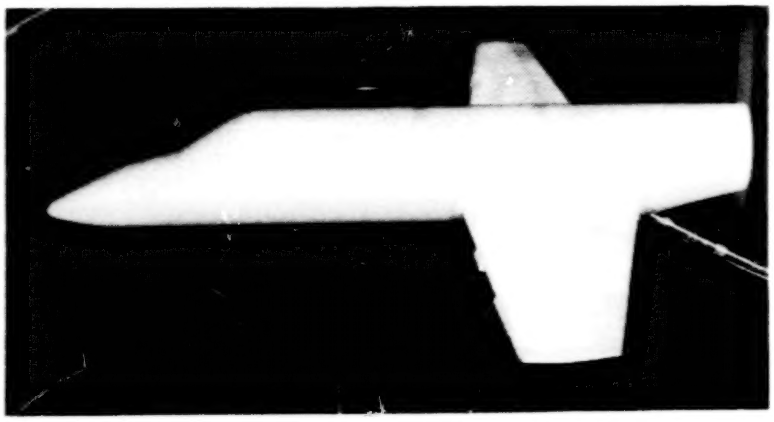

Figure 37.- Chemical sublimation studies on business jet in the 30- by 60-Foot Wind Tunnel.

ORIGINAL PAGE IS
OF POOR QUALITY

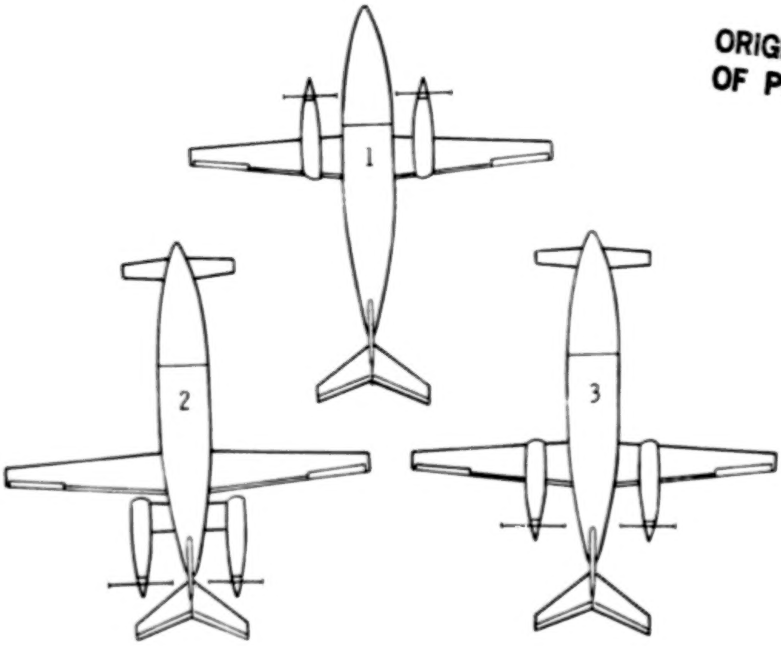

Figure 38.- Plan views of three-surface and conventional configurations.

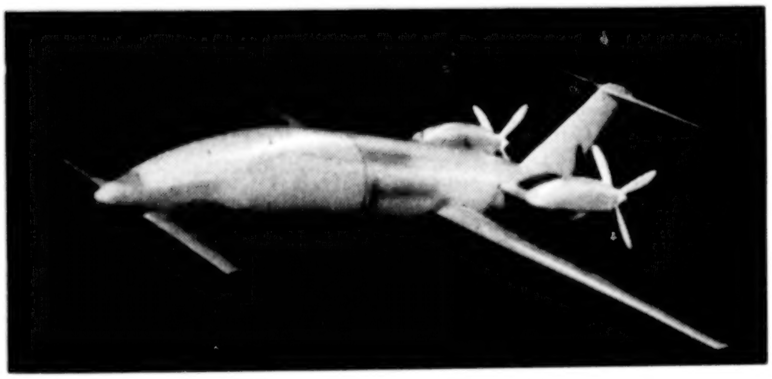

Figure 39.- Photograph of model of three-surface configuration.

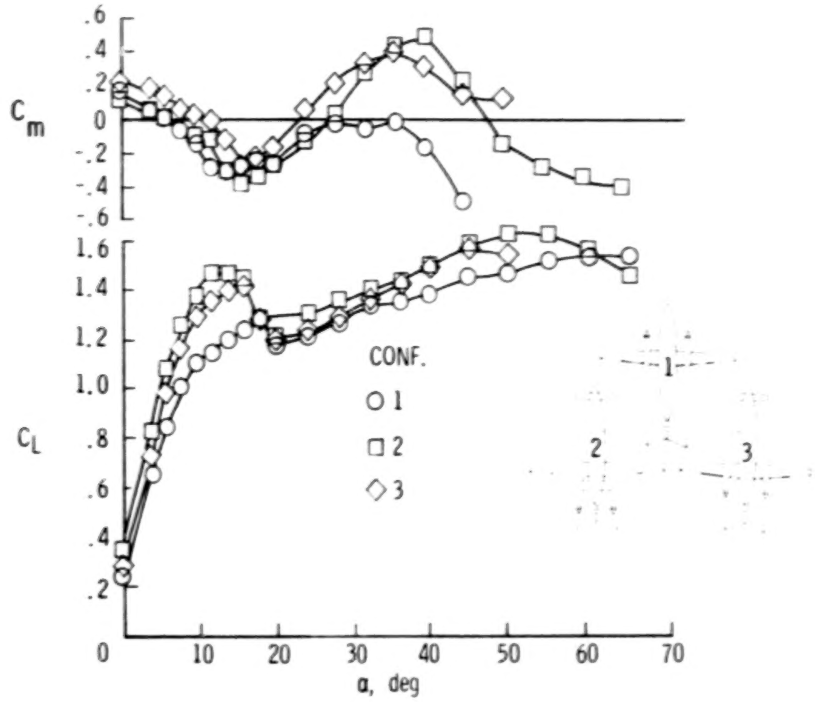

(a) Power off.

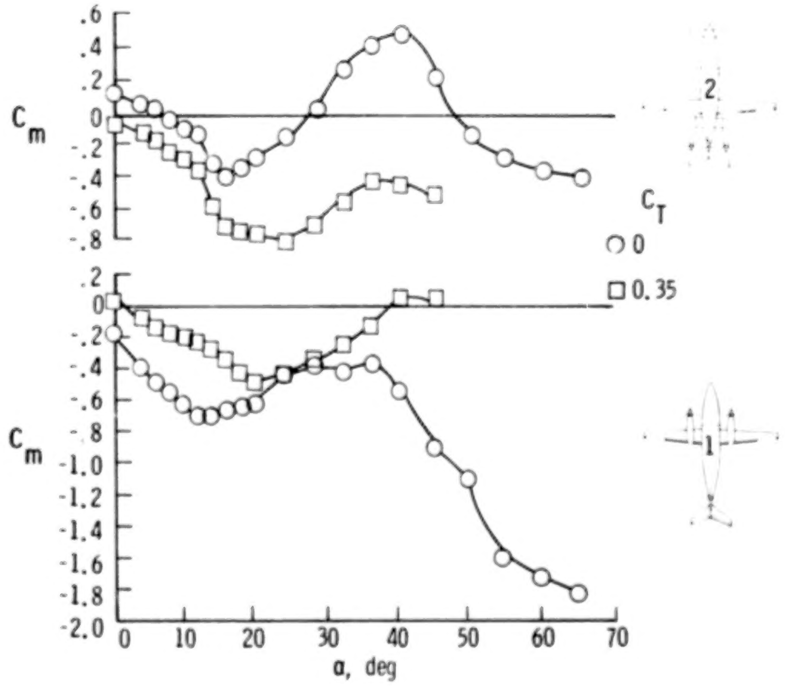

(b) Power on.

Figure 40.- Effects of power on longitudinal characteristics.

ORIGINAL PAGE IS
OF POOR QUALITY

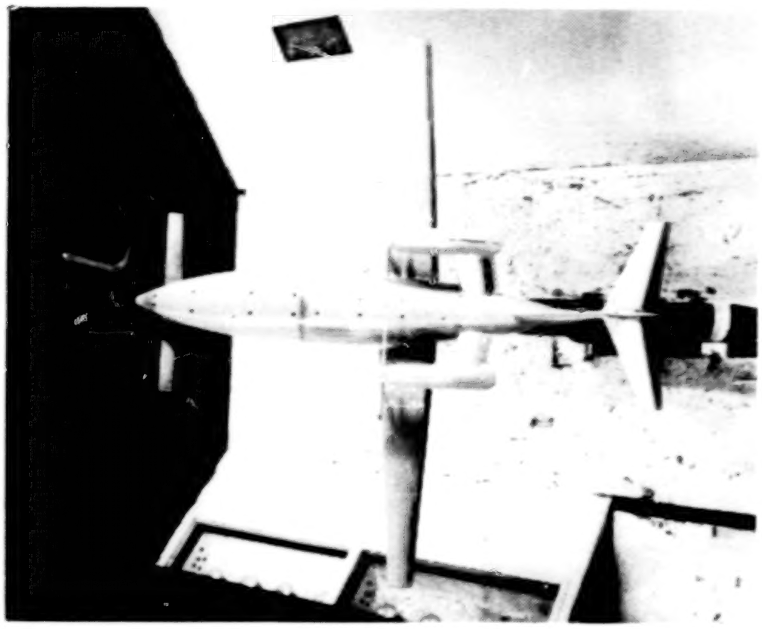

Figure 41.- Photograph of three-surface over-the-wing propeller configuration.

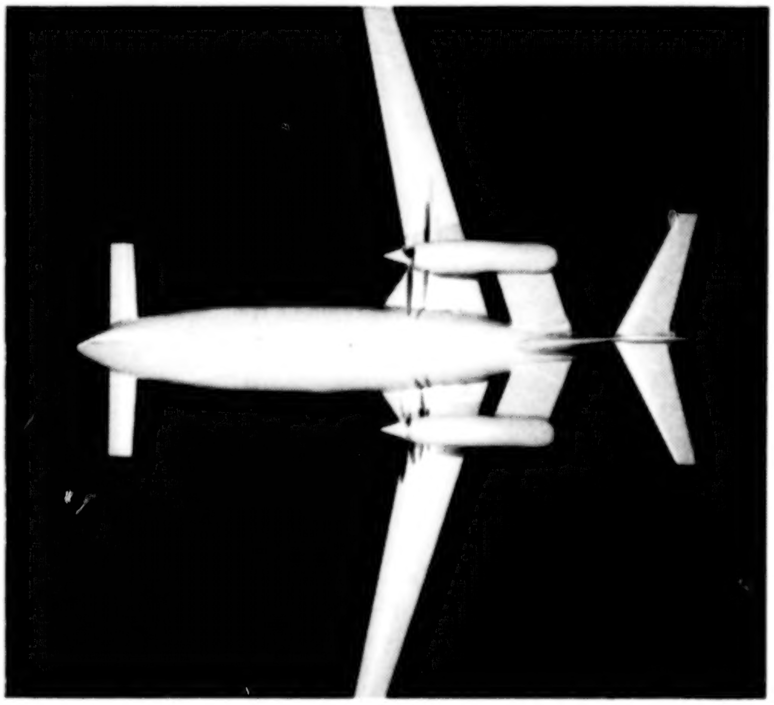

Figure 42.- Plan view photograph of three-surface over-the-wing propeller configuration with forward-swept wing.

N88-23747

NATURAL LAMINAR FLOW AND AIRPLANE STABILITY AND CONTROL*

S10-08
155

C. P. van Dam
Vigyan Research Associates, Inc.
Hampton, Virginia 23665

ABSTRACT

Location and mode of transition from laminar to turbulent boundary-layer flow have a dominant effect on the aerodynamic characteristics of an airfoil section. In this paper, the influences of these parameters on the sectional lift and drag characteristics of three airfoils are examined. Both analytical and experimental results demonstrate that when the boundary-layer transitions near the leading edge as a result of surface roughness, extensive trailing-edge separation of the turbulent boundary layer may occur. If the airfoil has a relatively sharp leading edge, leading-edge stall due to laminar separation can occur after the leading-edge suction peak is formed. These two-dimensional results are used to examine the effects of boundary-layer transition behavior on airplane longitudinal and lateral-directional stability and control.

INTRODUCTION

In recent years, airplane construction materials and fabrication methods have improved greatly, resulting in the production of airframe surfaces which are essentially free of roughness and waviness and which accurately match the design shape. Flight tests (e.g., refs. 1 and 2) have demonstrated that extensive runs of laminar flow can be obtained over the region of favorable pressure gradient on smooth airplane surfaces and provide a significant reduction in profile drag.

The application of natural laminar flow (NLF) to improve airplane speed and range, however, has also resulted in concerns about a new set of problems in airplane handling qualities. In order to exhibit satisfactory handling qualities, an airplane must possess a certain measure of both stability and controllability. Recently, a number of airplane stability and control problems have been encountered due to loss of laminar flow in some composite home-built airplanes and this has resulted in articles such as references 3 and 4. In flight, the loss of laminar flow can be the result of leading-edge surface contamination due to insects or moisture.

The purpose of this paper is to examine the effects of NLF on airplane stability and control. The first part of the paper will discuss the manner in which the aerodynamic characteristics of airfoil sections depend on location and mode of transition from laminar to turbulent boundary-layer flow. In the second part, the influence of airfoil aerodynamic characteristics on airplane longitudinal and lateral-directional stability and control will be discussed.

NOMENCLATURE

b	wing span, ft

---

*This research was conducted under NASA Contract No. NAS1-17797.

PRECEDING PAGE BLANK NOT FILMED

N86 [illegible]

C_D	airplane drag coefficient
$C_{D,0}$	airplane zero-lift drag coefficient
C_L	airplane lift coefficient
C_{L_α}	lift-curve slope, deg^{-1} or rad^{-1}
C_m	airplane pitching-moment coefficient
C_{m_q}	variation of pitching-moment coefficient with pitch rate
C_{m_α}	variation of pitching-moment coefficient with angle of attack, deg^{-1} or rad^{-1}
C_n	airplane yawing-moment coefficient
C_{n_β}	variation of yawing-moment coefficient with angle of sideslip, deg^{-1} or rad^{-1}
C_p	pressure coefficient, $(p - p_\infty)/q_\infty$
c	chord length, ft
$\bar{c}$	mean aerodynamic chord, ft
c_d	section drag coefficient
c_ℓ	section lift coefficient
c_{ℓ_α}	section lift-curve slope, deg^{-1} or rad^{-1}
c_m	section pitching-moment coefficient
H	boundary-layer shape parameter, δ^*/θ
I_{yy}	airplane moment of inertia about Y-axis, slug-ft^2
M	Mach number
N	airplane yawing moment, ft-lb
p	static pressure, psf
q	dynamic pressure, psf
R	chord Reynolds number
S	lifting surface reference area, ft^2
s	surface length, ft
U_∞	free-stream velocity, ft/sec
V_i	indicated airspeed, knots
v	local velocity, ft/sec
$\bar{X}$	nondimensional longitudinal location, $X/\bar{c}$
x	airfoil abscissa, ft
α	angle of attack, deg
β	angle of sideslip, deg
δ^*	boundary-layer displacement thickness, ft
δ_e	elevator deflection, deg
δ_f	flap deflection, deg
ζ	damping ratio
θ	boundary-layer momentum thickness, ft
ρ	air density, lb/ft^3
ω_n	undamped natural frequency, rad/sec

Subscripts:

ac	aerodynamic center
C	foreplane
cg	center of gravity
max	maximum

P	phugoid mode
SP	short-period mode
t	transition location
WB	wing body
WLT	winglet
∞	free-stream condition

BOUNDARY-LAYER TRANSITION AND AIRFOIL AERODYNAMIC CHARACTERISTICS

The two parameters which have a dominant effect on the aerodynamic characteristics of an airfoil section are boundary-layer transition location and boundary-layer transition mode. The transition modes of most practical interest include transition by inflectional instability at laminar separation or with crossflow vorticity, and transition by viscous (Tollmien-Schlichting) instability.

In most cases, the laminar boundary layer separates quickly when it encounters a slight pressure rise. Boundary-layer transition will take place in the separated boundary layer, and a laminar-separation bubble is formed when the turbulent boundary layer reattaches to the surface. Until recently, it has been assumed that only for Reynolds numbers of less than about 5 million would transition occur at laminar separation. (See e.g., refs. 5 and 6.) However, flight results reported in reference 2 indicate that for surfaces with minimal three-dimensional flow effects, transition occurs downstream of the point of minimum pressure, where laminar separation would be expected, even at relatively large transition Reynolds numbers. An extreme example presented in reference 2 is the case of a high-speed business-jet airplane, where transition has been measured at the 40-percent chord location for a chord Reynolds number of 30 million with the point of minimum pressure located at 35 percent of the chord.

Transition can also take place in the attached boundary layer due to the growth of two-dimensional disturbances in the laminar boundary layer. This growth of the two-dimensional disturbances can be accelerated by surface roughness and waviness. The initial conditions for the turbulent boundary layer which originates in the free-shear layer (due to laminar separation) are quite different as compared to the initial conditions of a turbulent boundary layer which originates in the attached boundary layer.

As mentioned before, transition location is another important parameter when examining the aerodynamic characteristics of an airfoil section. A turbulent boundary layer which originates near an airfoil leading edge produces a very different boundary-layer thickness and profile in the pressure-recovery region than a turbulent boundary layer which originates from transition near the point of minimum pressure. Depending on the pressure distribution in the pressure recovery region, a variation in initial conditions for the turbulent boundary layer can produce turbulent boundary-layer separation and consequently a change in airfoil aerodynamic characteristics. The influence of transition location and transition mode on aerodynamic characteristics can best be demonstrated by examining these characteristics for three airfoil sections.

In figure 1, the geometry and two inviscid velocity distributions for the GU 25-5(11)8 airfoil section are shown. The airfoil section characteristics have been calculated using the low-speed airfoil design and analysis method developed by Eppler and Somers (refs. 7 and 8). The surface pressure can be obtained from the local velocity ratio as follows:

$$C_p = 1 - \left(\frac{v}{U_\infty}\right)^2 \qquad (1)$$

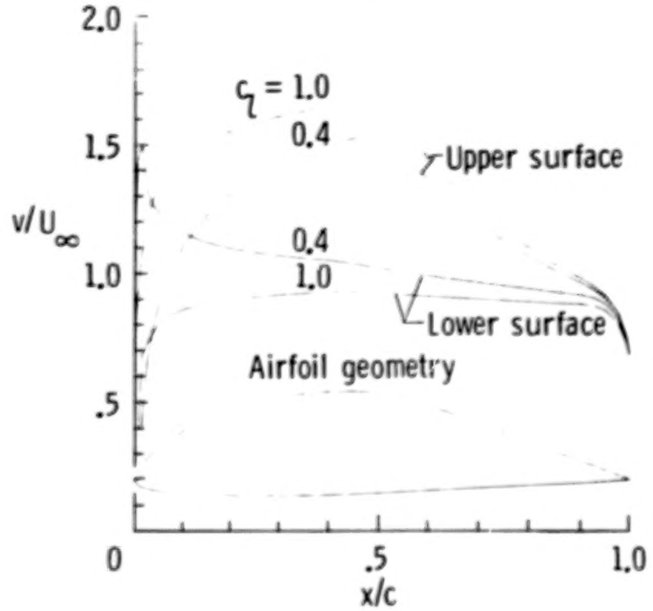

Figure 1.- Geometry and inviscid velocity distributions of GU25-5(11)8 airfoil.

This airfoil section is one of a series of low-drag airfoils designed (ref. 9) and wind-tunnel tested (refs. 10 and 11) at the University of Glasgow during the 1960's. The GU 25-5(11)8 airfoil section has a maximum thickness ratio of 0.20, occurring at 41.6 percent of the chord. The airfoil section is capable of generating a high maximum lift coefficient at relatively low Reynolds numbers. Wind-tunnel data in references 10 and 11 indicate a maximum section lift coefficient of 1.93 at a chord Reynolds number of 0.41 million. Because of these characteristics, a large number of foreplane designs for homebuilt canard configurations have used this airfoil section. The velocity distributions in figure 1 indicate that at approximately 50 percent of the chord the favorable accelerating flow condition over the front portion of the airfoil abruptly changes into an adverse decelerating flow condition over the aft portion of the airfoil. This type of discontinuity in the velocity distribution causes the laminar boundary layer to separate. Transition will occur in the free-shear layer, and the boundary layer will reattach in the form of a turbulent boundary layer.

The main disadvantage of laminar separation in this location will be an increment in section drag. The size of the laminar separation bubble is a function of Reynolds number. With decreasing Reynolds number, the boundary-layer reattachment point moves downstream and the bubble becomes more elongated. Eventually, for a low enough Reynolds number (R < 200,000 according to ref. 6), reattachment of the turbulent boundary layer will not occur before the trailing edge of the airfoil, and airfoil stall takes place. The results in references 10 and 11 show that in the case of a 12-in.-chord GU 25-5(11)8 airfoil section, a laminar separation bubble of about 1.5-in. length ($x/c = 0.13$) is formed at the onset of pressure recovery at $R = 0.63$ million. In order to eliminate this separation bubble, transition was fixed ahead of the point of minimum pressure by means of a trip wire located at $x/c = 0.455$.

In figure 2, the influence of the laminar separation bubble on the pressure distribution of the GU 25-5(11)8 is clearly visible. Wortmann (ref. 12) was the first to solve the problem of laminar separation bubbles by introducing an instability ramp upstream of the pressure recovery region. The flow condition across the instability ramp is such that the growth of the two-dimensional disturbances in the laminar boundary layer is so strongly accelerated that transition in the attached boundary layer occurs at the end of the instability ramp prior to the steep adverse pressure-gradient flow condition.

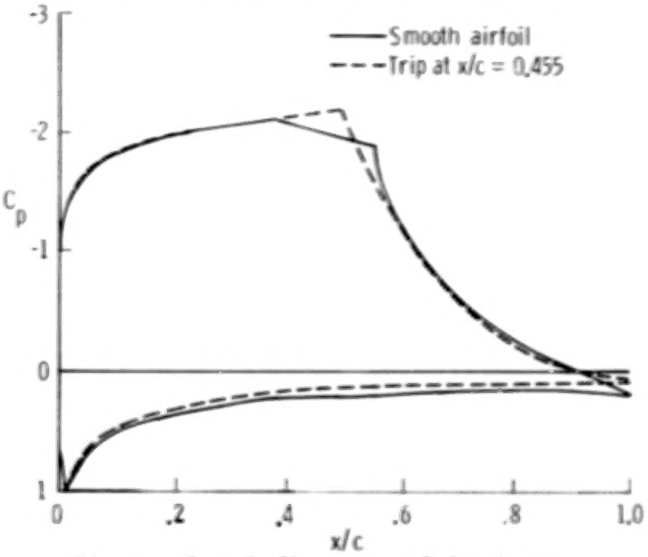

Figure 2.- Influence of laminar separation bubble on pressure distribution of GU 25-5(11)8 at α = 7.4° and R = 0.63 million (ref. 12).

Recently, Horstmann and Quast (ref. 6) have introduced pneumatic turbulators to produce premature boundary-layer transition. Small air jets are used to produce highly unstable three-dimensional disturbances in the laminar boundary layer at the onset of the pressure recovery region, thus preventing laminar separation bubbles. An excellent description of the laminar separation bubble and techniques to prevent them are presented in reference 6. With increasing Reynolds number, the size of the laminar separation bubble decreases, and consequently its effect becomes smaller.

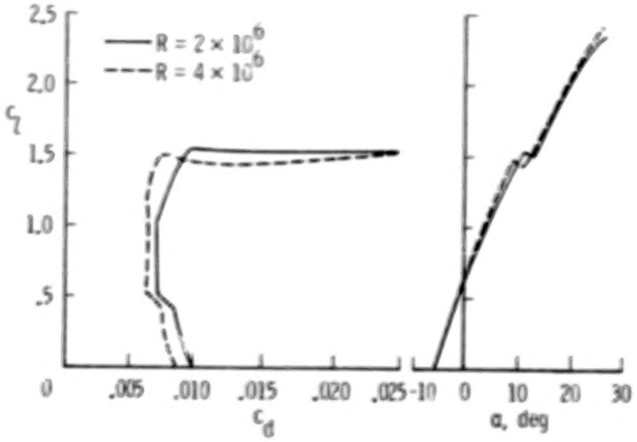

(a) Free transition.

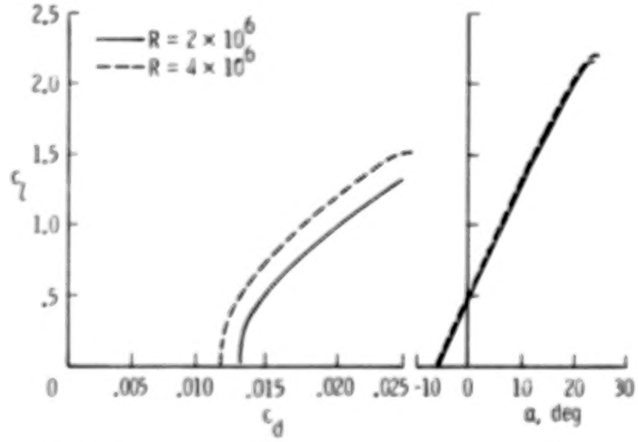

(b) Fixed transition at x/c = 0.075.

Figure 3.- Calculated aerodynamic characteristics of GU 25-5(11)8 airfoil.

In figure 3, the calculated lift and drag characteristics for this airfoil section are presented for R = 2.0 and 4.0 million. In figures 3(a) and 3(b), the results are shown for free boundary-layer transition and fixed transition at x/c = 0.075, respectively. The results for free transition show that airfoil aerodynamic characteristics change dramatically at an angle of attack of approximately

10°. At that angle of attack, a sharp suction peak near the leading edge causes transition to move forward suddenly. Due to this forward shift of transition, trailing-edge separation of the turbulent boundary layer increases, and a loss in lift is encountered. Also, forward movement of transition location and turbulent separation produces a large increment in section drag. The maximum sectional lift coefficients produced by the airfoil are very large in the case of free transition. However, the aerodynamic characteristics change drastically when boundary-layer transition is fixed near the leading edge. The latter simulates the condition when the leading edge of the airfoil section is critically contaminated by insects or moisture. The drag of the GU 25-5(11)8 increases significantly, as expected. However, the lift characteristics of the airfoil section are also affected as is clearly shown in figure 4.

The results in figure 4 indicate that both sectional lift-curve slope, c_{ℓ_α}, and section maximum lift coefficient, $c_{\ell,max}$, are reduced due to fixed boundary-layer transition. Techniques such as instability ramps, trip wires and strips, and pneumatic turbulators have a negligible influence and will not prevent this premature loss in lift when early transition occurs. Much larger devices such as vortex generators are required to prevent or reduce separation of the turbulent boundary layer.

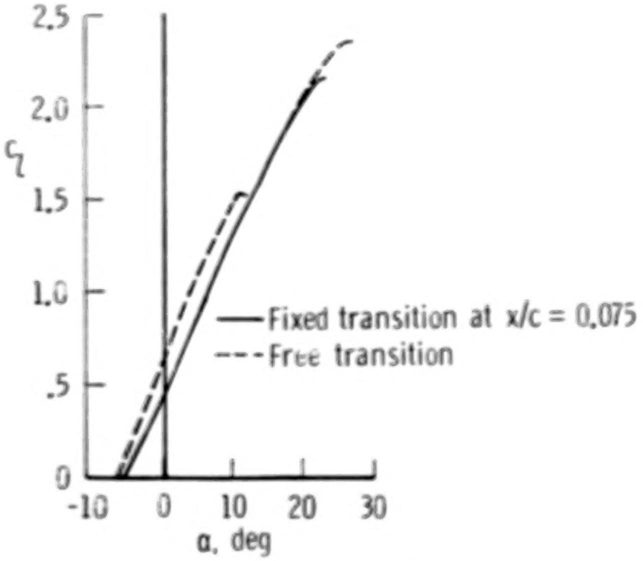

(a) R = 2 x 10^6.

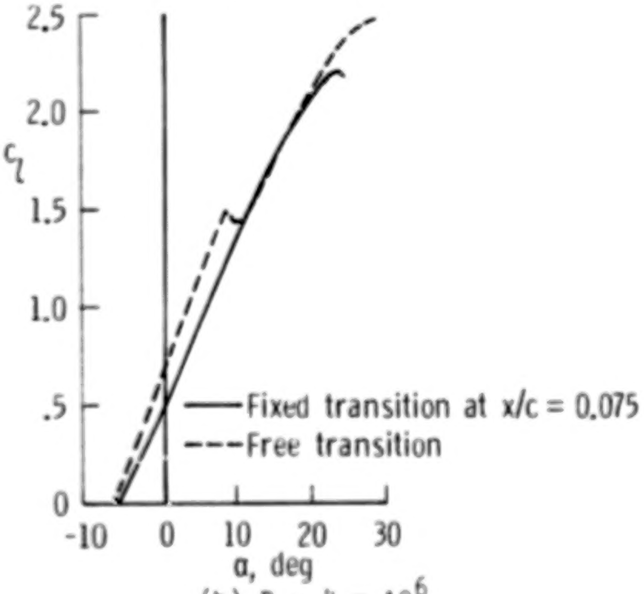

(b) R = 4 x 10^6.

Figure 4.- Influence of transition location on lift characteristics of GU 25-5(11)8 airfoil.

The influence of fixed transition on the boundary-layer development is shown in figure 5. In this figure, nondimensional boundary-layer displacement thickness, δ^*/c, nondimensional boundary-layer momentum thickness, θ/c, and boundary-layer shape factor, $H = \delta^*/\theta$, are plotted as a function of nondimensional distance, s/c, from the stagnation point along the upper surface of the GU 25-5(11)8 airfoil section at α = 3° and R = 2.0 million. Displacement thickness, δ^*, indicates the distance that the streamlines are displaced from the surface due to the reduced velocities within the boundary layer. Momentum thickness, θ, is representative of the loss in momentum of the air, $\rho U^2\theta$, due to the presence of the boundary layer. In figure 5(a), the boundary-layer development is plotted for the case of free transition. Transition occurs at s/c = 0.558 due to laminar separation, and it is followed by a steep drop in the value of H.

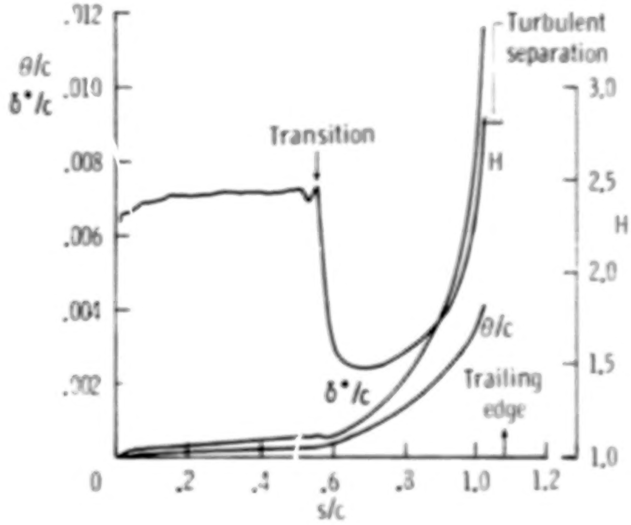

(a) Free transition.

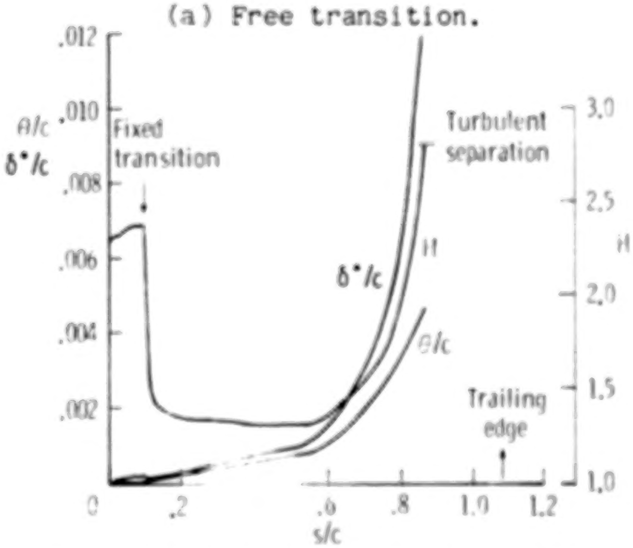

(b) Fixed transition at x/c = 0.075.

Figure 5.- Calculated boundary-layer parameters for upper surface of GU 25-5(11)8 at $\alpha = 3°$ and $R = 2 \times 10^6$.

In the pressure recovery region, displacement thickness and momentum thickness increase rapidly, and turbulent separation is predicted when the boundary-layer shape parameter H reaches a value of 2.8 at s/c = 1.033. In figure 5(b), the boundary-layer development is plotted when transition is fixed at x/c = 0.075 or s/c = 0.116. Downstream of s/c = 0.116, the boundary layer is turbulent, and displacement thickness and momentum thickness grow more rapidly as compared to the laminar case. At the onset of pressure recovery, s/c = 0.524, the displacement thickness and momentum thickness are about 2 to 4 times larger as compared to the laminar case shown in figure 5(a). The steep negative velocity gradient in the pressure recovery region causes these boundary-layer parameters to increase very rapidly resulting in turbulent separation at s/c = 0.873. Thus, for the GU 25-5(11)8 airfoil section, boundary-layer transition near the leading edge results in premature separation of the turbulent boundary layer.

Similar airfoil characteristics have also been shown by Althaus in reference 5. Althaus shows the influence of premature transition caused by leading-edge roughness to be even more

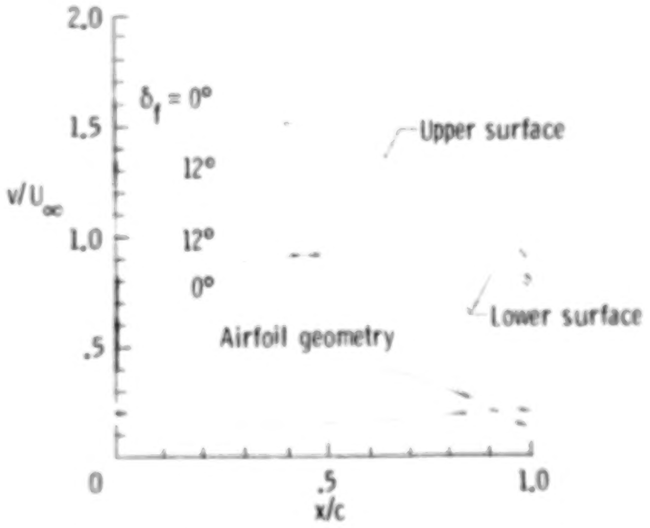

Figure 6.- Geometry and inviscid velocity distributions of FX 67-K-150/17 at $c_\ell = 1.0$.

dramatic for certain airfoils with flaps. In figure 6, the geometry and inviscid velocity distribution are shown for the FX 67-K-150/17 airfoil section with and without flap deflection at a constant angle of attack of 9.12° relative to the zero-lift line (inviscid $c_\ell = 1.0$). This airfoil was designed by F. X. Wortmann and wind-tunnel tested by D. Althaus at the University of Stuttgart (ref. 13). The airfoil has a maximum thickness ratio of 15 percent at 40.2 percent of the chord. The flap occupies the final 17 percent of the chord, and the gap between the airfoil and the flap has been sealed. An extensive set of wind-tunnel data for the smooth airfoil is presented in reference 13. Althaus, however, also performed wind-tunnel tests with a simulated pattern for insect debris established on the leading edge. This insect-roughness pattern was simulated by using small pieces of Mylar with bumps which were fastened on the airfoil nose.

Wind-tunnel data for the FX 67-K-150/17 airfoil section with and without his leading-edge roughness pattern are plotted in figure 7. As shown, large changes were measured in the lift and drag characteristics of the airfoil; sectional drag coefficient, c_d, increases while section lift-curve slope, c_{ℓ_α}, decreases significantly due to the loss of NLF. In figure 7(b), the results are shown for a Reynolds number of 1 million and 12° of flap deflection. In addition to the previously mentioned changes in the aerodynamic characteristics of the airfoil, a loss in section maximum lift coefficient can also be noted.

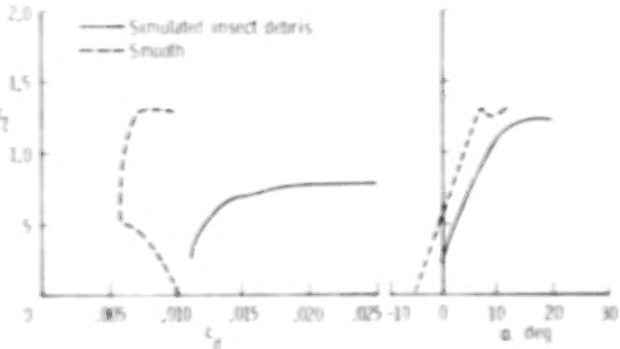

(a) $R = 2.5 \times 10^6$ and $\delta_f = 0°$.

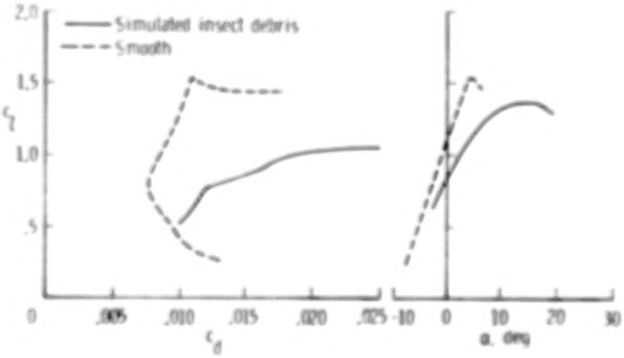

(b) $R = 1 \times 10^6$ and $\delta_f = 12°$.

Figure 7.- Influence of leading-edge contamination on aerodynamic characteristics of FX 67-K-150/17 airfoil (ref. 5).

As part of the discussion of the aerodynamic characteristics of the GU 25-5(11)8 airfoil section, the problem of laminar separation was explained. If the airfoil has a relatively sharp leading edge, however, laminar separation can also occur after the leading-edge suction peak is formed. The laminar boundary layer passes around the leading edge, through the suction peak, and separates. Transition occurs in the separated boundary layer, and initially a laminar separation bubble is formed when the boundary layer reattaches as a turbulent boundary layer. With increasing angle of attack, the suction peak grows rapidly because of high leading-edge curvature. As a result, the pressure gradient downstream of the point of minimum pressure becomes steeper, and turbulent reattachment becomes more difficult. Sufficient increase in angle of attack can eventually prevent the boundary layer from reattaching to the surface after transition, and leading-edge stall has then occurred. Generally, leading-edge stall is associated with angles of attack larger than those encountered in the cruise flight regime. However, separation near the leading edge can also occur at angles of attack below those encountered in cruise, as will be demonstrated in the following discussion.

Initial airfoil sections recommended for winglet applications on high-speed transport aircraft were developed to operate at supercritical high Mach number design conditions and were cambered to obtain satisfactory high-lift characteristics (ref. 14). In order to avoid producing shock waves on the upper winglet surface and to minimize the added induced velocities on the wing-tip upper surface associated with the winglet, the thickness ratio of the winglet airfoil was held to 8 percent. In a number of cases, subsequent winglet designs for low-speed airplanes have also used this airfoil section. However, this airfoil was not specifically designed for low Reynolds number, low-speed applications, and the airfoil performance under these conditions can be improved.

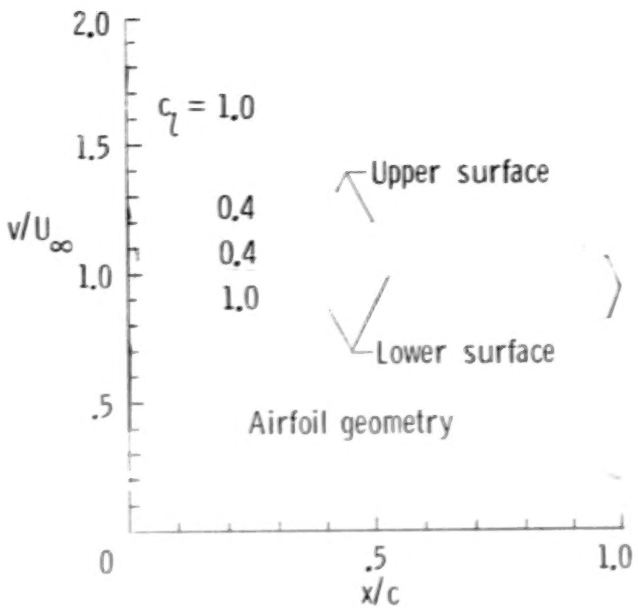

Figure 8.- Geometry and inviscid velocity distributions of supercritical winglet airfoil.

In figure 8, the airfoil section shape and two inviscid velocity distributions for the original supercritical airfoil are shown. At a cruise lift coefficient of 0.4, the velocity gradient on the upper surface is favorable up to 65 percent of the chord. On the lower surface, however, a sharp suction peak occurs near the leading edge. This suction peak grows with decreasing angle of attack, and the integral boundary-layer method of reference 7 predicts leading-edge flow separation on the lower surface for chord angles of attack lower than approximately -5°. The loss in lift and increment in drag associated with boundary-layer separation can have a significant influence on airplane lateral-directional stability and control. As shown in figure 9, a high maximum sectional lift coefficient is achieved, but the laminar-flow drag bucket is relatively narrow and starts and ends very abruptly. The results also indicate that minimum drag is obtained at a section lift coefficient of 0.6. The combination of a high design lift coefficient and a narrow drag bucket makes this airfoil section less desirable for winglet application on low-speed airplanes. Due to the shallow pressure recovery, however, section lift characteristics are not influenced by the loss of NLF, as shown in figure 9.

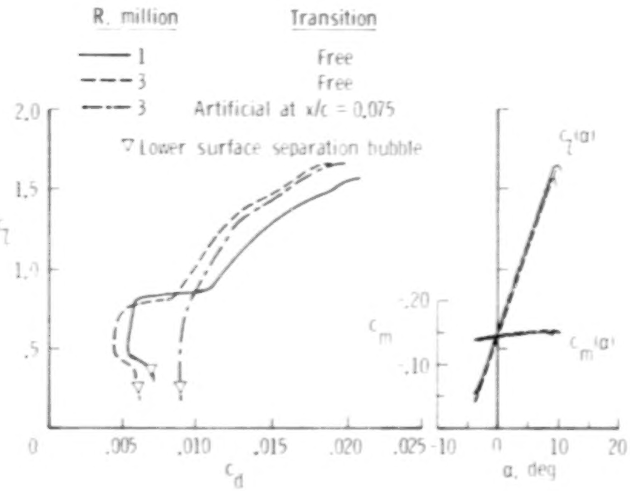

Figure 9.- Calculated aerodynamic characteristics of supercritical winglet airfoil.

The three airfoil sections discussed in this paper should not be viewed as "inferior" or "dangerous" airfoils. These airfoils have been developed with certain design objectives and constraints in mind and are very successful at meeting these design objectives. Airplane designers, however, sometimes select these airfoils to produce lift in operating conditions which violate the original airfoil design conditions.

TRANSITION AND AIRPLANE STABILITY AND CONTROL

In the previous section, the influence of location and mode of transition from laminar to turbulent boundary-layer flow on airfoil aerodynamic characteristics has been discussed. It has been shown that for certain airfoils, if the boundary layer becomes turbulent near the leading edge, extensive trailing-edge separation of the turbulent boundary layer can occur. This boundary-layer separation results in a loss of section lift, and the resulting effects on airplane longitudinal and lateral-directional stability and control characteristics are discussed in the following section. In addition, the influence of winglet airfoil section characteristics on airplane lateral-directional stability and control characteristics is also discussed.

LONGITUDINAL STABILITY AND CONTROL

Generally, longitudinal static stability is required for airplane airworthiness certification. However, too much static stability can have a negative influence on the controllability of an airplane. Dynamic stability is associated with the response behavior of an airplane as a result of a disturbance, and therefore, the damping and frequency of the response motion are examined. Generally, airplanes must also have some form of dynamic stability, i.e., the amplitudes of the motion should diminish progressively as a function of time. Motion damping has a strong effect on airplane handling qualities. If it is too low, then the airplane is too easily excited by disturbances, and if it is too high, then the airplane has a tendency to become too sluggish.

Wind-tunnel experiments have been conducted with the Rutan VariEze. This airplane has a high-aspect-ratio foreplane which uses the GU 25-5(11)8 airfoil section. In references 2 and 15, wind-tunnel data are presented depicting the effect of fixed transition on foreplane lift characteristics and airplane longitudinal aerodynamic characteristics. In the previous section, it was shown that transition location has a dramatic influence on the lift characteristics of the GU 25-5(11)8 airfoil section. Notably, a loss in section lift-curve slope due to fixed boundary-layer transition was shown (fig. 4). In subsonic flow conditions, the lift-curve slope of the foreplane, $C_{L_{\alpha,C}}$, is a function of the sectional lift-curve slope, c_{ℓ_α}, Mach number, and several planform parameters. Therefore, a reduction in c_{ℓ_α} will reduce the gradient of the foreplane lift curve $C_{L_{\alpha,C}}$.

In figure 10, airplane pitching-moment coefficient, C_m, results clearly demonstrate the large influence of fixed transition on the longitudinal static stability of the airplane.

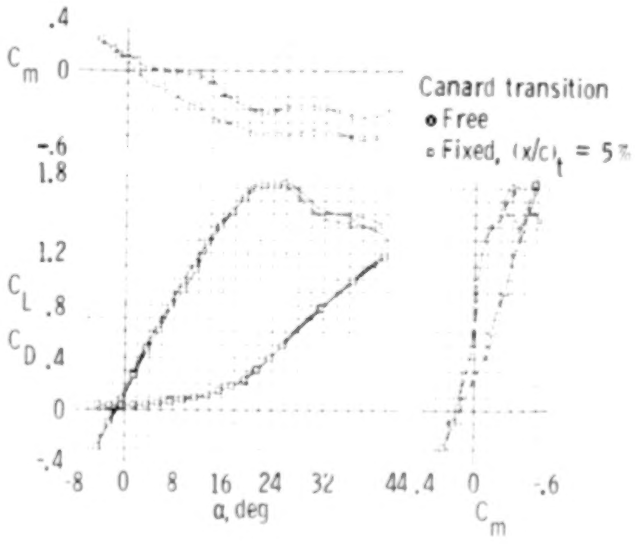

Figure 10.- Longitudinal aerodynamic characteristics of VariEze model as tested in Langley 30- by 60-Foot Tunnel (ref. 2).

For a canard configuration, airplane longitudinal static stability can be written as follows:

$$C_{m_\alpha} = C_{L_{\alpha,C}} \left(\bar{X}_{cg} - \bar{X}_{ac,C}\right) \frac{S_C}{S} + C_{L_{\alpha,WB}} \left(\bar{X}_{cg} - \bar{X}_{ac,WB}\right) \quad (2)$$

where $\bar{X}_{ac,WB} > \bar{X}_{cg} > \bar{X}_{ac,C}$, and $\bar{X}_{cg}$ and $\bar{X}_{ac}$ are defined as the longitudinal location of center of gravity and aerodynamic center, respectively, in terms of airplane mean aerodynamic chord $\bar{c}$. A reduction in $C_{L_{\alpha,C}}$ due to flow separation on the foreplane makes the first term on the right-hand side of equation (2) less positive, and consequently, C_{m_α} becomes more negative. Equation (2) can also be written in the following form:

$$C_{m_\alpha} = C_{L_\alpha} \left(\bar{X}_{cg} - \bar{X}_{ac}\right) \quad (3)$$

where C_{L_α} is defined as airplane lift-curve slope, and $\bar{X}_{ac}$ indicates the longitudinal location of the airplane aerodynamic center in terms of the airplane mean aerodynamic chord. The wind-tunnel results of figure 10 are for a fixed foreplane control surface deflection ($\delta_e = 0°$), and therefore, $\bar{X}_{cg} - \bar{X}_{ac}$ can be defined as stick-fixed static margin of the airplane. The effect of fixed foreplane transition on airplane lift-curve slope is relatively small, as shown in figure 10. In the angle-of-attack range from 3° to 13°, the wind-tunnel data show that airplane static margin (stick fixed) is approximately 0.10 $\bar{c}$ in the case of free transition. When transition is fixed near the leading edge of the foreplane, however, the airplane becomes much more stable and the static margin is approximately 0.30 $\bar{c}$. Thus, airplane aerodynamic center shifts rearward over a distance of 0.20 $\bar{c}$ as a result of foreplane trailing-edge flow separation.

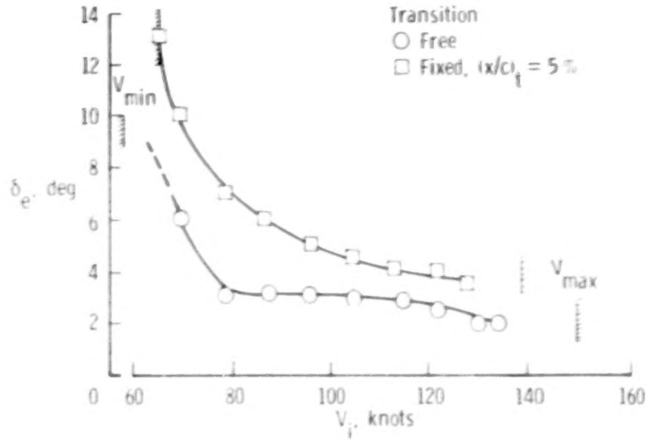

(a) VariEze airplane.

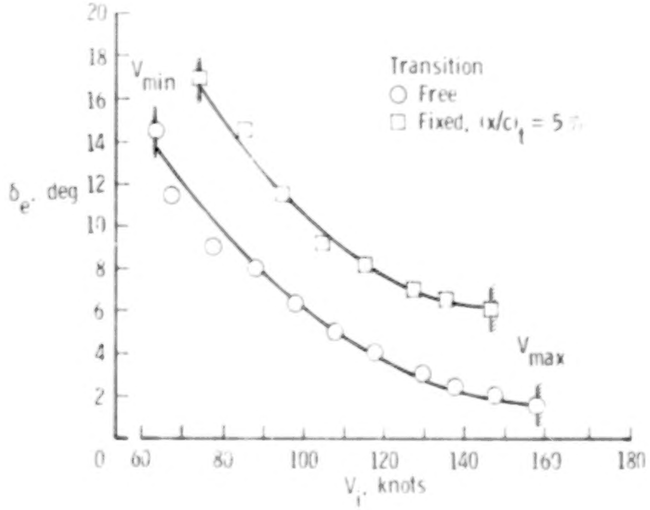

(b) Long-EZ airplane.

Figure 11.- Comparison of fixed versus free transition performance and longitudinal control characteristics as measured in flight (ref. 2).

The wind-tunnel-measured changes in airplane longitudinal aerodynamic characteristics due to fixed transition have also been observed in flight. The original versions of the Rutan VariEze and Long-EZ airplane both use the GU 25-5(11)8 airfoil for the foreplane. Both airplanes have been tested in flight with and without artificial surface roughness near the leading edge of the foreplane in order to measure the changes in airplane longitudinal aerodynamic characteristics caused by loss of NLF. The changes in foreplane lift characteristics with fixed transition come into view when examining elevator deflection required to trim the airplane for a given airspeed, as shown in figure 11. For both airplanes, fixed leading-edge transition induces flow separation on the foreplane, and consequently, increased positive elevator deflection is required to obtain a foreplane lift coefficient which provides longitudinal trim.

In the case of a canard configuration, the influence of wing lift characteristics on the longitudinal static stability is opposite as compared to the influence of foreplane lift characteristics. Therefore, selection of a wing airfoil section shape with lift characteristics which are affected by transition location will result in reduced longitudinal static stability of the airplane. The longitudinal stability and control of both the Rutan VariEze and Long-EZ airplanes appear to be almost unaffected by wing boundary-layer transition location.

For the VariEze and Long-EZ airplanes, the effect of fixed transition on airplane lift-curve slope is shown in figure 12. For both airplanes, the gradient of the lift-curve slope becomes less steep by 7 to 13 percent (ref. 2). The wind-tunnel results, however, only indicate a reduction in lift-curve slope of less than 4 percent. The reason for this

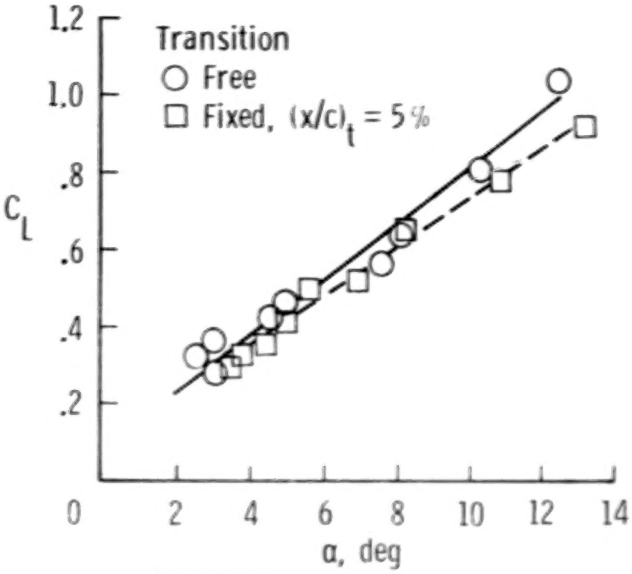

(a) VariEze airplane.

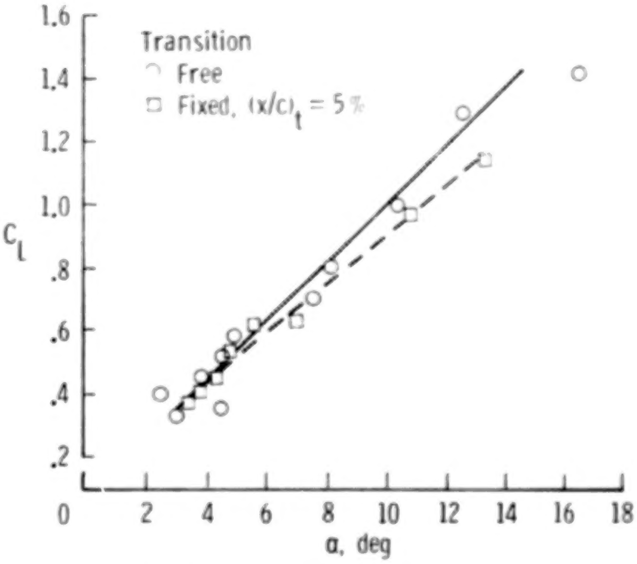

(b) Long-EZ airplane.

Figure 12.- Effect of fixed versus free transition on airplane lift-curve slope as measured in flight (ref. 2).

discrepancy is that the wind-tunnel data of figure 10 have been obtained for a constant elevator deflection δ_e = 0°, while the flight data of figure 12 have been obtained for elevator deflections required to trim the airplane. In flight, lower airspeed results in higher airplane lift coefficient, and therefore, more positive elevator deflection is required for airplane trim, as shown in figure 11. Apparently, trailing-edge flow separation increases with increasing elevator deflection, and consequently the lift loss is augmented at higher airplane lift coefficients. A second contributing factor is the influence of Reynolds number. Flight data at high lift coefficients are obtained at relatively low Reynolds numbers as compared to the Reynolds numbers encountered at low lift coefficients. The following expression depicts this effect more clearly:

$$\frac{R_1}{R_2} = \frac{C_{L_2}}{C_{L_1}} \qquad (4)$$

where it has been assumed that airplane weight and flight altitude are constant and R defines chord Reynolds number. The reduced Reynolds numbers at higher lift coefficients enhance the foreplane separation problem.

The previous results demonstrate the influence of premature boundary-layer separation on airplane longitudinal trim requirements and stick-fixed neutral point location (center-of-gravity location at which $C_{m_\alpha} = 0$).

Stick-fixed maneuvering margin is larger than stick-fixed static margin, and the difference between neutral point and maneuver point is proportional to the pitch-damping stability derivative, C_{m_q}. Therefore, if pitch damping is zero, then the difference between neutral point and maneuver point is zero. In the case of canard and conventional configurations, reduced gradients of the lift curve due to flow separation of airplane wing and/or tail will reduce airplane pitch damping and, consequently, reduce the difference between stick-fixed static margin and stick-fixed maneuvering margin.

Generally, longitudinal transient airplane response consists of two oscillatory terms. The first oscillatory term is called the short-period mode which is highly damped and has a high frequency. The second term describes a very slowly damped, low frequency oscillation which is called the phugoid mode. In the case of the VariEze, a large change in the variation of pitching-moment coefficient with angle of attack, C_{m_α}, is produced due to premature foreplane separation. This stability derivative has a very strong influence on the longitudinal transient behavior of an airplane. According to reference 16, the undamped natural frequency of the short period, $\omega_{n_{SP}}$, is approximately proportional to $\sqrt{-C_{m_\alpha}/I_{yy}}$ where I_{yy} defines the moment of inertia about the airplane Y-axis. Therefore, the influence of C_{m_α} on the undamped natural frequency can be estimated as follows:

$$\frac{\omega_{n_{SP,1}}}{\omega_{n_{SP,2}}} = \frac{C_{m_{\alpha,1}}}{C_{m_{\alpha,2}}} \qquad (5)$$

Thus, an increase of a factor 3 in the value of C_{m_α}, as observed in figure 10, causes the undamped natural

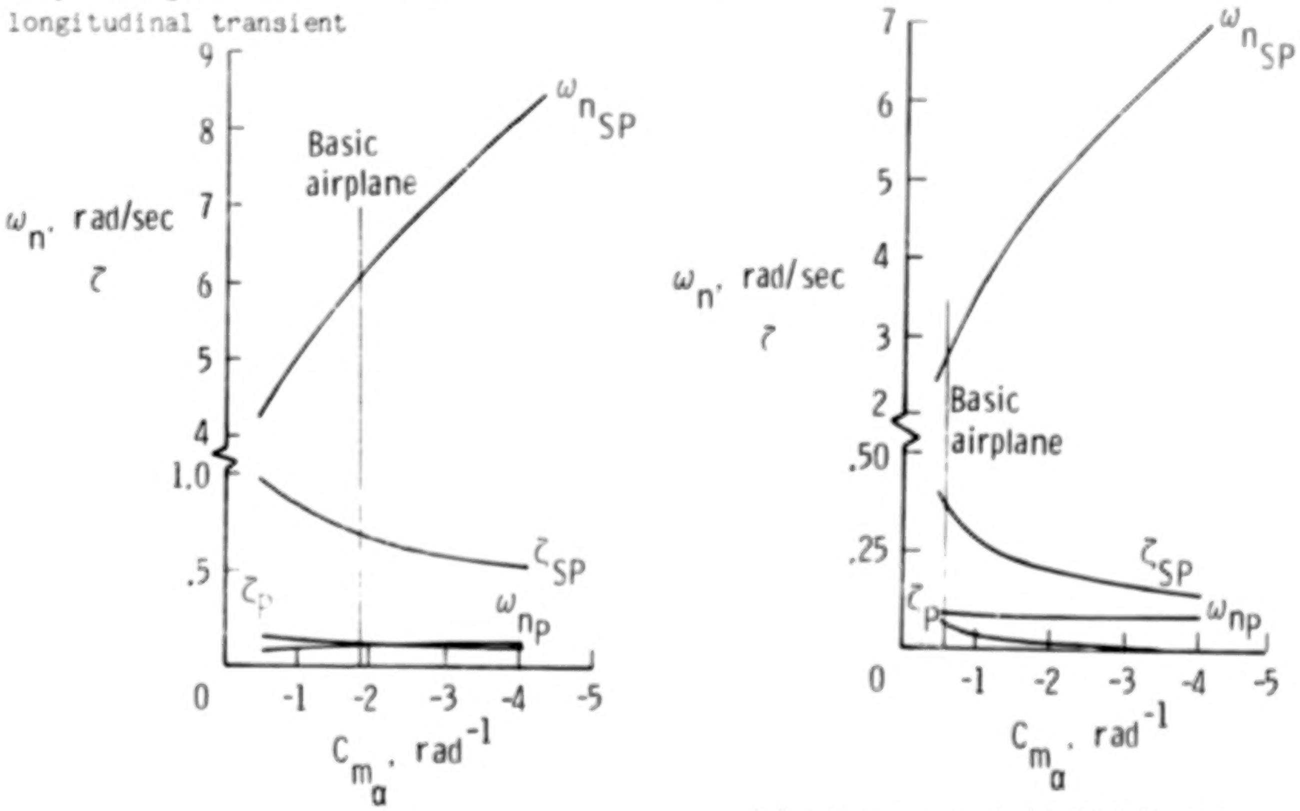

(a) Airplane B at 5,000 ft and M = 0.31.

(b) Airplane D at 40,000 ft and M = 0.7.

Figure 13.- Effect of airplane pitching-moment coefficient curve slope on the dynamic stability characteristics.

frequency of the short period to increase by more than 70 percent.

A complete set of stability derivatives was not available for a canard-type airplane. Therefore, a sensitivity analysis was conducted to illustrate the potential influences of $C_{D,0}$ on stability behavior. The results appear in figure 13. The stability derivatives used are presented in reference 16. Airplane B (fig. 13(a)) is representative of Beechcraft B99 type airplanes, while Airplane D (fig. 13(b)) is representative of Gates Learjet Model 24 type airplanes. The results of figure 13 indicate that undamped natural frequency of the short period is strongly influenced by C_{m_α}. Also, short-period damping decreases due to enhanced longitudinal static stability.

As previously mentioned, in general the phugoid mode has a low frequency and is lightly damped. The results in figure 13 verify this statement, and the sensitivity analysis shows that phugoid damping is reduced due to increased longitudinal static stability. This observation matches unpublished flight results obtained with the Rutan Long-EZ by Brown, Holmes, and van Dam. When evaluating airplane handling qualities with fixed foreplane transition, a noticeable reduction in phugoid damping was observed as compared to the phugoid damping with free transition on the foreplane. This effect appears to be more dominant than the influence of airplane drag coefficient on phugoid damping. The latter is sketched in figure 14. If airplane propulsion effects are assumed to be negligible, then phugoid-damping ratio can be approximated as follows (ref. 16):

$$\zeta_P = \frac{C_D}{2\,C_L\sqrt{2}} \qquad (6)$$

According to equation (6), an increase in drag due to transition near the leading edge appears to enhance phugoid damping.

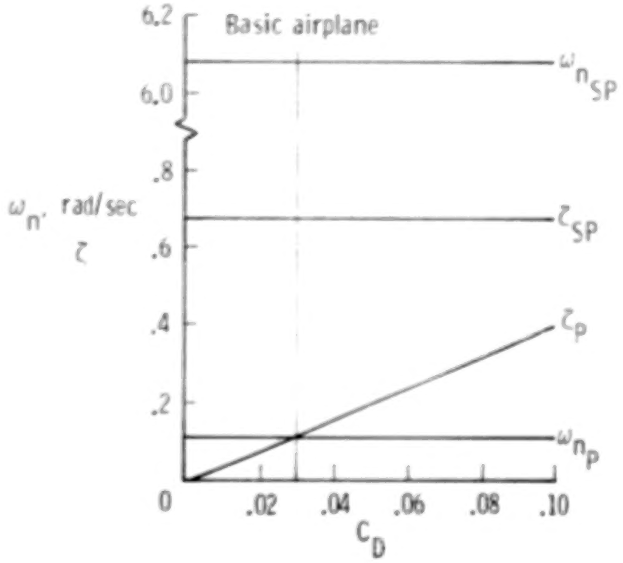

Figure 14.- Effect of airplane drag coefficient on the dynamic longitudinal stability characteristics of airplane B at 5,000 ft and M = 0.31.

Lateral-Directional Stability and Control

Wind-tunnel and flight tests have demonstrated that the use of winglets can provide increased aerodynamic efficiency by reducing lift-induced drag without overly penalizing wing structural weight (ref. 14). A more recent development in the area of airplane design is the utilization of wing-tip-mounted winglets to provide directional stability and control in addition to reducing lift-induced drag. The design of winglet airfoil sections, however, has not received much attention and some winglet designs for low-speed airplanes have used the airfoil section shown in figure 8. As mentioned previously, this airfoil was developed for winglet application at supercritical, high Mach number conditions. Further, this airfoil was designed with the assumption that the flow over the entire airfoil would be turbulent, primarily as a result of roughness of construction. However, the pressure gradients around $c_\ell = 0.6$ are favorable to NLF as is also indicated by the section drag characteristics in figure 9. The narrow drag bucket is a concern when the winglets also provide directional stability.

The sketch in figure 15 shows the drag polar of the winglet airfoil section and illustrates the potential problem.

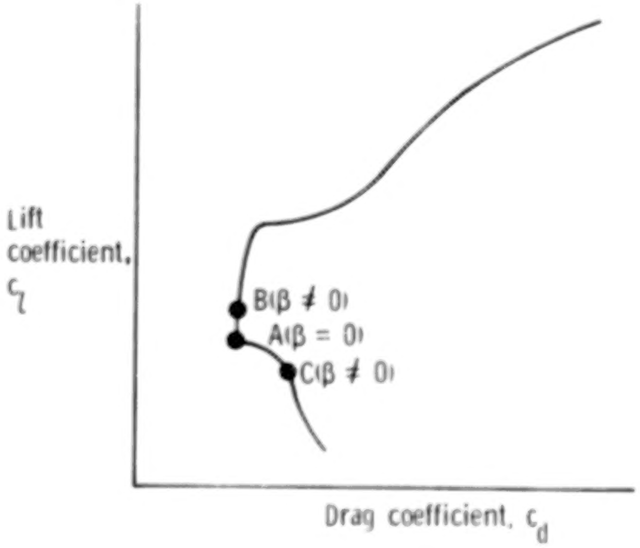

Figure 15.- Drag polar of a winglet airfoil with a sharply defined drag bucket.

Point A in figure 15 indicates the cruise condition at a sideslip angle, β, of 0°. A small positive excursion in sideslip angle causes an increase in angle of attack and as a result enhanced c_ℓ (point B) for the upwind winglet and reduced angle of attack and therefore decreased c_ℓ (point C) for the downwind winglet. For the airfoil of figure 8, section drag at the onset of the drag bucket changes rapidly and abruptly. A significant profile drag differential between the two winglets is produced due to the rapid chordwise movement of boundary-layer transition on the lower surface of the airfoil. This force differential produces a destabilizing yawing moment and can produce undesirable airplane handling qualities. The yawing moment produced by the profile drag differential is ($\beta > 0$)

$$N = -\Delta C_D \, q \, S_{WLT} \frac{b}{2} \tag{7}$$

where S_{WLT} is the area of one winglet and ΔC_D is the profile drag differential between the two winglets. As a result, the change in yawing-moment coefficient is ($\beta > 0$)

$$\Delta C_n = -\frac{\Delta C_D}{4} \Big/ \frac{S_{WLT}}{\frac{S}{2}} \tag{8}$$

For conventional airplane configurations, the ratio $S_{WLT}/(S/2)$ has a value of 0.02 to 0.10, and as a result, the effect of this destabilizing yawing moment will be small. Some canard configurations, however, use wing-tip-mounted winglets to provide directional stability and control, and because of the relatively short moment arm, the winglet area must be large to provide sufficient directional stability. In that case, $S_{WLT}/(S/2)$ can be larger than 0.20. An area ratio of that value combined with a ΔC_D of about 50 drag counts can generate a destabilizing yawing moment ($\beta > 0$) $\Delta C_n = -0.00025$. This is a relatively small value. However, it may be produced as a result of a sideslip excursion as small as 0.5°. Therefore, for small sideslip angles, the contribution to the airplane direction stability derivative may be of the order of $\Delta C_{n_\beta} = -0.03$ rad^{-1}. This value is large enough to produce significant nonlinearities in the rudder force and rudder deflection variation with sideslip angle.

In order to prevent changes in airplane directional stability, it is important that the lift characteristics of the surfaces which provide directional stability are not affected by premature boundary-layer transition near the leading edge. A reduction in the lift-curve slope of such a lifting surface due to leading-edge roughness will reduce the value of the directional stability derivative C_{n_β} significantly. This derivative has an important influence on the lateral-directional transient response characteristics of the airplane. Generally, all three modes of motion (spiral, roll, and Dutch roll) are affected by a reduction in C_{n_β}. The effects of winglets on the lateral-directional stability characteristics of the Rutan VariEze are clearly depicted in the wind-tunnel results of reference 15 and these results will be used to provide an example. For the angle-of-attack range from 0° to 8°, the destabilizing contribution of the airplane without winglets is $C_{n_\beta} = -0.057$ rad^{-1}. In this angle-of-attack range, the winglets produce a $C_{n_{\beta,WLT}} = 0.115$ rad^{-1} resulting in an airplane $C_{n_\beta} = 0.058$ rad^{-1}. A 10-percent reduction in winglet lift-curve slope due to premature flow separation results in a 10-percent reduction in $C_{n_{\beta,WLT}}$ and a 20-percent reduction in airplane C_{n_β}. The lift characteristics of the VariEze winglets, however, are not sensitive to the transition location from laminar to turbulent boundary layer. Additional information on the design considerations for vertical wing-tip-mounted lifting surfaces on low-speed airplanes is provided in reference 17.

CONCLUSIONS

The analytical and experimental results presented in this paper demonstrate that the location and mode of transition from laminar to turbulent boundary-layer flow can have a significant influence on the lift and drag characteristics of airfoil sections. For airfoils with a relatively steep pressure recovery, it has been shown that boundary-layer transition near the leading edge due to surface contamination can result in trailing-edge separation of the turbulent boundary layer. This premature separation produces a reduction in section lift-curve slope and it can also affect sectional maximum lift coefficient. If the leading edge of the airfoil is relatively sharp, separation of the laminar boundary layer can occur after the leading-edge suction peak is formed. Leading-edge stall arises when the boundary layer after transition does not reattach to the surface.

The two-dimensional results have been used to examine the effects of boundary-layer transition behavior on airplane longitudinal and lateral-directional stability and control. The analyses indicate that both trailing-edge separation of the turbulent boundary layer due to leading-edge contamination and leading-edge separation of the laminar boundary layer due to the suction peak have a detrimental effect on airplane stability and controllability. Therefore, for horizontal lifting surfaces such as fore-and tailplanes and wings it is essential to design airfoil section shapes which are not susceptible to boundary-layer separation if no laminar flow exists from the leading edge. For vertical lifting surfaces such as winglets which provide directional stability, an additional design requirement is that transition location on the upper and lower surface should move slowly and steadily with changing angle of attack. The examples given illustrate the importance of proper care in the selection of NLF airfoil characteristics to preclude difficulties with airplane stability and control changes due to the loss of laminar flow.

REFERENCES

1. Holmes, B. J.; Obara, C. J.; Gregorek, G. M.; Hoffman, M. J.; and Freuhler, R. J.: Flight Investigation of Natural Laminar Flow on the Bellanca Skyrocket. SAE paper 830717, April 1983.

2. Holmes, B. J.; Obara, C. J.; and Yip, L. P.: Natural Laminar Flow Experiments on Modern Airplane Surfaces. NASA TP 2256, June 1984.

3. Dwiggins, D.: Dangerous When Wet?. Homebuilt Aircraft, Part 1 and 2, March and April 1983.

4. Hewes, D.: Effects of Rain and Bugs on Flight Behavior of Tail-First Airplanes. Sport Aviation, Part 1, 2, and 3, May, June, and July 1983.

5. Althaus, D.: Influencing Transition on Airfoils. Technical Soaring, December 1981, pp. 82-93.

6. Horstmann, K. H.; and Quast, A.: Drag Reduction by Means of Pneumatic Turbulators. European Space Agency Technical Translation 743, September 1982.

7. Eppler, R.; and Somers, D. M.: A Computer Program for the Design and Analysis of Low-Speed Airfoils. NASA TM-80210, 1980.

8. Eppler, R.; and Somers, D. M.: Supplement to a Computer Program for the Design and Analysis of Low-Speed Airfoils. NASA TM-81862, December 1980.

9. Nonweiler, T.: A New Series of Low-Drag Aerofoils. University of Glasgow, Department of Aeronautics and Fluid Mechanics, Report No. 6801, 1968.

10. Kelling, F. H.: Experimental Investigation of a High-Lift Low-Drag Aerofoil. Aeronautical Research Council Current Papers 1187, 1971.

11. Kelling, F. H.: Experimental Investigation of a High-Lift Low-Drag Aerofoil. University of Glasgow, Department of Aeronautics and Fluid Mechanics, Report No. 6802, September 1968.

12. Wortmann, F. X.: Experimental Investigation on New Laminar Profiles for Gliders and Helicopters. Ministry of Aviation Translation TIL/T. 4906, 1960.

13. Althaus, D.; and Wortmann, F. X.: Stuttgarter Profilkatalog I, Friedr. Vieweg & Sohn Verlagsgesellschaft mbH, Braunschweig, West Germany, 1981.

14. Whitcomb, Richard T.: A Design Approach and Selected Wind-Tunnel Results at High-Subsonic Speeds for Wing-Tip Mounted Winglets. NASA TN D-8260, July 1976.

15. Yip, Long P.: Wind-Tunnel Investigation of a Full-Scale Canard-Configured General Aviation Airplane. NASA TP 2382, March 1985.

16. Roskam J.: Airplane Flight Dynamics and Automatic Flight Controls. Published by Roskam Aviation Engineering Corporation, 1979.

17. van Dam, C. P.: Natural Laminar Flow Airfoil Design Considerations for Winglets on Low-Speed Airplanes. NASA CR 3853, December 1984.

N88-23748

OPERATIONAL CONSIDERATIONS FOR LAMINAR FLOW AIRCRAFT

511-05

Dal V. Maddalon and Richard D. Wagner
NASA Langley Research Center
Hampton, Virginia 23665

SUMMARY

Considerable progress has been made in the development of laminar flow technology for commercial transports during the NASA Aircraft Energy Efficiency (ACEE) laminar flow program. Practical, operational laminar flow control (LFC) systems have been designed, fabricated, and are undergoing flight testing. New materials, fabrication methods, analysis techniques, and design concepts were developed and show much promise. The laminar flow control systems now being flight tested on the NASA Jetstar aircraft are complemented by natural laminar flow flight tests to be accomplished with the F-14 variable-sweep transition flight experiment. This paper presents an overview of some operational aspects of this exciting program.

SYMBOLS

ACEE	Aircraft Energy Efficiency
D	drag
EBP	electron beam perforated
GASP	Global Atmospheric Sampling Program
G/E	graphite-epoxy
L	lift
LEFT	leading-edge flight test
LFC	laminar flow control
M	free-stream Mach number
$M(L/D)_{MAX}$	aerodynamic efficiency
NLF	natural laminar flow
PGME	propylene glycol methyl ether

INTRODUCTION

Attainment of laminar boundary layer flow over transport aircraft has significant potential for drag reduction and fuel savings. The concept originated in the 1930's when boundary layer stability analyses showed that laminar flow could be stabilized by either a favorable pressure gradient or by a small amount of wall suction. Many efforts have been undertaken to achieve laminar flow using these two methods. Pressure gradient stabilization became known as natural laminar flow (NLF)

PRECEDING PAGE BLANK NOT FILMED

and led to the development of the 6-series NACA natural laminar flow airfoils. Suction stabilization, referred to as laminar flow control (LFC), was intensively researched during the 1960's with flight tests of an unswept suction glove on an F-94 aircraft (ref. 1) and the swept wing X-21 tests (refs. 2-5) on a reconfigured WB-66.

Although these flight tests showed that laminar flow could be repeatedly achieved to chord Reynolds numbers as high as 47 million, LFC system maintenance and reliability concerns prevented serious consideration of LFC as a design option for aircraft at that time. In 1976, NASA initiated the Aircraft Energy Efficiency (ACEE) program to develop fuel-conserving technology for commercial transports. One program objective was to expand viscous drag reduction technology through laminar flow control applications. Although including LFC as part of the ACEE effort was based on previous flight success, other prime considerations were the large potential LFC fuel saving coupled with the impact of increasing fuel price on airline economics. New materials, fabrication techniques, and airfoil technology developed since the X-21 program offered hope of resolving practical concerns such as the need to produce and maintain smooth wing surfaces during typical airline flight operations. Throughout the ACEE program, NASA worked closely with industry. Impressive progress was made, particularly in the areas of practical LFC leading-edge systems and wing construction. These developments could lead to near-term application of laminar flow technology.

OPERATIONAL CONSIDERATIONS

Important factors that can affect the transition of a boundary layer from laminar to turbulent flow are given in figure 1. Most fundamental are the Reynolds number at which laminar flow becomes turbulent, the degree of wing sweep used, and the airfoil geometry. If velocity and altitude are constant, the larger the airplane, the higher the Reynolds number, and the more difficult it is to keep flow laminar over significant lengths of wing chord. If the airplane is also designed for high speed, weight considerations dictate that the wing have a significant degree of sweep. Sweep introduces three dimensional cross-flow boundary layer disturbances that may amplify, interact with two dimensional Tollmien-Schlichting waves, and cause transition. Airfoil geometry determines both favorable pressure gradient extent and suction requirements needed for boundary layer stabilization. Ideally, a laminar flow wing should achieve the drag divergence Mach number, thickness ratio, and lift capability attainable with turbulent supercritical wing technology. (Some compromises may be necessary to achieve extensive lengths of favorable pressure gradient.) New aircraft materials such as graphite-epoxy composites offer the promise of wing sections of nearly perfect shape, tolerance, and smoothness at reasonable cost -- provided fabrication methods and deformation under load result in surface deviations small enough to prevent occurrence of local pressure waves which can cause transition (ref. 6). Propulsion system noise is another disturbance source which can be amplified by the boundary layer and lead to transition. Other operational concerns include the surface suction system (used to stabilize the wing boundary layer) which typically has very fine surface openings that must be easy to clean and repair while resistant to clogging and corrosion. Atmospheric conditions such as ice crystals and rain are known to influence boundary layer stability and must be thoroughly studied, since a fleet of LFC aircraft would operate throughout the world at a variety of climates, altitudes, and weather conditions.

Insect impacts in the leading-edge region are a particular concern, since surface residue can prevent attainment of laminar flow during cruise. Some preliminary answers to the insect contamination question were provided by NASA flight tests early in the LFC program with the NASA Jetstar aircraft (ref. 7). These tests also evaluated the effectiveness of superslick surface coatings and a liquid spray washing system for preventing or minimizing insect contamination. An outboard wing leading-edge test panel (with four chordwise strips of different surface coatings) was equipped with upper surface total head tubes to detect transition in the leading edge, and with lower surface water spray nozzles to coat both upper and lower surfaces with protective fluid film. Airline-type flights conducted at major U.S. airports (with no protective spray) indicated that insects can contaminate the wing leading edge and prevent laminar flow. Surface coatings (Teflon tape and spray-on, organo-silicone, and radome rain repellant) were not effective in preventing contamination. Degree of contamination experienced was seasonal and dependent on geographical location (ref. 8). Flights in agricultural areas heavily populated with insects showed that water spray injection which maintained a wet surface was effective in preventing leading edge insect contamination. This preliminary work indicated that a prudent course would be to develop and test a practical anti-contamination system.

Laminar flow impact on aerodynamic performance is given in figure 2 for a transport aircraft designed for a speed of $M = 0.75$, a Reynolds number of about 27 million, and a sweep of 27.5 degrees (ref. 9). If laminar flow extends over the entire wing section, more than an 80 percent profile drag reduction is possible -- with two-thirds of the reduction resulting from the upper surface. NASA-sponsored work by aircraft manufacturers quantified the effect of laminar flow loss on aircraft performance. Some results for aerodynamic efficiency, $M(L/D)_{MAX}$, are given in figure 2. Aerodynamic efficiency increases from 16 to over 20 for the full-chord laminar flow case. Conversely, should operations result in laminar flow loss, performance deterioration will be equally dramatic -- but acceptable. Maximum range is reduced from 6500 nmi to about 5200 nmi (fig. 3) for a Lockheed-Georgia-designed 400-passenger, $M = 0.80$ aircraft (ref. 8). Detection of laminar flow loss and flight management will be necessary in such circumstances.

LAMINAR FLOW CONTROL SYSTEMS

Prevention of laminar flow loss will depend heavily on the systems provided by the designer. Over the course of the ACEE program, NASA worked with industry to develop such systems and to incorporate them into both perforated and slotted LFC wing structure designs (fig. 4).

In the Douglas Aircraft Company (DAC) LFC concept (ref. 9), the main wing box covers are internal blade-stiffened G/E skin panels. Perforated suction panels are gloved to the main wing box, and suction air collection is external to the wing box. Suction panels are attached to generally chordwise oriented blades on the wing box cover outer surface. The blades form shallow ducts for suction air collection into trunk ducts in the leading-edge box. This collection scheme is advantageous over spanwise air collection because air flow quantity and collection distance are such that ducts can be very shallow and wing structural depth loss is minimized. Behind the rear spar and in the leading-edge box, air collection is in spanwise ducts. Suction is applied only on the upper surface wing, and a leading-edge Krueger flap is used. Acceptable low-speed aircraft performance is achieved with a small trailing-edge flap system which allows laminar flow to 85 percent chord on the wing upper surface in cruise. If suction is desired on the lower surface, the Krueger flap would not be used because of surface smoothness concerns in the stowed condition. In this instance, a powerful 30 percent chord trailing-edge flap and larger wing are required to meet acceptable low-speed performance. The trailing-edge flap limits laminar flow to 70 percent chord and the larger wing degrades cruise performance. Douglas trade studies show that upper surface laminarization is the most effective LFC suction application. Upper surface suction also provides practical solutions to potential manufacturing and maintenance concerns. The wing assembly can be accomplished from the lower surface using internal fasteners that do not penetrate the upper wing surface. Maintenance access can be done through the lower surface, and since most ducting is in the leading-edge box, ducting would be accessible by Krueger flap deployment on the ground. LFC impact damage maintenance is minimized since the upper surface is least exposed to foreign object damage. Finally, the Krueger flap can shield the leading edge from insects and debris on takeoff and landing.

Details of the Douglas perforated suction surface are given in figure 5. Surface perforations, drilled by an electron beam into titanium sheet, are finely spaced circular (or elliptic) holes as small as 0.0025 in. in diameter. Holes taper to about twice that size on the opposite surface. Figure 5 shows the remarkable regularity and circularity of the holes which are more than an order of magnitude smaller than the perforation sizes possible with practical manufacturing methods during the X-21 era. At that time, slotted suction surfaces were favored over perforations as wind tunnel and flight tests had shown that unless suction holes were very small, suction-induced flow disturbances would cause premature transition.

The tiny holes used in the DAC design mean that provisions must be made for periodically cleaning the suction surface. A steam-cleaning technique was developed with porosity results given in figure 6, for which the specimen was exposed to an airport environment for approximately 15 weeks. An initial steam-cleaning returned the sample to nearly virgin porosity, and three steam-cleanings returned air passage to the initial ultrasonic cleaning level.

Contamination prevention efforts include use of a cleaning fluid consisting of 60 percent PGME and 40 percent water during takeoff and at low altitudes in both Douglas and Lockheed concepts. Use of cleaning fluid may require purging systems to clear suction ducting. Douglas ground tests show a purging pressure near 1 psig (fig. 7) is sufficient to rapidly clear both suction ducting and surface.

In the Lockheed-Georgia Company concept (refs. 8, 10, 11), the LFC ducting network is integrated into primary structure, and wing surface suction is through spanwise slots (fig. 4). Extensive use is made of graphite-epoxy (G/E) composite material. Primary load-carrying structure is thick G/E wing skin stiffened with G/E hat section stiffeners. Titanium sheet is bonded to G/E wing skins to present a tough, damage-tolerant, noncorrosive surface -- and for lightning protection to the substructure. After bonding, spanwise slots are cut in the titanium sheet with a high-speed steel jeweler's saw. Suction air passes through the slots into small plenums molded into the G/E skins and then through metering holes to spanwise ducts formed by the hat stiffeners. At every other rib station, suction air is metered into ducts formed by rib caps of truss ribs. The rib cap ducts penetrate the front spar web to transfer suction air into trunk ducts in the leading-edge box. Trunk ducts collect suction air into suction pumps driven by independent gas turbine power units; both pumps and power units are located under the wing roots. To evaluate the wing-box design, an extensive fabrication and testing program examined materials, adhesives, cure process variables, structural characteristics, and fabrication techniques. No significant problems were uncovered.

Investigations of laminar flow loss from, for example, leading-edge surface roughness caused by insect impact, were made in wind tunnels by both Douglas and

Lockheed-Georgia. Conditions were representative of the altitude and speed of subsonic transport operations.

The Douglas approach used the Krueger high-lift flap as a protective shield against insect impact. Tests (ref. 9) in the NASA Lewis Icing Research Tunnel (fig. 8) evaluated Krueger effectiveness in protecting the leading edge from insect contamination. These tests (supported by trajectory analysis) demonstrated that the Krueger flap serves as an effective line-of-sight shield for heavy insects (fig. 9) and suggest that a supplemental spray might be necessary to protect against possible impingement of lighter insects in some wing areas. In particular, wing twist can result in direct impacts in the outboard region, and high inboard lift can deflect lighter insects onto the wing.

The Lockheed approach injects cleaning fluid through slots above and below the attachment line. Concept feasibility was verified during wind tunnel tests in their low-speed wind tunnel facility (ref. 8). A partial-span full-scale leading-edge section was subjected to insects injected in the tunnel free stream at number densities much higher than expected at actual flight takeoff and landing conditions. Cleaning fluid injected through leading-edge slots completely covered and protected upper and lower surfaces. Insects did not adhere to the wet surface.

Together, the Douglas and Lockheed tests show that although the need for an active "anti-contamination" system is not conclusive, the prudent course would be to develop potential systems and assess their need in actual operations.

LEADING-EDGE FLIGHT TEST OPERATIONS

Integration of either the Douglas or Lockheed concepts with insect protection, leading edge anti-icing, and suction systems is a formidable design challenge. Indeed, most difficult problems in achieving laminar flow on commercial transports are associated with the leading edge. Practical solutions to these problems will remove many laminar flow concerns. A laminar flow control Leading-Edge Flight Test (LEFT) was therefore begun to evaluate the effectiveness of integrated leading-edge LFC systems. Under NASA contract, both Douglas and Lockheed designed, fabricated, and installed on a Jetstar aircraft LFC leading-edge test articles (fig. 10) which demonstrate that these systems can be packaged into a leading-edge section representative of future LFC commercial transport aircraft. A further purpose was to show that these systems can operate reliably with minimum maintenance in an airline-type flight environment.

The Douglas leading-edge concept (fig. 11) consists of an electron-beam perforated (EBP) titanium sheet bonded to a fiberglass sandwich substructure which forms a removable suction panel (refs. 12, 13) attached to ribbed supporting substructure. Areas where the EBP skin bonds to the corrugated substructure are impervious to flow. Thus, suction is through perforated strips. Alternate substructure flutes are used for suction air collection. Suction is applied only on the upper surface from just below the attachment line to the front spar. The Krueger-type flap protects against insect impact. Supplemental spray nozzles on the underside of the Krueger flap coat the leading edge with a fluid freezing point depressant to guard against impingement of lighter insects. In icing conditions, the Krueger flap serves as the primary leading-edge anti-icing protection system -- supplemented as required with spray nozzles. The shield leading edge is equipped with a commercially available ice protection system. As previously discussed, a system for purging fluid from the suction flutes and surface perforations is provided.

The Lockheed leading-edge concept is illustrated in figure 12 (ref. 14). The leading-edge box structure is of sandwich construction with 0.016-in. thick titanium outer sheet bonded to a substructure of graphite-epoxy face sheets with a Nomex-honeycomb core. Suction is through fine spanwise slots (0.004-in. width) on both upper and lower surfaces and extends to the front spar. Suction flow is routed through the structure by a combination of slot ducts, metering holes, and collector ducts embedded in the honeycomb. The insect protection system is integrated with the anti-icing system and dispenses a cleaning/anti-icing fluid over the surface through slots above and below the attachment line. Slots which provide suction to achieve laminar boundary layer flow at cruise are purged of fluid during climbout. Actual fabrication of this configuration presented some extremely difficult problems that led to a suction surface only marginally acceptable in meeting LFC smoothness and waviness criteria (see ref. 14).

Flight acceptance testing on the LEFT aircraft began in late 1983 at the NASA Ames-Dryden Flight Research Facility. Figure 13 shows the aircraft in flight. Reference 15 contains a detailed program description.

Evaluation and optimization of the individual performance of each Jetstar LFC system are currently underway. The best laminar flow performance has been achieved on the Douglas article, but we are continuing to improve the Lockheed article performance. The aircraft will soon be placed in the simulated airline service flight testing phase wherein the aircraft operates out of "home base" areas throughout the Unites States (fig. 14). Plans are to fly two or more flights daily with test article condition and laminar flow results documented after each flight. These simulated airline service flights are designed to provide operational experience with LFC systems operated in a "hands off" mode, so that a maintenance and reliability data base can be established. In the Jetstar flight testing, the DAC test article purge begins before takeoff and continues until an altitude of about 23,000 ft is reached (fig. 15). The Lockheed slotted design also uses purging system air but only from about 6,000 to 23,000 ft. For both test articles, suction system operation begins at 32,000 ft with the surface clear of fluids.

ICE PARTICLE DEGRADATION OF LAMINAR FLOW

Laminar flow is usually lost in visible cloud penetrations. To determine visible cloud encounter probability along various airline routes, a program was initiated to study how cloud frequency varies with altitude, latitude, longitude, and season (ref. 16). Cloud-encounter data were available from the NASA Global Atmospheric Sampling Program (GASP) archive (ref. 17). In the GASP program, meteorological and trace-constituent measurements of ambient atmospheric conditions were taken worldwide aboard four Boeing 747's during routine commercial service to obtain detailed measurements of the upper troposphere and the lower stratosphere. Measurements made from 1975 to 1979 on some 3,000 flights included about 88,000 cloud encounters. Using this data, an analysis was made of LFC loss due to visible cloud encounters on major airline routes (fig. 16). Calculations assumed that all cloud encounters result in laminar flow loss and that no cloud avoidance measures (flight management) were taken. Using these conservative assumptions, results show that laminar flow should be lost at most about 8 percent of world-wide flight time (fig. 16). Hence, although infrequent, visible cloud encounters are not negligible and some flight management to avoid clouds could be desirable. This seems practical since at cruise altitudes these clouds usually occur in thin strata only a few thousand feet in depth.

During the X-21 program, it was found that high altitude ice particles could promote laminar boundary layer transition when either visible or invisible cirrus clouds were encountered. To help explain these results, Hall developed a theory to predict the effect of ice particle encounter on laminar flow (as discussed in ref. 16). Hall's theory assumes turbulent vortices shed in the wake of ice particles entering the laminar boundary layer will trigger transition (fig. 17). Key factors that determine whether a given cloud ice particle encounter will cause total, partial, or no loss of laminar flow are particle size, concentration, and residence time in the boundary layer. The theoretical analysis indicated that, for $M = 0.75$ and 40,000 ft altitude, particles smaller than 4 microns (μm) length will not impinge on the airfoil surface since aerodynamic forces predominate over inertia forces and particles follow streamlines which do not enter the boundary layer. As the ice particles become large, they penetrate the laminar boundary layer but do not cause a breakdown to turbulent flow until some critical size is attained. Concentration of particles of this critical dimension or larger will determine the persistence of boundary layer transition. Even with visibility as great as 50 miles, partial loss of laminar flow is predicted by the Hall criteria (fig. 18). This concentration certainly does not constitute a visible cloud and this suggests that the ice cloud problem is more extensive than suggested by the visible cloud analysis from the GASP program. In the X-21 program, erratic achievement of laminar flow was observed in light haze conditions, qualitatively verifying the Hall prediction. Pfenninger (ref. 18) has suggested that this effect is strongly dependent upon wing sweep. F-94 aircraft flights with a laminar flow control glove and 10 degrees of leading-edge sweep showed no evidence of erratic laminar flow due to ice crystals. (The X-21 had 33 degrees of leading-edge sweep.) To assess the ice particle problem, Jetstar flights include cloud measurements using a Knollenberg probe mounted on a pylon on the aircraft fuselage (fig. 18). Small ice particle concentrations due to cirrus conditions are monitored. These data will be correlated with the degree of laminar flow achieved.

A charge plate particle detector mounted on the leading edge of the Jetstar fuselage upper surface pylon (fig. 18) is also used to determine when ice particles impact the surface (by way of the aircraft charge produced). In earlier LFC flights, a similar device (ref. 4) detected clouds and laminar flow loss. Successful further development of this device may provide a low cost means of cloud identification and resultant laminar flow loss (for future aircraft use).

The influence of sweep will also be evaluated as part of a flight program to provide a transition data base for laminar flow wing designs (also, see ref. 19). An F-14 aircraft with variable wing sweep capability is being modified with full-span gloves to produce a range of upper wing surface pressure distributions (fig. 19). The gloves are constructed of foam and fiberglass (no suction provisions) gloved onto the existing wing surface. Gloves extend from below the attachment line to the upper surface rear spar (≈60 percent chord). The first glove is a simple fiberglass cover of the basic wing (which was a strong favorable pressure gradient). The fiberglass cover gives the wing a smooth, nearly wave-free surface which meets laminar flow criteria. Current plans are to begin flight testing of the basic wing glove in mid-1985. As part of the flight test, the Jetstar aircraft with mounted Knollenberg probe and charge patch (fig. 13) will be flown with the F-14 to allow correlation of cloud particulate size and concentration with the amount of natural laminar flow achieved (at different wing sweep angles).

CONCLUDING REMARKS

The NASA Jetstar laminar flow control leading-edge flight test program will soon provide day-to-day operational experience on laminar flow reliability and maintenance. Leading-edge suction concepts are being evaluated to resolve industry concerns about laminar flow practicality. Efforts such as the variable sweep transition flight test will provide additional insights with regard to laminar flow flight operations. Potential benefits from transport laminar flow operations are great. Accomplishments to date show that they may be achieveable.

REFERENCES

1. Groth, E. E.; Carmichael, B. H.; Whites, R. C.; and Pfenninger, W.: Low Drag Boundary Layer Suction Experiments in Flight on the Wing Glove of a F94-A Airplane - Phase II: Suction Through 69 Slots. NAI-57-318, BLC-94 (Contract AF-33 (616)-3168), Northrop Aircraft, Inc., 1957.

2. Antonatos, P. P.: Laminar Flow Control - Concepts and Applications. Astronautics and Aeronautics, vol. 4, no. 1, July 1966.

3. Nenni, J. P.; and Gluyas, G. L.: Aerodynamic Design and Analysis on an LFC Surface. Astronautics and Aeronautics, vol. 4, no. 1, July 1966.

4. White, R. C.; Sudderth, R. W.; and Weldan, W. G.: Laminar Flow Control on the X-21. Astronautics and Aeronautics, vol. 4, no. 1, July 1966.

5. Pfenninger, W.; and Reed, V. D.: Laminar-Flow Research and Experiments. Astronautics and Aeronautics, vol. 4, no. 1, July 1966.

6. Pfenninger, W.; Reed, H. L; and Dagenhart, J. R.: Design Considerations of Advanced Supercritical Low Drag Suction Airfoils. AIAA Technical Papers (A81-24501), 1980, vol. 72 of Progress in Astronautics and Aeronautics, pp. 249-271.

7. Peterson, J. B., Jr.; and Fisher, D. F.: Flight Investigation of Insect Contamination and Its Alleviation. NASA CP 2036, Part I, 1978, pp. 357-373.

8. Sturgeon, R. F.; et al.: Evaluation of Laminar Flow Control System Concepts for Subsonic Commercial Transport Aircraft. NASA CR-159253, 1980.

9. Douglas Aircraft Co. Staff: Evaluation of Laminar Flow Control System Concepts for Subsonic Commercial Transport Aircraft. NASA CR-159251, 1983.

10. Lineberger, L. B; et al.: Development of Laminar Flow Control Wing Surface Composite Structures. NASA CR-172330, 1984.

11. Lineberger, L. B.; et al.: Structural Tests and Development of a Laminar Flow Control Wing Surface Composite Chordwise Joint. NASA CR-172462, 1984.

12. Douglas Aircraft Co. Staff: Laminar Flow Control Leading Edge Glove Flight Test Article Development. NASA CR-172137, 1984.

13. Anderson, C. B.; et al.: Development of Laminar Flow Control Wing Surface Porous Structure. NASA CR-172424, 1984.

14. Etchberger, F. R.: Laminar Flow Control Leading Edge Glove Flight - Aircraft Modification Design, Test Article Development, and Systems Integration. NASA CR-172136, 1983.

15. Fischer, M. C.; Wright, A. S., Jr.; and Wagner, R. D.: A Flight Test of Laminar Flow Control Leading-Edge Systems. NASA TM-85712, 1983.

16. Davis, R. E.; and Fischer, M. C.: Cloud Particle Effects on Laminar Flow and Instrumentation for Their Measurement Aboard a NASA LFC Aircraft. AIAA Paper No. 83-2734, 1983.

17. Jasperson, W. H.; Nastrom, G. D.; Davis, R. E.; and Holdeman, J. D.: Cloud GASP Cloud - and Particle - Encounter Statistics, and their Application to LFC Aircraft Studies. NASA TM 85835, vol. I and II, 1984.

18. Pfenninger, W.: Design Considerations of Long-Range and Endurance LFC Airplanes with Practically All Laminar Flow. NASA CR-173234, 1982

19. Montoya, L. C.; Steers, L. L.; Christopher, D.; and Trujillo, B.: F-111 TACT Natural Laminar Flow Glove Flight Results. NASA CP-2208, 1981.

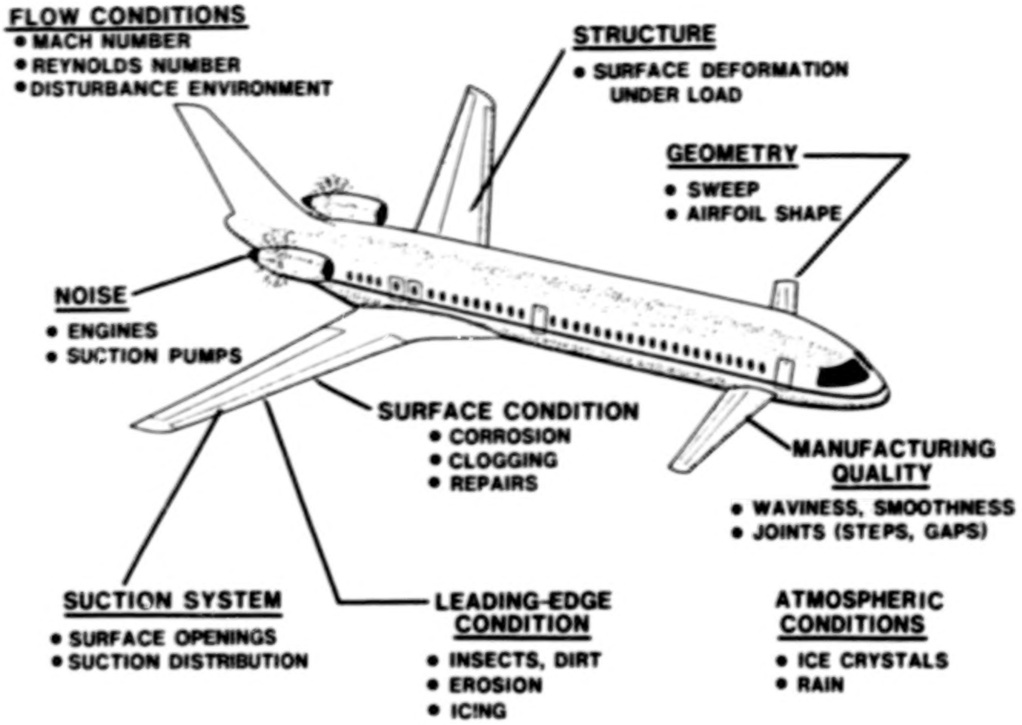
FLOW CONDITIONS
• MACH NUMBER
• REYNOLDS NUMBER
• DISTURBANCE ENVIRONMENT
STRUCTURE
• SURFACE DEFORMATION UNDER LOAD
GEOMETRY
• SWEEP
• AIRFOIL SHAPE
NOISE
• ENGINES
• SUCTION PUMPS
SURFACE CONDITION
• CORROSION
• CLOGGING
• REPAIRS
MANUFACTURING QUALITY
• WAVINESS, SMOOTHNESS
• JOINTS (STEPS, GAPS)
SUCTION SYSTEM
• SURFACE OPENINGS
• SUCTION DISTRIBUTION
LEADING-EDGE CONDITION
• INSECTS, DIRT
• EROSION
• ICING
ATMOSPHERIC CONDITIONS
• ICE CRYSTALS
• RAIN

Figure 1.- Factors affecting laminar flow in flight.

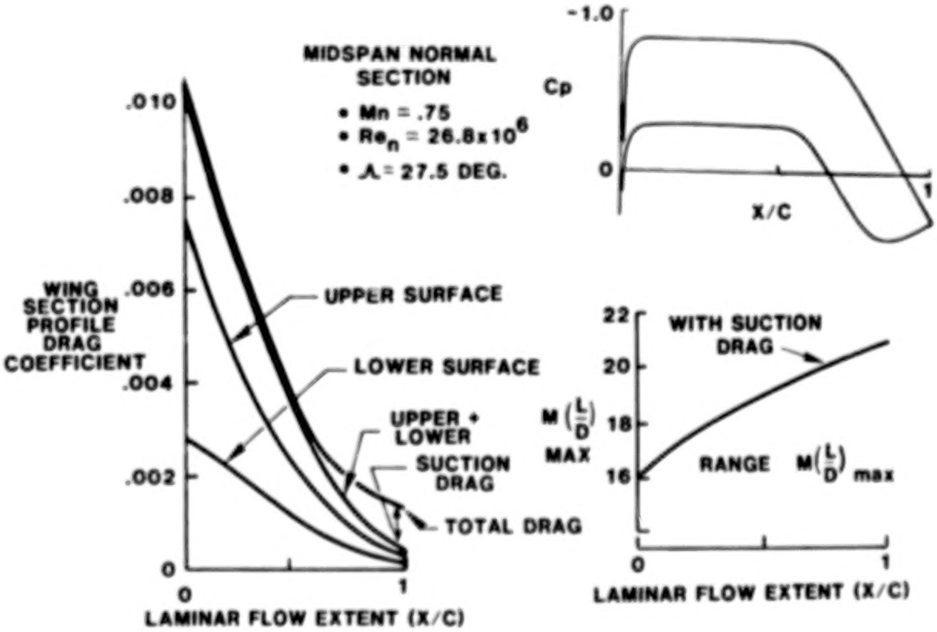

Figure 2.- Wing performance versus extent of laminar flow.

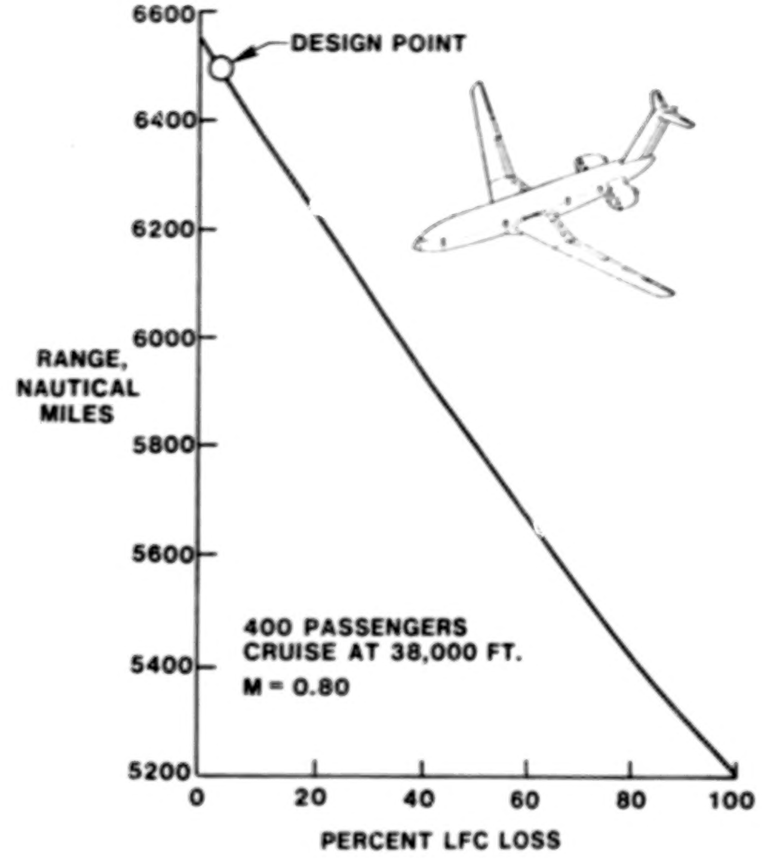

Figure 3.- Effect of laminar flow control system loss on range capability.

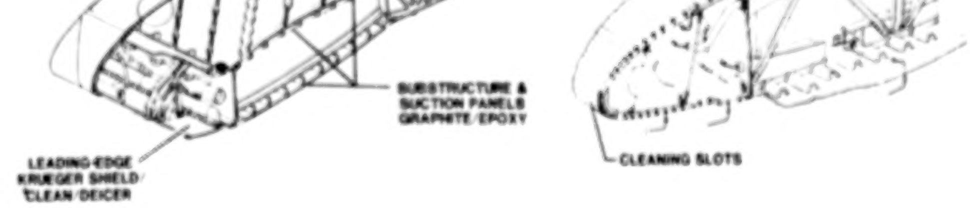
DOUGLAS DESIGN
PERFORATED
LOCKHEED DESIGN
SLOTTED
ELECTRON BEAM PERFORATED TITANIUM SKIN
SUBSTRUCTURE & SUCTION PANELS GRAPHITE/EPOXY
LEADING-EDGE KRUEGER SHIELD/CLEAN/DEICER
SUCTION SLOT
CLEANING SLOTS

Figure 4.- Laminar flow control structural development.

ORIGINAL PAGE IS
OF POOR QUALITY

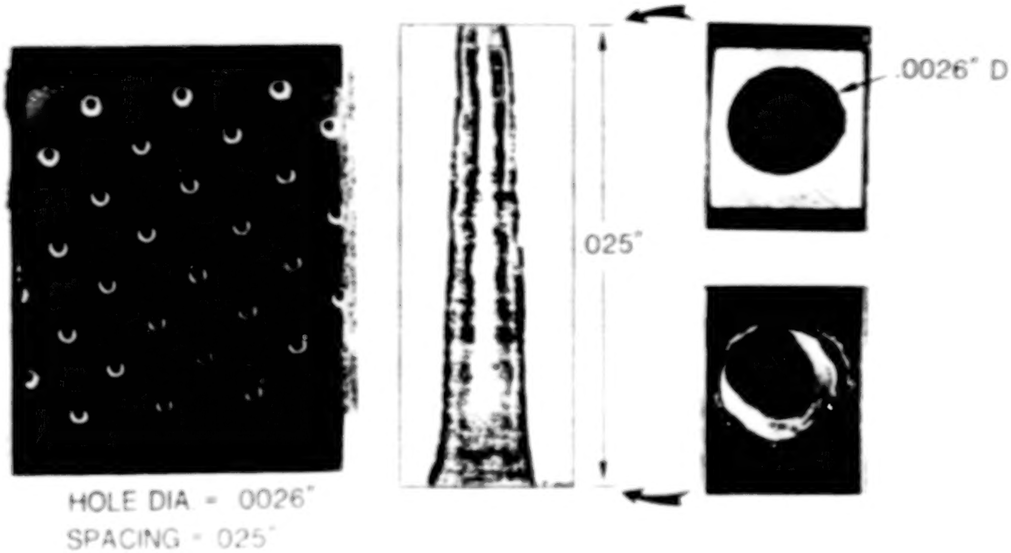
.0026" D
.025"
HOLE DIA = .0026"
SPACING = .025"

Figure 5.- Microphotograph of electron beam perforated holes.

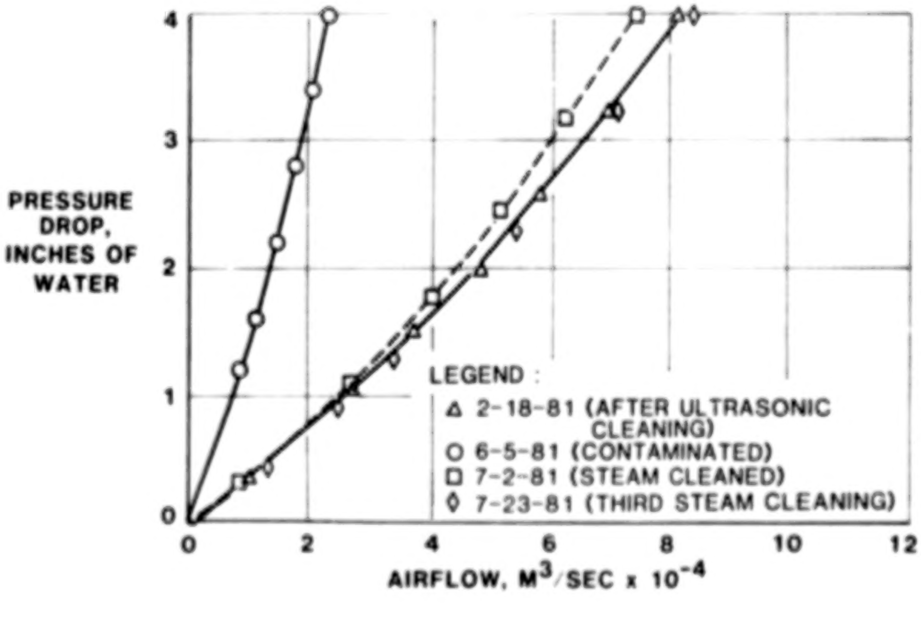

Figure 6.- Electron beam perforated titanium cleaning techniques.

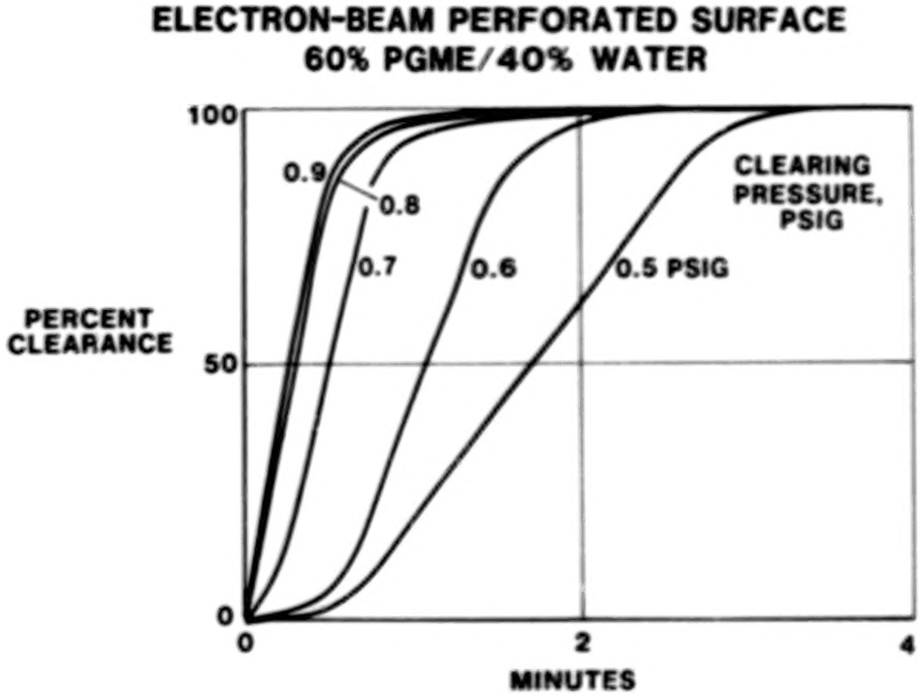

Figure 7.- Electron beam perforated surface purging system results.

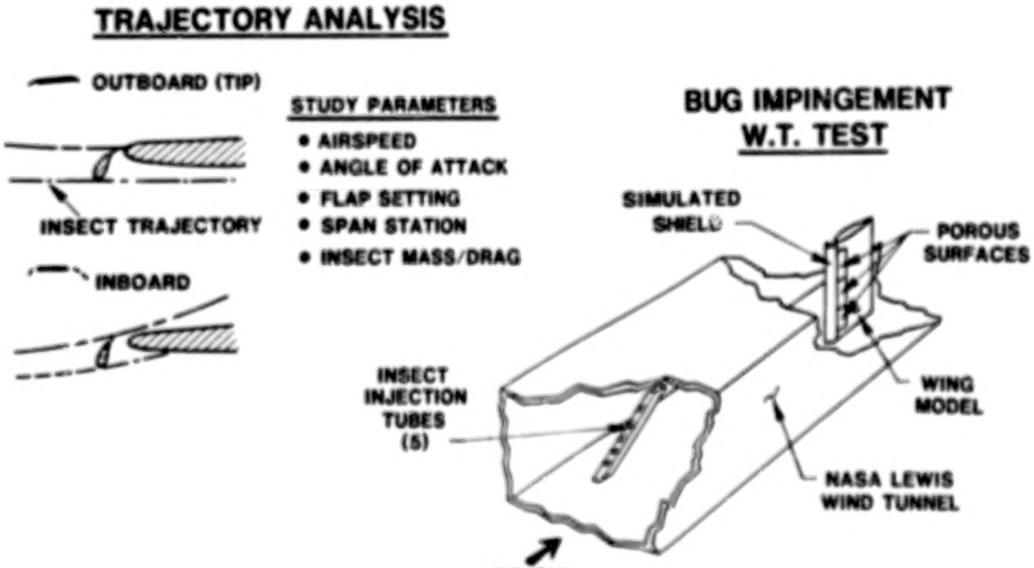
TRAJECTORY ANALYSIS
OUTBOARD (TIP)
INSECT TRAJECTORY
INBOARD
STUDY PARAMETERS
• AIRSPEED
• ANGLE OF ATTACK
• FLAP SETTING
• SPAN STATION
• INSECT MASS/DRAG
BUG IMPINGEMENT
W.T. TEST
SIMULATED SHIELD
POROUS SURFACES
WING MODEL
INSECT INJECTION TUBES (5)
NASA LEWIS WIND TUNNEL
AIRFLOW

Figure 8.- Douglas Krueger shield insect trajectory analysis and wind tunnel test.

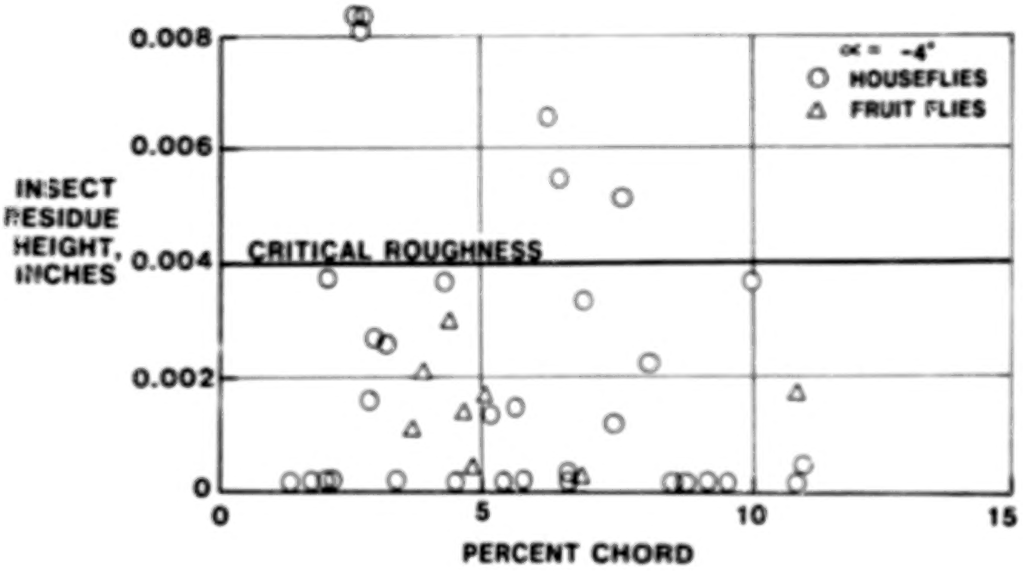

Figure 9.- Douglas insect residue wind tunnel test results.

OBJECTIVE: DEMONSTRATE THE EFFECTIVENESS AND PRACTICALITY OF L.E. SYSTEMS IN MAINTAINING LAMINAR FLOW UNDER REPRESENTATIVE FLIGHT CONDITIONS

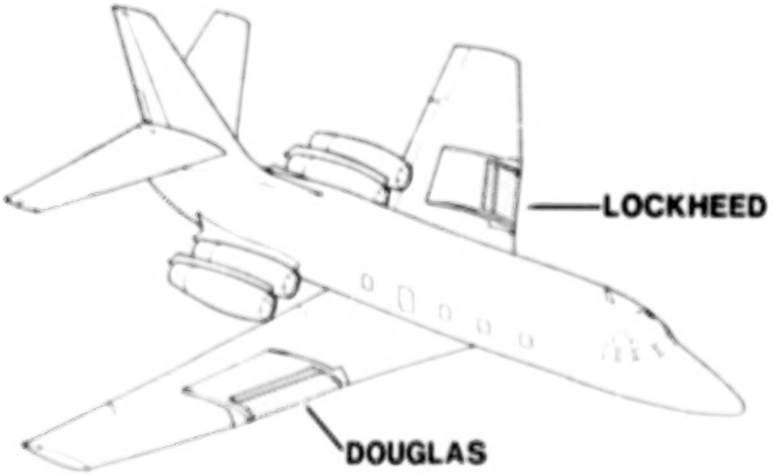

Figure 10.- Leading-edge flight test Jetstar configuration.

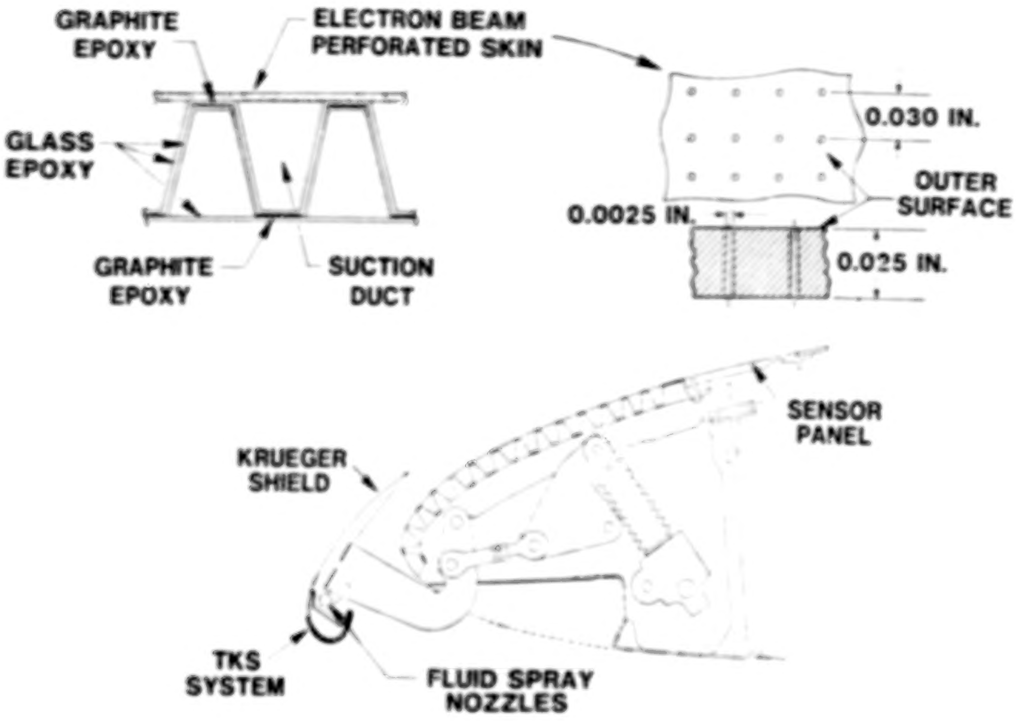
GRAPHITE EPOXY
ELECTRON BEAM PERFORATED SKIN
GLASS EPOXY
GRAPHITE EPOXY
SUCTION DUCT
0.030 IN.
OUTER SURFACE
0.0025 IN.
0.025 IN.
SENSOR PANEL
KRUEGER SHIELD
TKS SYSTEM
FLUID SPRAY NOZZLES

Figure 11.- Douglas leading-edge flight test article.

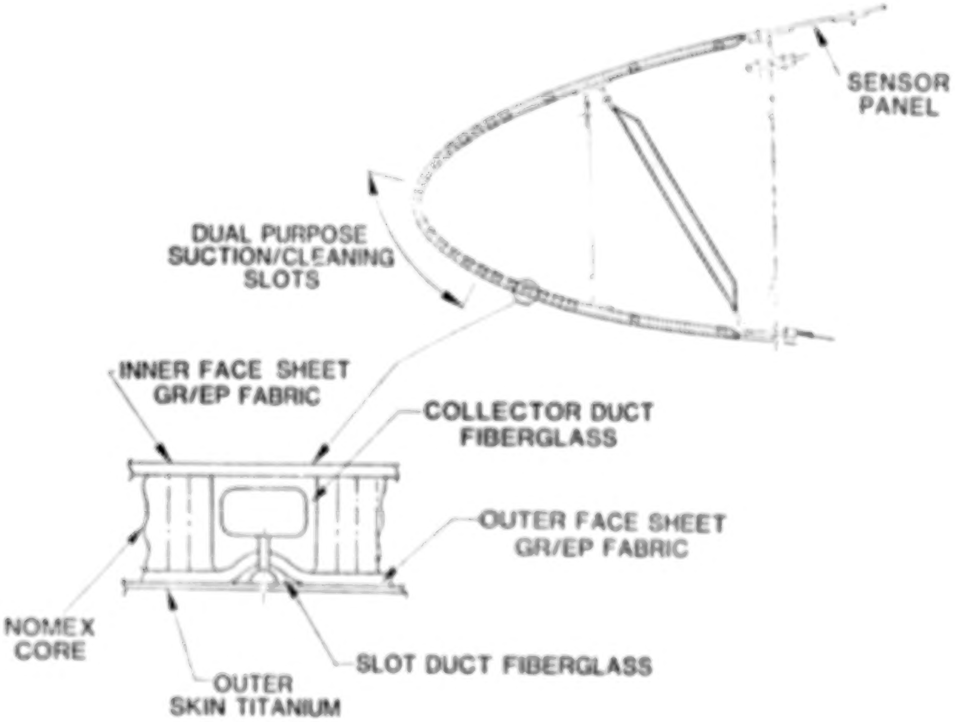
SENSOR PANEL
DUAL PURPOSE SUCTION/CLEANING SLOTS
INNER FACE SHEET GR/EP FABRIC
COLLECTOR DUCT FIBERGLASS
OUTER FACE SHEET GR/EP FABRIC
NOMEX CORE
OUTER SKIN TITANIUM
SLOT DUCT FIBERGLASS

Figure 12.- Lockheed leading-edge flight test article.

ORIGINAL PAGE IS
OF POOR QUALITY

Figure 13.- NASA DFRF Jetstar in flight.

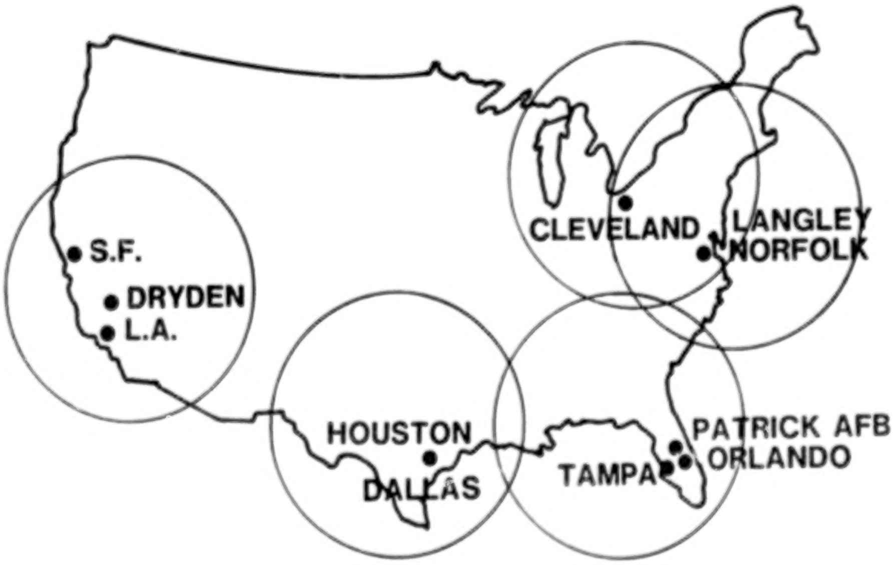
S.F.
DRYDEN
L.A.
CLEVELAND
LANGLEY
NORFOLK
HOUSTON
DALLAS
TAMPA
PATRICK AFB
ORLANDO

Figure 14.- LEFT simulated airline service homes bases.

	LOCKHEED	**DOUGLAS**
Takeoff	**Liquid on**	**Shield extended** **Liquid on** **Secondary purge on**
6,000 ft.	**Liquid off** **Secondary purge on**	**Liquid off** **Retract shield** **Secondary purge on**
12,000 ft.	**Secondary purge off** **Primary purge on**	**Secondary purge off** **Primary purge on**
20,000 ft.	**Suction pump start**	**Suction pump start**
23,000 ft.	**Primary purge off**	**Primary purge off**
32,000 ft.	**Beginning of suction on test article**	**Beginning of suction on test article**

Figure 15.- Leading-edge flight test operations.

GASP DATA BASE

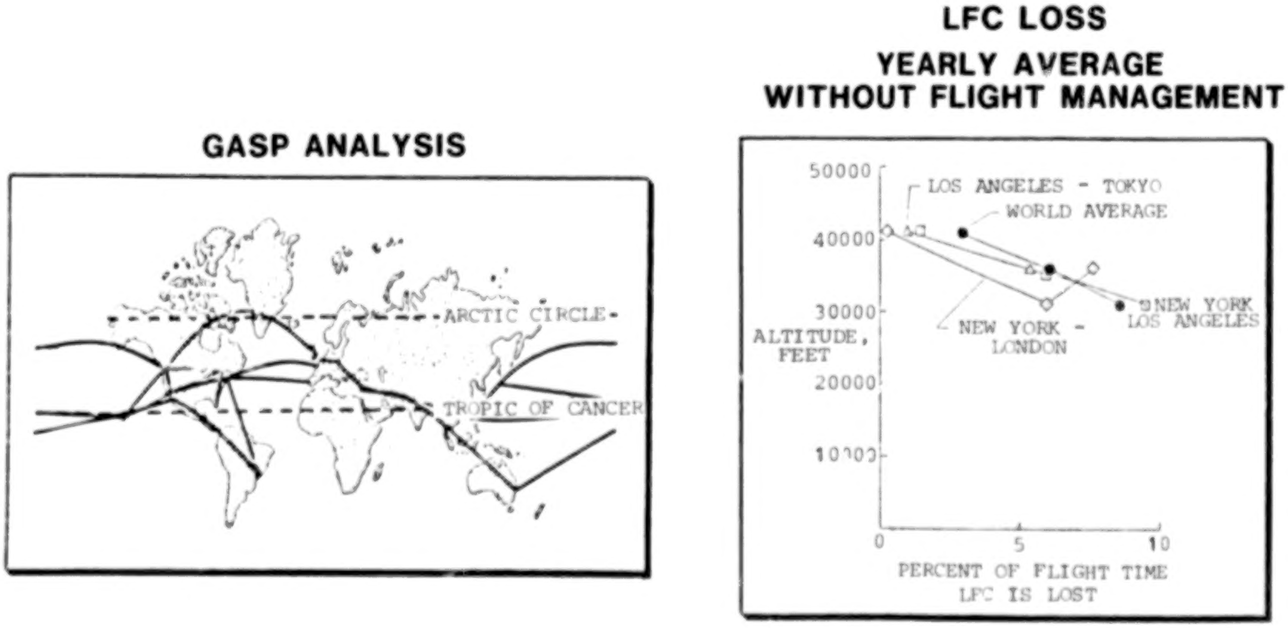

GASP ANALYSIS

LFC LOSS
YEARLY AVERAGE
WITHOUT FLIGHT MANAGEMENT

Figure 16.- Cloud particle impact on laminar flow loss from GASP data base analysis.

ORIGINAL PAGE IS
OF POOR QUALITY

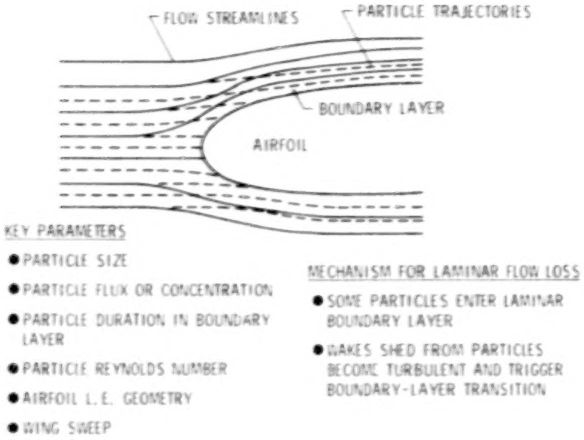
FLOW STREAMLINES
PARTICLE TRAJECTORIES
BOUNDARY LAYER
AIRFOIL
KEY PARAMETERS
● PARTICLE SIZE
● PARTICLE FLUX OR CONCENTRATION
● PARTICLE DURATION IN BOUNDARY LAYER
● PARTICLE REYNOLDS NUMBER
● AIRFOIL L. E. GEOMETRY
● WING SWEEP
MECHANISM FOR LAMINAR FLOW LOSS
● SOME PARTICLES ENTER LAMINAR BOUNDARY LAYER
● WAKES SHED FROM PARTICLES BECOME TURBULENT AND TRIGGER BOUNDARY-LAYER TRANSITION

Figure 17.- Ice particle penetration and breakdown of the laminar boundary layer.

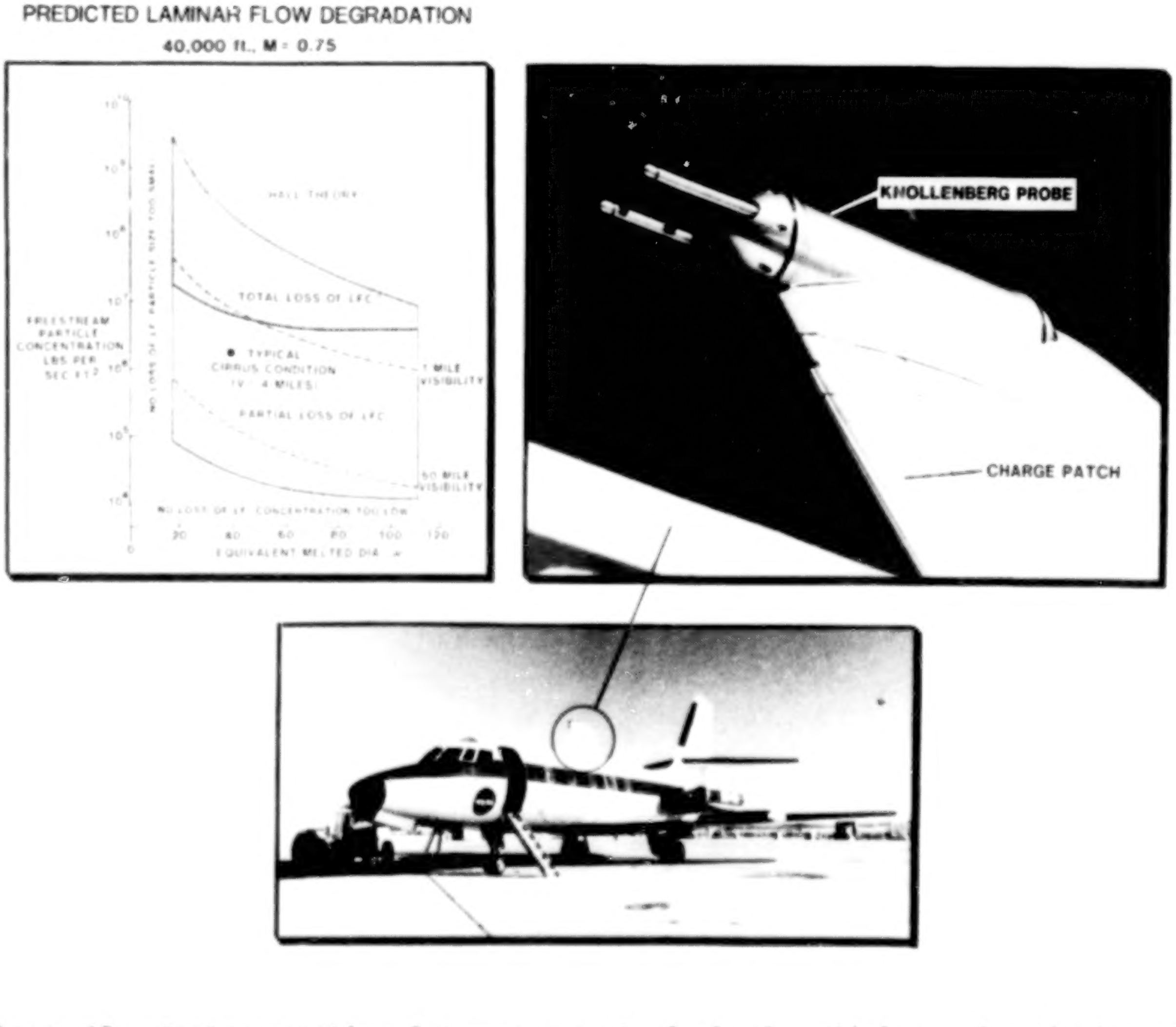

Figure 18.- Instrumentation for measurement of cloud particles and estimates of their effect on laminar flow loss.

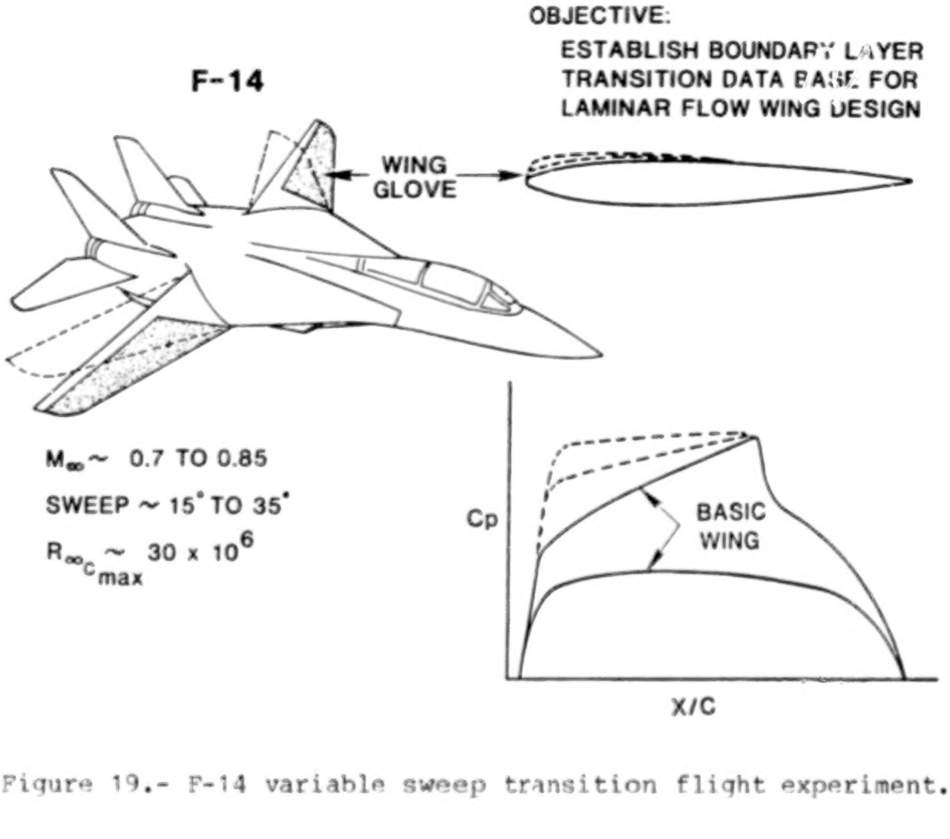
OBJECTIVE:
ESTABLISH BOUNDARY LAYER TRANSITION DATA BASE FOR LAMINAR FLOW WING DESIGN
F-14
WING GLOVE
$M_\infty \sim$ 0.7 TO 0.85
SWEEP ~ 15° TO 35°
$R_{\infty c_{max}} \sim 30 \times 10^6$
Cp
BASIC WING
X/C

Figure 19.- F-14 variable sweep transition flight experiment.

INDUSTRY PERSPECTIVE

Stanley J. Green, Vice President
General Aviation Manufacturers Association
Washington, D.C. 20005

I am limiting my views to natural laminar flow (NLF) aspects of this workshop and the obvious question concerning the certification issue, "is there anything about NLF technology that justifies new FAA rulemaking"? My answer is "NO".

The technology is not new - we started to develop natural laminar flow technology in the early 1930's though it wasn't described as such. The series six and similar airfoils have been around for a long time and we have learned a bit from them. Look at the airplanes in the "laminar flow fleet."

Transports

- Convair 240/340/580
- Martin 202-404
- Fairchild F27
- Grumman Gulfstream I
- Learjet

Lightplanes USA

- Mooney M-20 (1953)
- Piper Comanche (1957)
  - Twin Comanche (1963)
- Piper Cherokee (1961)
  - Cherokee Derivatives
- Piper Navajo (1966)
  - Navajo Derivatives including Cheyenne
- Cessna Model 2106 (1966)
  - Model 210 Derivatives
- Beech Musketeer (1962)
  - Musketeer Derivatives

Foreign

- Siai - Marchetti S.205 (1966)
- Siai - Marchetti SF 260 (1966)

Sailplanes

Virtually all high performance production sailplanes built in the past 20 years.

These aircraft and others, when measured, show considerable areas of or patches of natural laminar flow.

The perceived problem with NLF came about when some glider designs started out with lots of NLF (and performance). The NLF was lost due to rain or bug contamination, and the performance fell off rapidly. Handling qualities did not degrade. Another aircraft, a noncertificatable canard design, had a downward pitching moment when flying in rain (whether from loss of NLF, some canard effect, or other performance-related airfoil design factor was not determined).

NLF has potential to improve an airplane's utility from an energy-saving or economics point of view. NLF will extend the range of the aircraft if NLF is not lost. NLF will allow a lower power setting to attain the same speed as a nonlaminar flow airplane, or will allow a greater speed for the same fuel costs and thus save time - all other factors being equal. Speed and efficiency are factors that differentiate among airplanes today. If NLF becomes a marketing factor, it will be touted as "my airplane gets 20 miles to the gallon at 175 knots," or some other numbers appropriate to the airplane. This is no different from any of today's airplane marketing. An airplane won't be sold as my airplane is "60 percent NLF."

First and foremost, from an industry viewpoint, we recommend that you keep the work going in all areas of NLF research. This research has the potential of bringing about significant improvements in the economy and speed of flight for all newly designed planes. The industry needs all the research that NASA and the universities can provide.

Second, we need to define what data will be collected and provided to the FAA and to the airplane operator. With respect to the data we provide to the FAA to meet the FAA's current requirements, we see no need for additional regulation because the present normal performance information is adequate and will be provided to the FAA with the NLF tripped. The information will cover the takeoff, climb, and landing modes. In addition, we will have to show the FAA that the stall characteristics are about the same with and without NLF (NLF tripped). This is the conservative way to develop and present information, and this is what we do today. There is no need to show, for certification, performance with NLF, any more than there is a need to show performance up to the physical limits of the airplane (or any area beyond) which the manufacturer chooses to certify.

For the customer, the operator, we will provide information for flight planning purposes, with NLF and without it. It is likely that in the examples in the Pilot's Operating Handbook, we will present the fuel required charts, at various power settings, with 100 percent of that airplane's NLF, some intermediate percentages of this NLF, and without any NLF. This information will be supplemented with sufficient information to best estimate what percentage of NLF the operator might get based on the condition of the airplane, enroute weather, and other phenomena. There will, of course, be all of the appropriate cautions about stretching fuel. We will be telling the operator that, if available, NLF is a fuel-saving drag reducer.

The characteristics of and differences between an NLF airfoil and one that does not have any significant amount of NLF - a good airfoil that is not an NLF airfoil - are within the margins of FAR 23 requirements for handling qualities, controllability, and stability.

In summary, within today's regulations, we can design and test an airplane with NLF and with the NLF tripped. No new FAA certification regulations are needed, as evidenced by the many safe NLF airplanes now flying. Opportunity exists to build substantially more fuel efficient airplanes, using NLF technology, that will meet the FAA's rules on handling qualities, performance, and stall characteristics. Further research, as indicated by this workshop, will bring these improvements in airplane efficiency to fruition.

Thank you, on behalf of GAMA, for the opportunity to participate in this seminar.

N88-23749

CERTIFICATION ASPECTS OF AIRPLANES WHICH MAY OPERATE WITH SIGNIFICANT NATURAL LAMINAR FLOW

S12-05

Edward A. Gabriel
and
Earsa L. Tankesley

FAA Small Airplane Certification Directorate
Kansas City, Missouri

INTRODUCTION

Recent research by NASA indicates that extensive natural laminar flow (NLF) is attainable on modern high performance airplanes currently under development. Modern airframe construction methods and materials, such as milled aluminum skins, bonded aluminum skins, and composite materials, offer the potential for production aerodynamic surfaces having waviness and roughness below the values which are critical for boundary layer transition. In addition, the current trend is to higher wing loadings, higher aspect ratios, and higher cruise altitudes, all of which produce lower chord Reynolds numbers and, therefore, the possibility for more extensive laminar flow. We also expect to see an increasing application of modern computer designed airfoils which can be tailored to promote more extensive NLF.

The purpose of this paper is to identify areas of concern with the certification aspects of NLF and to stimulate thought and discussion of the possible problems at an early date. During its development, consideration has been given to the recent research information available on several small business and experimental airplanes and the certification and operating rules for general aviation airplanes. The certification considerations discussed are generally applicable to both large and small airplanes. However, from the information available at this time, we expect more extensive NLF on small airplanes because of their lower operating Reynolds numbers and cleaner leading edges (due to lack of leading-edge high lift devices). Further, the employment of composite materials for aerodynamic surfaces, which will permit incorporation of NLF technology, is currently beginning to appear in small airplanes.

The Certification Process

When a new airplane employing advanced technology is being developed, the FAA should be advised at the earliest possible time. This will permit an early identification of the certification issues and, if required, the timely development of any special conditions which may be necessary to provide a level of safety equivalent to that established in the regulations. Under the provision of the Federal Aviation Regulations (FAR) Part 21, Certification Procedures for Products and Parts, section 21.16, special conditions (SC) may be imposed when the applicable airworthiness regulations do not contain adequate or appropriate standards because of a novel or unusual design feature. These imposed SC become part of the airplane tape certification basis. The airworthiness regulations are updated and amended at intervals, with public participation, to cover recent aeronautical progress and thereby preclude the need for special conditions in subsequent airplane type certification projects.

General Concerns

The general concern in certification of airplanes having extensive NLF is that the extent of laminar flow may change during the airplane's operation, because of surface contamination due to: an accumulation of insects or dirt, condensation or rain, and frost or ice. Also, the original surface quality, as certificated, may change because of minor service damage, paint chipping or peeling, or changes in paint schemes or paint application techniques. Since extensive NLF is attainable, but not assured, consideration must be given to the effects of loss of a significant portion of laminar flow.

The following trends have been observed on airfoil sections where extensive NLF is possible:

- o The upper and lower surface local pressures may be significantly different for natural transition than when the transition point is fixed close to the leading edge.
- o The lift curve slope may be higher.
- o The pitching moment coefficient may be more positive.
- o The drag is normally lower at cruise angle of attack.

Loss of NLF may result in adverse changes in performance (including stall speed, rate of climb, and range), flying qualities, and airloads. If significant NLF is expected to be attainable, the applicant should present information early in the certification process on the possible extent of NLF, how maintenance of NLF will be assured, and the consequences of the loss of a significant portion of NLF. Verification by test will likely be necessary. Flight testing techniques, such as the use of sublimation chemicals to determine the extent of NLF, and artificial means to force boundary layer transition may be required. Wind tunnel testing done at much lower than normal flight Reynolds numbers will likely not be accepted.

PERFORMANCE

Stall Speed (FAR Part 23 - Airworthiness Standards; Normal, Utility and Acrobatic Category Airplanes - section 23.49)

For airfoils having appreciable NLF, the maximum lift may be adversely affected by loss of laminar flow with a corresponding increase in stall speed. However, this depends on the sensitivity of the airfoil and whether flow separation is involved. For a single engine composite structure airplane with an NACA 63_2-215 airfoil, test data provided in Reference 1, the maximum lift coefficient actually increased about 4 percent when boundary layer transition was fixed at 5 percent chord. However, other research has shown a reduction of maximum lift on airfoils designed for maintaining a laminar boundary layer, when transition was fixed near the leading edge (Reference 2).

Loss of NLF on a canard or tandem wing airplane may have severe adverse aerodynamic effects. This was shown in the tests of both canard configured airplanes reported in Reference 1. For the more severe case, fixed transition on the wings, winglets, and nose caused an 11 knot increase in minimum trim speed, corresponding to a 27 percent decrease in maximum lift.

The current certification regulations applicable to single-engine airplanes and to multiengine airplanes of 6,000 pounds or less maximum weight which do not have one-engine inoperative climb performance require a stall speed of 61 knots or less with the airplane in the landing configuration at maximum weight. For an NLF airplane of this type that may have a stall speed close to the 61 knot limit, an increase in stall speed due to loss of NLF may result in the design not being able to comply with this requirement.

Takeoff and Landing (FAR sections 23.51 and 23.75)

These sections of the FAR require the landing approach speed and the climb speed attained at the end of the takeoff distance (50 foot height) to be 30 percent greater than the stall speeds in the takeoff and landing configurations, respectively. If the stall speed increases because of loss of NLF, the takeoff and landing distances will also increase. If flight planning does not allow for this possibility, an intended destination runway may be too short for a safe landing.

Climb (FAR sections 23.65, 23.67 and 23.77)

A loss of NLF could result in a significant drag increase and may result in a lift curve slope decrease. Thus, the lift to drag ratio and the rate of climb could decrease. Section 23.67 contains one-engine inoperative climb requirements which are related to stall speed squared. Therefore, if a loss of NLF causes the stall speed to increase, the minimum rate of climb required will increase, with the possibility that this requirement will not be met.

FLIGHT CHARACTERISTICS

From review of the results of NASA research reported in References 1 and 3, it does not appear that testing of conventional configured airplanes included an evaluation of the effects of the loss of NLF on stability and control. The FAA would be concerned about how NLF and its loss change these parameters.

For the two canard configured airplanes tested in References 1 and 3, significant effects on longitudinal handling qualities were found when extensive NLF was changed to turbulent flow by fixing transition near the leading edge on both lifting surfaces. Full scale wind tunnel tests show a large increase in the trim elevator deflections required at any airspeed, a 7 to 11 knot increase in minimum trim speed, and some reduction in short period damping at cruise speed. These changes were attributed to loss of lift on the forward surface caused by turbulent flow separation near the trailing edge when NLF was lost. The forward wing was designed for a laminar boundary layer with attached flow. Loss of NLF and loss of forward wing lift also occurred with water sprayed on the wings to simulate rain during wind tunnel testing. These effects of fixed transition on the lifting surfaces (resulting in loss of NLF) were also seen in flight testing the canard configured airplanes reported in Reference 1.

Part 23 of the FAR contains the certification standards for controllability and maneuverability in sections 23.143 to 23.157, for trim in section 23.161, and for stability in sections 23.171 to 23.181. Loss of NLF may have a significant or even critical effect on the airplane's ability to meet these standards. A significant change in airfoil pressure distribution and moment coefficient due to loss of NLF could change the stabilizing and control forces which must be provided by the horizontal tail. Such a change would be evaluated to determine that the current standards and criteria are met for longitudinal control, control during landings, elevator control force in maneuvers, trim, static longitudinal stability, and dynamic stability.

Lateral handling characteristics may be adversely affected by asymmetric loss of NLF on a wing using an airfoil section which is sensitive to surface roughness and waviness. This could be a particular problem if the construction methods, skin thickness, etc., are not adequate to ensure that both right and left wing panels are within the tolerances required for maintenance of NLF. It is possible that such critical variations may not be present in the certification test airplane but may appear later on production airplanes and could become a problem on in-service airplanes if both wings are not maintained to the same standards.

For conventional airplane configurations, a loss of NLF on the wings would not be expected to have significant effects on the directional handling characteristics, unless it were an asymmetric loss, as discussed above, which would cause a spanwise asymmetric distribution of drag. However, a change of boundary layer state and possible associated flow separation on the vertical tail, due to high yaw angles or contaminated surface condition, could result in significant changes in directional stability and control and a higher minimum control speed (for multiengine airplanes). Canard or tandem wing configurations having winglets which obtain significant NLF and which also serve as the vertical tail surfaces pose a more difficult design problem in this respect because the winglets are normally cambered and set at an angle of incidence (with respect to the airplane centerline) to minimize the wing induced drag.

Stall and spin certification standards are contained in FAR sections 23.201 to 23.221. Airfoil section aerodynamic characteristics are known to directly affect stall and spin characteristics. The shape of the lift curve top (C_l versus α) is one of the most important design considerations for low-speed flight because it directly reflects the potential seriousness of the stall-spin characteristics of the airplane (Reference 4). A sharp lift curve top where lift decreases rapidly with angle of attack (due to large areas of flow separation) usually results in a large bank angle (roll-off) at stall. Laminar flow airfoil sections usually have a favorable shape of the lift curve top because flow separation normally starts at the trailing edge. However, cases of leading edge flow separation stalls have been observed on laminar flow airfoils which have been improperly designed.

It should be shown by flight test with fixed transition that loss of NLF will not affect the stall and spin recovery characteristics to the extent that the applicable certification FAR sections will not be met. For a laminar flow wing, the importance of limiting differences in right and left lifting surface panels due to manufacturing tolerances for airfoil contour, skin waviness, and roughness should be emphasized. An asymmetric loss of NLF may have an adverse effect on lateral handling characteristics at stall, and possibly on spin recovery. For wings having significant NLF, it will be necessary to investigate the likelihood or effects of asymmetric loss of laminar flow on stall and spin recovery characteristics.

FLIGHT LOADS

Certification standards for flight loads including control surface and tail surface loads are contained in Part 23 of the FAR, sections 23.321 through 23.459. As discussed in previous paragraphs, the boundary layer state, i.e., laminar or turbulent, may have a significant effect on the airfoil pressure distribution, lift curve slope, moment coefficient, and profile drag. Buckling or distortion of airfoil skins under maneuver or gust loading may cause a change in the boundary layer state. These factors will affect the distribution of air loads chordwise and possibly spanwise (symmetric and asymmetric), the gust loads, and the balancing tail loads. The extent of NLF is dependent on the surface condition and accuracy of the airfoil contours which, in turn, are dependent on factors in design, manufacture, maintenance, and operations.

During certification, the applicant should present type design data showing the extent of NLF expected, the likelihood of loss of NLF, the extent of NLF loss that may occur, and the maintenance necessary to assure that NLF is retained. Structural design flight loads should include the extremes defined by natural transition and by fixed transition near the leading edge. Flight testing using a technique such as the use of sublimating chemicals to determine the extent of NLF and artificial means to cause boundary layer transition may be required.

FLUTTER

FAR section 23.629 requires that the airplane be free from flutter, control reversal, and divergence. The FAA is not aware of any research that has indicated that a changing boundary layer may result in a flutter problem. However, this is an area that should be researched to determine the potential for flutter problems or to alleviate concerns about such problems arising. Two possible factors to consider are as follows:

(a) The effect of a changing pressure distribution on wing torsion loads and hence elastic wing twist.

(b) Pressure loadings on control surfaces can change significantly with change in boundary layer state, particularly if trailing edge separation occurs.

RANGE

For several airplanes tested in Reference 1, an increase of about 25 percent in cruise drag was measured due to loss of laminar flow caused by artificially fixing boundary layer transition near the leading edge. This drag increase would result in a 20 percent loss of range according to the Breguet Range Formula, assuming the propeller efficiency and power setting are unchanged. If flight planning is based on the range which can be achieved with full laminar flow existing, then adequate cautions and cruise performance information should be provided to the pilot in the event laminar flow is lost or only partially existing, due to surface contamination (insects, moisture, dirt, ice, etc.).

It would be desirable to provide the pilot with direct information on the boundary layer state. A simple boundary layer state indicator is now available for gliders. This system includes a total pressure averaging rake which is mounted at the trailing edge of the wing. When the boundary layer flow is laminar, the total pressure ports of the rake are outside the boundary layer and sense essentially free stream total pressure. When the flow is turbulent, the rake is immersed in the thickened boundary layer and senses a much lower average total pressure. The rake is connected by a single tube to a pressure indicator on the instrument panel which is referenced to the airspeed system total pressure. This provides a direct reading to the pilot on boundary layer state.

There are no present requirements for providing range performance data in the FAA approved flight manual. This information is normally provided by the airplane manufacturer in the Pilot's Operating Handbook. The pilot uses the cruise performance information to determine the fuel requirements for a particular flight. Because of the possible range differences that may be realized due to the boundary layer being either laminar or turbulent, special conditions may be needed in the type certification basis to provide a level of safety equivalent to that established in the regulations.

FAA operating regulations regarding fuel requirements for General Aviation are contained in FAR Part 91, General Operating and Flight Rules (sections 91.22 and 91.23); for Air Taxi and Commercial Operators in FAR Part 135 (sections 135.209, 135.217, and 135.233); and for Domestic and Flag Air Carriers in FAR Part 121.

PROPELLERS

In Reference 1, considerable laminar flow was shown to exist on a metal propeller operating at a Reynolds number of about 1.5 million at the 50 percent blade radius (2700 RPM, CAS = 133 kts, advance ratio = .84). For radial stations between 25 and 75 percent radius, the transition location on the forward face of the propeller blade was at 38 percent chord and 80 percent chord on the aft face.

FAR section 23.33 contains standards for propeller speed and pitch limits for fixed pitch, controllable pitch, and constant speed propellers. The blade element drag (which determines torque required) can change as a function of the amount of NLF being achieved. The changing surface roughness of propellers, due to nicks, pitting, insects, etc., would have an effect on the NLF achieved, particularly on propellers designed to use laminar flow airfoil sections. The resulting change in blade element drag could be substantial, thus affecting the relationship between propeller pitch and engine RPM.

FAR section 23.45 requires that performance testing be accomplished with the approved power, less installation and accessory losses. For reasons discussed above, the relationship of thrust and power setting for a propeller may vary depending on the amount of NLF existing. This would likely be an important consideration if the propeller was specifically designed to achieve large amounts of NLF.

ICE PROTECTION AND DEICING EQUIPMENT

FAR sections 23.1416 and 23.1419 contain standards for deicing and ice protection systems. The existence of NLF has no effect on the performance of these systems. However, icing equipment is sometimes added (by a Supplemental Type Certificate approval) after an airplane has been type certificated. For an airplane designed to achieve significant NLF, addition of deicing boots, fluid outlets, etc., could produce changes in the boundary layer that could dramatically change the vehicle's performance, flying qualities, and aerodynamic loads.

Porous-fluid-exuding leading edges have been studied (Reference 3) as a means of providing protection against both ice and insect contamination which may trip the laminar boundary layer. Such equipment would have to comply with FAR section 23.1419 for ice protection systems, and in addition, there may be reliability considerations in its use for maintaining a laminar boundary layer.

FLIGHT MANUAL

The airplane flight manual contains information necessary for safe operation of the airplane as required by FAR sections 23.1581 through 23.1589. The performance effects of NLF (including loss of NLF), which were discussed earlier, will need to be reflected in the flight manual material as follows:

(a) Recommended climb speed.

(b) Approach speeds.

(c) One engine inoperative procedures including minimum control speeds, landing and go around with one engine inoperative, and effects of airplane configuration.

(d) Stalling speeds for the clean configuration and for landing gear and flaps down.

(e) Takeoff distance.

(f) Landing distance.

(g) Rate of climb or climb gradient.

DESIGN AND CONSTRUCTION

Previously we noted that modern airframe construction methods and materials, such as milled aluminum skins, bonded aluminum skins, and composite materials, offer the potential for production aerodynamic surfaces having waviness and roughness below the values which are critical for boundary layer transition.

Conversely, a decision to reduce airframe drag by employing NLF will likely influence structural design, e.g., rib spacing, stiffer skins, and elimination of skin laps.

Since airplane performance, flying qualities, and flight loads may change significantly with boundary layer state, the fabrication methods used to manufacture each production article on an airplane designed for extensive laminar flow may be considered a critical process. An example of a possible problem would be a composite structure wing laid up in a mold with the possibility of the mold contour changing significantly with age. This has been known to occur in the production of composite structure high performance gliders.

FAR section 23.605 requires an approved process specification for fabrication processes requiring close control to produce consistently sound structures. Traditionally, this requirement has been related to structural strength, but in the case of NLF technology it would also relate to achieving the required surface contour, smoothness, and waviness. The production method of painting an airplane is an example of a process that might also be critical to achieving NLF.

MAINTENANCE OF AERODYNAMIC SURFACES

FAR section 21.50 requires that instructions for continued airworthiness be provided, and for small airplanes, FAR section 23.1529 requires that they be prepared in accordance with Appendix G of FAR 23. This applies to both Type Certificates and Supplemental Type Certificates for which application was made after January 28, 1981. Appendix G of FAR Part 23 contains requirements for a maintenance manual. It would be necessary, for an airplane designed for operation with extensive NLF, to have information in the maintenance manual concerning routine care, repair, repainting, etc., of the aerodynamic surfaces and maintenance information relative to any laminar flow instrumentation that might be installed.

CONCLUDING REMARKS

In previous paragraphs, we have discussed the possible effects that the boundary layer state, laminar or turbulent, and loss of NLF may have on airplane performance, flying qualities, and flight loads. These effects would be more likely, or more pronounced, for airplanes with airfoils and surface quality designed for extensive NLF and for canard and tandem wing configurations with such airfoils and surface quality. The main effects of NLF evident to the pilot will be on performance and to some extent on flying qualities. Significant adverse effects on flying qualities and on flight loads must be avoided or corrected during the design and certification process.

If significant NLF is expected to be attainable, the applicant should present information early in the certification process on the possible extent of NLF, how maintenance of NLF will be assured, and the consequences of loss of a significant portion of NLF. Verification by test will likely be necessary. Flight testing techniques, such as the use of sublimating chemicals to determine the extent of NLF, and artificial means to force boundary layer transition may be required.

REFERENCES

1. Holmes, B. J., Obara, C. J., and Yip, L. P.: "Natural Laminar Flow Experiments on Modern Airplane Surfaces," NASA TP 2256, June 1984.

2. Somers, Dan M.: "Design and Experimental Results for a Flapped NLF Airfoil for General Aviation Application." NASA TP 1865, June 1981.

3. Holmes, B. J., and Obara, C. J.: "Observations and Implications of Natural Laminar Flow on Practical Airplane Surfaces," AIAA Journal of Aircraft, vol. 20, December 1983.

4. Anderson, Seth B.: "Historical Overview of Stall/Spin Characteristics of General Aviation Aircraft," AIAA Journal of Aircraft, vol. 16, July 1979.

TEST TECHNIQUES WORKING GROUP SUMMARY AND RECOMMENDATIONS

Bruce J. Holmes, Chairman

The certification of natural laminar flow aircraft may entail new or different testing procedures and equipment as compared to certification of "turbulent" aircraft in the past. It is understood that with proper care in design, NLF airplanes can be manufactured and maintained with flying qualities essentially no different from those of turbulent airplanes. However, as illustrated in several of the technical presentations given at the workshop, selection of unsuitable NLF airfoils can produce undesirable flying qualities upon the loss of NLF. For a properly designed NLF airplane, the loss of laminar flow can be treated operationally by the pilot in the same manner headwinds are treated in turbulent airplanes (i.e., reduced range). The goal of these working group discussions was to identify the research and development (R & D) needed to provide the test techniques for flight and wind-tunnel testing of NLF airplanes to prove compliance with parts 23, 25, 91, and 135 of the FAR airworthiness and operating regulations. In addition to R & D needs related to certification, the recommendations also include R & D needs for NLF test techniques which do not necessarily directly affect certification. The recommendations given are limited to identification of topics in need of further research; time did not permit delineation of proposed research approaches, resources, and organizations. Details of these and other topics were identified which should be dealt with in follow-on negotiations between the airframe industries and the FAA.

Five topics were identified that need further research to facilitate the certification of NLF aircraft. These topics are discussed below.

Transition Fixing

The certification flight testing of NLF airplanes will probably require some matrix of tests with transition artificially fixed near the leading edges of the laminar surfaces. However, the definition of what constitutes a natural laminar flow airplane is unclear, since even some turbulent airfoils (for example the NACA 23012) will support NLF over 20 to 30 percent of the chord. It was recommended by the working group that discussions between industry and the FAA be held to determine a functional definition for natural laminar flow airplanes. This definition would serve the purpose of establishing which airplanes would require fixed transition testing during certification.

The working group recommended that research be conducted to establish standardized, acceptable means for fixing transition (for example by trips such as grit and by tape). The description of these means should include definitions of both location and sizing procedures for transition trips. In addition, agreement between the industry and the FAA should be reached on which airframe surfaces should have trips. The matrix of flight conditions for which fixed transition would be required should also be negotiated.

The working group further recommended that research be conducted to determine effective means for simulation of insect debris effects on transition and airfoil performance and simulation of "worst case" roughness (rain, for example). Research on correlations between wind-tunnel and flight aerodynamics of NLF airframes was supported.

PRECEDING PAGE BLANK NOT FILMED

The topic of transition fixing was the only one discussed by the working group which directly affects the certification of NLF airplanes. The remaining topics were recommended by the group as useful to facilitate the application of NLF technology.

Validation of Insect Contamination System Performance

Recent NASA flight research results have demonstrated the potential effectiveness of fluid-wetted porous leading-edge systems for use in the prevention of insect debris accumulation on airplane wings. Such systems could be useful on laminar flow airframes for maintaining NLF. The working group recommended that test procedures be established and agreed upon for the validation of the performance characteristics and limitations of such systems. This performance information would be particularly useful in the aircraft owner's manual (AOM).

Transition Instrumentation

In order to fully understand the aerodynamics of an NLF airplane, it is necessary to know both the locations and causes of boundary-layer transition. Because transition depends on Mach number, Reynolds number, and pressure gradient, it must be determined at each condition of practical interest throughout the airplane flight envelope. Thus, transition measurements must be made at the altitudes and flight conditions of interest. The group recommended continued research on high altitude (cold temperature) flow visualization test techniques and on electronic sensors for the measurement of both transition mode and location.

Pilot Instrumentation Transition Sensors

The group recommended research be conducted to develop simple, reliable sensors and displays for use by NLF airplane pilots to determine the extent of laminar flow at any given time during a flight. The purpose of this information is to assist in real-time flight management.

Measurement and Long-Term Behavior of Airframe Surface Quality

Recommendations by the working group included development of improved methods for the measurement of airframe waviness. An additional recommendation was made to study the long-term characteristics of airframe surface quality over periods of time on the order of an airframe life cycle.

AERODYNAMIC RESEARCH WORKING GROUP
SUMMARY AND RECOMMENDATIONS

Percy J. Bobbitt, Chairman

The aerodynamic research working group of the Laminar Flow Aircraft Certification Workshop sponsored by NASA, AIAA, SAE, and the FAA was divided into a number of panels to define the status and research needs for a variety of configurational and general research areas. The areas chosen along with the individuals who submitted material for inclusion in this white paper are listed below in the order they are presented.

I.	Wing Design Considerations and Procedures	Edgar G. Waggoner and W. E. Pearce
II.	NLF Airfoil Design, Analysis, and Testing	H. L. Morgan, Jr.
III.	Design Considerations for Laminar Nacelles	Roger J. Nyenhuis
IV.	Performance and Stability and Control Considerations	Joseph L. Johnson, Jr., Harry P. Stough, and Joseph W. Stickle
V.	Manufacturing Tolerances for Laminar Surfaces	Paul Vijgen and Bruce J. Holmes
VI.	Environmental Effects on Laminar Flow Aircraft	Michael B. Bragg and Parma Munger
VII.	Propeller Slipstream	Bruce J. Holmes
VIII.	Boundary-Layer Transition	Percy J. Bobbitt
IX.	Certification Aspects of NLF Airplanes	Mike O'Connor

A complete list of the members of the aerodynamic research working group is given in the front matter.

I. Wing Design Considerations and Procedures

This section addresses considerations and procedures necessary to design wings which can attain significant extents of laminar flow. These various aspects are considered in the light of true wing design where three-dimensional effects must be addressed successfully. A brief discussion of the current state of the art leads to a more detailed discussion of the four broad areas addressed: boundary-layer transition, wing design considerations and procedures, computational analysis and design techniques, and systems and operational considerations.

State of the Art

When progressing beyond designs for relatively unswept medium- to high-aspect-ratio low-speed wings, one quickly discovers there are few answers but many questions with regard to laminar flow wing design procedures or methodologies. Basically, as far as laminar flow wing design capability is concerned, it ends where airfoil design capability ends. That is, sections can be designed for significant laminar flow; however, the technology to integrate these designs into a three-dimensional flow environment while maintaining laminar flow and acceptable aerodynamic characteristics is just recently being developed. While industry and government research laboratories are investigating pieces of this complex puzzle, we are just now starting to understand how to effectively put the pieces together. This is not intended to discredit the excellent research that is being conducted but to point out the current limitations. The subsequent sections will delineate many of the critical technology areas and point out their impact on practical laminar flow wing design.

Boundary-Layer Transition

To design efficient wings with appreciable laminar flow, a thorough understanding of the factors influencing boundary-layer transition is required. It is important that the designer have at his disposal the boundary-layer and stability codes so that reasonably accurate predictions of transition can be made. In general, the various factors interact with each other to influence transition, and to the degree possible, this interaction must also be understood. A detailed description of the state of the art of predicting boundary-layer transition is given in section VIII, entitled Boundary-Layer Transition.

A major concern is the effect of wing surface quality and surface contamination on boundary-layer transition. Effects of waviness, surface roughness, gaps, and steps need to be systematically quantified relative to transition. (See section V, Manufacturing Tolerances for Laminar Surfaces.) In addition, transition effects because of surface contamination due to insects, dirt, paint chipping, etc., need to be quantified. These effects are rather insidious, since they can adversely affect a wing which through its design is capable of significant laminar flow.

The integration of the propulsion system into the configuration needs to be considered relative to the impact on the wing design and influence on laminar flow. Some of the boundary-layer transition concerns are acoustical disturbances and interferences from engine nacelles and propeller wakes. (See section III, Design Considerations for Laminar Nacelles, and section VII, Propeller

Slipstream.) This points out the need to integrate the propulsion system into the wing design at an early stage in the design process.

Wing-body juncture flows need to be understood in relation to their effect on the local boundary layers. As the flows are more thoroughly understood, the influences of the juncture flow disturbances on the wing boundary layer should be investigated. This is an extremely difficult problem, which is gaining more attention and requires higher order boundary-layer theory or Navier-Stokes solvers to generate realistic computational results.

Wing Design Considerations and Procedures

Wing design considerations will be addressed from the standpoint of integrating laminar flow airfoil sections into a practical, efficient, and safe wing. The overall performance of the aircraft is of paramount importance. The loss of laminar flow over the wing can result in significant changes in the performance and stability and control of the configuration. Wings must be designed which have acceptable aerodynamic characteristics independent of the extent of laminar flow actually realized, and this applies throughout the flight envelope. The key here is the design and utilization of airfoil sections in the design which, while promoting significant regions of laminar flow, have performance and flying qualities which do not change drastically as a function of transition location. (See section IV, Performance and Stability and Control Considerations.) The wings must have acceptable off-design characteristics as well. This includes low- and over-speed characteristics, climb performance, high-lift characteristics, and maximum lift. The wings must possess adequate buffet and stall margins. Again, these considerations are emphasized for a range of boundary-layer transition locations over the flight envelope.

Finally, wing design must address areas such as the effects of fences, leading-edge extensions, flap systems, and vortex generators. For practical wing designs these are often necessary design features. The influence of these features on transition must be understood as well as how to effectively incorporate them into the design process.

Computational Analysis and Design Techniques

Accurate, dependable computational techniques are required for efficient laminar flow wing design. This requirement obviously includes the effects of viscosity through boundary-layer solutions. Computational analysis and design may be more important for laminar flow wings than for conventional wings. This arises from increased sensitivity of design objectives to viscous effects and the limitations of conventional wind tunnels to accurately account for Reynolds number effects. Computer codes proposed to be used in this area must be rigorously validated by correlations with experimental data. State-of-the-art linear and nonlinear potential flow analysis methods have proven to be sufficiently accurate for laminar flow types of wing design application. Euler equation and Navier-Stokes equation solvers should be more accurate, but they are in the early stages of development. An inviscid technique must be coupled to three-dimensional boundary-layer solvers to yield truly reliable results. Both the coupling of the viscous and inviscid solvers and the accuracy of the viscous solvers are critical and for the most part are not adequately validated. Codes such as the TAWFIVE code, reference 1, are showing encouraging results but do require more extensive validation.

Automated design techniques will be relied upon to augment conventional design procedures. It is envisioned that design techniques will be a useful guide in making minor modifications to a wing to alleviate adverse three-dimensional effects. Codes which allow systematic contour changes to yield specified surface pressure distributions are ideally suited for this application. Exploitation of the capability of codes such as the NYU design code, reference 2, is encouraged. These extensions include spanwise and chordwise constraints on surface modifications, improved leading-edge treatment, and improved viscous interactions. Boundary-layer codes need to be validated by comparison with experimental data as do codes which predict the transition and stability. In general, for wing applications, boundary-layer codes have been relied upon to predict first-order viscous effects. However, the accuracy of these predictions becomes more important when stability calculations must be relied upon. The sensitivity of inviscid and viscous interactions must be investigated in the light of their influence on transition.

Systems and Operational Considerations

One cannot address wing design considerations without addressing the practical aspects of system integration and operational concerns. A high-lift system will have to be incorporated into a wing design if wing size and weight are to be minimized. This may dictate leading- and trailing-edge devices. Consequently, the effect of a leading-edge device on laminar flow will have to be addressed. To achieve desired benefits of laminar flow, a novel leading-edge device or leading-edge suction system may be required. Each of these has cost, weight, structural, and performance trade-offs to be considered.

Operational considerations involve the practicality of keeping the wing surface free from contamination which would adversely affect laminar flow. This could possibly involve surface coatings, anti-icing systems, anti-insect systems, or the use of special materials. Again, trade-offs must be considered based on such factors as cost, complexity, and maintenance.

Goals

Long- and short-term goals are identified below for the achievement of increased capability in the design of wings with significant extents of laminar flow.

1. Increased experimental data base for boundary-layer transition studies on

    Disturbance interaction, TS, CF(cross flow), noise

    Surface quality and finish

    Wing/body juncture flow effects

2. Development of airfoil sections with good laminar and turbulent characteristics over a wide range of flight conditions.

3. Experimental data to help understand the effect of fences, vortex generators, and leading-edge extensions on boundary-layer transition.

4. Experimental data to validate three-dimensional boundary-layer codes.

5. Development of efficient Euler codes coupled with viscous solvers and Navier-Stokes codes for two- and three-dimensional applications.

6. Development of robust and efficient automated wing design procedures.

7. Integration techniques which do not degrade laminar flow for

    High lift systems

    Anti-icing or anti-insect systems

    Hybrid laminar flow systems

References

1. Melson, N. D.; and Streett, C. L.: TAWFIVE: A User's Guide. NASA TM-84619, September 1983.

2. Bauer, F.; Garabedian, P.; and McFadden, G.: The NYU Inverse Swept Wing Code. NASA CR-3662, January 1983.

II. NLF Airfoil Design, Analysis, and Testing

Background

NASA and its predecessor, NACA, have been involved in airfoil research almost continuously since 1938. During the 1930's and early 1940's, NACA developed the well known and widely used NACA 4- and 5-digit turbulent airfoil sections. Also, during this same period and into the late 1940's and the early 1950's, NACA developed the low-drag 1- through 7-series airfoils. The most successful of these low-drag series are the 6-series which are used on many aircraft today. During most of the 1960's and the early 1970's, NASA discontinued the airfoil development effort. With the introduction of the supercritical airfoil concept by Dr. R. T. Whitcomb, the development of a new family of high-speed transonic airfoils was undertaken. This effort also led to the development of a new series of highly aft-loaded airfoils known as the GA airfoils. These GA airfoils were designed to have improved climb lift-drag ratios and high maximum lift, and they had mostly turbulent boundary layers. Since 1970, NASA has also developed four new low-drag natural laminar flow (NLF) airfoil sections. These NLF airfoils have many of the same performance characteristics of the earlier NACA low-drag sections but were designed to have broader drag buckets and higher maximum lift coefficients. The designers of the earlier NACA low-drag sections relied primarily on experimental trial-and-error methods to obtain sections with the desired characteristics. Today's designer has available several very accurate and highly reliable computer programs to help optimize the airfoil performance characteristics. These programs included subsonic design and analysis methods such as those found in the Eppler and MCARF programs and transonic methods such as those found in the KORN, GRUMFOIL, and TRANSEP programs. Several excellent boundary-layer stability and transition prediction programs are also available to aid the design of NLF airfoils which have large regions of laminar flow.

Recommendations for Additional Research

The newly developed NLF airfoils have rather large regions of laminar flow over both upper and lower surfaces. This laminar flow is obtained by shaping the airfoil to have very favorable pressure gradients over most of the forward portion of the airfoil. This produces airfoil shapes with the maximum thickness locations more rearward than those of conventional turbulent airfoils. The need for a rapid recovery of the pressure from the maximum thickness location to the trailing edge results in thin highly cambered aft thicknesses which produce considerable regions of separated flow at the off-design conditions. This separation can be controlled with the incorporation of a small-chord plain flap commonly referred to as a "cruise flap". Most of the newly developed NLF airfoils have been tested equipped with a cruise flap. A systematic research program needs to be conducted to determine the optimum size of the cruise flap. Additional experimental research is needed to obtain a set of test data on an NLF airfoil equipped with both single- and double-slotted trailing-edge flaps and Kreuger-type leading-edge devices. Experimental research is also needed to determine the effects of airfoil surface irregularities such as forward- and aft-facing steps, gaps, waviness, and roughness on the laminar transition characteristics of a typical NLF airfoil. The FAA has indicated the probable need to certify an aircraft with large extents of laminar flow with the laminar regions tripped to produce turbulent flow. Methods for tripping the flow during tests on small-scale wind-tunnel models are well established, but there are not established methods for tripping large-scale free-flight models. Experimental research is therefore needed to determine the proper size and material needed to trip the laminar boundary layer on large-scale aircraft.

III. Design Considerations for Laminar Nacelles

This section is concerned with defining what additional information would be useful for designing a nacelle having a large percentage of laminar boundary-layer flow on its external surface. The FAA certification requirements for a laminar flow nacelle would be the same as those which currently apply to nacelle designs in verifying adequate engine operation throughout an aircraft operating envelope.

In general, engine nacelles are either placed in front of the wing or located on the aft fuselage. The placement forward of the wing allows the nacelle to operate in a relatively undisturbed flow field and improves the possibility for attaining an extended run of natural laminar flow on the forward cowl. The aft-fuselage-mounted nacelle is located in a complex flow field influenced by the wing and fuselage and has a greater probability of needing suction to maintain the laminar boundary layer than a forward-mounted nacelle.

Areas in which theoretical and experimental research is required in order to provide guidance for laminar flow nacelle design are as follows:

NOISE

1. The extent to which the laminar boundary layer is affected by engine inlet and exhaust noise must be determined.
2. For aft-mounted nacelles, the noise originating from the turbulent fuselage boundary layer is a consideration in maintaining laminar flow on the nacelle. Data are required on these fuselage boundary-layer effects together with the influence of riblets and/or large-eddy breakup devices which may be applied to the fuselage.

PRESSURE GRADIENTS

1. The beneficial effect of decreasing surface pressure on maintaining control of the laminar boundary layer is well established; however, determining the extent to which a favorable pressure gradient can be designed into a nacelle cowl, while maintaining an adequate lip shape for cross-wind and high-angle-of-attack operating conditions, requires additional test data.
2. The nacelle angle of attack at which cross-flow instability becomes a limitation on maintaining laminar flow must also be determined experimentally.
3. The development of analytical methods for determining the laminar boundary-layer stability limits on bodies at small angle of attack should also be pursued.

LAMINAR FLOW CONTROL

1. Experimental test data are needed to describe the suction required for maintaining a laminar boundary layer on a nacelle located in a flow field representative of an aircraft mounting.
2. Analytical methods should be extended to enable the calculation of suction required to maintain a laminar boundary layer on a body, such as a nacelle, at realistic incidence angles.

IV. Performance and Stability and Control Considerations

Performance

Flight and wind-tunnel natural laminar flow (NLF) experiments have shown that significant regions of NLF can be achieved on modern aircraft designs, and that the boundary-layer behavior is more persistent and durable than previously expected. In recent years, there have been significant performance improvements in general aviation and business aircraft from the realization of increased amounts of natural laminar flow. This result was achieved in part through advanced NLF airfoil design, modern construction materials and fabrication techniques, and bonded aluminum skins. In addition, there have been design trends toward unconventional aircraft arrangements incorporating unusual features such as canards, tandem wings, and multiple-surfaces to obtain performance gains. Preliminary results suggest that the use of some of these features provides weight savings, improved cabin layouts, and improved aerodynamic characteristics which can provide significant performance benefits and increased overall operating efficiency and utility. Although the advanced aircraft designs with new technology features and modern construction techniques appear very promising from performance considerations, information on the aerodynamic characteristics of NLF configurations, particularly those with strong flow-field interactions, is very limited. For this reason, several system studies and wind-tunnel investigations have been undertaken to provide a technology base for evaluating the aerodynamic characteristics of the advanced NLF designs.

Stability and Control

The results of early tests have shown that while all configurations incur drag penalties due to loss of NLF, some configuration and airfoil combinations are subject to changes in lift performance and stability and control. For example, flight measurements from several aircraft types have indicated that transition from laminar to turbulent conditions increased cruise drag as much as 24 percent, decreased maximum trimmed lift coefficient as much as 27 percent, and decreased the lift-curve slope as much as 13 percent. Stability and control of conventional designs appear to be less sensitive to the changing of laminar to turbulent boundary-layer conditions than on some of the advanced canard configurations. Changes in airspeed and altitude and/or changes in surface conditions such as roughness due to insect strikes, local repair, rain effects, or weathering of surfaces can cause surface boundary layers to change from laminar to turbulent conditions. On some laminar flow airfoils, fixed transition near the leading edge can cause flow separation near the trailing edge and consequently a reduction in lift and control effectiveness. Water spray simulating heavy rain has also been found to cause separation patterns similar to that observed by fixing the boundary-layer transition near the wing leading edge.

At low Reynolds numbers, laminar separation of the boundary layer on thick airfoils can cause abrupt and significant lift losses and changes in airplane stability and control. With changes in airspeed and angle of attack, a dynamic lag effect may be introduced between the airfoil aerodynamics and the airplane motion which may severely alter the dynamic stability and control characteristics of the aircraft. On newer NASA-designed laminar flow airfoils, the objective is to have boundary-layer transition move slowly and steadily toward the leading edge with increasing angle of attack and thereby reduce the impact on dynamic stability and control.

The significant changes in performance and handling qualities, which could occur as the result of loss of laminar flow on some NLF configurations, suggest that both fixed and free transition tests be conducted for any airplane with surfaces smooth enough to support natural laminar flow. Model dynamic tests and airplane flight tests of configurations having extensive laminar flow will provide insight to the severity of such effects, particularly under dynamic conditions. These tests should address both symmetric and asymmetric transition of surfaces.

NLF and Spin Resistance

Lateral stability and controllability at the stall of typical general aviation airplanes with unswept wings are characterized by the tendency of such wings to experience separated flow, which can lead to unstable damping in roll and autorotation near the stall. One approach for providing improved spin resistance of general aviation aircraft is to provide means of eliminating or postponing autorotation to higher angles of attack. One such means is the use of a leading-edge modification to maintain attached flow on the outer wing panels. Such a concept has been shown to be effective on a number of existing aircraft, and recent research has indicated promising results for leading-edge modifications on advanced high-aspect-ratio wing designs employing NLF airfoils. A second approach for providing spin resistance is to use multiple lifting surfaces with the pitch control surface designed to stall before the main wing does and to limit vehicle angle of attack so that the main wing cannot be stalled. Both canard and three-surface configurations embodying this concept are under development. For low and moderate angles of attack, the performance benefits of NLF will be available. At high angles of attack near stall, however, all configurations transition to turbulent and separated flow. Because stalling and spinning involve mostly separated flow, no fundamental differences in departure/spin characteristics are anticipated for NLF configurations, and the current approach to investigating stall/spin characteristics is considered to be generally adequate.

Although NLF wings are not generally expected to experience stall/spin characteristics of unusual nature, there are some transition patterns of NLF airfoils wich may produce stability, control, and trim changes and, in turn, affect the onset of stall. For example, near stall angles of attack, flow transition for some airfoils can affect the magnitude of the maximum lift coefficient and, therefore, affect the airplane stall speed. For conventional configurations, the wing aerodynamics dominate the stall, departure, and spin resistant characteristics. For canard and other multiple-lifting-surface configurations, the forward wing (canard) pitch aerodynamics dominate the aircraft stall/departure limiting characteristics. For multiple-lifting-surface designs, pitch-up and deep stall are the primary high-angle-of-attack concerns. The large moment arms in multiple-lifting-surface configurations amplify the effects of lift changes on longitudinal stability characteristics. The initial results of wind-tunnel investigations indicate the importance of recognizing the strong aerodynamic interactions that can result from placing control surfaces or propulsion systems in unconventional locations.

Wing leading-edge modifications have proven very effective for improving the high-angle-of-attack aerodynamics and spin resistance of conventional and unconventional airplane configurations. Model tests of advanced configurations having high aspect ratio wings designed for extensive regions of natural laminar flow have indicated similar potential benefits for increased spin resistance through proper wing leading-edge design. Adoption of higher aspect ratio planforms, along with natural laminar flow airfoil sections, requires a further look at leading-edge design. Limited model tests indicate that multi-segment discontinuous leading-edge droops may be needed to maximize spin resistance of high aspect ratio wings. Achievement of laminar flow over the drooped sections is possible if the droop sections are themselves natural laminar flow airfoil shapes. Tests of a series of wings of varying aspect ratio having both conventional and natural laminar flow airfoil sections are currently under investigation, and the results will provide the initial data base for future designs.

In summary, recent aerodynamic research on advanced designs has revealed significant performance improvements in general aviation and business aircraft from the realization of increased amounts of natural laminar flow. This result was achieved in part through advanced NLF airfoil design and modern construction materials and fabrication techniques. The research also showed that all configurations incurred drag penalties due to loss of NLF and that some configurations and airfoil combinations were subject to change in lift performance and stability and control. Conventional configurations appear to be less sensitive than advanced canard or multi-surface configurations to changes in stability and control from laminar to turbulent boundary-layer transition. For canard and other multiple-lifting-surface configurations, results of recent research have shown the importance of recognizing the strong aerodynamic interactions that can result from placing propulsion systems or control surfaces in unconventional locations. The use of wing leading-edge modifications, such as leading-edge droop, may be required to offset undesirable high-angle-of-attack aerodynamic effects and improve stall/spin resistance of advanced general aviation design. Recent test results pointed out that increased stall departure resistance of advanced configurations could be achieved with mimimum NLF degradation through the use of a properly designed discontinuous wing leading-edge droop.

Proposed NLF Aerodynamic Research

From a review of recent NLF aerodynamic research needs and an assessment of the impact of NLF on performance, stability and control, and stall departure/spin resistance of current and advanced aircraft, it appears that near- and far-term NLF research plans should include activities in the following areas:

1. Continue advanced-configuration aerodynamic research on conventional and unconventional configurations, including studies of the effects of aft-mounted engine locations.

2. Continue theoretical and experimental NLF airfoil development with specific applications to wings of increased aspect ratio.

3. Place emphasis on theoretical and experimental development of stall/spin resistant NLF wings incorporating the discontinuous wing leading-edge droop.

4. Conduct research on the unsteady aerodynamics associated with possible lag effects between boundary-layer transition and airplane motion.

5. Conduct aerodynamic control research on advanced NLF airfoils with activities directed at spoiler and conventional aileron control.

6. Continue research on methods of achieving protection from insects such as that obtained with porous, fluid-exuding wing leading edges on aircraft.

7. Conduct full-scale wind-tunnel and flight-test experiments to validate performance, stability and control, and stall departure/spin resistance characteristics of advanced NLF airplane configurations.

V. Manufacturing Tolerances for Laminar Surfaces

Modern metal and composite airframe manufacturing techniques can provide surface smoothness which is compatible with requirements for natural laminar flow (NLF). Surface smoothness requirements for NLF refer to (a) waviness, (b) two-dimensional steps and gaps, and (c) three-dimensional roughness elements. The present consensus on requirements for these potential disturbances to NLF will be summarized and used as a starting point for recommendations for future work in this area. The only impact of manufacturing tolerances in the certification of laminar flow aircraft involves quality control in production and long term maintenance of the laminar surfaces.

Present Knowledge of Effects of Manufacturing Tolerances for NLF

Extensive cooperation between the general aviation industry and NASA has resulted in an improved understanding of requirements for the achievement of NLF on modern, smooth airframe surfaces. The following discussion reviews these requirements.

Waviness

Waves on a laminar surface cause local changes in pressure gradients, and if these waves are of sufficient magnitude, they can cause laminar separation. Reference 1 provides criteria for allowable wave height-to-length ratios to avoid premature transition for waves over swept and unswept surfaces. References 2 and 3 indicate that, in general, measured waviness over certain modern practical airframe surfaces is compatible with NLF requirements for many subsonic aircraft. (See figure 1.) The impact of a surface wave on the stability of the laminar boundary layer strongly depends on the slope of the potential-flow pressure gradient and the effect of compressibility on the boundary-layer flow (ref. 4). The existing waviness criterion (Carmichael, X-21A criterion (ref. 1)) is empirical in nature and only crudely accounts for these effects.

Two-Dimensional Steps and Gaps

The effect of steps and gaps in a laminar surface is to cause local laminar separation regions which cause pressure gradient disturbances and boundary-layer velocity profile inflections. These changes affect laminar flow stability. The critical step height or gap width to induce premature transition is expressed in a critical Reynolds number, $R_{h,crit}$. Historically, $R_{h,crit}$ has been determined for regular square-edged steps. A powerful method to increase $R_{h,crit}$, and thus to increase the allowable step height, is to shape the step to alter or prevent formation of separation bubbles associated with the step (ref. 5). Recent numerical and flight-test experiments at NASA Langley show a potential of shaping forward-facing steps to reduce the induced adverse pressure gradient (ref. 6). The existing criteria do not accurately account for pressure gradient, sweep, and compressibility effects.

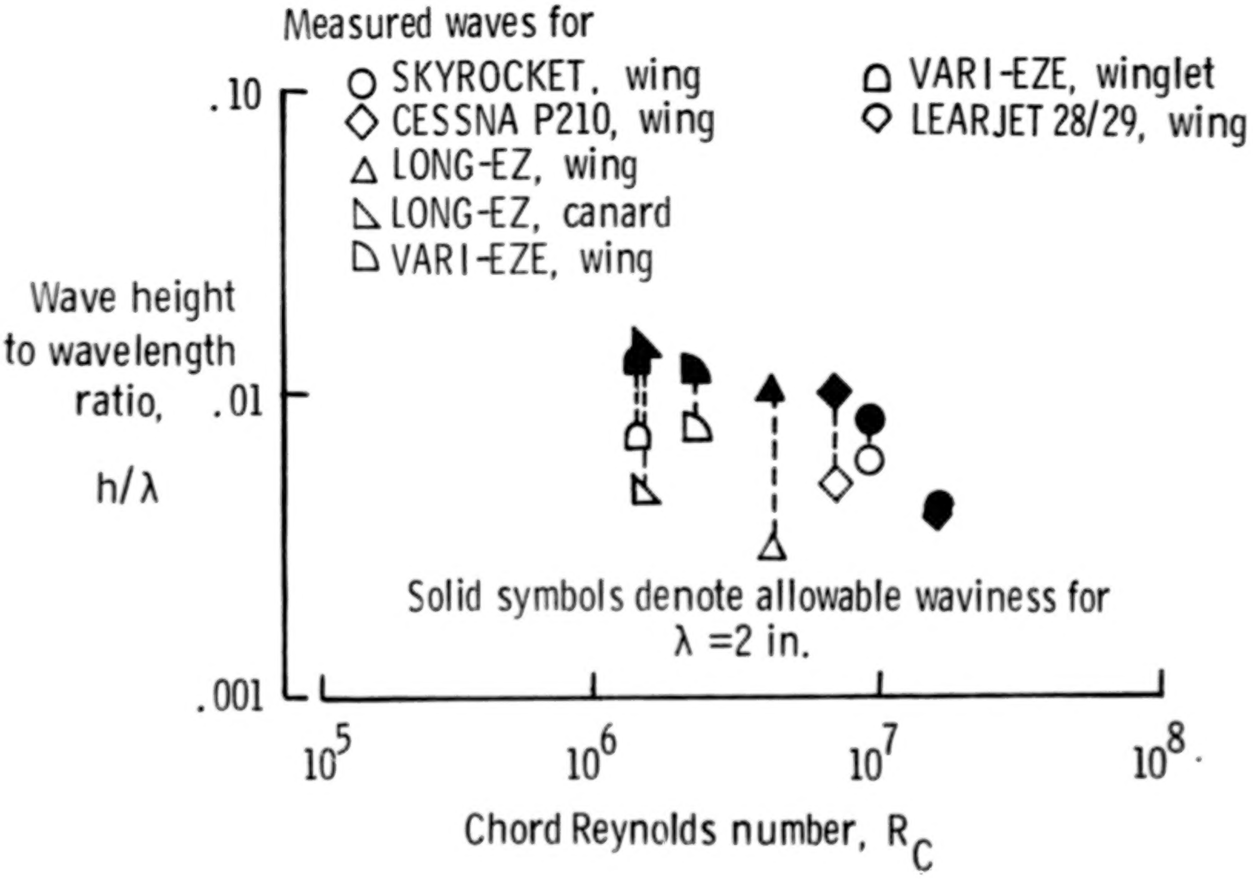

Figure 1. Comparison of allowable and actual waviness measured on airplanes used for NLF flight experiments (ref. 1).

Three-Dimensional Roughness Elements

Three-dimensional roughness elements (related to manufacturing tolerances) can take the forms of rivet heads, screw slots, and surface erosion, among other causes. These roughness elements shed vorticity into the laminar layer which can cause sustained transition to turbulence. The effect of three-dimensional roughness elements on disturbing NLF is expressed in a critical Reynolds number based on roughness height. References 6 and 7 present simplified methods to determine the critical roughness height for given flow conditions on both 2-D and 3-D (e.g., fuselage) surfaces. References 8 and 9 summarize major experiments to determine the effect of particular roughness elements. Past research has dealt primarily with roughness elements of various shapes which protrude above the surface; little data are available on "roughness" in the form of slots or holes below the surface, such as caused by screw slots.

In summary, a limited but practical data base exists today for waviness and two- and three-dimensional roughness elements. This data base can provide the manufacturer of NLF surfaces with conservative estimates for allowable roughness and waviness in extensive runs of laminar flow. Areas for future work in this area will be discussed next.

Need for Future Work

The previous discussion identified the limitations in the data and criteria available for determination of NLF manufacturing tolerances on waviness, two-dimensional roughness (steps and gaps), and three-dimensional roughness.

Needs for research will be formulated in the areas of both fundamental and applied research.

Waviness

(1) Fundamental Research Areas:

- a. Analysis of the laminar boundary layer over single and multiple waves.
- b. Analysis and verification of the transition process over single and multiple waves.
- c. Effect of sweep, compressibility and pressure gradient, and Reynolds number on the stability and the transition process.
- d. Effect of three-dimensional surface waves on the stability and transition process over axisymmetric and non-axisymmetric fuselages and nacelles.

(2) Practical Research Areas:

- a. Measurement of static waviness of existing fuselages and nacelles.
- b. Waviness of windshields of pressurized fuselages under pressurization loads.

c. Waviness of lifting and nonlifting surfaces under flight loads.

Two-Dimensional Steps and Gaps

(1) Fundamental Research Areas:

a. Application of numerical analysis (Navier-Stokes solution) combined with experimental research to define practical shapes of steps and gaps that will not lead to laminar separation in the step area.

b. Further development of an understanding of the transition process to predict laminar reattachment of the separation bubble on top of the step. Laminar reattachment can possibly lead to a relief in the constraints resulting from the laminar separation criterion.

c. Effect of compressibility on laminar boundary-layer development and stability in the step area.

d. Effect of sweep (up to 90° relative to the local potential flow streamline) of two-dimensional steps and gaps on the stability of the laminar boundary layer.

e. Effect of steps and gaps in swept wings on crossflow stability.

f. Effects of coupling of acoustic disturbances with laminar boundary-layer stability over steps and gaps.

g. Establishment of tolerances for steps and gaps in a three-dimensional surface (e.g., a fuselage nose).

(2) Practical Research Areas:

a. Impact of erosion of desired optimal shapes of steps over a period of time even though erosion might lead to more favorably shaped steps.

b. Change of step size (and step shape in cases of complicated shapes, see ref. 5) under loaded conditions and varying temperatures.

c. Investigations of the size and shape of practical steps for doors, windows, hatches, etc.

Roughness Elements

(1) Fundamental Research Area:

a. Numerical analysis to model laminar flow over three-dimensional roughness shapes in three-dimensional compressible flow.

(2) Practical Research Areas:

a. Investigation of the conditions for which rivets pose a problem to the achievability of a laminar boundary layer.

b. Extension of older data to include roughness elements such as screw heads, vent holes, panel access openings, paint chips, and lettering.

c. Investigation of erosion characteristics of three-dimensional roughness elements over a period of time.

d. Investigation of practical kinds of impact damage and the effects of scratches, dents, etc., on the maintainability of laminar flow.

In summary, a wider numerical and experimental data base on the manufacturing disturbances must be established that will provide guidelines in the design, maintenance, and operational stages of an airplane with extensive amounts of NLF.

Certification Concerns Related to Manufacturing Tolerances

Concept of Laminar Flow Surface Zoning

The sensitivity of NLF to surface imperfections depends on the location and geometry of the imperfection; that is, it depends on the history of the laminar boundary layer and the local pressure gradient. Accordingly, zoning of airframe surfaces to account for sensitivity of the laminar boundary layer can be used to indicate the maximum allowable size of each kind of surface imperfection on various portions of a laminar airframe. Manufacturing techniques that satisfy these requirements will result in surfaces over which laminar flow can be achieved at minimum cost. For a well-designed laminar surface, i.e., a surface with a predetermined aerodynamic tolerance to a moderate violation of the surface smoothness, emphasis is then placed on quality control and maintenance of the production technique.

Maintenance and Damage Tolerance

Following this zoning concept, maintenance and damage tolerances can be established for the different zones. Extensive repairs in critical NLF areas (i.e., generally in the nose region of NLF surfaces) might require a flow-visualization test to estimate the amount of NLF that can be attained in the condition for the highest unit Reynolds number of interest. A standardized means for determination of surface waviness and roughness following repairs may be useful.

Conclusion

The only impact of manufacturing tolerances in the certification of laminar flow aircraft involves specific quality control in the production of the laminar surfaces and maintenance of the production technique over the course of time. Damage tolerance and repair maintenance procedures for well-designed zoned laminar surfaces should be included in the Pilots' Operator Manual (POM) to enable the pilot to take the full benefit of natural laminar flow.

References

1. Holmes, B. J.; Obara, C. J.; Martin, G. L.; and Domack, C. J.: Manufacturing Tolerances for Natural Laminar Flow Airframe Surfaces. SAE Paper 850863, April 1985.

2. Holmes, B. J.; Obara, C. J.; and Yip, L. P.: Natural Laminar Flow Experiments on Modern Airplane Surfaces. NASA Technical Paper 2256, June 1984.

3. Holmes, B. J.; and Obara, C. J.: Observations and Implications of Natural Laminar Flow on Practical Airplane Surfaces. Journal of Aircraft, Vol. 20, No. 12, December 1983.

4. Obara, C. J.; and Holmes, B. J.: Flight-Measured Laminar Boundary-Layer Transition Phenomena Including Stability Theory Analysis. NASA Technical Paper 2417, April 1985.

5. Holmes, B. J.: Geometries for Roughness Shapes in Laminar Flow. Patent Application (NASA) NASA-Case-LAR-13255-1.

6. Braslow, A. L.; and Knox, E. C.: Simplified Method for Determination of Critical Heights of Distributed Roughness Particles for Boundary-Layer Transition at Mach Numbers from 0 to 5. NACA Technical Note 4363, August 1958.

7. von Doenhoff, A. E.; and Braslow, A. L.: The Effects of Laminar Flow, Boundary Layer and Flow Control, Its Principles and Application. Lachmann, G. V., ed. Pergamon Press, 1961.

8. Tani, I.: Effects of Two-Dimensional and Isolated Roughness on Laminar Flow, Boundary Layer and Flow Control, Its Principles and Application. Lachmann, G. V., ed. Pergamon Press, 1961.

9. Young, A. D.; Paterson, J. H.; and Jones, J. L.: Aircraft Excrescence Drag. AGARDograph No. 264, July 1981.

VI. Environmental Effects on Laminar Flow Aircraft

The most important environmental effects on laminar flow aircraft appear at this time to be to surface frost and ice, moisture due to rain or condensation, insect contamination, and acoustic noise.

Frost and Ice

Frost and ice problems are, of course, not unique to laminar flow wings but have been and are continuing to be researched on "turbulent flow" sections. Research areas which apply specifically to laminar flow that need to be addressed are 1) Do laminar flow airfoils accrete ice or suffer a performance penalty due to ice any differently than other airfoils? 2) How does the residual ice after the use of deicing system affect laminar flow? 3) How can ice protection systems be designed so as not to trip the laminar flow due to irregularities?

Rain

All rain effects are not well understood. Heavy rain problems on transport-type wings are currently being explored. This research needs to be extended to laminar flow profiles. The mechanisms of the beading of rain drops on an airfoil surface or the waviness in a surface water film can cause early boundary-layer transition. More work is needed in this area to better understand the surface physics involved and to study the design of airfoils which suffer no lift penalty due to rain or other roughness effects.

Insects

Insect contamination presents an operational problem for laminar flow aircraft. An encouraging recent development is the use of a weeping fluid anti-icing system on take-off and landing to reduce insect contamination. More work in the area of insect contamination protection is needed to support this effort. More fundamental research on the effect of 3-D roughness near the stagnation point of an airfoil to include insect accretion data would aid in the development of insect contamination numerical simulations. Little research in this area has been conducted since the 1950's, and with some additional research, perhaps ways can be found to reduce airfoil sensitivity to insects and improve the operational efficiency of laminar flow aircraft.

Noise

One of the significant problems in the maintenance of laminar flow was determined during the X-21A Laminar Flow Control Demonstration Program to be the adverse effect of the aircraft's own noise in causing premature transition. These and other succeeding studies have pointed out the need for the development of better understanding and improved prediction methods, both for cruise noise prediction and laminar flow acoustic criteria.

Noise is a part of the environment that accompanies the aerodynamic surface over which laminar flow is desired unlike free-stream turbulence and insects, which reduce in intensity with increasing altitude. Some progress has been made in the analytical development of sound-induced transition; these models, which predict critical sound pressure level spectra, require refinements and validation under idealized and practical environments.

Steps and gaps are known to cause premature transition for dimensions exceeding certain critical values. Specification of such critical dimensions is important in specifying manufacturing tolerances. It is also believed, but not firmly proven, that the critical dimensions of steps and gaps may be a function of the acoustic field. This is due to possible generation of acoustically induced vorticity in the vortical flow field ahead of and behind a step and inside a gap.

The recommendations for improvement in the laminar flow acoustic criteria are as follows:

1. Initiate and support noise prediction programs for laminar flow applications.

2. Support development and refinement of noise and boundary-layer disturbance coupling analyses in idealized and practical laminar flow applications.

3. Initiate and support an experimental program to validate items 1 and 2 above. Additionally, this will provide an experimental data base on critical sound pressure spectra on smooth and practical surfaces.

4. Initiate a program for the study of the impact of noise on critical roughness dimensions in the maintenance of laminar flow.

VII. Propeller Slipstream

Recent flight, wind tunnel, and analytical investigations have documented the behavior of the laminar boundary layer on surfaces immersed in propeller slipstreams. The results showed that some of the benefits of laminar drag reduction can be achieved in propeller slipstreams. These investigations were conducted on two- and three-bladed propellers at moderate to low disk loadings representative of general aviation propeller operating conditions. The aerodynamic research working group recommendations focused on expanded investigations of NLF behavior in slipstreams behind more highly loaded propeller disks (e.g., multibladed counterrotating propellers) and on other surfaces such as engine nacelles and fuselages. These recommended R&D needs are viewed not as directly related to NLF aircraft certification, but rather as research needed to facilitate NLF applications.

VIII. Boundary-Layer Transition

The design of laminar flow airfoils, wings, nacelles, and bodies is critically dependent on the "intelligent" use of flow stability methodology. Three types of instability are of concern: Tollmien-Schlichting (T-S) waves, crossflow (C-F), and Taylor-Görtler (T-G) vortices. For most aerodynamic configurations, only the first two are of concern, since the T-G instability only becomes a factor where the surface is concave and the fluid is subjected to centrifugal effects. Many airfoils have a slight concavity near the trailing edge, e.g., the underside of aft-loaded supercritical airfoils, but normally the flow is already turbulent due to the earlier onset of an unfavorable pressure gradient, and they pose no stability problem. Airfoils with an undercut leading edge (ref. 1) may well have T-G vortices that originate in the concave region unless one applies suction. For large concavities, geometric tailoring may also be required to maintain laminar flow through and beyond it. Suction is applied largely to maintain attached flow over the compression half of the concave region. While suction has a stabilizing influence on T-G vortices, large levels may be required to accomplish an appreciable stabilization of the flow. Geometric control has been attempted by dividing the curved surface into a series of flat segments connected by small-radius arcs. The hope was that the integrated amplification over a given turning angle could be minimized by making the radius of curvature of the arcs as small as possible. (See later subsection for more detailed discussion of Taylor-Görtler instability.)

Another concern in the design of laminar wings is "leading-edge contamination." This is the terminology used when the flow becomes turbulent along the attachment line of a swept leading edge. It occurs when the turbulent boundary layer on the fuselage moves out along the swept leading edge or when the spanwise flow along a leading edge becomes turbulent. Accelerating the flow rapidly from the attachment line to keep the momentum thickness Reynolds number on the attachment line to values less than 100 has been found (ref. 2) to be necessary to avoid the latter difficulty.

Determination of Transition

Linear theory provides a method of determining the amplitude of a disturbance relative to the disturbance amplitude at the neutral point. The natural logarithm of this ratio is termed the amplification, or n-factor, and when this quantity reaches a value on the order of 10, the conventional wisdom is that one can expect transition to occur. In hostile wind-tunnel environments, the amplification factor at transition will be lower depending on the noise and vorticity levels as well as their spectral content. Mack (ref. 3) gives an empirical equation for the relationship of the n-factor with onset flow disturbance level.

A wide range of numbers have been suggested for the amplification factor; flight data on the King Cobra (ref. 4) have yielded values as high as 18 when analyzed for the T-S type of transition using the Sally code (ref. 5) . However, a word of caution regarding the interpretation of n-factor results is in order. The significance of linear stability results, especially those using the parallel flow assumption, in the latter stages of the transition process is unclear. The final stages of transition are nonlinear; the mean flow is nonparallel, and boundary-layer/inviscid flow interactions do not properly account for the transition process. Linear stability calculations will often show a rapid increase in the n-factor near the experimentally determined transition point. Thus, over a very short chordwise distance, the n-factor may jump for example from 6 to 8 up to 20 or 25. However, this does not imply that these large numbers should be accepted as "calibrated" n-factors and used in design. This is especially true in laminar-flow-control applications when some type of control mechanism is used to retard the growth of disturbances. In such situations, "limiting" n-factors in the range of 6 to 8 are employed. For swept wings, interactions of T-S and C-F disturbances may require that the allowable n-factors be lowered still further.

It is well known that the location of transition may frequently coincide with the point of laminar separation. Certainly this is most likely to occur at low Reynolds numbers and high C_L values and when there are long runs of laminar boundary layer terminated by a rapid onset of the pressure recovery. In many cases the laminar separation will be followed by almost immediate attachment (a small separation bubble), and it is difficult to know whether the flow becomes turbulent because of the natural growth of a disturbance in the attached boundary layer or because of the destabilizing effect of a thin small separation bubble.

Tollmien-Schlichting Instability

The original concept of flow instability goes back to O. Reynolds in a Royal Society paper of 1895. A few years later, Lord Raleigh and L. Prandtl and his associates started to put those ideas on a firm mathematical basis and identified the importance of inflection points in stability. While A. Sommerfeld was the first to attempt a viscous stability calculation, it was left for Tollmien to put together a physically consistent solution (ref. 6). Schlichting is credited with a number of important contributions to stability theory including various extensions of Tollmien's two-dimensional linear perturbation analyses. All of the stability methods currently in regular use depend on small perturbation linear stability theory.

Stability analyses pertaining to T-S waves have progressed steadily in capability and complexity during the past 8 to 10 years. Two-dimensional incompressible parallel codes have been replaced in an evolutionary way by three-dimensional compressible parallel and nonparallel codes (refs. 5 and 7-14). Numerous investigations have shown that incompressible analyses yield faster disturbance growth rates than compressible analyses and that parallel analyses yield a slower growth rate than nonparallel analyses (refs. 9, 10, 15, and 16). In addition, our understanding through theory and experiment of the effect of the external environment on transition has greatly increased (ref. 17).

Present day T-S stability codes provide for the solution of the Orr-Sommerfeld equation or its compressible equivalent, which is derived, in turn, from a perturbation of the Navier-Stokes equation and the usual small-disturbance assumption. For compressible flow there is also an energy equation to contend with. In arriving at these equations, the flow is usually assumed to be parallel, i.e., the boundary-layer profiles at points surrounding the point being analyzed are the same. Both spatial and temporal disturbances can be assumed; however, spatial growth is considered by most analysts to be more appropriate for boundary-layer stability. The calculation of amplification rates requires the solution to an eigenvalue problem for either a fourth-order or a sixth-order system of ordinary differential equations, depending on whether the flow is incompressible or compressible. Actually the compressible stability equations are eighth order, but the neglect of the dissipation term and the correct choice of dependent variables reduce the system to sixth order. Typically a range of frequencies are analyzed for a specific wave orientation angle to obtain growth rates and amplitude ratios. The envelope of integrated growth rates is determined and when an amplitude ratio on the order of exp (10) is reached, transition is said to occur.

At incompressible speeds, the maximum amplification occurs in a direction very close to the potential flow direction. When compressibility becomes important, it is in the direction of the group velocity (ref. 9), which may be 40 to 60 degrees off to one side. Still, the low sensitivity of growth rate to propagation angle is such that a reasonable approximation is the potential flow direction.

Crossflow Instability

Wings with little or no sweep have been designed, built, and tested using this technology; several are in everyday service. Swept wing designs and tests requiring not only T-S analyses but crossflow have also been carried out (refs. 1, 18, and 19), but uncertainties in the coupling of crossflow with T-S instabilities have degraded the precision of predictions and the interpretation of results. Considerable research is in progress specifically aimed at improving our understanding of this important problem; some inroads have already been made (refs. 20-22).

Crossflow vortices, first identified by Gray (ref. 23), arise primarily on swept wings and in regions where there is a strong pressure gradient. These vortices all have the same sense of rotation and move in the general direction of the inviscid flow with very little change in spacing. Crossflow instabilities are unstable waves in a direction that is nearly 90° to the flow direction and result from the inflection point in crossflow profiles. Problems with C-F vortices usually arise as wing sweep is increased beyond 15°, but this can vary considerably depending on the pressure distribution and Reynolds number. Good design practice dictates that swept wing airfoil sections be configured to minimize the growth of C-F disturbances particularly in regions where the amplitude of T-S waves has become significant (refs. 19 and 24). In this way the various modes can be treated separately, and the coupling or interaction of the modes, which as we noted previously is not well understood, can be avoided.

As indicated earlier, the crossflow instability is associated with the so-called "crossflow" velocity profile. This is the profile of velocity components perpendicular to the local potential flow in the streamline direction and results from a three-dimensional pressure field such as that on a swept wing. By definition, the velocity in the crossflow direction must be zero both at the surface and at the outer edge of the boundary layer. Thus, a nonzero velocity profile must contain an inflection point, which in turn leads to a dynamic (or inviscid) instability. A low critical Reynolds number and relatively large amplification rates are typical of this type of instability. Furthermore, since suction cannot eliminate the inflection point in the profile (unless the whole boundary layer is removed), the crossflow instability is less amenable to control by suction than is the Tollmien-Schlichting instability.

There are three characteristic parameters in the crossflow stability problem: 1) frequency, 2) wavelength, and 3) wave orientation angle. Flow visualization studies have indicated the presence of essentially fixed wavelength, stationary crossflow vortices on swept wings. For a particular calculation, two of these three parameters may be specified, while the third parameter is a part of the solution along with the local amplification rate. A typical solution procedure consists of specifying a frequency (usually zero for stationary crossflow vortices) and a fixed wavelength with the wave orientation angle allowed to vary over the range of the calculation. The disturbance amplification for any point beyond the neutral point is determined as the running integral of the local amplification rate. This procedure must be repeated for a range of disturbance wavelengths to find the maximum amplified disturbance at the given frequency. It may also be necessary to consider a range of disturbance frequencies which correspond to moving crossflow vortices. Compressibility seems to have little effect on the vortex spacing or growth, with differences on the order of 10 percent from incompressible calculations being typical. El-Hady (ref. 10) indicates that C-F vortex spacing may grow slightly with increasing distance along the chord and in proportion to boundary-layer thickness.

Taylor-Görtler Instability

As noted earlier, Görtler vortices arise in boundary layers along concave surfaces due to centrifugal effects. Centrifugal instability in boundary layers was first treated analytically by Görtler (ref. 25), and many studies have since been devoted to the improvement and extension of Görtler's analysis (refs. 26 and 27). Several experiments have been conducted to observe the development and growth of Görtler vortices (refs. 28-30). In spite of these theoretical and experimental studies, there is a dearth of data to describe or explain the role of centrifugal instability on boundary-layer transition. Görtler vortices are stationary, grow in the streamwise direction, and distort the mean flow velocity profile that could make the boundary layer more unstable with respect to T-S waves. It is thus difficult to treat boundary-layer transition due to Görtler instability in isolation. Laminar boundary layers have been observed (ref. 30), even in the presence of large disturbances due to Görtler vortices. According to Wortmann (ref. 28) and Bippes (ref. 29), different types of instabilities follow the onset of the centrifugal instability but precede the burst of turbulence; the exact sequence of events is a function of the flow field geometry. The complexity of the process did not allow Bippes to define the transition Görtler number. Smith found that under ideal conditions, the amplitude of the vortices had to grow by a factor of exp (10), that is, an n-factor of 10, for transition to occur. This method is still the most widely used technique to predict boundary-layer transition along concave walls (ref. 31).

According to the existing literature, transition from laminar to turbulent boundary layer in the presence of Görtler vortices occurs in conjunction with one or more of the following:

1. Deformation by Görtler vortices of the mean flow field and induction of a spanwise variation in the boundary-layer thickness. This results in the development of velocity profiles having varying stability characteristics along the span and the consequent three-dimensional distortion of Tollmien-Schlichting waves (ref. 32).

2. Meandering motion of Görtler vortices before the breakdown of laminar flow (ref. 29).

3. Periodic formation of horseshoe-type vortices interconnecting the pairs of Görtler vortices (ref. 33).

Although a clear picture is yet to emerge, it could be reasonably concluded that any technique to predict transition in the presence of Görtler vortices should include the interaction of the Görtler vortices among themselves and with Tollmien-Schlichting waves. Higher eigenstates of Görtler vortices may well be important in laminar-turbulent transition (ref. 34). The presence of streamwise crossflow vortices only adds an additional dimension to an already complex flow situation. One of the first studies on the effect of streamwise vortices on Tollmien-Schlichting waves was reported by Nayfeh (ref. 20). Further research, theoretical as well as experimental, on this complex and challenging fundamental problem in fluid mechanics is very essential.

Enhanced Laminar Flow

There are several things that can be done to extend the run of laminar flow over a wing. Favorable pressure gradient is most often the remedy of choice for natural laminar flow, but at high Reynolds numbers, high sweep angles, and high cruise lift coefficients, it may be necessary to employ suction. Airfoils employing pressure gradient for flow stabilization have been used on production aircraft since the late 1930's; production aircraft with suction surfaces to promote the run of laminar flow have not yet materialized. Nevertheless, there have been several research aircraft tested that have demonstrated the feasibility of the concept (refs. 35 and 36). The recent test of an LFC supercritical airfoil in the Langley 8-Foot Transonic Pressure Tunnel and a leading-edge glove test on the Jetstar (refs. 1, 37, and 38) are indicative of renewed interest in the possibilities of LFC using the latest technologies in aerodynamics and structures. In the former test, spanwise suction slots were distributed over the top and bottom surfaces. Also of interest are combinations of LFC and natural laminar flow, usually termed "hybrid laminar flow," where suction is applied ahead of the wing box (and possibly behind), and pressure gradient is used over the wing box to reduce Tollmien-Schlichting wave growth.

It is well known that cooling the surface of a wing is another way of reducing the growth of disturbances and, thus, of obtaining longer runs of laminar flow or maintaining a given amount of laminar flow to higher Reynolds numbers (refs. 39-42). For subsonic, transonic, and possibly low-supersonic Mach numbers, cooling seems to stabilize the first T-S mode, which is the dominant mode. However, at higher supersonic Mach numbers, Mack (ref. 3) has shown that cooling apparently destabilizes the second and possibly higher T-S modes which come to dominate the first T-S mode. Several wind-tunnel experiments have been performed to obtain quantitative data, but like the LFC approach, no production aircraft have been built employing this technique.

Active Transition Control

There has been a surge of interest in the active control or retardation of transition with the successful water experiments of Liepmann and Nosenchuck (ref. 43). In their experiment, a heated strip, imbedded in the surface, was activated in a controlled manner to effectively cancel a two-dimensional disturbance induced upstream. Navier-Stokes simulations for air, using out-of-phase "sucking/blowing" (ref. 44) and "heating/cooling" (ref. 45), have indicated that there are control possibilities in air as well. The effects of sound have been examined experimentally by Maestrello with beneficial results (ref. 46). Whether any of these concepts yield practical flight systems should be of little concern at this time. We need to do much more research to find out what can and cannot be done in a laboratory environment.

Simulation

Another theoretical approach for determining transition is gradually emerging with the increasing power (speed and storage) of our supercomputers. That approach is the numerical simulation of transition using the time-dependent three-dimensional Navier-Stokes equations. A number of investigations have shown the efficacy of these simulations through comparisons with stability theory and detailed diagnostic experiments (ref. 47). These computations require computers with extremely large storage capacities because of the resolution required as one approaches a turbulent flow. Only low-speed (incompressible) results for flows in a channel or over a flat plate have been produced. Initial conditions are usually prescribed from the two-dimensional and three-dimensional eigen-solutions of the Orr-Sommerfeld equation.

Computers that are even faster and have considerably more storage than those now available will be coming on-line in the next few years to enable transition simulation about two-dimensional objects such as airfoils. With this, our understanding of the interaction between the various stability modes, the effect of the external environment, and the utility of a number of transition-control schemes can be examined and understood as never before.

Research Needs

Stability theory and boundary-layer codes now exist that take into account most of the important physics contributing to, or affecting the growth of, disturbances leading to transition. However, this only applies to instability modes which grow from the neutral stability point in the absence of other modes. Several analyses have shown that when two modes are assumed to exist simultaneously, they will have a double exponential growth (refs. 20, 21, and 48). We can expect then, without careful tailoring of pressure distributions to prevent Tollmien-Schlichting and crossflow or Tollmien-Schlichting and Taylor-Görtler disturbances from becoming large at the same time, to get earlier transition than linear theory predicts. The need clearly exists for an improved understanding of these interactions. Hopefully the F-14 laminar flow glove experiments, to be carried out this year, will provide this understanding as well as some empirical relationships for design (ref. 49). Theoretical attempts to solve this most difficult nonlinear problem are being made. Some hope is also provided by increasing ability to accurately simulate the transition process on our supercomputers, as noted in the previous section.

Most of the laminar boundary-layer codes used with three-dimensional stability codes are for an infinite span, yawed wing with a constant airfoil section across the span. Three-dimensional laminar codes exist, but the most accurate ones employ finite difference solution techniques. Interactive calculations of these codes with a high quality external inviscid flow code can be very time consuming and expensive. "Integral" three-dimensional boundary-layer codes, on the other hand, are very fast but do not seem to provide crossflow profiles with the necessary precision. The required understanding is available, and it is clearly feasible to formulate such a code.

Experiments aimed at the investigation of isolated instability mechanisms, as well as the interaction of one mode with another, are on the increase, but more are needed. Improvements in laser-system and thin-film gauge technology along with the advances in flow visualization techniques offer the possibility of measuring the onset and growth of the various instabilities with much greater precision than before (refs. 30 and 50). Of course, when these measurements are made, the quality of the surface (roughness and waviness) and the detailed characteristics of the environment must be determined. In connection with the latter, efforts to build diagnostic tunnels with "superquiet" test sections are well founded and should be increased.

Research needed in three additional areas is given below:

1. Receptivity

   Controlled free-stream disturbances should be introduced to examine their influence on boundary-layer disturbance generation and development. The theoretical researchers should strive to determine the types of free-stream disturbance which are important so that experimentalists can search for these specific types of disturbances.

2. Curvature Effects on Stability

   The first-order interaction of crossflow and centrifugal effects should receive both theoretical and experimental attention. The possible stabilizing effect of convex curvature on Görtler vortices should be evaluated. The vortex stretching problem in the leading-edge region should be examined.

3. Interaction of Transonic Shock With Laminar Boundary Layer

   The transonic shock interaction with the laminar boundary layer should be examined both theortically and experimentally. The theoretical examinations should include interacting outer flow and boundary-layer solutions, including stability computations. The influence of trailing-edge effects on the shock unsteadiness should be included. Suction surfaces with a large surface pressure drop and distributed suction which approaches area suction should be investigated.

Finally, there are a number of excellent papers which summarize the state of the art in boundary-layer stability and transition (refs. 51-53).

References

1. Harvey, W. D.; and Pride, J. D.: The NASA-Langley Laminar Flow Control Experiment. AIAA Paper No. 82-0567, 1982.

2. Poll, D. I. A.: Leading Edge Transition on Swept Wings. Laminar-Turbulent Transition. AGARD-CP-224, pp. 21-1 - 21-11, 1977.

3. Mack, L. M.: Transition Prediction and Linear Stability Theory. Laminar-Turbulent Transition. AGARD-CP-224, pp. 1-1 - 1-22, 1977.

4. Gray, W. E.: Transition in Flight on a Laminar-Flow Wing of Low Waviness (King Cobra). R. A. E. Report No. 2364, March 1950.

5. Srokowsky, A.; and Orszag, S. A.: Mass Flow Requirements for LFC Wing Design. AIAA Paper No. 77-1222, 1977.

6. Schlichting, Herman (J. Kestin, transl.): Boundary-Layer Theory. New York: McGraw-Hill Book Co., Sixth Edition, 1968.

7. Cebeci, T.; and Stewartson, K.: On Stability and Transition of Three-Dimensional Flows. AIAA Journal, Vol. 18, No. 4, pp. 398-405, 1980.

8. Nayfeh, A. H.: Stability of Three-Dimensional Boundary Layers. AIAA Journal, Vol. 18, No. 4, pp. 406-416, 1980.

9. Mack, L. M.: On the Stability of the Boundary Layer on a Transonic Swept Wing. AIAA Paper No. 79-0264, 1979.

10. El-Hady, N. M.: On the Stability of Three-Dimensional, Compressible Nonparallel Boundary Layers. AIAA Paper No. 80-1374, 1980.

11. Lekoudis, S. G.: Stability of Three-Dimensional Compressible Boundary Layers Over Wings With Suction. AIAA Paper No. 79-0265, 1979.

12. Malik, Mujeeb R.: COSAL--A Black Box Compressible Stability Analysis Code for Transition Prediction in Three-Dimensional Boundary Layers. NASA CR-165925, May 1982.

13. Malik, M. R.; and Poll, D. I. A.: Effect of Curvature on Three-Dimensional Boundary Layer Stability. AIAA Paper No. 84-1672, 1984.

14. Gaster, M.: Propagation of Linear Wave Packets in Laminar Boundary Layers. AIAA Journal, Vol. 19, No. 4, pp. 419-423, April 1981.

15. El-Hady, N. M.; and Nayfeh, A. H.: Non-parallel Stability of Compressible Boundary-Layer Flows. AIAA Paper No. 80-0277, 1980.

16. Saric, W. S.; and Nayfeh, A. H.: Non-Parallel Stability of Boundary Layers with Pressure Gradients and Suction. Laminar-Turbulent Transition, AGARD-CP-224, pp. 6-1 - 6-21, May 1977.

17. Pate, Samuel R.: Effects of Wind Tunnel Disturbances on Boundary-Layer Transition with Emphasis on Radiated Noise: A Review. AIAA Paper No. 80-0431, 1980.

18. Saric, W. S.; and Yeates, L. G.: Experiments on the Stability of Crossflow Vortices in Swept Wing Flows. AIAA Paper No. 85-0493, 1985.

19. Viken, J. K.: Boundary Layer Stability and Airfoil Design. Laminar Flow Aircraft Certification - 1985, NASA CP-2413, 1986.

20. Nayfeh, A. H.: Effect of Streamwise Vortices on Tollmien-Schlichting Waves. Journal of Fluid Mechanics, Vol. 107, pp. 441-453, 1981.

21. Reed, H. L.: Wave Interactions in Swept Wing Flows. AIAA Paper No. 84-1678, 1984.

22. Reed, H. L.: Disturbance Wave Interactions in Flows With Crossflow. AIAA Paper No. 85-0494, 1985.

23. Gray, W. E.: The Effect of Wing Sweep on Laminar Flow. Royal Aircraft Establishment, TM Aero 255, 1952.

24. Pfenninger, Werner: Laminar Flow Control Laminarization. Special Course on Concepts for Drag Reduction, AGARD-4-654, pp. 3-1 thru 3-75, June 1977.

25. Görtler, H.: Instabilität laminaren Grenzehichten an konkaven Wanden gengenüber gewissen dreidimensionalen Storungen. ZAMM, Vol. 21, No. 1, pp. 250-252, 1941.

26. Herbert, T. H.: On the Stability of The Boundary Layer Along a Concave Wall. Arch. Mechaniki Stosowanej, Vol. 28, No. 5-6, pp. 1039-1055, 1976.

27. Floryan, H. M.; and Saric, W. S.: Stability of Görtler Vortices in Boundary Layers. AIAA Journal, Vol. 20, No. 3, pp. 316-324, March 1985.

28. Wortmann, F. X.: Visualization of Transition. J. Fluid Mech., Vol. 38, Part 3, 1969, pp. 473-480.

29. Bippes, H.: Experimental Study of the Laminar-Turbulent Transition on a Concave Wall in a Parallel Flow. NASA TM-75243, 1978.

30. Mangalam, S. M.; Dagenhart, J. R.; Hepner, T. E.; and Meyers, J. F.: The Görtler Instability on an Airfoil. AIAA Paper No. 85-0491, 1985.

31. Smith, A. M. O.: On the Growth of Taylor-Görtler Vortices Along Highly Concave Walls. Quart. Applied Math., Vol. 13, No. 3, pp. 233-262, October 1955.

32. Tani, I.; and Aihara, Y.: Görtler Vortices and Boundary-Layer Transition. ZAMP, Vol. 20, pp. 609-618, 1969.

33. Aihara, Y.; and Koyama, H.: Secondary Instability of Görtler Vortices-Formation of Periodic Three-Dimensional Coherent Structure. Trans. Japan Soc. Aeron. Astron., Vol. 24, 1981.

34. Herbert, T. H.: Higher Eigen States of Görtler Vortices. In Theoretical and Experimental Fluid Mechanics, ed., U. Muller et al., Springer-Verlag, pp. 322-330, 1979.

35. Antonatos, P. P.: Laminar Flow Control - Concepts and Applications. Astronautics and Aeronautics, Vol. 4, No. 7, pp. 32-36, 1966.

36. Whites, R. C.; Sudderth, R. W.; and Wheldon, W. G.: Laminar Flow Control on the X-21. Astronautics and Aeronautics, Vol. 4, No. 7, pp. 38-43, 1966.

37. Wagner, R. D.; and Fischer, M. C.: Fresh Attack on Laminar Flow. Aerospace America, Vol. 22, No. 3, pp. 72-76, 1984.

38. Wagner, R. D.; Maddalon, D. V.; and Fischer, M. C.: Technology Development for Laminar Boundary Control on Subsonic Transport Aircraft. AGARD-CP-365, pp. 16-14 to 16-13, 1984.

39. Wazzan, A. R.; Okamura, T. T.; and Smith, A. M. O.: The Stability and Transition of Heated and Cooled Incompressible Laminar Boundary Layers. Proc. 4th Int. Heat Transfer Conf., ed., U. Grigull and E. Hahne, vol. 2, FC 1.4, Elsovier, 1970.

40. Reshotko, E.: Drag Reduction by Cooling in Hydrogen-Fueled Aircraft. Jour. Aircraft, vol. 16, No. 9, pp. 584-590, Sept. 1979.

41. Boehman, L. I.; and Mariscalco, M. G.: The Stability of Highly Cooled Compressible Laminar Boundary Layers. AFFDL Technical Report 76-148, 1976.

42. Lekoudis, S.: The Stability of the Boundary Layer on a Swept Wing with Wall Cooling. AIAA Paper No. 79-1495, 1979.

43. Liepmann, H. W.; and Nosenchuck, D. M.: Active Control of Laminar-Turbulent Transition. J. Fluid Mech., Vol. 118, pp. 201-204, 1982.

44. Biringen, S.; and Maestrello, L.: Development of Spot-Light Turbulence in Plain Channel Flow. Physics of Fluids 27-2, pp. 318-321, February 1984.

45. Bayliss, A.; Maestrello, L.; Parikh, P.; and Turkel, E.: Numerical Simulation of Boundary Layer Excitation by Surface Heating/Cooling. AIAA Paper No. 85-0565, 1985.

46. Maestrello, L.: Active Transition Fixing and Control of the Boundary Layer in Air. AIAA Paper No. 85-0564, 1985.

47. Biringen, S.: Final Stages of Transition to Turbulence in Plane Channel Flow. Journal of Fluid Mechanics, Vol. 148, pp. 413-432, 1984.

48. Herbert, T.; and Morkovin, M. V.: Dialogue on Bridging Some Gaps in Stability and Transition Research, in R. Eppler and H. Fasel, eds., Laminar-Turbulent Transition, Springer-Verlag, pp. 37-46, 1980.

49. Waggoner, E. G.: Computational Wing Design Studies Relating to Natural Laminar Flow, Laminar Flow Aircraft Certification - 1985, NASA CP-2413, 1986.

50 Saric, W. S.; Kizlov; V. V.; and Levchenko, V. Ya.: Forced and Unforced Subharmonic Resonance in Boundary-Layer Transition. AIAA Paper 84-0007, 1984.

51. Morkovin, M. V.: Instability, Transition to Turbulence and Predictability. Keynote Paper, AGARD Conference on Laminar-Turbulent Transition, AGARDograph No. 236, May 1977.

52. Reshotko, E.: Boundary Layer Stability and Transition. Annual Review of Fluid Mechanics, Vol. 8, pp. 311-349, 1976.

53. Reshotko, Eli: Control of Boundary Layer Transition. AIAA Paper No. 85-0562, 1985.

IX. Certification Aspects of NLF Airplanes

Introduction

It would appear that the certification of aircraft which are designed to achieve a high degree of natural laminar flow raises concerns if the flow changes during the operation of the airplane. Such changes could occur by flight into rain; by accumulation of ice, frost, insects, or dirt; or because of in-service damage and even paint applications. Consideration should therefore be given to the effects of loss of significant portions of laminar flow. Such loss of NLF has been seen to affect airplane performance and flying qualities and could also change airloads.

During Design

Early in the certification process, the application for certification should present to the FAA the likely extent of NLF and the possible consequences of loss of significant portions of NLF. Flight testing and other research being conducted by the company and elsewhere would be used to determine the extent of NLF. For example, the stall speeds and characteristics may change as a result of loss of NLF, which could affect take-off and landing performance and the flying qualities of the airplane during these phases. Special attention may be required for forward-wing aircraft, since these configurations have shown some adverse aerodynamic effects of a loss of NLF. In short, significant adverse effects of a loss of NLF on flying qualities, performance, or flight loads should be minimized or corrected during the design process.

During Certification

Here it would seem that any loss of NLF should be covered in the same way that the accumulation of ice is treated on non-laminar flow airplanes being certified to fly under these conditions. Performance, handling qualities, and stall characteristics have to be evaluated with simulated and natural ice, and the effects documented for incorporation into the approved Aircraft Flight Manual (AFM) or into the Pilots Operating Handbook (POH). If the aircraft is especially sensitive to surface smoothness, waviness, or contour limits for the maintaining of NLF, recommendations for in-service inspection and maintenance would have to be formulated for inclusion in the maintenance and repair manuals. Also, the Approved Process Specification (APS) could include reference to the requirements for achieving NLF.

Conclusions

1. The certification of airplanes designed for significant areas of natural laminar flow (NLF) should not necessitate any special requirements, other than recognizing the effects of a loss of all or a portion of the NLF and making sure that these effects are reflected in the appropriate documentation.

2. Research should be directed towards maximizing the favorable characteristics of NLF, while minimizing any adverse effects of a loss of NLF during normal operation.

3. Recommendations should be formulated for the in-service inspection and maintenance of airplanes designed for a significant degree of NLF, and these recommendations should be included in the appropriate manuals.

OPERATIONAL PROCEDURES WORKING GROUP SUMMARY AND RECOMMENDATIONS

Charles E. Arnold, Chairman

I. General

The operational procedures group met to focus on what factors should be considered when operating an airplane which has been designed with extensive runs of natural laminar flow (NLF). For the purposes of this workshop, augmented laminar flow was not addressed. The group concentrated on defining the types of information operators of NLF airplanes should be aware of and the best way of presenting the information to ensure that the operators' needs are met and that design objectives of the manufacturer are achieved.

After a brief discussion, it became apparent that all considerations of the impact of NLF characteristics would be dependent upon the objectives of the manufacturer in certificating the airplane. If the airplane is certificated so that all factors of certification are predicated on the existence of extensive NLF, then a high degree of attention to actions necessary to retain NLF would be required. Conversely, if the certification process ensured that loss of NLF had no adverse impact on the standards of certification, then operational considerations could be minimized to just an information process. The operational considerations would then be analogous to the effects of wind on planning and operation; that is, if proper preflight procedures are followed, one could expect some advantages from NLF; however, like the wind, it may not develop, and contingencies should be planned. However, if the airplane has been certificated and operations are predicated on the benefits of extensive NLF, then detailed procedures must be defined to assure that the aircraft will continuously meet certification standards. Since contaminants on the airfoil(s) are known to affect characteristics of lift, drag, and pitching moments, procedures or processes for controlling the results produced by contaminants must be addressed. Also, since performance, controllability, and stability will have been established on the assumption of having extensive NLF, the pilot must have some means of determining when the boundary layer has become turbulent and be provided proper emergency procedures that must be applied for continued safe flight.

II. Aircraft Certificated Without Significant Natural Laminar Flow

Discussions in this section will be limited to those airplanes having aerodynamic surfaces that do have significant runs of natural laminar flow (NLF) but have been certificated such that loss of NLF has been shown to produce no significant impact on the certification standards. It will be necessary in the certification process to examine all significant flight parameters with the boundary layer tripped to ensure that no hazard exists and that all information published in the airplane flight manual represents "tripped" conditions. The airplane flight manual should contain sufficient discussion on the subject of NLF to assure that information is provided to the pilot on the airplane characteristics and performance with and without NLF and on what precautions are appropriate with the existence and loss of NLF.

The following types of information should be considered in the airplane flight manual or POH:

1. Preflight procedures to include planning considerations, inspection of aerodynamic surfaces and propellers, and cleaning procedures for each. Consideration of taxi and take-off surfaces and avoidance of surface conditions that would contaminate any part of the airplane that would be critical to laminar flow.

PRECEDING PAGE BLANK NOT FILMED

2. Performance data should be presented for both laminar and turbulent conditions, or at least the incremental difference for the laminar condition, presuming only turbulent data were provided to meet certification requirements. Particular precautions should advise on the effect of laminar flow existing or not existing. For example, if all landing data are presented on the basis of a turbulent boundary layer, approach speeds may be slightly higher, drag may be slightly higher, and lift slope curves may be lower than those existing for a laminar condition. If the approach is made in a laminar state, additional float may occur and result in longer landing distances than published data currently indicate.

3. Any effect on controllability or stability should be discussed. This may be particularly significant if control or balancing surfaces are subject to NLF transitions. This has been a noted significance on certain canard or tandem wing installations. Also, the impact of asymmetric tripping or transition should be considered.

4. The servicing and maintenance sections of the flight manual are perhaps the most important concerns for a person desiring to ensure that the benefits of NLF are to be available during flight. The inspection, cleaning, maintenance, and repair procedures should be clearly and distinctly set forth in all appropriate sections of the airplane flight manual as well as the maintenance manual. The General Aviation Manufacturers Association Specification No. 1 may be used as a guide to the types of information to be provided. Particular attention should be paid to the differentiation between "preventive maintenance" as defined in FAR Part 43 and that maintenance required to be performed by a licensed mechanic.

III. Aircraft Certificated with Significant Natural Laminar Flow

The discussions in this section will concentrate only on airplanes having significant runs of natural laminar flow, where compliance with all certification standards and performance data is predicated on maintaining continuous laminar flow. As with aircraft certificated without benefit of natural laminal flow, the certification process will have significant impact on what information is necessary and how it is handled in the airplane flight and maintenance manuals. If the certification process reveals little impact from transition between laminar and turbulent conditions, it is probable that advisory information as described in section II above would be adequate. However, if the existence of a turbulent boundary layer compromises performance, controllability, stability, or other certification standards, the emphasis of the manual will be distinctly different. Also of distinct importance would be the need for the pilot to know when the boundary layer is tripped and either what actions are necessary to restore laminar flow or what emergency or diversionary actions are appropriate.

The considerations to be used in the airplane flight manual or POH are about the same as those enumerated in section II. The major difference is in emphasis. The procedures would now become authoritative and be written in the imperative mood. Also, certain limitations may be necessary both from the operator's perspective as well as from the maintenance perspective. Maintenance procedures and appropriate airworthiness limitations are required by FAR Part 23.1529 and may contain specific procedures prior to flight if found necessary in the certification process. Inspection and repair criteria and tolerances should receive careful attention to ensure surface smoothness is retained.

IV. Education Concerns

The discussions in sections II and III concentrated on information pertaining to a specific airplane design. Most of the information necessary for the pilot to properly operate an airplane with significant runs of natural laminar flow is cited because this type of information is not currently available to the average pilot. It will be necessary to begin building a foundation of knowledge that is widely published in all normal sources for pilot education. The FAA Advisory Circular System should be an early target to provide information in laymen's terms as well as a compendium of references.

Another concern where education will be necessary is the FAA Air Traffic Control System (ATC). The ATC system should become sensitive to the needs of a pilot to avoid certain climatic conditions if laminar flow is to be retained and predicted speeds maintained. Again, this could be the subject of appropriate Advisory Circulars.

MANUFACTURING TECHNOLOGY WORKING GROUP SUMMARY AND RECOMMENDATIONS

Bert Overfield, Chairman

Introduction

Aircraft manufacturers, along with technical societies and government agencies, are concentrating very heavily on improvements in operating efficiencies. One of the latest areas to be pursued is aerodynamic design for maximum utilization of laminar flow. Partial laminar flow has been an aerodynamic characteristic of numerous airplane wings, including sailplanes, for many years. The intent of these recent efforts is to greatly improve the laminar flow over wings and expand its use to empennage and canard surfaces, and eventually to the fuselage. The result would be significant improvements in speed, range, and fuel efficiency. The purpose of the manufacturing technology working group was to review the requirements of laminar flow design and compare them to current state-of-the-art fabrication methods. We would then establish short- and long-term development requirements and make specific recommendations regarding design for producibility.

State-of-the-Art Fabrication Methods

In the past few years, there have been significant improvements in the equipment and machine tools necessary for the tooling and manufacture of aircraft structures and components. One of the most important is the expanded use and improvements in computer-aided design (CAD) and computer-aided manufacturing (CAM). Of equal significance is the expansion of capabilities of computer numerically controlled (CNC) machine tools.

Sheet metal forming, the old standby of aircraft construction, has improved significantly. CAD and CAM provide us with the means to make close tolerance master tools and forming tools. Metal forming equipment, such as high-pressure bag presses, computerized stretch presses, and automatic riveters, is used extensively for smooth aerodynamic surfaces. Metal bonded skins provide even further refinements.

Milled wing and empennage skin panels have been around for some time, but improvements continue to be made in CNC controlled three-, four-, and five-axis gantry mills. Thinner panels can be machined flat and roll formed or shot peen formed to contour.

The last few years have shown great improvements in the use of composites and bonded honeycomb structures for aerodynamic surfaces. Advances are continually being made in layup and bond tooling to provide extremely smooth outer surfaces. Additional improvements are being made to control laminate thickness after cure.

The consensus of opinion of the workshop members was that the technology currently exists to meet virtually any laminar flow design requirement. The major concern of the group was the manufacturing costs associated with meeting these design parameters.

Development Requirements

As previously stated, manufacturing costs are of great concern for the attainment of laminar flow. As we all know, tooling and production costs increase dramatically, some exponentially, as tolerances become tighter. Initial tolerance

PRECEDING PAGE BLANK NOT FILMED

requirements for laminar flow were set extremely tight, some beyond manufacturing capability. Recent R & D efforts have provided some relaxation, but the costs of compliance are, in many cases, prohibitive. The cost factor is extremely important, especially in general aviation aircraft, which are very price sensitive.

In the short term, R & D effort should be expended to determine the maximum allowable tolerances for the required laminar flow characteristics. These should include surface roughness, waviness, steps and gaps, and contour. In addition, procedures must be developed for rework or repair in the event the required tolerances are exceeded. Recent developments of shaped steps and gaps are a good starting point. Improvements must be made in fastener design and installation. This is especially critical to leading-edge attachment.

Of equal importance is the development of quality assurance (QA) procedures and equipment that are suitable for these criteria on a production basis. Once the tolerances are firmly established by design, it becomes necessary to prove that the finished article conforms to type design.

In the long term, the design criteria for laminar flow must be broken down for discrete areas and conditions. Specific questions need to be addressed, such as:

Over what portion of the surface is laminar flow attainable?

What are the basic contour tolerances? Can cusps be straightened and trailing edges thickened without large penalties?

Do the surface irregularity tolerances (i.e., gaps, laps, fasteners, etc.) change downstream? If so, which way?

Are the requirements different for wings, empennage surfaces, canards, fuselage, etc.?

Is laminar flow over the fuselage feasible? If so, are the benefits worth the cost?

Conclusions

Manufacturing of airplanes for laminar flow is certainly achievable if the cost is not prohibitive. A very close interaction is needed between aerodynamics, structures, design, and manufacturing. Considerable development effort is needed to be assured of cost effective production. Careful consideration should be given to the probable condition of the airplanes after years of service. Are current maintenance and field repair techniques going to be adequate to assure continuation of laminar flow characteristics? Special maintenance manual material may need to be developed to meet the requirements for continued airworthiness.

1. Report No. NASA CP-2413	**2. Government Accession No.**	**3. Recipient's Catalog No.**

4. Title and Subtitle LAMINAR FLOW AIRCRAFT CERTIFICATION	**5. Report Date** May 1986
	6. Performing Organization Code 505-61-41-02
7. Author(s) Louis J. Williams, Compiler	**8. Performing Organization Report No.** L-16111
9. Performing Organization Name and Address NASA Langley Research Center Hampton, VA 23665-5225	**10. Work Unit No.**
	11. Contract or Grant No.
12. Sponsoring Agency Name and Address National Aeronautics and Space Administration Washington, DC 20546-0001	**13. Type of Report and Period Covered** Conference Publication
	14. Sponsoring Agency Code

15. Supplementary Notes

16. Abstract

This workshop on laminar flow aircraft certification was an outgrowth of the NASA/AIAA General Aviation Technology Conference held at the NASA Langley Research Center in 1984. At that conference, several people from NASA Langley, the Federal Aviation Administration, industry, and universities expressed the desire for a forum to discuss the effect of laminar flow aerodynamics on certification procedures for future aircraft. It was felt that such a forum should bring together researchers, concerned with maximizing the benefits of laminar flow aerodynamics; manufacturers, concerned with developing significantly improved new aircraft; and regulators, concerned with applying proper certification procedures to insure safety. By bringing together these diverse interests to address the common goal of developing new aircraft with superior efficiency, it was hoped that an improved understanding of laminar flow aerodynamics technology would be obtained and that improved communications between the participants would serve to guide future efforts.

The workshop was structured to review the state of the art in laminar flow aerodynamics technology and explore technology needs in four areas: test techniques, aerodynamics research, operational procedures, and manufacturing technology.

17. Key Words (Suggested by Author(s)) Laminar flow Aircraft certification General aviation Flight experiments	**18. Distribution Statement** [redacted] Subject Category 02

19. Security Classif. (of this report) Unclassified	**20. Security Classif. (of this page)** Unclassified	**21. No. of Pages** 333	**22. Price**

[redacted]

NASA-Langley, 19